Cancer Cell

Best of 2014

Featuring a Snapshot Collection

CellPress
www.cell.com

“ WE’RE BRINGING A NEW PERSPECTIVE TO

cancer metabolism research

XF technology provides the easiest and most comprehensive assessment of cancer cell metabolism, measuring glucose and glutamine metabolism, and fatty acid oxidation of cancer cells in a microplate, in real time! ”

— Kacey Caradonna PhD,
Applications Scientist
Seahorse Bioscience

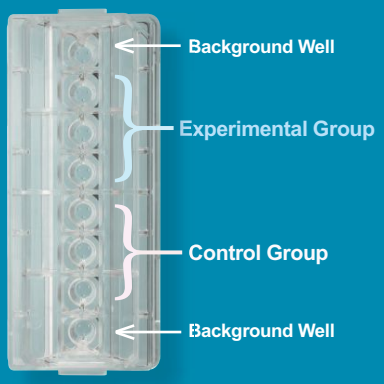

The Seahorse XFp Extracellular Flux Analyzer

Measurements of cellular glycolysis are essential to understanding cancer. The XFp Analyzer and XFp Glycolysis Stress Test Kit make it easy to measure the three key parameters of cellular glycolysis in a microplate: glycolysis, glycolytic capacity, and glycolytic reserve, revealing critical information not evident in mitochondrial respiration measurements alone.

See what’s possible.

Scan this QR code to view videos and see what the XF technology can achieve. Visit www.seahorsebio.com/cancercell for more information!

Seahorse Bioscience

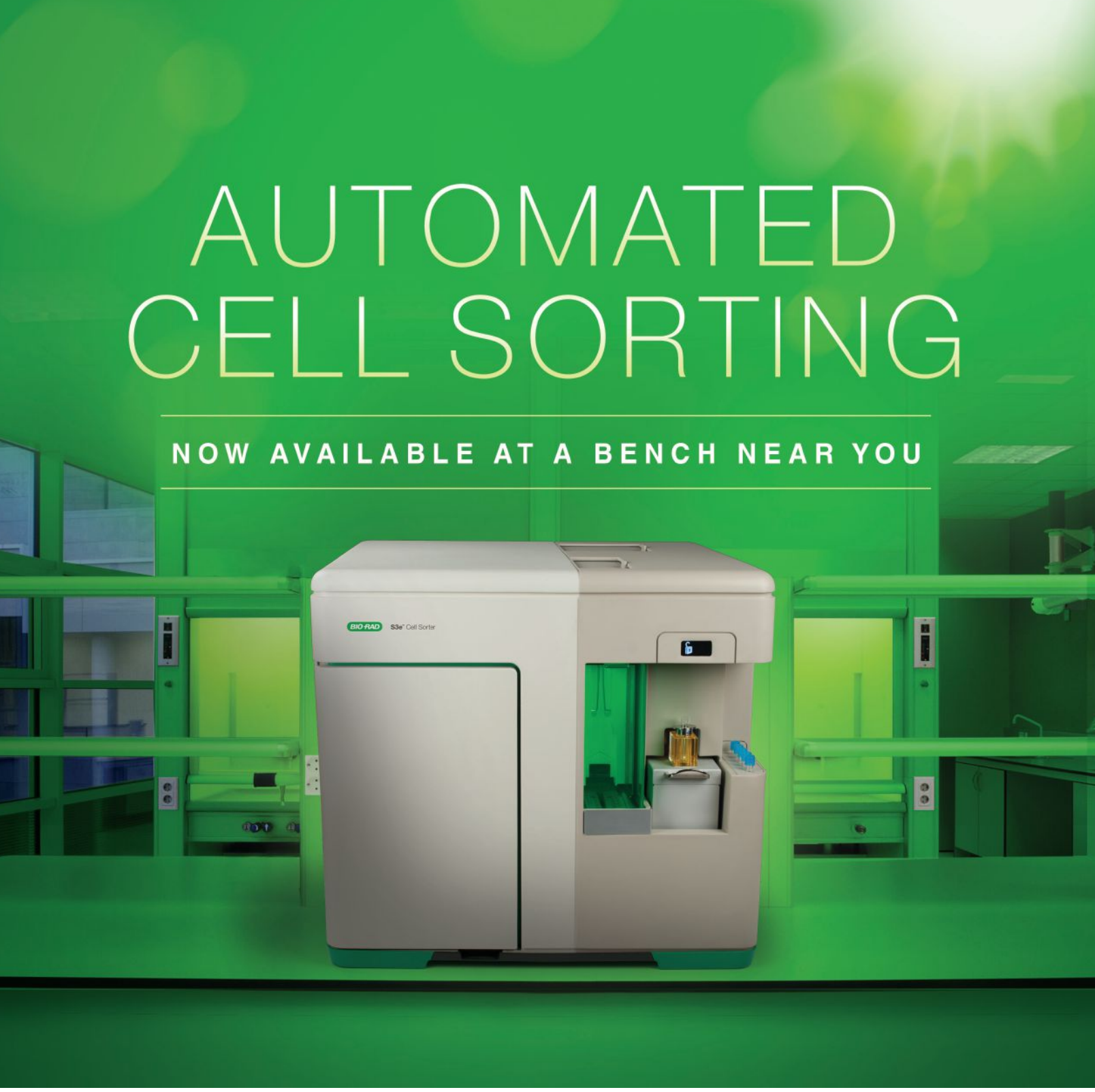

Presenting automation that lets you sort cells right in your lab.

The S3e™ Cell Sorter is designed to make cell sorting simple and accessible to all. Advanced automation features eliminate the need for extensive flow cytometry expertise by allowing instrument setup and operation with minimal user input while a small footprint and affordable price ensure that the S3e fits into almost any lab. It's time to put the focus on research and take the how, when, and where out of cell sorting.

Learn more about the S3e Cell Sorter at **bio-rad.com/info/BenchNearYou**

BIO-RAD

Introducing

bio-techne®

HIGHEST QUALITY PRODUCT PORTFOLIO

TRUSTED GLOBAL BRANDS

R&D systems NOVUS BIOLOGICALS™ TOCRIS

bio-techne® LEARN MORE bio-techne.com/launch

Building Innovation Opportunities

bio-techne.com
info@bio-techne.com
techsupport@bio-techne.com

North America
TEL 800 343 7475

Europe • Middle East • Africa
TEL +44 (0)1235 529449

China
info.cn@bio-techne.com
TEL +86 (21) 52380373

Rest of World
bio-techne.com/find-us/distributors
TEL +1 612 379 2956

Personalis®
ACE Services *for* Cancer Research & Clinical Trials

VISIT US AT
AACR 2015 | Booth 2156

Personalis @ AACR 2015

Exhibitor Spotlight Theater A

TUESDAY, APRIL 21
@ **10:00 AM**
Exhibit Hall

ACE Extended Cancer Panel for DNA and RNA

The Most Complete and Accurate Tumor Profiling

Designed for both cancer research and clinical trials

The **Accuracy and Content Enhanced (ACE) Extended Cancer Panel** has been designed to support both cancer research and clinical trials. It provides more coverage of gene pathways and functions known to be involved in cancer biology than any other panel commercially available. Up until now discovery researchers have had to make a choice between the breadth of sequencing used to find novel variants in cancer-related genes, and the depth of sequencing needed to identify variants present at low allelic fraction. The Personalis ACE Extended Cancer Panel is the first service to combine the breadth of coverage for novel variant discovery across key cancer pathway genes, with the sequencing depth needed to detect variants present at low allelic fraction.

- Comprehensive coverage of key cancer pathway genes
- >500x mean coverage over the extended footprint (DNA)
- Sensitivity for both known and novel fusion events (RNA)
- The most advanced and complete informatics analysis

enhanced coverage of
over 1,300+ cancer genes
and
over 200+ miRNA genes

www.personalis.com/cancer
info@personalis.com
+1 855 436-6634 | **+1 650 752-1300**

Personalis®
Pioneering Genome-Guided Medicine

EMD MILLIPORE

Simple, affordable flow cytometry – now at your side.

Sophisticated cancer cell analysis doesn't have to be exclusive, complicated, or costly. With the Muse® Cell Analyzer, you can now achieve highly quantitative results with statistical power, cell by cell. The Muse® Cell Analyzer packs 3-parameter analysis into a compact, easy-to-use benchtop device, making flow cytometry accessible to anyone, anytime. A user-friendly touchscreen interface, intuitive software, and reagents optimized for critical cancer research assays are engineered to simplify your work.

Discover the Muse® Cell Analyzer

www.emdmillipore.com/muse

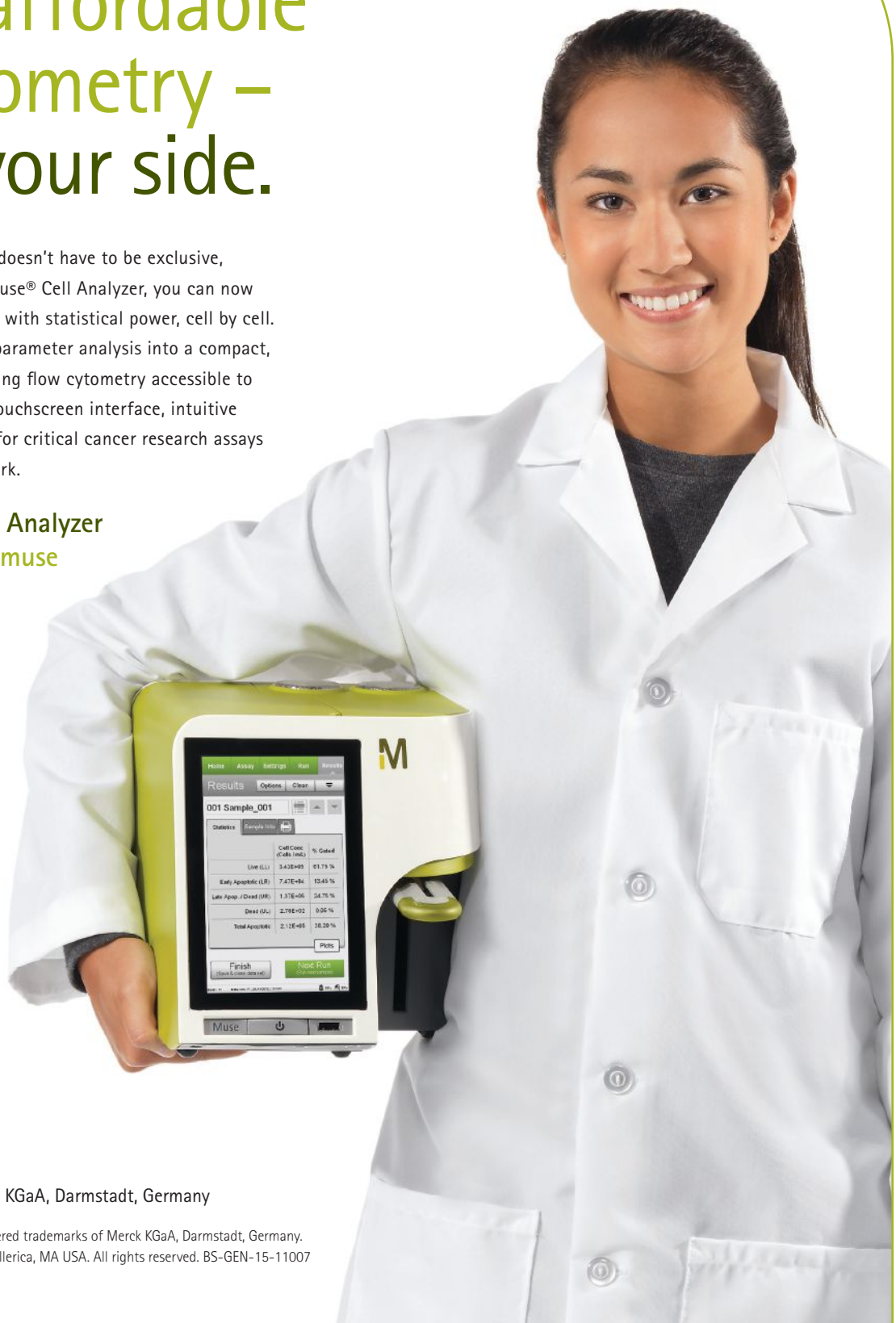

EMD Millipore is a division of Merck KGaA, Darmstadt, Germany

Foreword

In 2012 we introduced *Best of Cancer Cell 2011* as one of the first "Best of" reprint collections from Cell Press. Last year's third edition, *Best of Cancer Cell 2013*, continued to surpass our expectations and received even greater attention than any prior, with downloads of the digital edition exceeding 45,000. We are pleased to offer the fourth installment of this collection, *Best of Cancer Cell 2014,* in timing for the 2015 AACR annual meeting.

Cancer Cell is published monthly in two volumes each year. In order to account for the amount of time since publication, we have selected a mix of the most highly accessed research articles, perspectives, and reviews from volumes 25 and 26, which cover the first and second halves of 2014, respectively. We use the number of requests for PDF and full-text HTML versions of a given article to identify the "most-accessed" articles, taking into consideration the range of topic areas presented to provide our readers with a clearer sense of *Cancer Cell*'s breadth and scope. It is also extremely gratifying to see that the works featured in this collection come from around the world, reflecting the forefront of a global fight against cancer. Of course, no single measurement can be accurately indicative of "the best" research papers over a given period of time. This is especially true for new publications because the community hasn't had enough time to fully appreciate the relative importance of the findings. That said, we are confident that you will still find this collection informative and exciting.

Prior to the start of the articles, you will find four SnapShots examining various cancer biologies: hepatocellular carcinoma, medulloblastoma, chronic lymphocytic leukemia, and diffuse large B cell lymphoma. *Cancer Cell* is proud to feature these extraordinary collaborative efforts by researchers, editors, and our graphic artists.

We hope that you will enjoy reading this special collection. You can access the entire "Best of" Cell Press collection online at www.cell.com/bestof. Visit www.cell.com/cancer-cell to learn about the latest findings that *Cancer Cell* has had the privilege to publish and www.cell.com to find other high-quality cancer-relevant papers published in the full portfolio of Cell Press journals. Please feel free to contact us at cancer@cell.com to tell us about your latest work or to provide feedback. We look forward to working with you in 2015 and beyond!

Finally, we are grateful for the generosity of our sponsors, who helped to make this reprint collection possible.

Cancer Cell

For information for the Best of Series, please contact:
Jonathan Christison
Program Director, Best of Cell Press
e: jchristison@cell.com
p: 617-397-2893
t: @CellPressBiz

Molecular Probes®

Exhibit the brightest cell images using Alexa Fluor® secondary antibodies

With over 30,000 citations, it's no secret Alexa Fluor® dye–labeled secondary antibodies are the leader in fluorescence. Consistently dependable and available in 20 different colors, their brilliant hues have helped scientists visualize their research for nearly two decades.

Find out more about Alexa Fluor® secondary antibodies at **lifetechnologies.com/alexafluor**

life technologies

A **Thermo Fisher Scientific** Brand

MBL International Corporation

Cancer Epigenetics

Enrich. Detect. Discover. Identify.

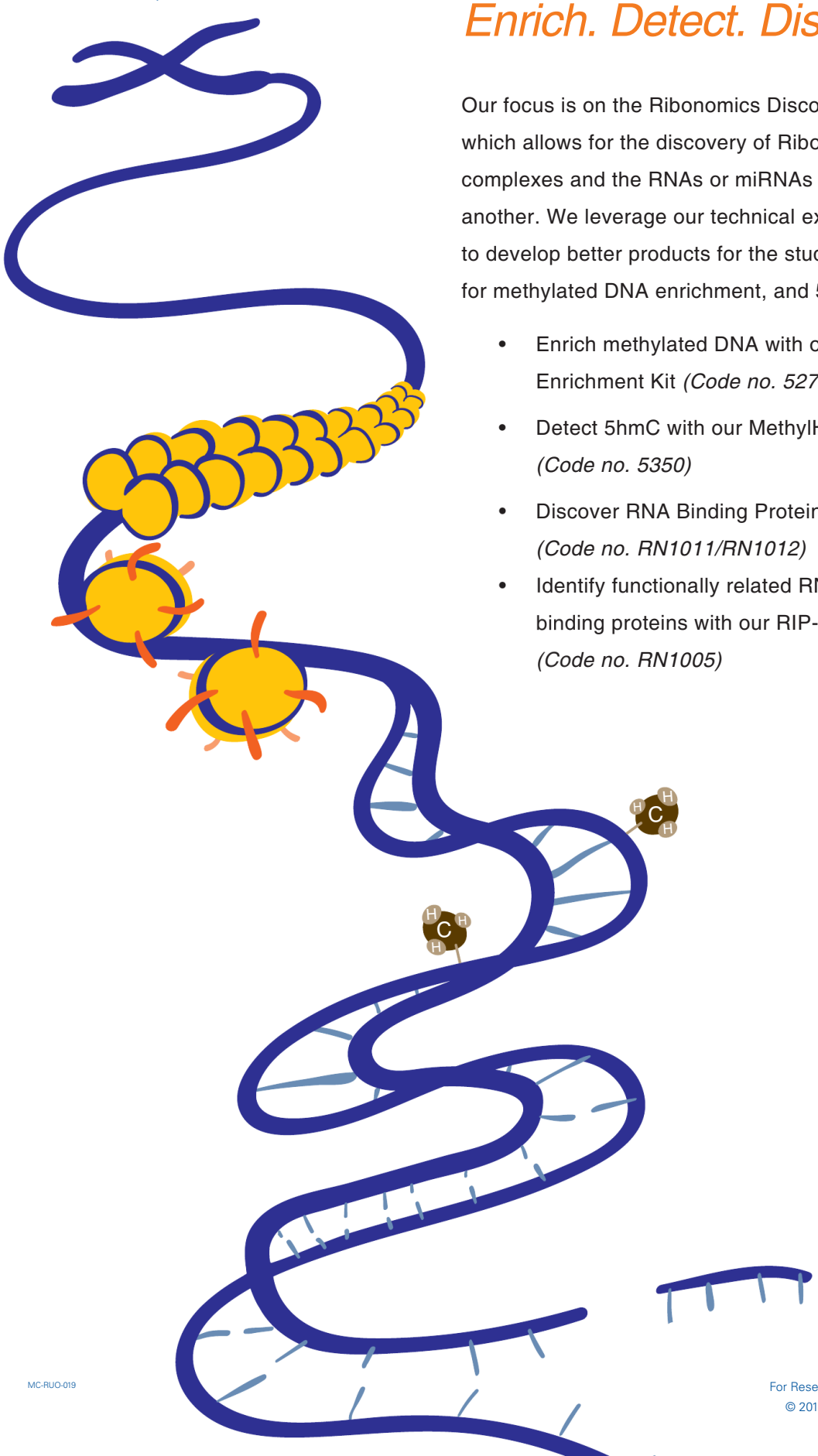

Our focus is on the Ribonomics Discovery Cycle, a process which allows for the discovery of Ribonucleoprotein (RNP) complexes and the RNAs or miRNAs which regulate one another. We leverage our technical expertise in RNA technology to develop better products for the study of DNA, products for methylated DNA enrichment, and 5hmC detection.

- Enrich methylated DNA with our MethylHunter™ MBD1 Enrichment Kit *(Code no. 5275)*
- Detect 5hmC with our MethylHunter™ 5hmC Detection Kit *(Code no. 5350)*
- Discover RNA Binding Proteins with our RiboTrap Kit *(Code no. RN1011/RN1012)*
- Identify functionally related RNAs and miRNA of RNA binding proteins with our RIP-Assay™ Kit *(Code no. RN1005)*

mblintl.com
800-200-5459
781-939-6964

MC-RUO-019

Detection this specific. Even in unpurified samples.

High throughput protein quantification and quality assessment

The Octet platform lets you screen bioprocess samples quickly and accurately, with little to no prep.

- **Antibody and protein concentration.** Measure 96 titers in 2 minutes directly from supernatants or lysates.
- **Host cell protein and residual protein A detection.** Analyze 96 samples in under 2 hours with a fully-automated workflow.
- **Protein quality.** Profile molecules based on differences in glycosylation and binding affinities.

fortebio.com | 888-OCTET-75

fortéBIO
A Division of Pall Life Sciences

PALL Life Sciences

The BD Accuri™ C6 for Cancer Research

Flow cytometry on the benchtop for a more complete view of the cell

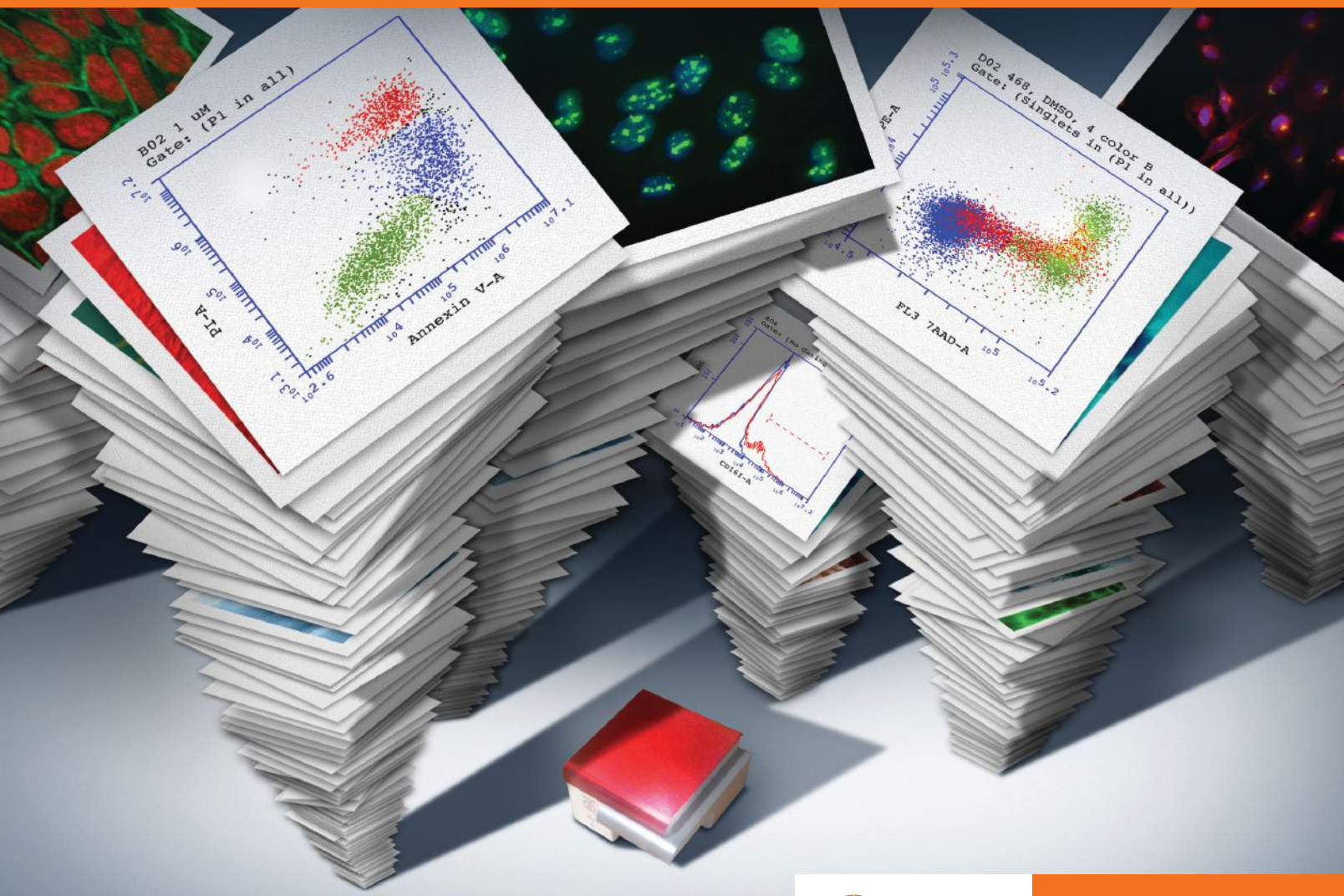

BD

Helping all people live healthy lives

A small space on your benchtop that speaks volumes about the cancer cell

The BD Accuri™ C6 personal flow cytometer takes up less than 0.5 cubic meter of bench space but gives cutting-edge data from multiparametric cell analysis. It's an indispensable tool for the cancer researcher, enabling immunophenotyping, cell function and signaling, and dose-response applications right in your own lab.

The BD Accuri C6 is affordable, easy to learn, easy to use, and transportable.

Free, downloadable software templates and BD reagents and kits provide simplified setup and analysis. And, the BD Accuri C6 is inexpensive to operate and simple to maintain.

Find out how you can transform a small space on your benchtop into your most valued tool and take advantage of **unprecedented special offers** that put flow cytometry even more within reach at **bdbiosciences.com/go/cancerbiology.**

BD Biosciences
2350 Qume Drive
San Jose, CA 95131
bdbiosciences.com

affymetrix
Biology for a better world

Distinguish between cancer drivers and passengers

Analytes to insight in less than one week

Introducing the new Concurrent Molecular Analysis Profiling (CoMAP™) capability in Chromosome Analysis Suite 3.0 software

CoMAP™ capability, in combination with Affymetrix' assays for copy number, gene expression, and miRNA expression, delivers

- Rapid co-analysis and visualization of genomic and transcriptomic data to identify and prioritize cancer driver events
- Accurate and robust results from limited and degraded FFPE tissues
- Biological insights from FFPE samples in less than one week

Visit www.affymetrix.com/CoMAP

#CoAnalyze

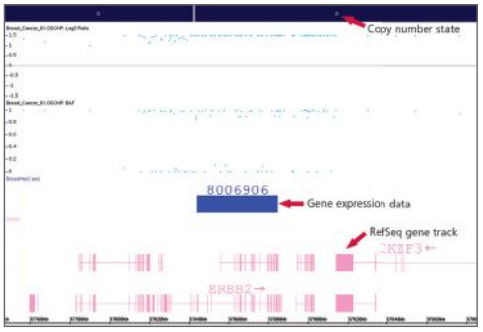

CoMAP™ capability
Get a single, comprehensive view of copy number, gene expression, and miRNA expression data.

eBioscience GeneChip USB

Cancer Cell

Best of 2014

(continued)

Disrupting the Interaction of BRD4 with Diacetylated Twist Suppresses Tumorigenesis in Basal-like Breast Cancer	*Jian Shi, Yifan Wang, Lei Zeng, Yadi Wu, Jiong Deng, Qiang Zhang, Yiwei Lin, Junlin Li, Tiebang Kang, Min Tao, Elena Rusinova, Guangtao Zhang, Chi Wang, Haining Zhu, Jun Yao, Yi-Xin Zeng, B. Mark Evers, Ming-Ming Zhou, and Binhua P. Zhou*
Stromal Elements Act to Restrain, Rather Than Support, Pancreatic Ductal Adenocarcinoma	*Andrew D. Rhim, Paul E. Oberstein, Dafydd H. Thomas, Emily T. Mirek, Carmine F. Palermo, Stephen A. Sastra, Erin N. Dekleva, Tyler Saunders, Claudia P. Becerra, Ian W. Tattersall, C. Benedikt Westphalen, Jan Kitajewski, Maite G. Fernandez-Barrena, Martin E. Fernandez-Zapico, Christine Iacobuzio-Donahue, Kenneth P. Olive, and Ben Z. Stanger*
Targeting Tumor-Associated Macrophages with Anti-CSF-1R Antibody Reveals a Strategy for Cancer Therapy	*Carola H. Ries, Michael A. Cannarile, Sabine Hoves, Jörg Benz, Katharina Wartha, Valeria Runza, Flora Rey-Giraud, Leon P. Pradel, Friedrich Feuerhake, Irina Klaman, Tobin Jones, Ute Jucknischke, Stefan Scheiblich, Klaus Kaluza, Ingo H. Gorr, Antje Walz, Keelara Abiraj, Philippe A. Cassier, Antonio Sica, Carlos Gomez-Roca, Karin E. de Visser, Antoine Italiano, Christophe Le Tourneau, Jean-Pierre Delord, Hyam Levitsky, Jean-Yves Blay, and Dominik Rüttinger*
Identification of Distinct Basal and Luminal Subtypes of Muscle-Invasive Bladder Cancer with Different Sensitivities to Frontline Chemotherapy	*Woonyoung Choi, Sima Porten, Seungchan Kim, Daniel Willis, Elizabeth R. Plimack, Jean Hoffman-Censits, Beat Roth, Tiewei Cheng, Mai Tran, I-Ling Lee, Jonathan Melquist, Jolanta Bondaruk, Tadeusz Majewski, Shizhen Zhang, Shanna Pretzsch, Keith Baggerly, Arlene Siefker-Radtke, Bogdan Czerniak, Colin P.N. Dinney, and David J. McConkey*
Metabolic Reprogramming of Stromal Fibroblasts through p62-mTORC1 Signaling Promotes Inflammation and Tumorigenesis	*Tania Valencia, Ji Young Kim, Shadi Abu-Baker, Jorge Moscat-Pardos, Christopher S. Ahn, Miguel Reina-Campos, Angeles Duran, Elias A. Castilla, Christian M. Metallo, Maria T. Diaz-Meco, and Jorge Moscat*

affymetrix
eBioscience

Detect RNA and protein in millions of single cells

Enter a new dimension of single-cell analysis

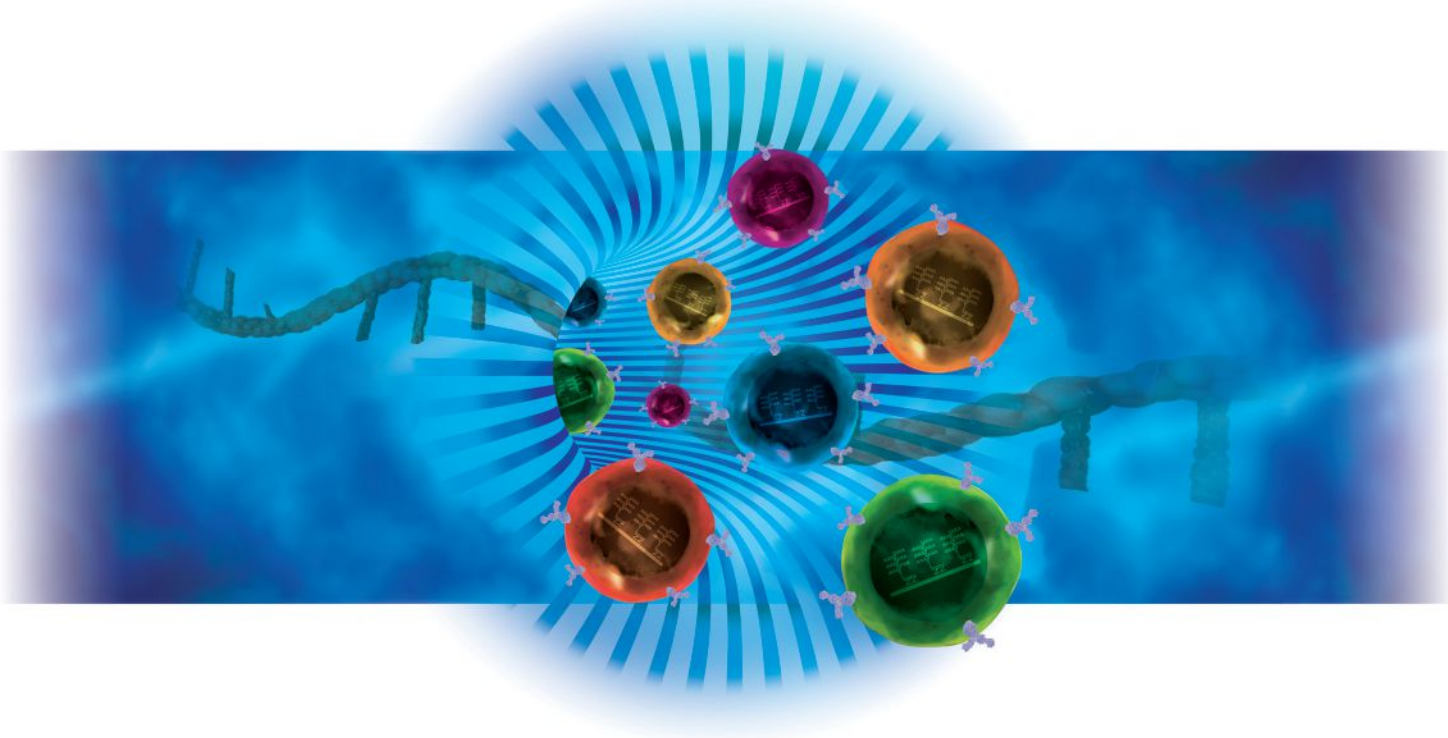

Detect RNA and protein simultaneously by flow cytometry to:

- See gene expression heterogeneity at the single-cell level
- Compare RNA and protein in the same cell
- Evaluate viral RNA within infected cells
- Detect non-coding RNA in cell subsets
- Analyze mRNA expression levels when antibody selection is limited

Real insight starts with single cells.
View webinar on demand "Detection of RNA with flow cytometry"
www.ebioscience.com/primeflow-tech-webinar-ccell

Biology for a better world.

NORTH AMERICA: 888-999-1371 ▪ EUROPE: +43 1 796 40 40-305 ▪ JAPAN: +81 (0)3 6430 4020 ▪ INQUIRIES: info@ebioscience.com

eBioscience GeneChip USB

BAKER

Environments For Science™

From the moment when
the pieces fell into place,
and you saw the big picture,

through late nights reviewing literature,
designing procedures,
testing hypotheses —

nothing fell through the cracks,
because too much was at stake.

The work you did then
advanced your field,
and your career.

We are proud to have been there,
protecting your work, and you,
with the very best in air containment,
contamination control, and
controlled environment technology.

Now, as your work gives rise
to new discoveries —

We can't wait to see what you do next.

bakerco.com

Biological Safety Cabinets • Clean Benches • Fume Hoods • CO_2 Incubators • Hypoxia & Anaerobic Workstations

The Inquiry-to-Insight Solution for Immune System Profiling

NOW available as a Research Use Only Kit, offering you the convenience and control of immunosequencing in your own lab

Harness the power of the adaptive immune system - in our lab or yours - to profile T- and B-cell receptors with groundbreaking sensitivity, accuracy, and specificity

Learn more at adaptivebiotech.com or by calling 855-466-8667

For Research Use Only. Not for use in diagnostic procedures.

immunoSEQ™

Amplify **Discovery**

Adaptive™ biotechnologies

1551 Eastlake Avenue East, Suite 200 • Seattle, WA 98102

P: 855.466.8667 **W:** adaptivebiotech.com

Introducing shERWOOD-UltramiR shRNA

Sensor-based shERWOOD algorithm
+ UltramiR scaffold
= Unrivaled Knockdown Performance

Find shRNA-mir constructs targeting your gene of interest using

FETCH my *gene*

www.transomic.com

Developed by Dr. Greg Hannon and colleagues at Cold Spring Harbor Laboratory, and available exclusively through transOMIC technologies, new generation shERWOOD UltramiR shRNA provide superior and more consistent gene knockdown than early generation shRNA designs. By incorporating advances in shRNA design (shRNA-specific shERWOOD algorithm) with optimized small RNA processing (UltramiR scaffold) these shRNA reagents produce unparalleled knockdown efficiencies to provide greater confidence in RNAi based studies-from single gene based phenotypes to large scale screens *in vitro* and *in vivo*.

- **shERWOOD Algorithm designs - Potent single copy knockdown**
- **UltramiR scaffold - Optimized small RNA processing for consistent knockdown**
- **100% Guarantee - Every shRNA is guaranteed to knockdown its intended target**

shERWOOD-UltramiR shRNA are available in lentiviral, inducible lentiviral or retroviral vectors to target human, mouse and rat genomes. Contact us at info@transomic.com to inquire about testing new shERWOOD-UltramiR shRNA today!

Visit www.transomic.com/shERWOOD-UltramiR for more information and to place your order

transOMIC technologies

www.transomic.com

Enabling Discovery Across the Genome

SnapShot: Hepatocelluar Carinoma

Jens U. Marquardt[1] and Snorri S. Thorgeirsson[2]
[1]Department of Medicine I, Johannes Gutenberg University of Mainz, 55131 Mainz, Germany
[2]Laboratory of Experimental Carcinogenesis, CCR/NCI/NIH, Bethesda, MD 20892, USA

Cancer Cell

CLINICAL PROGRESSION OF LIVER CANCER

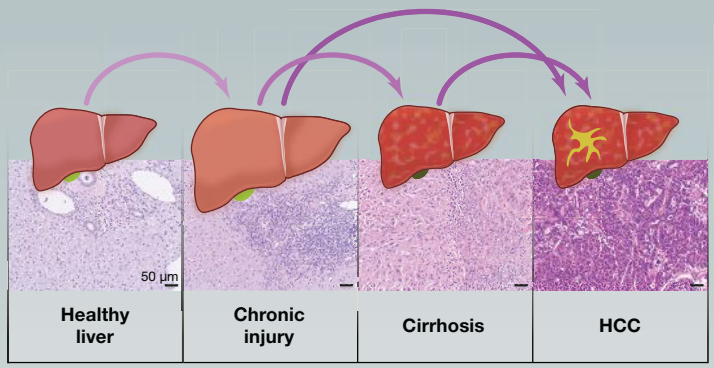

UNIFOCAL HCC

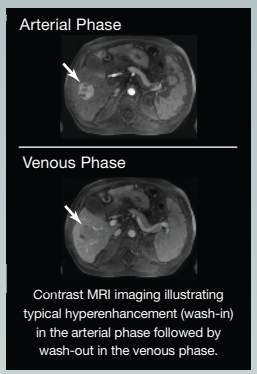

CELL TYPES OF ORIGIN FOR HCC

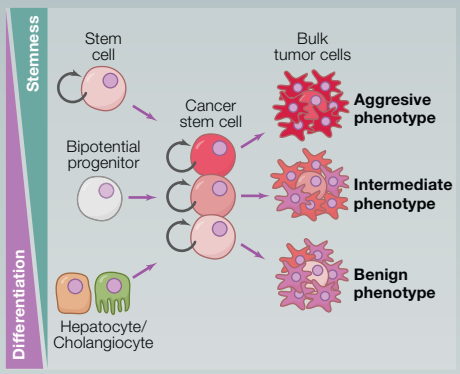

PROGNOSTIC CLASSIFICATION

	Favorable Outcome	Poor Outcome
Clinical/ Morphological features	▪ ECOG 0–1 Well-preserved liver function ▪ High differentiation Hepatocyte morphology ▪ Smaller tumors No vascular invasion	▪ ECOG >2 ▪ Poor liver function Poor differentiation CK19 positive ▪ Larger tumors Vascular invasion Extrahepatic spread
Molecular features	▪ Genomic stability Telomerase repression ▪ *CTNNB1* mutation Polysomy 7 ▪ High miR-122 Low miR-517a ▪ Expression of differentiation factors: HNF4α, CYPs ▪ Low Nault 5-gene score ▪ Beneficial subclass: G4-G5, S3 ▪ Beneficial metabolic profile	▪ Genomic instability Telomerase reactivation ▪ Loss of 8p Global hypomethylation ▪ Low miR-122 High miR-517a ▪ Stemness features: EpCAM, SALL4 ▪ High Nault 5-gene score ▪ Adverse subclass: G1-G3, S1-2, proliferation, HA subtype ▪ Adverse metabolic profile: stearoyl-CoA-desaturase activity, palmitate signaling ▪ Adverse signaling: HGF/MET, TGF-β, CK19, mTOR, IGF, MYC, AKT, WNT, loss of p53

BCLC STAGING & THERAPY

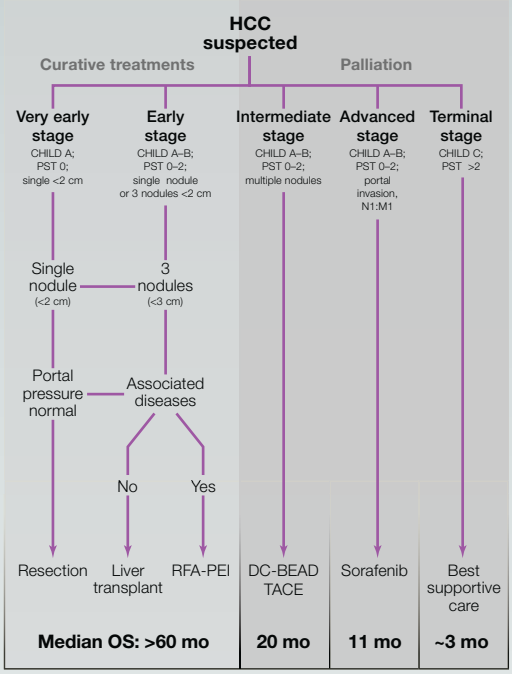

KEY GENETIC ALTERATIONS

Telomere Maintanance
Genes: ***TERT***
Cumulative frequency: **20%-60%**

WNT/β-Catenin
Genes: ***CTNNB1, AXIN1/2, APC***
Cumulative frequency: **2%-33%**

Cell Cycle
Genes: ***TP53, CKN2A/B, CCND/E1, CDKs, RB1***
Cumulative frequency: **4%-35%**

Apoptosis
Genes: ***TNFRSF10A/B, TRADD, CASP3/9, XIAP***
Cumulative frequency: **8%-20%**

Epigenetic Modifiers
Genes: ***ARID1A, ARID2, MLL genes***
Cumulative frequency: **10%-24%**

Proliferation
Genes: ***FGF19, RPS6KA, IRF2, KRAS***
Cumulative frequency: **2%-15%**

Immune Response
Genes: ***IL6R, IL20, IL6, JAK1***
Cumulative frequency: **2%-26%**

Oxidative Stress Regulation
Genes: ***NFEL2, KEAP1***
Cumulative frequency: **6%-8%**

EMERGING MOLECULAR TARGETS

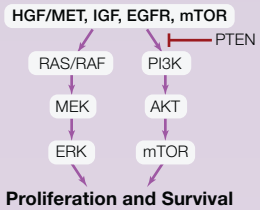

Tivantinib, cixutumumab, erlotinib, everolimus, selumetinib

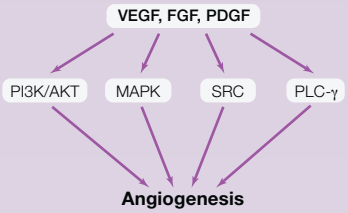

Sorafenib, brivanib, sunitinib, regorafenib

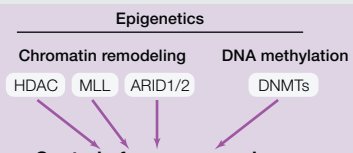

Resminostat, vorinostat, belinostat, zebularine

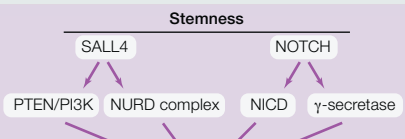

12-AA peptide, resminostat, γ-secretase inhibitors

CHALLENGES & OUTLOOK

- HCC develops on the basis of a predisposing liver disease that causes a chronically altered microenvironment.
- HCC is characterized by phenotypic and molecular heterogeneity reflecting a diverse cellular origin.
- Biopsies are not mandatory to establish the diagnosis. However, biopsies are of utmost importance for molecular classification and individualized therapeutic approaches.
- Our understanding of (epi)genetic pathophysiology is incomplete.
- The most common genetic alterations affect hTERT, β-catenin, and p53. No clear evidence for oncogene addiction has been demonstrated.
- In clinical routine, liver function frequently limits therapeutic options.
- Recurrence rate is high despite curative therapeutic intentions.
- There is an unmet need for new therapies and improved understanding of cancer biology.
- Novel innovative therapeutic strategies involve targeting of stem cell features as well as immune response.

Cancer Cell *25*, April 14, 2014 ©2014 Elsevier Inc. DOI 10.1016/j.ccr.2014.04.002

See online version for legend and references.

Because there's only one

BEST ANSWER.

Eliminate cross-reactivity concerns: UltraMAB® uniquely validated antibodies.

What is UltraMAB®?

OriGene UltraMAB® antibodies are highly specific monoclonal antibodies directed towards important diagnostic targets and known cancer biomarkers. OriGene's monoclonal antibodies are systematically screened on high-density human protein array chips (>17,000 proteins expressed). UltraMAB® antibody performance is also tested with over 25 types of normal and cancer human tissues in applications including WB, IHC, IF/ICC, and FACS.

Why use UltraMAB®?

Simply: High-specificity UltraMAB® antibodies reduce the risk of false positive results.
(British J. of Cancer, 2013, v109 p2096-2105).

IHC results of selected OriGene antibodies

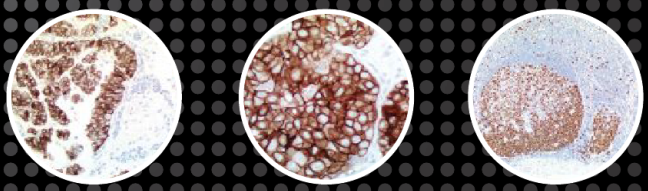

anti-ALK, NSCLC | anti-Her2, breast cancer | anti-Ki-67, tonsil

Antibodies were incubated on HIER pretreated paraffin embedded tissue at a 1:100 (ALK and Her2) or 1:200 (Ki-67) dilution for 30 minutes at room temperature. Detection was done with RTU polymer detection kit (POLINK-2 Broad HRP, GBI Labs) with the DAB chromogen.

Go to UltraMAB.com to review the full list of RUO antibody offers.

UltraMAB®

Contact us at antibody@origene.com
OriGene Technologies, Inc • 9620 Medical Center Dr., Suite 200 • Rockville, MD 20850 • 1-888-267-4436

SnapShot: Medulloblastoma

Jessica M. Rusert,[1] Xiaochong Wu,[2] Charles G. Eberhart,[3] Michael D. Taylor,[2] and Robert J. Wechsler-Reya[1]
[1]Tumor Initiation and Maintenance Program, NCI-Designated Cancer Center, Sanford-Burnham Medical Research Institute, La Jolla, CA 92037, USA
[2]Division of Neurosurgery, Hospital for Sick Children, University of Toronto, Toronto, ON M5G 1X8, Canada
[3]Departments of Pathology, Ophthalmology, and Oncology, Johns Hopkins University School of Medicine, Baltimore, MD 21205, USA

Cancer Cell

Origins - Embryo

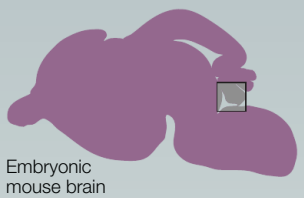

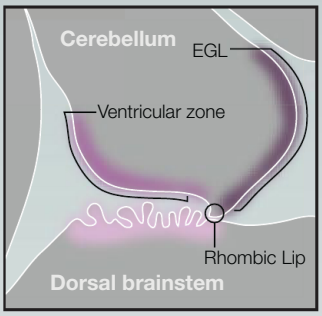

- EGL and rhombic lip granule neuron precursors
- Ventricular zone neural progenitors
- Dorsal brainstem neuronal progenitors

Medulloblastoma Subgroups and Subgroup-Based Risk Stratification

SHH

Most common in Infants/Adults
~75% survival
PTCH, SUFU, GLI2, TP53
Cells of origin =

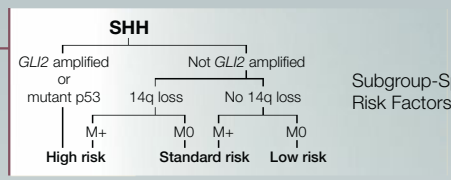

M0 = no metastasis; M+ = metastasis

FREQUENCY OF SUBGROUPS

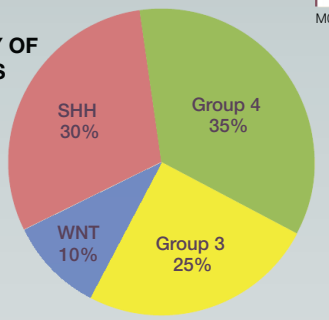

WNT

Most common in children
~95% survival (5 years)
CTNNB1, TP53, monosomy 6
Cells of origin =

Group 4

Most common in children
~75% survival
MYCN,CDK6, SNCAIP
~35%–40% metastasis

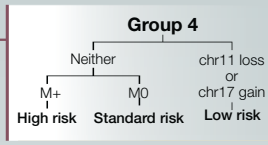

Group 3

Most common in children
~50% survival
MYC, GFI1/1B
~40%–45% metastasis
Cells of origin =

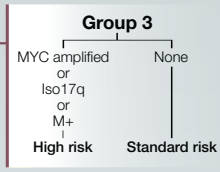

Histopathology

*Not shown: Extensively nodular tumors are known as medulloblastoma with extensive nodularity (MBEN)

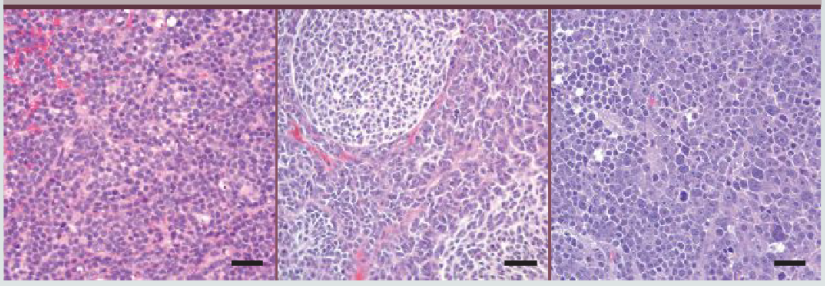

Classic medulloblastoma
Uniform sheets of poorly differentiated cells

Desmoplastic/nodular medulloblastoma
Differentiated nodules surrounded by more cellular internodular regions

Large Cell/Anaplastic medulloblastoma
Round cells with prominent nucleoli

Metastasis

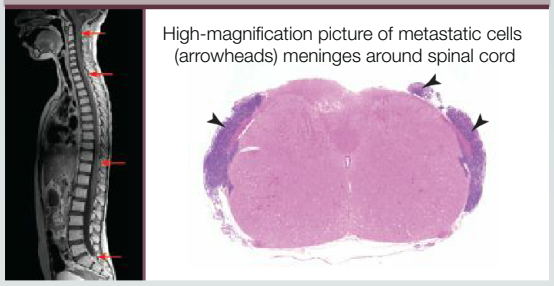

High-magnification picture of metastatic cells (arrowheads) meninges around spinal cord

Local Spread vs. Distal Spread
Leptomeningeal metastases are usually impossible to surgically remove and contain mutations distinct from those in the primary tumor.

Conventional Therapy

(5 year survival rate is 60%-80%)

Surgery
Radiation:
Craniospinal
Chemotherapy:
Cytotoxics e.g.,
Vincristine, Cisplatin,
Cyclophosphamide

Long-Term Effects of Conventional Therapy

Cognitive Decline
Endocrine Disorders
Secondary Cancers

Targeted Therapy

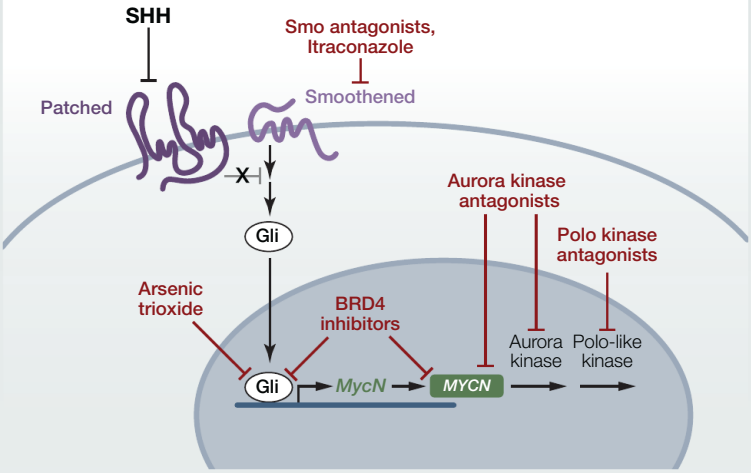

Moving Beyond Genomics

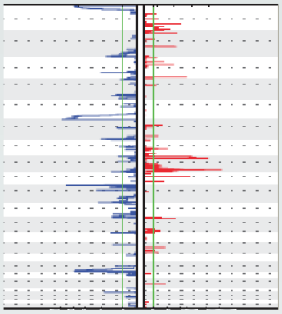

Decoding the many genomic events (gains, red; losses, blue) in each subgroup by determining which are driver events, and identifying new targeted therapies, will transform how MB patients are treated in the future.

Cancer Cell *26,* December 8, 2014 ©2014 Elsevier Inc. DOI http://dx.doi.org/10.1016/j.ccell.2014.11.015

See online version for legend and references.

Dharmacon™
part of GE Healthcare

CRISPR-Cas9 gene editing

Simplify your workflow with synthetic RNA. The Dharmacon™ Edit-R™ CRISPR-Cas9 platform eliminates time-consuming cloning tasks and sequencing steps – saving you time and money. With transfection-ready, endotoxin-free DNA and synthetic RNA components, our platform allows you to rapidly target several sites per gene, for multiple genes.

Fast, scalable, and efficient gene editing

gelifesciences.com/CRISPR

SnapShot: Chronic Lymphocytic Leukemia

Cancer Cell

Maria Ciccone,[1] Alessandra Ferrajoli,[1] Michael J. Keating,[1] and George A. Calin[1,2]
[1]Department of Leukemia, [2]Department of Experimental Therapeutics
The University of Texas MD Anderson Cancer Center, Houston, TX 77030, USA

Cell of Origin

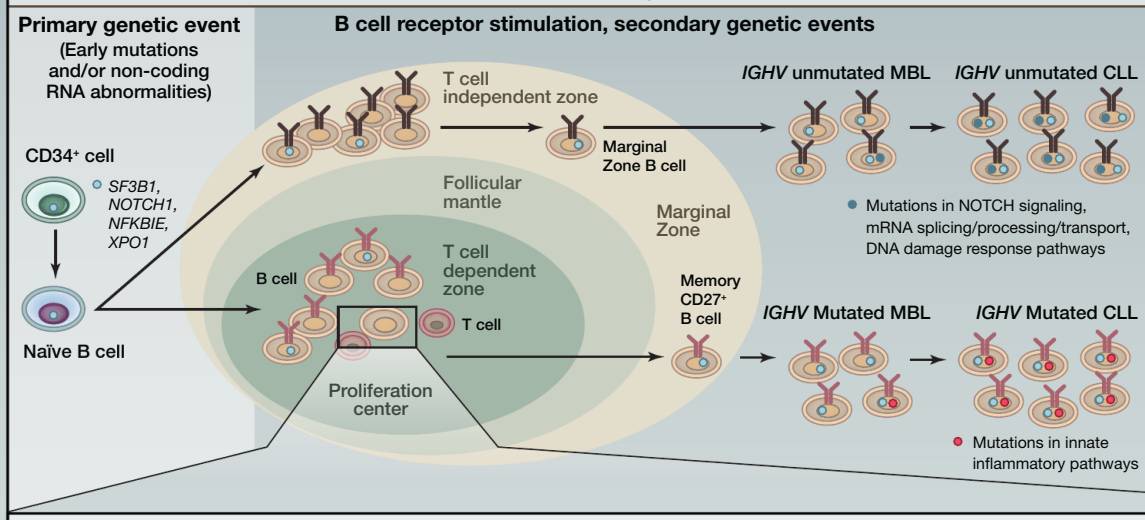

Evolutionary biology

MBL: Monoclonal B cell lymphocytosis

↓ Clonal expansion, antigen stimulation, early genetic events: del(13q), high miR-155

CLL: Chronic lymphocytic leukemia

↓ Secondary genetic events: del(13q), del(11q) (*ATM, miR-34b/c*), trisomy 12, del(17p), *TP53* and *NOTCH1* mutations

Progressed CLL

↓ Expansion of resistant clones and additional genetic abnormalities: del(17p)/*TP53* mutations, *NOTCH1, SF3B1, BIRC3, ATM* mutations, abnormal MYC levels, high miR-155 and miR-181 family

Refractory CLL or Richter transformation

Therapy from the bench to the bedside

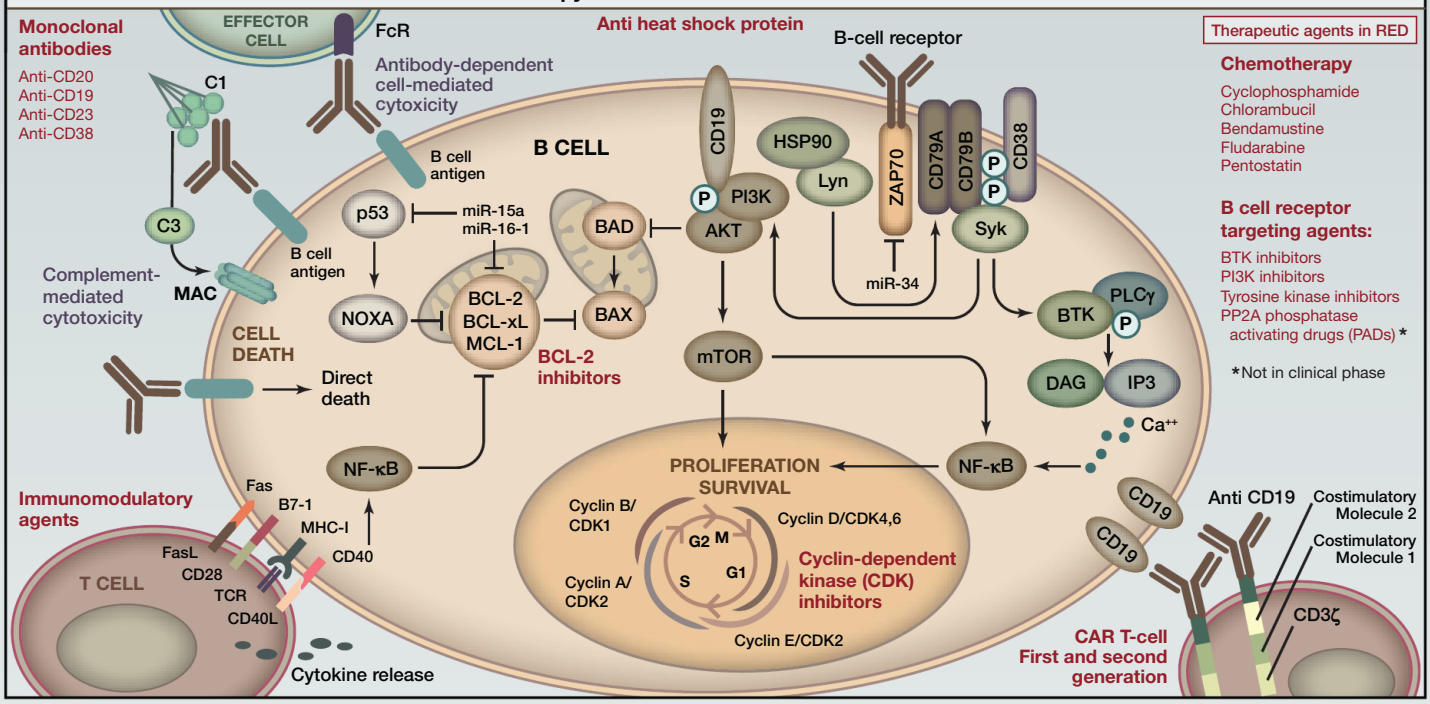

Prognostic factors

Risk category	Patient-related markers	Disease-related markers		
Low	Age ≤ 60 years	β_2 microglobulin < 3.5 mg/L	Normal FISH or deletion 13q-	CD38 ≤ 30%
	ECOG PS 0	Rai stage 0-1	Mutated *IGVH*	ZAP70 ≤ 20%
	Female	Serum Thymidine Kinase < 10.0 U/L	MYD88	
High	Age > 60 years	β_2 microglobulin > 3.5 mg/L	Unmutated *IGVH* and *IGHV4-39*	CD38 > 30%
	ECOG PS > 0	Rai stage 2-4	Deletion 11q- and deletion 17p	ZAP70 > 20%
	Male	Serum Thymidine Kinase > 10.0 U/L	Short telomere	Stereotyped CDR3
		ATM, TP53, NOTCH1, and/or *BIRC* abnormalities		

CLL mouse models

Models	Mutant gene/driver	B cell phenotype	CLL subtype
Eμ-*TCL1* transgenic	T cell leukemia/lymphoma protein 1A (*TCL1*)	$CD5^+IgM^+B220^+$ Unmutated stereotypic CDR3	Aggressive
TRAF2DN/BCL-2 transgenic	TNF receptor associated factor 2 (*TRAF2*) and *BCL-2*	$CD5^+IgM^{high}IgD^{low/-}B220^{moderate}CD21^{low/-}CD23^-CD11b^{low}$	N/A
Irf4$^{-/-}$*Vh11*	Interferon regulatory factor 4 (IRF4) deficiency	$CD5^+IgM^+CD19^+B220^{low/-}CD23^-CD21^-IgD^{low}CD1d^{int}$	MBL, indolent and aggressive
TNFSF13/APRIL transgenic	A proliferation-inducing ligand APRIL	$IgM^+CD5^+B220^+$	Indolent
Altered microRNA	Deletion of *DLEU2/miR-15a/16-1* cluster or transgenic miR-29a	$IgM^+CD5^+B220^+$	Indolent
New Zealand Black	Age-associated	$IgM^+B220^{dim}CD5^{dim}$	Indolent, familial

See online version for legend and references.

Perform Cancer Research under *in vivo* Cell Culture Conditions

Closed cell culture with O_2, CO_2, temperature & humidity control

HYPOXYstation

Define Your Environment

H45

H35

Cancer Researchers are using the HypOxystation to investigate:

- ER stress and the unfolded protein response *(University of Toronto)*
- The role of AMP Kinase in glioblastoma *(Cincinnati Children's Hospital)*
- Apoptosis and the adaptive hypoxic response in multiple myeloma *(VA Hospital Los Angeles)*
- Effects of tumor microenvironment on protein synthesis *(University of Miami)*
- Optical imaging of ovarian cancer to monitor therapy efficacy *(MD Anderson Cancer Center)*

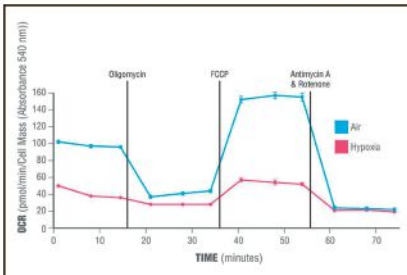

From: Ayse Latif, Experimental Oncology Group, University of Manchester, "Interrogating gynecological cancer cell metabolism at different oxygen tensions: Results using a novel atmosphere handling system"

i2 Instrument Workstation

See the HypOxystation & i2 Workstation at AACR Booth #1835

HYPOXYGEN

877-497-6994

www.HypOxygen.com

SnapShot: Diffuse Large B Cell Lymphoma

Laura Pasqualucci[1,2,5] and Riccardo Dalla-Favera[1,2,3,4,5]
[1]Institute for Cancer Genetics, [2]Department of Pathology and Cell Biology, [3]Department of Genetics, [4]Department of Microbiology and Immunology, [5]Herbert Irving Comprehensive Cancer Center, Columbia University, New York, NY 10032, USA

Cancer Cell

	Loss of function / Gain of function	% of DLBCL	Mutations	Deletions	Translocations	Amplifications	CN gains
Shared GCB- & ABC-DLBCL	**Altered histone/ chromatin modifications**						
	CREBBP/EP300	32	■	■			
	MLL2/MLL3	32-38	■				
	Immune escape						
	B2M	29	■	■			
	CD58	21	■	■			
	Deregulated BCL6 activity						
	BCL6	20-40			■		
	MEF2B	11	■				
	Other						
	FOXO1	8	■				
	TP53	20	■	■			
		% of subtype					
GCB-DLBCL	**Proliferation/ Apoptosis**						
	BCL2	34-45	■		■		
	MYC	10	■		■		
	miR-17~92	6-12.5					■
	Signaling						
	TNFRSF14	13	■				
	GNA13	11	■				
	SGK1	13	■				
	PTEN	6-11		■			
	Other						
	EZH2	22	■				
	BCL6 BSE1 sites	15	■				
	2p16.1	16				■	
ABC-DLBCL	**Constitutive NF-κB/BCR activity**						
	TNFAIP3	30	■	■			
	MYD88	30-37	■				
	CD79A/B	21	■				
	CARD11	10	■				
	Terminal differentiation block						
	PRDM1/BLIMP1	25-32	■	■			
	Apoptosis						
	BCL2	13				■	
	Cell cycle checkpoint						
	CDKN2A/B	24-30		■			
	Other						
	SPIB	26				■	■
PMBCL	**JAK/STAT activation**						
	JAK2/JMJD2C	30-45				■	■
	SOCS1	45	■				
	STAT6	36	■				
	Constitutive NF-κB activity						
	TNFAIP3	36	■	■			
	Immune escape						
	PDL1/PDL2	30-45				■	■
	CIITA	38	■		■		
	Deregulated BCL6 activity						
	BCL6	33*			■		

*Based on analysis of 12 cases only

CELL OF ORIGIN

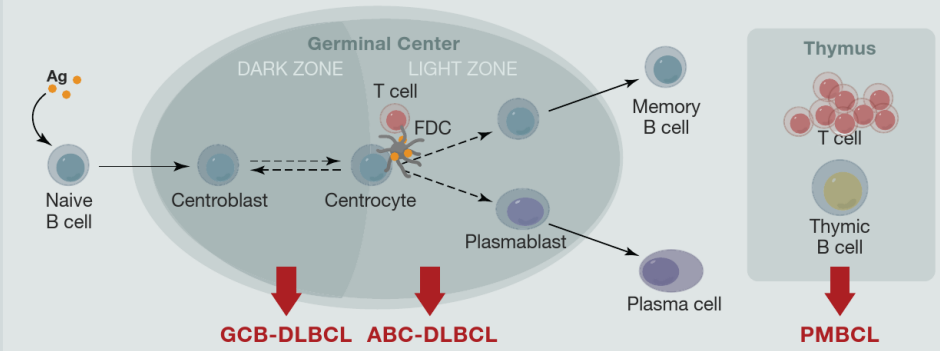

IMMUNE ESCAPE

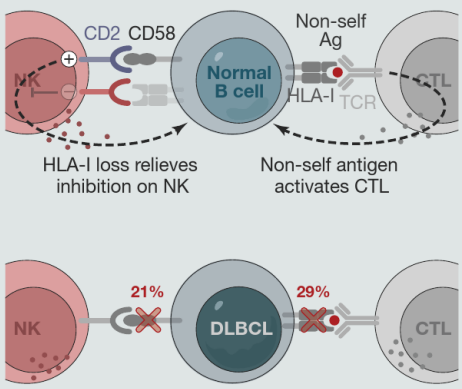

DEREGULATED BCL6 ACTIVITY

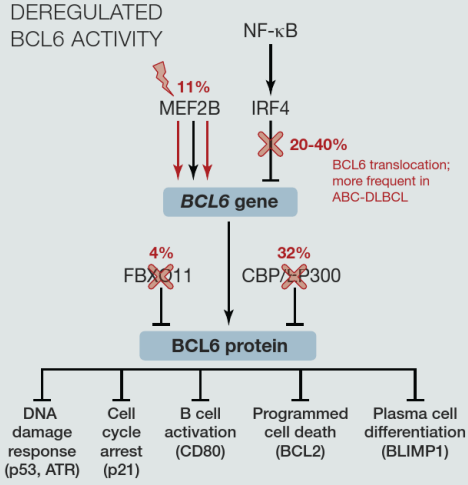

ABERRANT HISTONE/ CHROMATIN MODIFICATIONS

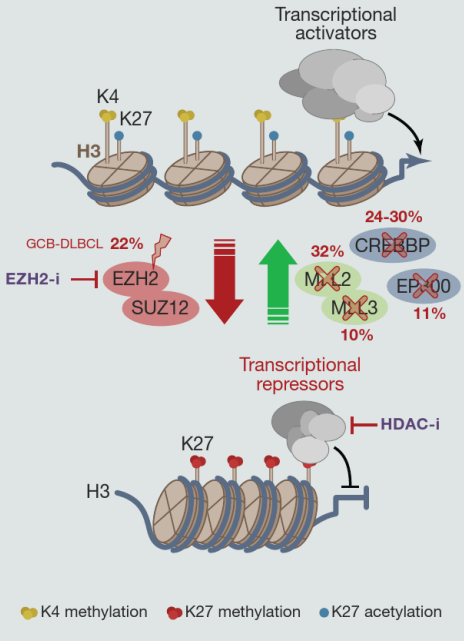

CONSTITUTIVE BCR AND NF-κB SIGNALING

ABC-DLBCL

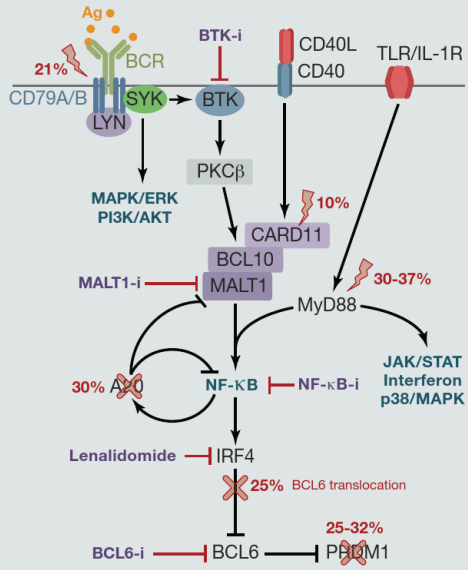

 DOI 10.1016/j.ccr.2013.12.012

See online version for legend and references.

89 NORTH®

PhotoFluor® LM-75

The world's first direct-mounted metal halide light source.

89 North's PhotoFluor LM-75 is designed for extended use with minimal down time and maximum benefits.

Direct mounting eliminates need for unreliable liquid light guides

As much or more **stable power** at the sample than a 200W metal halide light source

Broad spectrum with strong UV is **compatible with any filter set**

Pre-aligned, **user-exchangeable lamp** with a long lifetime

Extremely quiet operation with **minimal heat** production in rooms with multiple microscopes

Built-in DC ballast eliminates need for external control box, **reducing needed bench space**

Low up-front cost and lower overall cost of ownership than other fluorescence light sources

Contact 89 North for your ideal light source for *fluorescence in situ hybridization.*

PHONE +1-802-881-0302 1-877-417-8313

WEB sales@89north.com 89north.com

CHROMA®

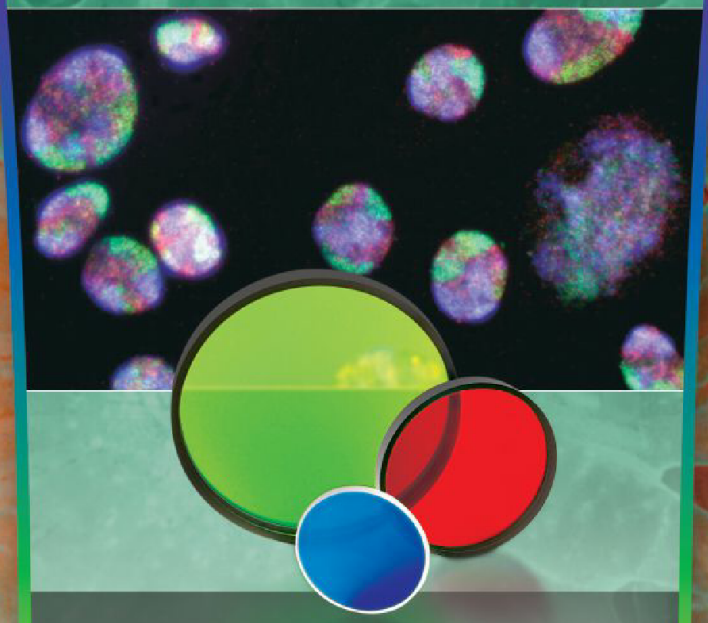

ET FISH Filter Sets

High-performance filter sets for fluorescence in situ hybridization.

Chroma's ET FISH filter sets provide brighter signals and excellent color separation for accurate scoring.

Eliminate bleedthrough of Gold and Aqua from Green signals to reliably discriminate between Aqua/Green/Gold/Red

Dual Band Sets with **balanced Green/Orange and Green/Red** signals for different light sources

Zero-pixel-shift sets for **perfect image registration**

Special Red and Orange filter sets to **separate Orange from Red signals** (advanced expertise required)

Less eye fatigue thanks to brighter fluorescent signals

No need for filter replacement – **lifetime warranty**

Contact Chroma for assistance in choosing filters for your fluorescent genetic testing application.

PHONE +1-802-428-2500 1-800-824-7662

WEB sales@chroma.com chroma.com

Rethink Possible

Is your flow too slow?
Is your ELISA content too low?

From combinatorial profiling, to screening cells and beads together, the iQue® Screener delivers the:

- Lowest Volume Assays
- Fastest Time to Results
- Richest Content
- Easiest Software You'll Ever Love

Leaders in immunotherapy, immune target screening, and antibody discovery are uncovering new possibilities with IntelliCyt.
What's stopping **you**?

Explore your possibilities at
www.intellicyt.com/Immunity

Rich Content

Fast Time to Results

Cost Effective

Better Insight

intellicyt®

www.intellicyt.com/Immunity

True Screening for Immunology

25th ANNIVERSARY

World-class innovation.
German engineering.
Local support.

It always seems impossible until it is done.

Nelson Mandela

LVF Monochromator™ technology.

BMG LABTECH

The Microplate Reader Company

www.bmglabtech.com

REPROCELL

INTEGRATED TOOLS FOR TRANSLATIONAL RESEARCH

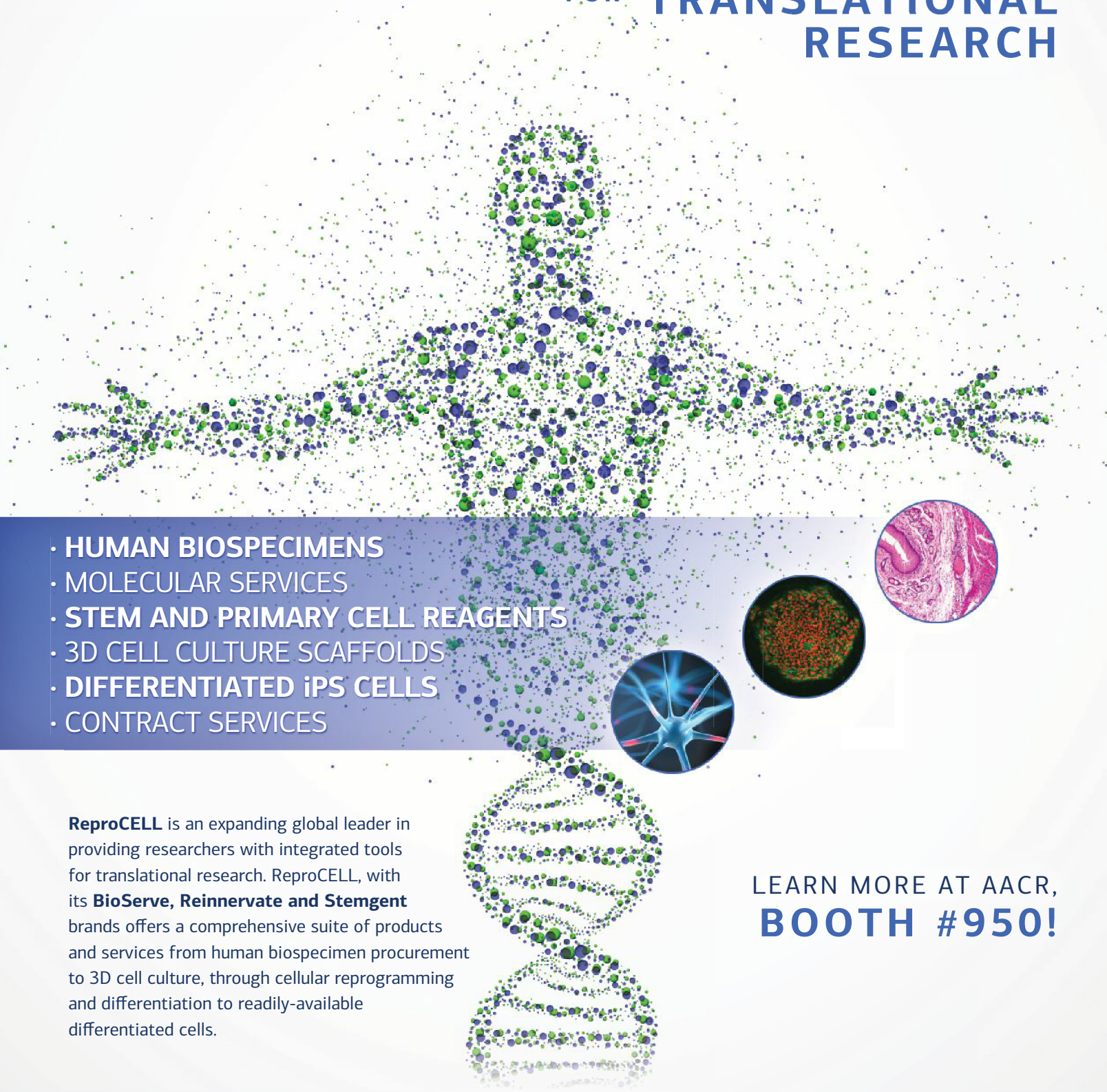

- **HUMAN BIOSPECIMENS**
- MOLECULAR SERVICES
- **STEM AND PRIMARY CELL REAGENTS**
- 3D CELL CULTURE SCAFFOLDS
- **DIFFERENTIATED iPS CELLS**
- CONTRACT SERVICES

ReproCELL is an expanding global leader in providing researchers with integrated tools for translational research. ReproCELL, with its **BioServe, Reinnervate and Stemgent** brands offers a comprehensive suite of products and services from human biospecimen procurement to 3D cell culture, through cellular reprogramming and differentiation to readily-available differentiated cells.

LEARN MORE AT AACR,
BOOTH #950!

REPROCELL GROUP COMPANIES

bioserve stemgent reinnervate

www.reprocell.com · www.bioserve.com · www.stemgent.com · www.reinnervate.com

proteintech™

ANTIBODY WISH LIST

- WORKS IN ALL MY APPLICATIONS
- HIGH SENSITIVITY AND BINDING AFFINITY
- EXTENSIVELY VALIDATED IN UNMODIFIED SAMPLES
- ALL VALIDATION DATA AVAILABLE ONLINE
- SUITABLE FOR USE IN MULTIPLE SPECIES
- SATISFACTION GUARANTEED OR MY GRANT MONEY BACK
- 100% ORIGINAL PRODUCT FROM THE ORIGINAL MANUFACTURER

PROTEINTECH GROUP FULFILS EVERY SCIENTIST'S ANTIBODY WISH LIST

Find out more at ptglab.com

Cancer Cell
Perspective

ERBB Receptors: From Oncogene Discovery to Basic Science to Mechanism-Based Cancer Therapeutics

Carlos L. Arteaga[1,*] and Jeffrey A. Engelman[2,*]
[1]Vanderbilt-Ingram Cancer Center, Vanderbilt University School of Medicine, Nashville, TN 37232, USA
[2]Massachusetts General Hospital Cancer Center, Harvard Medical School, Boston, MA 02114, USA
*Correspondence: carlos.arteaga@vanderbilt.edu (C.L.A.), jengelman@mgh.harvard.edu (J.A.E.)
http://dx.doi.org/10.1016/j.ccr.2014.02.025

ERBB receptors were linked to human cancer pathogenesis approximately three decades ago. Biomedical investigators have since developed substantial understanding of the biology underlying the dependence of cancers on aberrant ERBB receptor signaling. An array of cancer-associated genetic alterations in ERBB receptors has also been identified. These findings have led to the discovery and development of mechanism-based therapies targeting ERBB receptors that have improved outcome for many cancer patients. In this Perspective, we discuss current paradigms of targeting ERBB receptors with cancer therapeutics and our understanding of mechanisms of action and resistance to these drugs. As current strategies still have limitations, we also discuss challenges and opportunities that lie ahead as basic scientists and clinical investigators work toward more breakthroughs.

ERBB Family: EGFR, HER2, HER3, and HER4

The ERBB family of transmembrane receptor tyrosine kinases (RTKs) consists of the epidermal growth factor receptor EGFR (ERBB1), HER2 (ERBB2), HER3 (ERBB3), and HER4 (ERBB4). Binding of ligands to the extracellular domain of EGFR, HER3, and HER4 induces the formation of kinase active hetero-oligomers (Yarden and Sliwkowski, 2001). HER2 does not bind any of the ERBB ligands directly, but it is in a conformation that resembles a ligand-activated state and favors dimerization (Cho et al., 2003; Garrett et al., 2003). Activation of HER2 and EGFR induces transphosphorylation of the ERBB dimer partner and stimulates intracellular pathways such as RAS/RAF/MEK/ERK, PI3K/AKT/TOR, Src kinases, and STAT transcription factors (reviewed in Yarden and Pines, 2012). Although HER3 can bind ATP and catalyze autophosphorylation, it has a weak kinase activity compared to that of its ERBB coreceptors (Shi et al., 2010). However, upon transphosphorylation by another ERBB family member, HER3 serves as an efficient phosphotyrosine scaffold, leading to potent activation of downstream signaling. The specificity and potency of intracellular signaling cascades are determined by the expression of positive and negative regulators, the specific composition of activating ligand(s), receptor dimer constituents, and the array of proteins that associate with the tyrosine phosphorylated C-terminal domain of the ERBB receptors (Avraham and Yarden, 2011).

Over the past several years, it has become evident the ERBB family members have a prominent role in the initiation and maintenance of several solid tumors. This has led to the development and widespread implementation of specific ERBB inhibitors as cancer therapies. In this Perspective, we will focus on the therapeutic approaches for targeting ERBB family members in cancer, with a particular emphasis on *HER2*-amplified breast cancer and *EGFR* mutant lung cancer.

Links to Cancer

HER2

The first evidence for a role of ERBB2 or HER2 (for *h*uman *EGFR2*) in cancer was inferred from the connection to its rat ortholog, Neu, a mutant cDNA isolated from carcinogen-induced neuroblastomas (Schechter et al., 1984). (Please note that in this Perspective, ERBB2 and HER2 will be used when discussing mouse and human ERBB2, respectively.) Although rodent *Neu* is mutated, human *HER2* is typically amplified in human cancers such as breast, gastric, and esophageal cancer (Table 1). Overexpression of either rat or human wild-type ERBB2 was shown to transform diploid cells. Consistent with its oncogenic activity, overexpression of wild-type Neu or HER2 under the control of a mammary-specific promoter leads to metastatic mammary tumors in transgenic mice (Andrechek et al., 2000; Finkle et al., 2004). In a seminal study, Slamon et al. found that *HER2* is amplified in about 20% of breast cancers (Slamon et al., 1987). This was the first report of an oncogenic alteration associated with poor outcome in cancer patients, suggesting a causal relationship to cancer virulence. Further evidence linking HER2 with cancer progression is the improvement in survival of patients with *HER2*-amplified early-stage breast cancer treated with the HER2 antibody trastuzumab. More-recent studies using next-generation sequencing have identified less-frequent activating mutations in *HER2* in several cancer types without *HER2* gene amplification (discussed below).

A recent study of >500 breast tumors by The Cancer Genome Atlas (TCGA) Network has shed light into the biological heterogeneity of clinical HER2-overexpressing cancers ($HER2^+$ as defined by gene amplification) by further parsing into HER2-enriched (HER2E) and luminal subtypes as defined by gene expression (Cancer Genome Atlas Network, 2012). HER2E-$HER2^+$ tumors had higher frequencies of aneuploidy, somatic mutation, and *TP53* mutation, as well as amplification of FGFRs, EGFR, CDK4, and cyclin D1. Luminal-$HER2^+$ breast cancers

Table 1. Alterations of ERBB Receptors and Ligands in Human Cancer

Molecule	Alteration	Cancer Types	Notes	References
EGFR	mutation (L858R, etc.)	NSCLC (adenocarcinoma)	substitutions, deletions and insertions	Lynch et al., 2004; Paez et al., 2004; Pao et al., 2004
EGFR	vIII	glioma	deletion of exons 2–7 in the ectodomain	Sugawa et al., 1990
EGFR	amplification	NSCLC (squamous), head and neck, glioma, esophageal, colorectal, anal (?)		Yarden and Pines, 2012
HER2	amplification	breast, gastric, esophageal		Cancer Genome Atlas Network, 2012
HER2	mutation	breast (lobular), lung, gastric, bladder, endometrial	unclear whether all those reported are activating or gain of function	Cancer Genome Atlas Network, 2012
HER3	mutation	breast, gastric		Jaiswal et al., 2013
HER4	mutation	melanoma, NSCLC, medulloblastoma		Gilbertson et al., 2001; Prickett et al., 2009
TGF-α	overexpression	prostate, lung, pancreas, ovary, colon, head and neck	androgen-independent prostate cancer; poor prognosis when associated with high EGFR	Rubin Grandis et al., 1998; Yarden and Sliwkowski, 2001
Neuregulin-1	overexpression	colorectal, head and neck	linked to sensitivity to ERBB3 inhibitors and resistance to EGFR inhibitors	Wilson et al., 2011; Yonesaka et al., 2011

showed higher expression of a luminal gene cluster including GATA3, BCL2, and ESR1 and harbored a higher rate of GATA3 mutations. It is anticipated that because of these molecular differences, the clinical management of HER2E and luminal subtypes of $HER2^+$ breast cancers will also be different. Finally, not all tumors of the HER2E gene expression subtype are *HER2* amplified. One implication of these data is that some breast cancers with a single copy of *HER2* harbor an expression signature of HER2 dependence and, as such, may benefit from anti-HER2 therapy. Consistent with this speculation are the results of the NSABP B-31 adjuvant trastuzumab trial, in which 9.7% of patients that did not meet criteria for HER2 overexpression by fluorescence in situ hybridization (FISH) or immunohistochemistry (IHC) also benefitted from adjuvant trastuzumab (Paik et al., 2008).

Somatic mutations in HER2 have been reported in several human cancers (Table 1). Most are missense mutations in the tyrosine kinase and extracellular domains or duplications/insertions in a small stretch within exon 20. *HER2* mutations are almost exclusively observed in cancers without *HER2* gene amplification. Several of these mutants have increased signaling activity, and are most commonly associated with lung adenocarcinoma and lobular breast, bladder, gastric, and endometrial cancers (Cancer Genome Atlas Network, 2012).

EGFR

The EGF receptor was originally identified as an oncogene because of its homology to v-ERBB, a retroviral protein that enables the avian erythroblastosis virus to transform chicken cells (Downward et al., 1984). Subsequently, EGFR overexpression was shown to be transforming in laboratory models, and *EGFR* gene amplification was reported in a wide range of carcinomas. Early studies by Mendelsohn and colleagues demonstrated that antibodies directed against EGFR block growth of A431 cells, demonstrating that EGFR signaling could drive cancer cell growth and setting the stage for clinical use of EGFR inhibitors (Kawamoto et al., 1983).

An oncogenic mutation that deletes exons 2–7 in the receptor ectodomain, denoted *EGFRvIII*, is found in about 40% of high-grade gliomas with wild-type *EGFR* amplification (Sugawa et al., 1990). EGFRvIII exhibits constitutive dimerization, impaired downregulation, and aberrant tyrosine kinase activity, all resulting in enhanced tumorigenicity (Nishikawa et al., 1994). In addition to glioblastoma multiforme (GBM), EGFRvIII has been found in a fraction of breast, lung, head and neck, ovarian, and prostate cancers (Moscatello et al., 1995). Because its expression is restricted to tumor tissues, EGFRvIII has been therapeutically targeted with specific antibodies and vaccines. There is clinical evidence suggesting that the presence of EGFRvIII can predict clinical responses of GBMs to the EGFR tyrosine kinase inhibitors (TKIs) gefitinib and erlotinib (Haas-Kogan et al., 2005; Mellinghoff et al., 2005). The second most common EGFR variant in GBM is EGFRc958, observed in about 20% of tumors with wild-type *EGFR* amplification. EGFRc958 lacks amino acids 521–603 and displays increased, ligand-dependent kinase activity (Frederick et al., 2000).

The causal role of EGFR in tumorigenesis was further solidified in 2004 when somatic, activating mutations in EGFR were discovered in a subset of non-small-cell lung cancers (NSCLCs) (Lynch et al., 2004; Paez et al., 2004; Pao et al., 2004) (Table 1). The discovery was spurred by efforts to understand why occasional NSCLCs were highly sensitive to small-molecule EGFR TKIs. It is now well established that lung cancers harboring these *EGFR* mutations are highly responsive to single-agent EGFR inhibitors with RECIST response rates of ~55%–75% (Mok et al., 2009; Rosell et al., 2012; Sequist et al., 2013b). *EGFR* mutations are primarily localized within two hot spots of the kinase domains, a series of overlapping deletions in exon 19 and a leucine-to-arginine substitution at amino acid position 858 (L858R) (reviewed in Pao and Chmielecki, 2010). In addition,

mutations are also rarely observed elsewhere in the kinase domain, including insertions in exon 20 (Yasuda et al., 2013). The prevalence of the mutations differs among distinct human populations. They are found in ~8%–10% of Caucasians, but in a higher proportion of East Asians. Lung cancers with *EGFR* mutations are most highly associated with adenocarcinoma histology and in patients with a minimal smoking history. Of note, cancers with *EGFR* mutations often have amplification of the mutant *EGFR* allele as well (Cappuzzo et al., 2005). Cell culture and transgenic mouse model studies have shown that mutant EGFR has transforming activity (Greulich et al., 2005; Ji et al., 2006; Politi et al., 2006).

EGFR is important for the growth of some colorectal cancers (CRCs) and head and neck cancers. In these cancers, genetic alterations in *EGFR* have not been consistently identified. However, the efficacy of the EGFR antibody cetuximab demonstrates the importance of EGFR signaling in these tumors. Although some reports suggest that *EGFR* amplification correlates with response to cetuximab (Moroni et al., 2005), this alteration is not currently used as a predictive biomarker. Importantly, cetuximab provides clinical benefit primarily in colorectal cancers that do not harbor *KRAS* mutations (Cunningham et al., 2004) and in those with high expression of the EGFR ligands amphiregulin and epiregulin (Khambata-Ford et al., 2007). Presumably, cetuximab is effective in sensitive cancers because it blocks ligand-dependent activation of EGFR and downregulates the receptor from the cell surface (Fan et al., 1994). Thus, in these colorectal cancers, we suspect that ligand-dependent activation of EGFR drives progression of these cancers. Currently, cetuximab is most often administered with chemotherapy in *KRAS* wild-type colorectal cancers. Similarly, in head and neck cancers, cetuximab is primarily used in conjunction with chemotherapy (Vermorken et al., 2008) and radiotherapy (Bonner et al., 2006). Despite conflicting reports on the utility of EGFR expression by IHC for patient selection in head and neck cancers (and CRCs), there currently are no validated predictive biomarkers of response to EGFR inhibitors in head and neck cancers (Burtness et al., 2005; Cunningham et al., 2004; Licitra et al., 2011, 2013; Vermorken et al., 2008). It is notable that cetuximab appears to be more effective than EGFR TKIs in cancers with ligand-dependent activation of EGFR, whereas TKIs are more effective in cancers with *EGFR* mutations. We speculate that this is so because mutant EGFR activation is not ligand dependent and because TKIs have higher affinity for mutant EGFR than for wild-type EGFR, thus leading to a significant therapeutic window. In contrast, antibodies such as cetuximab are more effective in EGFR wild-type cancers because they are highly effective at blocking ligand-dependent activation of EGFR and are pharmacologically stable.

ERBB3 and ERBB4

ERBB3 has been linked to cancer, primarily due to its mechanistic role in promoting signaling from oncogenic HER2 and EGFR (discussed below). However, somatic mutations scattered throughout the *ERBB3* gene were recently identified in subsets of breast and gastric cancers (Table 1). Many of the mutations were located in the extracellular domain, and they appear to have oncogenic potential, function in a ligand-independent manner, and require heterodimerization with HER2 for transforming activity (Jaiswal et al., 2013). Future studies are needed to determine whether cancers with ERBB3 mutations are particularly sensitive to ERBB3- and/or HER2-targeted drugs. Similarly, mutations in ERBB4 were identified in cancer, particularly melanoma (Prickett et al., 2009), lung adenocarcinoma (Ding et al., 2008), and medulloblastoma (Gilbertson et al., 2001). Although laboratory studies demonstrated that melanoma cell lines harboring ERBB4 mutations were sensitive to lapatinib, it remains unknown whether targeting of ERBB4, or any other ERBB family member, will have therapeutic value in these cancers.

ERBB Ligands

Overproduction of ligands is one mechanism by which cancers aberrantly activate ERBB receptors. The source of these can be tumor cells or the tumor stroma. There are three groups of ligands. One group specifically binds EGFR and includes EGF, transforming growth factor α (TGF-α), amphiregulin (AR), and epigen (EPG). A second group binds both EGFR and HER4 and includes betacellulin (BTC), HB-EGF, and epiregulin (EPR). The third group includes all of the neuregulins (NRG1–NRG4), of which NRG1 and NRG2 bind HER3 and HER4, whereas NRG3 and NRG4 only bind HER4 (Hynes and MacDonald, 2009).

In transgenic mouse studies, mice that coexpress TGF-α and Neu in mammary epithelium developed multifocal mammary cancers that arise after a significantly shorter latency than those expressing either gene alone (Muller et al., 1996). TGF-α is also co-overexpressed with EGFR in lung, colorectal, ovary, and head and neck squamous cancers, where it is associated with poor patient prognosis (Rubin Grandis et al., 1998; Yarden and Sliwkowski, 2001) (Table 1). Recent reports suggest that in addition to overexpression, mistrafficking, and/or ''extracrine'' (*ex*osomal *t*argeting *r*eceptor *a*ctivation) signaling by ERBB ligands may also contribute to epithelial cell transformation (Singh and Coffey, 2014). For example, altered trafficking of EREG to the apical cell surface leads to prolonged EGFR phosphorylation and more proliferative and more invasive tumors (Singh et al., 2013). Further, significantly enhanced levels of invasiveness are observed when breast cancer cells are incubated with exosomes containing high levels of AREG compared to incubation of cells with exosomes containing low levels of AREG or recombinant EGFR ligands (Higginbotham et al., 2011), suggesting a gain-of-function mode of EGFR signaling that might act in more distant environments. Other roles of ligand-dependent activation of EGFR were discussed above.

An autocrine loop has been described in ovarian cancer cells and tumors that overexpress NRG1 and HER3, where suppression of HER3 with RNAi or with a neutralizing HER3 antibody suppressed ovarian cancer growth in laboratory models (Sheng et al., 2010) (Table 1). A NRG1-mediated autocrine loop inducing HER3 activation was also discovered in head and neck cancer cells without *HER2* amplification. These cells were particularly sensitive to the EGFR/HER2 TKI lapatinib (Wilson et al., 2011), suggesting that NRG1-driven tumors depend on HER3 activated by HER2 and/or EGFR. Finally, Hegde et al. found high levels of NRG1 and its receptor, HER4, in NSCLC residual tumor cells that remained after cytotoxic chemotherapy. Inhibition of HER3/HER4 signaling with a NRG1-blocking antibody increased the magnitude and duration of response to chemotherapy in these in vivo models (Hegde et al., 2013). This causal association of ERBB ligand overexpression and drug resistance is not limited to NRG1 or to chemotherapy. For example, HGF has been found

to confer resistance to the BRAF inhibitor vemurafenib in BRAF mutant melanoma cells (Wilson et al., 2012).

Downstream Signaling

Oncogenic addiction to EGFR and HER2 are intimately linked to regulation of downstream signaling. In cancers highly sensitive to inhibition of EGFR or HER2 inhibitors, EGFR or HER2 is the main driver of downstream signaling, particularly via the PI3K/AKT and MEK/ERK pathways. Thus, in cancers addicted to EGFR or HER2, inhibition of the respective RTK leads to concomitant loss of flux through these pathways. Loss of these signaling events leads to growth arrest and converges on the BCL-2 family of proteins to promote apoptosis (reviewed in Niederst and Engelman, 2013).

In EGFR and HER2 driven cancers, HER3 is an important heterodimer partner because it potently activates the phosphatidylinositide-3 kinase (PI3K)/AKT survival pathway via its six docking sites for the p85 regulatory subunit of PI3K. Although HER2 potently activates ERK signaling, it does not bind p85 or directly activate PI3K/AKT. Thus, HER2-mediated activation of HER3 is essential for stimulation of the PI3K/AKT pathway. In transgenic mice, genetic ablation of ERBB3 in the mammary gland via Cre-mediated recombination abrogates ERBB2-driven mammary hyperplasias, DCIS, invasive cancers, and metastases (Vaught et al., 2012). Similarly, small hairpin RNA (shRNA)-mediated knockdown of HER3 but not EGFR inhibits viability of HER2-overexpressing breast cancer cells. Further, HER3 but not EGFR, is always phosphorylated in human *HER2*-amplified breast cancers (Lee-Hoeflich et al., 2008), suggesting that it is an obligatory cobiomarker of aberrant HER2 activity and dependence. More recently, an inducible HER3 shRNA (Lee-Hoeflich et al., 2008) and a HER3-neutralizing antibody (Garrett et al., 2013b) were shown to inhibit growth of established *HER2*-amplified xenografts, further suggesting that HER3 is essential for the survival of HER2-dependent tumors. Analogous to HER2-induced signal transduction, mutant EGFR often activates PI3K via HER3 (Engelman et al., 2005), and maintenance of HER3 signaling can promote resistance to EGFR inhibitors (Engelman et al., 2007; Schoeberl et al., 2010). However, unlike HER2, EGFR is also able to signal to PI3K via GAB1 in a HER3-independent manner (Mattoon et al., 2004; Turke et al., 2010), suggesting that *EGFR* mutant cancers may be better equipped than *HER2*-amplified cancers to adapt to the loss of HER3 function.

HER2-amplified tumors have a strong dependence on PI3K/AKT signaling, as sustained blockade of this pathway appears to be required for the antitumor effect of HER2 antagonists (Chakrabarty et al., 2013; Yakes et al., 2002). Comprehensive cancer cell line panels screened for sensitivity to pan-PI3K, p110α-specific, and AKT inhibitors have consistently shown preferential activity of these drugs against *HER2*-amplified breast cancer lines (Heiser et al., 2012; O'Brien et al., 2010). Further, genetic ablation of p110α has been shown to abrogate ERBB2-induced mammary tumor formation in transgenic mice (Utermark et al., 2012). Preclinical studies have shown that, compared to HER2-amplified cancers, *EGFR* mutant cancers are less sensitive to single-agent PI3K/AKT inhibitors. Rather, inhibition of the PI3K and MEK pathways is necessary in order to induce apoptosis and cause tumor regressions (Faber et al., 2010). Importantly, mechanisms of de novo and acquired resistance to HER2- and EGFR-directed therapies involve persistence or reactivation of PI3K/AKT signaling via alternate amplified RTKs and/or mutations in the PI3K pathway (Rexer and Arteaga, 2013).

Other downstream signaling pathways, such as Src kinases, JAK/STAT, and WNT, are also activated by ERBB receptors (Yarden and Sliwkowski, 2001). Examples below suggest that they are involved in and/or mediate resistance to ERBB-receptor-targeted therapies. However, evidence that ERBB receptors depend on Src, JAK/STAT, or WNT for their effects on transformation and cancer progression is less clear and will not be discussed further.

Feedback Activation of ERBB Signaling Promoting Resistance to Inhibition of Alternative Kinases

More recently, EGFR and HER3 activation have been observed as important cellular adaptations to inhibitors of downstream signaling. For example, in *BRAF* mutant CRC, BRAF inhibitors fail to inhibit ERK signaling in sustained fashion due to activation of EGFR which, in turn, reactivates ERK in the presence of the BRAF inhibitor (Corcoran et al., 2012; Prahallad et al., 2012). However, combined inhibition of EGFR and BRAF blocks reactivation of ERK and leads to regressions of BRAF mutant CRC in vivo. This combination is now being actively developed in clinic for this subset of CRCs. Similarly, inhibition of the MEK pathway in many cancers, including KRAS mutant cancers, activates ERBB signaling by releasing a negative feedback on ERBB dimerization (Turke et al., 2012). This further suggests the ERBB activation could mitigate the responsiveness of other cancers to MEK inhibition.

Analogous to the effects of inhibition of the MEK pathway, inhibition of the PI3K pathway leads to potent activation of HER3-dependent signaling in *HER2*-amplified breast cancers (Chakrabarty et al., 2012; Chandarlapaty et al., 2011). In these cancers, coinhibition of HER3 and PI3K provided substantially greater antitumor efficacy. In other examples, EGFR activation has been observed as a resistance mechanism to small molecules targeting other tyrosine kinases. For example, EGFR activation is a resistance mechanism to ALK and MET inhibitors in *ALK*-positive lung and *MET*-amplified gastric cancers, respectively. Inhibition of EGFR resensitizes the resistant cancers to their respective TKI (Katayama et al., 2012; McDermott et al., 2010; Qi et al., 2011; Sasaki et al., 2011). Thus, activation of ERBB family members has emerged as a common mechanism of adaptation upon inhibition of downstream signaling, and inhibition of ERBB family members may be used to augment the efficacy of other pathway inhibitors.

Mechanisms of Action of EGFR and HER2 Inhibitors

HER2

Trastuzumab is a humanized immunoglobulin G_1 (IgG_1) antibody that binds to an epitope in juxtamembrane region IV of the HER2 receptor. It inhibits cleavage of the HER2 ectodomain, uncouples ligand-independent HER2-containing dimers leading to partial inhibition of downstream signaling, and triggers antibody-dependent, cell-mediated cytotoxicity (ADCC) (Clynes et al., 2000; Ghosh et al., 2011; Junttila et al., 2009; Molina et al., 2001; Yakes et al., 2002) (Table 2). This last mechanism cooperates with the recruitment of a T cell population mediating an adaptive immune (memory) response that enhances tumor

Table 2. ERBB Receptor Inhibitors: Mechanisms of Action and Key Clinical Trials

Drug	Type of Molecule	Mechanism of Action	FDA Approval	Key Clinical Trial(s)
Trastuzumab	humanized IgG_1, binds juxtamembrane domain IV	inhibits ectodomain cleavage and ligand-independent HER2-containing dimers; ADCC and adaptive immunity to HER2	1998 (metastatic breast); 2006 (adjuvant early breast); 2010 (advanced gastric)	Slamon et al., 2001; Piccart-Gebhart et al., 2005; Robert et al., 2006; Romond et al., 2005; Bang et al., 2010
Pertuzumab	humanized IgG_1, binds heterodimerization domain II	inhibits ligand-induced HER2-containing dimers	2012 (metastatic breast); 2013 (neoadjuvant breast)	Baselga et al., 2012b; Gianni et al., 2012; Schneeweiss et al., 2013
Lapatinib	small molecule	reversible, ATP-competitive TKI	2006 (advanced breast)	Geyer et al., 2006
Trastuzumab emtansine (T-DM1)	antibody-drug conjugate	same as trastuzumab plus inhibition of microtubules and cell lysis (DM-1)	2013 (advanced breast)	Verma et al., 2012
Erlotinib	small molecule	reversible, ATP-competitive TKI of EGFR	2004 (third-line advanced NSCLC); 2005 (pancreas cancer); 2013 (first-line EGFR mutant NSCLC)	Mok et al., 2009; Moore et al., 2007; Shepherd et al., 2005
Afatinib	small molecule	irreversible, ATP-competitive TKI of EGFR and HER2	2013 (metastatic EGFR mutant NSCLC)	Sequist et al., 2013b
Neratinib	small molecule	irreversible, ATP-competitive TKI of HER2	N/A	trials in patients with HER2 mutant tumors in progress
Cetuximab	human-murine chimeric IgG_2, binds ligand-binding domain	inhibits ligand-dependent activation of EGFR	2004 (originally for late line $EGFR^+$ CRC, but now only used in earlier-line wild-type KRAS CRC); 2006 (head and neck with radiotherapy or chemotherapy)	Van Cutsem et al., 2009; Vermorken et al., 2008; Bonner et al., 2006
Panitumumab	human IgG_1, binds ligand-binding domain	inhibits ligand-dependent activation of EGFR	2006 (originally for late-line $EGFR^+$ CRC, but now only used in earlier-line wild-type KRAS CRC)	Van Cutsem et al., 2007
AZD9291	small molecule	irreversible, ATP-competitive TKI of mutant EGFR (third generation)	NA	trials in EGFR mutant lung cancer in progress
CLO-1686	small molecule	irreversible, ATP-competitive TKI of mutant EGFR (third generation)	NA	trials in EGFR mutant lung cancer in progress

NA, not applicable.

eradication (Park et al., 2010; Stagg et al., 2011). The importance of the immune response is underscored by the finding that the therapeutic effect of trastuzumab was markedly diminished in mice that were engineered to be deficient in natural killer (NK) cells and macrophages capable of binding the Fc region of trastuzumab (Clynes et al., 2000). Pertuzumab is a monoclonal antibody that recognizes an epitope in heterodimerization domain II of HER2, thus blocking ligand-induced HER2-HER3 dimerization, resulting in partial inhibition of PI3K/AKT signaling (Agus et al., 2002). Because pertuzumab and trastuzumab bind to different epitopes in the HER2 ectodomain (Franklin et al., 2004), hence their complementary abilities to disrupt HER2-containing dimers, the combination of pertuzumab and trastuzumab has shown synergy in preclinical studies (Scheuer et al., 2009) and clinical trials (Baselga et al., 2012b; Gianni et al., 2012) and is now approved for treatment of patients with $HER2^+$ breast cancer. *T*rastuzumab-*d*erivative of *m*aytansine 1 (T-DM1 or trastuzumab emtansine) is an antibody-drug conjugate in which one molecule of trastuzumab is covalently bonded via a noncleavable linker to 3.5 molecules of a maytansinoid that inhibits microtubule polymerization (DM1). After binding to the receptor, the T-DM1/HER2 complex is internalized followed by degradation in lysosomes, release of DM1, and subsequent cell lysis (Lewis Phillips et al., 2008). T-DM1 binds to HER2 with similar affinity as trastuzumab, thus retaining the ability of the naked antibody to inhibit ligand-independent HER2-containing dimers and signal transduction as well as to mediate ADCC (Junttila et al., 2011).

Lapatinib is an ATP-competitive, reversible small-molecule inhibitor of the HER2 and EGFR tyrosine kinases (Konecny et al., 2006). In $HER2^+$ breast cancers, lapatinib quickly disables HER2 signaling, resulting in inhibition of the PI3K/AKT and MAPK pathways, and it has shown clinical activity in $HER2^+$ breast cancers that have progressed on trastuzumab (Geyer et al., 2006). Lapatinib also binds the inactive conformation of EGFR (Wood et al., 2004), but it has not been active against cancers for which EGFR antibodies or TKIs are approved. Afatinib (Minkovsky and Berezov, 2008) and neratinib (Burstein et al., 2010) are irreversible, covalent HER2/EGFR TKIs with activity against HER2, HER4,

EGFR, and some HER2 insertion mutants (Bose et al., 2013). Of note, the clinical efficacy of all therapeutic inhibitors of HER2 has been predominantly limited to breast cancers that overexpress HER2 as measured by intense membrane staining in the majority of tumor cells with HER2 antibodies (3+ by IHC) or excess copies of the *HER2* gene determined by FISH.

EGFR

Gefitinib and erlotinib are ATP-competitive EGFR TKIs (Table 2). Biochemical and crystallography analyses demonstrate that the mutants possess a higher affinity for the first-generation EGFR inhibitors gefitinib and erlotinib compared to the wild-type receptor (Carey et al., 2006; Yun et al., 2007). Thus, the mutant enzymes are inhibited at lower concentrations of drug, which leads to a favorable therapeutic index. As will be discussed in greater detail below, EGFR mutant lung cancers often develop a second mutation in the gatekeeper residue, T790M, as they become resistant to gefitinib or erlotinib. Thus, there have been intense efforts to develop a drug that can inhibit T790M EGFR to overcome resistance. One such effort was the development of second-generation EGFR inhibitors, such as afatinib and dacomitinib. These drugs are irreversible ATP competitors that form covalent links with the Cys773 residue of EGFR. Although these second-generation drugs have the capacity to inhibit the EGFR T790M, they do so at concentrations that also inhibit wild-type EGFR. Thus, there is not a favorable therapeutic index, and dose-limiting toxicities due to inhibition of wild-type EGFR (such as rash and diarrhea) prevent increasing doses high enough to fully suppress T790M. Thus, they have been largely ineffective at overcoming T790M-mediated resistance in the clinic. Pao et al. found that mouse lung transgenic tumors expressing T790M EGFR are sensitive to the combination of afatinib and cetuximab (Regales et al., 2009). This combination has progressed to the clinic, where it has demonstrated significant clinical activity against T790M EGFR lung cancers, although it is also associated with significant toxicity (Janjigian et al., 2011).

More recently, third-generation EGFR inhibitors have been developed. The first of such compounds, WZ-4002, was designed to be much more potent against the resistant T790M mutation than the wild-type receptor, thus restoring a favorable therapeutic index in which the drugs can be dosed high enough to inhibit T790M without inducing toxicity from inhibiting wild-type EGFR (Walter et al., 2013; Zhou et al., 2009). Of note, this drug is not a quinazoline derivative like the first- and second-generation EGFR inhibitors. WZ-4002 has not been developed clinically, whereas two drugs with similar properties, AZD9291 and CLO-1686, have been (Walter et al., 2013). Clinical data are emerging for these compounds, and the high rate of clinical responses, with minimal toxicity, is increasing enthusiasm for the class of drugs (Ranson et al., 2013; Sequist et al., 2013a; Soria et al., 2013).

In contrast to the EGFR TKIs, the EGFR-neutralizing antibody cetuximab blocks ligand binding to the EGFR. Thus, it is most effective in cancers that harbor ligand-activated, wild-type *EGFR*. In colorectal cancers with wild-type *KRAS*, inhibition of EGFR leads mainly to loss of downstream ERK signaling. However, since mutant KRAS directly activates ERK, cetuximab fails to suppress ERK in these cancers, most likely explaining the lack of clinical activity (Ebi et al., 2011). As a result, cetuximab is now used primarily in cancers with wild-type *KRAS*. Panitumumab is another EGFR-targeted antibody that has activity in wild-type *KRAS* CRC. Unlike cetuximab, it is an IgG_2, and is predicted not to engage immune effector cells to mediate ADCC. Despite this difference, phase III studies have demonstrated clinical efficacy similar to that of cetuximab (Douillard et al., 2014; Jonker et al., 2007; Van Cutsem et al., 2007, 2009). Thus, it seems plausible that the primary mechanism of action of cetuximab and panitumumab is due to its inhibition of EGFR signaling and not engagement of ADCC.

HER3 Inhibitors

Several HER3-neutralizing antibodies are in clinical development. MM-121 and U3-1287 (formerly AMG-888) bind the extracellular domain of HER3, block heregulin-induced phosphorylation, and reduce expression of HER3 at the cell surface (Garrett et al., 2011; Schoeberl et al., 2010). MM-121 (IgG_2) is most effective against tumors with ligand-dependent activation of HER3 (Sheng et al., 2010). U3-1287 synergizes with trastuzumab and lapatinib to suppress the growth of *HER2*-amplified xenografts (Garrett et al., 2013a) and has single-agent activity against transgenic mouse mammary cancers induced by Polyomavirus middle T antigen (Cook et al., 2011). RG7116 is an IgG_1 that selectively binds domain 1 of human HER3. It blocks ligand binding and downregulates HER3 from the cell surface. Through glycoengineering of its Fc moiety, RG7116 mediates enhanced ADCC that correlates with HER3 receptor density (Mirschberger et al., 2013). At this time, these antibodies have completed phase I safety and dose-finding trials, but their clinical efficacy remains to be shown.

LJM716 is a novel anti-HER3 antibody that binds an epitope within domains 2 and 4 in the receptor's extracellular domain, thus trapping HER3 in an inactive conformation. In contrast to the other anti-HER3 antibodies, it blocks both ligand-induced and ligand-independent HER3 dimerization and activation (Garner et al., 2013). This property may be particularly advantageous in *HER2*-amplified breast cancers, in which HER2 appears to activate HER3 in a ligand-independent manner. Accordingly, in laboratory studies, LJM716 reduced growth of established *HER2*-amplified xenografts when given as a single agent and synergized with PI3K inhibitors to suppress growth of *HER2*-amplified/*PIK3CA* mutant tumors (Garrett et al., 2013b).

More recently, bispecific antibodies targeting HER3 have been introduced. MM-111 is an antibody that docks onto HER2 and subsequently binds HER3, thus blocking ligand-dependent activation of HER2/HER3 dimers (McDonagh et al., 2012). Finally, MEHD7945A is a two-in-one IgG_1 generated by phage display engineering that specifically binds HER3 and EGFR with high affinity, thus blocking TGF-α- and HRG-induced activation of both receptors and downstream PI3K/AKT and ERK signaling. MEHD7945A mediates ADCC in vivo and demonstrates superior antitumor activity against multiple tumor models compared to monospecific antibodies (Schaefer et al., 2011). Currently, HER3 inhibitors are being developed in combination with trastuzumab, EGFR antibodies and TKIs, PI3K inhibitors, and cytotoxic chemotherapy. In addition to *HER2* amplification and *EGFR* mutation, high heregulin expression and *HER3* mutations are being explored as predictive biomarkers of response in clinical trials.

Mechanisms of Resistance to ERBB Inhibitors

Although ERBB-targeted therapies have provided substantial benefit to patients with advanced cancer, cancers ultimately

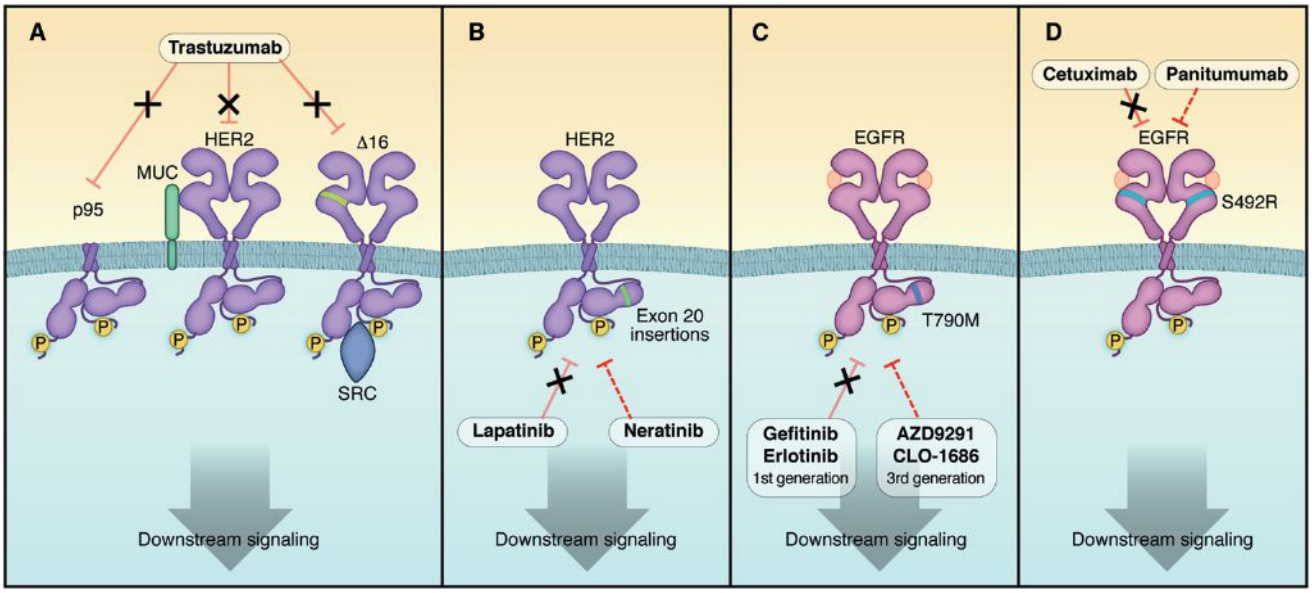

Figure 1. Schema Depicting Intragenic Alterations Leading to Resistance to HER2 and EGFR Inhibitors

(A) HER2 truncations (p95) and splice variants (Δ16) are not inhibited by trastuzumab. In addition, expression of specific mucin isoforms can prevent trastuzumab from binding HER2 (Price-Schiavi et al., 2002). Not shown in the figure, pertuzumab and T-DM1 cannot recognize p95 either.

(B) HER2s harboring exon 20 insertions are not inhibited by lapatinib, but may be sensitive to irreversible HER2 inhibitors afatinib and neratinib. They are also resistant to trastuzumab.

(C) The EGFR T790M gatekeeper mutation leads to acquired resistance to first generation EGFR inhibitors, but is effectively inhibited by third-generation EGFR inhibitors.

(D) An EGFR mutation in the extracellular domain is associated with acquired resistance to cetuximab, but may still be sensitive to another anti-EGFR antibody, panitumumab. Dashed lines indicate inhibition via alternative antibodies and inhibitors.

have developed resistance to the current approaches. In this Perspective, we will discuss both de novo and acquired resistance. The distinction is primarily a clinical one: de novo or intrinsic resistance refers to cancers that do not exhibit an initial response, whereas acquired resistance develops after an initial, often marked and durable, clinical response. It is important to appreciate that the same molecular mechanism may cause both types of resistance, underscoring the robustness of the biological principles underlying how cancers evade these therapies.

Mechanisms of resistance have been discovered by several approaches, including the maintenance of cell lines and xenografts in the presence of drug until resistance emerges or infection of sensitive cell lines with open reading frame (ORF) or shRNA libraries to identify genes whose expression or loss leads to resistance. These efforts have also been coupled to biopsy programs, in which cancers are systematically biopsied upon the development of resistance to interrogate acquired molecular changes upon treatment pressures (Sequist et al., 2011; Yano et al., 2011; Yu et al., 2013). However, there are significant limitations with many of the laboratory studies. Although EGFR TKIs are primarily used as single agents for *EGFR* mutant lung cancers, HER2-directed therapies and EGFR antibodies are generally used in combination with chemotherapy in the clinic. However, most laboratory studies have modeled resistance to these agents as single therapies, thus not recapitulating the selective pressure of combination therapies applied in the clinic. Other data about potential resistance mechanisms have been derived from correlative clinical trials in which patients have been treated with anti-HER2 drug(s) in combination with chemotherapy, a variable not always considered in the interpretation of the studies of drug resistance. Finally, even though combinations of HER2 antagonists are increasingly used in the clinic, resistance to these combinations has yet to be modeled widely in the laboratory.

Intrinsic HER2 Alterations

Some resistance mechanisms affect the capacity for HER2 inhibitors to directly engage HER2. Anido et al. described p95-HER2, a truncated form of HER2 lacking the trastuzumab binding region, which may arise from alternate transcription initiation sites in *HER2* (Anido et al., 2006) (Figure 1A). Patients with metastatic breast cancer harboring cytosolic expression of p95-HER2 exhibit a very low response rate to trastuzumab compared to those patients without p95-HER2 in their tumors (Scaltriti et al., 2007). This form of HER2 retains kinase activity, and tumors with p95-HER2 may still be susceptible to kinase inhibition with a TKI, as suggested by the observation that p95-HER2 tumors exhibit a similar response rate to the combination of capecitabine and lapatinib compared to breast cancers expressing full-length HER2 (Scaltriti et al., 2010).

A splice variant that eliminates exon 16 in the extracellular domain of the HER2 receptor has also been identified in $HER2^{+}$ primary breast cancers and cell lines (Kwong and Hung, 1998) (Figure 1A). This variant does not eliminate the trastuzumab epitope on HER2, but stabilizes HER2 homodimers and prevents their disruption upon binding by the antibody, resulting in trastuzumab resistance in cell lines. The Δ16 isoform was found to interact directly with Src, and treatment with the Src inhibitor dasatinib overcame the resistance to the antibody

conferred by the alternative splicing variant (Mitra et al., 2009). However, clinical evidence of an association between HER2-Δ16 and resistance to trastuzumab has not been shown.

HER2 mutations have been found in a small proportion of lung, gastric, colorectal, breast, and head and neck cancers (Lee et al., 2006; Ross et al., 2013; Stephens et al., 2004; Willmore-Payne et al., 2006). These mutants of HER2 are resistant to lapatinib and trastuzumab (Figure 1B), but are sensitive to the covalent HER2 TKI neratinib (Bose et al., 2013; Wang et al., 2006). To the best of our knowledge, *HER2* mutations in *HER2* gene-amplified breast tumors are very rare. As such, they have not been identified as a resistance mechanism to trastuzumab. One possible reason is that these mutations may comprise only a portion of the amplified HER2 alleles and, therefore, exist below the limits of sensitivity of traditional DNA sequencing methods (Zito et al., 2008). It is possible that cancer cells harboring these mutations will be selected, or acquired, after the selective pressure of anti-HER2 treatment. If so, they may only be detected in tumors that are progressing after primary HER2-targeted therapy. However, comprehensive studies profiling $HER2^+$ tumors that have progressed on primary anti-HER2 therapies have not been reported.

Intrinsic EGFR Alterations

In EGFR mutant lung cancer, the most common mechanism of acquired resistance to EGFR inhibitors is the development of a mutation in the gatekeeper residue of EGFR, T790M (Kobayashi et al., 2005; Pao et al., 2005). T790M abrogates the inhibitor effects of gefitinib and erlotinib by increasing the affinity of the receptor for ATP (Yun et al., 2008), thereby lessening the potency of first-generation EGRF inhibitors (Figure 1C). At least 50% of biopsies from patients with acquired resistance harbor the T790M mutation. Recent studies suggest that highly sensitive methods can detect the T790M mutation in ~35% of pretreatment biopsies. This suggests, but does not prove, that it preexists in a small fraction of cells and that those cells are selected for during the course of treatment (Maheswaran et al., 2008; Rosell et al., 2011). Currently, the third-generation EGFR inhibitors (discussed above) are in early clinical trials to overcome this resistance.

An analogous finding has been observed in wild-type KRAS CRCs that develop resistance to cetuximab. A small study reported the development of a S492R mutation in the extracellular domain of EGFR that interferes with cetuximab binding, but does not interfere with ligand-dependent activation or abrogate receptor engagement by panitumumab (Montagut et al., 2012) (Figure 1D).

Bypass Track Resistance

Other than the immune effects of ERBB antibodies, it is believed that most of activity of these drugs is due to suppression of downstream signaling, particularly PI3K/AKT and MEK/ERK. Thus, many cancers are resistant to single-agent ERBB inhibitors because at least one of these critical downstream pathways is maintained despite inhibition of the targeted receptor. This type of resistance, also termed "bypass track" resistance, is often used to describe resistance resulting from maintenance of these key downstream signaling pathways despite adequate inhibition of the respective RTK (reviewed in Niederst and Engelman, 2013; Figure 2).

Ligand- and RTK-Mediated Resistance. One of the earliest validated observations that RTK bypass signaling induces resistance to ERBB inhibitors was in *EGFR*-mutant NSCLCs. Amplification of the *MET* gene was found in *EGFR* mutant cancers with acquired resistance to EGFR TKIs but not in pretreatment biopsies (Bean et al., 2007; Engelman et al., 2007). In these resistant cancers, MET reactivates both PI3K/AKT and MEK/ERK signaling despite the inhibition of EGFR. The combination of MET and EGFR inhibitors was sufficient to block downstream signaling and induce marked tumor regressions (Engelman et al., 2007; Turke et al., 2010). Activation of MET by its ligand hepatic growth factor (HGF) was also sufficient to promote resistance through activation of downstream signaling (Yano et al., 2008). MET has also been implicated in trastuzumab resistance. HGF-induced signaling through MET was shown to abrogate the action of trastuzumab (Shattuck et al., 2008; Turke et al., 2010). Further, gene amplification of MET and HGF was reported in a cohort of $HER2^+$ patients who did not respond to trastuzumab and chemotherapy (Minuti et al., 2012). Thus, MET activation by either gene amplification or ligand stimulation can cause bypass resistance to EGFR and HER2 inhibitors.

Reactivation of EGFR and HER3 can also serve as a mechanism of resistance to ERBB inhibitors. In laboratory models of *HER2*-amplified breast cancer treated with trastuzumab, increased levels of EGFR and ERBB ligands led to an increase in active EGFR/HER3 and EGFR/HER2 dimers to promote resistance (Ritter et al., 2007). This is consistent with data showing that trastuzumab is unable to block ligand-induced HER2-containing heterodimers (Agus et al., 2002). Similarly, activation of TGFβ receptors can increase ERBB ligand production and cleavage, particularly TGF-α, amphiregulin, and heregulin, via activation of the TACE/ADAM17 sheddase; this results in activation of HER3 and PI3K and promotes drug resistance (Wang et al., 2008). Further, a gene signature of TGFβ activity was developed and shown to correlate with resistance to trastuzumab and poor clinical outcome in patients (Wang et al., 2008).

Similarly, in *EGFR* mutant cancers, *MET* amplification leads to resistance to EGFR TKIs through reactivation of HER3 (Engelman et al., 2007). In a subset of *EGFR* mutant lung cancers, amplification of HER2, presumably involving HER3 reactivation, was also identified as a resistance mechanism to EGFR TKIs (Takezawa et al., 2012). Consistent with these data, blockade of HER3 with the neutralizing antibody MM-121 increases the efficacy of cetuximab in a mouse model of EGFR mutant lung cancer (Schoeberl et al., 2010). Along those lines, a selective ADAM inhibitor, INCB3619, which prevents the processing and activation of multiple ERBB ligands including heregulin, inhibits HER3 signaling and enhances gefitinib-mediated inhibition of EGFR in NSCLC (Zhou et al., 2006). Further supporting a role of amplified HER2-HER3 signaling in resistance to EGFR-targeted therapies, colorectal cancer patients with de novo or acquired resistance to cetuximab-based therapy exhibit HER2 amplification in their tumor or high levels of circulating heregulin (Yonesaka et al., 2011). Finally, using patient-derived colon cancer xenografts, Bertotti et al. identified *HER2* gene amplification as a predictor of resistance to cetuximab among KRAS wild-type tumors (Bertotti et al., 2011).

IGF-I receptors have also been implicated in driving resistance to both EGFR and HER2 inhibitors. Overexpression of IGF-1R or an increase in levels of IGF-1R/HER2 heterodimers can potently activate PI3K/AKT signaling and confer resistance to

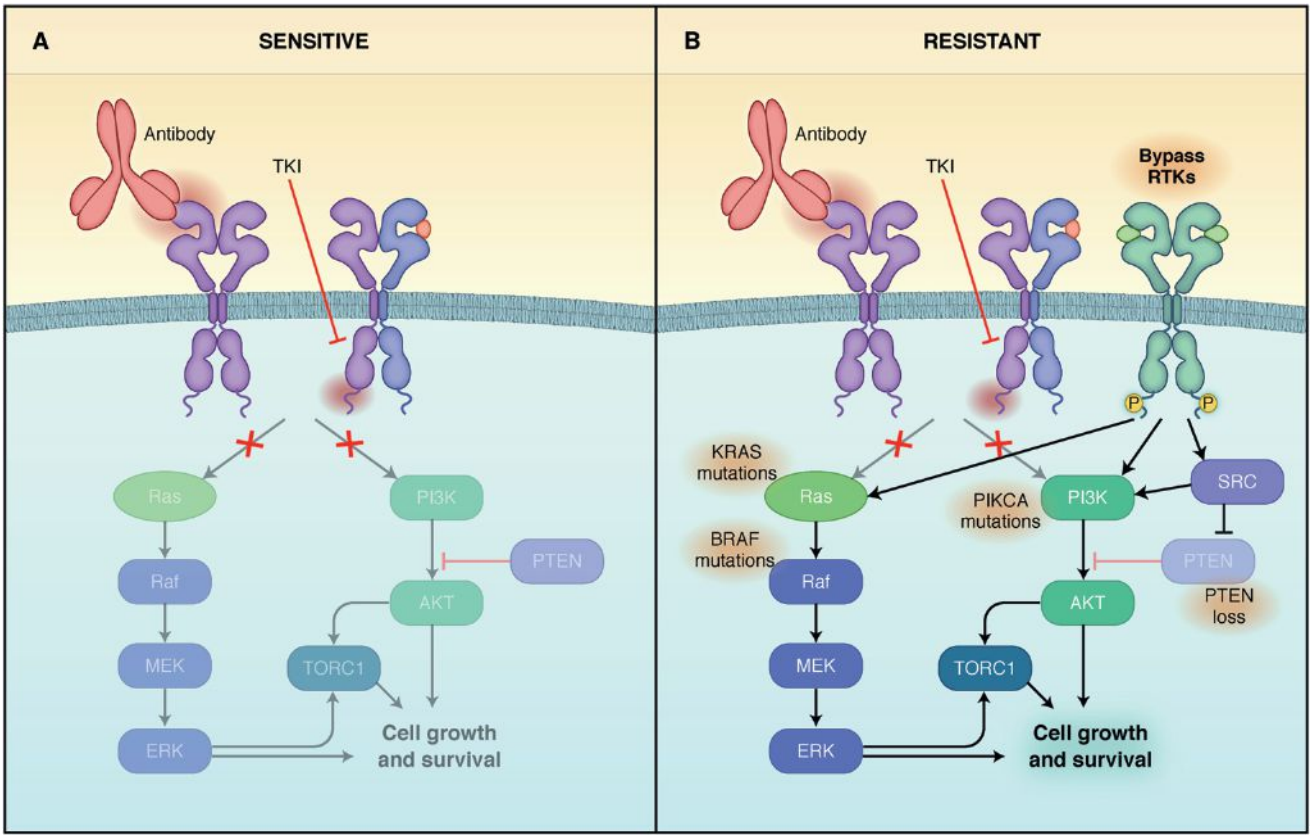

Figure 2. Schematic Depicting Resistance to EGFR and HER2 Inhibitors due to Activation of Bypass Track Signaling
(A) Model of a sensitive EGFR or HER2-addicted cancer treated with an ERBB small-molecule inhibitor or antibody resulting in suppression of downstream signaling. EGFR or HER2 homodimers and heterodimers are shown.
(B) Model of a EGFR mutant or *HER2*-amplified cancer with resistance due to maintenance of downstream signaling in the presence of the EGFR or HER2 inhibitors. Activation of signaling can be caused by activation of other RTKs or mutational activation of downstream signaling.

trastuzumab in laboratory studies (Huang et al., 2010). Inhibition of IGF-1R with a neutralizing antibody or a small-molecule TKI, or targeting of the HER2 kinase with lapatinib was found to overcome IGF-1R-mediated resistance to trastuzumab (Nahta et al., 2007). In a neoadjuvant trial of chemotherapy plus trastuzumab, a high level of IGF-1R expression measured by IHC correlated with a poor clinical response (Harris et al., 2007). Similarly, activation of IGFIR, via loss of expression of *IGFBP3* and *IGFBP4*, which encode insulin-like growth factor binding proteins 3 and 4, respectively, maintains PI3K/AKT signaling despite blockade of EGFR and promotes resistance to EGFR inhibitors in multiple cell lines (Guix et al., 2008). In these cases, inhibition of IGF1R resensitized to EGFR inhibition. In addition, inhibition of IGF-IR also suppressed the development of "persistor cells," the small population of PC9 EGFR mutant cells that survives the initial inhibition of EGFR, described by Settleman and colleagues (Sharma et al., 2010).

In addition to the bypass pathways mentioned above, numerous other RTK-mediated resistance mechanisms have been observed. The EphA2 receptor has been shown to confer resistance to trastuzumab in cell lines, and EphA2 expression was shown to predict poor outcome patients with $HER2^+$ breast cancer (Zhuang et al., 2010). Most recently, the erythropoietin (Epo) receptor was found to be coexpressed in cell lines and primary tumors that overexpress HER2. In these cell lines, concurrent treatment with recombinant erythropoietin conferred trastuzumab resistance. In patients with $HER2^+$ breast cancer, the concurrent administration of erythropoietin and trastuzumab correlated with a shorter progression-free and overall survival compared to patients not receiving erythropoietin (Liang et al., 2010). Finally, in erlotinib-resistant *EGFR* mutant lung cancer cells and lapatinib-resistant *HER2*-amplified breast cancer cells, levels of the AXL RTK were markedly increased (Liu et al., 2009; Zhang et al., 2012). Targeting of AXL was able to resensitize some of these resistant cancers to the original TKI.

We should note that most of these RTK-mediated mechanisms do not necessarily involve genetic activation of the RTK, as mainly protein assays (i.e., IHC for IGF-IR, AXL, EphA2, etc.) have been employed to measure their levels in tumor tissues. Such correlations do not *prove* that the putative bypass RTK is causal to drug resistance in the clinic or in a particular patient. Ultimately, clinical efficacy using specific drugs that target the bypass RTK will be needed for true validation.

Intracellular Kinases. Molecules in the pathways downstream of RTKs can be aberrantly activated as a result of genetic alterations, also resulting in drug resistance (Figure 2). Somatic alterations in the PI3K/AKT pathway are the most frequent in breast cancer, occurring in approximately 30% of $HER2^+$ tumors. These

include mutation and/or amplification of the genes encoding the PI3K catalytic subunits p110α (*PIK3CA*) and p110β (*PIK3CB*), the PI3K regulatory subunit p85α (*PIK3R1*), the PI3K effectors AKT1, AKT2, and PDK1, and loss of the lipid phosphatases PTEN and INPP4B (reviewed in Engelman, 2009). It is generally accepted that the antitumor activity of HER2 inhibitors depends on inhibition of PI3K-AKT downstream of HER2. Thus, one would expect that activating mutations in the PI3K pathway would confer resistance to HER2 inhibitors.

Constitutive activation of PI3K, via overexpression of *PIK3CA* mutants, conferred resistance to the antibody in laboratory studies (Chakrabarty et al., 2010; Eichhorn et al., 2008; Serra et al., 2008). Patients with "hot-spot" *PIK3CA* mutations and undetectable or low PTEN measured by IHC exhibited a poorer outcome after treatment with chemotherapy and trastuzumab compared to patients without those alterations (Berns et al., 2007; Dave et al., 2011; Esteva et al., 2010). In the EMILIA and Neo-ALTTO randomized trials in $HER2^+$ breast cancer, patients with *PIK3CA* mutant tumors did not benefit from lapatinib and capecitabine (Baselga et al., 2013b) and from lapatinib and trastuzumab (Baselga et al., 2013a), respectively. It remains to be determined whether T-DM1, because of its ability to deliver high levels of cytotoxic chemotherapy to HER2-overexpressing cells, trumps this mechanism of resistance.

One of the first discoveries linking constitutive activation of PI3K signaling and resistance to HER2 inhibitors was accomplished by Berns et al. Using a large-scale small interfering RNA genetic screen, they identified PTEN as the only gene whose knockdown conferred trastuzumab resistance (Berns et al., 2007). However, the association of PTEN loss with drug resistance in the clinic is less clear. In one early study in patients with metastatic breast cancer, loss or low levels of PTEN correlated with a lower response to trastuzumab (Nagata et al., 2004). This correlation was not found in patients with early breast cancer treated with adjuvant trastuzumab (Perez et al., 2013). We speculate that this was because of the concomitant administration of chemotherapy in an adjuvant setting (Rexer et al., 2013).

Similar findings have been observed in cancers with acquired resistance to EGFR inhibitors. Introduction of *PIK3CA* mutations into EGFR mutant lung cancer cell lines is sufficient to maintain PI3K signaling and promote resistance (Engelman et al., 2006). Accordingly, PIK3CA mutations have been identified in biopsies of *EGFR* mutant cancers with acquired resistance to EGFR inhibitors (Sequist et al., 2011). Similarly, a report found that *PTEN* loss may be associated with resistance to EGFR inhibitors (Sos et al., 2009). In addition to reactivation of PI3K, reactivation of ERK signaling can promote resistance to EGFR inhibitors, as evidenced by the finding of a *BRAF* mutation in an *EGFR* mutant lung cancer with acquired resistance (Ohashi et al., 2012). In a second example, an *EGFR* mutant cell line made resistant to third-generation EGFR inhibitors developed amplification of ERK and was resensitized upon inhibition of MEK (Ercan et al., 2012).

A compelling recent discovery underlying this type of resistance mechanism was the study of KRAS wild-type colorectal cancers that had developed resistance to cetuximab. By performing repeat biopsies and evaluating circulating tumor DNA, investigators observed the emergence of *KRAS* mutations as a resistance mechanism (Diaz et al., 2012; Misale et al., 2012). From a signaling perspective, one would expect that the *KRAS* mutant clones fail to downregulate the ERK pathway in response to cetuximab, underlying the resistance. As the presence of KRAS mutations predicts for lack of initial response to cetuximab, these findings underscore the convergence of intrinsic and acquired resistance mechanisms.

Src family kinase (SFK) signaling has been implicated by several studies in promoting resistance to HER2 inhibitors. In $HER2^+$ breast cancer cells with acquired resistance to lapatinib, upregulation of SFK activity, particularly Yes, was observed in several resistant cell lines. Resistance was associated with recovery of PI3K/AKT signaling despite inhibition of HER2. Addition of a Src TKI partially blocked PI3K/AKT and restored sensitivity to lapatinib (Rexer et al., 2011). In another study, the authors suggest that PTEN was no longer capable of dephosphorylating and suppressing Src in trastuzumab-resistant $HER2^+$ cells, and the addition of a Src kinase inhibitor overcame trastuzumab resistance (Zhang et al., 2011). Src activity is also involved in the resistance conferred by the Δ16 HER2 isoform and the EpoR (Mitra et al., 2009). Src is thought to mediate resistance in part via phosphorylation and inhibition of PTEN, leading to constitutive PI3K signaling (Liang et al., 2010).

Defects in Apoptosis and Cell-Cycle Control

Inhibition of a driver oncogene such as EGFR and HER2 results in proliferation arrest and apoptosis. Therefore, alterations in the normal apoptotic machinery can also induce resistance to EGFR- and HER2-targeted therapies. Indeed, we observed that levels of the proapoptotic BH3-only Bcl2 family member, BIM, are predictive of response to targeted therapy in *EGFR* mutant lung cancers, *HER2*-amplified breast cancers, and *PIK3CA* mutant cancers (Faber et al., 2011). BIM protein normally is induced after inhibition of EGFR and HER2 in these cancers. In this study, although erlotinib or lapatinib inhibited EGFR and HER2 and downstream signaling in *EGFR* mutant and *HER2*-amplified cancers, respectively, only those cell lines with high levels of BIM underwent marked apoptosis. This suggests that BIM levels are a biomarker predictive of response to a TKI in an oncogene-addicted cancer. Other groups have reported similar results in EGFR mutant lung cancers (Ng et al., 2012) and *HER2* gene-amplified breast cell lines with and without activating mutations (Tanizaki et al., 2011). In cancers with concurrent *PIK3CA* mutant cells, however, both the growth inhibitory effect and induction of BIM after treatment with lapatinib were blunted (Tanizaki et al., 2011).

Survivin, a member of the inhibitor of apoptosis (IAP) protein family that inhibits the activity of caspases, has been shown to be a point of convergence of several pathways that can lead to resistance to HER2 inhibitors. In $HER2^+$ breast cancer cells, inhibition of HER2-PI3K reduces survivin expression resulting in apoptosis. *HER2*-amplified breast cancer cells with acquired resistance to lapatinib upregulate ERα, which, in turn, induces FoxO3a-mediated transcription of survivin (Xia et al., 2006). In turn, high survivin levels allow for escape from lapatinib. Accordingly, elevated levels of survivin and MCL-1 have been found in trastuzumab-resistant cells (Chakrabarty et al., 2013).

Altered control of progression through the cell cycle in response to HER2 inhibition also plays a role in resistance. Cell lines made resistant to trastuzumab by chronic exposure

exhibited focal amplification of cyclin E. CDK2 inhibitors reduced growth of these trastuzumab-resistant xenografts (Scaltriti et al., 2011). Further, in a cohort of patients with $HER2^+$ breast cancers treated with trastuzumab, amplification of cyclin E was associated with a diminished clinical response. Downregulation of the Cdk inhibitor $p27^{KIP1}$ and a resulting increase in Cdk activity has also been associated with trastuzumab resistance (Nahta et al., 2004; Yakes et al., 2002). Indeed, modulation of levels of $p27^{KIP1}$ appears to be a common endpoint for several of the resistance pathways noted above, including signaling from IGF-1R and MET (Nahta et al., 2005; Shattuck et al., 2008).

Tumor Host Factors

Host factors that affect the immunomodulatory function of trastuzumab can also contribute to trastuzumab resistance. In mice lacking FcγRIII and, thus, deficient in NK cells and macrophages capable of binding the Fc region of trastuzumab, the therapeutic effect of trastuzumab was markedly diminished (Clynes et al., 2000). Polymorphisms in the gene encoding FcγRIII in humans were associated with resistance to trastuzumab in patients with metastatic $HER2^+$ breast cancer (Musolino et al., 2008). In the same study, PBMCs from patients with *FCGR3* polymorphisms associated with an improved outcome after trastuzumab induce a stronger trastuzumab-mediated ADCC in vitro. A follow-up study found that the quantity and lytic efficiency of $CD16^+$ lymphocytes are the major factors affecting the level of ADCC induced by trastuzumab. This, in turn, correlates with tumor response (Gennari et al., 2004). We should note, however, that a large trial of trastuzumab-based adjuvant chemotherapy in patients with early $HER2^+$ breast cancer did not show an association between *FCGR3A* and *FCGR2A* polymorphisms with patient outcome (Hurvitz et al., 2012).

Strategies to Overcome Resistance: Combination Therapies

Clinical experience has validated EGFR and HER2 as effective drug targets. However, in the metastatic setting, these inhibitors do not lead to cures, and cancers ultimately develop resistance. Thus, there is a great need to identify therapeutic strategies that will improve upon the current approaches. We believe that one strategy will include maximal blockade of the oncogene target itself as well as inhibition of the key bypass tracks that promote resistance. The growing number of escape routes will likely necessitate combinations of multiple agents, whose delivery will require innovative dosing and scheduling.

HER2

All currently available HER2 inhibitors target or exploit mechanisms of HER2 function. As single drugs, however, they do not potently suppress HER2 signaling. This may explain the generally short-lived responses of metastatic $HER2^+$ breast cancers to single-agent HER2 inhibitors. Trastuzumab and pertuzumab, in particular, are each weak signaling inhibitors, possibly because they incompletely block HER2-containing dimers (Junttila et al., 2009). Treatment with lapatinib (and most likely other HER2 TKIs) leads to an increase in HER2 and HER2-containing dimers at the plasma membrane and fails to completely and persistently inhibit the HER2 kinase (Garrett et al., 2011; Scaltriti et al., 2009). This may be explained by both the narrow therapeutic index of current HER2 TKIs and the challenge of complete and sustained inhibition of an amplified drug target, i.e., HER2, with small molecules. Moreover, inhibition of the HER2 kinase leads to an initial reduction of PI3K/AKT signaling, which releases negative feedbacks resulting in upregulation of HER3 and other RTKs, as well as survival factors such as BCL2 and ERα, thereby mitigating the efficacy of HER2 inhibitors (Chakrabarty et al., 2012; Chandarlapaty et al., 2011; Garrett et al., 2011; Muranen et al., 2012; Xia et al., 2006). We also recognize that *HER2*-amplified breast cancers vary with respect to their addiction to HER2 signaling, although they are grouped together using clinical criteria (FISH, IHC) for HER2 overexpression. Thus, we speculate many *HER2*-gene-amplified cancers are not truly "addicted" to HER2 signaling and, as such, are not sensitive to HER2 TKIs. Finally, resistance to T-DM1 may be due to several reasons, including the sparing of $HER2^-$ tumor cells within heterogeneous cancers containing $HER2^+$ and HER^- tumor cells, a scenario not uncommon in clinical practice. Finally, T-DM1, trastuzumab, and pertuzumab cannot bind p95-HER2 and, thus, would be inactive against tumor cells with an abundance of cytosolic fragments of HER2.

One strategy to address the limitations of anti-HER2 drugs as single agents has been to combine multiple HER2 antagonists that have different but complementary mechanisms of action. Clinical experience had suggested that trastuzumab-refractory tumors remained dependent on HER2 as continuing trastuzumab in new treatment regimens beyond progression to trastuzumab demonstrated clinical benefit (von Minckwitz et al., 2009). Currently, dual blockade of HER2 is well entrenched in the clinic. For example, the combination of trastuzumab and lapatinib is superior to each agent alone in both the metastatic (Blackwell et al., 2010) and neoadjuvant (Baselga et al., 2012a) settings. Similarly, the combination of trastuzumab and pertuzumab was shown to be superior to each antibody alone in both neoadjuvant trials in patients with early disease (Gianni et al., 2012) and in patients with advanced disease (Baselga et al., 2012b), as assessed by progression-free survival. The combination of T-DM1 and pertuzumab is also in progress. This novel approach would incorporate dual receptor blockade with two HER2 antibodies (trastuzumab and pertuzumab) plus the delivery of a potent cytotoxic (DM1) to *HER2*-amplified cells while mostly sparing host tissues (Phillips et al., 2014).

At the time of writing this Perspective, several novel anti-HER2 combinations are being tested in clinical trials. Some of these include a third drug targeted to the HER2 network (Table 3). It is anticipated that for a cohort of $HER2^+$ breast cancers that escape anti-HER2 dual therapy, a third drug targeted against a signaling hub in the receptor network might be necessary. Supporting this possibility, a recent study showed that transgenic mammary tumors expressing HER2 and $PIK3CA^{H1047R}$ were completely resistant to the combinations of trastuzumab plus pertuzumab and trastuzumab plus lapatinib. Addition of the pan-PI3K inhibitor BKM120 to each combination resulted in inhibition of tumor growth, but only partially and temporarily (Hanker et al., 2013). Currently, a main clinical focus is the addition of PI3K inhibitors and/or HER3-neutralizing antibodies (Garrett et al., 2013b) to the established combinations of anti-HER2 therapies (Table 3). More-recent data suggest that blockade of mTOR downstream HER2 with the TORC1 inhibitor everolimus, while maintaining trastuzumab therapy, can induce clinical responses in $HER2^+$ cancers that have progressed on trastuzumab (Hurvitz et al., 2013; Morrow et al., 2011; O'Regan et al., 2013).

Table 3. Anti-ERBB Combinations

Combination	Mechanism(s) of Action	Relevant Clinical Trials
Trastuzumab + lapatinib (or neratinib, afatinib)	ADCC, partial disruption of HER2-HER3 dimers, inhibition of HER2 and EGFR tyrosine kinases	Baselga et al., 2012a; Blackwell et al., 2010
Trastuzumab + pertuzumab (only approved combination)	More-complete inhibition of ligand-induced and ligand-independent HER2-containing heterodimers, ADCC, downregulation of HER2 from cell surface	Baselga et al., 2012b; Gianni et al., 2012; Schneeweiss et al., 2013
T-DM1 + pertuzumab	Same as above plus inhibition of polymerization of microtubules with DM1	MARIANNE (NCT01120184)
Trastuzumab + everolimus	ADCC, disruption of ligand-independent HER2-HER3 dimers, inhibition of TORC1	BOLERO-3 (NCT01007942)
Trastuzumab + pertuzumab + PI3K inhibitor	Inhibition of ligand-induced and ligand-independent HER2-containing heterodimers, ADCC, ATP-competitive inhibition of catalytic activity of p110	
Trastuzumab + HER3-neutralizing antibody	ADCC, partial disruption of HER2-HER3 dimers, inhibition of heregulin binding, downregulation of HER3 and/or HER3 dimerization	
Trastuzumab + HER3 antibody + PI3K inhibitor	Same as above plus direct inhibition of p110	
T-DM1 + PI3K inhibitor	ADCC, partial disruption of HER2-HER3 dimers, inhibition of polymerization of microtubules, direct inhibition of p110	
Afatinib + cetuximab	Combined targeting of EGFR T790M to compensate for complete inhibition of target by either approach alone. Afatinib may also target resistance due to HER2 activation	NCT01090011
EGFR + PI3K inhibitor	Block resistance due to reactivation of PI3K signaling	
Erlotinib + MET inhibitor	Block MET-dependent resistance to EGFR inhibitors	MetLung Trial and others
EGFR inhibitor + IGF-IR antibody	Block IGF-IR-dependent resistance to EGFR inhibitors	
Erlotinib + hydroxychloroquine	Effort to block the survival of "drug-tolerant" cells after treatment with EGFR TKIs (Sharma et al., 2010)	Goldberg et al., 2012
Irreversible EGFR inhibitor + MET inhibitor	Overcome both T790M- and MET-mediated resistance	

Along the same lines, neratinib in combination with the TORC1 inhibitor temsirolimus recently demonstrated clinical activity in HER2 mutant lung cancers (Gandhi et al., 2014). Finally, one proposed novel strategy is the combination of trastuzumab with anti-PD1 and anti-CD37 monoclonal antibodies. In this case, anti-PD1 would inhibit IFNγ-activated T cells, and anti-CD37 would block $CD8^+$ T cells; both of these T cell subtypes are required for the adaptive immune response triggered by trastuzumab (Stagg et al., 2011).

EGFR

One major mechanism of resistance to EGFR inhibitors in EGFR mutant cancers is the development of the T790M gatekeeper residue. The newer third-generation EGFR TKIs that suppress T790M are showing remarkable progress in this subset of cancers (Ranson et al., 2013; Sequist et al., 2013a; Soria et al., 2013). Ultimately, clinical trials will be needed to determine whether third-generation EGFR inhibitors become first-line therapy for *EGFR* mutant lung cancers. We anticipate that metastatic *EGFR* mutant lung cancers will likely become resistant to drugs that target T790M since there are several additional potential resistance mechanisms. Thus, it will most likely be necessary to combine inhibitors of bypass tracks with T790M-specific inhibitors to provide greater durations of remission and prolongation of patient survival.

In general, combinations that overcome resistance to EGFR inhibitors have generally required continued inhibition of EGFR combined with a drug that blocks the bypass track (reviewed in Niederst and Engelman, 2013). For example, in *EGFR* mutant lung cancers that are resistant via *MET* amplification, combined EGFR and MET inhibition is required to suppress downstream PI3K/AKT and MEK/ERK and induce tumor regressions in vivo (Turke et al., 2010). In similar examples of resistance mediated by IGF-IR and AXL, inhibition of the bypass RTK in combination with the EGFR is needed to overcome resistance (Cortot et al., 2013; Guix et al., 2008; Zhang et al., 2012). Thus, one central strategy involving combinations centers on maintaining potent inhibition mutant EGFR while adding different inhibitors to these accessory pathways. This has been employed in early clinical trials that have combined EGFR inhibitors with MET inhibitors, PI3K inhibitors, and IGF-IR inhibitors (Table 3). However, none of these trials utilized third-generation EGFR inhibitors, which are the only drugs that appear to be capable of overcoming T790M. The advent of these third-generation inhibitors may now unleash the potential of targeting bypass tracks once T790M is effectively inhibited.

In *KRAS* wild-type colorectal cancers, the recent finding that resistant cancers develop EGFR mutations that abrogate cetuximab binding or *KRAS* mutations suggests approaches analogous to those discussed above. Again, the development of point mutations in EGFR suggests that alternative approaches to suppress EGFR may be warranted. Preclinical studies suggest panitumumab may overcome this type of resistance (Montagut et al., 2012). In colorectal cancers that develop *KRAS* mutations upon development of resistance, current trials are examining the

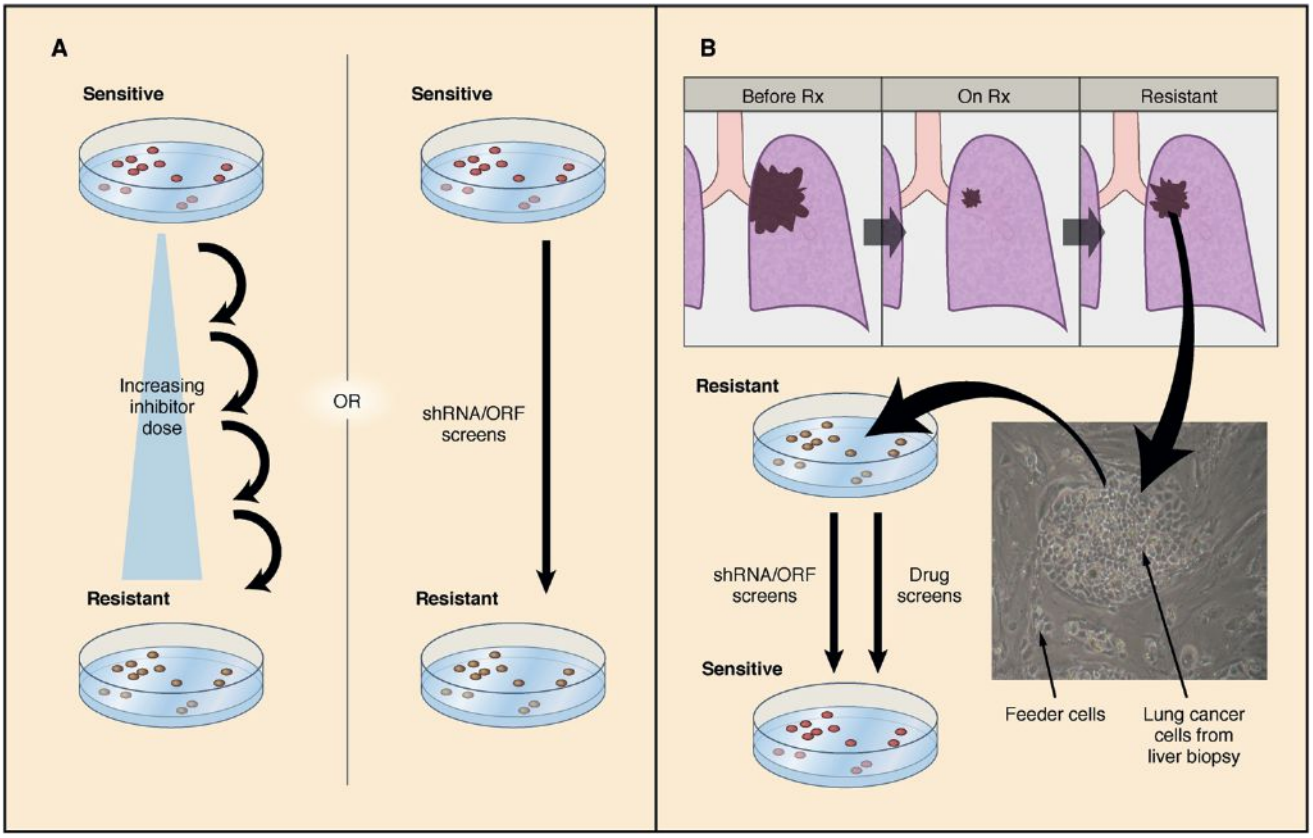

Figure 3. Developing Laboratory Models to Discover Mechanisms of Resistance
(A) Resistance mechanisms can be discovered by culture of sensitive cell lines in the presence of a specific HER2 or EGFR inhibitor until resistance develops or by introduction of shRNA or ORF libraries to determine genes whose overexpression or suppression will lead to resistance.
(B) Alternatively, when resistance develops in the clinic, a cell line can be generated from a biopsy of the resistant lesion, and the resulting resistant line can be screened with drugs and/or shRNA libraries to determine strategies to resensitize them.

efficacy of EGFR inhibitors in combination with inhibitors to overcome resistance (Misale et al., 2014).

Projections to the Future: Novel Approaches

Monitoring Tumor Evolution

One of the major challenges will be to determine the optimal combinations for individual patients. Some examples have clear biomarkers pointing to specific combinations, such as the use of combined HER2 and PI3K inhibitors for *HER2*-amplified breast cancers harboring *PIK3CA* mutations, as well as EGFR and MET inhibitors for *EGFR* mutant lung cancers harboring *MET* amplifications. However, several of the other combinations do not have straightforward biomarkers for patient selection. In the cases of IGF-IR and AXL, it is quite unlikely that expression of the RTK alone will accurately identify those cancers in which those proteins are driving resistance. Thus, more-precise assessments of RTK and signaling activation via novel proteomic methods would be potentially valuable to identify the most appropriate combinations.

As the cancers progress through therapies, there will be a need to continually interrogate the cancer to understand how it has adapted to treatment pressures and become drug resistant. Many centers have utilized repeat biopsy programs to perform biopsies after the development of resistance to targeted therapies to determine how the cancer has evolved. Indeed, with the increasing use of next-generation sequencing approaches, it is likely that the genetic landscape for resistance mechanisms will increase dramatically over the coming years. Even though this approach has great promise to discover resistance mechanism, it may also have potential limitations when the results are used to determine the next course of therapy for an individual patient as the (acquired) alterations identified in a single biopsy may not reflect all of the resistant clones in multiple metastatic sites in an individual patient (Bean et al., 2007; Engelman et al., 2007; Turke et al., 2010). Thus, noninvasive measures such as molecular interrogation of circulating tumor cells or plasma DNA may help capture the heterogeneity of resistance in patients, as was done to identify the development of *KRAS* mutations in colorectal cancers that acquire resistance to cetuximab (Diaz et al., 2012; Misale et al., 2012). As efforts to identify new therapeutic strategies to overcome resistance are intensified, the development of cell lines and patient-derived xenografts from resistant biopsies may facilitate the identification of new therapeutic strategies. Recent advances in technology may help bring these "live" biopsies directly into the laboratory for interrogation (Liu et al., 2012). Such models could be interrogated by high-throughput shRNA and drug screens to identify novel therapeutic approaches to overcome resistance (Figure 3).

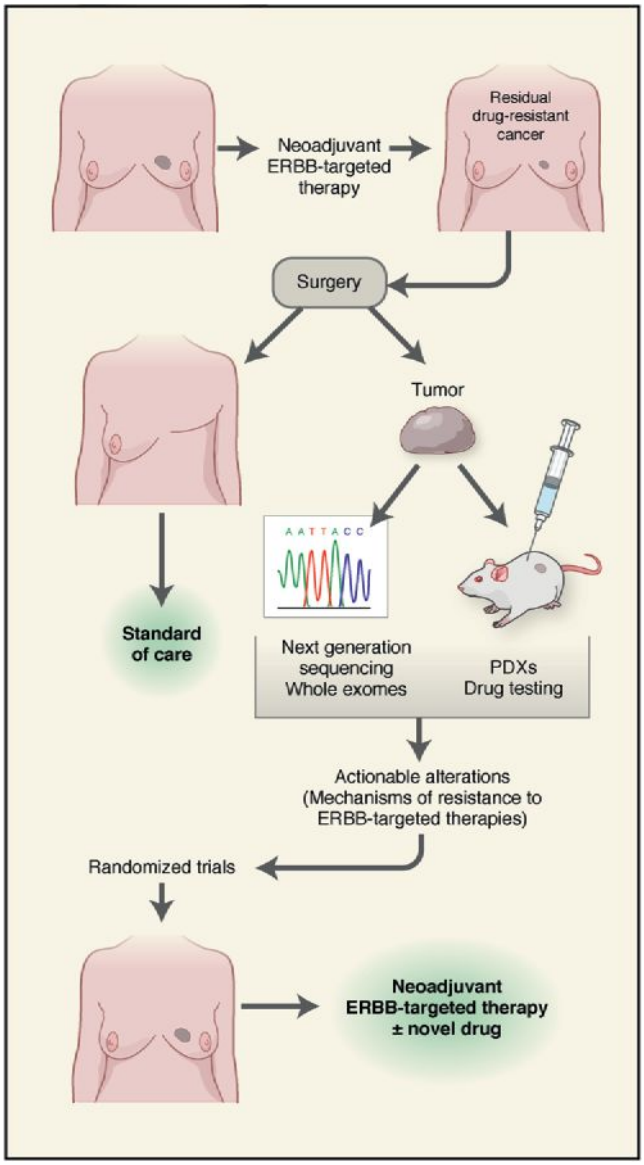

Figure 4. Targetable Alterations in Residual Breast Cancers after Neoadjuvant Anti-HER2 Therapy May Identify Actionable Mechanisms of Drug Resistance

Systemic neoadjuvant anti-HER2 therapy reduces or eliminates the primary HER2$^+$ tumor as well as micrometastases (top row). We propose that "drug-resistant" residual cancers in the breast after neoadjuvant therapy harbor targetable genomic alterations causally associated with resistance to HER2 inhibitors. Molecular profiling of these residual tumors should identify these genomic alterations. Further, patient-derived xenografts (PDXs) generated with these residual cancers can be used to test novel combinations with activity against these drug-resistant cancers that can be later applied to patients on an individual basis. Drugs that target novel mechanisms of resistance identified in the residual tumors can be examined in subsequent neoadjuvant trials (bottom row).

In addition to profiling of metastatic recurrences, the increasing use of neoadjuvant anti-HER2 therapy in patients with newly diagnosed HER2$^+$ breast cancers provides a novel platform for discovery of mechanisms of resistance and tumor heterogeneity. At least two studies have shown that some patients with HER2$^+$ tumors convert to HER2$^-$ after neoadjuvant trastuzumab and chemotherapy, and these patients exhibit a shorter relapse-free survival compared to those with residual tumors that remain HER2 amplified (Hurley et al., 2006; Mittendorf et al., 2009). These results suggest, first, that with heterogeneity in HER2 overexpression in the primary tumor, the antioncogene therapy eliminates the HER2-dependent compartment and enriches for HER2-negative clones. Second, patients with HER2$^+$ tumors that change to HER2$^-$ upon primary anti-HER2 therapy are at a high risk of early recurrence. This neoadjuvant approach facilitates interrogation of the drug-resistant cancer and the identification of targetable mechanisms potentiallly driving subsequent metastatic recurrences (discussed below).

Innovative Trial Designs

For both HER2- and EGFR-driven cancers, it is becoming apparent that new treatment paradigms will be necessary to lead to durable remissions or even cures. Ultimately, we posit that combination therapies will be needed and that it is more rational to consider a proactive regimen that employs alternating regimens of combinations that eliminate cancer cells before they adapt and become resistant rather than treating cancers after the development of clinically overt resistance. However, the large number of potential resistance mechanisms will most likely necessitate the use of more drugs than will be tolerable if they are all delivered simultaneously and each drug is dosed to achieve continual target suppression. In the development of combinations, the use of mutant specific inhibitors will be highly attractive components because of their greater therapeutic windows. However, even with such an approach, given the large number of potential resistance mechanisms, it may become necessary to use even more-creative approaches to proactively kill the various resistant clones as they emerge. In the future, we envision developing regimens that rotate and intercalate tolerable combinations to prevent or substantially delay the development of resistance. In particular, regimens that include immunotherapy and other disparate approaches may be needed.

In breast cancer, the increasing use of neoadjuvant therapy lends itself to some innovative possibilities to develop novel therapeutic regimens, accelerate drug approvals, and discover mechanisms of drug resistance. Achievement of a pathological complete response (path CR) in the breast and axillary lymph nodes after neoadjuvant trastuzumab or chemotherapy has been associated with improved long-term outcome (Gianni et al., 2010; Liedtke et al., 2008). Because of this association, the FDA recently proposed that randomized neoadjuvant trials can be considered for accelerated drug approval using path CR as a surrogate that is "reasonably likely to predict longer term benefit," at least for some subtypes of breast cancer, particularly the HER2$^+$ subtype (Prowell and Pazdur, 2012). Recently, the FDA approved the HER2 antibody pertuzumab as neoadjuvant treatment in patients with HER2$^+$ early breast cancer (http://www.fda.gov/NewsEvents/Newsroom/PressAnnouncements/ucm370393.htm). This approval was based on the results of two neoadjuvant studies, NeoSphere and TRYPHAENA, where the combination of pertuzumab and trastuzumab was superior to trastuzumab alone. The potential impact of this recommendation is quite transformative, as it can accelerate the approval of novel and effective combinations. Further, the early delivery of these anti-HER2 combinations to patients with treatment-naive HER2$^+$ tumors should at least

partially trump acquired drug resistance. The use of the preoperative therapy setting as a clinical research platform in which novel combinations and regimens can be compared and triaged using path CR as a clinical endpoint predictive of long-term outcome has been discussed recently (Bardia and Baselga, 2013).

Another benefit of a preoperative approach is that, except for patients who experience a complete response, tumor tissue is always available at the time of surgery. These "drug-resistant" residual cancers should harbor mechanisms and/or biomarkers of resistance to the primary therapy and, potentially, a similar molecular profile to that of drug-resistant micrometastases that can be interrogated with massive parallel sequencing of DNA extracted from the mastectomy specimen (Balko et al., 2012, 2014). Thus, we propose that "drug-resistant" $HER2^+$ residual cancers in the breast harbor targetable genomic alterations causally associated with resistance to neoadjuvant anti-HER2 therapy (Figure 4). Molecular profiling of these residual tumors should identify these alterations. In addition, patient-derived xenografts generated with these residual cancers can be used to test novel combinations with activity against these drug-resistant cancers that can be later applied to patients on an individual basis. Drugs that target novel mechanisms of resistance identified in the residual tumors can be examined in subsequent randomized neoadjuvant trials. In the future, we anticipate that tumor types other than HER2-overexpressing breast cancer could also effectively utilize neoadjuvant trials to accelerate drug development and discover mechanisms of resistance.

Conclusions

Ultimately, to cure ERBB-dependent cancers, we will most likely have to incorporate therapeutics that are toxic to cancer cells via mechanisms that are not solely based on suppressing ERBB signaling, the associated bypass tracks, and antibodies targeting ERBB receptors to induce ADCC. The timing of treatment may also make a difference. For example, deploying ERBB-targeted combinations early in the natural history of these cancers, i.e., in the adjuvant setting to treat micrometastatic subclinical disease, may yield better outcomes than treating patients with metastatic disease, where the effect will not be curative. We feel that optimizing the timing and intensity of this approach will provide substantial clinical benefit to patients and will serve as the foundation for incorporating complementary, independent therapeutic strategies that may ultimately lead to highly durable responses and further cures.

ACKNOWLEDGMENTS

This work was supported by NCI grants R01 CA80195 (C.L.A.), R01 CA137008 (J.A.E.), R01 CA164273 (J.A.E.), and R01 CA140954 (J.A.E.), ACS Clinical Research Professorship Grant CRP-07-234 (C.L.A.), Breast Cancer SPORE grant P50 CA98131, GI Cancer SPORE grant P50 CA127003, the Department of Defense (J.A.E.), and Vanderbilt-Ingram Cancer Center Support grant P30 CA68485.

REFERENCES

Agus, D.B., Akita, R.W., Fox, W.D., Lewis, G.D., Higgins, B., Pisacane, P.I., Lofgren, J.A., Tindell, C., Evans, D.P., Maiese, K., et al. (2002). Targeting ligand-activated ErbB2 signaling inhibits breast and prostate tumor growth. Cancer Cell *2*, 127–137.

Andrechek, E.R., Hardy, W.R., Siegel, P.M., Rudnicki, M.A., Cardiff, R.D., and Muller, W.J. (2000). Amplification of the neu/erbB-2 oncogene in a mouse model of mammary tumorigenesis. Proc. Natl. Acad. Sci. USA *97*, 3444–3449.

Anido, J., Scaltriti, M., Bech Serra, J.J., Santiago Josefat, B., Todo, F.R., Baselga, J., and Arribas, J. (2006). Biosynthesis of tumorigenic HER2 C-terminal fragments by alternative initiation of translation. EMBO J. *25*, 3234–3244.

Avraham, R., and Yarden, Y. (2011). Feedback regulation of EGFR signalling: decision making by early and delayed loops. Nat. Rev. Mol. Cell Biol. *12*, 104–117.

Balko, J.M., Cook, R.S., Vaught, D.B., Kuba, M.G., Miller, T.W., Bhola, N.E., Sanders, M.E., Granja-Ingram, N.M., Smith, J.J., Meszoely, I.M., et al. (2012). Profiling of residual breast cancers after neoadjuvant chemotherapy identifies DUSP4 deficiency as a mechanism of drug resistance. Nat. Med. *18*, 1052–1059.

Balko, J.M., Giltnane, J.M., Wang, K., Schwarz, L.J., Young, C.D., Cook, R.S., Owens, P., Sanders, M.E., Kuba, M.G., Sánchez, V., et al. (2014). Molecular profiling of the residual disease of triple-negative breast cancers after neoadjuvant chemotherapy identifies actionable therapeutic targets. Cancer Discov. *4*, 232–245.

Bang, Y.J., Van Cutsem, E., Feyereislova, A., Chung, H.C., Shen, L., Sawaki, A., Lordick, F., Ohtsu, A., Omuro, Y., Satoh, T., et al.; ToGA Trial Investigators (2010). Trastuzumab in combination with chemotherapy versus chemotherapy alone for treatment of HER2-positive advanced gastric or gastro-oesophageal junction cancer (ToGA): a phase 3, open-label, randomised controlled trial. Lancet *376*, 687–697.

Bardia, A., and Baselga, J. (2013). Neoadjuvant therapy as a platform for drug development and approval in breast cancer. Clin. Cancer Res. *19*, 6360–6370.

Baselga, J., Bradbury, I., Eidtmann, H., Di Cosimo, S., de Azambuja, E., Aura, C., Gómez, H., Dinh, P., Fauria, K., Van Dooren, V., et al.; NeoALTTO Study Team (2012a). Lapatinib with trastuzumab for HER2-positive early breast cancer (NeoALTTO): a randomised, open-label, multicentre, phase 3 trial. Lancet *379*, 633–640.

Baselga, J., Cortés, J., Kim, S.B., Im, S.A., Hegg, R., Im, Y.H., Roman, L., Pedrini, J.L., Pienkowski, T., Knott, A., et al.; CLEOPATRA Study Group (2012b). Pertuzumab plus trastuzumab plus docetaxel for metastatic breast cancer. N. Engl. J. Med. *366*, 109–119.

Baselga, J., Majewski, I., Nuciforo, P., Eidtmann, H., Holmes, E., Sotiriou, C., Fumagalli, D., Diaz Delgado, M.C., Piccart-Gebhart, M., and Bernards, R. (2013a). PIK3CA mutations and correlation with pCR in the NeoALTTO trial (BIG 01-06). European Cancer Congress 2013.

Baselga, J., Verma, S., Ro, J., Huober, J., Guardino, E., Fang, L., Olsen, S., Lewis Phillips, G., de Haas, S., and Pegram, M. (2013b). Relationship between tumor biomarkers (BM) and efficacy in EMILIA, a phase III study of trastuzumab emtansine (T-DM1) in HER2-positive metastatic breast cancer (MBC). Cancer Res. *73* (*Suppl.*), LB-63.

Bean, J., Brennan, C., Shih, J.Y., Riely, G., Viale, A., Wang, L., Chitale, D., Motoi, N., Szoke, J., Broderick, S., et al. (2007). MET amplification occurs with or without T790M mutations in EGFR mutant lung tumors with acquired resistance to gefitinib or erlotinib. Proc. Natl. Acad. Sci. USA *104*, 20932–20937.

Berns, K., Horlings, H.M., Hennessy, B.T., Madiredjo, M., Hijmans, E.M., Beelen, K., Linn, S.C., Gonzalez-Angulo, A.M., Stemke-Hale, K., Hauptmann, M., et al. (2007). A functional genetic approach identifies the PI3K pathway as a major determinant of trastuzumab resistance in breast cancer. Cancer Cell *12*, 395–402.

Bertotti, A., Migliardi, G., Galimi, F., Sassi, F., Torti, D., Isella, C., Corà, D., Di Nicolantonio, F., Buscarino, M., Petti, C., et al. (2011). A molecularly annotated platform of patient-derived xenografts ("xenopatients") identifies HER2 as an effective therapeutic target in cetuximab-resistant colorectal cancer. Cancer Discov. *1*, 508–523.

Blackwell, K.L., Burstein, H.J., Storniolo, A.M., Rugo, H., Sledge, G., Koehler, M., Ellis, C., Casey, M., Vukelja, S., Bischoff, J., et al. (2010). Randomized study of Lapatinib alone or in combination with trastuzumab in women with ErbB2-positive, trastuzumab-refractory metastatic breast cancer. J. Clin. Oncol. *28*, 1124–1130.

Bonner, J.A., Harari, P.M., Giralt, J., Azarnia, N., Shin, D.M., Cohen, R.B., Jones, C.U., Sur, R., Raben, D., Jassem, J., et al. (2006). Radiotherapy plus

cetuximab for squamous-cell carcinoma of the head and neck. N. Engl. J. Med. *354*, 567–578.

Bose, R., Kavuri, S.M., Searleman, A.C., Shen, W., Shen, D., Koboldt, D.C., Monsey, J., Goel, N., Aronson, A.B., Li, S., et al. (2013). Activating HER2 mutations in HER2 gene amplification negative breast cancer. Cancer Discov. *3*, 224–237.

Burstein, H.J., Sun, Y., Dirix, L.Y., Jiang, Z., Paridaens, R., Tan, A.R., Awada, A., Ranade, A., Jiao, S., Schwartz, G., et al. (2010). Neratinib, an irreversible ErbB receptor tyrosine kinase inhibitor, in patients with advanced ErbB2-positive breast cancer. J. Clin. Oncol. *28*, 1301–1307.

Burtness, B., Goldwasser, M.A., Flood, W., Mattar, B., and Forastiere, A.A.; Eastern Cooperative Oncology Group (2005). Phase III randomized trial of cisplatin plus placebo compared with cisplatin plus cetuximab in metastatic/recurrent head and neck cancer: an Eastern Cooperative Oncology Group study. J. Clin. Oncol. *23*, 8646–8654.

Cancer Genome Atlas Network (2012). Comprehensive molecular portraits of human breast tumours. Nature *490*, 61–70.

Cappuzzo, F., Varella-Garcia, M., Shigematsu, H., Domenichini, I., Bartolini, S., Ceresoli, G.L., Rossi, E., Ludovini, V., Gregorc, V., Toschi, L., et al. (2005). Increased HER2 gene copy number is associated with response to gefitinib therapy in epidermal growth factor receptor-positive non-small-cell lung cancer patients. J. Clin. Oncol. *23*, 5007–5018.

Carey, K.D., Garton, A.J., Romero, M.S., Kahler, J., Thomson, S., Ross, S., Park, F., Haley, J.D., Gibson, N., and Sliwkowski, M.X. (2006). Kinetic analysis of epidermal growth factor receptor somatic mutant proteins shows increased sensitivity to the epidermal growth factor receptor tyrosine kinase inhibitor, erlotinib. Cancer Res. *66*, 8163–8171.

Chakrabarty, A., Rexer, B.N., Wang, S.E., Cook, R.S., Engelman, J.A., and Arteaga, C.L. (2010). H1047R phosphatidylinositol 3-kinase mutant enhances HER2-mediated transformation by heregulin production and activation of HER3. Oncogene *29*, 5193–5203.

Chakrabarty, A., Sánchez, V., Kuba, M.G., Rinehart, C., and Arteaga, C.L. (2012). Feedback upregulation of HER3 (ErbB3) expression and activity attenuates antitumor effect of PI3K inhibitors. Proc. Natl. Acad. Sci. USA *109*, 2718–2723.

Chakrabarty, A., Bhola, N.E., Sutton, C., Ghosh, R., Kuba, M.G., Dave, B., Chang, J.C., and Arteaga, C.L. (2013). Trastuzumab-resistant cells rely on a HER2-PI3K-FoxO-survivin axis and are sensitive to PI3K inhibitors. Cancer Res. *73*, 1190–1200.

Chandarlapaty, S., Sawai, A., Scaltriti, M., Rodrik-Outmezguine, V., Grbovic-Huezo, O., Serra, V., Majumder, P.K., Baselga, J., and Rosen, N. (2011). AKT inhibition relieves feedback suppression of receptor tyrosine kinase expression and activity. Cancer Cell *19*, 58–71.

Cho, H.S., Mason, K., Ramyar, K.X., Stanley, A.M., Gabelli, S.B., Denney, D.W., Jr., and Leahy, D.J. (2003). Structure of the extracellular region of HER2 alone and in complex with the Herceptin Fab. Nature *421*, 756–760.

Clynes, R.A., Towers, T.L., Presta, L.G., and Ravetch, J.V. (2000). Inhibitory Fc receptors modulate in vivo cytotoxicity against tumor targets. Nat. Med. *6*, 443–446.

Cook, R.S., Garrett, J.T., Sánchez, V., Stanford, J.C., Young, C., Chakrabarty, A., Rinehart, C., Zhang, Y., Wu, Y., Greenberger, L., et al. (2011). ErbB3 ablation impairs phosphatidylinositol 3-kinase (PI3K)/AKT-dependent mammary tumorigenesis. Cancer Res. *71*, 3941–3951.

Corcoran, R.B., Ebi, H., Turke, A.B., Coffee, E.M., Nishino, M., Cogdill, A.P., Brown, R.D., Della Pelle, P., Dias-Santagata, D., Hung, K.E., et al. (2012). EGFR-mediated re-activation of MAPK signaling contributes to insensitivity of BRAF mutant colorectal cancers to RAF inhibition with vemurafenib. Cancer Discov. *2*, 227–235.

Cortot, A.B., Repellin, C.E., Shimamura, T., Capelletti, M., Zejnullahu, K., Ercan, D., Christensen, J.G., Wong, K.K., Gray, N.S., and Jänne, P.A. (2013). Resistance to irreversible EGF receptor tyrosine kinase inhibitors through a multistep mechanism involving the IGF1R pathway. Cancer Res. *73*, 834–843.

Cunningham, D., Humblet, Y., Siena, S., Khayat, D., Bleiberg, H., Santoro, A., Bets, D., Mueser, M., Harstrick, A., Verslype, C., et al. (2004). Cetuximab monotherapy and cetuximab plus irinotecan in irinotecan-refractory metastatic colorectal cancer. N. Engl. J. Med. *351*, 337–345.

Dave, B., Migliaccio, I., Gutierrez, M.C., Wu, M.F., Chamness, G.C., Wong, H., Narasanna, A., Chakrabarty, A., Hilsenbeck, S.G., Huang, J., et al. (2011). Loss of phosphatase and tensin homolog or phosphoinositol-3 kinase activation and response to trastuzumab or lapatinib in human epidermal growth factor receptor 2-overexpressing locally advanced breast cancers. J. Clin. Oncol. *29*, 166–173.

Diaz, L.A., Jr., Williams, R.T., Wu, J., Kinde, I., Hecht, J.R., Berlin, J., Allen, B., Bozic, I., Reiter, J.G., Nowak, M.A., et al. (2012). The molecular evolution of acquired resistance to targeted EGFR blockade in colorectal cancers. Nature *486*, 537–540.

Ding, L., Getz, G., Wheeler, D.A., Mardis, E.R., McLellan, M.D., Cibulskis, K., Sougnez, C., Greulich, H., Muzny, D.M., Morgan, M.B., et al. (2008). Somatic mutations affect key pathways in lung adenocarcinoma. Nature *455*, 1069–1075.

Douillard, J.Y., Zemelka, T., Fountzilas, G., Barone, C., Schlichting, M., Heighway, J., Eggleton, S.P., and Srimuninnimit, V. (2014). FOLFOX4 With Cetuximab vs. UFOX With Cetuximab as First-Line Therapy in Metastatic Colorectal Cancer: The Randomized Phase II FUTURE Study. Clin. Colorectal Cancer *13*, 14–26.e1.

Downward, J., Yarden, Y., Mayes, E., Scrace, G., Totty, N., Stockwell, P., Ullrich, A., Schlessinger, J., and Waterfield, M.D. (1984). Close similarity of epidermal growth factor receptor and v-erb-B oncogene protein sequences. Nature *307*, 521–527.

Ebi, H., Corcoran, R.B., Singh, A., Chen, Z., Song, Y., Lifshits, E., Ryan, D.P., Meyerhardt, J.A., Benes, C., Settleman, J., et al. (2011). Receptor tyrosine kinases exert dominant control over PI3K signaling in human KRAS mutant colorectal cancers. J. Clin. Invest. *121*, 4311–4321.

Eichhorn, P.J., Gili, M., Scaltriti, M., Serra, V., Guzman, M., Nijkamp, W., Beijersbergen, R.L., Valero, V., Seoane, J., Bernards, R., and Baselga, J. (2008). Phosphatidylinositol 3-kinase hyperactivation results in lapatinib resistance that is reversed by the mTOR/phosphatidylinositol 3-kinase inhibitor NVP-BEZ235. Cancer Res. *68*, 9221–9230.

Engelman, J.A. (2009). Targeting PI3K signalling in cancer: opportunities, challenges and limitations. Nat. Rev. Cancer *9*, 550–562.

Engelman, J.A., Jänne, P.A., Mermel, C., Pearlberg, J., Mukohara, T., Fleet, C., Cichowski, K., Johnson, B.E., and Cantley, L.C. (2005). ErbB-3 mediates phosphoinositide 3-kinase activity in gefitinib-sensitive non-small cell lung cancer cell lines. Proc. Natl. Acad. Sci. USA *102*, 3788–3793.

Engelman, J.A., Mukohara, T., Zejnullahu, K., Lifshits, E., Borrás, A.M., Gale, C.M., Naumov, G.N., Yeap, B.Y., Jarrell, E., Sun, J., et al. (2006). Allelic dilution obscures detection of a biologically significant resistance mutation in EGFR-amplified lung cancer. J. Clin. Invest. *116*, 2695–2706.

Engelman, J.A., Zejnullahu, K., Mitsudomi, T., Song, Y., Hyland, C., Park, J.O., Lindeman, N., Gale, C.M., Zhao, X., Christensen, J., et al. (2007). MET amplification leads to gefitinib resistance in lung cancer by activating ERBB3 signaling. Science *316*, 1039–1043.

Ercan, D., Xu, C., Yanagita, M., Monast, C.S., Pratilas, C.A., Montero, J., Butaney, M., Shimamura, T., Sholl, L., Ivanova, E.V., et al. (2012). Reactivation of ERK signaling causes resistance to EGFR kinase inhibitors. Cancer Discov. *2*, 934–947.

Esteva, F.J., Guo, H., Zhang, S., Santa-Maria, C., Stone, S., Lanchbury, J.S., Sahin, A.A., Hortobagyi, G.N., and Yu, D. (2010). PTEN, PIK3CA, p-AKT, and p-p70S6K status: association with trastuzumab response and survival in patients with HER2-positive metastatic breast cancer. Am. J. Pathol. *177*, 1647–1656.

Faber, A.C., Wong, K.K., and Engelman, J.A. (2010). Differences underlying EGFR and HER2 oncogene addiction. Cell Cycle *9*, 851–852.

Faber, A.C., Corcoran, R.B., Ebi, H., Sequist, L.V., Waltman, B.A., Chung, E., Incio, J., Digumarthy, S.R., Pollack, S.F., Song, Y., et al. (2011). BIM expression in treatment-naive cancers predicts responsiveness to kinase inhibitors. Cancer Discov. *1*, 352–365.

Fan, Z., Lu, Y., Wu, X., and Mendelsohn, J. (1994). Antibody-induced epidermal growth factor receptor dimerization mediates inhibition of autocrine proliferation of A431 squamous carcinoma cells. J. Biol. Chem. *269*, 27595–27602.

Finkle, D., Quan, Z.R., Asghari, V., Kloss, J., Ghaboosi, N., Mai, E., Wong, W.L., Hollingshead, P., Schwall, R., Koeppen, H., and Erickson, S. (2004). HER2-targeted therapy reduces incidence and progression of midlife mammary tumors in female murine mammary tumor virus huHER2-transgenic mice. Clin. Cancer Res. *10*, 2499–2511.

Franklin, M.C., Carey, K.D., Vajdos, F.F., Leahy, D.J., de Vos, A.M., and Sliwkowski, M.X. (2004). Insights into ErbB signaling from the structure of the ErbB2-pertuzumab complex. Cancer Cell *5*, 317–328.

Frederick, L., Wang, X.Y., Eley, G., and James, C.D. (2000). Diversity and frequency of epidermal growth factor receptor mutations in human glioblastomas. Cancer Res. *60*, 1383–1387.

Gandhi, L., Bahleda, R., Tolaney, S.M., Kwak, E.L., Cleary, J.M., Pandya, S.S., Hollebecque, A., Abbas, R., Ananthakrishnan, R., Berkenblit, A., et al. (2014). Phase I study of neratinib in combination with temsirolimus in patients with human epidermal growth factor receptor 2-dependent and other solid tumors. J. Clin. Oncol. *32*, 68–75.

Garner, A.P., Bialucha, C.U., Sprague, E.R., Garrett, J.T., Sheng, Q., Li, S., Sineshchekova, O., Saxena, P., Sutton, C.R., Chen, D., et al. (2013). An antibody that locks HER3 in the inactive conformation inhibits tumor growth driven by HER2 or neuregulin. Cancer Res. *73*, 6024–6035.

Garrett, T.P., McKern, N.M., Lou, M., Elleman, T.C., Adams, T.E., Lovrecz, G.O., Kofler, M., Jorissen, R.N., Nice, E.C., Burgess, A.W., and Ward, C.W. (2003). The crystal structure of a truncated ErbB2 ectodomain reveals an active conformation, poised to interact with other ErbB receptors. Mol. Cell *11*, 495–505.

Garrett, J.T., Olivares, M.G., Rinehart, C., Granja-Ingram, N.D., Sánchez, V., Chakrabarty, A., Dave, B., Cook, R.S., Pao, W., McKinely, E., et al. (2011). Transcriptional and posttranslational up-regulation of HER3 (ErbB3) compensates for inhibition of the HER2 tyrosine kinase. Proc. Natl. Acad. Sci. USA *108*, 5021–5026.

Garrett, J.T., Sutton, C.R., Kuba, M.G., Cook, R.S., and Arteaga, C.L. (2013a). Dual blockade of HER2 in HER2-overexpressing tumor cells does not completely eliminate HER3 function. Clin. Cancer Res. *19*, 610–619.

Garrett, J.T., Sutton, C.R., Kurupi, R., Bialucha, C.U., Ettenberg, S.A., Collins, S.D., Sheng, Q., Wallweber, J., Defazio-Eli, L., and Arteaga, C.L. (2013b). Combination of antibody that inhibits ligand-independent HER3 dimerization and a p110α inhibitor potently blocks PI3K signaling and growth of HER2+ breast cancers. Cancer Res. *73*, 6013–6023.

Gennari, R., Menard, S., Fagnoni, F., Ponchio, L., Scelsi, M., Tagliabue, E., Castiglioni, F., Villani, L., Magalotti, C., Gibelli, N., et al. (2004). Pilot study of the mechanism of action of preoperative trastuzumab in patients with primary operable breast tumors overexpressing HER2. Clin. Cancer Res. *10*, 5650–5655.

Geyer, C.E., Forster, J., Lindquist, D., Chan, S., Romieu, C.G., Pienkowski, T., Jagiello-Gruszfeld, A., Crown, J., Chan, A., Kaufman, B., et al. (2006). Lapatinib plus capecitabine for HER2-positive advanced breast cancer. N. Engl. J. Med. *355*, 2733–2743.

Ghosh, R., Narasanna, A., Wang, S.E., Liu, S., Chakrabarty, A., Balko, J.M., González-Angulo, A.M., Mills, G.B., Penuel, E., Winslow, J., et al. (2011). Trastuzumab has preferential activity against breast cancers driven by HER2 homodimers. Cancer Res. *71*, 1871–1882.

Gianni, L., Eiermann, W., Semiglazov, V., Manikhas, A., Lluch, A., Tjulandin, S., Zambetti, M., Vazquez, F., Byakhow, M., Lichinitser, M., et al. (2010). Neoadjuvant chemotherapy with trastuzumab followed by adjuvant trastuzumab versus neoadjuvant chemotherapy alone, in patients with HER2-positive locally advanced breast cancer (the NOAH trial): a randomised controlled superiority trial with a parallel HER2-negative cohort. Lancet *375*, 377–384.

Gianni, L., Pienkowski, T., Im, Y.H., Roman, L., Tseng, L.M., Liu, M.C., Lluch, A., Staroslawska, E., de la Haba-Rodriguez, J., Im, S.A., et al. (2012). Efficacy and safety of neoadjuvant pertuzumab and trastuzumab in women with locally advanced, inflammatory, or early HER2-positive breast cancer (NeoSphere): a randomised multicentre, open-label, phase 2 trial. Lancet Oncol. *13*, 25–32.

Gilbertson, R., Hernan, R., Pietsch, T., Pinto, L., Scotting, P., Allibone, R., Ellison, D., Perry, R., Pearson, A., and Lunec, J. (2001). Novel ERBB4 juxtamembrane splice variants are frequently expressed in childhood medulloblastoma. Genes Chromosomes Cancer *31*, 288–294.

Goldberg, S.B., Supko, J.G., Neal, J.W., Muzikansky, A., Digumarthy, S., Fidias, P., Temel, J.S., Heist, R.S., Shaw, A.T., McCarthy, P.O., et al. (2012). A phase I study of erlotinib and hydroxychloroquine in advanced non-small-cell lung cancer. J. Thorac. Oncol. *7*, 1602–1608.

Greulich, H., Chen, T.H., Feng, W., Jänne, P.A., Alvarez, J.V., Zappaterra, M., Bulmer, S.E., Frank, D.A., Hahn, W.C., Sellers, W.R., and Meyerson, M. (2005). Oncogenic transformation by inhibitor-sensitive and -resistant EGFR mutants. PLoS Med. *2*, e313.

Guix, M., Faber, A.C., Wang, S.E., Olivares, M.G., Song, Y., Qu, S., Rinehart, C., Seidel, B., Yee, D., Arteaga, C.L., and Engelman, J.A. (2008). Acquired resistance to EGFR tyrosine kinase inhibitors in cancer cells is mediated by loss of IGF-binding proteins. J. Clin. Invest. *118*, 2609–2619.

Haas-Kogan, D.A., Prados, M.D., Tihan, T., Eberhard, D.A., Jelluma, N., Arvold, N.D., Baumber, R., Lamborn, K.R., Kapadia, A., Malec, M., et al. (2005). Epidermal growth factor receptor, protein kinase B/Akt, and glioma response to erlotinib. J. Natl. Cancer Inst. *97*, 880–887.

Hanker, A.B., Pfefferle, A.D., Balko, J.M., Kuba, M.G., Young, C.D., Sánchez, V., Sutton, C.R., Cheng, H., Perou, C.M., Zhao, J.J., et al. (2013). Mutant PIK3CA accelerates HER2-driven transgenic mammary tumors and induces resistance to combinations of anti-HER2 therapies. Proc. Natl. Acad. Sci. USA *110*, 14372–14377.

Harris, L.N., You, F., Schnitt, S.J., Witkiewicz, A., Lu, X., Sgroi, D., Ryan, P.D., Come, S.E., Burstein, H.J., Lesnikoski, B.A., et al. (2007). Predictors of resistance to preoperative trastuzumab and vinorelbine for HER2-positive early breast cancer. Clin. Cancer Res. *13*, 1198–1207.

Hegde, G.V., de la Cruz, C.C., Chiu, C., Alag, N., Schaefer, G., Crocker, L., Ross, S., Goldenberg, D., Merchant, M., Tien, J., et al. (2013). Blocking NRG1 and other ligand-mediated Her4 signaling enhances the magnitude and duration of the chemotherapeutic response of non-small cell lung cancer. Sci. Transl. Med. *5*, 71ra18.

Heiser, L.M., Sadanandam, A., Kuo, W.L., Benz, S.C., Goldstein, T.C., Ng, S., Gibb, W.J., Wang, N.J., Ziyad, S., Tong, F., et al. (2012). Subtype and pathway specific responses to anticancer compounds in breast cancer. Proc. Natl. Acad. Sci. USA *109*, 2724–2729.

Higginbotham, J.N., Demory Beckler, M., Gephart, J.D., Franklin, J.L., Bogatcheva, G., Kremers, G.J., Piston, D.W., Ayers, G.D., McConnell, R.E., Tyska, M.J., and Coffey, R.J. (2011). Amphiregulin exosomes increase cancer cell invasion. Curr. Biol. *21*, 779–786.

Huang, X., Gao, L., Wang, S., McManaman, J.L., Thor, A.D., Yang, X., Esteva, F.J., and Liu, B. (2010). Heterotrimerization of the growth factor receptors erbB2, erbB3, and insulin-like growth factor-i receptor in breast cancer cells resistant to herceptin. Cancer Res. *70*, 1204–1214.

Hurley, J., Doliny, P., Reis, I., Silva, O., Gomez-Fernandez, C., Velez, P., Pauletti, G., Powell, J.E., Pegram, M.D., and Slamon, D.J. (2006). Docetaxel, cisplatin, and trastuzumab as primary systemic therapy for human epidermal growth factor receptor 2-positive locally advanced breast cancer. J. Clin. Oncol. *24*, 1831–1838.

Hurvitz, S.A., Betting, D.J., Stern, H.M., Quinaux, E., Stinson, J., Seshagiri, S., Zhao, Y., Buyse, M., Mackey, J., Driga, A., et al. (2012). Analysis of Fcγ receptor IIIa and IIa polymorphisms: lack of correlation with outcome in trastuzumab-treated breast cancer patients. Clin. Cancer Res. *18*, 3478–3486.

Hurvitz, S.A., Dalenc, F., Campone, M., O'Regan, R.M., Tjan-Heijnen, V.C., Gligorov, J., Llombart, A., Jhangiani, H., Mirshahidi, H.R., Tan-Chiu, E., et al. (2013). A phase 2 study of everolimus combined with trastuzumab and paclitaxel in patients with HER2-overexpressing advanced breast cancer that progressed during prior trastuzumab and taxane therapy. Breast Cancer Res. Treat. *141*, 437–446.

Hynes, N.E., and MacDonald, G. (2009). ErbB receptors and signaling pathways in cancer. Curr. Opin. Cell Biol. *21*, 177–184.

Jaiswal, B.S., Kljavin, N.M., Stawiski, E.W., Chan, E., Parikh, C., Durinck, S., Chaudhuri, S., Pujara, K., Guillory, J., Edgar, K.A., et al. (2013). Oncogenic ERBB3 mutations in human cancers. Cancer Cell *23*, 603–617.

Janjigian, Y.Y., Groen, H.J., Horn, L., Smit, E.F., Fu, Y., Wang, F., Shahidi, M., Denis, L.J., Pao, W., and Miller, V.A. (2011). Activity and tolerability of afatinib (BIBW 2992) and cetuximab in NSCLC patients with acquired resistance to erlotinib or gefitinib. J. Clin. Oncol. *29* (*Suppl.*), abstr. 7525.

Ji, H., Li, D., Chen, L., Shimamura, T., Kobayashi, S., McNamara, K., Mahmood, U., Mitchell, A., Sun, Y., Al-Hashem, R., et al. (2006). The impact of human EGFR kinase domain mutations on lung tumorigenesis and in vivo sensitivity to EGFR-targeted therapies. Cancer Cell *9*, 485–495.

Jonker, D.J., O'Callaghan, C.J., Karapetis, C.S., Zalcberg, J.R., Tu, D., Au, H.J., Berry, S.R., Krahn, M., Price, T., Simes, R.J., et al. (2007). Cetuximab for the treatment of colorectal cancer. N. Engl. J. Med. *357*, 2040–2048.

Junttila, T.T., Akita, R.W., Parsons, K., Fields, C., Lewis Phillips, G.D., Friedman, L.S., Sampath, D., and Sliwkowski, M.X. (2009). Ligand-independent HER2/HER3/PI3K complex is disrupted by trastuzumab and is effectively inhibited by the PI3K inhibitor GDC-0941. Cancer Cell *15*, 429–440.

Junttila, T.T., Li, G., Parsons, K., Phillips, G.L., and Sliwkowski, M.X. (2011). Trastuzumab-DM1 (T-DM1) retains all the mechanisms of action of trastuzumab and efficiently inhibits growth of lapatinib insensitive breast cancer. Breast Cancer Res. Treat. *128*, 347–356.

Katayama, R., Shaw, A.T., Khan, T.M., Mino-Kenudson, M., Solomon, B.J., Halmos, B., Jessop, N.A., Wain, J.C., Yeo, A.T., Benes, C., et al. (2012). Mechanisms of acquired crizotinib resistance in ALK-rearranged lung Cancers. Sci. Transl. Med. *4*, 20ra17.

Kawamoto, T., Sato, J.D., Le, A., Polikoff, J., Sato, G.H., and Mendelsohn, J. (1983). Growth stimulation of A431 cells by epidermal growth factor: identification of high-affinity receptors for epidermal growth factor by an anti-receptor monoclonal antibody. Proc. Natl. Acad. Sci. USA *80*, 1337–1341.

Khambata-Ford, S., Garrett, C.R., Meropol, N.J., Basik, M., Harbison, C.T., Wu, S., Wong, T.W., Huang, X., Takimoto, C.H., Godwin, A.K., et al. (2007). Expression of epiregulin and amphiregulin and K-ras mutation status predict disease control in metastatic colorectal cancer patients treated with cetuximab. J. Clin. Oncol. *25*, 3230–3237.

Kobayashi, S., Boggon, T.J., Dayaram, T., Jänne, P.A., Kocher, O., Meyerson, M., Johnson, B.E., Eck, M.J., Tenen, D.G., and Halmos, B. (2005). EGFR mutation and resistance of non-small-cell lung cancer to gefitinib. N. Engl. J. Med. *352*, 786–792.

Konecny, G.E., Pegram, M.D., Venkatesan, N., Finn, R., Yang, G., Rahmeh, M., Untch, M., Rusnak, D.W., Spehar, G., Mullin, R.J., et al. (2006). Activity of the dual kinase inhibitor lapatinib (GW572016) against HER-2-overexpressing and trastuzumab-treated breast cancer cells. Cancer Res. *66*, 1630–1639.

Kwong, K.Y., and Hung, M.C. (1998). A novel splice variant of HER2 with increased transformation activity. Mol. Carcinog. *23*, 62–68.

Lee, J.W., Soung, Y.H., Seo, S.H., Kim, S.Y., Park, C.H., Wang, Y.P., Park, K., Nam, S.W., Park, W.S., Kim, S.H., et al. (2006). Somatic mutations of ERBB2 kinase domain in gastric, colorectal, and breast carcinomas. Clin. Cancer Res. *12*, 57–61.

Lee-Hoeflich, S.T., Crocker, L., Yao, E., Pham, T., Munroe, X., Hoeflich, K.P., Sliwkowski, M.X., and Stern, H.M. (2008). A central role for HER3 in HER2-amplified breast cancer: implications for targeted therapy. Cancer Res. *68*, 5878–5887.

Lewis Phillips, G.D., Li, G., Dugger, D.L., Crocker, L.M., Parsons, K.L., Mai, E., Blättler, W.A., Lambert, J.M., Chari, R.V., Lutz, R.J., et al. (2008). Targeting HER2-positive breast cancer with trastuzumab-DM1, an antibody-cytotoxic drug conjugate. Cancer Res. *68*, 9280–9290.

Liang, K., Esteva, F.J., Albarracin, C., Stemke-Hale, K., Lu, Y., Bianchini, G., Yang, C.Y., Li, Y., Li, X., Chen, C.T., et al. (2010). Recombinant human erythropoietin antagonizes trastuzumab treatment of breast cancer cells via Jak2-mediated Src activation and PTEN inactivation. Cancer Cell *18*, 423–435.

Licitra, L., Mesia, R., Rivera, F., Remenár, E., Hitt, R., Erfán, J., Rottey, S., Kawecki, A., Zabolotnyy, D., Benasso, M., et al. (2011). Evaluation of EGFR gene copy number as a predictive biomarker for the efficacy of cetuximab in combination with chemotherapy in the first-line treatment of recurrent and/or metastatic squamous cell carcinoma of the head and neck: EXTREME study. Ann. Oncol. *22*, 1078–1087.

Licitra, L., Störkel, S., Kerr, K.M., Van Cutsem, E., Pirker, R., Hirsch, F.R., Vermorken, J.B., von Heydebreck, A., Esser, R., Celik, I., and Ciardiello, F. (2013). Predictive value of epidermal growth factor receptor expression for first-line chemotherapy plus cetuximab in patients with head and neck and colorectal cancer: analysis of data from the EXTREME and CRYSTAL studies. Eur. J. Cancer *49*, 1161–1168.

Liedtke, C., Mazouni, C., Hess, K.R., André, F., Tordai, A., Mejia, J.A., Symmans, W.F., Gonzalez-Angulo, A.M., Hennessy, B., Green, M., et al. (2008). Response to neoadjuvant therapy and long-term survival in patients with triple-negative breast cancer. J. Clin. Oncol. *26*, 1275–1281.

Liu, L., Greger, J., Shi, H., Liu, Y., Greshock, J., Annan, R., Halsey, W., Sathe, G.M., Martin, A.M., and Gilmer, T.M. (2009). Novel mechanism of lapatinib resistance in HER2-positive breast tumor cells: activation of AXL. Cancer Res. *69*, 6871–6878.

Liu, X., Ory, V., Chapman, S., Yuan, H., Albanese, C., Kallakury, B., Timofeeva, O.A., Nealon, C., Dakic, A., Simic, V., et al. (2012). ROCK inhibitor and feeder cells induce the conditional reprogramming of epithelial cells. Am. J. Pathol. *180*, 599–607.

Lynch, T.J., Bell, D.W., Sordella, R., Gurubhagavatula, S., Okimoto, R.A., Brannigan, B.W., Harris, P.L., Haserlat, S.M., Supko, J.G., Haluska, F.G., et al. (2004). Activating mutations in the epidermal growth factor receptor underlying responsiveness of non-small-cell lung cancer to gefitinib. N. Engl. J. Med. *350*, 2129–2139.

Maheswaran, S., Sequist, L.V., Nagrath, S., Ulkus, L., Brannigan, B., Collura, C.V., Inserra, E., Diederichs, S., Iafrate, A.J., Bell, D.W., et al. (2008). Detection of mutations in EGFR in circulating lung-cancer cells. N. Engl. J. Med. *359*, 366–377.

Mattoon, D.R., Lamothe, B., Lax, I., and Schlessinger, J. (2004). The docking protein Gab1 is the primary mediator of EGF-stimulated activation of the PI-3K/Akt cell survival pathway. BMC Biol. *2*, 24.

McDermott, U., Pusapati, R.V., Christensen, J.G., Gray, N.S., and Settleman, J. (2010). Acquired resistance of non-small cell lung cancer cells to MET kinase inhibition is mediated by a switch to epidermal growth factor receptor dependency. Cancer Res. *70*, 1625–1634.

McDonagh, C.F., Huhalov, A., Harms, B.D., Adams, S., Paragas, V., Oyama, S., Zhang, B., Luus, L., Overland, R., Nguyen, S., et al. (2012). Antitumor activity of a novel bispecific antibody that targets the ErbB2/ErbB3 oncogenic unit and inhibits heregulin-induced activation of ErbB3. Mol. Cancer Ther. *11*, 582–593.

Mellinghoff, I.K., Wang, M.Y., Vivanco, I., Haas-Kogan, D.A., Zhu, S., Dia, E.Q., Lu, K.V., Yoshimoto, K., Huang, J.H., Chute, D.J., et al. (2005). Molecular determinants of the response of glioblastomas to EGFR kinase inhibitors. N. Engl. J. Med. *353*, 2012–2024.

Minkovsky, N., and Berezov, A. (2008). BIBW-2992, a dual receptor tyrosine kinase inhibitor for the treatment of solid tumors. Curr. Opin. Investig. Drugs *9*, 1336–1346.

Minuti, G., Cappuzzo, F., Duchnowska, R., Jassem, J., Fabi, A., O'Brien, T., Mendoza, A.D., Landi, L., Biernat, W., Czartoryska-Arłukowicz, B., et al. (2012). Increased MET and HGF gene copy numbers are associated with trastuzumab failure in HER2-positive metastatic breast cancer. Br. J. Cancer *107*, 793–799.

Mirschberger, C., Schiller, C.B., Schräml, M., Dimoudis, N., Friess, T., Gerdes, C.A., Reiff, U., Lifke, V., Hoelzlwimmer, G., Kolm, I., et al. (2013). RG7116, a therapeutic antibody that binds the inactive HER3 receptor and is optimized for immune effector activation. Cancer Res. *73*, 5183–5194.

Misale, S., Yaeger, R., Hobor, S., Scala, E., Janakiraman, M., Liska, D., Valtorta, E., Schiavo, R., Buscarino, M., Siravegna, G., et al. (2012). Emergence of KRAS mutations and acquired resistance to anti-EGFR therapy in colorectal cancer. Nature *486*, 532–536.

Misale, S., Arena, S., Lamba, S., Siravegna, G., Lallo, A., Hobor, S., Russo, M., Buscarino, M., Lazzari, L., Sartore-Bianchi, A., et al. (2014). Blockade of EGFR and MEK Intercepts Heterogeneous Mechanisms of Acquired Resistance to Anti-EGFR Therapies in Colorectal Cancer. Sci. Transl. Med. *6*, 24ra26.

Mitra, D., Brumlik, M.J., Okamgba, S.U., Zhu, Y., Duplessis, T.T., Parvani, J.G., Lesko, S.M., Brogi, E., and Jones, F.E. (2009). An oncogenic isoform of HER2 associated with locally disseminated breast cancer and trastuzumab resistance. Mol. Cancer Ther. *8*, 2152–2162.

Mittendorf, E.A., Wu, Y., Scaltriti, M., Meric-Bernstam, F., Hunt, K.K., Dawood, S., Esteva, F.J., Buzdar, A.U., Chen, H., Eksambi, S., et al. (2009). Loss of HER2 amplification following trastuzumab-based neoadjuvant systemic therapy and survival outcomes. Clin. Cancer Res. *15*, 7381–7388.

Mok, T.S., Wu, Y.L., Thongprasert, S., Yang, C.H., Chu, D.T., Saijo, N., Sunpaweravong, P., Han, B., Margono, B., Ichinose, Y., et al. (2009). Gefitinib or carboplatin-paclitaxel in pulmonary adenocarcinoma. N. Engl. J. Med. *361*, 947–957.

Molina, M.A., Codony-Servat, J., Albanell, J., Rojo, F., Arribas, J., and Baselga, J. (2001). Trastuzumab (herceptin), a humanized anti-Her2 receptor monoclonal antibody, inhibits basal and activated Her2 ectodomain cleavage in breast cancer cells. Cancer Res. *61*, 4744–4749.

Montagut, C., Dalmases, A., Bellosillo, B., Crespo, M., Pairet, S., Iglesias, M., Salido, M., Gallen, M., Marsters, S., Tsai, S.P., et al. (2012). Identification of a mutation in the extracellular domain of the Epidermal Growth Factor Receptor conferring cetuximab resistance in colorectal cancer. Nat. Med. *18*, 221–223.

Moore, M.J., Goldstein, D., Hamm, J., Figer, A., Hecht, J.R., Gallinger, S., Au, H.J., Murawa, P., Walde, D., Wolff, R.A., et al.; National Cancer Institute of Canada Clinical Trials Group (2007). Erlotinib plus gemcitabine compared with gemcitabine alone in patients with advanced pancreatic cancer: a phase III trial of the National Cancer Institute of Canada Clinical Trials Group. J. Clin. Oncol. *25*, 1960–1966.

Moroni, M., Veronese, S., Benvenuti, S., Marrapese, G., Sartore-Bianchi, A., Di Nicolantonio, F., Gambacorta, M., Siena, S., and Bardelli, A. (2005). Gene copy number for epidermal growth factor receptor (EGFR) and clinical response to antiEGFR treatment in colorectal cancer: a cohort study. Lancet Oncol. *6*, 279–286.

Morrow, P.K., Wulf, G.M., Ensor, J., Booser, D.J., Moore, J.A., Flores, P.R., Xiong, Y., Zhang, S., Krop, I.E., Winer, E.P., et al. (2011). Phase I/II study of trastuzumab in combination with everolimus (RAD001) in patients with HER2-overexpressing metastatic breast cancer who progressed on trastuzumab-based therapy. J. Clin. Oncol. *29*, 3126–3132.

Moscatello, D.K., Holgado-Madruga, M., Godwin, A.K., Ramirez, G., Gunn, G., Zoltick, P.W., Biegel, J.A., Hayes, R.L., and Wong, A.J. (1995). Frequent expression of a mutant epidermal growth factor receptor in multiple human tumors. Cancer Res. *55*, 5536–5539.

Muller, W.J., Arteaga, C.L., Muthuswamy, S.K., Siegel, P.M., Webster, M.A., Cardiff, R.D., Meise, K.S., Li, F., Halter, S.A., and Coffey, R.J. (1996). Synergistic interaction of the Neu proto-oncogene product and transforming growth factor alpha in the mammary epithelium of transgenic mice. Mol. Cell. Biol. *16*, 5726–5736.

Muranen, T., Selfors, L.M., Worster, D.T., Iwanicki, M.P., Song, L., Morales, F.C., Gao, S., Mills, G.B., and Brugge, J.S. (2012). Inhibition of PI3K/mTOR leads to adaptive resistance in matrix-attached cancer cells. Cancer Cell *21*, 227–239.

Musolino, A., Naldi, N., Bortesi, B., Pezzuolo, D., Capelletti, M., Missale, G., Laccabue, D., Zerbini, A., Camisa, R., Bisagni, G., et al. (2008). Immunoglobulin G fragment C receptor polymorphisms and clinical efficacy of trastuzumab-based therapy in patients with HER-2/neu-positive metastatic breast cancer. J. Clin. Oncol. *26*, 1789–1796.

Nagata, Y., Lan, K.H., Zhou, X., Tan, M., Esteva, F.J., Sahin, A.A., Klos, K.S., Li, P., Monia, B.P., Nguyen, N.T., et al. (2004). PTEN activation contributes to tumor inhibition by trastuzumab, and loss of PTEN predicts trastuzumab resistance in patients. Cancer Cell *6*, 117–127.

Nahta, R., Takahashi, T., Ueno, N.T., Hung, M.C., and Esteva, F.J. (2004). P27(kip1) down-regulation is associated with trastuzumab resistance in breast cancer cells. Cancer Res. *64*, 3981–3986.

Nahta, R., Yuan, L.X., Zhang, B., Kobayashi, R., and Esteva, F.J. (2005). Insulin-like growth factor-I receptor/human epidermal growth factor receptor 2 heterodimerization contributes to trastuzumab resistance of breast cancer cells. Cancer Res. *65*, 11118–11128.

Nahta, R., Yuan, L.X., Du, Y., and Esteva, F.J. (2007). Lapatinib induces apoptosis in trastuzumab-resistant breast cancer cells: effects on insulin-like growth factor I signaling. Mol. Cancer Ther. *6*, 667–674.

Ng, K.P., Hillmer, A.M., Chuah, C.T., Juan, W.C., Ko, T.K., Teo, A.S., Ariyaratne, P.N., Takahashi, N., Sawada, K., Fei, Y., et al. (2012). A common BIM deletion polymorphism mediates intrinsic resistance and inferior responses to tyrosine kinase inhibitors in cancer. Nat. Med. *18*, 521–528.

Niederst, M.J., and Engelman, J.A. (2013). Bypass mechanisms of resistance to receptor tyrosine kinase inhibition in lung cancer. Sci. Signal. *6*, re6.

Nishikawa, R., Ji, X.D., Harmon, R.C., Lazar, C.S., Gill, G.N., Cavenee, W.K., and Huang, H.J. (1994). A mutant epidermal growth factor receptor common in human glioma confers enhanced tumorigenicity. Proc. Natl. Acad. Sci. USA *91*, 7727–7731.

O'Brien, C., Wallin, J.J., Sampath, D., GuhaThakurta, D., Savage, H., Punnoose, E.A., Guan, J., Berry, L., Prior, W.W., Amler, L.C., et al. (2010). Predictive biomarkers of sensitivity to the phosphatidylinositol 3′ kinase inhibitor GDC-0941 in breast cancer preclinical models. Clin. Cancer Res. *16*, 3670–3683.

O'Regan, R., Ozguroglu, M., Andre, F., Toi, M., Jerusalem, G., Wilks, S., Isaacs, C., Xu, B., Masuda, N., Arena, F.P., Yardley, D.A., Yap, Y.S., Mukhopadhyay, P., Douma, S., El-Hashimy, M., Taran, T., Sahmoud, T., Lebwohl, D.E., and Gianni, L. (2013). Phase III randomized, double-blind, placebo-controlled, multicenter trial of daily everolimus plus weekly trastuzumab and vinorelbine in trastuzumab-resistant, advanced breast cancer (BOLERO-3). J. Clin. Oncol. *31* (*Suppl.*), abstr. 505.

Ohashi, K., Sequist, L.V., Arcila, M.E., Moran, T., Chmielecki, J., Lin, Y.L., Pan, Y., Wang, L., de Stanchina, E., Shien, K., et al. (2012). Lung cancers with acquired resistance to EGFR inhibitors occasionally harbor BRAF gene mutations but lack mutations in KRAS, NRAS, or MEK1. Proc. Natl. Acad. Sci. USA *109*, E2127–E2133.

Paez, J.G., Jänne, P.A., Lee, J.C., Tracy, S., Greulich, H., Gabriel, S., Herman, P., Kaye, F.J., Lindeman, N., Boggon, T.J., et al. (2004). EGFR mutations in lung cancer: correlation with clinical response to gefitinib therapy. Science *304*, 1497–1500.

Paik, S., Kim, C., and Wolmark, N. (2008). HER2 status and benefit from adjuvant trastuzumab in breast cancer. N. Engl. J. Med. *358*, 1409–1411.

Pao, W., and Chmielecki, J. (2010). Rational, biologically based treatment of EGFR-mutant non-small-cell lung cancer. Nat. Rev. Cancer *10*, 760–774.

Pao, W., Miller, V., Zakowski, M., Doherty, J., Politi, K., Sarkaria, I., Singh, B., Heelan, R., Rusch, V., Fulton, L., et al. (2004). EGF receptor gene mutations are common in lung cancers from "never smokers" and are associated with sensitivity of tumors to gefitinib and erlotinib. Proc. Natl. Acad. Sci. USA *101*, 13306–13311.

Pao, W., Miller, V.A., Politi, K.A., Riely, G.J., Somwar, R., Zakowski, M.F., Kris, M.G., and Varmus, H. (2005). Acquired resistance of lung adenocarcinomas to gefitinib or erlotinib is associated with a second mutation in the EGFR kinase domain. PLoS Med. *2*, e73.

Park, S., Jiang, Z., Mortenson, E.D., Deng, L., Radkevich-Brown, O., Yang, X., Sattar, H., Wang, Y., Brown, N.K., Greene, M., et al. (2010). The therapeutic effect of anti-HER2/neu antibody depends on both innate and adaptive immunity. Cancer Cell *18*, 160–170.

Perez, E.A., Dueck, A.C., McCullough, A.E., Chen, B., Geiger, X.J., Jenkins, R.B., Lingle, W.L., Davidson, N.E., Martino, S., Kaufman, P.A., et al. (2013). Impact of PTEN protein expression on benefit from adjuvant trastuzumab in early-stage human epidermal growth factor receptor 2-positive breast cancer in the North Central Cancer Treatment Group N9831 trial. J. Clin. Oncol. *31*, 2115–2122.

Phillips, G.D., Fields, C.T., Li, G., Dowbenko, D., Schaefer, G., Miller, K., Andre, F., Burris, H.A., 3rd, Albain, K.S., Harbeck, N., et al. (2014). Dual Targeting of HER2-Positive Cancer with Trastuzumab Emtansine and Pertuzumab: Critical Role for Neuregulin Blockade in Antitumor Response to Combination Therapy. Clin. Cancer Res. *20*, 456–468.

Piccart-Gebhart, M.J., Procter, M., Leyland-Jones, B., Goldhirsch, A., Untch, M., Smith, I., Gianni, L., Baselga, J., Bell, R., Jackisch, C., et al.; Herceptin Adjuvant (HERA) Trial Study Team (2005). Trastuzumab after adjuvant chemotherapy in HER2-positive breast cancer. N. Engl. J. Med. *353*, 1659–1672.

Politi, K., Zakowski, M.F., Fan, P.D., Schonfeld, E.A., Pao, W., and Varmus, H.E. (2006). Lung adenocarcinomas induced in mice by mutant EGF receptors found in human lung cancers respond to a tyrosine kinase inhibitor or to down-regulation of the receptors. Genes Dev. *20*, 1496–1510.

Prahallad, A., Sun, C., Huang, S., Di Nicolantonio, F., Salazar, R., Zecchin, D., Beijersbergen, R.L., Bardelli, A., and Bernards, R. (2012). Unresponsiveness of colon cancer to BRAF(V600E) inhibition through feedback activation of EGFR. Nature *483*, 100–103.

Price-Schiavi, S.A., Jepson, S., Li, P., Arango, M., Rudland, P.S., Yee, L., and Carraway, K.L. (2002). Rat Muc4 (sialomucin complex) reduces binding of

anti-ErbB2 antibodies to tumor cell surfaces, a potential mechanism for herceptin resistance. Int. J. Cancer *99*, 783–791.

Prickett, T.D., Agrawal, N.S., Wei, X., Yates, K.E., Lin, J.C., Wunderlich, J.R., Cronin, J.C., Cruz, P., Rosenberg, S.A., and Samuels, Y. (2009). Analysis of the tyrosine kinome in melanoma reveals recurrent mutations in ERBB4. Nat. Genet. *41*, 1127–1132.

Prowell, T.M., and Pazdur, R. (2012). Pathological complete response and accelerated drug approval in early breast cancer. N. Engl. J. Med. *366*, 2438–2441.

Qi, J., McTigue, M.A., Rogers, A., Lifshits, E., Christensen, J.G., Jänne, P.A., and Engelman, J.A. (2011). Multiple mutations and bypass mechanisms can contribute to development of acquired resistance to MET inhibitors. Cancer Res. *71*, 1081–1091.

Ranson, M., Pao, W., Kim, D.-W., Kim, S.-W., Ohe, Y., Felip, E., Planchard, D., Ghiorghiu, S., Cantarini, M., Cross, D., et al. (2013). AZD9291: an irreversible, potent and selective tyrosine kinase inhibitor (TKI) of activating (EGFRm+) and resistance (T790M) mutations in advanced NSCLC. J. Thorac. Oncol. *8*, s389.

Regales, L., Gong, Y., Shen, R., de Stanchina, E., Vivanco, I., Goel, A., Koutcher, J.A., Spassova, M., Ouerfelli, O., Mellinghoff, I.K., et al. (2009). Dual targeting of EGFR can overcome a major drug resistance mutation in mouse models of EGFR mutant lung cancer. J. Clin. Invest. *119*, 3000–3010.

Rexer, B.N., and Arteaga, C.L. (2013). Optimal targeting of HER2-PI3K signaling in breast cancer: mechanistic insights and clinical implications. Cancer Res. *73*, 3817–3820.

Rexer, B.N., Ham, A.J., Rinehart, C., Hill, S., Granja-Ingram, Nde.M., González-Angulo, A.M., Mills, G.B., Dave, B., Chang, J.C., Liebler, D.C., and Arteaga, C.L. (2011). Phosphoproteomic mass spectrometry profiling links Src family kinases to escape from HER2 tyrosine kinase inhibition. Oncogene *30*, 4163–4174.

Rexer, B.N., Shyr, Y., and Arteaga, C.L. (2013). Phosphatase and tensin homolog deficiency and resistance to trastuzumab and chemotherapy. J. Clin. Oncol. *31*, 2073–2075.

Ritter, C.A., Perez-Torres, M., Rinehart, C., Guix, M., Dugger, T., Engelman, J.A., and Arteaga, C.L. (2007). Human breast cancer cells selected for resistance to trastuzumab in vivo overexpress epidermal growth factor receptor and ErbB ligands and remain dependent on the ErbB receptor network. Clin. Cancer Res. *13*, 4909–4919.

Robert, N., Leyland-Jones, B., Asmar, L., Belt, R., Ilegbodu, D., Loesch, D., Raju, R., Valentine, E., Sayre, R., Cobleigh, M., et al. (2006). Randomized phase III study of trastuzumab, paclitaxel, and carboplatin compared with trastuzumab and paclitaxel in women with HER-2-overexpressing metastatic breast cancer. J. Clin. Oncol. *24*, 2786–2792.

Romond, E.H., Perez, E.A., Bryant, J., Suman, V.J., Geyer, C.E., Jr., Davidson, N.E., Tan-Chiu, E., Martino, S., Paik, S., Kaufman, P.A., et al. (2005). Trastuzumab plus adjuvant chemotherapy for operable HER2-positive breast cancer. N. Engl. J. Med. *353*, 1673–1684.

Rosell, R., Molina, M.A., Costa, C., Simonetti, S., Gimenez-Capitan, A., Bertran-Alamillo, J., Mayo, C., Moran, T., Mendez, P., Cardenal, F., et al. (2011). Pretreatment EGFR T790M mutation and BRCA1 mRNA expression in erlotinib-treated advanced non-small-cell lung cancer patients with EGFR mutations. Clin. Cancer Res. *17*, 1160–1168.

Rosell, R., Carcereny, E., Gervais, R., Vergnenegre, A., Massuti, B., Felip, E., Palmero, R., Garcia-Gomez, R., Pallares, C., Sanchez, J.M., et al.; Spanish Lung Cancer Group in collaboration with Groupe Français de Pneumo-Cancérologie and Associazione Italiana Oncologia Toracica (2012). Erlotinib versus standard chemotherapy as first-line treatment for European patients with advanced EGFR mutation-positive non-small-cell lung cancer (EURTAC): a multicentre, open-label, randomised phase 3 trial. Lancet Oncol. *13*, 239–246.

Ross, J.S., Wang, K., Sheehan, C.E., Boguniewicz, A.B., Otto, G., Downing, S.R., Sun, J., He, J., Curran, J.A., Ali, S., et al. (2013). Relapsed classic E-cadherin (CDH1)-mutated invasive lobular breast cancer shows a high frequency of HER2 (ERBB2) gene mutations. Clin. Cancer Res. *19*, 2668–2676.

Rubin Grandis, J., Melhem, M.F., Gooding, W.E., Day, R., Holst, V.A., Wagener, M.M., Drenning, S.D., and Tweardy, D.J. (1998). Levels of TGF-alpha and EGFR protein in head and neck squamous cell carcinoma and patient survival. J. Natl. Cancer Inst. *90*, 824–832.

Sasaki, T., Koivunen, J., Ogino, A., Yanagita, M., Nikiforow, S., Zheng, W., Lathan, C., Marcoux, J.P., Du, J., Okuda, K., et al. (2011). A novel ALK secondary mutation and EGFR signaling cause resistance to ALK kinase inhibitors. Cancer Res. *71*, 6051–6060.

Scaltriti, M., Rojo, F., Ocaña, A., Anido, J., Guzman, M., Cortes, J., Di Cosimo, S., Matias-Guiu, X., Ramon y Cajal, S., Arribas, J., and Baselga, J. (2007). Expression of p95HER2, a truncated form of the HER2 receptor, and response to anti-HER2 therapies in breast cancer. J. Natl. Cancer Inst. *99*, 628–638.

Scaltriti, M., Verma, C., Guzman, M., Jimenez, J., Parra, J.L., Pedersen, K., Smith, D.J., Landolfi, S., Ramon y Cajal, S., Arribas, J., and Baselga, J. (2009). Lapatinib, a HER2 tyrosine kinase inhibitor, induces stabilization and accumulation of HER2 and potentiates trastuzumab-dependent cell cytotoxicity. Oncogene *28*, 803–814.

Scaltriti, M., Chandarlapaty, S., Prudkin, L., Aura, C., Jimenez, J., Angelini, P.D., Sánchez, G., Guzman, M., Parra, J.L., Ellis, C., et al. (2010). Clinical benefit of lapatinib-based therapy in patients with human epidermal growth factor receptor 2-positive breast tumors coexpressing the truncated p95HER2 receptor. Clin. Cancer Res. *16*, 2688–2695.

Scaltriti, M., Eichhorn, P.J., Cortés, J., Prudkin, L., Aura, C., Jiménez, J., Chandarlapaty, S., Serra, V., Prat, A., Ibrahim, Y.H., et al. (2011). Cyclin E amplification/overexpression is a mechanism of trastuzumab resistance in HER2+ breast cancer patients. Proc. Natl. Acad. Sci. USA *108*, 3761–3766.

Schaefer, G., Haber, L., Crocker, L.M., Shia, S., Shao, L., Dowbenko, D., Totpal, K., Wong, A., Lee, C.V., Stawicki, S., et al. (2011). A two-in-one antibody against HER3 and EGFR has superior inhibitory activity compared with monospecific antibodies. Cancer Cell *20*, 472–486.

Schechter, A.L., Stern, D.F., Vaidyanathan, L., Decker, S.J., Drebin, J.A., Greene, M.I., and Weinberg, R.A. (1984). The neu oncogene: an erb-B-related gene encoding a 185,000-Mr tumour antigen. Nature *312*, 513–516.

Scheuer, W., Friess, T., Burtscher, H., Bossenmaier, B., Endl, J., and Hasmann, M. (2009). Strongly enhanced antitumor activity of trastuzumab and pertuzumab combination treatment on HER2-positive human xenograft tumor models. Cancer Res. *69*, 9330–9336.

Schneeweiss, A., Chia, S., Hickish, T., Harvey, V., Eniu, A., Hegg, R., Tausch, C., Seo, J.H., Tsai, Y.F., Ratnayake, J., et al. (2013). Pertuzumab plus trastuzumab in combination with standard neoadjuvant anthracycline-containing and anthracycline-free chemotherapy regimens in patients with HER2-positive early breast cancer: a randomized phase II cardiac safety study (TRYPHAENA). Ann. Oncol. *24*, 2278–2284.

Schoeberl, B., Faber, A.C., Li, D., Liang, M.C., Crosby, K., Onsum, M., Burenkova, O., Pace, E., Walton, Z., Nie, L., et al. (2010). An ErbB3 antibody, MM-121, is active in cancers with ligand-dependent activation. Cancer Res. *70*, 2485–2494.

Sequist, L.V., Waltman, B.A., Dias-Santagata, D., Digumarthy, S., Turke, A.B., Fidias, P., Bergethon, K., Shaw, A.T., Gettinger, S., Cosper, A.K., et al. (2011). Genotypic and histological evolution of lung cancers acquiring resistance to EGFR inhibitors. Sci. Transl. Med. *3*, 75ra26.

Sequist, L.V., Soria, J.-C., Gadgeel, S.M., Wakelee, H.A., Camidge, D.R., Varga, A., Fidias, P., Wozniak, A.J., Neal, J.W., Doebele, R.C., et al. (2013a). First-in-human evaluation of CO-1686, an irreversible, selective, and potent tyrosine kinase inhibitor of EGFR T790M. J. Clin. Oncol. *31* (*Suppl.*), abstr. 2524.

Sequist, L.V., Yang, J.C., Yamamoto, N., O'Byrne, K., Hirsh, V., Mok, T., Geater, S.L., Orlov, S., Tsai, C.M., Boyer, M., et al. (2013b). Phase III study of afatinib or cisplatin plus pemetrexed in patients with metastatic lung adenocarcinoma with EGFR mutations. J. Clin. Oncol. *31*, 3327–3334.

Serra, V., Markman, B., Scaltriti, M., Eichhorn, P.J., Valero, V., Guzman, M., Botero, M.L., Llonch, E., Atzori, F., Di Cosimo, S., et al. (2008). NVP-BEZ235, a dual PI3K/mTOR inhibitor, prevents PI3K signaling and inhibits the growth of cancer cells with activating PI3K mutations. Cancer Res. *68*, 8022–8030.

Sharma, S.V., Lee, D.Y., Li, B., Quinlan, M.P., Takahashi, F., Maheswaran, S., McDermott, U., Azizian, N., Zou, L., Fischbach, M.A., et al. (2010). A chromatin-mediated reversible drug-tolerant state in cancer cell subpopulations. Cell *141*, 69–80.

Shattuck, D.L., Miller, J.K., Carraway, K.L., 3rd, and Sweeney, C. (2008). Met receptor contributes to trastuzumab resistance of Her2-overexpressing breast cancer cells. Cancer Res. *68*, 1471–1477.

Sheng, Q., Liu, X., Fleming, E., Yuan, K., Piao, H., Chen, J., Moustafa, Z., Thomas, R.K., Greulich, H., Schinzel, A., et al. (2010). An activated ErbB3/NRG1 autocrine loop supports in vivo proliferation in ovarian cancer cells. Cancer Cell *17*, 298–310.

Shepherd, F.A., Rodrigues Pereira, J., Ciuleanu, T., Tan, E.H., Hirsh, V., Thongprasert, S., Campos, D., Maoleekoonpiroj, S., Smylie, M., Martins, R., et al.; National Cancer Institute of Canada Clinical Trials Group (2005). Erlotinib in previously treated non-small-cell lung cancer. N. Engl. J. Med. *353*, 123–132.

Shi, F., Telesco, S.E., Liu, Y., Radhakrishnan, R., and Lemmon, M.A. (2010). ErbB3/HER3 intracellular domain is competent to bind ATP and catalyze autophosphorylation. Proc. Natl. Acad. Sci. USA *107*, 7692–7697.

Singh, B., and Coffey, R.J. (2014). Trafficking of epidermal growth factor receptor ligands in polarized epithelial cells. Annu. Rev. Physiol. *76*, 275–300.

Singh, B., Bogatcheva, G., Washington, M.K., and Coffey, R.J. (2013). Transformation of polarized epithelial cells by apical mistrafficking of epiregulin. Proc. Natl. Acad. Sci. USA *110*, 8960–8965.

Slamon, D.J., Clark, G.M., Wong, S.G., Levin, W.J., Ullrich, A., and McGuire, W.L. (1987). Human breast cancer: correlation of relapse and survival with amplification of the HER-2/neu oncogene. Science *235*, 177–182.

Slamon, D.J., Leyland-Jones, B., Shak, S., Fuchs, H., Paton, V., Bajamonde, A., Fleming, T., Eiermann, W., Wolter, J., Pegram, M., et al. (2001). Use of chemotherapy plus a monoclonal antibody against HER2 for metastatic breast cancer that overexpresses HER2. N. Engl. J. Med. *344*, 783–792.

Soria, J.-C., Sequist, L.V., Gadgeel, S., Goldman, J., Wakelee, H., Varga, A., Fidias, P., Wozniak, A.J., Neal, J.W., Doebele, R.C., et al. (2013). First-in-human evaluation of CO-1686, an irreversible, highly selective tyrosine kinase inhibitor of mutations of EGFR (activating and T790M). J. Thorac. Oncol. *8*, s141.

Sos, M.L., Koker, M., Weir, B.A., Heynck, S., Rabinovsky, R., Zander, T., Seeger, J.M., Weiss, J., Fischer, F., Frommolt, P., et al. (2009). PTEN loss contributes to erlotinib resistance in EGFR-mutant lung cancer by activation of Akt and EGFR. Cancer Res. *69*, 3256–3261.

Stagg, J., Loi, S., Divisekera, U., Ngiow, S.F., Duret, H., Yagita, H., Teng, M.W., and Smyth, M.J. (2011). Anti-ErbB-2 mAb therapy requires type I and II interferons and synergizes with anti-PD-1 or anti-CD137 mAb therapy. Proc. Natl. Acad. Sci. USA *108*, 7142–7147.

Stephens, P., Hunter, C., Bignell, G., Edkins, S., Davies, H., Teague, J., Stevens, C., O'Meara, S., Smith, R., Parker, A., et al. (2004). Lung cancer: intragenic ERBB2 kinase mutations in tumours. Nature *431*, 525–526.

Sugawa, N., Ekstrand, A.J., James, C.D., and Collins, V.P. (1990). Identical splicing of aberrant epidermal growth factor receptor transcripts from amplified rearranged genes in human glioblastomas. Proc. Natl. Acad. Sci. USA *87*, 8602–8606.

Takezawa, K., Pirazzoli, V., Arcila, M.E., Nebhan, C.A., Song, X., de Stanchina, E., Ohashi, K., Janjigian, Y.Y., Spitzler, P.J., Melnick, M.A., et al. (2012). HER2 amplification: a potential mechanism of acquired resistance to EGFR inhibition in EGFR-mutant lung cancers that lack the second-site EGFRT790M mutation. Cancer Discov. *2*, 922–933.

Tanizaki, J., Okamoto, I., Fumita, S., Okamoto, W., Nishio, K., and Nakagawa, K. (2011). Roles of BIM induction and survivin downregulation in lapatinib-induced apoptosis in breast cancer cells with HER2 amplification. Oncogene *30*, 4097–4106.

Turke, A.B., Zejnullahu, K., Wu, Y.L., Song, Y., Dias-Santagata, D., Lifshits, E., Toschi, L., Rogers, A., Mok, T., Sequist, L., et al. (2010). Preexistence and clonal selection of MET amplification in EGFR mutant NSCLC. Cancer Cell *17*, 77–88.

Turke, A.B., Song, Y., Costa, C., Cook, R., Arteaga, C.L., Asara, J.M., and Engelman, J.A. (2012). MEK inhibition leads to PI3K/AKT activation by relieving a negative feedback on ERBB receptors. Cancer Res. *72*, 3228–3237.

Utermark, T., Rao, T., Cheng, H., Wang, Q., Lee, S.H., Wang, Z.C., Iglehart, J.D., Roberts, T.M., Muller, W.J., and Zhao, J.J. (2012). The p110α and p110β isoforms of PI3K play divergent roles in mammary gland development and tumorigenesis. Genes Dev. *26*, 1573–1586.

Van Cutsem, E., Peeters, M., Siena, S., Humblet, Y., Hendlisz, A., Neyns, B., Canon, J.L., Van Laethem, J.L., Maurel, J., Richardson, G., et al. (2007). Open-label phase III trial of panitumumab plus best supportive care compared with best supportive care alone in patients with chemotherapy-refractory metastatic colorectal cancer. J. Clin. Oncol. *25*, 1658–1664.

Van Cutsem, E., Köhne, C.H., Hitre, E., Zaluski, J., Chang Chien, C.R., Makhson, A., D'Haens, G., Pintér, T., Lim, R., Bodoky, G., et al. (2009). Cetuximab and chemotherapy as initial treatment for metastatic colorectal cancer. N. Engl. J. Med. *360*, 1408–1417.

Vaught, D.B., Stanford, J.C., Young, C., Hicks, D.J., Wheeler, F., Rinehart, C., Sánchez, V., Koland, J., Muller, W.J., Arteaga, C.L., and Cook, R.S. (2012). HER3 is required for HER2-induced preneoplastic changes to the breast epithelium and tumor formation. Cancer Res. *72*, 2672–2682.

Verma, S., Miles, D., Gianni, L., Krop, I.E., Welslau, M., Baselga, J., Pegram, M., Oh, D.Y., Diéras, V., Guardino, E., et al.; EMILIA Study Group (2012). Trastuzumab emtansine for HER2-positive advanced breast cancer. N. Engl. J. Med. *367*, 1783–1791.

Vermorken, J.B., Mesia, R., Rivera, F., Remenar, E., Kawecki, A., Rottey, S., Erfan, J., Zabolotnyy, D., Kienzer, H.R., Cupissol, D., et al. (2008). Platinum-based chemotherapy plus cetuximab in head and neck cancer. N. Engl. J. Med. *359*, 1116–1127.

von Minckwitz, G., du Bois, A., Schmidt, M., Maass, N., Cufer, T., de Jongh, F.E., Maartense, E., Zielinski, C., Kaufmann, M., Bauer, W., et al. (2009). Trastuzumab beyond progression in human epidermal growth factor receptor 2-positive advanced breast cancer: a german breast group 26/breast international group 03-05 study. J. Clin. Oncol. *27*, 1999–2006.

Walter, A.O., Sjin, R.T., Haringsma, H.J., Ohashi, K., Sun, J., Lee, K., Dubrovskiy, A., Labenski, M., Zhu, Z., Wang, Z., et al. (2013). Discovery of a mutant-selective covalent inhibitor of EGFR that overcomes T790M-mediated resistance in NSCLC. Cancer Discov. *3*, 1404–1415.

Wang, S.E., Narasanna, A., Perez-Torres, M., Xiang, B., Wu, F.Y., Yang, S., Carpenter, G., Gazdar, A.F., Muthuswamy, S.K., and Arteaga, C.L. (2006). HER2 kinase domain mutation results in constitutive phosphorylation and activation of HER2 and EGFR and resistance to EGFR tyrosine kinase inhibitors. Cancer Cell *10*, 25–38.

Wang, S.E., Xiang, B., Guix, M., Olivares, M.G., Parker, J., Chung, C.H., Pandiella, A., and Arteaga, C.L. (2008). Transforming growth factor beta engages TACE and ErbB3 to activate phosphatidylinositol-3 kinase/Akt in ErbB2-overexpressing breast cancer and desensitizes cells to trastuzumab. Mol. Cell. Biol. *28*, 5605–5620.

Willmore-Payne, C., Holden, J.A., and Layfield, L.J. (2006). Detection of EGFR- and HER2-activating mutations in squamous cell carcinoma involving the head and neck. Mod. Pathol. *19*, 634–640.

Wilson, T.R., Lee, D.Y., Berry, L., Shames, D.S., and Settleman, J. (2011). Neuregulin-1-mediated autocrine signaling underlies sensitivity to HER2 kinase inhibitors in a subset of human cancers. Cancer Cell *20*, 158–172.

Wilson, T.R., Fridlyand, J., Yan, Y., Penuel, E., Burton, L., Chan, E., Peng, J., Lin, E., Wang, Y., Sosman, J., et al. (2012). Widespread potential for growth-factor-driven resistance to anticancer kinase inhibitors. Nature *487*, 505–509.

Wood, E.R., Truesdale, A.T., McDonald, O.B., Yuan, D., Hassell, A., Dickerson, S.H., Ellis, B., Pennisi, C., Horne, E., Lackey, K., et al. (2004). A unique structure for epidermal growth factor receptor bound to GW572016 (Lapatinib): relationships among protein conformation, inhibitor off-rate, and receptor activity in tumor cells. Cancer Res. *64*, 6652–6659.

Xia, W., Bacus, S., Hegde, P., Husain, I., Strum, J., Liu, L., Paulazzo, G., Lyass, L., Trusk, P., Hill, J., et al. (2006). A model of acquired autoresistance to a potent ErbB2 tyrosine kinase inhibitor and a therapeutic strategy to prevent its onset in breast cancer. Proc. Natl. Acad. Sci. USA *103*, 7795–7800.

Yakes, F.M., Chinratanalab, W., Ritter, C.A., King, W., Seelig, S., and Arteaga, C.L. (2002). Herceptin-induced inhibition of phosphatidylinositol-3 kinase and Akt Is required for antibody-mediated effects on p27, cyclin D1, and antitumor action. Cancer Res. *62*, 4132–4141.

Yano, S., Wang, W., Li, Q., Matsumoto, K., Sakurama, H., Nakamura, T., Ogino, H., Kakiuchi, S., Hanibuchi, M., Nishioka, Y., et al. (2008). Hepatocyte growth factor induces gefitinib resistance of lung adenocarcinoma with epidermal growth factor receptor-activating mutations. Cancer Res. *68*, 9479–9487.

Yano, S., Yamada, T., Takeuchi, S., Tachibana, K., Minami, Y., Yatabe, Y., Mitsudomi, T., Tanaka, H., Kimura, T., Kudoh, S., et al. (2011). Hepatocyte growth factor expression in EGFR mutant lung cancer with intrinsic and acquired resistance to tyrosine kinase inhibitors in a Japanese cohort. J. Thorac. Oncol. *6*, 2011–2017.

Yarden, Y., and Pines, G. (2012). The ERBB network: at last, cancer therapy meets systems biology. Nat. Rev. Cancer *12*, 553–563.

Yarden, Y., and Sliwkowski, M.X. (2001). Untangling the ErbB signalling network. Nat. Rev. Mol. Cell Biol. *2*, 127–137.

Yasuda, H., Park, E., Yun, C.H., Sng, N.J., Lucena-Araujo, A.R., Yeo, W.L., Huberman, M.S., Cohen, D.W., Nakayama, S., Ishioka, K., et al. (2013). Structural, biochemical, and clinical characterization of epidermal growth factor receptor (EGFR) exon 20 insertion mutations in lung cancer. Sci. Transl. Med. *5*, ra177.

Yonesaka, K., Zejnullahu, K., Okamoto, I., Satoh, T., Cappuzzo, F., Souglakos, J., Ercan, D., Rogers, A., Roncalli, M., Takeda, M., et al. (2011). Activation of ERBB2 signaling causes resistance to the EGFR-directed therapeutic antibody cetuximab. Sci. Transl. Med. *3*, 99ra86.

Yu, H.A., Arcila, M.E., Rekhtman, N., Sima, C.S., Zakowski, M.F., Pao, W., Kris, M.G., Miller, V.A., Ladanyi, M., and Riely, G.J. (2013). Analysis of tumor specimens at the time of acquired resistance to EGFR-TKI therapy in 155 patients with EGFR-mutant lung cancers. Clin. Cancer Res. *19*, 2240–2247.

Yun, C.H., Boggon, T.J., Li, Y., Woo, M.S., Greulich, H., Meyerson, M., and Eck, M.J. (2007). Structures of lung cancer-derived EGFR mutants and inhibitor complexes: mechanism of activation and insights into differential inhibitor sensitivity. Cancer Cell *11*, 217–227.

Yun, C.H., Mengwasser, K.E., Toms, A.V., Woo, M.S., Greulich, H., Wong, K.K., Meyerson, M., and Eck, M.J. (2008). The T790M mutation in EGFR kinase causes drug resistance by increasing the affinity for ATP. Proc. Natl. Acad. Sci. USA *105*, 2070–2075.

Zhang, S., Huang, W.C., Li, P., Guo, H., Poh, S.B., Brady, S.W., Xiong, Y., Tseng, L.M., Li, S.H., Ding, Z., et al. (2011). Combating trastuzumab resistance by targeting SRC, a common node downstream of multiple resistance pathways. Nat. Med. *17*, 461–469.

Zhang, Z., Lee, J.C., Lin, L., Olivas, V., Au, V., LaFramboise, T., Abdel-Rahman, M., Wang, X., Levine, A.D., Rho, J.K., et al. (2012). Activation of the AXL kinase causes resistance to EGFR-targeted therapy in lung cancer. Nat. Genet. *44*, 852–860.

Zhou, B.B., Peyton, M., He, B., Liu, C., Girard, L., Caudler, E., Lo, Y., Baribaud, F., Mikami, I., Reguart, N., et al. (2006). Targeting ADAM-mediated ligand cleavage to inhibit HER3 and EGFR pathways in non-small cell lung cancer. Cancer Cell *10*, 39–50.

Zhou, W., Ercan, D., Chen, L., Yun, C.H., Li, D., Capelletti, M., Cortot, A.B., Chirieac, L., Iacob, R.E., Padera, R., et al. (2009). Novel mutant-selective EGFR kinase inhibitors against EGFR T790M. Nature *462*, 1070–1074.

Zhuang, G., Brantley-Sieders, D.M., Vaught, D., Yu, J., Xie, L., Wells, S., Jackson, D., Muraoka-Cook, R., Arteaga, C., and Chen, J. (2010). Elevation of receptor tyrosine kinase EphA2 mediates resistance to trastuzumab therapy. Cancer Res. *70*, 299–308.

Zito, C.I., Riches, D., Kolmakova, J., Simons, J., Egholm, M., and Stern, D.F. (2008). Direct resequencing of the complete ERBB2 coding sequence reveals an absence of activating mutations in ERBB2 amplified breast cancer. Genes Chromosomes Cancer *47*, 633–638.

Cancer Cell
Perspective

Mutant p53 in Cancer: New Functions and Therapeutic Opportunities

Patricia A.J. Muller[1,*] and Karen H. Vousden[2,*]
[1]Medical Research Council Toxicology Unit, Hodgkin Building, Lancaster Road, Leicester LE1 9HN, UK
[2]CR-UK Beatson Institute, Garscube Estate, Switchback Road, Glasgow G61 1BD, UK
*Correspondence: pm292@le.ac.uk (P.A.J.M.), k.vousden@beatson.gla.ac.uk (K.H.V.)
http://dx.doi.org/10.1016/j.ccr.2014.01.021

Many different types of cancer show a high incidence of *TP53* mutations, leading to the expression of mutant p53 proteins. There is growing evidence that these mutant p53s have both lost wild-type p53 tumor suppressor activity and gained functions that help to contribute to malignant progression. Understanding the functions of mutant p53 will help in the development of new therapeutic approaches that may be useful in a broad range of cancer types.

p53 is one of the most intensively studied tumor suppressor proteins, with mutations that lead to loss of wild-type p53 activity frequently detected in many different tumor types. Perturbations in p53 signaling pathways are believed to be required for the development of most cancers, and there is evidence to suggest that restoration or reactivation of p53 function will have significant therapeutic benefit. For the first 10 years of investigation, p53 was considered to be the product of an oncogene, with many studies describing proliferative and transforming activities for p53. This mistake in the initial classification of p53 was the result of a simple error; the *TP53* gene that had been cloned and used in the initial experiments encoded a mutant version of the wild-type gene. The tumor suppressor credentials of wild-type p53 are no longer in doubt, but the early studies provided a tantalizing hint of what has become an extremely active area of study—the suggestion that mutations in p53 can result in both loss of wild-type activity and gain of a novel transforming function. Moving in a circle in the past 30 years, we have come back around to considering that p53, albeit mutant versions of p53, can function as oncoproteins. In this review, we highlight recent progress in our understanding of how mutant p53 functions, discuss the avenues that are being explored to target mutant p53 tumors, and explore future directions for mutant p53 research.

TP53 is the most commonly mutated gene in human cancer (Kandoth et al., 2013). Alterations have been found in virtually every region of the protein (Leroy et al., 2013), but only a handful of the most frequently occurring mutations have been studied in depth for their contribution to cancer progression. In some cases, frameshift or nonsense mutations result in the loss of p53 protein expression, as seen with other tumor suppressors. However, more frequently, the tumor-associated alterations in p53 result in missense mutations, leading to the substitution of a single amino acid in the p53 protein that can be stably expressed in the tumor cell. These substitutions occur throughout the p53 protein, but most commonly cluster within the DNA binding region of p53, with six "hotspot" amino acids that are most frequently substituted. These mutations generally lead to a loss or diminution of the wild-type activity of p53, and because p53 normally acts as a tetramer, these mutant proteins may also function as dominant negative inhibitors over any remaining wild-type p53. Indeed, in a mouse model, the expression of mutant p53 has been shown to dampen (but not prevent) the therapeutic response to restoration of wild-type p53 (Wang et al., 2011). However, it is becoming clear that at least some of these mutant p53 proteins give rise to a more aggressive tumor profile, indicating that they have acquired novel functions in promoting tumorigenesis.

Gain of Function of Mutant p53

The concept that mutant p53 may show a neomorphic gain of function (GOF) was first suggested 20 years ago (Dittmer et al., 1993), when the introduction of mutant p53 into p53 null cells was shown to give rise to a new phenotype. Since then, a large number of publications have demonstrated many GOFs in numerous cell lines with a variety of p53 mutations, summarized in Table 1. The GOF acquired by mutant p53 is further supported by the finding that patients carrying a *TP53* missense mutation (leading to expression of a mutant p53 protein) in the germline have a significantly earlier cancer onset than patients with mutations in *TP53* that result in loss of p53 protein expression (Bougeard et al., 2008; Zerdoumi et al., 2013). Consistently, in vivo experiments showed that mice expressing mutant p53 display a tumor profile that is more aggressive and metastatic than p53 null or p53 wild-type mice (Doyle et al., 2010; Lang et al., 2004; Morton et al., 2010; Olive et al., 2004), although some tissue specificity of this effect has been suggested by further studies showing that introduction of similar p53 mutations in the lung did not reveal any detectable GOF activity over p53 loss (Jackson et al., 2005). Nevertheless, numerous in vitro and xenograft models have confirmed the ability of mutant p53s to drive enhanced invasion and motility, with evidence that mutant p53 can enhance signaling through receptors such as transforming growth factor β (TGF-β) receptor, epidermal growth factor receptor, and MET (Adorno et al., 2009; Grugan et al., 2013; Muller et al., 2009, 2012; Sauer et al., 2010; Wang et al., 2013a). In part,

Table 1. The Different GOF Roles of Mutant p53 in Cells

Mutation	Cell Line	Mutant p53 Expression	Reference
Invasion			
R172H (human R175H), 175H	PDAC	endogenous (also stable/transient)	Muller et al., 2012
R175H	KLE	endogenous (also stable/transient)	Dong et al., 2009
R175H, R273H, R248Q, R280K,	H1299	stable/transient	Adorno et al., 2009; Coffill et al., 2012; Muller et al., 2009; Noll et al., 2012; Yoshikawa et al., 2010
G266E	MDA MB435	endogenous	Yeudall et al., 2012
R273H	A431	endogenous	Muller et al., 2009
R280K	MDA MB231	endogenous	Coffill et al., 2012; Girardini et al., 2011; Muller et al., 2009
Increased (Altered) Migration[a]			
R172H	MEF	endogenous	Adorno et al., 2009
R175H, H179L, R248Q, R273H, D281G	H1299	stable/transient	Adorno et al., 2009; Muller et al., 2009, 2012; Noll et al., 2012; Yeudall et al., 2012
R175H, R248Q	HEC-50	stable/transient	Dong et al., 2012
R248Q	HEC-1	endogenous	Dong et al., 2012
R248W	HCT116$^{-/-}$	endogenous	Muller et al., 2012
R249S	KNS-62	endogenous	Vaughan et al., 2012b
R267P	H1437	endogenous	Vaughan et al., 2012b
R273H	HT29, A431, U373, SNB19	endogenous	Huang et al., 2013; Muller et al., 2012
R280K	MDA MB231	endogenous	Adorno et al., 2009; Girardini et al., 2011; Li et al., 2011a
Proliferation, Propagation of Cell Cycle			
P278S	ABC1	endogenous	Vaughan et al., 2012a
R172H (human R175H)	MEF	endogenous	Lang et al., 2004
R175H	SK-BR3, VMRC	endogenous	Bossi et al., 2006; Vaughan et al., 2012a
R175H, R248H	BE-13	stable/transient	Hsiao et al., 1994
R175H, R273H, D281G	H1299	stable/transient	Liu et al., 2011; Scian et al., 2004b)
C176F, P223L, R273H, R282Q	PC-3	stable/transient	Shi et al., 2002
M246I	H23	endogenous	Vaughan et al., 2012b
R248W, D281G	10(3)	stable/transient	Loging and Reisman, 1999; Scian et al., 2004a
R249S	KNS-62	endogenous	Vaughan et al., 2012a
R267P	H1437	endogenous	Vaughan et al., 2012a; Vaughan et al., 2012b
R273C	H1048	endogenous	Vaughan et al., 2012b
R273H	HT-29, MDA MB468, H2405	endogenous	Bossi et al., 2006; Gurtner et al., 2010; Vaughan et al., 2012a; Wang et al., 2013a
R273H/ P309S	SW480	endogenous	Bossi et al., 2006; Yan et al., 2008
R273H/ R248W	Mia-Paca-2	endogenous	Yan et al., 2008
R280T	SWO-38	endogenous	Lin et al., 2012
Drug Resistance/Avoidance of Cell Death			
A135V, R248W, R273H	M1/2 cells, LN-308	stable/transient	Li et al., 1998; Matas et al., 2001; Pohl et al., 1999; Trepel et al., 1998
R175H	MEC, 10(3), HEC-50	stable/transient	Dong et al., 2012; Murphy et al., 2000; Pugacheva et al., 2002
R175H	SK-BR3	endogenous	Bossi et al., 2006; Di Agostino et al., 2006; Vaughan et al., 2012b
R175H, P223L + V274F	Pc-3	stable/transient	Gurova et al., 2003; Zalcenstein et al., 2003

(*Continued on next page*)

Table 1. *Continued*

Mutation	Cell Line	Mutant p53 Expression	Reference
R175H, R245S, R273H, D281G	Saos-2	stable/transient	Atema and Chène, 2002; El-Hizawi et al., 2002; Kawamata et al., 2007; Tsang et al., 2005; Wong et al., 2007
R175H, R248W, R273H	SKOV-3	stable/transient	Buganim et al., 2006; Liu et al., 2011; Pugacheva et al., 2002
R175H, R248W, R273H	H1299	stable/ transient	Blandino et al., 1999; Di Como et al., 1999; Pugacheva et al., 2002; Zalcenstein et al., 2006
Y220S	fibroblasts	stable/transient	Capponcelli et al., 2005
M237?	T98G	endogenous	Wang et al., 2013b
R248Q	HEC-1	endogenous	Dong et al., 2012
G266E	MDA MB435	endogenous	Vaughan et al., 2012b
R273?	U138	endogenous	Wang et al., 2013b
R273C	C33A, H1048	endogenous	Liu et al., 2011; Vaughan et al., 2012b
R273H	C33A	endogenous	Liu et al., 2011
R273H	HT-29, MDA MB468	endogenous	Bossi et al., 2006; Vaughan et al., 2012b
R273H/ P309S	SW480	endogenous	Bossi et al., 2006; Di Agostino et al., 2006
R273H/ R248W	Mia-Paca-2	endogenous	Do et al., 2012
V143A, R175H, R248W, R273H	Hep3B	stable/transient	Schilling et al., 2010
Anchorage-Independent Growth/Anoikis			
Y126C, R175H, H214R, G245S, R273C, R273H, V273F, R280T, R282Q	SAOS-2	stable/transient	Dittmer et al., 1993; Shi et al., 2002; Sun et al., 1993
P151S	TU-138	endogenous	Xie et al., 2013
Increased Colony Formation			
V143A	BEAS-2B	stable/transient	Gerwin et al., 1992
V143A, R175H, R248W, R273H	H1299	stable/transient	Kalo et al., 2012; Liu et al., 2011; Weisz et al., 2004
V143A, Y163C, R175H, L194R, R273H, D281G, R282W	10(3)	stable/transient	Scian et al., 2004a
G144P, R158H, Y163N, H168Y, V173L, Y234C, R248W	REF[b]	stable/transient	Smith et al., 1999
C174Y	Saos-2	stable/transient	Preuss et al., 2000
R172H (human R175H)	MEF	endogenous	Lang et al., 2004
R175H	SK-BR3	endogenous	Bossi et al., 2006
C194T	T47D	endogenous	Nguyen et al., 2013; Vikhanskaya et al., 2007
A220G	Huh-7	endogenous	Vikhanskaya et al., 2007
R270C	IP3	stable/transient	Halevy et al., 1990
R273H	HT-29, MDA MB 468, U373, SNB19	endogenous	Bossi et al., 2006, 2008; Huang et al., 2013; Wang et al., 2013a
R273H	MCF10A[b]	stable/transient	Nguyen et al., 2013
R273H/ P309S	SW480	endogenous	Bossi et al., 2006; Yan and Chen, 2009, 2010; Yan et al., 2008
R273H/ R248W	Mia-Paca-2	endogenous	Yan and Chen, 2009; Yan et al., 2008
Genomic Instability			
R172H (human R175H)	primary mouse oral tumor	endogenous	Acin et al., 2011
R175H	MEC	stable/transient	Murphy et al., 2000
R175H, R248W, R273H	MEF	stable/transient	Agapova et al., 1996
N236S (human N239S)	MEF	endogenous	Jia et al., 2012

(*Continued on next page*)

Table 1. *Continued*

Mutation	Cell Line	Mutant p53 Expression	Reference
R248W	primary mouse cells	endogenous	Song et al., 2007
R248W, R273H	K562 KMV	stable/transient	Restle et al., 2008
Spheroid Disorganization/Mammary Architecture Disruption			
R273H, R280K	MDA MB 468, MDA MB231	endogenous	Freed-Pastor et al., 2012
R175H, G245S, R248W, R273H	MCF10A[b]	stable/transient	Zhang et al., 2011
Stem Cell Dedifferentiation/Propagation			
V143A, R175H, R273H	10(3)	stable/transient	Yi et al., 2012
R172H (human R175H)	MEF	endogenous	Sarig et al., 2010
Xenograft Growth (Cell Line Injected Subcutaneously or in the Mammary Fat Pad)			
V143A, R175H, R248W, R273H, R281D, D281G	(10) 3	stable/transient	Dittmer et al., 1993; Lányi et al., 1998
R172H (human R175H)	primary mouse oral tumor	endogenous	Acin et al., 2011
R175H, R273H,	H1299	stable/transient	Liu et al., 2011
N236S (human N239S)	MEF	endogenous	Jia et al., 2012
R267P	H1437	endogenous	Vaughan et al., 2012a
R273C	H1048	endogenous	Vaughan et al., 2012b
R273H	HT29, MDA MB 468	endogenous	Bossi et al., 2008; Wang et al., 2013a
P278S	ABC1	endogenous	Vaughan et al., 2012a
R280K	MDA MB 231	endogenous	Adorno et al., 2009
R280T	SAOS-2	stable/transient	Sun et al., 1993
Intravenous Injection (Formation of Lung Metastasis)			
R175H, R248G, R213G	BE-13[c]	stable/transient	Hsiao et al., 1994
C236F	D3S2	endogenous	Adorno et al., 2009
R280K	MDA MB231	endogenous	Adorno et al., 2009
Elongated Cell Morphology/EMT			
C135Y, R175H, R273H	HEC-50	stable/transient	Dong et al., 2012
V143A	HCT116$^{-/-}$	stable/transient	Roger et al., 2010
R175H	H1299	stable/transient	Adorno et al., 2009
R175H, R273H	10(3)	stable/transient	Gloushankova et al., 1997
R248Q	HEC-1	endogenous	Dong et al., 2012
R273H	SW620	endogenous	Roger et al., 2010
R175H, G245S, R248W, R273H	MCF10A[b]	stable/transient	Zhang et al., 2011
Polyploidy			
V143A	NHF3 cells[b]	stable/transient	Gualberto et al., 1998
R248W, R249S, R175H	H1299	stable/transient	Noll et al., 2012
Angiogenesis			
Δ126	T24	endogenous	Zhu et al., 2013
R175H[d]	H1299	stable/transient	Fontemaggi et al., 2009
Y220S	fibroblasts	stable/transient	Capponcelli et al., 2005
Cell Survival			
V157F	Hs578T	endogenous	Braicu et al., 2013
C194T	T47D	endogenous	Lim et al., 2009
P223L/V274F	DU-145	endogenous	Zhu et al., 2011
R273H	MDA MB468, U373, SNB19	endogenous	Huang et al., 2013; Lim et al., 2009
R273H	H1299	stable/transient	Kalo et al., 2012

(*Continued on next page*)

Table 1. *Continued*

Mutation	Cell Line	Mutant p53 Expression	Reference
R280K	MDA MB231	endogenous	Ali et al., 2013; Hui et al., 2006
R280T	5637	endogenous	Zhu et al., 2013
Mammosphere Formation			
R175H	MESC, HEC-50	endogenous	Lu et al., 2013; Dong et al., 2012
R248Q	HEC-1	endogenous	Dong et al., 2012

The different cellular processes in which mutant p53 has been shown to play a role are indicated. Literature was selected based on the following search criteria in Pubmed: "Mutant p53" and "Gain of Function" or "Mutant p53" and "acquired functions." Only studies in which a clear gain of function effect was shown are included (i.e., mutant p53 compared to a p53 null in the same cell line). These comprise studies in which mutant p53 was overexpressed in a p53 null cell line and compared to a vector control, or studies in which endogenous mutant p53 was knocked down or knocked out compared to control cells. Studies describing the activity of mutant p53 in cells that express wild-type p53 are not included to avoid complications from possible dominant negative effects. Indicated are the different mutations, cell lines, endogenous expression, or stable/transient transfection, and the references. The studies in this table were manually selected from >400 publications and we apologize to those authors whose papers we have inadvertently missed.

[a]Increased (altered) migration comprises wound scratch assays, scattering, migration in three-dimensional culture conditions, and Boyden chamber migration (frequently referred to as transwell invasion without addition of a matrix such as Matrigel).

[b]Cells were depleted for endogenous wild-type p53 expression.

[c]These are T cell acute lymphoblastic leukemia cells and therefore increased hematological disease rather than promoted lung metastases.

[d]H1299 cells expressing p53 R175H promoted the angiogenesis of HUVEC cells.

these responses reflect an ability of mutant p53 to promote integrin/RCP driven recycling (Muller et al., 2009, 2012) or increase the expression of growth factor receptors (Sauer et al., 2010; Wang et al., 2013a). Although mutant p53s have generally lost the ability to bind consensus p53 DNA binding regions in target gene promoters, their activity appears to reflect an ability to regulate gene expression directly (Weisz et al., 2007), although cytoplasmic and mitochondrial activities of mutant p53 in regulating apoptosis and autophagy have also been described (Chee et al., 2013; Frank et al., 2011; Morselli et al., 2008). Whereas various different mutant p53s can bind directly to DNA with some degree of selectivity (Brázdová et al., 2013; Göhler et al., 2005; Quante et al., 2012) and may thereby directly control the transcription of some genes (Weisz et al., 2007), there is increasing evidence that an indirect effect on gene expression through binding to other transcription factors underlies the novel activities of mutant p53s. For example, several studies have revealed a role for TAp63, a p53 family protein and transcription factor, which interacts with mutant but not wild-type p53 (Gaiddon et al., 2001; Strano et al., 2002). By inhibiting TAp63, mutant p53 can regulate a pro-invasive transcription program that includes regulation of the expression of Dicer, DEPDC1, Cyclin G2, and Sharp1 (Adorno et al., 2009; Girardini et al., 2011). The Dicer regulation by mutant p53 may be of particular importance, because several miRNAs that can in turn regulate genes involved in invasion have been described to be regulated by mutant p53, although this may not always involve TAp63 or Dicer inhibition (Dong et al., 2012; Neilsen et al., 2012; Tucci et al., 2012; Wang et al., 2013a).

Mutant p53 inhibition of TAp63 can be modeled by deletion of TAp63, which results in an aggressive tumor profile and metastases similar to that seen in mice expressing mutant p53 (Su et al., 2010). However, a direct comparison of mutant p53 expression with loss of TAp63 in a mouse model of pancreatic ductal adenocarcinoma (PDAC) showed that loss of TAp63 is less potent in inducing metastases, suggesting that mutant p53 does more than inhibiting TAp63 (Tan et al., 2013). This is not surprising, because mutant p53 interacts with a wide variety of other proteins, resulting in interference in a multitude of cellular pathways, some of which are likely to contribute to metastasis (Freed-Pastor and Prives, 2012; Muller and Vousden, 2013; Walerych et al., 2012). Besides inhibiting p63, mutant p53 inhibits and interacts with other proteins including the MRE11-Rad51-NSB complex, p73, and SP-1 to induce genomic instability, chemoresistance, or proliferation (Chicas et al., 2000; Gaiddon et al., 2001; Song et al., 2007). Furthermore, mutant p53 can also promote the function of proteins including SREBP, NF-Y, VDR, ETS2, or NRF2, resulting in increased proliferation, cholesterol synthesis, accumulation of reactive oxygen species, and enhanced cell survival (Do et al., 2012; Freed-Pastor et al., 2012; Kalo et al., 2012; Liu et al., 2011; Stambolsky et al., 2010). All of these proteins and pathways affected by mutant p53 are thoroughly described in three recent reviews (Freed-Pastor and Prives, 2012; Muller and Vousden, 2013; Walerych et al., 2012).

More recent studies are identifying further GOF activities of mutant p53, such as a role in cell reprogramming and expansion or in the maintenance and interaction with tumor stroma. Wild-type p53 was characterized as a suppressor of somatic stem cell reprogramming, the process in which differentiated somatic cells can be reprogrammed into a pluripotent stem cell to allow for unlimited expansion (Kawamura et al., 2009; Marión et al., 2009). Loss of p53 promoted the dedifferentiation of somatic cells and some, but not all, mutant p53s could potentiate the reprogramming (Sarig et al., 2010; Yi et al., 2012). An expansion of hematopoietic and mesenchymal stem cell progenitors is also seen in mutant p53 R248Q transgenic mice (Hanel et al., 2013). Consistently, in breast tissue with a *Wnt* transgene, loss of wild-type p53 generally promoted the formation of one distinct tumor, whereas mutant p53 R175H expression promoted the initiation of multiple different tumors that could be expanded in mammosphere assays (Lu et al., 2013). Together, these data suggest that mutant p53 can initiate tumor formation by promoting the generation and expansion of pluripotent stem cells.

The role of stroma tissue, including extracellular matrix, proteases, cytokines, immune cells, epithelial cells, and cancer-associated fibroblasts (CAFs), in tumorigenesis has become very evident (Pietras and Ostman, 2010). CAFs, the most abundant cell type in the stroma, secrete cytokines, hormones, and growth factors including hepatocyte growth factor and TGF-β (Bhowmick et al., 2004; Ostman and Augsten, 2009), both of which have been shown to mediate mutant p53-dependent invasion and metastasis (Adorno et al., 2009; Muller et al., 2012). In addition, a recent report highlights an important function for mutant p53 in promoting the inflammatory environment of colorectal tumors by prolonging NF-κB activation and cell survival (Cooks et al., 2013). It seems clear, therefore, that the presence of a mutant p53 in tumor cells will have an influence on how the tumor and stromal cells interact. In co-culture experiments, H1299 cells (regardless of p53 status) upregulated interferon-β (IFN-β) secretion in CAFs. This would normally cause inhibition of cell migration, but mutant p53-expressing tumor cells counteracted this response by enhancing STAT phosphorylation to promote invasion (Madar et al., 2013). Although interesting, these experiments are difficult to interpret, because the IFN-β secreted by the fibroblasts also reduced mutant p53 expression (Madar et al., 2013). Alternatively, it is possible that *TP53* mutations occur in the stroma surrounding tumors to promote tumor growth (Narendran et al., 2003; Patocs et al., 2007). Mutant p53-expressing fibroblasts were shown to promote tumor growth better than p53 null fibroblasts, suggesting that mutant p53 has a pro-oncogenic GOF role not only in tumor cells, but also in stromal cells (Addadi et al., 2010). However, whether stromal cells that have sustained mutations in p53 are prevalent, and how they are affected by (or affect) tumor cells remains unclear.

Are All Mutant p53s the Same?

Although most experimental studies have focused on the activity of a few most commonly detected p53 mutations that are clustered at codons 175, 245, 248, 249, 273, and 282, almost every codon within the DNA binding domain of p53 has been found to be mutated in cancer. Mutations have also been found in other domains, but their contribution to carcinogenesis is largely unknown (Leroy et al., 2013). Different tumor types show different spectra of *TP53* mutations—in some cases, reflecting the mutagenic event was thought to contribute to that type of cancer (e.g., aflatoxin and liver, UV light, and skin) or geographic variation in other cases. The frequency of missense mutations also differs in different subclasses of tumors of the same organ. For example, luminal breast cancers almost all carry point mutations in *TP53*, while alterations resulting in p53 truncations were more frequently detected in basal breast tumors (Dumay et al., 2013).

Whereas p53 mutants are often considered to be equivalent, evidence is accumulating to indicate that different mutants show a distinct profile with respect to loss of wild-type p53 activity, the ability to inhibit wild-type p53, and the acquisition of gain of function (Table 1; Halevy et al., 1990; Petitjean et al., 2007). The large number of p53 mutations complicates such analyses, as does the realization that different mutants may function differently in different tissues, potentially reflecting differences in the expression of targets of mutant p53 such as TAp63. To date, mutant p53s have been considered in two different categories: the first affecting amino acids that contact DNA and so preventing wild-type transcriptional activity without dramatically affecting the conformation of the p53 protein (known as contact mutants), and the second comprising mutations that clearly disrupt the three-dimensional structure of the protein (termed conformational mutants). Data from cell lines suggest that conformational and contact mutants can cooperate via different mechanisms with the H-Ras signaling pathway, leading to similar gene expression profiles and tumorigenesis (Solomon et al., 2012). However, this classification of mutants is clearly an oversimplification, because different mutations can lead to subtly different alterations in the structure and conformational stability of the p53 protein (Joerger and Fersht, 2007). Various mouse models have shown that both conformational and contact mutants can promote metastasis compared to p53 null mice. These differences appear to be dependent on the nature of the substitution, but caution should be taken when interpreting data from mouse models using different strain backgrounds that are being studied in different laboratories, and in some cases mutate the mouse gene and in others examine humanized TP53 sequences in the mouse. Models of R172H or R270H (prototype examples of a conformation and a contact hotspot mutation, equivalent to R175H and R273H in humans) both showed GOF activity (Lang et al., 2004; Olive et al., 2004), whereas no GOF was seen in R246S (the mouse equivalent of human R249S) and the humanized G245S mutant p53 mouse models, although the R246S could dominant-negatively inhibit wild-type p53 to promote cell survival after radiation exposure (Hanel et al., 2013; Lee et al., 2012). R248Q (humanized) p53 knock-in mice showed an earlier onset of tumor formation with a significantly reduced lifespan compared to p53 null mice (Hanel et al., 2013), although this reduction in overall survival was not evident in any of the other mutant p53 models. Consistently, Li-Fraumeni patients carrying an R248Q mutation display an earlier onset of cancer compared to inherited null mutations or the G245S mutation (Hanel et al., 2013). These findings suggest that the R248Q p53 functions in a different manner than other p53 mutants that have been studied so far. Remarkably, not only the position of the mutation, but also the nature of the substitution may influence the activity of the resulting mutant protein. For example, both R248Q and R248W are structural mutants, but the humanized R248W p53 knock-in mouse does not display reduced lifespan or earlier disease onset (Song et al., 2007). Understanding the consequences of each p53 mutation in relationship to disease progression and response to therapy therefore promises to be an extremely complex undertaking.

Consequences of Mutant p53 Expression to Tumor Therapy

The realization that loss of p53 and expression of mutant p53 may not be analogous has also raised the question of whether the presence of a mutant p53 protein may affect the response to therapy. Whereas there is evidence that the presence of mutant p53 may dampen the response to restoration of wild-type p53 (Wang et al., 2011), reflecting a dominant negative activity of mutant p53, more recent studies have indicated that the retention of wild-type p53 can be detrimental to the therapeutic response in breast cancer. This effect is seen in tumors that express both mutant and wild-type p53 alleles (Jackson et al., 2012). Such studies highlight the possibility that in some

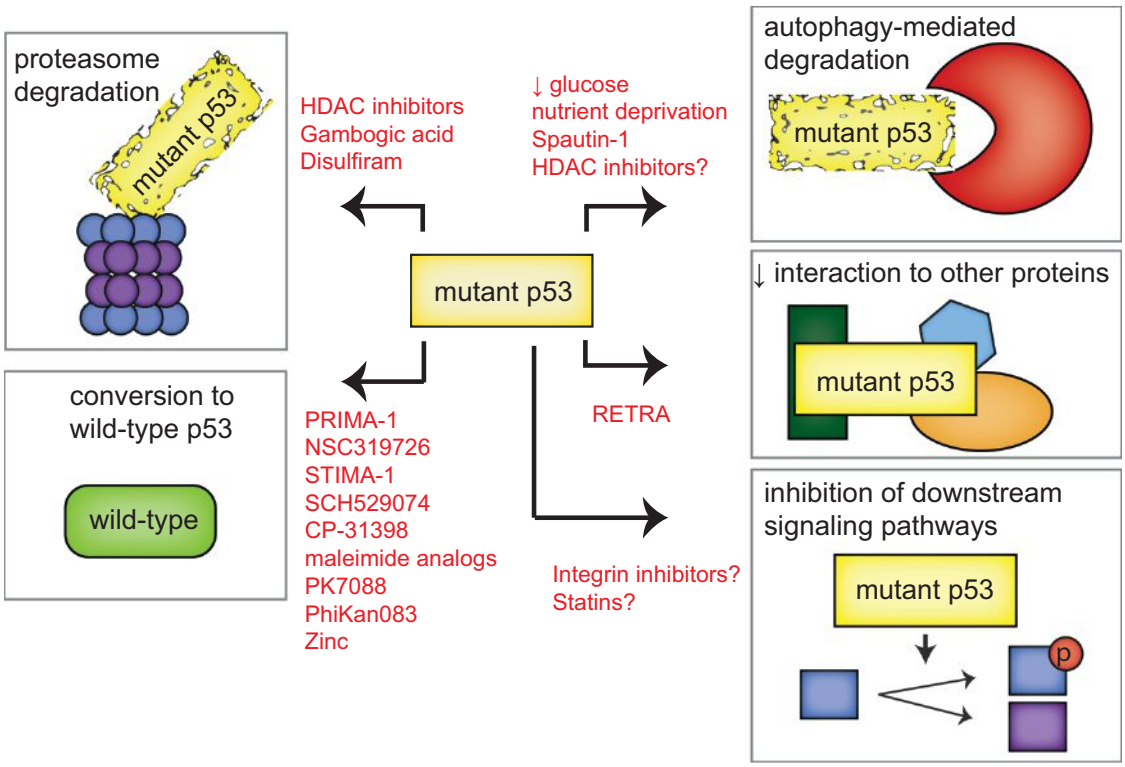

Figure 1. Strategies that Are Currently Being Explored to Target Mutant p53
Depicted in red are schematics of the strategies that are currently being explored to target p53 mutant-expressing cancers. These strategies include promotion of mutant p53 degradation through the proteasome and autophagy pathways, restoration of wild-type p53 activity, interference with the interaction between mutant p53 and other proteins, and interference in signaling pathways downstream of mutant p53.

tumor types wild-type p53 can be dominant over mutant, and that studies of patient response based on p53 status must take into account heterozygosity at the *TP53* locus, as well as the presence of mutant or wild-type p53 (Jackson and Lozano, 2013).

Therapeutic Strategies to Restore Wild-Type Activity to Mutant p53

With so many different mutations and phenotypes it is not surprising that a variety of strategies are being explored to target tumors expressing mutant p53s (summarized in Figure 1). Wild-type p53 is a potent inducer of apoptosis and senescence when expressed in tumor cells, making the reactivation of some level of wild-type function in mutant p53 (which is generally expressed at high levels in cancer cells) an attractive therapeutic avenue. Interestingly, loss of wild-type function introduced by some destabilizing tumor-derived mutations can be rescued by additional point mutations that serve to stabilize the conformation of p53 protein, showing that the loss of structure is intrinsically reversible (Joerger and Fersht, 2008). In addition, a variety of compounds that might restore wild-type p53 function have been characterized and are reviewed in several recent publications (Lehmann and Pietenpol, 2012; Maslon and Hupp, 2010; Wiman, 2010). Small molecules that bind to a site in p53 formed in the Y220C mutant (PhiKan083 and PK7088) function by stabilizing the structure of this mutant p53, and so increasing the level of p53 with a wild-type conformation and activity (Boeckler et al., 2008; Liu et al., 2013). Other compounds bind to multiple mutant p53 proteins (e.g., PRIMA-1, or the soluble derivative PRIMA-met/APR-246, CP-31398, and SCH29074; Bykov et al., 2002; Demma et al., 2010; Foster et al., 1999), interacting with the DNA binding domain, thereby promoting proper folding of the mutant protein and restoration of p53 function. However, the precise mechanistic function of these compounds and others, such as maleimide analogs and STIMA-1, remain to be elucidated (Bykov et al., 2005; Zache et al., 2008).

Whereas wild-type p53 requires binding to the metal ion Zn(2+) to fold correctly (Loh, 2010; Verhaegh et al., 1998), the R175H p53 mutant was found to be impaired in zinc binding (Butler and Loh, 2003). Loss of metallothioneins that chelate and store intracellular zinc promotes a wild-type conformation of misfolded p53 (Puca et al., 2009) and addition of zinc to the conformational mutants G245C and G245D p53 partially restored the wild-type conformation (Pintus et al., 2013). The potential use of zinc to recover wild-type folding has therefore been explored and this approach has been shown to restore chemosensitivity to anticancer drugs in cells expressing endogenous mutant p53 (Puca et al., 2011). In addition, the thiosemicarbazone metal ion chelator NSC31926 was found to restore wild-type function in a variety of different mutant p53-expressing cell lines, possibly through increasing the bioavailability of zinc to (mutant) p53 (Yu et al., 2012).

Of all the compounds that restore wild-type activity, the most progress has been made with PRIMA-1 analogs, with the

demonstration of safety in a phase I clinical study (Lehmann et al., 2012). PRIMA-1 is rapidly converted to other compounds, including MQ, which can bind to both mutant p53 and wild-type p53 (Lambert et al., 2009), although the precise mechanisms underlying the p53 reactivation are currently unknown. Under some circumstances, p53 can adopt an unfolded conformation and behave like a mutant p53 protein to promote invasion (Trinidad et al., 2013). Unfolded wild-type p53 seen in tumor cells grown under hypoxia (Gogna et al., 2012) could be restored by PRIMA-1 treatment (Rieber and Strasberg-Rieber, 2012). It will therefore be interesting to explore whether both wild-type and mutant p53 tumors might benefit from PRIMA-1 treatment.

Therapeutic Strategies to Promote Mutant p53 Degradation

An alternative approach to targeting mutant p53 is to remove the proteins by enhancing turnover (Figure 1). Both wild-type and mutant p53 can be targeted for proteasomal degradation in otherwise normal cells by the ubiquitin ligase MDM2. Inhibition of MDM2 in response to stress underlies the activation of wild-type p53, but is also thought to lead to the overexpression of mutant p53 seen in cancer cells. Indeed, stress induced stabilization of mutant p53 seems to be a prerequisite for its GOF (Suh et al., 2011). In addition to MDM2, another chaperone-associated E3 ubiquitin ligase, CHIP, was shown to be important for mutant p53 degradation (Esser et al., 2005; Lukashchuk and Vousden, 2007). To be stabilized, mutant p53 interacts with the Hsp70 and Hsp90 chaperone complex that requires an interaction with HDAC6 for proper functioning (Li et al., 2011b). Abrogation of HDAC6 binding results in the dissociation of the heat shock proteins from mutant p53 and allows for mutant p53 degradation by MDM2 and CHIP (Li et al., 2011b). HDAC inhibitors such as SAHA show promise in destabilizing mutant p53 by preventing HDAC6 from interacting with Hsp90 (Li et al., 2011a). However, SAHA and the pan-HDAC inhibitor NaB were recently shown to not only regulate mutant p53 stability, but also its transcription via the p53 activator HoxA5 (Yan et al., 2013). This activity was not confined to mutant p53 and also extended to decreasing wild-type p53 expression (Yan et al., 2013), indicating that care should be taken to determine the p53 status of tumors when HDAC inhibitors are used as therapeutic agents. Small molecule activators of SIRT1 have also been shown to lead to the deacetylation of p53 and reduction of overall mutant p53 levels (Yi et al., 2013). In other studies, Stathmin—a transcriptional target of wild-type p53 and mutant p53 (through the regulation of miR-223)—promoted mutant p53 activity by regulating phosphorylation and stability in ovarian cancers (Sonego et al., 2013).

Autophagy also plays a role in mutant p53 degradation. Macro-autophagy is the process by which intracellular contents such as proteins or organelles are engulfed and degraded through lysosomes. This can provide a means to recycling intracellular content, providing an alternative energy source to allow cells to survive transient starvation, and also functioning to remove damaged or excess organelles (Mizushima et al., 2008). The role of autophagy in cancer is complex and can both promote and inhibit tumor development, depending on the targets of the autophagic process and the timing during tumor evolution (Liu and Ryan, 2012). Macro-autophagy induced by glucose restriction selectively promoted mutant p53 degradation, whereas wild-type p53 was stabilized under similar conditions (Rodriguez et al., 2012). The degradation of mutant p53 was promoted by proteasomal inhibition and depended on functional autophagy machinery (Choudhury et al., 2013; Rodriguez et al., 2012). Glucose starvation combined with confluent growth conditions could promote mutant p53 degradation by a specialized form of autophagy known as chaperone-mediated autophagy (Vakifahmetoglu-Norberg et al., 2013). In contrast to the findings of Rodriguez et al. (2012), degradation of mutant p53 via this specialized autophagy pathway was enhanced by inhibition of macro-autophagy (Vakifahmetoglu-Norberg et al., 2013), suggesting conditional aspects to glucose deprived mutant p53 degradation. Furthermore, both mutant and wild-type p53 can inhibit autophagy when localized in the cytoplasm (Morselli et al., 2008; Tasdemir et al., 2008), indicating that the relationship between autophagy and mutant p53 is complex.

Therefore, while targeting mutant p53 for degradation seems feasible, there remains a concern as to how effective simple removal of mutant p53 (without replacement by degradation-resistant wild-type p53) might be in driving a therapeutic response. Some comfort has been provided by many studies showing reduction of mutant p53 levels (either by siRNA or spautin treatment) results in increased apoptosis, indicating that these cells may have become dependent on mutant p53 for their survival (Table 1; Ali et al., 2013; Braicu et al., 2013; Huang et al., 2013; Hui et al., 2006; Lim et al., 2009; Vakifahmetoglu-Norberg et al., 2013; Xie et al., 2013; Zhu et al., 2011, 2013). However, whether decreasing mutant p53 levels is sufficient as a means of therapy in vivo and in the long term requires confirmation.

Targeting Mutant p53 Regulated Pathways

Instead of targeting mutant p53 directly, another approach is to identify commonalities in the mechanisms through which mutant p53 proteins function and to target and exploit these downstream pathways (Figure 1). Despite the clear differences between mutant p53s, a large number of them interact and inhibit p63 and p73. A small molecule named RETRA, identified by serendipity in a screen to identify drugs to stabilize wild-type p53, has been suggested to destabilize the p73 mutant p53 interaction (Kravchenko et al., 2008). RETRA-induced release of p73 resulted in the activation of p73 target genes and a concomitant decreased tumor cell survival and suppression of xenograft tumor growth (Kravchenko et al., 2008). Whether RETRA impairs the interaction of mutant p53s with other target proteins has not been reported, but this could be a more general approach to block the oncogenic effect of mutant p53s that share binding partners.

Downstream pathways activated by mutant p53 may also be targets for therapeutic intervention. An attractive possibility here is the cholesterol synthesis pathway through which mutant p53 disrupts the morphology of mammary tumors (Freed-Pastor et al., 2012). Inhibition of cholesterol synthesis restored the morphology and decreased survival of mutant p53 cells (Freed-Pastor et al., 2012). This is of particular interest because statins (cholesterol inhibitors) are among the most commonly prescribed drugs worldwide to prevent cardiovascular diseases and have shown promise as preventive anticancer agents (Singh

and Singh, 2013). It will therefore be interesting and relatively straightforward to determine the utility of statins as a therapeutic strategy for mutant p53 tumors.

Finally, several studies have described a role for mutant p53 in enhancing receptor tyrosine kinase (RTK) signaling (Adorno et al., 2009; Muller et al., 2009; Sauer et al., 2010; Wang et al., 2013a). A multitude of inhibitors of the kinase activity of RTKs or their downstream mediators have been described, including EGFR inhibitors, MET inhibitors and MAPK inhibitors. Selective efficacy of these compounds in the treatment of mutant p53 expressing cancers remains to be explored. The specific role of RTK and integrin recycling may also provide an additional attractive target, since various integrin antibodies and drugs that inhibit integrin recycling are currently on the market and have shown some promise as anticancer agents (Desgrosellier and Cheresh, 2010).

Future Directions

A number of hurdles still need to be overcome before the studies of mutant p53 can be translated into clinical practice. While there is clear evidence that mutant p53 promotes various oncogenic responses, the relative importance of survival, motility, invasion, and metabolic changes, or the critical pathways through which these responses are mediated remain unclear. How different mutations affect p53 function also remains underexplored, as does the comparative importance of loss of wild-type, dominant-negative, and GOF phenotypes. The fact that most mutant p53s are expressed at very high levels in cancer cells (leading to the immunohistochemical detection of p53 being used as a proxy for the presence of mutant p53) makes these proteins tremendously attractive therapeutic targets, and the efficacy of inhibiting the activity of these mutant p53s or even re-establishing some wild-type function, as described above, holds great promise. Such approaches depend, however, on designing efficient mechanisms through which to target mutant p53, an understanding of the activities and function of the many different mutants, and the capacity to identify which mutation a tumor carries (the latter likely to be the most easily attainable goal).

Maybe a more effective approach will be to explore the possibility of synthetic lethality as a therapeutic strategy. Recently, a computational approach using gene expression from the NCI-60 panel, the GBM (glioblastoma multiforme) project and the TCGA (the cancer genome) project revealed a number of genes and pathways that may result in synthetic lethality when targeted in mutant p53-expressing tumors (Wang and Simon, 2013). The majority of these genes were involved in the cell cycle, perhaps reflecting the loss of wild-type p53 function, and an interesting candidate identified in several of the data sets is polo-like kinase 1 (PLK1), which is involved in the regulation of mitosis. PLK1 was found to be upregulated in breast cancers with mutant p53 expression; the presence of both coincided with a worse prognosis than cancers with either PLK1 upregulation or mutant p53 expression alone (King et al., 2012). Because PLK1 can be inhibited by a variety of compounds (Strebhardt, 2010), it will be interesting to follow up this lead.

Conclusions

Recent data reveal that mutant p53 is not just one protein, but a multitude of proteins that can contribute to a wide range of oncogenic processes. Designing drug strategies to target mutant p53 tumors is therefore highly challenging and will require a deeper understanding of the degradation pathways, interaction partners, and downstream signaling pathways in mutant p53 cells. However, we are optimistic that our ever-expanding knowledge of mutant p53 function will translate into some useful therapeutic strategies in the future.

ACKNOWLEDGMENTS

We thank Cancer Research UK, AICR, and the Royal Society/Wellcome trust for funding support.

REFERENCES

Acin, S., Li, Z., Mejia, O., Roop, D.R., El-Naggar, A.K., and Caulin, C. (2011). Gain-of-function mutant p53 but not p53 deletion promotes head and neck cancer progression in response to oncogenic K-ras. J. Pathol. *225*, 479–489.

Addadi, Y., Moskovits, N., Granot, D., Lozano, G., Carmi, Y., Apte, R.N., Neeman, M., and Oren, M. (2010). p53 status in stromal fibroblasts modulates tumor growth in an SDF1-dependent manner. Cancer Res. *70*, 9650–9658.

Adorno, M., Cordenonsi, M., Montagner, M., Dupont, S., Wong, C., Hann, B., Solari, A., Bobisse, S., Rondina, M.B., Guzzardo, V., et al. (2009). A Mutant-p53/Smad complex opposes p63 to empower TGFbeta-induced metastasis. Cell *137*, 87–98.

Agapova, L.S., Ilyinskaya, G.V., Turovets, N.A., Ivanov, A.V., Chumakov, P.M., and Kopnin, B.P. (1996). Chromosome changes caused by alterations of p53 expression. Mutat. Res. *354*, 129–138.

Ali, A., Wang, Z., Fu, J., Ji, L., Liu, J., Li, L., Wang, H., Chen, J., Caulin, C., Myers, J.N., et al. (2013). Differential regulation of the REGgamma-proteasome pathway by p53/TGF-beta signalling and mutant p53 in cancer cells. Nature communications *4*, 2667.

Atema, A., and Chène, P. (2002). The gain of function of the p53 mutant Asp281Gly is dependent on its ability to form tetramers. Cancer Lett. *185*, 103–109.

Bhowmick, N.A., Neilson, E.G., and Moses, H.L. (2004). Stromal fibroblasts in cancer initiation and progression. Nature *432*, 332–337.

Blandino, G., Levine, A.J., and Oren, M. (1999). Mutant p53 gain of function: differential effects of different p53 mutants on resistance of cultured cells to chemotherapy. Oncogene *18*, 477–485.

Boeckler, F.M., Joerger, A.C., Jaggi, G., Rutherford, T.J., Veprintsev, D.B., and Fersht, A.R. (2008). Targeted rescue of a destabilized mutant of p53 by an in silico screened drug. Proc. Natl. Acad. Sci. USA *105*, 10360–10365.

Bossi, G., Lapi, E., Strano, S., Rinaldo, C., Blandino, G., and Sacchi, A. (2006). Mutant p53 gain of function: reduction of tumor malignancy of human cancer cell lines through abrogation of mutant p53 expression. Oncogene *25*, 304–309.

Bossi, G., Marampon, F., Maor-Aloni, R., Zani, B., Rotter, V., Oren, M., Strano, S., Blandino, G., and Sacchi, A. (2008). Conditional RNA interference in vivo to study mutant p53 oncogenic gain of function on tumor malignancy. Cell Cycle *7*, 1870–1879.

Bougeard, G., Sesboüé, R., Baert-Desurmont, S., Vasseur, S., Martin, C., Tinat, J., Brugières, L., Chompret, A., de Paillerets, B.B., Stoppa-Lyonnet, D., et al.; French LFS working group (2008). Molecular basis of the Li-Fraumeni syndrome: an update from the French LFS families. J. Med. Genet. *45*, 535–538.

Braicu, C., Pileczki, V., Irimie, A., and Berindan-Neagoe, I. (2013). p53siRNA therapy reduces cell proliferation, migration and induces apoptosis in triple negative breast cancer cells. Mol. Cell. Biochem. *381*, 61–68.

Brázdová, M., Navrátilová, L., Tichý, V., Němcová, K., Lexa, M., Hrstka, R., Pečinka, P., Adámik, M., Vojtesek, B., Paleček, E., et al. (2013). Preferential binding of hot spot mutant p53 proteins to supercoiled DNA in vitro and in cells. PLoS ONE *8*, e59567.

Buganim, Y., Kalo, E., Brosh, R., Besserglick, H., Nachmany, I., Rais, Y., Stambolsky, P., Tang, X., Milyavsky, M., Shats, I., et al. (2006). Mutant p53 protects cells from 12-O-tetradecanoylphorbol-13-acetate-induced death by attenuating activating transcription factor 3 induction. Cancer Res. *66*, 10750–10759.

Butler, J.S., and Loh, S.N. (2003). Structure, function, and aggregation of the zinc-free form of the p53 DNA binding domain. Biochemistry *42*, 2396–2403.

Bykov, V.J., Issaeva, N., Shilov, A., Hultcrantz, M., Pugacheva, E., Chumakov, P., Bergman, J., Wiman, K.G., and Selivanova, G. (2002). Restoration of the tumor suppressor function to mutant p53 by a low-molecular-weight compound. Nat. Med. *8*, 282–288.

Bykov, V.J., Issaeva, N., Zache, N., Shilov, A., Hultcrantz, M., Bergman, J., Selivanova, G., and Wiman, K.G. (2005). Reactivation of mutant p53 and induction of apoptosis in human tumor cells by maleimide analogs. J. Biol. Chem. *280*, 30384–30391.

Capponcelli, S., Pedrini, E., Cerone, M.A., Corti, V., Fontanesi, S., Alessio, M., Bachi, A., Soddu, S., Ribatti, D., Picci, P., et al. (2005). Evaluation of the molecular mechanisms involved in the gain of function of a Li-Fraumeni TP53 mutation. Hum. Mutat. *26*, 94–103.

Chee, J.L., Saidin, S., Lane, D.P., Leong, S.M., Noll, J.E., Neilsen, P.M., Phua, Y.T., Gabra, H., and Lim, T.M. (2013). Wild-type and mutant p53 mediate cisplatin resistance through interaction and inhibition of active caspase-9. Cell Cycle *12*, 278–288.

Chicas, A., Molina, P., and Bargonetti, J. (2000). Mutant p53 forms a complex with Sp1 on HIV-LTR DNA. Biochem. Biophys. Res. Commun. *279*, 383–390.

Choudhury, S., Kolukula, V.K., Preet, A., Albanese, C., and Avantaggiati, M.L. (2013). Dissecting the pathways that destabilize mutant p53: the proteasome or autophagy? Cell Cycle *12*, 1022–1029.

Coffill, C.R., Muller, P.A., Oh, H.K., Neo, S.P., Hogue, K.A., Cheok, C.F., Vousden, K.H., Lane, D.P., Blackstock, W.P., and Gunaratne, J. (2012). Mutant p53 interactome identifies nardilysin as a p53R273H-specific binding partner that promotes invasion. EMBO Rep. *13*, 638–644.

Cooks, T., Pateras, I.S., Tarcic, O., Solomon, H., Schetter, A.J., Wilder, S., Lozano, G., Pikarsky, E., Forshew, T., Rosenfeld, N., et al. (2013). Mutant p53 prolongs NF-κB activation and promotes chronic inflammation and inflammation-associated colorectal cancer. Cancer Cell *23*, 634–646.

Demma, M., Maxwell, E., Ramos, R., Liang, L., Li, C., Hesk, D., Rossman, R., Mallams, A., Doll, R., Liu, M., et al. (2010). SCH529074, a small molecule activator of mutant p53, which binds p53 DNA binding domain (DBD), restores growth-suppressive function to mutant p53 and interrupts HDM2-mediated ubiquitination of wild type p53. J. Biol. Chem. *285*, 10198–10212.

Desgrosellier, J.S., and Cheresh, D.A. (2010). Integrins in cancer: biological implications and therapeutic opportunities. Nat. Rev. Cancer *10*, 9–22.

Di Agostino, S., Strano, S., Emiliozzi, V., Zerbini, V., Mottolese, M., Sacchi, A., Blandino, G., and Piaggio, G. (2006). Gain of function of mutant p53: the mutant p53/NF-Y protein complex reveals an aberrant transcriptional mechanism of cell cycle regulation. Cancer Cell *10*, 191–202.

Di Como, C.J., Gaiddon, C., and Prives, C. (1999). p73 function is inhibited by tumor-derived p53 mutants in mammalian cells. Mol. Cell. Biol. *19*, 1438–1449.

Dittmer, D., Pati, S., Zambetti, G., Chu, S., Teresky, A.K., Moore, M., Finlay, C., and Levine, A.J. (1993). Gain of function mutations in p53. Nat. Genet. *4*, 42–46.

Do, P.M., Varanasi, L., Fan, S., Li, C., Kubacka, I., Newman, V., Chauhan, K., Daniels, S.R., Boccetta, M., Garrett, M.R., et al. (2012). Mutant p53 cooperates with ETS2 to promote etoposide resistance. Genes Dev. *26*, 830–845.

Dong, P., Xu, Z., Jia, N., Li, D., and Feng, Y. (2009). Elevated expression of p53 gain-of-function mutation R175H in endometrial cancer cells can increase the invasive phenotypes by activation of the EGFR/PI3K/AKT pathway. Mol. Cancer *8*, 103.

Dong, P., Karaayvaz, M., Jia, N., Kaneuchi, M., Hamada, J., Watari, H., Sudo, S., Ju, J., and Sakuragi, N. (2012). Mutant p53 gain-of-function induces epithelial-mesenchymal transition through modulation of the miR-130b-ZEB1 axis. Oncogene.

Doyle, B., Morton, J.P., Delaney, D.W., Ridgway, R.A., Wilkins, J.A., and Sansom, O.J. (2010). p53 mutation and loss have different effects on tumourigenesis in a novel mouse model of pleomorphic rhabdomyosarcoma. J. Pathol. *222*, 129–137.

Dumay, A., Feugeas, J.P., Wittmer, E., Lehmann-Che, J., Bertheau, P., Espie, M., Plassa, L.F., Cottu, P., Marty, M., Andre, F., et al. (2013). Distinct tumor protein p53 mutants in breast cancer subgroups. International journal of cancer Journal international du cancer *132*, 1227–1231.

El-Hizawi, S., Lagowski, J.P., Kulesz-Martin, M., and Albor, A. (2002). Induction of gene amplification as a gain-of-function phenotype of mutant p53 proteins. Cancer Res. *62*, 3264–3270.

Esser, C., Scheffner, M., and Höhfeld, J. (2005). The chaperone-associated ubiquitin ligase CHIP is able to target p53 for proteasomal degradation. J. Biol. Chem. *280*, 27443–27448.

Fontemaggi, G., Dell'Orso, S., Trisciuoglio, D., Shay, T., Melucci, E., Fazi, F., Terrenato, I., Mottolese, M., Muti, P., Domany, E., et al. (2009). The execution of the transcriptional axis mutant p53, E2F1 and ID4 promotes tumor neoangiogenesis. Nat. Struct. Mol. Biol. *16*, 1086–1093.

Foster, B.A., Coffey, H.A., Morin, M.J., and Rastinejad, F. (1999). Pharmacological rescue of mutant p53 conformation and function. Science *286*, 2507–2510.

Frank, A.K., Pietsch, E.C., Dumont, P., Tao, J., and Murphy, M.E. (2011). Wild-type and mutant p53 proteins interact with mitochondrial caspase-3. Cancer Biol. Ther. *11*, 740–745.

Freed-Pastor, W.A., and Prives, C. (2012). Mutant p53: one name, many proteins. Genes Dev. *26*, 1268–1286.

Freed-Pastor, W.A., Mizuno, H., Zhao, X., Langerød, A., Moon, S.H., Rodriguez-Barrueco, R., Barsotti, A., Chicas, A., Li, W., Polotskaia, A., et al. (2012). Mutant p53 disrupts mammary tissue architecture via the mevalonate pathway. Cell *148*, 244–258.

Gaiddon, C., Lokshin, M., Ahn, J., Zhang, T., and Prives, C. (2001). A subset of tumor-derived mutant forms of p53 down-regulate p63 and p73 through a direct interaction with the p53 core domain. Mol. Cell. Biol. *21*, 1874–1887.

Gerwin, B.I., Spillare, E., Forrester, K., Lehman, T.A., Kispert, J., Welsh, J.A., Pfeifer, A.M., Lechner, J.F., Baker, S.J., Vogelstein, B., et al. (1992). Mutant p53 can induce tumorigenic conversion of human bronchial epithelial cells and reduce their responsiveness to a negative growth factor, transforming growth factor beta 1. Proc. Natl. Acad. Sci. USA *89*, 2759–2763.

Girardini, J.E., Napoli, M., Piazza, S., Rustighi, A., Marotta, C., Radaelli, E., Capaci, V., Jordan, L., Quinlan, P., Thompson, A., et al. (2011). A Pin1/mutant p53 axis promotes aggressiveness in breast cancer. Cancer Cell *20*, 79–91.

Gloushankova, N., Ossovskaya, V., Vasiliev, J., Chumakov, P., and Kopnin, B. (1997). Changes in p53 expression can modify cell shape of ras-transformed fibroblasts and epitheliocytes. Oncogene *15*, 2985–2989.

Gogna, R., Madan, E., Kuppusamy, P., and Pati, U. (2012). Chaperoning of mutant p53 protein by wild-type p53 protein causes hypoxic tumor regression. J. Biol. Chem. *287*, 2907–2914.

Göhler, T., Jäger, S., Warnecke, G., Yasuda, H., Kim, E., and Deppert, W. (2005). Mutant p53 proteins bind DNA in a DNA structure-selective mode. Nucleic Acids Res. *33*, 1087–1100.

Grugan, K.D., Vega, M.E., Wong, G.S., Diehl, J.A., Bass, A.J., Wong, K.K., Nakagawa, H., and Rustgi, A.K. (2013). A common p53 mutation (R175H) activates c-Met receptor tyrosine kinase to enhance tumor cell invasion. Cancer Biol. Ther. *14*, 14.

Gualberto, A., Aldape, K., Kozakiewicz, K., and Tlsty, T.D. (1998). An oncogenic form of p53 confers a dominant, gain-of-function phenotype that disrupts spindle checkpoint control. Proc. Natl. Acad. Sci. USA *95*, 5166–5171.

Gurova, K.V., Rokhlin, O.W., Budanov, A.V., Burdelya, L.G., Chumakov, P.M., Cohen, M.B., and Gudkov, A.V. (2003). Cooperation of two mutant p53 alleles contributes to Fas resistance of prostate carcinoma cells. Cancer Res. *63*, 2905–2912.

Gurtner, A., Starace, G., Norelli, G., Piaggio, G., Sacchi, A., and Bossi, G. (2010). Mutant p53-induced up-regulation of mitogen-activated protein kinase kinase 3 contributes to gain of function. J. Biol. Chem. *285*, 14160–14169.

Halevy, O., Michalovitz, D., and Oren, M. (1990). Different tumor-derived p53 mutants exhibit distinct biological activities. Science *250*, 113–116.

Hanel, W., Marchenko, N., Xu, S., Yu, S.X., Weng, W., and Moll, U. (2013). Two hot spot mutant p53 mouse models display differential gain of function in tumorigenesis. Cell Death Differ. *20*, 898–909.

Hsiao, M., Low, J., Dorn, E., Ku, D., Pattengale, P., Yeargin, J., and Haas, M. (1994). Gain-of-function mutations of the p53 gene induce lymphohematopoietic metastatic potential and tissue invasiveness. Am. J. Pathol. *145*, 702–714.

Huang, X., Zhang, Y., Tang, Y., Butler, N., Kim, J., Guessous, F., Schiff, D., Mandell, J., and Abounader, R. (2013). A novel PTEN/mutant p53/c-Myc/Bcl-XL axis mediates context-dependent oncogenic effects of PTEN with implications for cancer prognosis and therapy. Neoplasia *15*, 952–965.

Hui, L., Zheng, Y., Yan, Y., Bargonetti, J., and Foster, D.A. (2006). Mutant p53 in MDA-MB-231 breast cancer cells is stabilized by elevated phospholipase D activity and contributes to survival signals generated by phospholipase D. Oncogene *25*, 7305–7310.

Jackson, J.G., and Lozano, G. (2013). The mutant p53 mouse as a pre-clinical model. Oncogene *32*, 4325–4330.

Jackson, E.L., Olive, K.P., Tuveson, D.A., Bronson, R., Crowley, D., Brown, M., and Jacks, T. (2005). The differential effects of mutant p53 alleles on advanced murine lung cancer. Cancer Res. *65*, 10280–10288.

Jackson, J.G., Pant, V., Li, Q., Chang, L.L., Quintás-Cardama, A., Garza, D., Tavana, O., Yang, P., Manshouri, T., Li, Y., et al. (2012). p53-mediated senescence impairs the apoptotic response to chemotherapy and clinical outcome in breast cancer. Cancer Cell *21*, 793–806.

Jia, S., Zhao, L., Tang, W., and Luo, Y. (2012). The gain of function of p53 mutant p53S in promoting tumorigenesis by cross-talking with H-RasV12. Int. J. Biol. Sci. *8*, 596–605.

Joerger, A.C., and Fersht, A.R. (2007). Structure-function-rescue: the diverse nature of common p53 cancer mutants. Oncogene *26*, 2226–2242.

Joerger, A.C., and Fersht, A.R. (2008). Structural biology of the tumor suppressor p53. Annu. Rev. Biochem. *77*, 557–582.

Kalo, E., Kogan-Sakin, I., Solomon, H., Bar-Nathan, E., Shay, M., Shetzer, Y., Dekel, E., Goldfinger, N., Buganim, Y., Stambolsky, P., et al. (2012). Mutant p53R273H attenuates the expression of phase 2 detoxifying enzymes and promotes the survival of cells with high levels of reactive oxygen species. J. Cell Sci. *125*, 5578–5586.

Kandoth, C., McLellan, M.D., Vandin, F., Ye, K., Niu, B., Lu, C., Xie, M., Zhang, Q., McMichael, J.F., Wyczalkowski, M.A., et al. (2013). Mutational landscape and significance across 12 major cancer types. Nature *502*, 333–339.

Kawamata, H., Omotehara, F., Nakashiro, K., Uchida, D., Shinagawa, Y., Tachibana, M., Imai, Y., and Fujimori, T. (2007). Oncogenic mutation of the p53 gene derived from head and neck cancer prevents cells from undergoing apoptosis after DNA damage. Int. J. Oncol. *30*, 1089–1097.

Kawamura, T., Suzuki, J., Wang, Y.V., Menendez, S., Morera, L.B., Raya, A., Wahl, G.M., and Izpisúa Belmonte, J.C. (2009). Linking the p53 tumour suppressor pathway to somatic cell reprogramming. Nature *460*, 1140–1144.

King, S.I., Purdie, C.A., Bray, S.E., Quinlan, P.R., Jordan, L.B., Thompson, A.M., and Meek, D.W. (2012). Immunohistochemical detection of Polo-like kinase-1 (PLK1) in primary breast cancer is associated with TP53 mutation and poor clinical outcom. Breast Cancer Res. *14*, R40.

Kravchenko, J.E., Ilyinskaya, G.V., Komarov, P.G., Agapova, L.S., Kochetkov, D.V., Strom, E., Frolova, E.I., Kovriga, I., Gudkov, A.V., Feinstein, E., and Chumakov, P.M. (2008). Small-molecule RETRA suppresses mutant p53-bearing cancer cells through a p73-dependent salvage pathway. Proc. Natl. Acad. Sci. USA *105*, 6302–6307.

Lambert, J.M., Gorzov, P., Veprintsev, D.B., Söderqvist, M., Segerbäck, D., Bergman, J., Fersht, A.R., Hainaut, P., Wiman, K.G., and Bykov, V.J. (2009). PRIMA-1 reactivates mutant p53 by covalent binding to the core domain. Cancer Cell *15*, 376–388.

Lang, G.A., Iwakuma, T., Suh, Y.A., Liu, G., Rao, V.A., Parant, J.M., Valentin-Vega, Y.A., Terzian, T., Caldwell, L.C., Strong, L.C., et al. (2004). Gain of function of a p53 hot spot mutation in a mouse model of Li-Fraumeni syndrome. Cell *119*, 861–872.

Lányi, A., Deb, D., Seymour, R.C., Ludes-Meyers, J.H., Subler, M.A., and Deb, S. (1998). 'Gain of function' phenotype of tumor-derived mutant p53 requires the oligomerization/nonsequence-specific nucleic acid-binding domain. Oncogene *16*, 3169–3176.

Lee, M.K., Teoh, W.W., Phang, B.H., Tong, W.M., Wang, Z.Q., and Sabapathy, K. (2012). Cell-type, dose, and mutation-type specificity dictate mutant p53 functions in vivo. Cancer Cell *22*, 751–764.

Lehmann, B.D., and Pietenpol, J.A. (2012). Targeting mutant p53 in human tumors. Journal of clinical oncology: official journal of the American Society of Clinical Oncology *30*, 3648–3650.

Lehmann, S., Bykov, V.J., Ali, D., Andren, O., Cherif, H., Tidefelt, U., Uggla, B., Yachnin, J., Juliusson, G., Moshfegh, A., et al. (2012). Targeting p53 in vivo: a first-in-human study with p53-targeting compound APR-246 in refractory hematologic malignancies and prostate cancer. J Clin Oncol. *30*, 3633–3639.

Leroy, B., Fournier, J.L., Ishioka, C., Monti, P., Inga, A., Fronza, G., and Soussi, T. (2013). The TP53 website: an integrative resource centre for the TP53 mutation database and TP53 mutant analysis. Nucleic Acids Res. *41* (Database issue), D962–D969.

Li, R., Sutphin, P.D., Schwartz, D., Matas, D., Almog, N., Wolkowicz, R., Goldfinger, N., Pei, H., Prokocimer, M., and Rotter, V. (1998). Mutant p53 protein expression interferes with p53-independent apoptotic pathways. Oncogene *16*, 3269–3277.

Li, D., Marchenko, N.D., and Moll, U.M. (2011a). SAHA shows preferential cytotoxicity in mutant p53 cancer cells by destabilizing mutant p53 through inhibition of the HDAC6-Hsp90 chaperone axis. Cell Death Differ. *18*, 1904–1913.

Li, D., Marchenko, N.D., Schulz, R., Fischer, V., Velasco-Hernandez, T., Talos, F., and Moll, U.M. (2011b). Functional inactivation of endogenous MDM2 and CHIP by HSP90 causes aberrant stabilization of mutant p53 in human cancer cells. Mol. Cancer Res. *9*, 577–588.

Lim, L.Y., Vidnovic, N., Ellisen, L.W., and Leong, C.O. (2009). Mutant p53 mediates survival of breast cancer cells. Br. J. Cancer *101*, 1606–1612.

Lin, C., Liang, Y., Zhu, H., Zhang, J., and Zhong, X. (2012). R280T mutation of p53 gene promotes proliferation of human glioma cells through GSK-3β/PTEN pathway. Neurosci. Lett. *529*, 60–65.

Liu, E.Y., and Ryan, K.M. (2012). Autophagy and cancer—issues we need to digest. J. Cell Sci. *125*, 2349–2358.

Liu, K., Ling, S., and Lin, W.C. (2011). TopBP1 mediates mutant p53 gain of function through NF-Y and p63/p73. Mol. Cell. Biol. *31*, 4464–4481.

Liu, X., Wilcken, R., Joerger, A.C., Chuckowree, I.S., Amin, J., Spencer, J., and Fersht, A.R. (2013). Small molecule induced reactivation of mutant p53 in cancer cells. Nucleic Acids Res. *41*, 6034–6044.

Loging, W.T., and Reisman, D. (1999). Elevated expression of ribosomal protein genes L37, RPP-1, and S2 in the presence of mutant p53. Cancer Epidemiol Biomarkers Prev. *8*, 1011–1016.

Loh, S.N. (2010). The missing zinc: p53 misfolding and cancer. Metallomics: integrated biometal science *2*, 442–449.

Lu, X., Liu, D.P., and Xu, Y. (2013). The gain of function of p53 cancer mutant in promoting mammary tumorigenesis. Oncogene *32*, 2900–2906.

Lukashchuk, N., and Vousden, K.H. (2007). Ubiquitination and degradation of mutant p53. Mol. Cell. Biol. *27*, 8284–8295.

Madar, S., Harel, E., Goldstein, I., Stein, Y., Kogan-Sakin, I., Kamer, I., Solomon, H., Dekel, E., Tal, P., Goldfinger, N., et al. (2013). Mutant p53 attenuates the anti-tumorigenic activity of fibroblasts-secreted interferon beta. PLoS ONE *8*, e61353.

Marión, R.M., Strati, K., Li, H., Murga, M., Blanco, R., Ortega, S., Fernandez-Capetillo, O., Serrano, M., and Blasco, M.A. (2009). A p53-mediated DNA damage response limits reprogramming to ensure iPS cell genomic integrity. Nature *460*, 1149–1153.

Maslon, M.M., and Hupp, T.R. (2010). Drug discovery and mutant p53. Trends Cell Biol. *20*, 542–555.

Matas, D., Sigal, A., Stambolsky, P., Milyavsky, M., Weisz, L., Schwartz, D., Goldfinger, N., and Rotter, V. (2001). Integrity of the N-terminal transcription

domain of p53 is required for mutant p53 interference with drug-induced apoptosis. EMBO J. *20*, 4163–4172.

Mizushima, N., Levine, B., Cuervo, A.M., and Klionsky, D.J. (2008). Autophagy fights disease through cellular self-digestion. Nature *451*, 1069–1075.

Morselli, E., Tasdemir, E., Maiuri, M.C., Galluzzi, L., Kepp, O., Criollo, A., Vicencio, J.M., Soussi, T., and Kroemer, G. (2008). Mutant p53 protein localized in the cytoplasm inhibits autophagy. Cell Cycle *7*, 3056–3061.

Morton, J.P., Timpson, P., Karim, S.A., Ridgway, R.A., Athineos, D., Doyle, B., Jamieson, N.B., Oien, K.A., Lowy, A.M., Brunton, V.G., et al. (2010). Mutant p53 drives metastasis and overcomes growth arrest/senescence in pancreatic cancer. Proc. Natl. Acad. Sci. USA *107*, 246–251.

Muller, P.A., and Vousden, K.H. (2013). p53 mutations in cancer. Nat. Cell Biol. *15*, 2–8.

Muller, P.A., Caswell, P.T., Doyle, B., Iwanicki, M.P., Tan, E.H., Karim, S., Lukashchuk, N., Gillespie, D.A., Ludwig, R.L., Gosselin, P., et al. (2009). Mutant p53 drives invasion by promoting integrin recycling. Cell *139*, 1327–1341.

Muller, P.A., Trinidad, A.G., Timpson, P., Morton, J.P., Zanivan, S., van den Berghe, P.V., Nixon, C., Karim, S.A., Caswell, P.T., Noll, J.E., et al. (2012). Mutant p53 enhances MET trafficking and signalling to drive cell scattering and invasion. Oncogene *32*, 1252–1265.

Murphy, K.L., Dennis, A.P., and Rosen, J.M. (2000). A gain of function p53 mutant promotes both genomic instability and cell survival in a novel p53-null mammary epithelial cell model. FASEB journal: official publication of the Federation of American Societies for Experimental Biology *14*, 2291–2302.

Narendran, A., Ganjavi, H., Morson, N., Connor, A., Barlow, J.W., Keystone, E., Malkin, D., and Freedman, M.H. (2003). Mutant p53 in bone marrow stromal cells increases VEGF expression and supports leukemia cell growth. Exp. Hematol. *31*, 693–701.

Neilsen, P.M., Noll, J.E., Mattiske, S., Bracken, C.P., Gregory, P.A., Schulz, R.B., Lim, S.P., Kumar, R., Suetani, R.J., Goodall, G.J., and Callen, D.F. (2012). Mutant p53 drives invasion in breast tumors through up-regulation of miR-155. Oncogene *32*, 2992–3000.

Nguyen, C.H., Lang, B.J., Chai, R.C., Vieusseux, J.L., Kouspou, M.M., and Price, J.T. (2013). Heat-shock factor 1 both positively and negatively affects cellular clonogenic growth depending on p53 status. Biochem. J. *452*, 321–329.

Noll, J.E., Jeffery, J., Al-Ejeh, F., Kumar, R., Khanna, K.K., Callen, D.F., and Neilsen, P.M. (2012). Mutant p53 drives multinucleation and invasion through a process that is suppressed by ANKRD11. Oncogene *31*, 2836–2848.

Olive, K.P., Tuveson, D.A., Ruhe, Z.C., Yin, B., Willis, N.A., Bronson, R.T., Crowley, D., and Jacks, T. (2004). Mutant p53 gain of function in two mouse models of Li-Fraumeni syndrome. Cell *119*, 847–860.

Ostman, A., and Augsten, M. (2009). Cancer-associated fibroblasts and tumor growth—bystanders turning into key players. Curr. Opin. Genet. Dev. *19*, 67–73.

Patocs, A., Zhang, L., Xu, Y., Weber, F., Caldes, T., Mutter, G.L., Platzer, P., and Eng, C. (2007). Breast-cancer stromal cells with TP53 mutations and nodal metastases. N. Engl. J. Med. *357*, 2543–2551.

Petitjean, A., Achatz, M.I., Borresen-Dale, A.L., Hainaut, P., and Olivier, M. (2007). TP53 mutations in human cancers: functional selection and impact on cancer prognosis and outcomes. Oncogene *26*, 2157–2165.

Pietras, K., and Ostman, A. (2010). Hallmarks of cancer: interactions with the tumor stroma. Exp. Cell Res. *316*, 1324–1331.

Pintus, S.S., Ivanisenko, N.V., Demenkov, P.S., Ivanisenko, T.V., Ramachandran, S., Kolchanov, N.A., and Ivanisenko, V.A. (2013). The substitutions G245C and G245D in the Zn(2+)-binding pocket of the p53 protein result in differences of conformational flexibility of the DNA-binding domain. J. Biomol. Struct. Dyn. *31*, 78–86.

Pohl, U., Wagenknecht, B., Naumann, U., and Weller, M. (1999). p53 enhances BAK and CD95 expression in human malignant glioma cells but does not enhance CD95L-induced apoptosis. Cellular physiology and biochemistry: international journal of experimental cellular physiology, biochemistry, and pharmacology *9*, 29–37.

Preuss, U., Kreutzfeld, R., and Scheidtmann, K.H. (2000). Tumor-derived p53 mutant C174Y is a gain-of-function mutant which activates the fos promoter and enhances colony formation. Int. J. Cancer *88*, 162–171.

Puca, R., Nardinocchi, L., Bossi, G., Sacchi, A., Rechavi, G., Givol, D., and D'Orazi, G. (2009). Restoring wtp53 activity in HIPK2 depleted MCF7 cells by modulating metallothionein and zinc. Exp. Cell Res. *315*, 67–75.

Puca, R., Nardinocchi, L., Porru, M., Simon, A.J., Rechavi, G., Leonetti, C., Givol, D., and D'Orazi, G. (2011). Restoring p53 active conformation by zinc increases the response of mutant p53 tumor cells to anticancer drugs. Cell Cycle *10*, 1679–1689.

Pugacheva, E.N., Ivanov, A.V., Kravchenko, J.E., Kopnin, B.P., Levine, A.J., and Chumakov, P.M. (2002). Novel gain of function activity of p53 mutants: activation of the dUTPase gene expression leading to resistance to 5-fluorouracil. Oncogene *21*, 4595–4600.

Quante, T., Otto, B., Brázdová, M., Kejnovská, I., Deppert, W., and Tolstonog, G.V. (2012). Mutant p53 is a transcriptional co-factor that binds to G-rich regulatory regions of active genes and generates transcriptional plasticity. Cell Cycle *11*, 3290–3303.

Restle, A., Färber, M., Baumann, C., Böhringer, M., Scheidtmann, K.H., Müller-Tidow, C., and Wiesmüller, L. (2008). Dissecting the role of p53 phosphorylation in homologous recombination provides new clues for gain-of-function mutants. Nucleic Acids Res. *36*, 5362–5375.

Rieber, M., and Strasberg-Rieber, M. (2012). Hypoxia, Mn-SOD and H(2)O(2) regulate p53 reactivation and PRIMA-1 toxicity irrespective of p53 status in human breast cancer cells. Biochem. Pharmacol. *84*, 1563–1570.

Rodriguez, O.C., Choudhury, S., Kolukula, V., Vietsch, E.E., Catania, J., Preet, A., Reynoso, K., Bargonetti, J., Wellstein, A., Albanese, C., and Avantaggiati, M.L. (2012). Dietary downregulation of mutant p53 levels via glucose restriction: mechanisms and implications for tumor therapy. Cell Cycle *11*, 4436–4446.

Roger, L., Jullien, L., Gire, V., and Roux, P. (2010). Gain of oncogenic function of p53 mutants regulates E-cadherin expression uncoupled from cell invasion in colon cancer cells. J. Cell Sci. *123*, 1295–1305.

Sarig, R., Rivlin, N., Brosh, R., Bornstein, C., Kamer, I., Ezra, O., Molchadsky, A., Goldfinger, N., Brenner, O., and Rotter, V. (2010). Mutant p53 facilitates somatic cell reprogramming and augments the malignant potential of reprogrammed cells. J. Exp. Med. *207*, 2127–2140.

Sauer, L., Gitenay, D., Vo, C., and Baron, V.T. (2010). Mutant p53 initiates a feedback loop that involves Egr-1/EGF receptor/ERK in prostate cancer cells. Oncogene *29*, 2628–2637.

Schilling, T., Kairat, A., Melino, G., Krammer, P.H., Stremmel, W., Oren, M., and Müller, M. (2010). Interference with the p53 family network contributes to the gain of oncogenic function of mutant p53 in hepatocellular carcinoma. Biochem. Biophys. Res. Commun. *394*, 817–823.

Scian, M.J., Stagliano, K.E., Deb, D., Ellis, M.A., Carchman, E.H., Das, A., Valerie, K., Deb, S.P., and Deb, S. (2004a). Tumor-derived p53 mutants induce oncogenesis by transactivating growth-promoting genes. Oncogene *23*, 4430–4443.

Scian, M.J., Stagliano, K.E., Ellis, M.A., Hassan, S., Bowman, M., Miles, M.F., Deb, S.P., and Deb, S. (2004b). Modulation of gene expression by tumor-derived p53 mutants. Cancer Res. *64*, 7447–7454.

Shi, X.B., Nesslinger, N.J., Deitch, A.D., Gumerlock, P.H., and deVere White, R.W. (2002). Complex functions of mutant p53 alleles from human prostate cancer. Prostate *51*, 59–72.

Singh, S., and Singh, P.P. (2013). Statin a day keeps cancer at bay. World journal of clinical oncology *4*, 43–46.

Smith, P.D., Crossland, S., Parker, G., Osin, P., Brooks, L., Waller, J., Philp, E., Crompton, M.R., Gusterson, B.A., Allday, M.J., and Crook, T. (1999). Novel p53 mutants selected in BRCA-associated tumours which dissociate transformation suppression from other wild-type p53 functions. Oncogene *18*, 2451–2459.

Solomon, H., Buganim, Y., Kogan-Sakin, I., Pomeraniec, L., Assia, Y., Madar, S., Goldstein, I., Brosh, R., Kalo, E., Beatus, T., et al. (2012). Various p53 mutant proteins differently regulate the Ras circuit to induce a cancer-related gene signature. J. Cell Sci. *125*, 3144–3152.

Sonego, M., Schiappacassi, M., Lovisa, S., Dall'Acqua, A., Bagnoli, M., Lovat, F., Libra, M., D'Andrea, S., Canzonieri, V., Militello, L., et al. (2013). Stathmin regulates mutant p53 stability and transcriptional activity in ovarian cancer. EMBO molecular medicine *5*, 707–722.

Song, H., Hollstein, M., and Xu, Y. (2007). p53 gain-of-function cancer mutants induce genetic instability by inactivating ATM. Nat. Cell Biol. *9*, 573–580.

Stambolsky, P., Tabach, Y., Fontemaggi, G., Weisz, L., Maor-Aloni, R., Siegfried, Z., Shiff, I., Kogan, I., Shay, M., Kalo, E., et al. (2010). Modulation of the vitamin D3 response by cancer-associated mutant p53. Cancer Cell *17*, 273–285.

Strano, S., Fontemaggi, G., Costanzo, A., Rizzo, M.G., Monti, O., Baccarini, A., Del Sal, G., Levrero, M., Sacchi, A., Oren, M., and Blandino, G. (2002). Physical interaction with human tumor-derived p53 mutants inhibits p63 activities. J. Biol. Chem. *277*, 18817–18826.

Strebhardt, K. (2010). Multifaceted polo-like kinases: drug targets and antitargets for cancer therapy. Nat. Rev. Drug Discov. *9*, 643–660.

Su, X., Chakravarti, D., Cho, M.S., Liu, L., Gi, Y.J., Lin, Y.L., Leung, M.L., El-Naggar, A.K., Creighton, C.J., Suraokar, M.B., et al. (2010). TAp63 suppresses metastasis through coordinate regulation of Dicer and miRNAs. Nature *467*, 986–990.

Suh, Y.A., Post, S.M., Elizondo-Fraire, A.C., Maccio, D.R., Jackson, J.G., El-Naggar, A.K., Van Pelt, C., Terzian, T., and Lozano, G. (2011). Multiple stress signals activate mutant p53 in vivo. Cancer Res. *71*, 7168–7175.

Sun, Y., Nakamura, K., Wendel, E., and Colburn, N. (1993). Progression toward tumor cell phenotype is enhanced by overexpression of a mutant p53 tumor-suppressor gene isolated from nasopharyngeal carcinoma. Proc. Natl. Acad. Sci. USA *90*, 2827–2831.

Tan, E.H., Morton, J.P., Timpson, P., Tucci, P., Melino, G., Flores, E.R., Sansom, O.J., Vousden, K.H., and Muller, P.A. (2013). Functions of TAp63 and p53 in restraining the development of metastatic cancer. Oncogene.

Tasdemir, E., Maiuri, M.C., Galluzzi, L., Vitale, I., Djavaheri-Mergny, M., D'Amelio, M., Criollo, A., Morselli, E., Zhu, C., Harper, F., et al. (2008). Regulation of autophagy by cytoplasmic p53. Nat. Cell Biol. *10*, 676–687.

Trepel, M., Groscurth, P., Malipiero, U., Gulbins, E., Dichgans, J., and Weller, M. (1998). Chemosensitivity of human malignant glioma: modulation by p53 gene transfer. J. Neurooncol. *39*, 19–32.

Trinidad, A.G., Muller, P.A., Cuellar, J., Klejnot, M., Nobis, M., Valpuesta, J.M., and Vousden, K.H. (2013). Interaction of p53 with the CCT complex promotes protein folding and wild-type p53 activity. Mol. Cell *50*, 805–817.

Tsang, W.P., Ho, F.Y., Fung, K.P., Kong, S.K., and Kwok, T.T. (2005). p53-R175H mutant gains new function in regulation of doxorubicin-induced apoptosis. International journal of cancer Journal international du cancer *114*, 331–336.

Tucci, P., Agostini, M., Grespi, F., Markert, E.K., Terrinoni, A., Vousden, K.H., Muller, P.A.J., Dötsch, V., Kehrloesser, S., Sayan, B.S., et al. (2012). Loss of p63 and its microRNA-205 target results in enhanced cell migration and metastasis in prostate cancer. Proc. Natl. Acad. Sci. USA *109*, 15312–15317.

Vakifahmetoglu-Norberg, H., Kim, M., Xia, H.G., Iwanicki, M.P., Ofengeim, D., Coloff, J.L., Pan, L., Ince, T.A., Kroemer, G., Brugge, J.S., and Yuan, J. (2013). Chaperone-mediated autophagy degrades mutant p53. Genes Dev. *27*, 1718–1730.

Vaughan, C.A., Frum, R., Pearsall, I., Singh, S., Windle, B., Yeudall, A., Deb, S.P., and Deb, S. (2012a). Allele specific gain-of-function activity of p53 mutants in lung cancer cells. Biochem. Biophys. Res. Commun. *428*, 6–10.

Vaughan, C.A., Singh, S., Windle, B., Sankala, H.M., Graves, P.R., Andrew Yeudall, W., Deb, S.P., and Deb, S. (2012b). p53 mutants induce transcription of NF-κB2 in H1299 cells through CBP and STAT binding on the NF-κB2 promoter and gain of function activity. Arch. Biochem. Biophys. *518*, 79–88.

Verhaegh, G.W., Parat, M.O., Richard, M.J., and Hainaut, P. (1998). Modulation of p53 protein conformation and DNA-binding activity by intracellular chelation of zinc. Mol. Carcinog. *21*, 205–214.

Vikhanskaya, F., Lee, M.K., Mazzoletti, M., Broggini, M., and Sabapathy, K. (2007). Cancer-derived p53 mutants suppress p53-target gene expression—potential mechanism for gain of function of mutant p53. Nucleic Acids Res. *35*, 2093–2104.

Walerych, D., Napoli, M., Collavin, L., and Del Sal, G. (2012). The rebel angel: mutant p53 as the driving oncogene in breast cancer. Carcinogenesis *33*, 2007–2017.

Wang, X., and Simon, R. (2013). Identification of potential synthetic lethal genes to p53 using a computational biology approach. BMC Med. Genomics *6*, 30.

Wang, Y., Suh, Y.A., Fuller, M.Y., Jackson, J.G., Xiong, S., Terzian, T., Quintás-Cardama, A., Bankson, J.A., El-Naggar, A.K., and Lozano, G. (2011). Restoring expression of wild-type p53 suppresses tumor growth but does not cause tumor regression in mice with a p53 missense mutation. J. Clin. Invest. *121*, 893–904.

Wang, W., Cheng, B., Miao, L., Mei, Y., and Wu, M. (2013a). Mutant p53-R273H gains new function in sustained activation of EGFR signaling via suppressing miR-27a expression. Cell Death Dis. *4*, e574.

Wang, X., Chen, J.X., Liu, J.P., You, C., Liu, Y.H., and Mao, Q. (2013b). Gain of function of mutant TP53 in glioblastoma: prognosis and response to temozolomide. Ann. Surg. Oncol. Published online November 19, 2013. http://dx.doi.org/10.1245/s10434-013-3380-0.

Weisz, L., Zalcenstein, A., Stambolsky, P., Cohen, Y., Goldfinger, N., Oren, M., and Rotter, V. (2004). Transactivation of the EGR1 gene contributes to mutant p53 gain of function. Cancer Res. *64*, 8318–8327.

Weisz, L., Oren, M., and Rotter, V. (2007). Transcription regulation by mutant p53. Oncogene *26*, 2202–2211.

Wiman, K.G. (2010). Pharmacological reactivation of mutant p53: from protein structure to the cancer patient. Oncogene *29*, 4245–4252.

Wong, R.P., Tsang, W.P., Chau, P.Y., Co, N.N., Tsang, T.Y., and Kwok, T.T. (2007). p53-R273H gains new function in induction of drug resistance through down-regulation of procaspase-3. Mol. Cancer Ther. *6*, 1054–1061.

Xie, T.X., Zhou, G., Zhao, M., Sano, D., Jasser, S.A., Brennan, R.G., and Myers, J.N. (2013). Serine substitution of proline at codon 151 of TP53 confers gain of function activity leading to anoikis resistance and tumor progression of head and neck cancer cells. Laryngoscope *123*, 1416–1423.

Yan, W., and Chen, X. (2009). Identification of GRO1 as a critical determinant for mutant p53 gain of function. J. Biol. Chem. *284*, 12178–12187.

Yan, W., and Chen, X. (2010). Characterization of functional domains necessary for mutant p53 gain of function. J. Biol. Chem. *285*, 14229–14238.

Yan, W., Liu, G., Scoumanne, A., and Chen, X. (2008). Suppression of inhibitor of differentiation 2, a target of mutant p53, is required for gain-of-function mutations. Cancer Res. *68*, 6789–6796.

Yan, W., Liu, S., Xu, E., Zhang, J., Zhang, Y., Chen, X., and Chen, X. (2013). Histone deacetylase inhibitors suppress mutant p53 transcription via histone deacetylase 8. Oncogene *32*, 599–609.

Yeudall, W.A., Vaughan, C.A., Miyazaki, H., Ramamoorthy, M., Choi, M.Y., Chapman, C.G., Wang, H., Black, E., Bulysheva, A.A., Deb, S.P., et al. (2012). Gain-of-function mutant p53 upregulates CXC chemokines and enhances cell migration. Carcinogenesis *33*, 442–451.

Yi, L., Lu, C., Hu, W., Sun, Y., and Levine, A.J. (2012). Multiple roles of p53-related pathways in somatic cell reprogramming and stem cell differentiation. Cancer Res. *72*, 5635–5645.

Yi, Y.W., Kang, H.J., Kim, H.J., Kong, Y., Brown, M.L., and Bae, I. (2013). Targeting mutant p53 by a SIRT1 activator YK-3-237 inhibits the proliferation of triple-negative breast cancer cells. Oncotarget *4*, 984–994.

Yoshikawa, K., Hamada, J., Tada, M., Kameyama, T., Nakagawa, K., Suzuki, Y., Ikawa, M., Hassan, N.M., Kitagawa, Y., and Moriuchi, T. (2010). Mutant p53 R248Q but not R248W enhances in vitro invasiveness of human lung cancer NCI-H1299 cells. Biomed. Res. *31*, 401–411.

Yu, X., Vazquez, A., Levine, A.J., and Carpizo, D.R. (2012). Allele-specific p53 mutant reactivation. Cancer Cell *21*, 614–625.

Zache, N., Lambert, J.M., Rökaeus, N., Shen, J., Hainaut, P., Bergman, J., Wiman, K.G., and Bykov, V.J. (2008). Mutant p53 targeting by the low molecular weight compound STIMA-1. Mol. Oncol. *2*, 70–80.

Zalcenstein, A., Stambolsky, P., Weisz, L., Müller, M., Wallach, D., Goncharov, T.M., Krammer, P.H., Rotter, V., and Oren, M. (2003). Mutant p53 gain of

function: repression of CD95(Fas/APO-1) gene expression by tumor-associated p53 mutants. Oncogene *22*, 5667–5676.

Zalcenstein, A., Weisz, L., Stambolsky, P., Bar, J., Rotter, V., and Oren, M. (2006). Repression of the MSP/MST-1 gene contributes to the antiapoptotic gain of function of mutant p53. Oncogene *25*, 359–369.

Zerdoumi, Y., Aury-Landas, J., Bonaïti-Pellié, C., Derambure, C., Sesboüé, R., Renaux-Petel, M., Frebourg, T., Bougeard, G., and Flaman, J.M. (2013). Drastic effect of germline TP53 missense mutations in Li-Fraumeni patients. Hum. Mutat. *34*, 453–461.

Zhang, Y., Yan, W., and Chen, X. (2011). Mutant p53 disrupts MCF-10A cell polarity in three-dimensional culture via epithelial-to-mesenchymal transitions. J. Biol. Chem. *286*, 16218–16228.

Zhu, H., Mao, Q., Lin, Y., Yang, K., and Xie, L. (2011). RNA interference targeting mutant p53 inhibits growth and induces apoptosis in DU145 human prostate cancer cells. Med. Oncol. *28* (*Suppl 1*), S381–S387.

Zhu, H.B., Yang, K., Xie, Y.Q., Lin, Y.W., Mao, Q.Q., and Xie, L.P. (2013). Silencing of mutant p53 by siRNA induces cell cycle arrest and apoptosis in human bladder cancer cells. World J. Surg. Oncol. *11*, 22.

Cell Symposia

Cancer, Inflammation, and Immunity

June 14–16, 2015 — Sitges, Spain

Abstract submission deadline:

January 16 2015

Early bird deadline:

March 27 2015

This symposium will bring academic and industry researchers and clinicians together to explore the many facets of cancer immunology and discuss how tumor-associated inflammation can be reprogrammed for therapeutic benefit.

Keynote Speakers

James Allison, USA
Lisa Coussens, USA

Speakers

Rafi Ahmed, *USA*
Vincenzo Bronte, *ITA*
George Coukos, *SUI*
Mikala Egeblad, *USA*
Jerome Galon, *FRA*
Johanna Joyce, *USA*
Michael Karin, *USA*
Alberto Mantovani (co-organizer), *ITA*
Ignancio Melero, *ESP*
Ira Mellman (co-organizer), *USA*
Peter Murray, *USA*
Jeffrey Pollard, *UK*
Fiona Powrie, *UK*
Carola Ries, *GER*
Alexander Rudensky, *USA*
Michel Sadelain, *USA*
Giorgio Trinchieri, *USA*
Laurence Zitvogel, FRA

Organizers

Alberto Mantovani, *University of Milan, ITA*
Ira Mellman, *Genentech, USA*
Li-Kuo Su, *Editor, Cancer Cell*
Elizabeth Thompson, *Scientific Editor, Immunity*

cell-symposia-cancerandinflammation.com

Cancer Cell
Review

Endoplasmic Reticulum Stress in Malignancy

Hanna J. Clarke,[1] Joseph E. Chambers,[1] Elizabeth Liniker,[1] and Stefan J. Marciniak[1,*]
[1]Department of Medicine, Cambridge Institute for Medical Research (CIMR), Wellcome Trust/MRC Building, University of Cambridge, Hills Road, Cambridge CB2 0XY, UK
*Correspondence: sjm20@cam.ac.uk
http://dx.doi.org/10.1016/j.ccr.2014.03.015

The combination of relative nutrient deprivation and dysregulation of protein synthesis make malignant cells especially prone to protein misfolding. Endoplasmic reticulum stress, which results from protein misfolding within the secretory pathway, has a profound effect on cancer cell proliferation and survival. In this review, we examine the evidence implicating endoplasmic reticulum dysfunction in the pathology of cancer and discuss how recent findings may help to identify novel therapeutic targets.

In the crowded molecular environment of the endoplasmic reticulum (ER), protein maturation requires the coordinated activity of many chaperones and folding enzymes. BiP is an abundant ER HSP70 chaperone that binds to exposed stretches of hydrophobic residues of immature polypeptide chains, while GRP94 is an HSP90 chaperone involved in subsequent folding steps for a subset of ER client proteins. When the efficiency of secretory protein folding is threatened, the cell is said to experience "ER stress" and elicits a homeostatic "unfolded protein response" (UPR) (Figure 1) (Walter and Ron, 2011). The diverse substrate repertoire of BiP enables it to function as a master regulator of the UPR by binding to and inactivating the three ER stress sensors, PERK, IRE1, and ATF6. During ER stress, increased levels of unfolded substrates lead to the sequestration of BiP, freeing the sensors to initiate UPR signaling. PERK ameliorates ER stress through phosphorylation of the translation initiation factor eIF2α. This causes generalized attenuation of protein synthesis while also promoting the translation of a subset of UPR target proteins, including the transcription factor ATF4. ATF4 induces expression of the transcription factor CHOP and, subsequently, the phosphatase subunit GADD34, which specifically dephosphorylates eIF2α, enabling the recovery of protein translation (Marciniak et al., 2004). The induction of ER oxidase 1α (ERO1α) by CHOP promotes oxidative protein folding in the ER, but this increased formation of disulphide bonds can contribute to worsening cellular stress through the generation of reactive oxygen species (ROS). However, additional targets of ATF4 include enzymes necessary to withstand oxidative stress, which tend to limit this toxicity. Additional targets of ATF4 promote amino acid import and synthesis, thus playing a cytoprotective role during a variety of stressful insults. Because other eIF2α kinases responding to different stresses can trigger this pathway—for example, GCN2 responds to amino acid deprivation—it has been named the integrated stress response (ISR; Figure 2) (Harding et al., 2003).

Tumor Growth

As solid cancers grow, their nutrient requirements eventually exceed the capacity of the existing vascular bed. Although many cancers adapt by triggering angiogenesis, inevitably the cores of most tumors become hypoxic and nutrient depleted. Impaired generation of ATP compromises ER protein folding, thus leading to activation of the UPR and ISR, while amino acid starvation further contributes to ISR activation. Indeed, phosphorylation of eIF2α by PERK has been shown to be necessary for the growth of larger solid tumors (Bi et al., 2005).

During hypoxia, generation of ROS increases both in mitochondria (Brunelle et al., 2005) and the ER, partly through UPR-mediated induction of ERO1α (Marciniak et al., 2004; Song et al., 2008). Accordingly, a key function of the ISR is to defend against oxidative stress, primarily by increasing biosynthesis of the antioxidant glutathione (Harding et al., 2003). The resulting increased capacity for oxidative protein folding is beneficial for tumor growth. Levels of ERO1α correlate with a worse prognosis in breast cancer (Kutomi et al., 2013), and depleting breast carcinoma cells of PERK increases ROS production and impairs cell growth (Bobrovnikova-Marjon et al., 2010). Moreover, the loss of PERK promotes G2/M cell cycle delay due to oxidative damage of DNA (Bobrovnikova-Marjon et al., 2010). This PERK-mediated resistance to oxidative stress is also implicated in resistance to radiotherapy (Rouschop et al., 2013; Rouschop et al., 2010), an effect of tumor adaptation to preconditioned ER stress.

In addition to the ATF4-dependent antioxidant response, cells can induce antioxidant pathways via Nrf2. This transcription factor is normally held inactive within the cytosol through binding to Keap1, which promotes its ubiquitination by Cul3 and subsequent proteasomal degradation. Upon oxidative stress, Keap1 releases Nrf2 to transactivate target genes within the nucleus. It has been suggested that this interaction is modulated by PERK. Two early reports suggested that Nrf2 could be phosphorylated by PERK during ER stress, triggering dissociation from Keap1 and induction of antioxidant genes (Cullinan and Diehl, 2004; Cullinan et al., 2003). Indeed, Nrf2 appears to be beneficial during ER stress-induced oxidative stress. However, activation of PERK's kinase domain in the absence of ER stress leads to induction of ISR target genes in a manner that is entirely dependent on phosphorylation of eIF2α (Lu et al., 2004). This suggests either that phosphorylation of Nrf2 plays a minor role in the transcriptional response to ER stress or that it is important only when additional arms of the UPR are active.

Recent observations suggest that activation of the UPR in hypoxic tumors leads to increased autophagy (Rouschop et al., 2010). Autophagy is cytoprotective during stress by liberating amino acids from long-lived proteins and the removal of damaged organelles. Accordingly, hypoxic regions of human

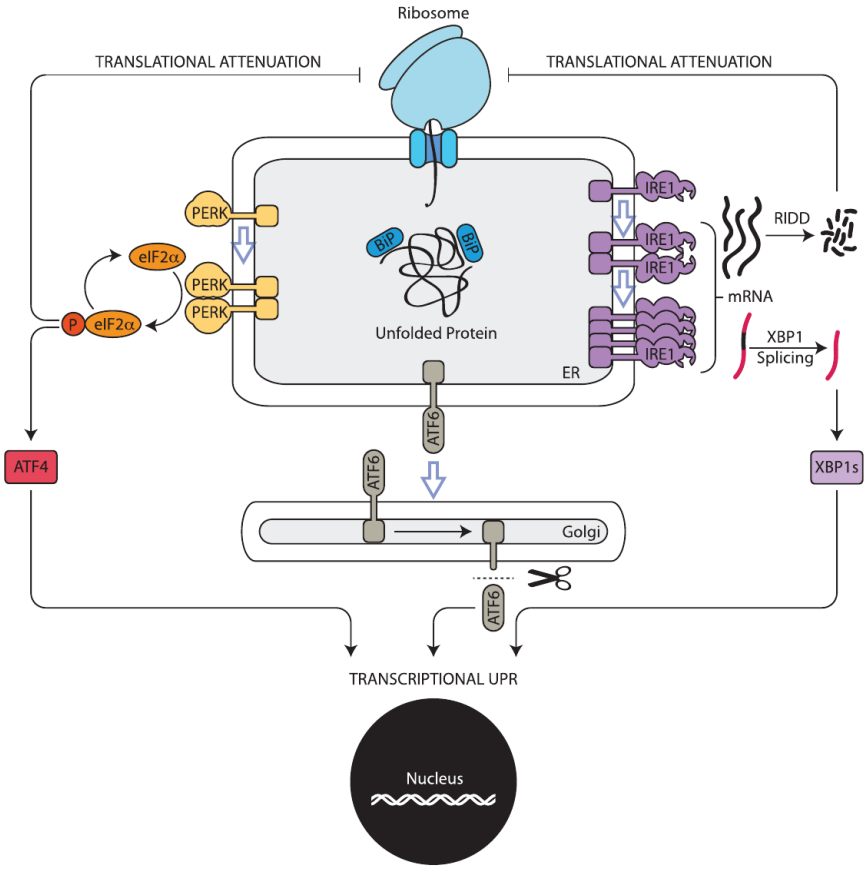

Figure 1. The UPR
Nascent secretory proteins synthesized by ER-bound ribosomes enter the ER lumen. When the load of unfolded protein threatens to exceed the capacity of the organelle to fold them, the cell is said to experience ER stress. This triggers three UPR signal transducers: PERK, IRE1, and ATF6. Activated PERK dimerizes, autophosphorylates, and then phosphorylates the translation initiation factor subunit eIF2α, causing general attenuation of translation that lessens ER protein client load while also increasing the translation of a subset of genes, including the transcription factor ATF4. Activated IRE1 oligomerizes, triggering its endonuclease activity to initiate splicing of *XBP1* mRNA and synthesis of the UPR transcription factor XBP1s. Activated IRE1 can also degrade a variety of mRNAs in proximity to the ER to reduced ER client protein load; a process termed regulated IRE1-dependent decay (RIDD). ATF6 traffics from the ER to the Golgi apparatus during stress and is cleaved to release a soluble UPR transcription factor, ATF6c.

tumor xenografts demonstrate increased expression of autophagy factors, such as LC3, and increased autophagy. In multiple cell lines, PERK mediates the upregulation of LC3 and autophagy-related gene 5 via ATF4 and CHOP, respectively, promoting phagophore formation (Rouschop et al., 2010). The inability of PERK-deficient cells to replenish LC3 correlates with impaired survival when subjected to hypoxia. Although PERK clearly plays an important role in the survival of hypoxic tumor cells, the IRE1 arm of the UPR is also important. During hypoxia-induced ER stress, IRE1-driven XBP1 splicing (to generate XBP1s) increases tumor cell tolerance to hypoxia, whereas loss of XBP1 impairs hypoxic tumor growth (Romero-Ramirez et al., 2004). Indeed, in breast cancer, increased splicing of *XBP1* is associated with a worse prognosis, perhaps reflecting an increased tolerance of tumor cells to hypoxia (Davies et al., 2008).

Angiogenesis and Invasion

It is well established that tumor hypoxia and glucose deprivation induce angiogenesis. Hypoxia achieves this via HIF, but the mechanism of nutrient limitation has remained obscure until recently. Evidence suggests that the PERK-ATF4 arm of the UPR directly upregulates vascular endothelial growth factor (VEGF) while downregulating inhibitors of angiogenesis (Blais et al., 2006; Wang et al., 2012). Depleting cells of PERK prevents upregulation of VEGF by glucose deprivation, whereas antagonism of HIF1α does not (Wang et al., 2012). Similarly, inhibition of PERK, which reduces the growth of xenograft tumors in mice, decreases tumor vascularity and perfusion (Wang et al., 2012). In addition, hypoxia-induced vascularization is modulated by IRE1α (Drogat et al., 2007). *Ire1α*$^{-/-}$ mouse embryonic fibroblasts and glioblastoma cells expressing dominant-negative IRE1α induce less VEGFA in ischemic conditions, limiting growth and angiogenesis of xenografts. In a human glioma model, it has been demonstrated that IRE1α is involved in the expression of angiogenic factors, including VEGFA and interleukin-6 (IL6), while suppressing the expression of antiangiogenic factors (Auf et al., 2010). Consequently, loss of IRE1α impairs glioma growth with increased overall survival of glioma-implanted animals. However, the relationship between IRE1α signaling and angiogenesis appears to be complex since, in nonmalignant models of ischemia, IRE1 has been shown to impair vascular regeneration by degrading mRNA encoding the neurovascular guidance cue netrin-1 via the process of regulated IRE1 dependent decay (RIDD) (Binet et al., 2013).

It is surprising that, although antagonism of IRE1 can impair tumor vascularity and improve survival, it may promote tumor invasion (Auf et al., 2010). Hypovascularity may contribute to invasiveness, but a more complex picture is likely, as the induction of angiogensis does not fully suppress the infiltrative properties of IRE1-deficient glioma cells. Recent analysis has revealed that the increased migratory phenotype likely reflects changes in the secretome via a reduction in RIDD (Dejeans et al., 2012b). For example, antagonism of IRE1 increases levels of the RIDD target BM-40, promoting cell adhesion and migration (Dejeans et al., 2012b). This suggests that, while suppression of IRE1 signaling may offer a novel approach to target tumor vascularization, it also risks promoting tumor invasion and so deserves further study.

Tumor invasion is also influenced by epithelial-to-mesenchymal transition (EMT), a known characteristic of ER-stressed

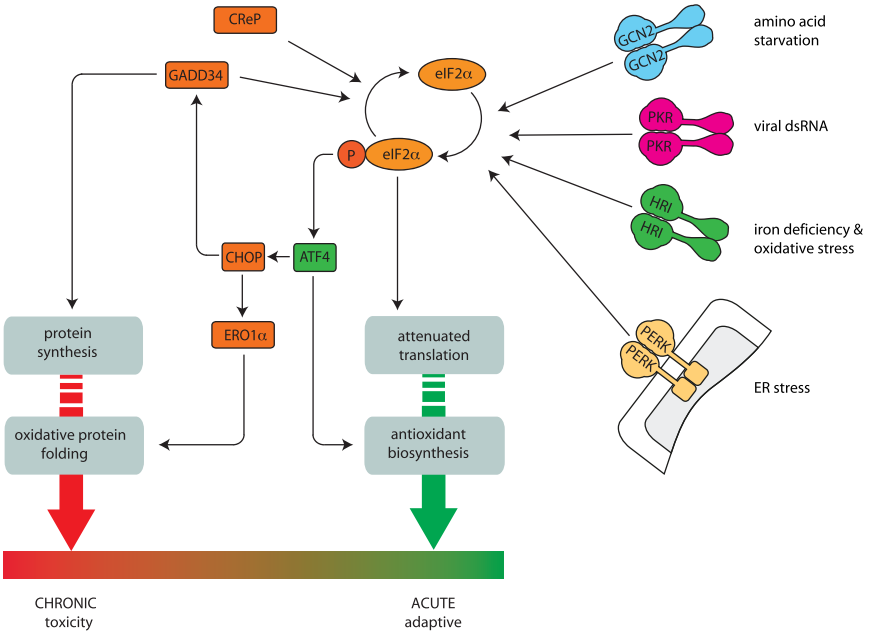

Figure 2. The ISR

Phosphorylation of eIF2α serves as a hub for integration of signals mediated by a family of kinases: PERK responds to ER stress, HRI responds to iron deficiency and to oxidative stress, PKR is activated by dsRNA during some viral infections, and GCN2 is activated during amino acid starvation (Harding et al., 2003). In unstressed conditions, eIF2α supports new protein synthesis as a component of the eIF2 complex that recruits initiator methionyl-tRNA to the ribosome. During its catalytic cycle, the eIF2 complex hydrolyzes bound GTP and must interact with the guanine nucleotide exchange factor eIF2B to be recharged with GTP. Once eIF2α is phosphorylated, it becomes a potent antagonist of eIF2B and thus attenuates the rate of protein translation. Low basal levels of eIF2α phosphorylation are antagonized by the constitutively expressed eIF2α phosphatase CReP, but during stress, this is overwhelmed and phospho-eIF2α accumulates. While translation of most mRNAs is reduced by phosphorylation of eIF2α, a subset is translated more efficiently, most notably, the transcript factor ATF4. This transactivates most genes of the ISR, including amino acid transporters and synthetases, which help counter amino acid limitation while providing the thiol moieties necessary for synthesis of the antioxidant glutathione. Subsequently, ATF4 induces another transcription factor CHOP, which induces the eIF2α phosphatase GADD34 leading to dephosphorylation of eIF2α and the resumption of normal rates of cap-dependent translation. CHOP also induces the ER oxidase ERO1α, thus promoting oxidative protein folding. While the induction of GADD34 and ERO1α can be seen as adaptive during the response to transient ER stress, their induction during chronic stressful circumstances can contributes to worsening stress and result in exaggerated toxicity.

cells. During embryonic development and in malignancy, HIF1α and Notch signaling link hypoxia with EMT, causing loss of epithelial integrity through downregulation of adhesion molecules such as E-cadherin (Lester et al., 2007; Sahlgren et al., 2008). Simultaneously, increased chemotaxis accompanies the induction of the chemokine receptor CXCR4 (Azab et al., 2012; Barriga et al., 2013). Thus, EMT promotes metastasis by removing impediments to the egress of cells from their original tumor while also honing them to new niches (reviewed in Hanahan and Weinberg, 2011). ER stress has been shown to drive EMT in vitro and in animal models of fibrosis through src-mediated signaling (Tanjore et al., 2011; Ulianich et al., 2008). It is therefore plausible that ER stress may contribute to EMT in cancer invasion, although more formal examinations of this are needed. A further consideration is that phenotypic change from epithelium to mesenchyme will affect the secretory capacity of a cell, thus altering its vulnerability to ER stress. Consistent with this, evidence suggests that expression of the ER stress markers CHOP and GADD34 change during dedifferentiation of mesothelioma cells (Dalton et al., 2013).

ER-Mitochondrial Communication

Through a proteostatic network, impaired protein folding in one cellular location leads to the propagation of cell-wide responses. The interplay between the mitochondrial HSP90 chaperone networks and the protein-folding environment of the ER exemplifies such a mechanism. HSP90 and its related chaperone, TRAP-1, are abundant in the mitochondria of tumor cells but not in those of most normal tissues, and they appear to antagonize mitochondrial death pathways (Chae et al., 2012). It is not surprising that impaired function of mitochondrial HSP90 leads to a mitochondrial UPR and the induction of autophagy (Siegelin et al., 2011). More recently, it has been shown that inhibition of mitochondrial HSP90 using the small molecule gamitrinib disrupts tumor bioenergetics to such an extent that ER stress pathways are activated (Chae et al., 2012). Notably, activation of the classical UPR of the ER was necessary for survival of mitochondrial proteotoxicity.

Direct communication between the mitochondrion and ER during stress serves to modulate the function of both organelles. PERK is enriched at mitochondrial-ER contact sites and appears to tether mitochondria to the ER membrane (Figure 3) (Verfaillie et al., 2012). Mitofusin 2 (Mfn2), a GTPase of the mitochondrial outer membrane that mediates mitochondrial fusion, has recently been shown to bind directly to PERK (Muñoz et al., 2013). Because cells lacking Mfn2 experience basal activation of PERK, it has been suggested that Mfn2 may normally inhibit PERK signaling. However, enhanced signaling in all three branches of the UPR in *Mfn2*$^{-/-}$ cells is difficult to explain by this dysinhibition of PERK alone, since exaggerated phosphorylation of eIF2α would reduce ER stress by attenuating protein translation. It therefore seems likely that ER-mitochondrial signaling is affected more extensively. Indeed, PERK modulates mitochondrial morphology and function, with overexpression of PERK causing mitochondrial fragmentation and reduced respiration, while depletion of PERK reduces mitochondrial calcium overload and ROS production in Mfn2-deficient cells (Muñoz et al., 2013). It is interesting that the tethering function of PERK appears independent of its kinase activity and facilitates ROS-mediated proapoptotic signaling between the ER and mitochondrion (Verfaillie et al., 2012). These organelles therefore function in tandem and can both contribute to oxidative stress through production of ROS.

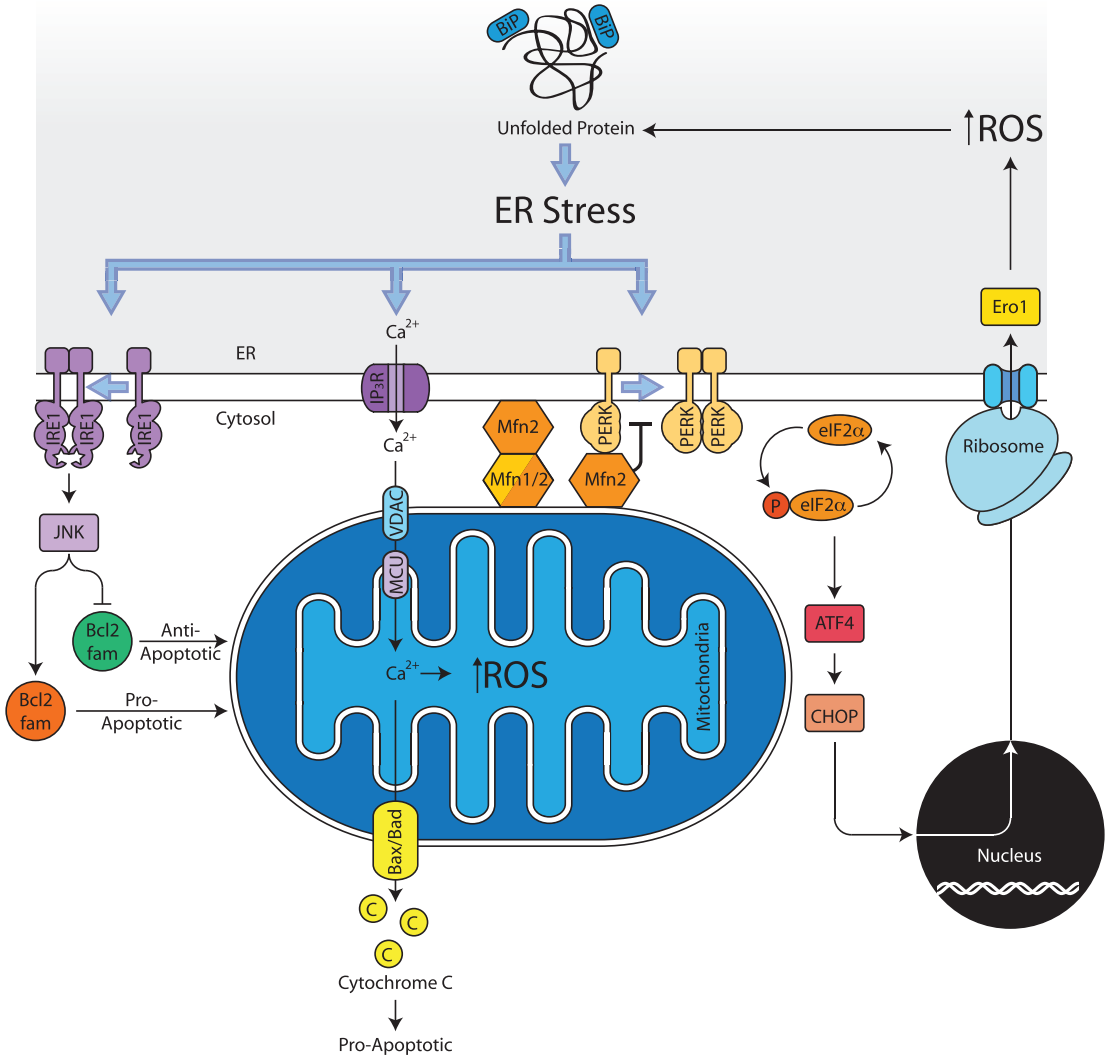

Figure 3. ER-Mitochondrial Communication during ER Stress

During ER stress, IRE1 mediates activation of c-Jun N-terminal kinase (JNK) and apoptosis via activation of pro-apoptotic BH3 only family Bcl-2 proteins, such as Bid, and inhibition of anti-apoptotic Bcl-2 (reviewed in Tabas and Ron, 2011). Calcium released from the ER is taken up by the mitochondrion to stimulate the production of ROS and the release of cytochrome c, both of which promote apoptosis. Prolonged PERK activation induces ERO1α leading to increased production of ROS within the ER. Mfn2, which along with mitofusin 1 (Mfn1) tethers mitochondria to the ER membrane (de Brito and Scorrano, 2008), is thought to inhibit PERK by direct interaction. Ablation of Mfn2 leads to gross mitochondrial dysfunction in a PERK dependent manner, suggesting the existence of further, yet to be discovered, interactions.

Intercellular Signaling

In addition to communication between organelles during failure of proteostasis, it has been suggested that, in cancer, ER stress signals may be transmissible from cell to cell. One proposed mechanism involves the tumor suppressor PAWR, which is known to promote prostate cancer cell apoptosis via WT1. Brief exposure to ER stress causes the secretion of PAWR into the extracellular space that can trigger the apoptosis of nearby cancer cells (Burikhanov et al., 2009). Controversially, the "receptor" on nearby cells has been reported to be the chaperone BiP (Burikhanov et al., 2009), and it has been suggested that ER stress induces surface presentation of ER chaperones that can then modulate the activity of other plasma membrane proteins, such as cripto (Kelber et al., 2009). The apparent surface translocation of ER chaperones in cancer cells must be subjected to further rigorous validation and would be greatly strengthened by further mechanistic insight. However, the observation that cripto-dependent SMAD signaling can be blocked by an antibody recognizing surface-exposed BiP raises the possibility that this putative cancer-cell-specific mechanism may offer novel therapeutic targets (Kelber et al., 2009).

Cancer Cell Death

Depending on the context of ER stress, including intensity and duration, the UPR can promote survival or trigger cell death. In B cell chronic lymphocytic lymphoma, ER stress has been implicated in causing spontaneous tumor cell apoptosis (Rosati et al.,

2010). The initiation of cell death by ER stress involves several partially redundant parallel pathways (reviewed in Tabas and Ron, 2011), but evidence implicates PERK as a major effector (Marciniak et al., 2004). Because loss of CHOP, a downstream target of PERK, renders cells and mice more resistant to ER stress, for some time it was believed that CHOP regulates a cell death program, a theory that was not supported by transcriptional analysis (Han et al., 2013; Marciniak et al., 2004). Instead, CHOP regulates a complex array of more than 200 genes, which promote ongoing protein secretion and autophagy (Marciniak et al., 2004; Rouschop et al., 2010). For example, by inducing the ISR targets GADD34 and ERO1α, PERK and CHOP trigger the upregulation of protein translation and protein oxidation that, in the face of ongoing protein misfolding, represent a worsening to the original toxic insult (Han et al., 2013; Marciniak et al., 2004). Although recovery of protein translation is a necessary part of the adaptive response to acute ER stress, in situations of chronic stress, increased protein synthesis can contribute to toxicity (Figure 2). Recovery of protein translation is brought about by dephosphorylation of eIF2α by GADD34 (Marciniak et al., 2004), and so antagonism of GADD34 protects cells from chronic ER-stress-induced cell death (Tsaytler et al., 2011). In a murine model of medulloblastoma, loss of GADD34 increased eIF2α phosphorylation and promoted tumor growth, invasiveness, and angiogenesis (Lin et al., 2011). This may reflect the increased induction of VEGFA observed in mice lacking functional GADD34.

Although mutation of the *GADD34* gene is a rare event in human carcinogenesis, there is increasing evidence that suppression of the CHOP-GADD34 axis may be a tumor survival mechanism. For example, in malignant mesothelioma, loss of GADD34 expression correlates well with the degree of tumor dedifferentiation and a worse prognosis (Dalton et al., 2013). Reduced expression of CHOP in mammary carcinoma, mediated by the PERK-induced microRNA mir211, promotes tumor cell survival (Chitnis et al., 2012), while attenuation of PERK-CHOP signaling by overexpression of the DNAJ cochaperone p58IPK enables malignant progression under conditions of nutrient limitation (Huber et al., 2013). It therefore appears likely that, while PERK-ATF4 signaling may promote tumor survival, the induction of GADD34 may have broadly tumor-suppressive effects (Figure 2). This hypothesis is testable, since *Gadd34* null mice are viable (Marciniak et al., 2004). It is noteworthy that, in addition to GADD34, which is normally induced by ER stress, cells also possess a constitutively expressed eIF2α phosphatase called CReP. Recently, this has been shown to be downregulated in cells deficient in the tumor suppressor PTEN (Zeng et al., 2011). The resulting increase in phosphorylated eIF2α in these cells leads to increased resistance to oxidative stress.

Tumor-Specific Mechanisms for the Induction of Endoplasmic Stress

A number of mechanisms contribute to cancer-specific induction of the UPR. For example, deficiencies of the tumor suppressors tuberous sclerosis complex (Tsc)-1 or Tsc2, which negatively regulate mTORC1, cause ER stress through uncontrolled protein synthesis (Ozcan et al., 2008). Constitutive activation of the serine/threonine kinase mTORC1 is common to many cancers and stimulates protein synthesis and cell growth. However, mTORC1 activity is often also repressed by homeostatic responses to features of the tumor microenvironment, such as hypoxia and nutrient deprivation, to promote cancer cell survival (Figure 4) (Brugarolas et al., 2004; Inoki et al., 2003). Recently, it has been recognized that an important function of Tsc2 is to enable the cell to regulate its rate of protein synthesis to match the availability of lipids (Düvel et al., 2010). In the secretory pathway, these two processes are intimately linked, since an increased demand for ER protein flux triggers an IRE1-XBP1-dependent expansion of ER membrane to accommodate more folding proteins. Defects in mTORC1 signaling can render hypoxic tumors dependent on exogenous desaturated lipids, an essential nutrient for hypoxic $Tsc2^{-/-}$ tumors (Young et al., 2013). Lipid-deprived $Tsc2^{-/-}$ cells experience an exaggerated ER stress response because IRE-1 activation fails to trigger adequate expansion of the ER (Young et al., 2013). When lipids are limiting, this leads to ER stress-induced cell death that can be blocked by inhibition of mTORC1 with rapamycin. This phenomenon was also seen in kidney tumors arising in $Tsc2^{+/-}$ mice, as well as in multiple cancer cell lines, suggesting that therapies targeting lipid desaturation machinery might enhance ER stress-induced cell death in a tumor-specific manner (Young et al., 2013).

Frequently, transformed cells depend on the activation of prosurvival pathways such as those mediated by the oncogene Myc (reviewed in Dang, 2010), which enhance proliferation through cell cycle deregulation and increased protein synthesis. Increased protein load leads to activation of the UPR, which promotes malignant transformation through PERK-mediated cytoprotective autophagy. Limiting protein synthesis by genetic manipulation abrogates UPR activation by Myc and attenuates lymphomagenesis in a murine model (Hart et al., 2012). Accordingly, PERK inhibition diminished the level of autophagy accompanying Myc activation, leading to reduced colony formation in vitro and decreasing tumor formation in vivo (Hart et al., 2012).

In some situations, ER stress responses appear to be used as antioncogenic mechanisms. In naevi of the skin, components of the MAPK pathways are commonly dysregulated, but although many naevi have oncogenic mutations, few develop into malignant melanomas. Instead, they senesce through incompletely understood mechanisms (Michaloglou et al., 2005). Oncogenic mutations of HRAS have been shown to trigger the UPR via activation of the AKT pathway (Denoyelle et al., 2006), and while the link between AKT and ER stress is unclear, the consequence of UPR activation is to induce senescence and prevent transformation.

The Role of Endoplasmic Reticulum Stress in Tumor Immunogenicity

In cancer, ER stress has the capacity to activate cells of the adaptive immune system (Wheeler et al., 2008) and is sufficient to trigger systemic inflammation by proteolytic activation of the transcription factor CREBH at the ER membrane (Zhang et al., 2006). ER stress in prostate cancer causes the release of proinflammatory cytokines such as IL6 and tumor necrosis factor α (Mahadevan et al., 2010), the promoters of which contain functional XBP1s binding sites (Martinon et al., 2010). These cytokines not only stimulate inflammation but also have been

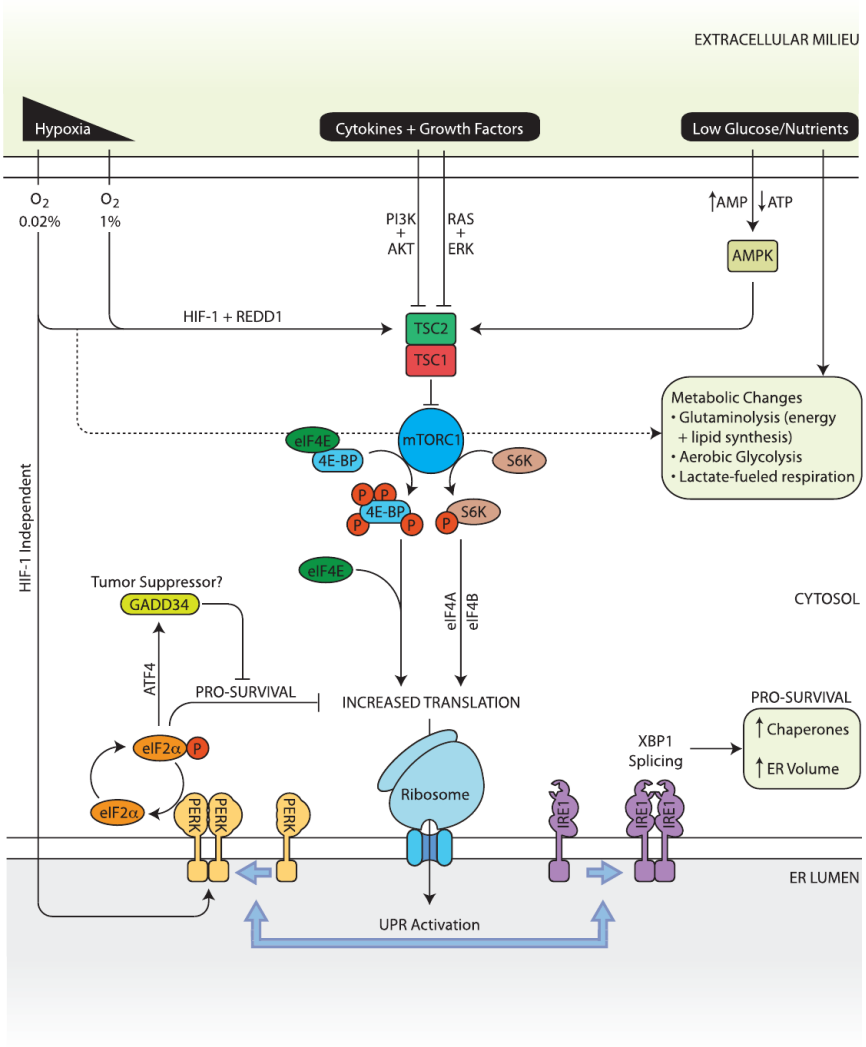

Figure 4. Regulation of Protein Synthesis in Cancer

mTORC1 stimulates protein translation at multiple levels. Release of eukaryotic initiation factor 4E (eIF4E) from its inhibitory binding partner 4E-BP is promoted by 4E-BP phosphorylation by mTORC1, while phosphorylation of S6K leads to activation of eIF4A and eIF4B. Tsc1/2 complex inhibits mTORC1 in response to cues from the tumor microenvironments, while mitogenic factors inhibit Tsc1/2 via PI3-kinase/Akt and Ras/Erk pathways to promoting protein synthesis and growth (reviewed in Mendoza et al., 2011). PERK and IRE1 limit protein synthesis and expand the ER capacity to match ER protein folding to the rate to protein synthesis. GADD34-induced recovery of protein synthesis can have toxic consequences during chronic stress and so may mediate tumor-suppressive effects. When glucose is limiting, reduced cytosolic ATP:AMP ratios trigger Tsc1/2 via AMPK, while hypoxia activates Tsc1/2 via HIF-1 and REDD1. Anoxia ($O_2 \leq 0.02\%$) additionally activates PERK in a HIF-1 independent manner, further limiting translation via eIF2α phosphorylation. Both hypoxia and nutrient deprivation alter cell metabolism, promoting aerobic glycolysis, lactate utilization, and glutaminolysis (reviewed in Dang, 2012).

implicated in promoting tumor survival (Kim et al., 2009; Pikarsky et al., 2004). Remarkably, ER stress appears to be transmissible from cancer cells to cells of the immune system. When cultured in media conditioned by murine cancer cells experiencing ER stress, macrophages show activation of the UPR in a TLR-dependent manner (Mahadevan et al., 2011). It is plausible that this acquired UPR of macrophages might cause the release of proinflammatory mediators and thus contribute to tumor inflammation.

Cell surface expression of damage-associated molecular patterns (DAMPs) offers novel targeting strategies for immunogenic killing of cancer cells. ER-stress-mediated cell surface presentation of calreticulin has emerged as a DAMP of potential importance in cancer (Garg et al., 2012; Obeid et al., 2007). For example, it has been proposed as a mechanism for immune surveillance of hyperploid cancer cells, which display constitutive ER stress (Senovilla et al., 2012). It is interesting that anthracycline chemotherapeutics efficiently induce calreticulin translocation to the cell surface, causing tumor immunogenicity, while knockdown of calreticulin prevents phagocytosis and antigen presentation by dendritic cells (Obeid et al., 2007). In contrast, agents such as cisplatin that do not cause relocalization of calreticulin fail to elicit an anticancer immune response. This therapeutic limitation can be rectified by the coadministration of ER-stress-inducing agents (Martins et al., 2011). The combined insult of ER stress and excess reactive oxygen species appears to be required for translocation of calreticulin in a PERK-dependent process (Garg et al., 2012; Martins et al., 2011; Panaretakis et al., 2009). Phosphorylation of eIF2α is likely to mediate this effect, although one report suggested this to be nonessential (Garg et al., 2012). Although calreticulin appears to be a key molecule in this response, the combination of reactive oxygen species and ER stress also causes surface exposure of additional DAMPs, the relative importance of which remains unexplored (Fucikova et al., 2011; Garg et al., 2012).

Endoplasmic Reticulum Stress as a Therapeutic Target

The homeostatic mechanisms that maintain proteostasis are now sufficiently well understood to be legitimate targets of novel anticancer strategies. For example, the HSP90 family of chaperones are required for the proper folding and stability of many kinases and transcription factors involved in tumor survival, and HSP90 inhibitors have already entered clinical trials. Many of the agents developed to target cytosolic HSP90s appear also to inhibit the ER localized homolog GRP94, but it is currently unclear which of these two targets is the most important for cancer cell toxicity. Elevated levels of GRP94 have been observed in many cancers and have been associated with

advanced clinical stage (Wang et al., 2005; Zheng et al., 2008). Reduction of GRP94 levels has been shown to augment the toxicity of etoposide (Reddy et al., 1999) and actinomycin D (Pan et al., 2009), while overexpression of GRP94 in breast cancer promoted cell proliferation and migration (Dejeans et al., 2012a). Inhibition of GRP94 within the ER lumen was first achieved with the prototype HSP90 inhibitor geldanamycin. This agent and many of its derivatives have been shown to induce ER stress and cell death (Marcu et al., 2002). Recently, agents displaying selectivity for GRP94 were developed but appeared to be less toxic than nonspecific inhibitors of HSP90 (Duerfeldt et al., 2012); however, drug combinations that maximize ER stress and proteotoxicity may prove to be more effective. When combined with rapamycin, the HSP90 inhibitor retaspimycin, or IPI-504, caused catastrophic ER stress and the regression of aggressive ras-driven tumors (De Raedt et al., 2011). Since inhibition of HSP90 induces a robust heat shock response through effects on cytosolic protein folding, cytoprotective induction of cytosolic HSP70-class chaperones is characteristically seen. Consequently, cells depleted of both HSC70 and HSP72 show enhanced toxicity during inhibition of HSP90 (Powers et al., 2008), offering further opportunities for synergistic drug combinations.

Prolonged inhibition of HSP90 may also disable the cell's ability to mount a cytoprotective UPR, since PERK and IRE1 are stabilized by this chaperone (Marcu et al., 2002). These ER stress sensors have been targets of a number of successful small molecule inhibitor screening programs. The specific PERK inhibitor GSK2656157 reduces cancer growth in vivo, most likely via impaired angiogenesis and amino acid metabolism (Atkins et al., 2013), while the inhibitors of IRE1, MKC-3946 and STF-083010, both show antimyeloma activity in animal models (Mimura et al., 2012; Papandreou et al., 2011). While it has been noted that oncolytic viral therapy induces a prosurvival UPR, the cytoprotective effects of this are diminished by inhibition of IRE1, leading to increased oncolytic efficacy (Mahoney et al., 2011). This represents one of many potential utilities of such compounds in combination therapies. It should be noted, however, that agents that antagonize the UPR, such as PERK inhibitors, are likely to cause some systemic toxicity, since conditional ablation of PERK in the adult murine pancreas causes diabetes through ER stress-induced β-cell death (Gao et al., 2012). In addition, administration of the PERK inhibitor GSK2656157 to mice for 2 weeks caused combined degeneration of the endocrine and exocrine components of the pancreas (Atkins et al., 2013). Following this brief treatment, the effects appeared to be reversible on withdrawal of the drug, but longer term effects have yet to be determined.

The proteasome inhibitor bortezomib can induce cell death in Burkitt lymphoma (Shirley et al., 2011) and multiple myeloma (Meister et al., 2007), at least in part via ER stress. It is likely the highly secretory nature of myeloma cells that renders them especially vulnerable to agents that promote ER stress, and in vitro studies have shown that inhibition of the proteasome synergizes with other therapies that increase the load of ER misfolded proteins, such as photodynamic therapy (Szokalska et al., 2009). In addition, bortezomib has been shown to kill hypoxic tumor cells, preferentially through overactivation of the UPR, since hypoxia is a cause of protein misfolding (Fels et al., 2008). The relative selectivity of bortezomib for a subset of cancer cells reflects the dependence of professional secretory cells on their ability to degrade proteins that have terminally misfolded within the ER; the process of ER-associated degradation (ERAD). In addition to direct inhibition of the proteasome, ERAD can be blocked by other means. Eeyarestatin I inhibits the p97-Ufd1-Npl4 complex that mediates dislocation of polyubiquitinated substrates out of the ER into the cytosol and also impairs their deubiquitination (Wang et al., 2008). This agent synergizes with bortezomib in tumor cell killing by inducing the proapoptotic protein NOXA in an ISR-dependent manner (Wang et al., 2009). Similar synergy has been observed with the combination of bortezomib and another p97 inhibitor, DBeQ (Auner et al., 2013).

While the introduction of bortezomib has led to an increased rate of remission in myeloma patients, acquired drug resistance has limited its use in the clinic. Cells cultured in the presence of proteasome inhibitors have been shown to acquire mutations of the bortezomib binding site on proteasome subunit PSMB5 or to overexpress this subunit, although such mutations are rarely observed in the clinical setting (Balsas et al., 2012; Oerlemans et al., 2008). An alternative mechanism involves increased basal expression levels of BiP that allows cells to withstand the accumulation of more misfolded proteins without activation of a cytotoxic UPR (Schewe and Aguirre-Ghiso, 2009). More recently, a subpopulation of bortezomib-refractory B-cell progenitors has been identified in which IRE1-XBP1s signaling is suppressed (Leung-Hagesteijn et al., 2013). It has been known for some time that XBP1s is necessary for the differentiation of B lymphocytes into plasma cells by enabling a dramatic expansion of the ER (Carrasco et al., 2007). Continued signaling by the IRE1-XBP1s axis was thought necessary to maintain healthy plasma cells, but a recent screen identified IRE1 loss of function as promoting bortezomib resistance in myeloma (Leung-Hagesteijn et al., 2013). Despite previous evidence that inhibition of IRE1 is toxic to myeloma (Mimura et al., 2012; Papandreou et al., 2011), knockdown of either IRE1 or XBP1 was surprisingly well tolerated by myeloma-derived cell lines and induced resistance to inhibition of the proteasome, while overexpression of XBP1s restored sensitivity (Leung-Hagesteijn et al., 2013). Moreover, XBP1 target genes were depressed in clinical samples from progressive myeloma. The protective effect of depleting myeloma cells of XBP1s correlated with a partial reversal of plasma cell differentiation, both morphologically and functionally, with a reduced capacity to secrete immunoglobin light chains. Moreover, XBP1s-deficient myeloma progenitors could be isolated from the bone marrow of patients with progressive disease, and it was suggested that these represent a pool of cells intrinsically resistant to proteasome inhibition owing to their arrested development. This may explain the inability of proteasome inhibition to induce an outright cure in myeloma and the appearance of resistance following initial remission. It is encouraging, however, that bortezomib resistance can be overcome in models of disease by potentiating the degree of ER stress with coadministration of an HSP90 inhibitor (Roué et al., 2011). The suppression of the UPR in some bortezomib-resistant cells is thought to be facilitated by reduced phosphorylation of eIF2α. Accordingly, promotion of phosph-eIF2α levels with the agent salubrinal was shown to enhance bortezomib-induced cell killing (Schewe

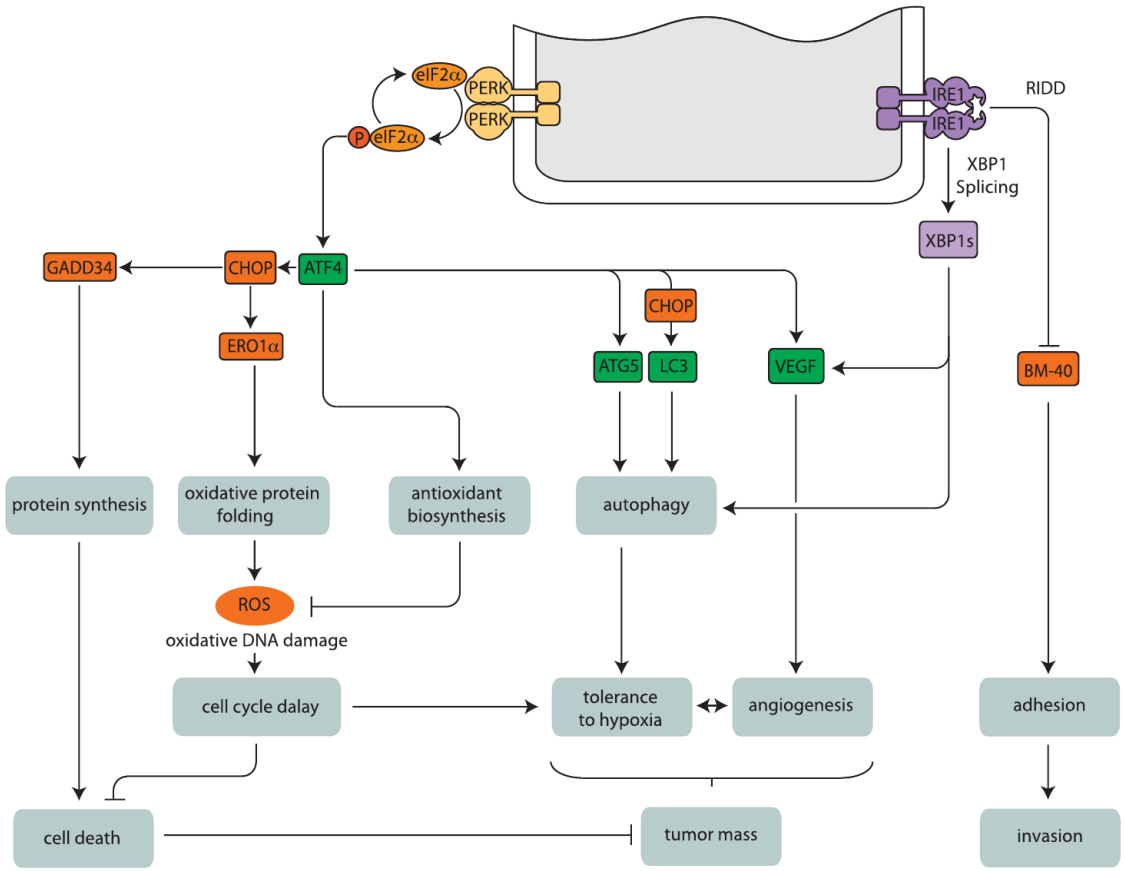

Figure 5. The UPR in Cancer

Activation of the UPR in malignancy results in complex signaling that is neither fully oncogenic nor tumor suppressive. The relative importance of each downstream pathway varies between cells depending on the chronicity of ER stress and on the relative expression of key factors; for example, GADD34. High rates of protein synthesis during ER stress lead to cell death through the accumulation of misfolded protein, which would reduce tumor mass. Loss of GADD34 may serve to antagonize this, leaving PERK unhindered in the attenuation of protein synthesis. Generation of ROS during ER stress, while potentially toxic, may help limit tumor growth to match nutrient supply by initiating DNA damage checkpoints. Excess toxicity from ROS is limited by ATF4-mediated induction of antioxidant pathways. Nutrient limitation within tumors is antagonized by autophagy and angiogenesis, which are induced by the PERK and IRE1 arms of the UPR. Reduced expression of extracellular matrix molecules, such as BM-40, may limit migration and invasion.

and Aguirre-Ghiso, 2009). Conversely, it has also been suggested that enhanced induction of ATF4 may have undesirable effects in the treatment of myeloma. Inhibition of the proteasome is associated with accumulation of the antiapoptotic protein Mcl-1, which can confer resistance to bortezomib (Hu et al., 2012). This accumulation does not reflect stabilization of the protein; instead, Mcl-1 appears to be induced by ATF4. Newer, more selective inhibitors of eIF2α phosphatases are under development and should help to clarify which effect, cytotoxicity or antiapoptotic, is dominant.

Concluding Remarks

Current understanding of the cellular responses to ER stress has made this a valid target for the development of rational therapies, but the role of the UPR in modulating many aspects of tumor behavior from cell proliferation and death to angiogenesis and invasion is becoming clearer (Figure 5). It is perhaps not surprising that the cellular response to ER stress is neither fully oncogenic nor completely tumor suppressive. For example, antioxidant pathways induced downstream of ATF4 appear to promote tumor survival and may largely account for the requirement for PERK in models of solid tumors; while induction of GADD34 may be toxic to cancers experiencing chronic ER stress. Such insights will contribute to better targeting of therapies while also informing our appreciation of the cell biology of physiological ER stress. Remarkably, the precise mechanisms of cell death during ER stress remain unclear, and so better understanding will be required if death pathways are to be invoked with selectivity to ER-stressed cancer cells. It is likely that the relative importance of these death pathways will depend both on the cancer type and on the tumor microenvironment, which will offer further possibilities for personalization of treatment.

Finally, it is important to bear in mind the heterogeneity of cancer as a disease, or rather as a group of diseases. The evolution of an individual tumor over time frequently leads to loss of differentiation and increased propensities for invasion and metastasis, which will affect secretory capacity and reliance on the UPR. Also, there is heterogeneity between subtypes of cancer originating from a single tissue type such the breast, which include basal-like, luminal-like, normal breast-like, and HER2 positive. Given that subtype-dependent differences will lead to differences in metabolic characteristics, it is to be

expected that the importance of ER protein homeostasis for each subtype will vary accordingly. This has already been demonstrated in the context of cytosolic protein folding. HER2 is a client protein of Hsp90, and so HER2-positive tumors are especially sensitive to inhibition of HSP90 (Rodrigues et al., 2012). The highly secretory natures of the rare mucinous and secretory breast cancers make them likely candidates for UPR dependence.

A number of areas require further study. Clearly, there is a need for a more sophisticated appreciation of the oncogenic and tumor-suppressive features of the UPR. This is well illustrated by the antagonism of IRE1 that, while attenuating tumor growth through impaired angiogenesis, might promote tumor invasion. It is unclear what role the mutational burden of a tumor cell plays in the induction of ER stress. Are specific mutations more likely to cause ER stress? A better understanding of how the UPR influences chemo- and radiosensitivity may also direct more effective interventions.

ACKNOWLEDGMENTS

H.J.C. is funded by the British Lung Foundation. E.L. is funded by Cancer Research UK via the Cambridge Cancer Centre.

REFERENCES

Atkins, C., Liu, Q., Minthorn, E., Zhang, S.Y., Figueroa, D.J., Moss, K., Stanley, T.B., Sanders, B., Goetz, A., Gaul, N., et al. (2013). Characterization of a novel PERK kinase inhibitor with antitumor and antiangiogenic activity. Cancer Res. *73*, 1993–2002.

Auf, G., Jabouille, A., Guérit, S., Pineau, R., Delugin, M., Bouchecareilh, M., Magnin, N., Favereaux, A., Maitre, M., Gaiser, T., et al. (2010). Inositol-requiring enzyme 1alpha is a key regulator of angiogenesis and invasion in malignant glioma. Proc. Natl. Acad. Sci. USA *107*, 15553–15558.

Auner, H.W., Moody, A.M., Ward, T.H., Kraus, M., Milan, E., May, P., Chaidos, A., Driessen, C., Cenci, S., Dazzi, F., et al. (2013). Combined inhibition of p97 and the proteasome causes lethal disruption of the secretory apparatus in multiple myeloma cells. PLoS ONE *8*, e74415.

Azab, A.K., Hu, J., Quang, P., Azab, F., Pitsillides, C., Awwad, R., Thompson, B., Maiso, P., Sun, J.D., Hart, C.P., et al. (2012). Hypoxia promotes dissemination of multiple myeloma through acquisition of epithelial to mesenchymal transition-like features. Blood *119*, 5782–5794.

Balsas, P., Galán-Malo, P., Marzo, I., and Naval, J. (2012). Bortezomib resistance in a myeloma cell line is associated to PSMβ5 overexpression and polyploidy. Leuk. Res. *36*, 212–218.

Barriga, E.H., Maxwell, P.H., Reyes, A.E., and Mayor, R. (2013). The hypoxia factor Hif-1α controls neural crest chemotaxis and epithelial to mesenchymal transition. J. Cell Biol. *201*, 759–776.

Bi, M., Naczki, C., Koritzinsky, M., Fels, D., Blais, J., Hu, N., Harding, H., Novoa, I., Varia, M., Raleigh, J., et al. (2005). ER stress-regulated translation increases tolerance to extreme hypoxia and promotes tumor growth. EMBO J. *24*, 3470–3481.

Binet, F., Mawambo, G., Sitaras, N., Tetreault, N., Lapalme, E., Favret, S., Cerani, A., Leboeuf, D., Tremblay, S., Rezende, F., et al. (2013). Neuronal ER stress impedes myeloid-cell-induced vascular regeneration through IRE1α degradation of netrin-1. Cell Metab. *17*, 353–371.

Blais, J.D., Addison, C.L., Edge, R., Falls, T., Zhao, H., Wary, K., Koumenis, C., Harding, H.P., Ron, D., Holcik, M., and Bell, J.C. (2006). Perk-dependent translational regulation promotes tumor cell adaptation and angiogenesis in response to hypoxic stress. Mol. Cell. Biol. *26*, 9517–9532.

Bobrovnikova-Marjon, E., Grigoriadou, C., Pytel, D., Zhang, F., Ye, J., Koumenis, C., Cavener, D., and Diehl, J.A. (2010). PERK promotes cancer cell proliferation and tumor growth by limiting oxidative DNA damage. Oncogene *29*, 3881–3895.

Brugarolas, J., Lei, K., Hurley, R.L., Manning, B.D., Reiling, J.H., Hafen, E., Witters, L.A., Ellisen, L.W., and Kaelin, W.G., Jr. (2004). Regulation of mTOR function in response to hypoxia by REDD1 and the TSC1/TSC2 tumor suppressor complex. Genes Dev. *18*, 2893–2904.

Brunelle, J.K., Bell, E.L., Quesada, N.M., Vercauteren, K., Tiranti, V., Zeviani, M., Scarpulla, R.C., and Chandel, N.S. (2005). Oxygen sensing requires mitochondrial ROS but not oxidative phosphorylation. Cell Metab. *1*, 409–414.

Burikhanov, R., Zhao, Y., Goswami, A., Qiu, S., Schwarze, S.R., and Rangnekar, V.M. (2009). The tumor suppressor Par-4 activates an extrinsic pathway for apoptosis. Cell *138*, 377–388.

Carrasco, D.R., Sukhdeo, K., Protopopova, M., Sinha, R., Enos, M., Carrasco, D.E., Zheng, M., Mani, M., Henderson, J., Pinkus, G.S., et al. (2007). The differentiation and stress response factor XBP-1 drives multiple myeloma pathogenesis. Cancer Cell *11*, 349–360.

Chae, Y.C., Caino, M.C., Lisanti, S., Ghosh, J.C., Dohi, T., Danial, N.N., Villanueva, J., Ferrero, S., Vaira, V., Santambrogio, L., et al. (2012). Control of tumor bioenergetics and survival stress signaling by mitochondrial HSP90s. Cancer Cell *22*, 331–344.

Chitnis, N.S., Pytel, D., Bobrovnikova-Marjon, E., Pant, D., Zheng, H., Maas, N.L., Frederick, B., Kushner, J.A., Chodosh, L.A., Koumenis, C., et al. (2012). miR-211 is a prosurvival microRNA that regulates chop expression in a PERK-dependent manner. Mol. Cell *48*, 353–364.

Cullinan, S.B., and Diehl, J.A. (2004). PERK-dependent activation of Nrf2 contributes to redox homeostasis and cell survival following endoplasmic reticulum stress. J. Biol. Chem. *279*, 20108–20117.

Cullinan, S.B., Zhang, D., Hannink, M., Arvisais, E., Kaufman, R.J., and Diehl, J.A. (2003). Nrf2 is a direct PERK substrate and effector of PERK-dependent cell survival. Mol. Cell. Biol. *23*, 7198–7209.

Dalton, L.E., Clarke, H.J., Knight, J., Lawson, M.H., Wason, J., Lomas, D.A., Howat, W.J., Rintoul, R.C., Rassl, D.M., and Marciniak, S.J. (2013). The endoplasmic reticulum stress marker CHOP predicts survival in malignant mesothelioma. Br. J. Cancer *108*, 1340–1347.

Dang, C.V. (2010). Enigmatic MYC Conducts an Unfolding Systems Biology Symphony. Genes Cancer *1*, 526–531.

Dang, C.V. (2012). Links between metabolism and cancer. Genes Dev. *26*, 877–890.

Davies, M.P., Barraclough, D.L., Stewart, C., Joyce, K.A., Eccles, R.M., Barraclough, R., Rudland, P.S., and Sibson, D.R. (2008). Expression and splicing of the unfolded protein response gene XBP-1 are significantly associated with clinical outcome of endocrine-treated breast cancer. Int. J. Cancer *123*, 85–88.

de Brito, O.M., and Scorrano, L. (2008). Mitofusin 2 tethers endoplasmic reticulum to mitochondria. Nature *456*, 605–610.

De Raedt, T., Walton, Z., Yecies, J.L., Li, D., Chen, Y., Malone, C.F., Maertens, O., Jeong, S.M., Bronson, R.T., Lebleu, V., et al. (2011). Exploiting cancer cell vulnerabilities to develop a combination therapy for ras-driven tumors. Cancer Cell *20*, 400–413.

Dejeans, N., Glorieux, C., Guenin, S., Beck, R., Sid, B., Rousseau, R., Bisig, B., Delvenne, P., Buc Calderon, P., and Verrax, J. (2012a). Overexpression of GRP94 in breast cancer cells resistant to oxidative stress promotes high levels of cancer cell proliferation and migration: implications for tumor recurrence. Free Radic. Biol. Med. *52*, 993–1002.

Dejeans, N., Pluquet, O., Lhomond, S., Grise, F., Bouchecareilh, M., Juin, A., Meynard-Cadars, M., Bidaud-Meynard, A., Gentil, C., Moreau, V., et al. (2012b). Autocrine control of glioma cells adhesion and migration through IRE1α-mediated cleavage of SPARC mRNA. J. Cell Sci. *125*, 4278–4287.

Denoyelle, C., Abou-Rjaily, G., Bezrookove, V., Verhaegen, M., Johnson, T.M., Fullen, D.R., Pointer, J.N., Gruber, S.B., Su, L.D., Nikiforov, M.A., et al. (2006). Anti-oncogenic role of the endoplasmic reticulum differentially activated by mutations in the MAPK pathway. Nat. Cell Biol. *8*, 1053–1063.

Drogat, B., Auguste, P., Nguyen, D.T., Bouchecareilh, M., Pineau, R., Nalbantoglu, J., Kaufman, R.J., Chevet, E., Bikfalvi, A., and Moenner, M. (2007). IRE1 signaling is essential for ischemia-induced vascular endothelial growth factor-A expression and contributes to angiogenesis and tumor growth in vivo. Cancer Res. *67*, 6700–6707.

Duerfeldt, A.S., Peterson, L.B., Maynard, J.C., Ng, C.L., Eletto, D., Ostrovsky, O., Shinogle, H.E., Moore, D.S., Argon, Y., Nicchitta, C.V., and Blagg, B.S. (2012). Development of a Grp94 inhibitor. J. Am. Chem. Soc. *134*, 9796–9804.

Düvel, K., Yecies, J.L., Menon, S., Raman, P., Lipovsky, A.I., Souza, A.L., Triantafellow, E., Ma, Q., Gorski, R., Cleaver, S., et al. (2010). Activation of a metabolic gene regulatory network downstream of mTOR complex 1. Mol. Cell *39*, 171–183.

Fels, D.R., Ye, J., Segan, A.T., Kridel, S.J., Spiotto, M., Olson, M., Koong, A.C., and Koumenis, C. (2008). Preferential cytotoxicity of bortezomib toward hypoxic tumor cells via overactivation of endoplasmic reticulum stress pathways. Cancer Res. *68*, 9323–9330.

Fucikova, J., Kralikova, P., Fialova, A., Brtnicky, T., Rob, L., Bartunkova, J., and Spísek, R. (2011). Human tumor cells killed by anthracyclines induce a tumor-specific immune response. Cancer Res. *71*, 4821–4833.

Gao, Y., Sartori, D.J., Li, C., Yu, Q.C., Kushner, J.A., Simon, M.C., and Diehl, J.A. (2012). PERK is required in the adult pancreas and is essential for maintenance of glucose homeostasis. Mol. Cell. Biol. *32*, 5129–5139.

Garg, A.D., Krysko, D.V., Verfaillie, T., Kaczmarek, A., Ferreira, G.B., Marysael, T., Rubio, N., Firczuk, M., Mathieu, C., Roebroek, A.J., et al. (2012). A novel pathway combining calreticulin exposure and ATP secretion in immunogenic cancer cell death. EMBO J. *31*, 1062–1079.

Han, J., Back, S.H., Hur, J., Lin, Y.H., Gildersleeve, R., Shan, J., Yuan, C.L., Krokowski, D., Wang, S., Hatzoglou, M., et al. (2013). ER-stress-induced transcriptional regulation increases protein synthesis leading to cell death. Nat. Cell Biol. *15*, 481–490.

Hanahan, D., and Weinberg, R.A. (2011). Hallmarks of cancer: the next generation. Cell *144*, 646–674.

Harding, H.P., Zhang, Y., Zeng, H., Novoa, I., Lu, P.D., Calfon, M., Sadri, N., Yun, C., Popko, B., Paules, R., et al. (2003). An integrated stress response regulates amino acid metabolism and resistance to oxidative stress. Mol. Cell *11*, 619–633.

Hart, L.S., Cunningham, J.T., Datta, T., Dey, S., Tameire, F., Lehman, S.L., Qiu, B., Zhang, H., Cerniglia, G., Bi, M., et al. (2012). ER stress-mediated autophagy promotes Myc-dependent transformation and tumor growth. J. Clin. Invest. *122*, 4621–4634.

Hu, J., Dang, N., Menu, E., De Bryune, E., Xu, D., Van Camp, B., Van Valckenborgh, E., and Vanderkerken, K. (2012). Activation of ATF4 mediates unwanted Mcl-1 accumulation by proteasome inhibition. Blood *119*, 826–837.

Huber, A.L., Lebeau, J., Guillaumot, P., Pétrilli, V., Malek, M., Chilloux, J., Fauvet, F., Payen, L., Kfoury, A., Renno, T., et al. (2013). p58(IPK)-mediated attenuation of the proapoptotic PERK-CHOP pathway allows malignant progression upon low glucose. Mol. Cell *49*, 1049–1059.

Inoki, K., Zhu, T., and Guan, K.L. (2003). TSC2 mediates cellular energy response to control cell growth and survival. Cell *115*, 577–590.

Kelber, J.A., Panopoulos, A.D., Shani, G., Booker, E.C., Belmonte, J.C., Vale, W.W., and Gray, P.C. (2009). Blockade of Cripto binding to cell surface GRP78 inhibits oncogenic Cripto signaling via MAPK/PI3K and Smad2/3 pathways. Oncogene *28*, 2324–2336.

Kim, S., Takahashi, H., Lin, W.W., Descargues, P., Grivennikov, S., Kim, Y., Luo, J.L., and Karin, M. (2009). Carcinoma-produced factors activate myeloid cells through TLR2 to stimulate metastasis. Nature *457*, 102–106.

Kutomi, G., Tamura, Y., Tanaka, T., Kajiwara, T., Kukita, K., Ohmura, T., Shima, H., Takamaru, T., Satomi, F., Suzuki, Y., et al. (2013). Human endoplasmic reticulum oxidoreductin 1-alpha is a novel predictor for poor prognosis of breast cancer. Cancer Sci. *104*, 1091–1096.

Lester, R.D., Jo, M., Montel, V., Takimoto, S., and Gonias, S.L. (2007). uPAR induces epithelial-mesenchymal transition in hypoxic breast cancer cells. J. Cell Biol. *178*, 425–436.

Leung-Hagesteijn, C., Erdmann, N., Cheung, G., Keats, J.J., Stewart, A.K., Reece, D.E., Chung, K.C., and Tiedemann, R.E. (2013). Xbp1s-negative tumor B cells and pre-plasmablasts mediate therapeutic proteasome inhibitor resistance in multiple myeloma. Cancer Cell *24*, 289–304.

Lin, W., Lin, Y., Li, J., Harding, H.P., Ron, D., and Jamison, S. (2011). A deregulated integrated stress response promotes interferon-γ-induced medulloblastoma. J. Neurosci. Res. *89*, 1586–1595.

Lu, P.D., Jousse, C., Marciniak, S.J., Zhang, Y., Novoa, I., Scheuner, D., Kaufman, R.J., Ron, D., and Harding, H.P. (2004). Cytoprotection by pre-emptive conditional phosphorylation of translation initiation factor 2. EMBO J. *23*, 169–179.

Mahadevan, N.R., Fernandez, A., Rodvold, J.J., Almanza, G., and Zanetti, M. (2010). Prostate cancer cells undergoing ER stress in vitro and in vivo activate transcription of pro-inflammatory cytokines. J. Inflamm. Res. *3*, 99–103.

Mahadevan, N.R., Rodvold, J., Sepulveda, H., Rossi, S., Drew, A.F., and Zanetti, M. (2011). Transmission of endoplasmic reticulum stress and pro-inflammation from tumor cells to myeloid cells. Proc. Natl. Acad. Sci. USA *108*, 6561–6566.

Mahoney, D.J., Lefebvre, C., Allan, K., Brun, J., Sanaei, C.A., Baird, S., Pearce, N., Grönberg, S., Wilson, B., Prakesh, M., et al. (2011). Virus-tumor interactome screen reveals ER stress response can reprogram resistant cancers for oncolytic virus-triggered caspase-2 cell death. Cancer Cell *20*, 443–456.

Marciniak, S.J., Yun, C.Y., Oyadomari, S., Novoa, I., Zhang, Y., Jungreis, R., Nagata, K., Harding, H.P., and Ron, D. (2004). CHOP induces death by promoting protein synthesis and oxidation in the stressed endoplasmic reticulum. Genes Dev. *18*, 3066–3077.

Marcu, M.G., Doyle, M., Bertolotti, A., Ron, D., Hendershot, L., and Neckers, L. (2002). Heat shock protein 90 modulates the unfolded protein response by stabilizing IRE1alpha. Mol. Cell. Biol. *22*, 8506–8513.

Martinon, F., Chen, X., Lee, A.H., and Glimcher, L.H. (2010). TLR activation of the transcription factor XBP1 regulates innate immune responses in macrophages. Nat. Immunol. *11*, 411–418.

Martins, I., Kepp, O., Schlemmer, F., Adjemian, S., Tailler, M., Shen, S., Michaud, M., Menger, L., Gdoura, A., Tajeddine, N., et al. (2011). Restoration of the immunogenicity of cisplatin-induced cancer cell death by endoplasmic reticulum stress. Oncogene *30*, 1147–1158.

Meister, S., Schubert, U., Neubert, K., Herrmann, K., Burger, R., Gramatzki, M., Hahn, S., Schreiber, S., Wilhelm, S., Herrmann, M., et al. (2007). Extensive immunoglobulin production sensitizes myeloma cells for proteasome inhibition. Cancer Res. *67*, 1783–1792.

Mendoza, M.C., Er, E.E., and Blenis, J. (2011). The Ras-ERK and PI3K-mTOR pathways: cross-talk and compensation. Trends Biochem. Sci. *36*, 320–328.

Michaloglou, C., Vredeveld, L.C., Soengas, M.S., Denoyelle, C., Kuilman, T., van der Horst, C.M., Majoor, D.M., Shay, J.W., Mooi, W.J., and Peeper, D.S. (2005). BRAFE600-associated senescence-like cell cycle arrest of human naevi. Nature *436*, 720–724.

Mimura, N., Fulciniti, M., Gorgun, G., Tai, Y.T., Cirstea, D., Santo, L., Hu, Y., Fabre, C., Minami, J., Ohguchi, H., et al. (2012). Blockade of XBP1 splicing by inhibition of IRE1α is a promising therapeutic option in multiple myeloma. Blood *119*, 5772–5781.

Muñoz, J.P., Ivanova, S., Sánchez-Wandelmer, J., Martínez-Cristóbal, P., Noguera, E., Sancho, A., Díaz-Ramos, A., Hernández-Alvarez, M.I., Sebastián, D., Mauvezin, C., et al. (2013). Mfn2 modulates the UPR and mitochondrial function via repression of PERK. EMBO J. *32*, 2348–2361.

Obeid, M., Tesniere, A., Ghiringhelli, F., Fimia, G.M., Apetoh, L., Perfettini, J.L., Castedo, M., Mignot, G., Panaretakis, T., Casares, N., et al. (2007). Calreticulin exposure dictates the immunogenicity of cancer cell death. Nat. Med. *13*, 54–61.

Oerlemans, R., Franke, N.E., Assaraf, Y.G., Cloos, J., van Zantwijk, I., Berkers, C.R., Scheffer, G.L., Debipersad, K., Vojtekova, K., Lemos, C., et al. (2008). Molecular basis of bortezomib resistance: proteasome subunit beta5 (PSMB5) gene mutation and overexpression of PSMB5 protein. Blood *112*, 2489–2499.

Ozcan, U., Ozcan, L., Yilmaz, E., Düvel, K., Sahin, M., Manning, B.D., and Hotamisligil, G.S. (2008). Loss of the tuberous sclerosis complex tumor suppressors triggers the unfolded protein response to regulate insulin signaling and apoptosis. Mol. Cell *29*, 541–551.

Pan, Z., Erkan, M., Streit, S., Friess, H., and Kleeff, J. (2009). Silencing of GRP94 expression promotes apoptosis in pancreatic cancer cells. Int. J. Oncol. *35*, 823–828.

Panaretakis, T., Kepp, O., Brockmeier, U., Tesniere, A., Bjorklund, A.C., Chapman, D.C., Durchschlag, M., Joza, N., Pierron, G., van Endert, P., et al.

(2009). Mechanisms of pre-apoptotic calreticulin exposure in immunogenic cell death. EMBO J. *28*, 578–590.

Papandreou, I., Denko, N.C., Olson, M., Van Melckebeke, H., Lust, S., Tam, A., Solow-Cordero, D.E., Bouley, D.M., Offner, F., Niwa, M., and Koong, A.C. (2011). Identification of an Ire1alpha endonuclease specific inhibitor with cytotoxic activity against human multiple myeloma. Blood *117*, 1311–1314.

Pikarsky, E., Porat, R.M., Stein, I., Abramovitch, R., Amit, S., Kasem, S., Gutkovich-Pyest, E., Urieli-Shoval, S., Galun, E., and Ben-Neriah, Y. (2004). NF-kappaB functions as a tumour promoter in inflammation-associated cancer. Nature *431*, 461–466.

Powers, M.V., Clarke, P.A., and Workman, P. (2008). Dual targeting of HSC70 and HSP72 inhibits HSP90 function and induces tumor-specific apoptosis. Cancer Cell *14*, 250–262.

Reddy, R.K., Lu, J., and Lee, A.S. (1999). The endoplasmic reticulum chaperone glycoprotein GRP94 with Ca(2+)-binding and antiapoptotic properties is a novel proteolytic target of calpain during etoposide-induced apoptosis. J. Biol. Chem. *274*, 28476–28483.

Rodrigues, L.M., Chung, Y.L., Al Saffar, N.M., Sharp, S.Y., Jackson, L.E., Banerji, U., Stubbs, M., Leach, M.O., Griffiths, J.R., and Workman, P. (2012). Effects of HSP90 inhibitor 17-allylamino-17-demethoxygeldanamycin (17-AAG) on NEU/HER2 overexpressing mammary tumours in MMTV-NEU-NT mice monitored by Magnetic Resonance Spectroscopy. BMC Res. Notes *5*, 250.

Romero-Ramirez, L., Cao, H., Nelson, D., Hammond, E., Lee, A.H., Yoshida, H., Mori, K., Glimcher, L.H., Denko, N.C., Giaccia, A.J., et al. (2004). XBP1 is essential for survival under hypoxic conditions and is required for tumor growth. Cancer Res. *64*, 5943–5947.

Rosati, E., Sabatini, R., Rampino, G., De Falco, F., Di Ianni, M., Falzetti, F., Fettucciari, K., Bartoli, A., Screpanti, I., and Marconi, P. (2010). Novel targets for endoplasmic reticulum stress-induced apoptosis in B-CLL. Blood *116*, 2713–2723.

Roué, G., Pérez-Galán, P., Mozos, A., López-Guerra, M., Xargay-Torrent, S., Rosich, L., Saborit-Villarroya, I., Normant, E., Campo, E., and Colomer, D. (2011). The Hsp90 inhibitor IPI-504 overcomes bortezomib resistance in mantle cell lymphoma in vitro and in vivo by down-regulation of the prosurvival ER chaperone BiP/Grp78. Blood *117*, 1270–1279.

Rouschop, K.M., van den Beucken, T., Dubois, L., Niessen, H., Bussink, J., Savelkouls, K., Keulers, T., Mujcic, H., Landuyt, W., Voncken, J.W., et al. (2010). The unfolded protein response protects human tumor cells during hypoxia through regulation of the autophagy genes MAP1LC3B and ATG5. J. Clin. Invest. *120*, 127–141.

Rouschop, K.M., Dubois, L.J., Keulers, T.G., van den Beucken, T., Lambin, P., Bussink, J., van der Kogel, A.J., Koritzinsky, M., and Wouters, B.G. (2013). PERK/eIF2α signaling protects therapy resistant hypoxic cells through induction of glutathione synthesis and protection against ROS. Proc. Natl. Acad. Sci. USA *110*, 4622–4627.

Sahlgren, C., Gustafsson, M.V., Jin, S., Poellinger, L., and Lendahl, U. (2008). Notch signaling mediates hypoxia-induced tumor cell migration and invasion. Proc. Natl. Acad. Sci. USA *105*, 6392–6397.

Schewe, D.M., and Aguirre-Ghiso, J.A. (2009). Inhibition of eIF2alpha dephosphorylation maximizes bortezomib efficiency and eliminates quiescent multiple myeloma cells surviving proteasome inhibitor therapy. Cancer Res. *69*, 1545–1552.

Senovilla, L., Vitale, I., Martins, I., Tailler, M., Pailleret, C., Michaud, M., Galluzzi, L., Adjemian, S., Kepp, O., Niso-Santano, M., et al. (2012). An immunosurveillance mechanism controls cancer cell ploidy. Science *337*, 1678–1684.

Shirley, C.M., Chen, J., Shamay, M., Li, H., Zahnow, C.A., Hayward, S.D., and Ambinder, R.F. (2011). Bortezomib induction of C/EBPβ mediates Epstein-Barr virus lytic activation in Burkitt lymphoma. Blood *117*, 6297–6303.

Siegelin, M.D., Dohi, T., Raskett, C.M., Orlowski, G.M., Powers, C.M., Gilbert, C.A., Ross, A.H., Plescia, J., and Altieri, D.C. (2011). Exploiting the mitochondrial unfolded protein response for cancer therapy in mice and human cells. J. Clin. Invest. *121*, 1349–1360.

Song, B., Scheuner, D., Ron, D., Pennathur, S., and Kaufman, R.J. (2008). Chop deletion reduces oxidative stress, improves beta cell function, and promotes cell survival in multiple mouse models of diabetes. J. Clin. Invest. *118*, 3378–3389.

Szokalska, A., Makowski, M., Nowis, D., Wilczynski, G.M., Kujawa, M., Wójcik, C., Mlynarczuk-Bialy, I., Salwa, P., Bil, J., Janowska, S., et al. (2009). Proteasome inhibition potentiates antitumor effects of photodynamic therapy in mice through induction of endoplasmic reticulum stress and unfolded protein response. Cancer Res. *69*, 4235–4243.

Tabas, I., and Ron, D. (2011). Integrating the mechanisms of apoptosis induced by endoplasmic reticulum stress. Nat. Cell Biol. *13*, 184–190.

Tanjore, H., Cheng, D.S., Degryse, A.L., Zoz, D.F., Abdolrasulnia, R., Lawson, W.E., and Blackwell, T.S. (2011). Alveolar epithelial cells undergo epithelial-to-mesenchymal transition in response to endoplasmic reticulum stress. J. Biol. Chem. *286*, 30972–30980.

Tsaytler, P., Harding, H.P., Ron, D., and Bertolotti, A. (2011). Selective inhibition of a regulatory subunit of protein phosphatase 1 restores proteostasis. Science *332*, 91–94.

Ulianich, L., Garbi, C., Treglia, A.S., Punzi, D., Miele, C., Raciti, G.A., Beguinot, F., Consiglio, E., and Di Jeso, B. (2008). ER stress is associated with dedifferentiation and an epithelial-to-mesenchymal transition-like phenotype in PC Cl3 thyroid cells. J. Cell Sci. *121*, 477–486.

Verfaillie, T., Rubio, N., Garg, A.D., Bultynck, G., Rizzuto, R., Decuypere, J.P., Piette, J., Linehan, C., Gupta, S., Samali, A., and Agostinis, P. (2012). PERK is required at the ER-mitochondrial contact sites to convey apoptosis after ROS-based ER stress. Cell Death Differ. *19*, 1880–1891.

Walter, P., and Ron, D. (2011). The unfolded protein response: from stress pathway to homeostatic regulation. Science *334*, 1081–1086.

Wang, Q., He, Z., Zhang, J., Wang, Y., Wang, T., Tong, S., Wang, L., Wang, S., and Chen, Y. (2005). Overexpression of endoplasmic reticulum molecular chaperone GRP94 and GRP78 in human lung cancer tissues and its significance. Cancer Detect. Prev. *29*, 544–551.

Wang, Q., Li, L., and Ye, Y. (2008). Inhibition of p97-dependent protein degradation by Eeyarestatin I. J. Biol. Chem. *283*, 7445–7454.

Wang, Q., Mora-Jensen, H., Weniger, M.A., Perez-Galan, P., Wolford, C., Hai, T., Ron, D., Chen, W., Trenkle, W., Wiestner, A., and Ye, Y. (2009). ERAD inhibitors integrate ER stress with an epigenetic mechanism to activate BH3-only protein NOXA in cancer cells. Proc. Natl. Acad. Sci. USA *106*, 2200–2205.

Wang, Y., Alam, G.N., Ning, Y., Visioli, F., Dong, Z., Nör, J.E., and Polverini, P.J. (2012). The unfolded protein response induces the angiogenic switch in human tumor cells through the PERK/ATF4 pathway. Cancer Res. *72*, 5396–5406.

Wheeler, M.C., Rizzi, M., Sasik, R., Almanza, G., Hardiman, G., and Zanetti, M. (2008). KDEL-retained antigen in B lymphocytes induces a proinflammatory response: a possible role for endoplasmic reticulum stress in adaptive T cell immunity. J. Immunol. *181*, 256–264.

Young, R.M., Ackerman, D., Quinn, Z.L., Mancuso, A., Gruber, M., Liu, L., Giannoukos, D.N., Bobrovnikova-Marjon, E., Diehl, J.A., Keith, B., and Simon, M.C. (2013). Dysregulated mTORC1 renders cells critically dependent on desaturated lipids for survival under tumor-like stress. Genes Dev. *27*, 1115–1131.

Zeng, N., Li, Y., He, L., Xu, X., Galicia, V., Deng, C., and Stiles, B.L. (2011). Adaptive basal phosphorylation of eIF2α is responsible for resistance to cellular stress-induced cell death in Pten-null hepatocytes. Mol. Cancer Res. *9*, 1708–1717.

Zhang, K., Shen, X., Wu, J., Sakaki, K., Saunders, T., Rutkowski, D.T., Back, S.H., and Kaufman, R.J. (2006). Endoplasmic reticulum stress activates cleavage of CREBH to induce a systemic inflammatory response. Cell *124*, 587–599.

Zheng, H.C., Takahashi, H., Li, X.H., Hara, T., Masuda, S., Guan, Y.F., and Takano, Y. (2008). Overexpression of GRP78 and GRP94 are markers for aggressive behavior and poor prognosis in gastric carcinomas. Hum. Pathol. *39*, 1042–1049.

CellPress

Cancer Cell
Article

A Long Noncoding RNA Activated by TGF-β Promotes the Invasion-Metastasis Cascade in Hepatocellular Carcinoma

Ji-hang Yuan,[1] Fu Yang,[1] Fang Wang,[1] Jin-zhao Ma,[1] Ying-jun Guo,[1] Qi-fei Tao,[2] Feng Liu,[1] Wei Pan,[1] Tian-tian Wang,[1] Chuan-chuan Zhou,[1] Shao-bing Wang,[1] Yu-zhao Wang,[1] Yuan Yang,[2] Ning Yang,[3] Wei-ping Zhou,[2] Guang-shun Yang,[3] and Shu-han Sun[1,*]

[1]Department of Medical Genetics, Second Military Medical University, Shanghai, 200433, China
[2]The Third Department of Hepatic Surgery, Eastern Hepatobiliary Hospital, Second Military Medical University, Shanghai, 200433, China
[3]The Fifth Department of Hepatic Surgery, Eastern Hepatobiliary Hospital, Second Military Medical University, Shanghai, 200433, China
*Correspondence: shsun@vip.sina.com
http://dx.doi.org/10.1016/j.ccr.2014.03.010

SUMMARY

The role of TGF-β-induced epithelial-mesenchymal transition (EMT) in cancer cell dissemination is well established, but the involvement of lncRNAs in TGF-β signaling is still unknown. In this study, we observed that the lncRNA-activated by TGF-β (lncRNA-ATB) was upregulated in hepatocellular carcinoma (HCC) metastases and associated with poor prognosis. lncRNA-ATB upregulated ZEB1 and ZEB2 by competitively binding the miR-200 family and then induced EMT and invasion. In addition, lncRNA-ATB promoted organ colonization of disseminated tumor cells by binding IL-11 mRNA, autocrine induction of IL-11, and triggering STAT3 signaling. Globally, lncRNA-ATB promotes the invasion-metastasis cascade. Thus, these findings suggest that lncRNA-ATB, a mediator of TGF-β signaling, could predispose HCC patients to metastases and may serve as a potential target for antimetastatic therapies.

INTRODUCTION

Hepatocellular carcinoma (HCC) is one of the most common and aggressive human malignancies in the world (Jemal et al., 2011). The poor prognosis and high recurrence rate of HCC is largely due to the high rate of intrahepatic and extrahepatic metastases (Budhu et al., 2006). This emphasizes the urgency of identifying these patients in advance and establishing new therapeutic targets for successful intervention. Metastasis is a complex process, and many cell-intrinsic identities and extrinsic microenvironment factors influence the metastatic potential of HCC cells (Fidler, 2003). However, the underlying molecular mechanisms that mediate the metastatic cascade remain largely unclear. Enhancing our understanding of the molecular mechanisms may promote the development of effective metastasis-targeted therapy and improve the overall prognosis of patients with HCC.

The multifunctional cytokine transforming growth factor β (TGF-β) orchestrates an intricate signaling network to modulate tumorigenesis and progression (Majumdar et al., 2012; Massagué, 2008). TGF-β exerts its tumor-suppressive role by inducing cell-cycle arrest and apoptosis (Pardali and Moustakas, 2007). Nevertheless, TGF-β also promotes tumor progression through enhancing proliferation, migration, and invasion, in part by its ability to induce epithelial-mesenchymal transition (EMT) (Akhurst and Hata, 2012). EMT has been shown to be of critical importance in the early events of tumor cell metastatic dissemination by endowing cells with a more motile, invasive potential (Thiery et al., 2009). However, the involvement of EMT and its reverse process, mesenchymal-epithelial transition (MET) in the late events of tumor cell metastasis, such as distant colonization, are still hotly debated (Ocaña et al., 2012; Tsai et al., 2012). The multiple and often contradictory functions of TGF-β necessitate both a better understanding of the special downstream effectors

Significance

Metastases account for the vast majority of cancer-associated deaths and TGF-β-induced EMT has been associated with tumor invasion. However, the tumor-suppressive role of TGF-β hinders the application of anti-TGF-β cancer treatments. The involvement of EMT in metastatic colonization is still hotly debated. We found that lncRNA activated by TGF-β (lncRNA-ATB) can mimic the prometastatic role of TGF-β. lncRNA-ATB induced EMT and tumor cell invasion and promoted the colonization of disseminated tumor cells. High expression of lncRNA-ATB is a robust predictor of poor survival. Therefore, lncRNA-ATB may serve as a target for therapeutic intervention against cancer metastases early in the metastatic process and when patients present with circulating tumor cells.

of TGF-β and a search for specific inhibitors of the different TGF-β-dependent pathways for HCC treatment.

Long noncoding RNAs (lncRNAs) are a class of transcripts longer than 200 nucleotides with limited protein coding potential. Recently, many studies have shown that lncRNAs are frequently deregulated in various diseases and have multiple functions in a wide range of biological processes, such as proliferation, apoptosis, or cell migration (Mercer et al., 2009; Ponting et al., 2009). Although several lncRNAs have been reported to modulate tumor metastases (Gupta et al., 2010; Prensner et al., 2013), the specific roles of lncRNAs in mediating the prometastatic role of TGF-β and regulating EMT are not well studied. In this study, we report the identification of lncRNA-AL589182.3 (ENST00000493038), which we have named lncRNA-activated by TGF-β (lncRNA-ATB), and focus on the role of lncRNA-ATB in TGF-β signaling and in the invasion-metastasis cascade of HCC.

RESULTS

lncRNA-ATB Is Upregulated by TGF-β and Is Physically Associated with the miR-200 Family

To identify lncRNAs that are regulated by TGF-β and mediated the role of TGF-β in inducing EMT, we treated SMMC-7721 hepatoma cells continuously with TGF-β for 21 days, which caused SMMC-7721 cells to undergo EMT, as indicated by a spindle-shaped appearance (Figure S1A available online), decreased expression of the epithelial marker CDH1, and increased expression of the mesenchymal markers and transcription factors CDH2, VIM, ZEB1, SNAI1, and TWIST1 (Figure S1B). We then used microarray analysis to compare lncRNA expression levels between TGF-β treated and untreated cells, and found 676 upregulated and 297 downregulated lncRNAs in the treated cells (Table S1). Microarray results also indicated that TGF-β treatment led to EMT gene expression signature (Figure S1C; Huang et al., 2012) and gene set enrichment analysis (GSEA; Subramanian et al., 2005) indicated that four published TGF-β response signatures (Calon et al., 2012; Kang et al., 2003; Padua et al., 2008) were significantly enriched in the treated cells (Figure S1D), which further confirmed that the microarray results were trustable and TGF-β treatment for 21 days indeed induced EMT.

Recently, many RNA transcripts have been reported to function as competing endogenous RNAs (ceRNA) by competitively binding common microRNAs (Cesana et al., 2011; Salmena et al., 2011; Tay et al., 2011). The miR-200 family, including miR-200a, miR-200b, miR-200c, miR-141, and miR-429, has been reported to repress EMT and tumor invasion by targeting the 3′UTRs of ZEB1 and ZEB2 (Burk et al., 2008; Gregory et al., 2008). Among the deregulated lncRNAs, we predicted 76 miR-200s targeting sites on 46 lncRNAs (Table S2) using the TargetScan prediction algorithm (Lewis et al., 2005; http://www.targetscan.org/). Interestingly, one of the upregulated lncRNAs, lncRNA-ATB, which has a relatively large fold change, has three predicted miR-200s targeting sites in a relatively short span (Figures 1A and 1B), indicating a strong possibility as a ceRNA (Tay et al., 2011).

To confirm the microarray result, we treated SMMC-7721 and the normal liver cell line QSG-7701 with TGF-β and measured the expression of lncRNA-ATB at various time points. TGF-β induced a robust increase of lncRNA-ATB in both cells, not only in the long-term treatment, but also in short-term treatment (Figures 1C–1F). In breast cancer cell line MCF7 and colorectal cancer cell line SW480, TGF-β also upregulated lncRNA-ATB (Figures S1E and S1F).

The sequence of full-length lncRNA-ATB is presented in Figures S1G and S1H. Northern blot analysis of lncRNA-ATB confirmed the expected size (Figure 1G). Using a BLAST search of the sequence of lncRNA-ATB against the human genome, we found another three highly homologous lncRNA-ATB loci on chromosomes 13, 14, and 22, suggesting there may be an lncRNA family, which includes lncRNA-ATB. lncRNA-ATB was poly (A)-negative and mainly located in the cytoplasm (Figures S1I and S1J). Analysis of the sequences by ORF Finder from the National Center for Biotechnology Information failed to predict a protein of more than 55 amino acids (Figure S1K). Moreover, lncRNA-ATB does not contain a valid Kozak sequence. In addition, we used txCdsPredict from UCSC and PhyloCSF (Lin et al., 2011) to calculate its coding potential. The txCdsPredict score of lncRNA-ATB is 309.5 and the codon substitution frequency score is lower than −500 (Figure S1L), which further supports that lncRNA-ATB has no protein-coding potential. An analysis with quantitative (q)RT-PCR revealed a significantly higher expression of lncRNA-ATB in HCC cells than in normal liver cells, especially in highly metastatic cells (Figures S1M and S1N).

To validate the direct binding between miR-200s and lncRNA-ATB at endogenous levels, we performed an RNA immunoprecipitation (RIP) to pull down endogenous microRNAs associated with lncRNA-ATB and demonstrated via qPCR analysis that the lncRNA-ATB RIP in SMMC-7721 cells was significantly enriched for miR-200s compared to the empty vector (MS2), IgG, nontargeting microRNA (miR-122), lncRNA-ATB with mutations in miR-200s targeting sites (henceforth named ATB-mut(miR-200)), and another lncRNA-ENST00000508851 (RP11-893F2.9; henceforth named lncRNA-508851), which is also induced by TGF-β, but does not have a predicated miR-200s targeting site (Figure 1H; Figure S1O). The specific association between miR-200s and lncRNA-ATB was further validated by affinity pull-down of endogenous miR-200s using in vitro transcribed biotin-labeled lncRNA-ATB (Figure 1I). For further confirmation, we constructed luciferase reporters containing the 3′ 500nt of lncRNA-ATB, which contains wild-type (WT) or mutated miR-200s binding sites. We found that overexpression of miR-200s reduced the luciferase activities of the WT reporter vector but not empty vector or mutant reporter vector (Figure 1J). However, we found no significant difference in lncRNA-ATB levels after overexpression of miR-200s (Figure S1P). The microRNAs are known to bind their targets and cause translational repression and/or RNA degradation in an AGO2-dependent manner. To determine whether lncRNA-ATB was regulated by miR-200s in such a manner, we conducted anti-AGO2 RIP in SMMC-7721 cells transiently overexpressing miR-200s. Endogenous lncRNA-ATB pull-down by AGO2 was specifically enriched in miR-200s-transfected cells (Figure 1K), supporting that miR-200s are bona fide lncRNA-ATB-targeting microRNAs. These data demonstrated that miR-200s bound to lncRNA-ATB but did not induce the degradation of lncRNA-ATB. Ectopically expressed lncRNA-ATB WT, but not the mutant or lncRNA-508851, reduced the levels of miR-200s (Figure S1Q). To function

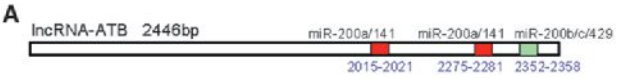

B

microRNA	matching	position
miR-200a	3' uguAGCAAUGGU- -CUGUCACAAu 5' 5' aacT TGTAGCCACCTTCAGTGTTt 3'	2015-2021
miR-141	3' ggUAGAA- AU- GGU- -CUGUCACAAu 5' 5' atAACTTGTAGCCACCTTCAGTGTTt 3'	2015-2021
miR-200a	3' uguagcaaugguCUGUCACAAu 5' 5' ga ta tccag t t tGACAGTGTTc 3'	2275-2281
miR-141	3' ggUAGAAAU-GGUCUGUCACAAu 5' 5' ggATATCCAGTT TGACAGTGTTc 3'	2275-2281
miR-200b	3' aguaguaaugguccgUCAUAAU 5' 5' aacagagaguaacagAGUAUUA 3'	2352-2358
miR-200c	3' agguaguaaugggccgUCAUAAU 5' 5' caacagagaguaacagAGUAUUA 3'	2352-2358
miR-429	3' ugccaaaauggucugUCAUAAU 5' 5' aacagagaguaacagAGUAUUA 3'	2352-2358

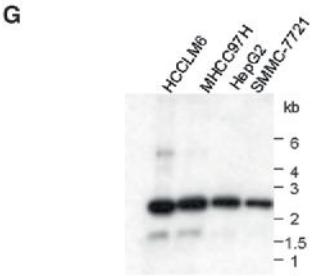

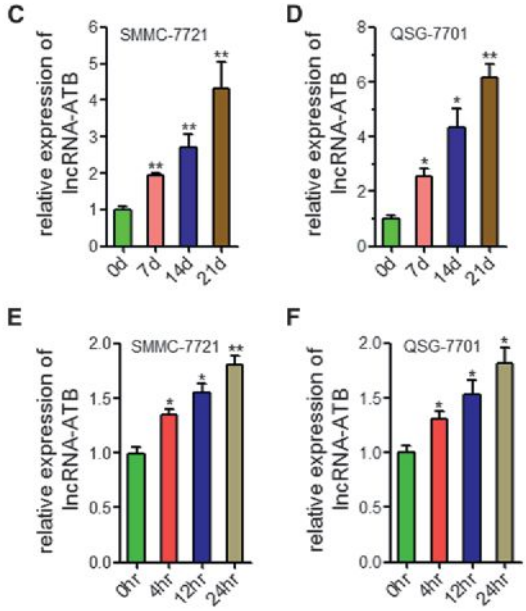

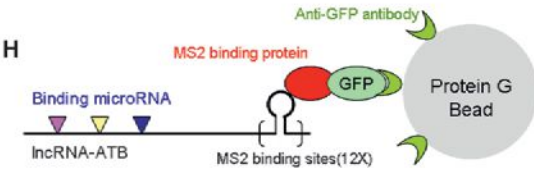

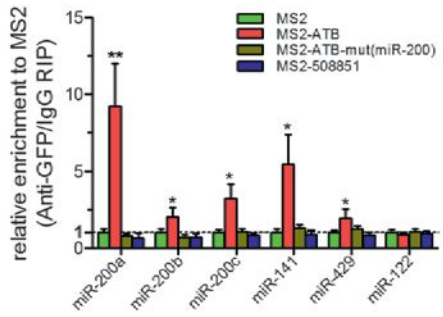

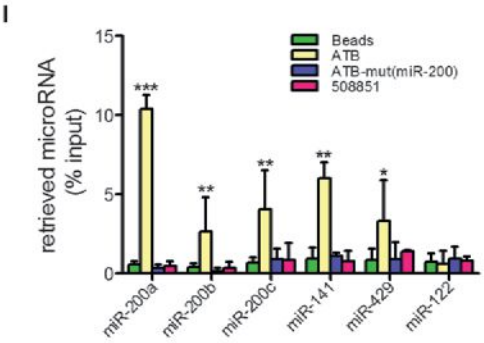

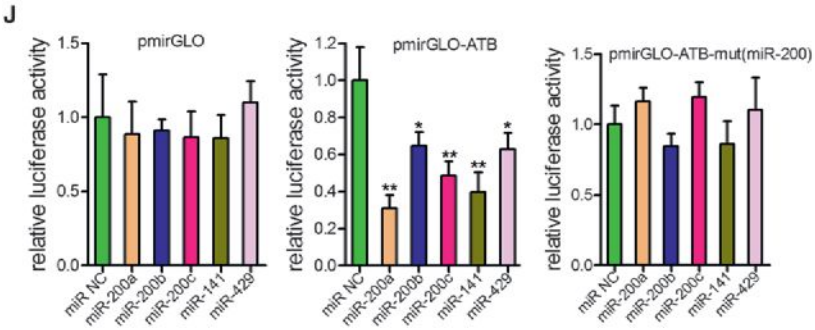

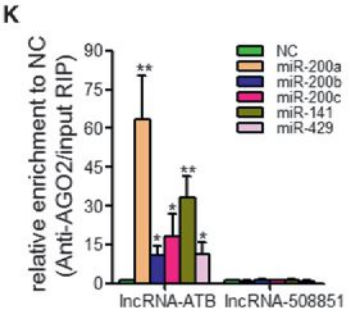

(legend on next page)

as a ceRNA, the abundance of lncRNA-ATB and miR-200s should be comparable. We therefore used quantitative real-time PCR to quantify the exact copy numbers of lncRNA-ATB and miR-200s per cell in TGF-β treated and untreated SMMC-7721 cells. We formulated standard curves with limit dilution approaches using lncRNA-ATB expressing vector pcDNA3.1-ATB and reverse-transcribed miR-200s cDNA as standard templates, and then the exact copy numbers of lncRNA-ATB and miR-200s per cell were calculated according to cell counts and molecular weights. As a result, we found that in the untreated cells, the expression level of lncRNA-ATB was approximately 100 copies per cell, and mature miR-200s levels were approximately 200 copies per cell. TGF-β treatment induced upregulation of lncRNA-ATB and downregulation of miR-200s (Figure S1R). This result implied that lncRNA-ATB may be able to function as a ceRNA for miR-200s. All these data demonstrated that lncRNA-ATB physically associated with the miR-200 family and may function as a ceRNA.

lncRNA-ATB Upregulates ZEB1 and ZEB2 Levels

Because lncRNA-ATB shares regulatory miR-200s with ZEB1 and ZEB2, we wondered whether lncRNA-ATB could modulate ZEB1 and ZEB2 and then EMT and invasion of HCC cells. We stably overexpressed lncRNA-ATB WT, lncRNA-ATB-mut(miR-200), and lncRNA-508851 in SMMC-7721 cells (Figure 2A; Figure S2A). The overexpression level of mutant clone is similar to that of WT overexpression clone 1, which is also comparable to that in highly metastatic HCCLM6 cells. For the rescue experiment, we stably overexpressed miR-200a in lncRNA-ATB overexpression clone 1 (Figure S2B). Overexpression of lncRNA-ATB WT, but not the mutant or lncRNA-508851, increased ZEB1 and ZEB2 transcript and protein levels in a dose-dependent manner. Ectopic expression of miR-200a abrogated this increase (Figures 2B and 2C). In QSG-7701 cells, stable overexpression of lncRNA-ATB also upregulated ZEB1 and ZEB2 (Figures 2D–2F). Additionally, HCCLM6 cells with stably downregulated lncRNA-ATB or lncRNA-508851 were also constructed, which do not have any effect on other family members of lncRNA-ATB (Figure 2G; Figures S2C and S2D). For the rescue experiment, we inhibited miR-200a in lncRNA-ATB downregulated HCCLM6 clone 1 (Figure S2E). The depletion of lncRNA-ATB, but not lncRNA-508851, decreased ZEB1 and ZEB2 in a dose-dependent manner. Inhibition of miR-200a overcame the decrease of ZEB1 and ZEB2 (Figures 2H and 2I).

To ascertain whether this observed effect depends on regulation of the ZEB1 and ZEB2 3′UTR, we constructed luciferase reporters containing either the ZEB1 or ZEB2 3′UTR (pmirGLO-ZEB1 or pmirGLO-ZEB2). Luciferase plasmid (pmirGLO-ZEB1, pmirGLO-ZEB2, or the control reporter [pmirGLO]) was transfected into the different SMMC-7721 and HCCLM6 cell clones. Overexpression of lncRNA-ATB, but not the mutant or lncRNA-508851, increased the luciferase activity of pmirGLO-ZEB1 and pmirGLO-ZEB2 in a dose-dependent manner. Ectopic expression of miR-200a abolished this upregulation (Figure 2J). Reciprocally, the depletion of lncRNA-ATB, but not lncRNA-508851, decreased the luciferase activity of pmirGLO-ZEB1 and pmirGLO-ZEB2, which were rescued by inhibition of miR-200a (Figure 2K).

Because lncRNA-ATB could upregulate ZEB1 and ZEB2, we next examined whether lncRNA-ATB is coexpressed with ZEB1 and ZEB2 in human HCC samples. We measured the expression levels of lncRNA-ATB, ZEB1, and ZEB2 in 86 human HCC tissues. As shown in Figures 2L and 2M, lncRNA-ATB transcript level was significantly correlated with ZEB1 or ZEB2 mRNA level. All these results suggest an important role of lncRNA-ATB in modulating ZEB1 and ZEB2 by competitively binding miR-200s.

lncRNA-ATB Induces EMT and Cell Invasion In Vitro

To investigate whether lncRNA-ATB regulates EMT through modulating ZEB1 and ZEB2, we first examined the effect of lncRNA-ATB on cell phenotypes. Overexpression of lncRNA-ATB WT, but not the mutant or lncRNA-508851, induced mesenchymal-like morphological feature in SMMC-7721 cells. Ectopic expression of miR-200a caused lncRNA-ATB overexpressed cells to revert to an epithelial phenotype (Figure 3A). Analysis of the epithelial markers E-cadherin and ZO-1 and the mesenchymal markers N-cadherin and vimentin revealed that overexpression of lncRNA-ATB, but not the mutant or lncRNA-508851, reduced E-cadherin and ZO-1 and increased N-cadherin and vimentin. Consistently, ectopic expression of miR-200a abolished the effects (Figures 3B and 3C). Immunofluorescence staining also revealed that overexpression of lncRNA-ATB, but not the mutant or lncRNA-508851, induced loss of E-cadherin and ZO-1 expression from the cell membrane, and increased N-cadherin and vimentin, which was also abolished by overexpression of miR-200a (Figure 3D). Conversely, the depletion of lncRNA-ATB, but not lncRNA-508851, induced an epithelial phenotype, upregulated E-cadherin and ZO-1, as well as downregulated N-cadherin and vimentin in HCCLM6 cells, which were also abrogated by inhibition of miR-200a (Figures 3E–3G). Moreover, depletion of lncRNA-ATB attenuated TGF-β-induced EMT in SMMC-7721 cells (Figure S3A; Figures 3H and 3I). Overexpression of lncRNA-ATB also induced EMT in QSG-7701 cells and MCF7 cells (Figures S3B–S3H). To further support this conclusion, we construct stable SMMC-7721 cell clone that overexpressed

Figure 1. lncRNA-ATB Is Upregulated by TGF-β and Interacts with miR-200s

(A) Schematic outlining the predicted binding sites of miR-200s on lncRNA-ATB.

(B) The prediction for miR-200s binding sites on lncRNA-ATB transcript. The red nucleotides are the seed sequences of microRNAs.

(C–F) Relative expression of lncRNA-ATB in SMMC-7721 cells or QSG-7701 cells treated with TGF-β1 for the indicated time was measured by qRT-PCR.

(G) Northern blot analysis of lncRNA-ATB in HCC cells.

(H) MS2-RIP followed by microRNA qRT-PCR to detect microRNAs endogenously associated with lncRNA-ATB.

(I) SMMC-7721 cell lysates were incubated with biotin-labeled lncRNA-ATB; after pull-down, microRNAs was extracted and assessed by qRT-PCR.

(J) Luciferase activity in SMMC-7721 cells cotransfected with miR-200s and luciferase reporters containing nothing, lncRNA-ATB or mutant transcript. Data are presented as the relative ratio of firefly luciferase activity to renilla luciferase activity.

(K) Anti-AGO2 RIP was performed in SMMC-7721 cells transiently overexpressing miR-200s, followed by qRT-PCR to detect lncRNA-ATB or lncRNA-508851 associated with AGO2.

Data are shown as mean ± SD; n = 3. *$p < 0.05$, **$p < 0.01$, ***$p < 0.001$ (Student's t test). See also Figure S1 and Tables S1 and S2.

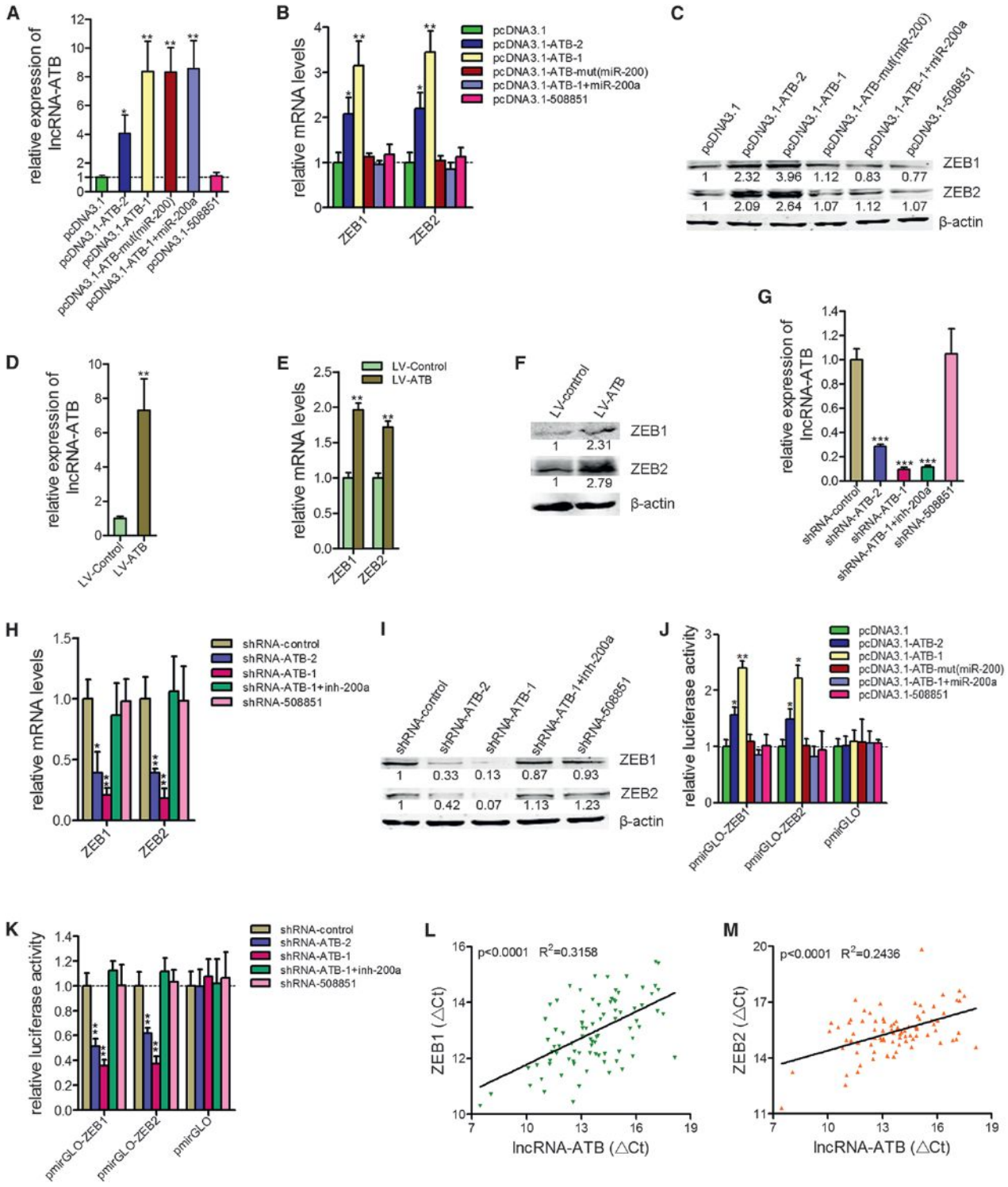

Figure 2. Regulation of ZEB1 and ZEB2 by lncRNA-ATB

(A) The expression of lncRNA-ATB in stable SMMC-7721 cell clones.

(B and C) The mRNA (B) or protein (C) levels of ZEB1 and ZEB2 in stable SMMC-7721 cell clones.

(D) The expression of lncRNA-ATB in stable QSG-7701 cell clones.

(E and F) The mRNA (E) or protein (F) levels of ZEB1 and ZEB2 in stable QSG-7701 cell clones.

(G) The expression of lncRNA-ATB in stable HCCLM6 cell clones.

(H and I) The mRNA (H) or protein (I) levels of ZEB1 and ZEB2 in stable HCCLM6 cell clones.

(legend continued on next page)

miR-200a with a similar overexpression level to the lncRNA-ATB and miR-200a simultaneously overexpressed clone 1 (Figure S3I). Our results indicate that overexpression of lncRNA-ATB rescued the downregulation of ZEB1 and ZEB2 and the inhibition of EMT caused by ectopic expression of miR-200a (Figures S3J and S3K). Taken together, these data suggest a functional role for lncRNA-ATB in inducing EMT. This inducing effect depends on the competitive binding of miR-200s.

Consistent with the different expression of lncRNA-ATB in the four HCC cells in Figure S1M, the expression of ZEB1, ZEB2, N-cadherin, and vimentin were higher and the expression of E-cadherin and ZO-1 were lower in lncRNA-ATB high expression cells (Figure S3L), indicating the expression of lncRNA-ATB was correlated with ZEB1, ZEB2, and EMT features.

To evaluate whether lncRNA-ATB overexpression induced global EMT-related changes, we performed gene expression microarray analysis on lncRNA-ATB overexpressed SMMC-7721 cells. GSEA indicated that three published EMT gene signatures (Alonso et al., 2007; Gotzmann et al., 2006; Huang et al., 2012) were significantly enriched in lncRNA-ATB overexpressed cells (Figure 3J), strongly suggesting that lncRNA-ATB overexpression induces a pervasive and sustained EMT signaling program.

To ascertain the pathological correlation between lncRNA-ATB and EMT in human HCC samples, we measured E-cadherin mRNA level in the same set of 86 HCC tissues shown in Figure 2L and found that lncRNA-ATB transcript level was inversely correlated with E-cadherin mRNA level (Figure 3K), consistent with a role of lncRNA-ATB in EMT.

To directly test whether lncRNA-ATB could promote invasive behavior by promoting EMT-like morphological changes, we determined the invasion ability of different SMMC-7721 and HCCLM6 cell clones using Matrigel-coated transwell experiments. We observed that overexpression of lncRNA-ATB, but not the mutant or lncRNA-508851, significantly increased the invasion potential of SMMC-7721 cells, and this invasion potential was completely abolished when miR-200a was overexpressed (Figure 3L). We also found that depletion of lncRNA-ATB, but not lncRNA-508851, reduced the invasion potential of HCCLM6 cells, which was abrogated by inhibition of miR-200a (Figure 3M). Altogether, these results show that lncRNA-ATB induces EMT and promotes a more invasive phenotype by competitively binding miR-200s.

Aberrant Expression of lncRNA-ATB in Human HCC Tissues

To further define the role of lncRNA-ATB in human HCC, we measured lncRNA-ATB expression level in the same set of HCC tissues shown in Figure 2L and in their pair-matched noncancerous hepatic tissues. The lncRNA-ATB transcript level was higher in the HCC tissues than in the paired adjacent noncancerous hepatic tissues (Figure 4A). We next examined the relationship between lncRNA-ATB expression levels and the clinicopathological characteristics of the 86 HCC samples (Table S3). Correlation regression analysis showed that high expression of lncRNA-ATB was significantly correlated with liver cirrhosis ($p = 0.006$), microvascular invasion ($p = 0.000$), macrovascular invasion ($p = 0.000$), and encapsulation ($p = 0.007$). Portal vein tumor thrombus (PVTT) is the main route for intrahepatic metastasis of HCC cells in human patients. We examined the expression of lncRNA-ATB in 40 pairs of PVTT and pair-matched primary tumor tissues. As shown in Figure 4B, the expression level of lncRNA-ATB was significantly higher in the PVTT tissues than in the primary tumor tissues. These data support that a high level of lncRNA-ATB is strongly associated with the metastasis of HCC cells.

We further examined whether the lncRNA-ATB expression level was correlated with the outcome of HCC after hepatectomy. Kaplan-Meier analysis in the 86 patients with HCC revealed that high lncRNA-ATB expression level in HCC tissues significantly correlated with a reduction in recurrence-free survival ($p < 0.001$; Figure 4C) and overall survival ($p = 0.004$; Figure 4D), consistent with the important roles of lncRNA-ATB in the pathogenesis of HCC and the prognosis of HCC.

lncRNA-ATB Promotes the Invasion-Metastasis Cascade of HCC Cells In Vivo

To evaluate the biological functions of lncRNA-ATB in vivo, we inoculated different clones of SMMC-7721 and HCCLM6 cells subcutaneously into nude mice. Neither the overexpression nor the depletion of lncRNA-ATB had a measurable effect on the growth of tumors and the proportion of proliferating (Ki67+) cancer cells (Figures S4A and S4B; data not shown). We then used subcutaneous tumor tissues to establish orthotopic tumor models. In this model system, lncRNA-ATB overexpression effectively promoted intrahepatic, mesenteric, pulmonic, and diaphragmatic metastases in SMMC-7721 cells. However, mutating the miR-200s binding sites or overexpressing miR-200a only partially abolished the prometastatic role of lncRNA-ATB (Figure 5A; Figures S4C and S4D). We next included a stable SMMC-7721 cell clone with inhibition of miR-200a (Figure S4E) and found that inhibition of miR-200a promoted metastases of SMMC-7721 cells, but the prometastatic role is weaker than that of lncRNA-ATB (Figure 5A; Figure S4C). The depletion of lncRNA-ATB inhibited intrahepatic, mesenteric, and pulmonic metastases in HCCLM6 cells, which was also partially abolished by inhibition of miR-200a (Figure 5B). This implies that miR-200s is most likely not the only functional downstream effector of the prometastatic role of lncRNA-ATB.

Because metastasis is a complex multistep process that involves the early step of tumor invasion and the late step of metastatic colonization in distant organs, we aimed to explore the influence of lncRNA-ATB and miR-200s on the different stages of metastasis. We labeled the different clones with green fluorescent protein (GFP) and established orthotopic tumor models,

(J and K) Luciferase activity in stable SMMC-7721 cell clones (J) or HCCLM6 cell clones (K) transfected with luciferase reporters containing ZEB1 3′UTR, ZEB2 3′UTR or nothing. Data are presented as the relative ratio of firefly luciferase activity to renilla luciferase activity. For (A–K), n = 3, mean ± SD. *$p < 0.05$, **$p < 0.01$, ***$p < 0.001$ (Student's t test).

(L and M) The correlation between lncRNA-ATB transcript level and ZEB1 (L) or ZEB2 (M) mRNA level was measured in 86 HCC tissues. The ΔCt values (normalized to 18S rRNA) were subjected to Pearson correlation analysis.

See also Figure S2.

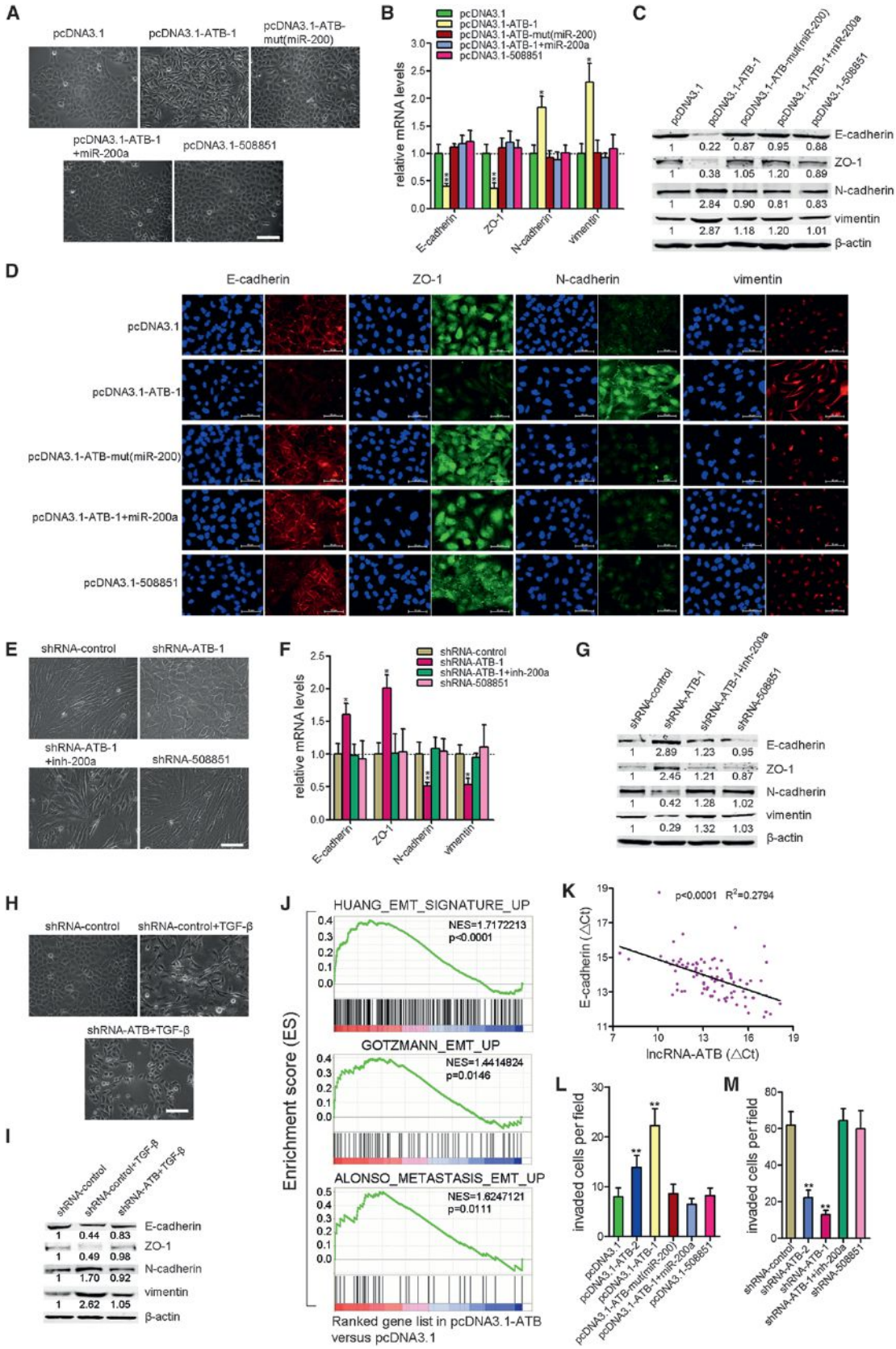

(legend on next page)

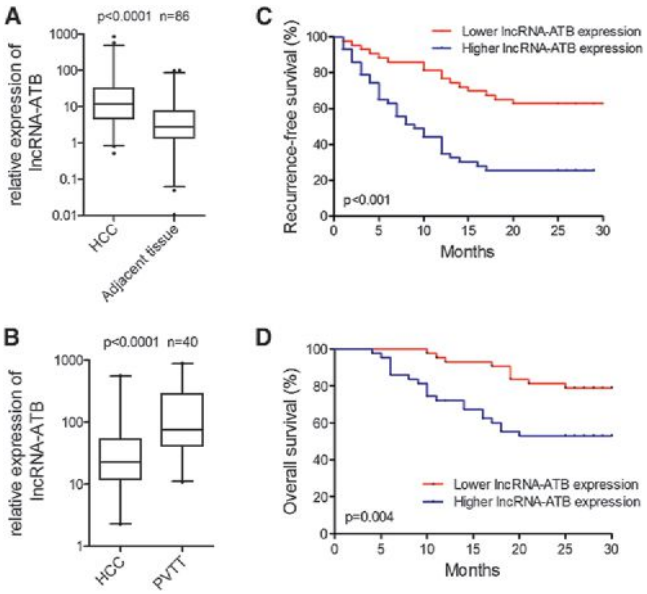

Figure 4. Aberrant Expression of lncRNA-ATB in Clinical Samples

(A) lncRNA-ATB expression in human HCC tissues and paired adjacent noncancerous hepatic tissues. (B) lncRNA-ATB expression in PVTT tissues and paired primary HCC tissues. For (A) and (B), the expression level of lncRNA-ATB was analyzed by qRT-PCR. The horizontal lines in the box plots represent the medians, the boxes represent the interquartile range, and the whiskers represent the 2.5th and 97.5th percentiles. The significant differences between samples were analyzed using the Wilcoxon signed-rank test.

(C and D) Kaplan-Meier analyses of the correlations between lncRNA-ATB expression level and recurrence-free survival (C) or overall survival (D) of 86 patients with HCC. The median expression level was used as the cutoff. Patients with lncRNA-ATB expression values below the 50th percentile were classified as having lower lncRNA-ATB levels. Patients with lncRNA-ATB expression values above the 50th percentile were classified as having higher lncRNA-ATB levels.

See also Table S3.

and 5 weeks later examined circulating tumor cells (CTCs) by flow cytometry from whole-blood samples. As shown in Figure 5C and Figure S4F, ectopic expression of lncRNA-ATB significantly increased the number of CTCs, and the mutation of the miR-200s binding sites or overexpressing miR-200a completely abolished the increase. Inhibition of miR-200a also increased the number of CTCs, which is comparable to that of overexpression of lncRNA-ATB. Reciprocally, the depletion of lncRNA-ATB significantly decreased the number of CTCs, which was abolished by inhibition of miR-200a (Figure 5D). We also analyzed the levels of human LINE1 DNA, another indicator of CTCs, by qPCR of genomic DNA from whole-blood samples. The results were consistent with that of measuring GFP-positive CTCs (Figures 5E and 5F). These data demonstrated that lncRNA-ATB promoted intravasation of HCC cells, which was dependent on the competitive binding of miR-200s.

Consistent with in vitro results, ZEB1, ZEB2, N-cadherin, and vimentin were upregulated, and E-cadherin and ZO-1 were reduced in the orthotopic tumor tissues with lncRNA-ATB overexpression or miR-200a inhibition. In addition, the mutation of the miR-200s binding sites or overexpression of miR-200a completely abolished the effects (Figures S4G–S4J). These data suggest that lncRNA-ATB upregulates ZEB1 and ZEB2, induces EMT, and promotes tumor invasion in vivo, all of which depend on miR-200s.

To explore the influence of lncRNA-ATB on liver colonization, we labeled the different clones with firefly luciferase and inoculated cells intrasplenically into nude mice. Overexpression of lncRNA-ATB resulted in greater liver metastases burden. The mutation of the miR-200s binding sites or overexpression of miR-200a, which induced MET in the liver metastases (Figure S4K), however, did not change this liver metastases-promoting role of lncRNA-ATB. Inhibition of miR-200a also did not influence liver metastases (Figures 5G and 5H; Figures S4L and S4M). The depletion of lncRNA-ATB reduced the liver metastases burden of HCCLM6 cells, which was also not abolished by inhibition of miR-200a (Figures 5I and 5J; Figures S4N and S4O). We further explored the role of lncRNA-ATB in lung colonization by inoculating cells directly into the tail veins of nude mice. We also observed an increase in the lung metastases burden generated by lncRNA-ATB-overexpressing SMMC-7721 cells. The mutation of the miR-200s binding sites or overexpression of miR-200a did not abolish this lung metastases-promoting role of lncRNA-ATB. Inhibition of miR-200a also did not influence lung metastases (Figures 5K and 5L; Figures S4P and S4Q). Reciprocally, the depletion of lncRNA-ATB significantly reduced the lung metastases burden of HCCLM6 cells, which was also not abolished by inhibition of miR-200a (Figures 5M and 5N; Figures S4R and S4S). These results demonstrate that lncRNA-ATB promotes the liver and lung colonization of HCC cells and that this effect is not dependent on miR-200s or EMT. This suggests that other genes or signaling pathways are likely to mediate the procolonization efficiency of lncRNA-ATB. Consistent with in vitro invasion assay results, the in vivo results also indicated that HCCLM6 is highly metastatic compared with SMMC-7721 cells.

Figure 3. The Effects of lncRNA-ATB on EMT and Invasion In Vitro

(A) Phase-contrast micrographs of indicated SMMC-7721 cell clones. Scale bars = 100 μm.

(B and C) The mRNA (B) or protein (C) levels of EMT markers in indicated SMMC-7721 cell clones.

(D) Immunofluorescence microscopy analysis of the localization and expression of EMT markers in indicated SMMC-7721 cell clones. Scale bars = 50 μm.

(E) Phase-contrast micrographs of indicated HCCLM6 cell clones. Scale bars represent 100 μm.

(F and G) The mRNA (F) or protein (G) levels of EMT markers in indicated HCCLM6 cell clones.

(H and I) Phase-contrast micrographs (H) or the protein levels of EMT markers (I) in control and lncRNA-ATB-knockdown SMMC-7721 cells undergoing TGF-induced EMT. Scale bars represent 100 μm.

(J) GSEA of EMT gene signatures in lncRNA-ATB overexpressed SMMC-7721 cells versus control cells. NES, normalized enrichment score.

(K) The correlation between lncRNA-ATB transcript level and E-cadherin mRNA level was measured in 86 HCC tissues. The ΔCt values (normalized to 18S rRNA) were subjected to Pearson correlation analysis.

(L and M) Indicated SMMC-7721 cell clones (L) or HCCLM6 cell clones (M) were added to the top of transwells coated with Matrigel. The number of invasive cells per field was counted after 48 hr. Data are shown as mean ± SD n = 3. *p < 0.05, **p < 0.01 (Student's t test). See also Figure S3.

A

SMMC-7721	Mets	Liver	Mesentery	Lung	Diaphragm
pcDNA3.1	1/10	1/10	0/10	0/10	0/10
pcDNA3.1-ATB-1	9/10**	9/10	5/10	3/10	1/10
pcDNA3.1-ATB-mut(miR-200)	5/10	5/10	2/10	1/10	0/10
pcDNA3.1-ATB-1+miR-200a	5/10	5/10	2/10	1/10	1/10
pcDNA3.1-508851	2/10	2/10	0/10	0/10	0/10
inh-NC	1/10	1/10	0/10	0/10	0/10
inh-200a	5/10	5/10	3/10	2/10	0/10

B

HCCLM6	Mets	Liver	Mesentery	Lung
shRNA-control	8/10	8/10	5/10	3/10
shRNA-ATB-1	1/10**	1/10	0/10	0/10
shRNA-ATB-1+inh-200a	4/10	4/10	2/10	1/10
shRNA-508851	9/10	9/10	5/10	4/10

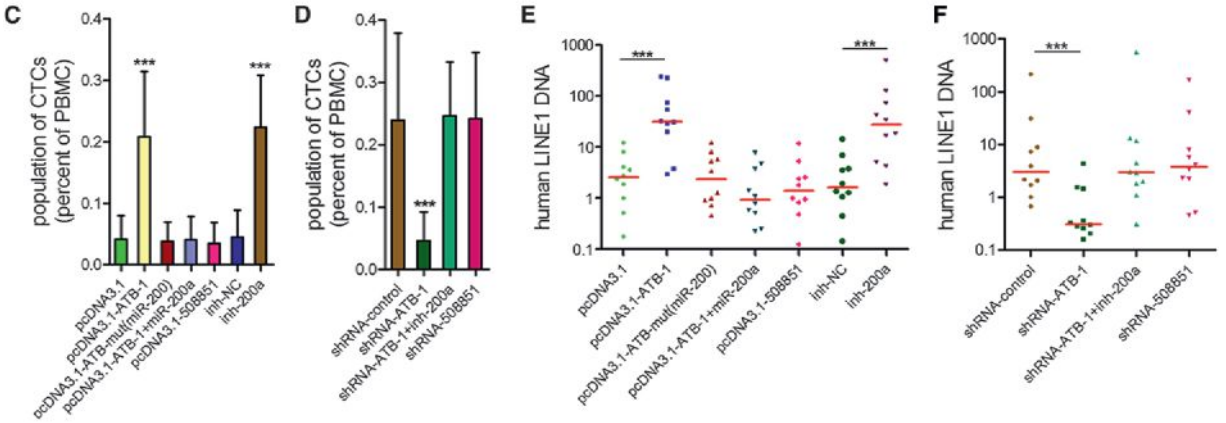

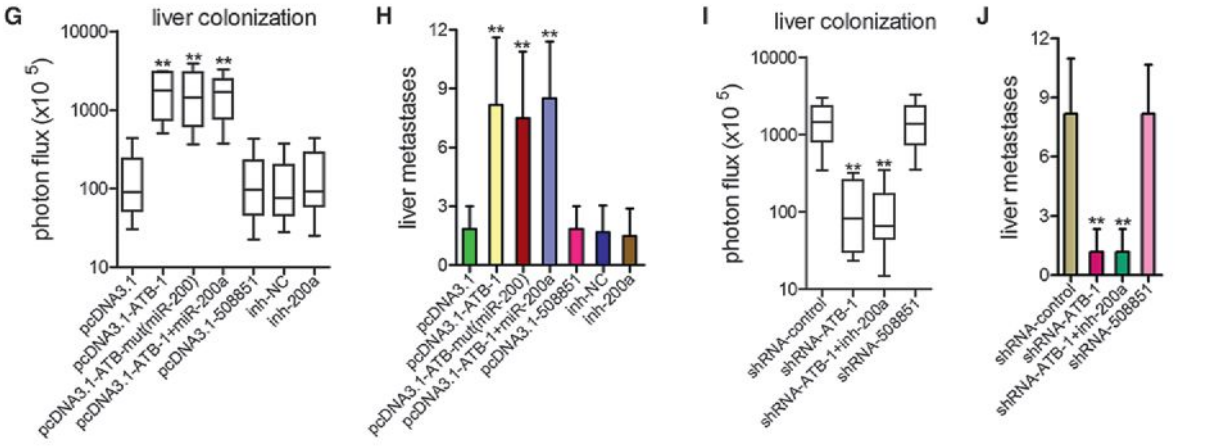

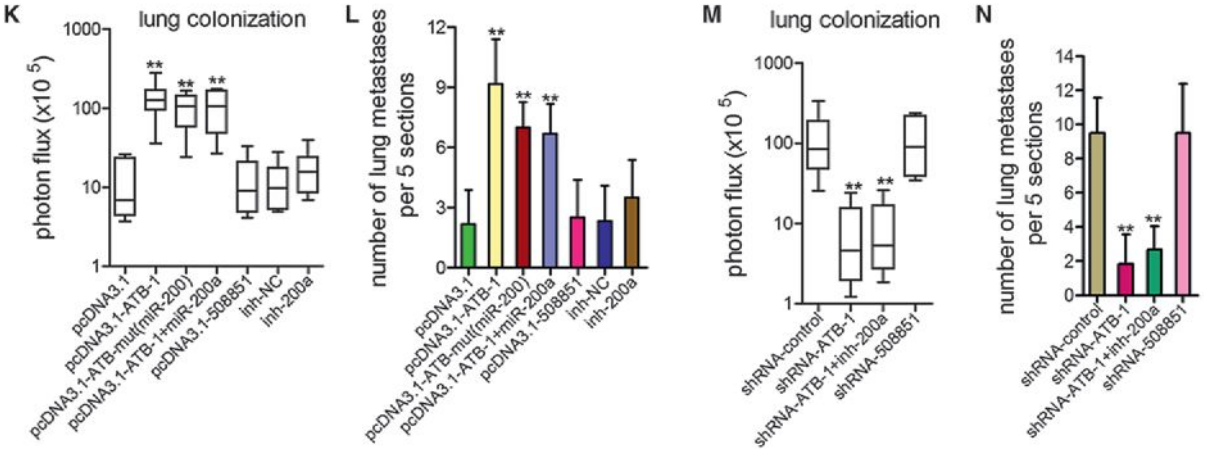

(legend on next page)

lncRNA-ATB Interacts with and Increases Stability of IL-11 mRNA

We next sought to explore the mechanisms behind the potent effect of lncRNA-ATB on metastatic colonization. Recently, many lncRNAs have been reported to interact with mRNA and increase the stability of mRNA (Faghihi et al., 2008; Yoon et al., 2012). To identify mRNA species bound by lncRNA-ATB, we performed an RIP to pull down endogenous mRNAs associated with lncRNA-ATB (Figure 6A) and sequenced the retrieved RNA. Interleukin-11 (IL-11) was one of the most enriched transcripts (Figure 6B; Figure S5A; Table S4), which has been reported to activate STAT3 signaling and confer a survival advantage to metastatic cells (Calon et al., 2012). Furthermore, GSEA indicated that KEGG_JAK_STAT signaling pathway from the Molecular Signatures Database (Liberzon et al., 2011) and published distinct IL-11/STAT3 upregulated gene signatures (Azare et al., 2007; Dauer et al., 2005; Putoczki et al., 2013) were significantly enriched in lncRNA-ATB overexpressed cells, whereas IL-11/STAT3 downregulated gene signature was negatively enriched (Figure 6C). We thus reasoned that lncRNA-ATB may promote metastatic cell survival through IL-11 mRNA binding, autocrine induction of IL-11, and activation of IL-11/STAT3 signaling. Promisingly, we discovered that the liver metastases generated in the intrasplenically inoculated model displayed higher expression of IL-11 and more accumulation of p-STAT3 when derived from the lncRNA-ATB-overexpressing SMMC-7721 cells, and lower expression of IL-11 and less accumulation of p-STAT3 derived from lncRNA-ATB-downregulated HCCLM6 cells (Figures S5B and S5C).

Using BLAST (http://blast.ncbi.nlm.nih.gov/), we identified six regions of high complementary between lncRNA-ATB and IL-11 mRNA, but none for β-actin mRNA (Figure 6D). We then mutated all six binding sites in lncRNA-ATB. To validate the direct interaction of lncRNA-ATB with IL-11 mRNA, we performed RIP-qPCR and the results demonstrated that the lncRNA-ATB RIP in SMMC-7721 cells is significantly enriched for IL-11 mRNA compared to the empty vector, IgG, β-actin mRNA, IL-11 binding sites mutated lncRNA-ATB (lncRNA-ATB-mut(IL-11)), or lncRNA-508851, which did not have a complementary region with IL-11 mRNA (Figure 6E). The specific association between lncRNA-ATB and IL-11 mRNA was further validated by affinity pull-down of endogenous IL-11 mRNA using in vitro transcribed biotin-labeled lncRNA-ATB (Figure 6F). These results suggest that lncRNA-ATB interacts with IL-11 mRNA.

To test whether lncRNA-ATB regulates the stability of IL-11 mRNA, we treated different clones of SMMC-7721 and HCCLM6 cells with α-amanitin to block new RNA synthesis and then measured the loss of IL-11, β-actin, and 18S rRNA over a 24 hr period. The overexpression of lncRNA-ATB, but not lncRNA-ATB-mut(IL-11) or lncRNA-508851, elongated the half-life of IL-11 mRNA, and conversely, the depletion of lncRNA-ATB shortened the half-life of IL-11 mRNA (Figure 6G). Collectively, these data demonstrate that lncRNA-ATB specially increases the stability of IL-11 mRNA, which depends on the binding of IL-11 mRNA.

lncRNA-ATB Activates IL-11/STAT3 Signaling

To further validate the effects of lncRNA-ATB on IL-11/STAT3 signaling in vitro, we measured IL-11 mRNA levels in different clones of SMMC-7721 and HCCLM6 cells and found that the overexpression of lncRNA-ATB, but not lncRNA-ATB-mut(IL-11) or lncRNA-508851, significantly increased IL-11 mRNA levels in a dose-dependent manner, and ectopic expression of miR-200a did not change the effects (Figure 6H). Reciprocally, the depletion of lncRNA-ATB significantly reduced IL-11 mRNA levels in a dose-dependent manner, which was also not changed by inhibition of miR-200a (Figure 6I). Consistent with the different expression of lncRNA-ATB in the four HCC cells in Figure S1M, the expression of IL-11 was higher in lncRNA-ATB high expression cells (Figure S5D). We also found that overexpression of lncRNA-ATB upregulated IL-11 mRNA level in QSG-7701 cells (Figure S5E). To examine whether lncRNA-ATB increases IL-11 secretion and activates IL-11/STAT3 signaling, we measured IL-11 levels in the cell supernatants and phosphorylation levels of STAT3 in different clones. The overexpression of lncRNA-ATB, but not lncRNA-ATB-mut(IL-11) or lncRNA-508851, leads to increased IL-11 levels in the cell supernatants and phosphorylation levels of STAT3 in a dose-dependent manner (Figures 6J and 6K). Reciprocally, the depletion of lncRNA-ATB leads to reduced IL-11 levels in the cell supernatants and phosphorylation levels of STAT3 in a dose-dependent manner (Figures 6L and 6M). Neither overexpression nor inhibition of miR-200a changed the effects (Figures 6J–6M). Overexpression of lncRNA-ATB also upregulated IL-11 levels in the cell

Figure 5. The Roles of lncRNA-ATB in the Invasion-Metastasis Cascade of HCC Cells

(A and B) Incidence of metastases 8 weeks after orthotopic xenografting in nude mice using indicated SMMC-7721 cell clones (A) or HCCLM6 cell clones (B) (Fisher's exact test).

(C and D) The number of GFP labeled CTCs was examined by flow cytometry from whole-blood samples 5 weeks after orthotopic xenografting using indicated SMMC-7721 cell clones (C) or HCCLM6 cell clones (D). PBMC, peripheral blood mononuclear cells.

(E and F) Relative levels of human LINE1 DNA were analyzed by qPCR of genomic DNA from the blood in (C) and (D), normalized to mouse LINE1 DNA. For (C–F), n = 10, nonparametric Mann-Whitney U test.

(G) Luciferase signal intensities of mice in each group 6 weeks after intrasplenic injection with 2×10^6 indicated SMMC-7721 cells. The horizontal lines in the box plots represent the medians, the boxes represent the interquartile range, and the whiskers represent the minimum and maximum values.

(H) Number of liver metastases in mice from (G).

(I) Luciferase signal intensities of mice in each group 6 weeks after intrasplenic injection with 2×10^6 indicated HCCLM6 cells. Data are shown as in (G).

(J) Number of liver metastases in mice from (I).

(K) Luciferase signal intensities of mice in each group 5 weeks after tail vein injection with 1×10^6 indicated SMMC-7721 cells. Data are shown as in (G).

(L) Number of metastatic nodules in the lungs from the mice in (K) (five sections evaluated per lung).

(M) Luciferase signal intensities of mice in each group 5 weeks after tail vein injection with 1×10^6 indicated HCCLM6 cells. Data are shown as in (G).

(N) Number of metastatic nodules in the lungs from the mice in (M) (five sections evaluated per lung). For (G–N), n = 6, nonparametric Mann-Whitney U test. Bars represent mean ± SD. $^{**}p < 0.01$, $^{***}p < 0.001$. See also Figure S4.

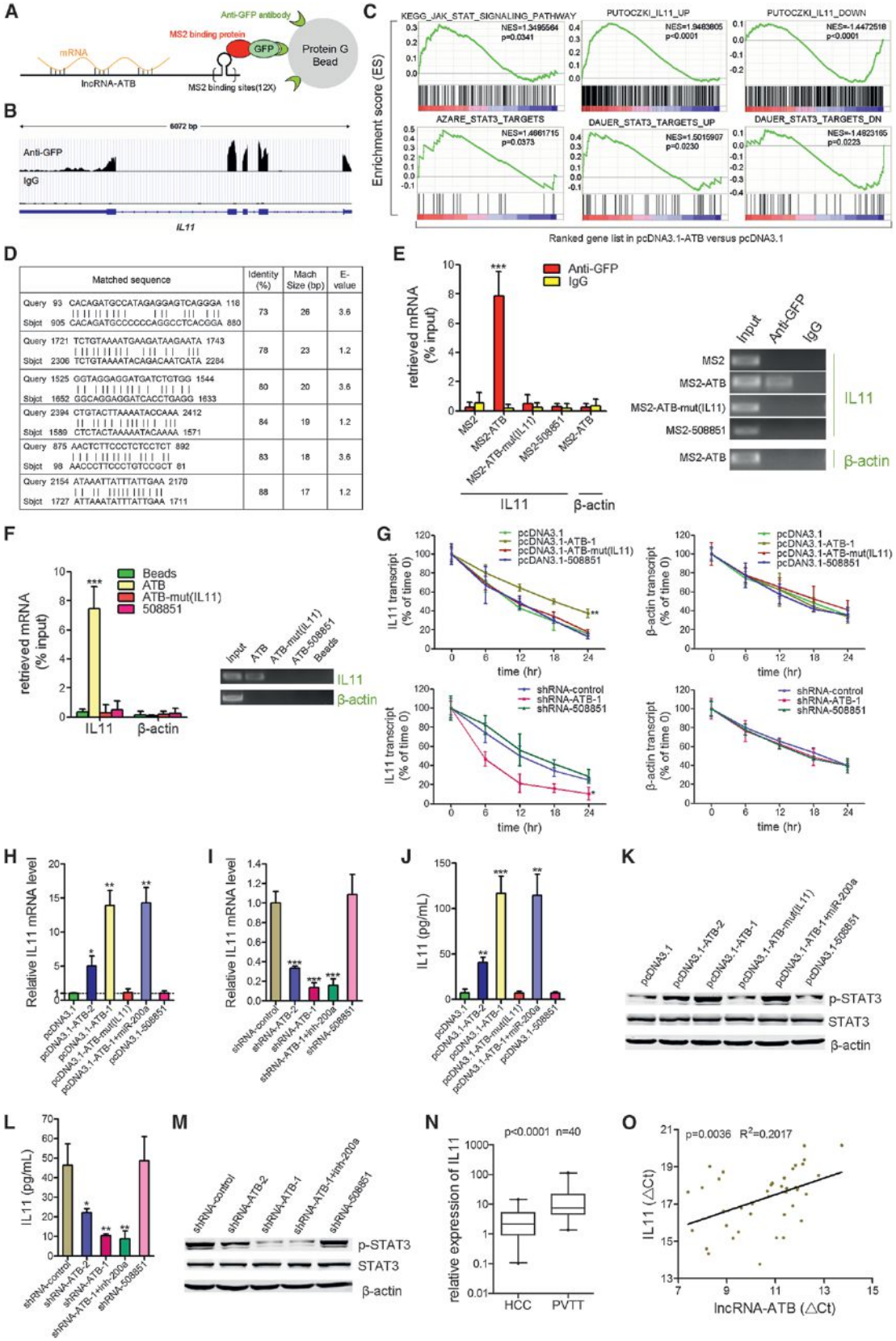

(legend on next page)

supernatants and phosphorylation levels of STAT3 in QSG-7701 cells (Figures S5F and S5G). STAT3 downstream target protein BCL2 was also upregulated by overexpression of lncRNA-ATB, but not lncRNA-ATB-mut(IL-11) or lncRNA-508851, and was downregulated by depletion of lncRNA-ATB (Figures S5H–S5J). These results indicate that lncRNA-ATB upregulated the expression of IL-11, increased IL-11 secretion, and activated STAT3 signaling in an autocrine manner. The effects of lncRNA-ATB on IL-11/STAT3 signaling are not dependent on miR-200s.

To confirm the regulation of IL-11 by lncRNA-ATB in human HCC tissues, we measured IL-11 mRNA level in the same set of 40 pairs of PVTT and pair-matched primary HCC tissues shown in Figure 4B and found that IL-11 mRNA level was significantly higher in the PVTT tissues than in the primary HCC tissues (Figure 6N). Importantly, the IL-11 mRNA level is correlated with the lncRNA-ATB transcript level in the PVTT tissues (Figure 6O). These clinical data demonstrated that IL-11 may be associated with the metastasis of HCC cells and were consistent with the role of lncRNA-ATB in the regulation of IL-11.

lncRNA-ATB Requires IL-11/STAT3 Signaling to Promote Colonization

To test the contribution of IL-11 to the procolonization role of lncRNA-ATB, we knocked down IL-11 in lncRNA-ATB-overexpressing SMMC-7721 clone 1. This knockdown has no significant effect on lncRNA-ATB expression (Figure 7A). We first measured the effects of IL-11 on EMT, and found that knockdown of IL-11 did not induce or invert EMT (Figure S6A). Next, we found that the mutation of IL-11 binding sites or knockdown of IL-11 also did not change the proinvasive efficiency of lncRNA-ATB (Figure S6B).

The cells were labeled with firefly luciferase and inoculated intrasplenically into nude mice. During the first few days following inoculation, most of the cells that reached the liver were progressively lost, and by 7 days, tumor cells were barely detectable. The overexpression of lncRNA-ATB, but not lncRNA-ATB-mut(IL-11), significantly increased the number of cells detected at the early time points and induced more metastatic foci in the liver at the late time point. The knockdown of IL-11 in lncRNA-ATB-overexpressing cells reduced the amounts to near those of the control cells (Figures 7B–7E). We further explored the role of lncRNA-ATB and IL-11 in lung colonization by injecting cells directly into the tail veins of nude mice. lncRNA-ATB overexpressing cells, but not that of lncRNA-ATB-mut(IL-11), displayed increased lung colonization rates at the early time points and formed more metastatic tumors in the lung at the late time point, whereas knockdown of IL-11 mostly abolished this increase (Figures 7F–7I). These data demonstrated that lncRNA-ATB enhances the colonization potential of HCC cells and this effect depends on IL-11.

DISCUSSION

In this study, we report that lncRNA-ATB, which could be activated by TGF-β, promotes HCC cell invasion by competitively binding the miR-200 family, upregulating ZEB1 and ZEB2, and then inducing EMT. On the other hand, lncRNA-ATB promotes HCC cell colonization at the site of metastasis by binding IL-11 mRNA, increasing IL-11 mRNA stability, causing autocrine induction of IL-11, and then activating STAT3 signaling. Therefore, lncRNA-ATB plays a prometastatic role in HCC (Figure 8). We also found that the expression of lncRNA-ATB was increased in HCC and was further increased in PVTT. Furthermore, a higher level of lncRNA-ATB was associated with tumor invasion in patients with HCC and was inversely correlated with prognosis. All these data support our conclusion that lncRNA-ATB has pleiotropic effects on HCC cell invasion, colonization, and metastasis. Therefore, lncRNA-ATB was determined to have oncogenic activity.

Our results indicated that a higher level of lncRNA-ATB was associated with liver cirrhosis in patients with HCC, which is consistent with the observation that TGF-β is also associated with liver cirrhosis (Yang et al., 2013). A recent report indicated that the level of TGF-β signaling activity was higher in PVTT tissues than the primary HCC tissues (Yang et al., 2012), which further supports the regulation of lncRNA-ATB by TGF-β in vivo. The biphasic activities of the TGF-β signaling pathway during

Figure 6. lncRNA-ATB Interacts with IL-11 mRNA and Activates IL-11/STAT3 Signaling in HCC Cells

(A) A schematic outline of the MS2-RIP strategy used to identify endogenous mRNA:lncRNA-ATB binding.

(B) lncRNA-ATB-MS2 RIP-seq identification of IL-11 enrichment in anti-GFP and nonspecific IgG groups.

(C) GSEA of KEGG_JAK_STAT signaling pathway and published IL-11/STAT3 regulated gene signatures in lncRNA-ATB overexpressed SMMC-7721 cells versus control cells. NES, normalized enrichment score.

(D) Regions of putative interaction between lncRNA-ATB (query) and IL-11 mRNA (subject).

(E) RIP-derived RNA was measured by qRT-PCR. The levels of qRT-PCR products were expressed as a percentage of input RNA.

(F) SMMC-7721 cell lysates were incubated with biotin-labeled lncRNA-ATB; after pull-down, mRNA was extracted and assessed by qRT-PCR. Data are shown as in (E).

(G) The stability of IL-11 and β-actin mRNA over time was measured by qRT-PCR relative to time 0 after blocking new RNA synthesis with α-amanitin (50 μM) in indicated SMMC-7721 cell clones or HCCLM6 cell clones and normalized to 18S rRNA (a product of RNA polymerase I that is unchanged by α-amanitin).

(H and I) Relative IL-11 mRNA levels in indicated SMMC-7721 cell clones (H) or HCCLM6 cell clones (I).

(J and K) Concentration of IL-11 in the culture medium measured by ELISA (J) or p-STAT3 levels determined by western blot (K) from indicated SMMC-7721 cell clones.

(L and M) Concentration of IL-11 in the culture medium measured by ELISA (L) or p-STAT3 levels determined by western blot (M) from indicated HCCLM6 cell clones. For (E–M), n = 3, mean ± SD, Student's t test, *$p < 0.05$, **$p < 0.01$, ***$p < 0.001$.

(N) IL-11 mRNA levels in primary HCC and PVTT tissues from the same set of patients as in Figure 4B were measured by qRT-PCR. The horizontal lines in the box plots represent the medians, the boxes represent the interquartile range, and the whiskers represent the 2.5th and 97.5th percentiles. Wilcoxon signed-rank test.

(O) The correlation between lncRNA-ATB transcript level and IL-11 mRNA level was measured in the same set of PVTT tissues as in (N). The ΔCt values (normalized to 18S rRNA) were subjected to Pearson correlation analysis.

See also Figure S5 and Table S4.

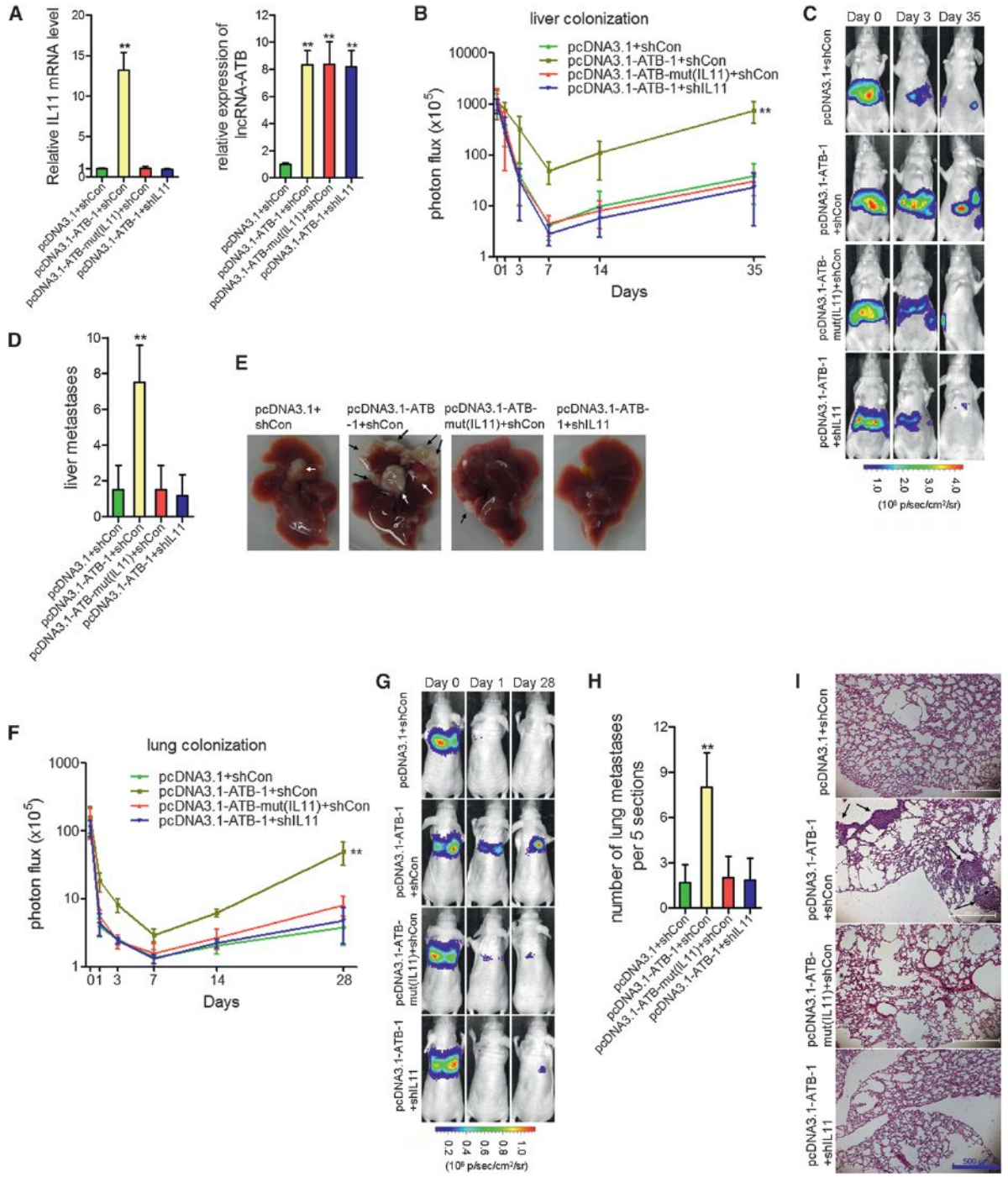

Figure 7. The Pro-Colonization Role of lncRNA-ATB Requires IL-11/STAT3 Signaling

(A) The expression levels of IL-11 and lncRNA-ATB were determined by qRT-PCR. n = 3, Student's t test.

(B) Luciferase signal intensities of the mice in each group over time after intrasplenic injection with 2 × 10^6 indicated SMMC-7721 cell clones.

(C) Representative images of mice from (B) over time.

(D) The number of liver metastases in the mice from (B) 35 days after intrasplenic injection.

(E) Representative livers from (D).

(F) Luciferase signal intensities of mice over time after tail vein injection with 1 × 10^6 indicated SMMC-7721 cell clones.

(G) Representative images of the mice from (F) over time.

(H) The number of metastatic nodules in the lungs from (F) 28 days after tail vein injection (five sections evaluated per lung).

(I) Hematoxylin and eosin-stained images of lung tissues isolated from the mice in (H). Scale bars represent 500 μm. For (B–I), n = 6, nonparametric Mann-Whitney U test; arrows indicate the metastasis nodules. Data are shown as mean ± SD, **p < 0.01. See also Figure S6.

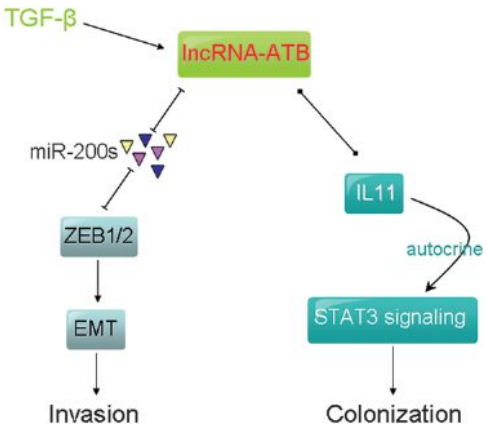

Figure 8. A Schematic Model of lncRNA-ATB Functions during the Invasion-Metastasis Cascade

lncRNA-ATB, which could be activated by TGF-β, promotes HCC cell invasion by competitively binding the miR-200 family, upregulating ZEB1 and ZEB2, and then inducing EMT. On the other hand, lncRNA-ATB promotes HCC cell colonization at the site of metastases by binding IL-11 mRNA, increasing IL-11 mRNA stability, causing autocrine induction of IL-11, and then activating STAT3 signaling.

tumorigenesis hinder its utilization in clinical treatment. Therefore, it would be beneficial to target the tumor-progressing arm of TGF-β action while avoiding the tumor-suppressing arm. Thus, the specific downstream effectors of the different TGF-β signaling pathways need to be explored further. In this study, we identified that lncRNA-ATB mediates the role of TGF-β in inducing EMT and promoting metastasis. Promisingly, lncRNA-ATB was activated by TGF-β and induced EMT not only in HCC cells, but also in colorectal cancer and breast cancer cells, indicating that lncRNA-ATB is a more general TGF-β mediator. Our results indicated that a short-term TGF-β treatment was sufficient to activate lncRNA-ATB, which implied that lncRNA-ATB may be a direct target of TGF-β/Smad pathway, but how TGF-β activates lncRNA-ATB requires further investigation.

In this study, we found that lncRNA-ATB shares miR-200s response elements with ZEB1 and ZEB2, the master inducers of EMT. In our in vitro system, an orthotopic xenograft model of nude mice and clinical HCC tissues, we observed that ectopic expression of lncRNA-ATB was sufficient to increase ZEB1 and ZEB2 and induce EMT. The mRNA expression profile after overexpressing of lncRNA-ATB fortified its role in inducing EMT. Notably, this role depends on the competitive binding of miR-200s, indicating that lncRNA-ATB functions as a ceRNA. Because there is a double negative feedback loop between miR-200s and ZEB1/ZEB2 (Burk et al., 2008), the upregulation of ZEB1 and ZEB2 by lncRNA-ATB could further augment the effects. It is widely recognized that EMT facilitates tumor invasion and dissemination (Massagué, 2008). Consistently, in our in vitro system, an orthotopic xenograft model of nude mice and clinical HCC tissues, we all found that by inducing EMT, lncRNA-ATB promotes HCC cell invasion.

In the orthotopic xenograft model in nude mice, we found that lncRNA-ATB promoted HCC cell metastases, which were not completely dependent on miR-200s or EMT. This implies that metastasis is not only determined by the invasion potential and that the miR-200-ZEB-EMT axis is not the only downstream effector of lncRNA-ATB. Metastasis is a complex multistep process that involves early invasion and late colonization of cancer cells (Tao et al., 2013). Clinical observations and animal model studies have indicated that, despite the significant and continuous tumor cell intravasation into the circulation, only a small minority of these cells colonize a distant organ (Gupta and Massagué, 2006). Therefore, colonization is a rather inefficient process and also has a critical influence on ultimate metastasis. In our tail vein injection and intrasplenic inoculation xenograft models, we found that the miR-200-EMT axis had no significant effect on colonization. Therefore, lncRNA-ATB exerts its procolonization effect through other pathways.

We combined RIP-seq and transcriptome analysis to identify that lncRNA-ATB bound IL-11 mRNA, increased IL-11 mRNA stability, and caused autocrine induction of IL-11, and activated IL-11/STAT3 signaling, which were further verified in our in vitro system, the xenograft metastasis model, and clinical HCC tissues. In our xenograft model using nude mice, IL-11 secreted by HCC cells contributes to the procolonization role of lncRNA-ATB, because the depletion of IL-11 in HCC cells abolished the procolonization effect of lncRNA-ATB. The depletion of IL-11 did not induce or invert EMT, indicating that the role of lncRNA-ATB or IL-11 in colonization is not dependent on EMT or MET.

Taken together, our research demonstrated that lncRNA-ATB acts as a key regulator of TGF-β signaling pathways and revealed roles of TGF-β in regulating long noncoding RNAs. The findings of this study have significant implications regarding our understanding of HCC metastasis pathogenesis. As direct targets of lncRNA-ATB, miR-200-ZEB and IL-11 mediated the role of lncRNA-ATB in local invasion and distant colonization, respectively. The pleiotropic effects of lncRNA-ATB on the early and late steps of the invasion-metastasis cascade suggest that lncRNA-ATB could be an effective target for antimetastasis therapies.

EXPERIMENTAL PROCEDURES

Patients

Frozen HCC tissues, normal liver tissues, and PVTT tissues were randomly obtained with informed consent from patients who underwent radical resections in the Eastern Hepatobiliary Surgery Hospital (Second Military Medical University, Shanghai, China). Ethical consent was granted from the Committees for Ethical Review of Research involving Human Subjects of Second Military Medical University.

Animal Studies

The animal studies were approved by the Institutional Animal Care and Use Committee of the Second Military Medical University. Male athymic BALB/c nude mice (4–5 weeks old) were used for animal studies. Subcutaneous tumor growth assays were performed as previously described (Yuan et al., 2011). Orthotopic xenograft model and metastasis model are described in the Supplemental Experimental Procedures.

Statistical Analysis

All statistical analyses were performed using the GraphPad Prism Software (GraphPad Software). For comparisons, Student's t test (two-tailed), Wilcoxon signed-rank test, Pearson chi-square test, Pearson correlation analysis, Log-rank test, Fisher's exact test, and nonparametric Mann-Whitney U test were performed as indicated. A p value < 0.05 was considered significant.

ACCESSION NUMBERS

The Gene Expression Omnibus accession numbers for the lncRNA microarray data for TGF-β-treated cells, gene expression data for lncRNA-ATB overexpressed SMMC-7721 cells, and RIP-seq data of lncRNA-ATB are GSE54797, GSE54798, and GSE54799, respectively.

SUPPLEMENTAL INFORMATION

Supplemental Information includes Supplemental Experimental Procedures, six figures, and four tables and can be found with this article online at http://dx.doi.org/10.1016/j.ccr.2014.03.010.

ACKNOWLEDGMENTS

We thank Dr. Xing He from Department of Tropical Infectious Diseases, Second Military Medical University for technical assistance and Dr. Xiao-zhi Wang from Gminix (Shanghai, China) for assistance with bioinformatic analyses. This work was supported by grants from the National Natural Science Foundation of China (grant nos. 81330037, 81372240, 81071680, 81071700, 81171936, 81171937, and 31171251), the National Natural Science Foundation of Shanghai (12ZR1437200), and the Youth start-up funding of SMMU (2011QN02).

Received: June 29, 2013
Revised: January 7, 2014
Accepted: March 11, 2014
Published: April 24, 2014

REFERENCES

Akhurst, R.J., and Hata, A. (2012). Targeting the TGFβ signalling pathway in disease. Nat. Rev. Drug Discov. *11*, 790–811.

Alonso, S.R., Tracey, L., Ortiz, P., Pérez-Gómez, B., Palacios, J., Pollán, M., Linares, J., Serrano, S., Sáez-Castillo, A.I., Sánchez, L., et al. (2007). A high-throughput study in melanoma identifies epithelial-mesenchymal transition as a major determinant of metastasis. Cancer Res. *67*, 3450–3460.

Azare, J., Leslie, K., Al-Ahmadie, H., Gerald, W., Weinreb, P.H., Violette, S.M., and Bromberg, J. (2007). Constitutively activated Stat3 induces tumorigenesis and enhances cell motility of prostate epithelial cells through integrin beta 6. Mol. Cell. Biol. *27*, 4444–4453.

Budhu, A., Forgues, M., Ye, Q.H., Jia, H.L., He, P., Zanetti, K.A., Kammula, U.S., Chen, Y., Qin, L.X., Tang, Z.Y., and Wang, X.W. (2006). Prediction of venous metastases, recurrence, and prognosis in hepatocellular carcinoma based on a unique immune response signature of the liver microenvironment. Cancer Cell *10*, 99–111.

Burk, U., Schubert, J., Wellner, U., Schmalhofer, O., Vincan, E., Spaderna, S., and Brabletz, T. (2008). A reciprocal repression between ZEB1 and members of the miR-200 family promotes EMT and invasion in cancer cells. EMBO Rep. *9*, 582–589.

Calon, A., Espinet, E., Palomo-Ponce, S., Tauriello, D.V., Iglesias, M., Céspedes, M.V., Sevillano, M., Nadal, C., Jung, P., Zhang, X.H., et al. (2012). Dependency of colorectal cancer on a TGF-β-driven program in stromal cells for metastasis initiation. Cancer Cell *22*, 571–584.

Cesana, M., Cacchiarelli, D., Legnini, I., Santini, T., Sthandier, O., Chinappi, M., Tramontano, A., and Bozzoni, I. (2011). A long noncoding RNA controls muscle differentiation by functioning as a competing endogenous RNA. Cell *147*, 358–369.

Dauer, D.J., Ferraro, B., Song, L., Yu, B., Mora, L., Buettner, R., Enkemann, S., Jove, R., and Haura, E.B. (2005). Stat3 regulates genes common to both wound healing and cancer. Oncogene *24*, 3397–3408.

Faghihi, M.A., Modarresi, F., Khalil, A.M., Wood, D.E., Sahagan, B.G., Morgan, T.E., Finch, C.E., St Laurent, G., 3rd, Kenny, P.J., and Wahlestedt, C. (2008). Expression of a noncoding RNA is elevated in Alzheimer's disease and drives rapid feed-forward regulation of beta-secretase. Nat. Med. *14*, 723–730.

Fidler, I.J. (2003). The pathogenesis of cancer metastasis: the 'seed and soil' hypothesis revisited. Nat. Rev. Cancer *3*, 453–458.

Gotzmann, J., Fischer, A.N., Zojer, M., Mikula, M., Proell, V., Huber, H., Jechlinger, M., Waerner, T., Weith, A., Beug, H., and Mikulits, W. (2006). A crucial function of PDGF in TGF-beta-mediated cancer progression of hepatocytes. Oncogene *25*, 3170–3185.

Gregory, P.A., Bert, A.G., Paterson, E.L., Barry, S.C., Tsykin, A., Farshid, G., Vadas, M.A., Khew-Goodall, Y., and Goodall, G.J. (2008). The miR-200 family and miR-205 regulate epithelial to mesenchymal transition by targeting ZEB1 and SIP1. Nat. Cell Biol. *10*, 593–601.

Gupta, G.P., and Massagué, J. (2006). Cancer metastasis: building a framework. Cell *127*, 679–695.

Gupta, R.A., Shah, N., Wang, K.C., Kim, J., Horlings, H.M., Wong, D.J., Tsai, M.C., Hung, T., Argani, P., Rinn, J.L., et al. (2010). Long non-coding RNA HOTAIR reprograms chromatin state to promote cancer metastasis. Nature *464*, 1071–1076.

Huang, S., Hölzel, M., Knijnenburg, T., Schlicker, A., Roepman, P., McDermott, U., Garnett, M., Grernrum, W., Sun, C., Prahallad, A., et al. (2012). MED12 controls the response to multiple cancer drugs through regulation of TGF-β receptor signaling. Cell *151*, 937–950.

Jemal, A., Bray, F., Center, M.M., Ferlay, J., Ward, E., and Forman, D. (2011). Global cancer statistics. CA Cancer J. Clin. *61*, 69–90.

Kang, Y., Chen, C.R., and Massagué, J. (2003). A self-enabling TGFbeta response coupled to stress signaling: Smad engages stress response factor ATF3 for Id1 repression in epithelial cells. Mol. Cell *11*, 915–926.

Lewis, B.P., Burge, C.B., and Bartel, D.P. (2005). Conserved seed pairing, often flanked by adenosines, indicates that thousands of human genes are microRNA targets. Cell *120*, 15–20.

Liberzon, A., Subramanian, A., Pinchback, R., Thorvaldsdóttir, H., Tamayo, P., and Mesirov, J.P. (2011). Molecular signatures database (MSigDB) 3.0. Bioinformatics *27*, 1739–1740.

Lin, M.F., Jungreis, I., and Kellis, M. (2011). PhyloCSF: a comparative genomics method to distinguish protein coding and non-coding regions. Bioinformatics *27*, i275–i282.

Majumdar, A., Curley, S.A., Wu, X., Brown, P., Hwang, J.P., Shetty, K., Yao, Z.X., He, A.R., Li, S., Katz, L., et al. (2012). Hepatic stem cells and transforming growth factor β in hepatocellular carcinoma. Nat Rev Gastroenterol Hepatol *9*, 530–538.

Massagué, J. (2008). TGFbeta in Cancer. Cell *134*, 215–230.

Mercer, T.R., Dinger, M.E., and Mattick, J.S. (2009). Long non-coding RNAs: insights into functions. Nat. Rev. Genet. *10*, 155–159.

Ocaña, O.H., Córcoles, R., Fabra, A., Moreno-Bueno, G., Acloque, H., Vega, S., Barrallo-Gimeno, A., Cano, A., and Nieto, M.A. (2012). Metastatic colonization requires the repression of the epithelial-mesenchymal transition inducer Prrx1. Cancer Cell *22*, 709–724.

Padua, D., Zhang, X.H., Wang, Q., Nadal, C., Gerald, W.L., Gomis, R.R., and Massagué, J. (2008). TGFbeta primes breast tumors for lung metastasis seeding through angiopoietin-like 4. Cell *133*, 66–77.

Pardali, K., and Moustakas, A. (2007). Actions of TGF-beta as tumor suppressor and pro-metastatic factor in human cancer. Biochim. Biophys. Acta *1775*, 21–62.

Ponting, C.P., Oliver, P.L., and Reik, W. (2009). Evolution and functions of long noncoding RNAs. Cell *136*, 629–641.

Prensner, J.R., Iyer, M.K., Sahu, A., Asangani, I.A., Cao, Q., Patel, L., Vergara, I.A., Davicioni, E., Erho, N., Ghadessi, M., et al. (2013). The long noncoding RNA SChLAP1 promotes aggressive prostate cancer and antagonizes the SWI/SNF complex. Nat. Genet. *45*, 1392–1398.

Putoczki, T.L., Thiem, S., Loving, A., Busuttil, R.A., Wilson, N.J., Ziegler, P.K., Nguyen, P.M., Preaudet, A., Farid, R., Edwards, K.M., et al. (2013). Interleukin-11 is the dominant IL-6 family cytokine during gastrointestinal tumorigenesis and can be targeted therapeutically. Cancer Cell *24*, 257–271.

Salmena, L., Poliseno, L., Tay, Y., Kats, L., and Pandolfi, P.P. (2011). A ceRNA hypothesis: the Rosetta Stone of a hidden RNA language? Cell *146*, 353–358.

Subramanian, A., Tamayo, P., Mootha, V.K., Mukherjee, S., Ebert, B.L., Gillette, M.A., Paulovich, A., Pomeroy, S.L., Golub, T.R., Lander, E.S., and Mesirov, J.P. (2005). Gene set enrichment analysis: a knowledge-based approach for interpreting genome-wide expression profiles. Proc. Natl. Acad. Sci. USA *102*, 15545–15550.

Tao, Z.H., Wan, J.L., Zeng, L.Y., Xie, L., Sun, H.C., Qin, L.X., Wang, L., Zhou, J., Ren, Z.G., Li, Y.X., et al. (2013). miR-612 suppresses the invasive-metastatic cascade in hepatocellular carcinoma. J. Exp. Med. *210*, 789–803.

Tay, Y., Kats, L., Salmena, L., Weiss, D., Tan, S.M., Ala, U., Karreth, F., Poliseno, L., Provero, P., Di Cunto, F., et al. (2011). Coding-independent regulation of the tumor suppressor PTEN by competing endogenous mRNAs. Cell *147*, 344–357.

Thiery, J.P., Acloque, H., Huang, R.Y., and Nieto, M.A. (2009). Epithelial-mesenchymal transitions in development and disease. Cell *139*, 871–890.

Tsai, J.H., Donaher, J.L., Murphy, D.A., Chau, S., and Yang, J. (2012). Spatiotemporal regulation of epithelial-mesenchymal transition is essential for squamous cell carcinoma metastasis. Cancer Cell *22*, 725–736.

Yang, P., Li, Q.J., Feng, Y., Zhang, Y., Markowitz, G.J., Ning, S., Deng, Y., Zhao, J., Jiang, S., Yuan, Y., et al. (2012). TGF-β-miR-34a-CCL22 signaling-induced Treg cell recruitment promotes venous metastases of HBV-positive hepatocellular carcinoma. Cancer Cell *22*, 291–303.

Yang, L., Inokuchi, S., Roh, Y.S., Song, J., Loomba, R., Park, E.J., and Seki, E. (2013). Transforming growth factor-β signaling in hepatocytes promotes hepatic fibrosis and carcinogenesis in mice with hepatocyte-specific deletion of TAK1. Gastroenterology *144*, 1042–1054, e4.

Yoon, J.H., Abdelmohsen, K., Srikantan, S., Yang, X., Martindale, J.L., De, S., Huarte, M., Zhan, M., Becker, K.G., and Gorospe, M. (2012). LincRNA-p21 suppresses target mRNA translation. Mol. Cell *47*, 648–655.

Yuan, J.H., Yang, F., Chen, B.F., Lu, Z., Huo, X.S., Zhou, W.P., Wang, F., and Sun, S.H. (2011). The histone deacetylase 4/SP1/microrna-200a regulatory network contributes to aberrant histone acetylation in hepatocellular carcinoma. Hepatology *54*, 2025–2035.

Cancer Cell
Article

Depletion of Carcinoma-Associated Fibroblasts and Fibrosis Induces Immunosuppression and Accelerates Pancreas Cancer with Reduced Survival

Berna C. Özdemir,[1,2] Tsvetelina Pentcheva-Hoang,[3] Julienne L. Carstens,[1] Xiaofeng Zheng,[1] Chia-Chin Wu,[4] Tyler R. Simpson,[3] Hanane Laklai,[5] Hikaru Sugimoto,[1,2] Christoph Kahlert,[1,2] Sergey V. Novitskiy,[6] Ana De Jesus-Acosta,[7] Padmanee Sharma,[3] Pedram Heidari,[8] Umar Mahmood,[8] Lynda Chin,[4] Harold L. Moses,[6] Valerie M. Weaver,[5] Anirban Maitra,[9] James P. Allison,[3] Valerie S. LeBleu,[1,2] and Raghu Kalluri[1,2,*]

[1]Department of Cancer Biology, Metastasis Research Center, University of Texas MD Anderson Cancer Center, Houston, TX 77054, USA
[2]Division of Matrix Biology, Department of Medicine, Beth Israel Deaconess Medical Center and Harvard Medical School, Boston, MA 02115, USA
[3]Department of Immunology, University of Texas MD Anderson Cancer Center, Houston, TX 77054, USA
[4]Department of Genomic Medicine, University of Texas MD Anderson Cancer Center, Houston, TX 77054, USA
[5]Department of Surgery, University of California, San Francisco, San Francisco, CA 94143, USA
[6]Department of Cancer Biology, Vanderbilt University School of Medicine, Nashville, TN 37232, USA
[7]Department of Medical Oncology, Johns Hopkins Hospital, Baltimore, MD 21287, USA
[8]Department of Radiology, Massachusetts General Hospital, Boston, MA 02114, USA
[9]Departments of Pathology and Translational Molecular Pathology, Ahmad Center for Pancreatic Cancer Research, University of Texas MD Anderson Cancer Center, Houston, TX 77030, USA
*Correspondence: rkalluri@mdanderson.org
http://dx.doi.org/10.1016/j.ccr.2014.04.005

SUMMARY

Pancreatic ductal adenocarcinoma (PDAC) is associated with marked fibrosis and stromal myofibroblasts, but their functional contribution remains unknown. Transgenic mice with the ability to delete αSMA$^+$ myofibroblasts in pancreatic cancer were generated. Depletion starting at either noninvasive precursor (pancreatic intraepithelial neoplasia) or the PDAC stage led to invasive, undifferentiated tumors with enhanced hypoxia, epithelial-to-mesenchymal transition, and cancer stem cells, with diminished animal survival. In PDAC patients, fewer myofibroblasts in their tumors also correlated with reduced survival. Suppressed immune surveillance with increased CD4$^+$Foxp3$^+$ Tregs was observed in myofibroblast-depleted mouse tumors. Although myofibroblast-depleted tumors did not respond to gemcitabine, anti-CTLA4 immunotherapy reversed disease acceleration and prolonged animal survival. This study underscores the need for caution in targeting carcinoma-associated fibroblasts in PDAC.

INTRODUCTION

Pancreatic ductal adenocarcinoma (PDAC) is a near uniformly lethal disease with a dismal median survival of 4 to 6 months (Hidalgo, 2010; Korc, 2007). Despite years of efforts to design therapeutic approaches for pancreatic cancer, the use of conventional chemotherapy combination regimens with modest benefit remains the only option for the overwhelming majority of patients who present with advanced neoplasms. Revisiting the complex biology of PDAC in an unbiased manner is thus urgently required if we are to develop more effective therapies. The progress in generating genetically engineered mouse models faithfully mimicking human PDAC provides a unique opportunity to interrogate the functional contribution of the desmoplastic

Significance

Pancreas cancer is associated with large amounts of stroma composed of collagen I and myofibroblasts, but their functional contribution remains unknown. Specific depletion of myofibroblasts using compound genetic mouse models of PDAC leads to aggressive tumors with diminished animal survival. Fewer myofibroblasts in human PDAC also correlate with reduced patient survival. Detailed studies show that myofibroblast loss decreases the ability of the immune system to control cancer associated with the persistence of regulatory T cells. Myofibroblast depletion did not improve gemcitabine's efficacy, but immunotherapy to revive immune attack prolonged mice's survival. This study demonstrates a protective role of myofibroblasts and suggests that targeting carcinoma-associated fibroblasts in pancreas cancer should be approached with caution.

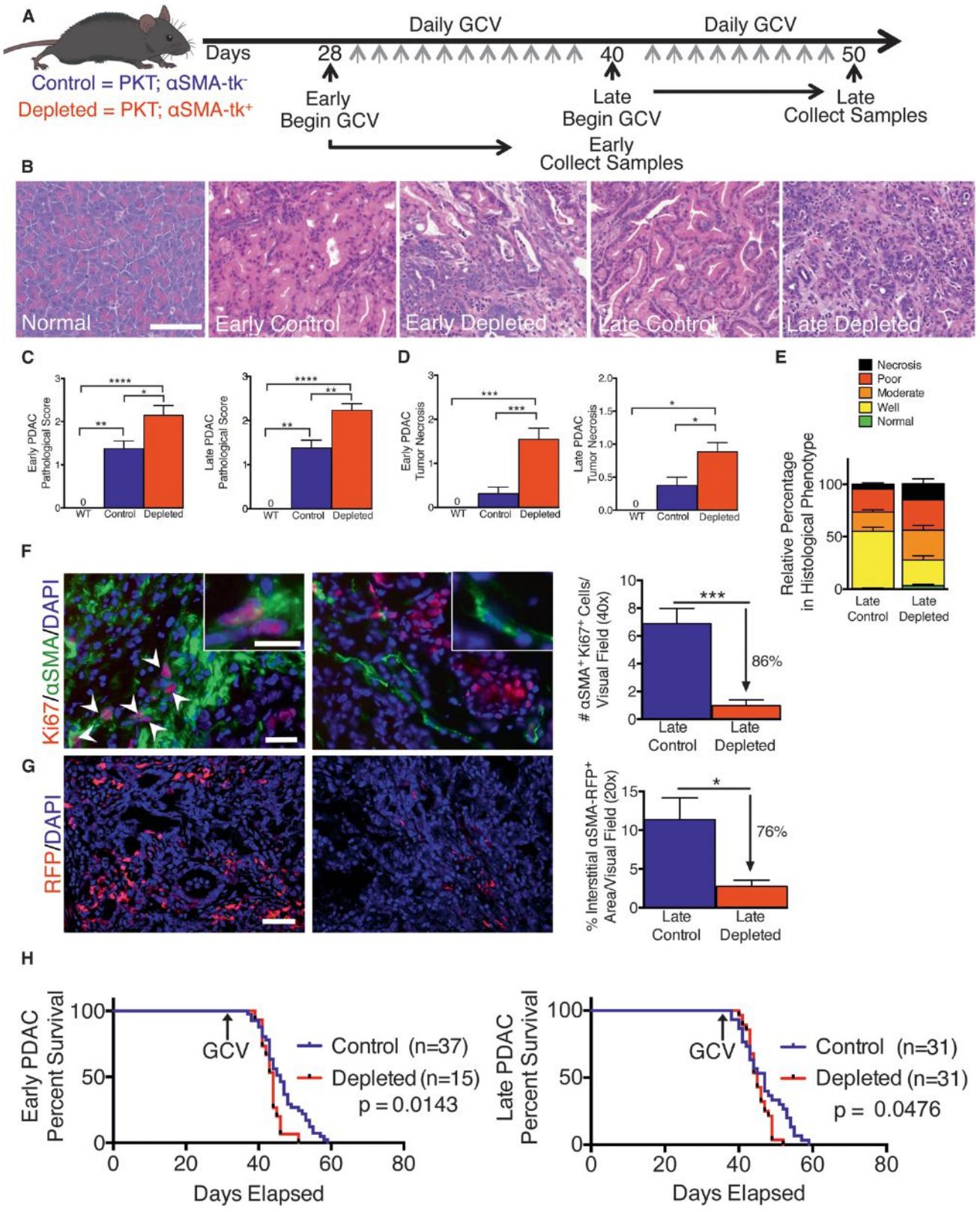

Figure 1. Myofibroblast Depletion Augments PDAC and Diminishes Overall Survival

(A) Tumor progression timeline with experimental treatment time points. GCV administration in PKT; αSMA-tk^{+} mice allows myofibroblast depletion, in contrast with control PKT; αSMA-tk^{-} mice.

(legend continued on next page)

stromal reaction in PDAC, a defining feature of this carcinoma, which accounts for the majority of the tumor tissue volume (Aguirre et al., 2003; Bardeesy et al., 2006a, 2006b; Gidekel Friedlander et al., 2009; Hingorani et al., 2003, 2005; Hruban et al., 2007; Ijichi et al., 2006).

The cellular component of the desmoplastic stroma in PDAC is composed primarily of myofibroblasts, characterized by αSMA expression (Feig et al., 2012; Rasheed et al., 2012). Recent studies have implicated the stroma as a physical barrier to the delivery of cytotoxic chemotherapies to the peritumoral milieu (Feig et al., 2012; Provenzano et al., 2012; Whatcott et al., 2012). Nonetheless, although preclinical models have demonstrated the benefit of stromal depletion through blockade of paracrine Hedgehog signaling in accentuating drug delivery (Olive et al., 2009), subsequent clinical trials targeting stromal myofibroblasts in human PDAC resulted in an apparent paradoxical accelerated disease progression, halting clinical trials (Amakye et al., 2013). These studies reinforced the need to critically evaluate the functional contribution of stroma in the initiation and progression of PDAC. In this regard, the functional role of αSMA^+ myofibroblasts and type I collagen in PDAC remains unknown.

RESULTS

Myofibroblast Depletion Leads to Increased Tumor Invasion Associated with Decreased Survival

To interrogate the functional contribution of αSMA^+ myofibroblasts in PDAC, we used a genetic strategy for selective in vivo depletion. *Ptf1a*$^{cre/+}$;*LSL-Kras*$^{G12D/+}$;*Tgfbr2*$^{flox/flox}$ (PKT) mice develop spontaneous PDAC with full penetrance that reliably recapitulates the clinical and histopathological features of the human disease (Ijichi et al., 2006). The mice consistently progress from pancreatic intraepithelial neoplasia (PanIN) at 4.5 weeks of age to invasive cancer at 6 weeks of age and die at 8 weeks of age, without much variation (Ijichi et al., 2006). These mice were crossed with αSMA-tk transgenic mice to selectively target proliferating αSMA^+ myofibroblasts upon systemic ganciclovir (GCV; InvivoGen) administration (PKT; αSMA-tk mice) (LeBleu et al., 2013). Daily GCV injections were initiated when mice developed PanIN lesions (early) and allowed to progress to PDAC (Figure 1A). Mice also received GCV injections starting at the established PDAC stage (late) until they developed significant signs of illness leading to their death or requiring euthanasia (Figure 1A). In both early and late myofibroblast depletion settings, PKT mice presented with significantly more invasive, undifferentiated, and necrotic tumors when myofibroblasts were depleted compared with control tumors (Figures 1B–1E). Immunohistochemical and immunofluorescence analyses revealed an average of 80% depletion of proliferating myofibroblasts (Figure 1F; Figures S1A and S1B available online). Direct visualization of interstitial myofibroblasts using the αSMA-RFP transgenic mice crossed with PKT; αSMA-tk mice also showed approximately 80% depletion of total myofibroblasts (Figure 1G). A significant reduction in αSMA transcript level was also noted in depleted tumors (Figure S1C). Extrapancreatic organs, such as the kidney, lung, small bowel, heart, and liver, did not show any depletion in αSMA^+ cells (Figures S1D and S1E). Notably, myofibroblast depletion in PDAC was associated with significant reduction in survival, in both the early and late depletion groups (Figure 1H). Tumor weight was significantly reduced by myofibroblast depletion and was associated with a reduced body weight specifically in PDAC mice with late myofibroblast depletion (Figures S1F and S1G). Mice with myofibroblast-depleted tumors exhibit an increased frequency of pulmonary emboli, likely contributing to diminished overall survival (Figure S1H).

Loss of one allele of *Tgfbr2* (versus both in the PKT mice) in the context of *Kras*^{G12D} activation (PKT^{Het} mice) leads to a similar PDAC phenotype, but with a slower progression rate, with PanIN lesions noted at 4 to 6 weeks of age and PDAC at 8 to 10 weeks of age (Ijichi et al., 2006). GCV treatment was initiated at the onset of PDAC in PKT^{Het}; αSMA-tk mice and continued until they died or were moribund, requiring euthanasia. Depletion of myofibroblasts resulted in undifferentiated tumors (Figures 2A–2E) and significantly diminished the survival of PKT^{Het}; αSMA-tk mice (Figure 2F). Similar findings were also observed when myofibroblasts were depleted in *Pdx1*$^{cre/+}$;*LSL-Kras*$^{G12D/+}$;*Trp53*$^{R172H/+}$ (KPC) mice crossed with αSMA-tk (KPC; αSMA-tk) mice. Myofibroblast depletion in this setting also resulted in poorly differentiated tumors and significantly diminished survival (Figures S2A–S2C). Because of the similar phenotypes of the PKT; αSMA-tk mice and KPC; αSMA-tk mice, the remaining experiments were carried out using the PKT mice because of their faster course of disease.

On the basis of the striking and somewhat unexpected impact of stromal depletion on survival in PDAC models, we next assessed whether a comparable impact of stromal content was observed in the cognate human setting. Immunohistochemical scoring for interstitial αSMA^+ cells from resected PDAC of untreated patients indicated that low αSMA is associated with

(B) Representative micrographs of H&E stained pancreatic samples (scale bar represents 100 μm).
(C) Pathological scores of early-depleted tumors (left: wild-type [WT], n = 5; control, n = 16; depleted, n = 17) and late-depleted tumors (right: WT, n = 5; control, n = 17; depleted, n = 26). Significance was determined by one-way ANOVA with Tukey post hoc analysis.
(D) Necrosis penetrance of early-depleted tumors (left: WT, n = 5; control, n = 16; depleted, n = 22) and late-depleted tumors (right: WT, n = 5; control, n = 17; depleted, n = 25).
(E) Relative percentages in histological phenotypes in late depleted tumors. Control, n = 17; depleted, n = 25.
(F) Representative micrographs (scale bar represents 50 μm) of Ki-67/αSMA dual-immunofluorescence (left, control; right, depleted) and corresponding quantification (n = 4 and n = 6 for control and depleted, respectively). Arrows point to double-positive cells and inserts show high-magnification images (scale bar represents 25 μm).
(G) Representative micrographs (scale bar represents 100 μm) of reporter αSMA-RFP tumor samples (left, control; right, depleted) and corresponding quantification (n = 3 in each group).
(H) Survival analysis of early (left) and late (right) treatment groups. GCV, GCV treatment was initiated.
Data are represented as mean ± SEM. Unless otherwise noted, significance was determined using t tests (*$p < 0.05$, **$p < 0.01$, ***$p < 0.001$, ****$p < 0.0001$). ns, not significant. See also Figure S1.

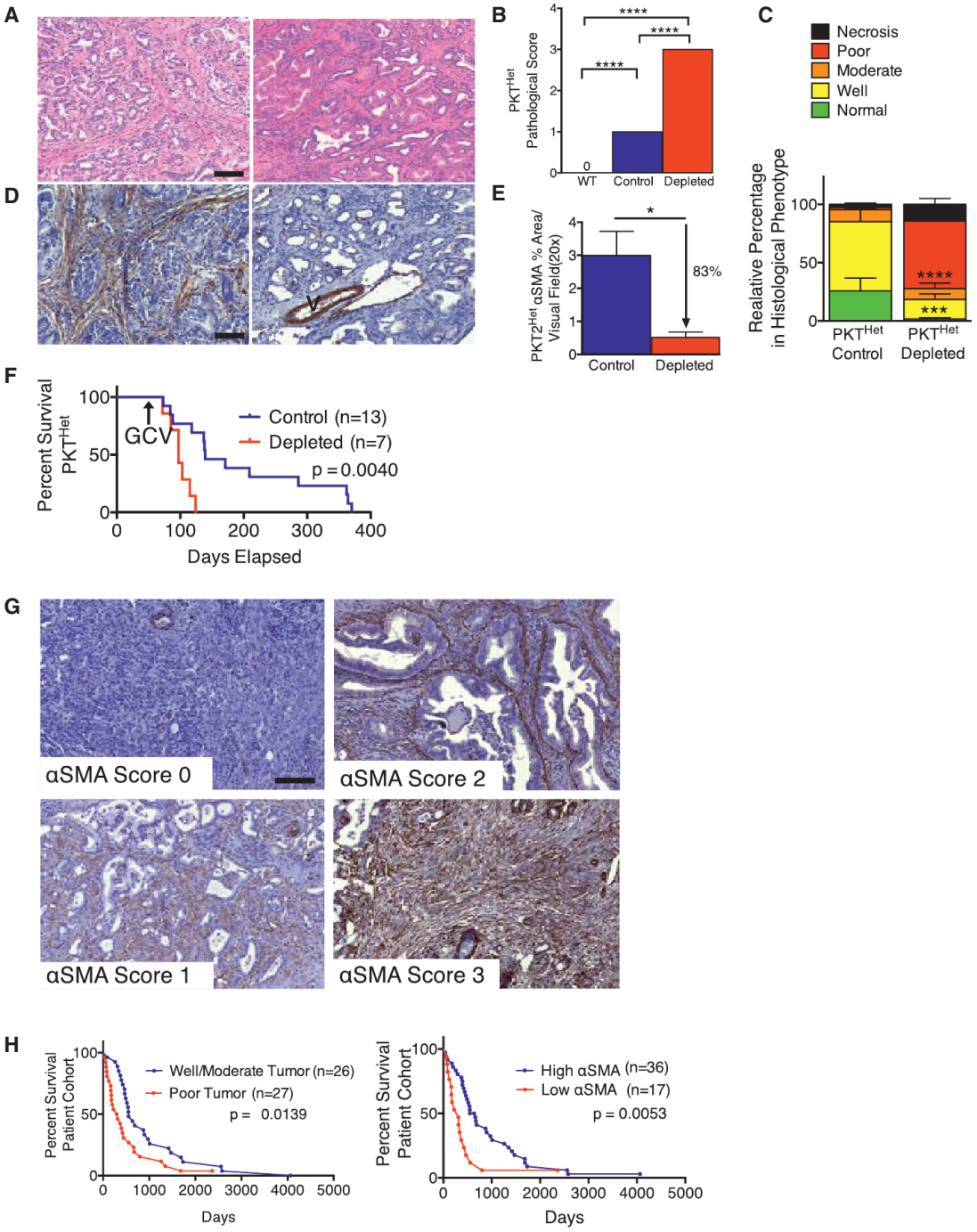

Figure 2. Decreased αSMA Correlates with Poor Prognosis and Overall Survival in Slow-Progressing Mice with PDAC and Patients with Pancreatic Cancer

(A and B) Representative micrographs of H&E stained PKT^{Het} tumors at 106 (control, left) and 103 (depleted, right) days old (A) (scale bar represents 100 μm) and pathological scores (B). WT, n = 5; control, n = 6; depleted, n = 4. Significance was determined by one-way ANOVA with Tukey post hoc analysis.

(C) Relative percentages in histological phenotypes (n = 6 and n = 4, respectively, for control and depleted).

(D and E) Representative micrographs of αSMA stained pancreatic samples as in (A) (D) (scale bar represents 100 μm) and corresponding quantification (E) (n = 6 and n = 4, respectively, for control and depleted). V, vessel.

(F) Survival analysis in PKT^{Het} mice. GCV, GCV treatment was initiated.

(G) Representative micrographs of αSMA stained pancreatic samples resected from patients in each score category: 0, 1, 2, and 3 (scale bar represents 200 μm).

(H) Survival analysis based on histopathological score (left) and αSMA score (right). Low αSMA: scores 0 and 1; high αSMA: scores 2 and 3.

Significance was determined using the Mantel-Cox test. Data are represented as mean ± SEM. Unless otherwise noted, significance was determined using t tests (*p < 0.05, ***p < 0.001, ****p < 0.0001). ns, not significant. See also Figure S2 and Table S1.

worse survival, supporting the observations in the PKT and KPC mice with myofibroblast depletion (Figure 2G; Table S1). Of note, patients with low αSMA scores present significantly more often with poorly differentiated cancers than tumors with well or moderate differentiation (Table S1), and yet despite this correlation, αSMA scoring offered greater significance in differential stratification of patients for survival than histopathological grade (Figure 2H), suggesting that stromal content likely has a direct impact on the natural history of human PDAC.

Myofibroblast Depletion Reduced Type I Collagen Content and Altered Extracellular Matrix Organization in PDAC

Global gene expression profiling of tumors from PKT mice without (control) and with myofibroblast depletion (depleted) revealed differentially expressed genes associated with remodeling of the extracellular matrix (ECM), epithelial-to-mesenchymal transition (EMT), angiogenesis, and immune response (Table S2). Comparative analyses of tumor transcriptomes revealed 4,393 differentially expressed genes in early-depleted versus age-matched control tumors (1,682 downregulated and 2,711 upregulated genes) and 2,344 differentially expressed genes in late-depleted versus age-matched control tumors (1,170 downregulated and 1,174 upregulated genes) (Figures S3A–S3D). Tumor collagen content assayed by type I collagen immunostaining (Figure 3A) was significantly decreased in myofibroblast-depleted tumors. Masson's trichrome staining (MTS) and picrosirius red staining revealed a significant reorganization of collagen fibrils, with decreased stiffness and elastic modulus in myofibroblast-depleted tumors compared with control tumors (Figures 3B–3D). Interestingly, collagen crosslinking and immunolabeling for the collagen crosslinking enzyme lysyl oxidase (LOX) were unchanged despite reduced stiffness of the ECM (Figures 3E and 3F), highlighting a complex regulation of type I collagen crosslinking mediated by multiple sources of LOX. These results are consistent with the ability of αSMA^+ myofibroblasts to produce type I collagen and induce fibrosis in PDAC. Despite extensive remodeling of type I collagen ECM in myofibroblast-depleted tumors, hyaluronic acid (HA) binding protein (HABP), a marker for total HA content, remained unchanged in the myofibroblast-depleted tumors (Figure S3E). Vimentin labeling, however, was significantly decreased in myofibroblast-depleted tumors (Figure S3F). Auditing of other mesenchymal cells in the PDAC tumor stroma revealed a decrease in the number of fibroblast-specific protein 1 (FSP1)/$S100A4^+$ cells in myofibroblast-depleted tumors (Figure S3G), while the number of fibroblast activation protein (FAP)-positive cells remained unchanged (Figure S3H). Colocalization of αSMA with FAP was not detectable in the PDAC tumors (Figure S3H).

Myofibroblast-Depleted PDAC Displays Suppression of Angiogenesis, Enhanced Tumor Hypoxia, EMT Program, and Cancer Stem Cell-like Phenotype

Histopathological analyses of myofibroblast-depleted tumors revealed highly undifferentiated, invasive-grade tumors with enhanced necrosis (Figures 1B–1E). These features are associated with tumor hypoxia and the acquisition of an EMT program. Myofibroblast depletion was associated with a decrease in the number of $CD31^+$ vessels, indicative of suppressed vessel density (Figure 4A; Figures S4A–S4C). Perivascular αSMA^+ cells appear unaffected by the αSMA-tk strategy (Figure S4A). Global gene expression profiling performed on normal pancreas fibroblasts and PDAC-associated fibroblasts (CAF) shows differences in pathways affecting ECM remodeling, angiogenesis, and immune response in PDAC (Figure S4D; Table S3). RNA sequencing analyses further validated the increased expression of several proangiogenic factors in CAF, supporting their proangiogenic role in PDAC (Table S3).

Although pericyte numbers, assayed by immunostaining analyses for the pericyte marker NG2 (Figure S4B), and vascular leakage, determined by extravascular fluorescein isothiocyanate (FITC)-dextran (Figure 4B; Figure S4E), were unchanged, tumor hypoxia assayed by staining for pimonidazole adduct formation was dramatically increased in myofibroblast-depleted tumors compared with control tumors (Figure 4C; Figure S4F). Lineage tracing of cancer cells using the LSL-YFP reporter together with immunolabeling for αSMA allowed the quantitative analysis of YFP^+ cancer cells that have acquired mesenchymal features ($YFP^+\alpha SMA^+$ cells). Tumors with 80% depletion of αSMA^+ interstitial myofibroblasts showed an increase in EMT program with increased $YFP^+\alpha SMA^+$ cells (Figure 4D; Figure S4G) and enhanced expression of the EMT transcriptional regulators, *Twist*, *Snail*, and *Slug* (Figure 4E). The enhanced acquisition of EMT was associated with the loss of mucin staining (Figure S4H), which is in alignment with the decreased histological differentiation within the neoplastic glands (Figures 1B–1E). YFP^+ cancer cells from myofibroblast-depleted tumors exhibited an increase in their capacity to form spheres in culture, a feature of cells with EMT program and potential cancer stem cell-like phenotype (Kalluri and Weinberg, 2009; Scheel and Weinberg, 2012) (Figure 4F; Figure S4I). Additionally, the number of $CD44^+CD133^+$ cells (suggestive of pancreatic cancer stem cells; Hermann et al., 2007; Simeone, 2008) was enhanced in myofibroblast-depleted tumors (Figure 4G). Fluorescence-activated cell sorted YFP^+ cells freshly isolated from myofibroblast-depleted tumors showed enhanced tumorigenic potential when implanted in nude mice (Figure 4H). Interestingly, cancer cells with EMT program and expression of αSMA were not eliminated in the PKT; αSMA-tk mice on GCV administration but increased in number (Figure 4D). This could be explained by the observation that cancer cells with EMT program likely do not proliferate (Tsai et al., 2012; Vega et al., 2004), further confirming their low-cycling-stem-cell status. Further, although overall apoptosis was significantly increased in myofibroblast-depleted tumors (Figures S4J and S4K), it was mostly localized within terminally differentiated compartments, such as islets (Figure S4K).

Reduction of Fibrosis Does Not Increase the Efficacy of Gemcitabine in PDAC

To test whether the decrease in myofibroblasts and type I collagen content along with reduced ECM stiffness leads to increased efficacy of gemcitabine (GEM), we treated control and myofibroblast-depleted mice with GEM. Histopathological score did not improve when PKT mice were treated with GEM alone or in combination with myofibroblast depletion (Figure 5A). $TUNEL^+$ cell number increased with myofibroblast depletion, independent of GEM treatment, and GEM treatment alone did not significantly increase tumor cell apoptosis (Figure 5B). Similarly,

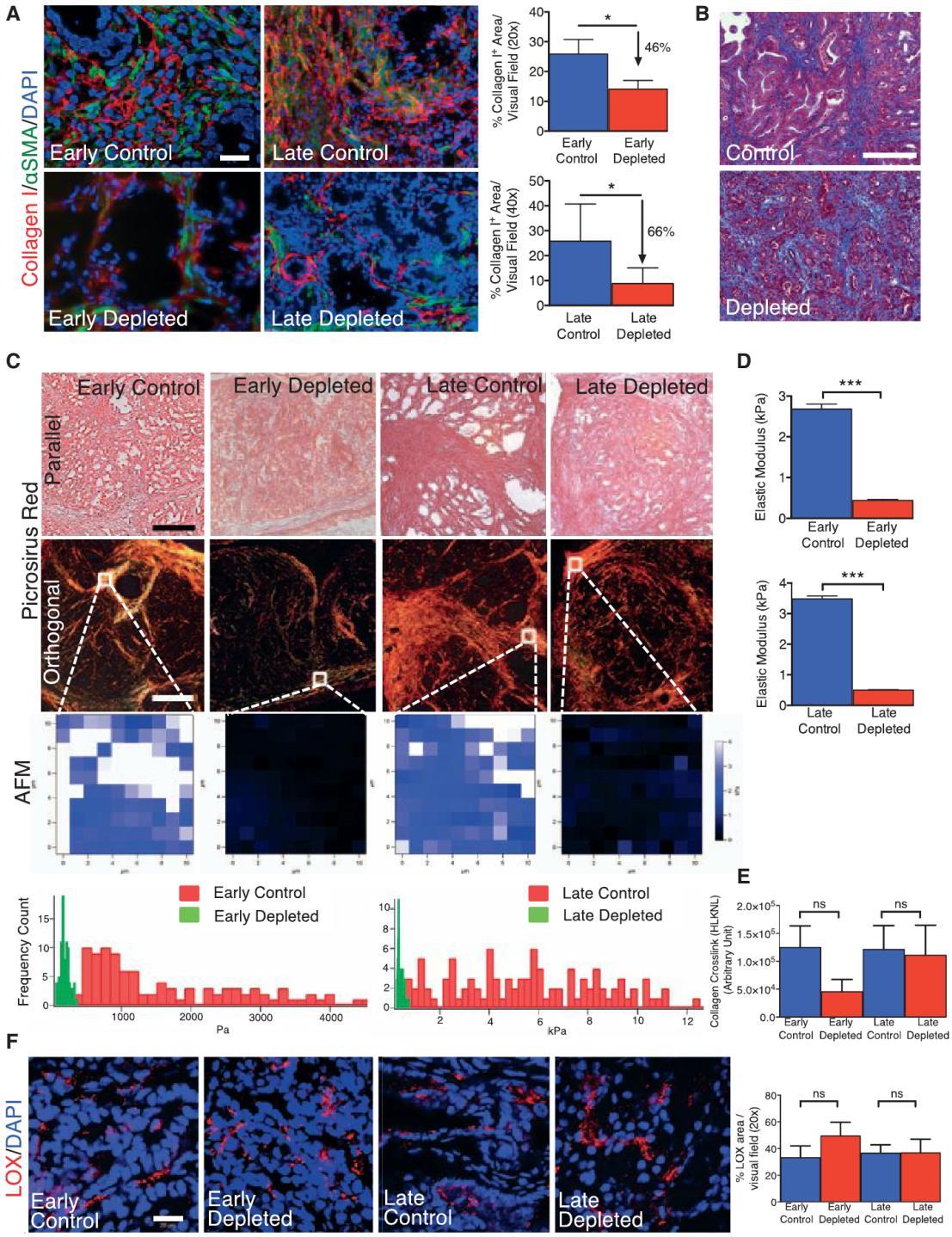

Figure 3. PDAC ECM Is Significantly Remodeled in Myofibroblast-Depleted Tumors

(A) Representative micrographs (scale bar represents 50 μm) of collagen I and αSMA and corresponding quantification (n = 4).

(B) Representative micrographs (scale bar represents 200 μm) of MTS in late control and late deleted mice.

(C) Representative images of picrosirius red staining of PKT pancreatic tissues samples viewed under parallel (top row) and polarized (second row) light (scale bar represents 75 μm) and representative images of stiffness distribution by atomic force microscopy measurement (AFM; third row) and quantification (bottom row, n = 3).

(D) Quantification of the elastic modulus of tumor matrix (n = 3).

(E) Collagen crosslinking quantification (n = 4).

(F) Representative micrographs for LOX (scale bar represents 20 μm) and quantification.

Data are represented as mean ± SEM. Significance was determined using t tests (*p < 0.05, ***p < 0.001). ns, not significant. See also Figure S3 and Table S2.

the change in FSP1$^+$ cells correlated only with myofibroblast depletion and was independent of GEM treatment (Figure 5C). Interestingly, CD31$^+$ cell numbers decreased with GEM therapy and decreased further with myofibroblast depletion (Figure 5D). Standard uptake values computed from ^{18}F-fluorodeoxyglucose positron emission tomography (PET)/computed tomography (CT) revealed comparable glycolysis per tumor volume in control, depleted, and GEM therapy in depleted tumors (Figure 5E). Despite a robust decrease in collagen content associated with myofibroblast depletion (fibrosis) (Figure 5F), GEM therapy did not improve overall survival (Figure 5G). Further, GEM therapy of PDAC compared with untreated mice did not result in improved survival, as previously reported using a different PDAC mouse model (Olive et al., 2009) (Figure 5G). GEM therapy in myofibroblast-depleted tumors compared with myofibroblast-depleted tumors also failed to improve overall survival (Figure 5G).

Myofibroblast Depletion Decreases Overall Immune Infiltration in PDAC but Results in Increased Frequency of FoxP3$^+$ Treg Cells

Gene expression profiling and RNA sequence analyses comparing control tumors with myofibroblast-depleted tumors revealed a significant change in the expression of genes associated with tumor immunity, including those associated with acute inflammatory responses, regulation of macrophage activation, regulation of T cell-mediated cytotoxicity, antigen presentation, and B cell activation (Figure 6A; Table S2). Tumors with myofibroblast depletion starting at the PanIN stage (early) present with significant decreases in overall peritumoral infiltration of CD45$^+$ cells and CD3$^+$ T cell and CD19$^+$ B cell infiltration compared with control tumors (Figure S5A). Such reductions in T cells and B cells were not observed in established PDAC with myofibroblast depletion (late-stage depletion) (Figure S5A). Natural killer (NK) cell infiltration with myofibroblast depletion was unchanged following myofibroblast depletion (Figure S5A). In both early and late depletion settings, myofibroblast depletion was associated with a significant suppression in the percentage of effector T cells (Teff, CD4$^+$Foxp3$^-$) together with an increase in the percentage of regulator T cells (Treg, CD4$^+$Foxp3$^+$), leading to an overall decrease in the Teff/Treg ratio (Figures 6B–6D). Myofibroblast depletion resulted in increased Foxp3 and *Ctla4* expression assayed by immunohistochemistry (IHC) (Figure S5B) and real-time PCR analysis (Figure 6E), respectively, consistent with the enhanced Treg infiltration. The cytotoxic CD8$^+$/Treg ratio was also decreased in the myofibroblast-depleted tumor (Figure 6F), as well as CD3$^+$/CD11b$^+$ ratio (early depletion; Figure 6G). The percentages of Teff and Treg, respectively, correlate with disease progression and acceleration of PDAC associated with myofibroblast depletion (Figures 6H and 6I). The percentages of CD11b$^+$Ly6G$^+$ cells and granulocytes (CD11b$^+$Gr1$^+$F4/80$^-$) were also increased in late myofibroblast-depleted tumors (Figures 6J and 6K), whereas the percentage of macrophages (CD11b$^+$Gr1$^-$ F4/80$^+$) was suppressed (Figure 6L). The differential tumor immune infiltration in early versus late depletion is also substantiated by distinct expression patterns in respective tumor immune gene expression signature, with a selectively downregulated tumor immunity gene signature in late-depleted tumor (Figure 6A).

Anti-CTLA-4 Antibody Therapy Rescues Enhanced PDAC Progression upon Myofibroblast Depletion and Increases Overall Survival

Myofibroblast depletion starting at early- and late-stage tumors resulted in a decreased Teff/Treg ratio associated with increased CTLA-4 expression (Figures 6D and 6E). Therefore, we tested whether the Teff/Treg ratio in PDAC mice with myofibroblast depletion can be rescued by CTLA-4 checkpoint blockade. Anti-CLTA-4 antibody administration significantly improved histopathological scores associated with a reduction in undifferentiated cancer cells (Figure 7A). Despite similar myofibroblast depletion (Figure 7B), suggesting that anti-CTLA-4 per se did not alter myofibroblast number, anti-CTLA-4 antibody treatment induced tumor clearance and replacement by normal parenchyma in up to 25% of the organ (Figure 7C). Treatment with anti-CTLA-4 antibodies in the setting of stromal depletion not only resulted in a rescue of the phenotype of myofibroblast-depleted tumors but also attenuated PDAC progression, which was associated with a significant extension in overall survival (an average increase of 60% in lifespan) (Figure 7D). Such elongation of lifespan was associated with reduced frequency of pulmonary emboli (Figure 7E). This was noticed in concordance with restored Teff and Treg percentages (Figure 7F) and diminished tumor sphere-forming ability within remnant cancer cells in age-matched mice (Figure 7G). Further, the transcriptome of myofibroblast-depleted tumors treated with anti-CTLA-4 clustered with the expression profiles of control tumor rather than myofibroblast-depleted tumors, suggesting that transcriptional reprogramming accompanies the observed phenotypic rescue (clustering using the 2,344 differentially expressed genes in late-depleted tumors versus control) (Figure 7H). Anti-CTLA-4 alone did not alter αSMA$^+$ content, and histopathological analyses revealed a modest increase in the percentage of normal parenchyma (Figures S6A and S6B). Treatment with anti-CTLA-4 alone improved overall survival (median survival of 49.5 days, compared with 47 days in the control group), albeit to a much lesser extent than anti-CTLA-4 treatment in combination with fibrosis depletion (median survival of 65 days) (Figure 7D).

DISCUSSION

The desmoplastic reaction is thought to represent a host defense mechanism, similar to wound healing and tissue regeneration, to repair or hopefully impede the conversion of a neoplastic lesion into invasive carcinoma (Bissell and Radisky, 2001; Dvorak, 1986; Lu et al., 2012). The function of desmoplastic stroma is likely dynamic during cancer progression, and its heterogeneous cellular and noncellular constituents change in relation to the evolving genetic landscape of cancer cells. In this regard, several studies have suggested that αSMA$^+$ myofibroblasts and type I collagen associated with tumor fibrosis are tumor promoting in solid tumors, including PDAC (Angeli et al., 2009; Karnoub et al., 2007; Merika et al., 2012; Vong and Kalluri, 2011). We demonstrate that depletion of αSMA$^+$ myofibroblasts resulted in multiple adverse outcomes leading to poor survival. These results suggest that at both early and late stages of pancreatic cancer, fibrosis associated with myofibroblasts and type I collagen constitutes a protective response from the host rather

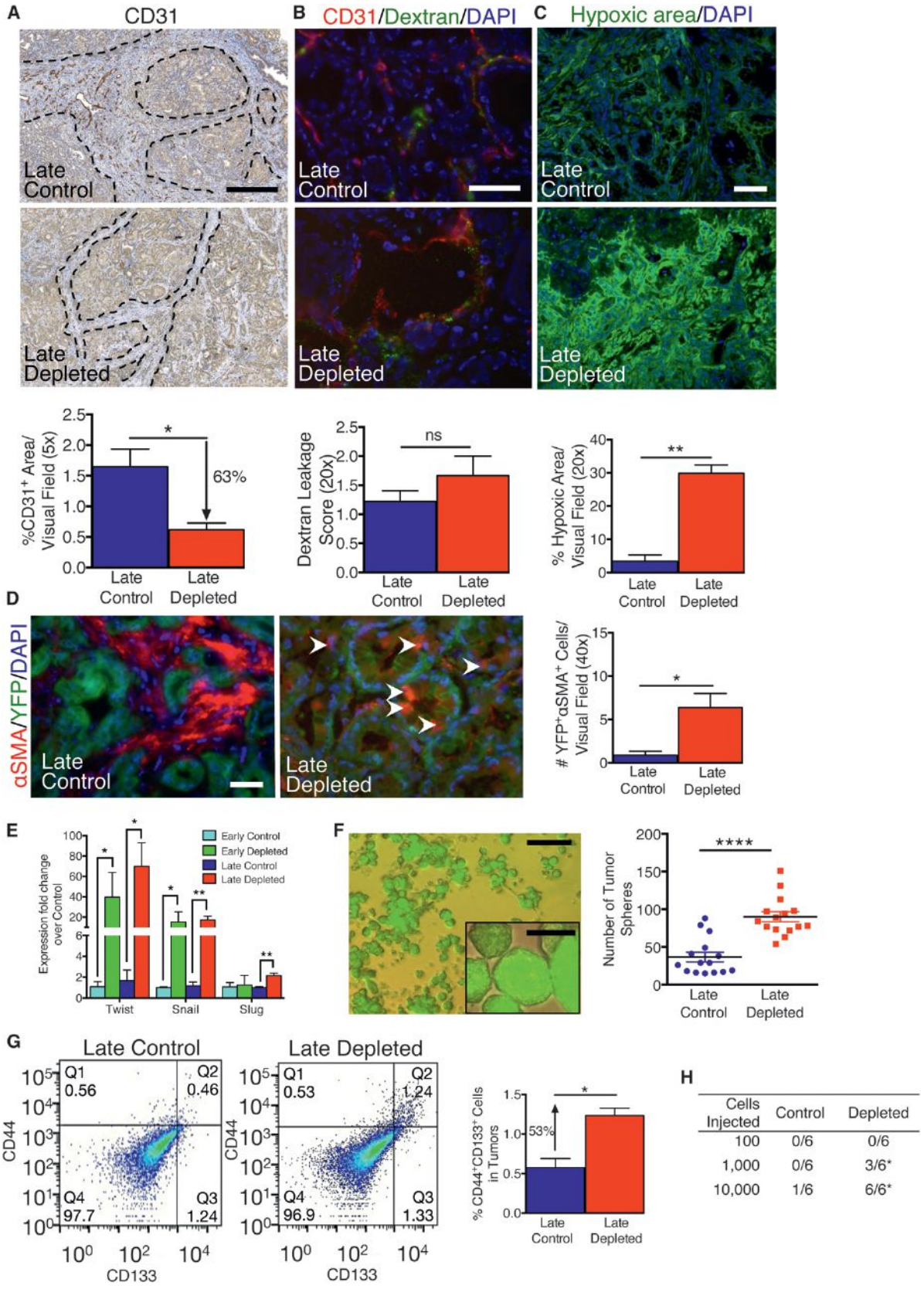

(legend on next page)

than offering an oncogenic supportive role, as speculated (Armstrong et al., 2004; Omary et al., 2007). This conclusion is supported by the clinical correlation between high αSMA and improved survival; a similar trend was previously reported from analyses also performed on resected tumors from treatment-naive patients (Wang et al., 2013). Although other studies have also attempted to specifically address the correlation between relative tumor content in αSMA^+ myofibroblasts and PDAC patient outcomes, potential therapeutic intervention prior to tumor resection makes interpretations unclear (Erkan et al., 2008; Mani et al., 2008).

Myofibroblast depletion leads to extensive remodeling of the tumor ECM, with a significant decrease in tumor tissue stiffness and total collagen content. Myofibroblasts contribute to the production of type I collagen, albeit likely not all of it. Contrary to previous assumptions, myofibroblasts do not contribute to the total production of LOX, an enzyme responsible for crosslinking of type I collagen. In this regard, we did not observe a difference in crosslinking, despite significant depletion and reorganization of tumor-associated collagen. Therefore, cancer cells or other stromal cells may compensate LOX expression. Similar to LOX, myofibroblast depletion did not affect HA content of the tumors, suggesting a nonmyofibroblast source for this matrix molecule. Targeting HA using PEGPH20, a modified enzyme that degrades HA, yielded promising results when combined with GEM (Jacobetz et al., 2013; Provenzano et al., 2012). In our study, ECM remodeling and the significant reduction in collagen content via myofibroblast depletion did not improve the treatment efficacy of GEM. Therefore, PDAC-associated myofibroblasts and type I collagen do not appear to serve as physical barriers to the exposure of cancer cells to GEM. In this regard, the potential role of HA, independent of type I collagen, in determining interstitial fluid pressure in PDAC tissue needs further mechanistic unraveling, and clinical trials with PEGPH20 will offer more insights in the future (Provenzano et al., 2012).

As noted above, significant depletion of myofibroblasts and type I collagen did not alter vessel permeability and perfusion. GEM efficacy was unaltered in myofibroblast and type I collagen-depleted tumors, suggesting that the increased efficacy observed in preclinical models treated with GEM and Smoothened inhibitor IPI-926 was likely due to mechanisms independent of myofibroblasts and type I collagen (Olive et al., 2009). It is likely that Smoothened inhibition was not myofibroblast specific and could also have affected other stromal cells, such as endothelial cells. In this regard, further analysis of the failed clinical trials could shed further light on this matter (Amakye et al., 2013). It is possible that if higher doses of IPI-926 combined with prolonged treatment period were used in the preclinical setting, potential adverse effects may have been encountered (Olive et al., 2009; Amakye et al., 2013). Nevertheless, our direct approach of targeting myofibroblasts and the associated fibrosis offers further insights into the complexity of using pharmacological targeting to derive specific answers related to target cells in tumors (Olive et al., 2009).

An interesting corollary that emerges from this study is the dominant contribution of cell division in the accumulation of myofibroblasts in PDAC. The origin of myofibroblasts in PDAC may be diverse (Phillips, 2012; Scarlett et al., 2011), yet using the αSMA-tk strategy to ablate proliferating myofibroblasts, we show 80% depletion of these cells, which account for the majority of myofibroblasts in PDAC tumors. These results offer an opportunity to speculate that drugs such as GEM and paclitaxel, which target proliferating cancer cells, may also target proliferating myofibroblasts. Such dual targeting may likely compromise the efficacy of GEM over time, because of progressive depletion of protective fibrosis along with proliferating cancer cells, resulting in the eventual emergence of resistant cancer cells with EMT program and stem cell-like phenotype.

Intratumoral hypoxia was dramatically increased in myofibroblast-depleted tumors. Decreased tumor vasculature, despite intact vessel structural integrity and permeability status, may have directly contributed to the increased tumor hypoxia when myofibroblasts are depleted, consequently promoting enhanced invasiveness and an undifferentiated phenotype of cancer cells (Cheresh and Stupack, 2008; Cooke et al., 2012; Pàez-Ribes et al., 2009). Impaired paracrine signaling between myofibroblasts and cancer cells and alteration of ECM microenvironment due to myofibroblast depletion might also have directly contributed to changes in cancer cells, lending to the acquisition of EMT program, stem cell-like phenotype, and an undifferentiated state. Many studies have indeed suggested that altered matrix microenvironment can influence the acquisition of epigenetic changes in epithelial cells (Bissell et al., 2005; Grassian et al., 2011; Guerra et al., 2011).

Figure 4. Myofibroblast-Depleted Tumors Display Increased Invasion Associated with Intratumoral Hypoxia

(A) Representative micrographs (scale bar represents 100 μm) of CD31 staining and corresponding quantification (n = 4). Dashed lines delineate the stromal compartment, where $CD31^+$ vessels are primarily found.

(B) Representative micrographs (scale bar represents 100 μm) and corresponding quantification (n = 4) of CD31 cells and intratumoral FITC-dextran leakage.

(C) Representative micrographs (scale bar represents 100 μm) of hypoxia indicator, Hypoxyprobe, and corresponding quantification (n = 4).

(D) Representative micrographs (scale bar represents 50 μm) of αSMA^+ cells in tumors with YFP^+ linage tagged cancer cells and corresponding quantification (n = 4). White arrowheads point to αSMA^+YFP^+ cells.

(E) Relative *Twist*, *Snail*, and *Slug* expression in tumors.

(F) Representative micrograph (scale bar represents 100 μm) of YFP^+ tumor spheres (insert shows higher magnification micrograph, scale bar represents 25 μm) and corresponding quantification (n = 15).

(G) Representative scatterplot and quantification of percentage $CD44^+CD133^+$ cancer cells (control: n = 2; depleted: n = 3). Q1: $CD44^+CD133^-$; Q2: $CD44^+CD133^+$; Q3: $CD44^-CD133^+$; Q4: $CD44^-CD133^-$.

(H) Tumorigenic ability of YFP^+ cells determined by limiting dilution assay. For each cell dose, six mice were injected with YFP^+ cancer cells from control or myofibroblast depleted tumors, and data are presented as the number of mice displaying tumors. Significance was assayed using χ^2 tests.

Data are represented as mean ± SEM. Unless otherwise noted, significance was determined using t tests (*$p < 0.05$, **$p < 0.01$, ****$p < 0.0001$). ns, not significant. See also Figure S4 and Table S3.

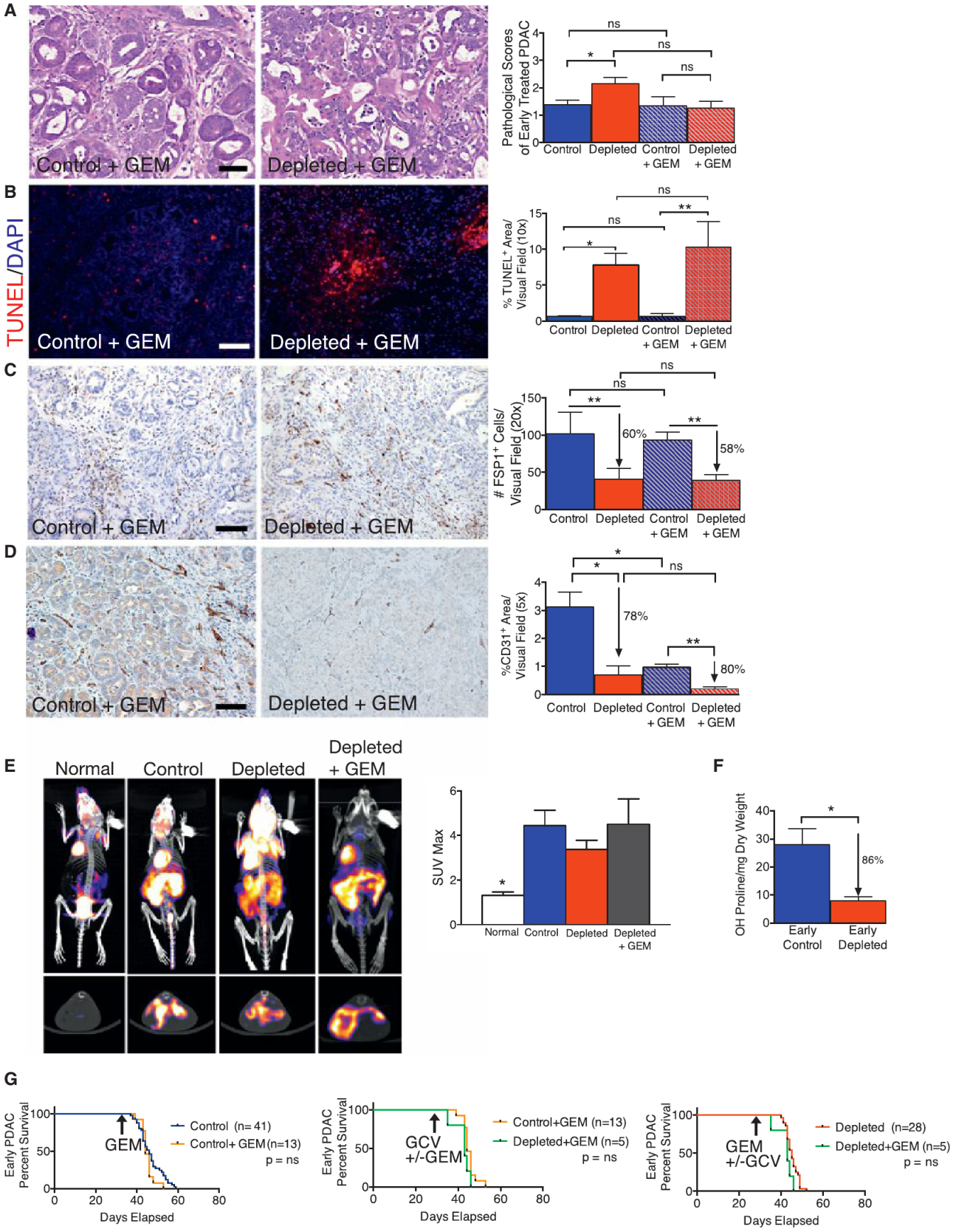

(legend on next page)

The most dramatic impact of myofibroblast depletion was on the composition of the immune infiltrate in the tumor microenvironment. The interplay between cancer-associated fibroblasts and immune cells has long been recognized as a major contributor of cancer development (Coussens and Werb, 2002; Erez et al., 2010; Kalluri and Zeisberg, 2006). Here, we demonstrate that the immune response (innate and adaptive) associated with PDAC tumors was significantly impaired when fibrosis was reduced starting at the PanIN stage or at the PDAC stage. Myofibroblast-depleted tumors are associated with a decreased Teff/Treg ratio and a significant elevation in *Ctla4* expression. Myofibroblast depletion coupled with inhibition of checkpoint blockade using anti-CTLA-4 antibodies significantly ameliorated tumor burden in mice with established PDAC and improved overall survival. Our data suggest that although myofibroblast depletion results in the suppression of immune surveillance, an opportunist immune profile dominated by suppressor T cells emerges in the tumor, offering a viable checkpoint blockade target using anti-CTLA-4 antibodies. Although this antibody shows marginal efficacy in control PDAC mice with normal levels of fibrosis, depletion of fibrosis unravels more robust efficacy, likely because of significant changes in the microenvironment. Small proof-of-concept trials with ipilimumab have revealed some anecdotal responses (Royal et al., 2010), and our study suggests that stratifying patients on the basis of their fibrosis scores might offer better responses. This is supported by the fact that ipilimumab showed dramatic efficacy in metastatic melanoma (Robert et al., 2011), a cancer with low levels of overall stroma.

In summary, our study, together with other ongoing efforts to elucidate pancreatic tumor immunity and immunotherapy (Bayne et al., 2012; Clark et al., 2007; Hiraoka et al., 2006; Roberts et al., 2013; Vonderheide et al., 2013), will likely offer insights into potential efficacy of combination therapies involving immunotherapy in patients with pancreas cancer.

EXPERIMENTAL PROCEDURES

Animal Studies

The disease progression and genotyping for the PKT mice was previously described (Ijichi et al., 2006). PKT mice were crossed to R26-*LSL*-EYFP (purchased from Jackson Laboratory), αSMA-tk (LeBleu et al., 2013), and αSMA-RFP (LeBleu et al., 2013) mice. Mice received daily intraperitoneal (i.p.) injections with 50 mg/kg body weight of GCV at 4 to 4.5 weeks of age (30.3 ± 1.7 days) for 14 days or less (early depletion) or at 6 weeks of age (40.7 ± 1.7 days) for 10 days or less (late depletion). One hour prior to sacrifice, mice were injected i.p. with 60 mg/kg body weight pimonidazole (Hypoxyprobe). KPC mice were previously described (Hingorani et al., 2005) and crossed to αSMA-tk mice. KPC mice were treated with GCV starting at 7 weeks of age (49 ± 2.5 days). GEM (50 μg/kg body weight; LC Laboratories) was given i.p. at day 1 and day 7, either alone or in combination with GCV. An initial 200 μg anti-CTLA-4 (BioXCell, clone 9H10, BE0131) antibody or 200 μg hamster immunoglobulin G (IgG) (BioXCell, BE0091) in 200 μl PBS was administered i.p., followed by two injections of 100 μg anti-CTLA-4 or 100 μg hamster IgG in 100 μl PBS every other day. All mice were housed under standard housing conditions at the Beth Israel Deaconess Medical Center (BIDMC) and MD Anderson Cancer Center (MDACC) animal facilities, and all animal procedures were reviewed and approved by the BIDMC and the MDACC institutional animal care and use committees. Acquisition and analysis of ^{18}F-FDG PET/CT in mice is detailed in Supplemental Experimental Procedures.

Histology and Histopathology

Formalin-fixed tumors were submitted to the BIDMC and MDACC histology core facilities, and paraffin-embedded sections were cut for hematoxylin and eosin (H&E) staining and MTS. For histopathological scoring, H&E-stained slides were scored for the penetrance of each histological hallmark on a scale of 0 to 3. The predominant tumor phenotype gave the pathological score for the whole tumor (1 = well differentiated, 2 = moderately differentiated, 3 = poorly differentiated). Necrosis was also scored on a scale of 0 to 3. Lung emboli were counted in one H&E lung section per mouse evaluated. Picrosirius red staining for collagen was achieved using 0.1% picrosirius red (Direct Red 80; Sigma) and counterstained with Weigert's hematoxylin. Mucin staining was achieved using mucicarmine and metalin yellow and counter-stained with Weigert's hematoxylin.

IHC

Harvested tumors were formalin fixed prior to paraffin embedding. Sections 4 to 5 μm thick were deparaffinized, rehydrated, and boiled for 1 hr in 10 mM citrate buffer at pH 6.0. Staining for αSMA was processed using the M.O.M. Kit (Vector Laboratories) according to the manufacturer's recommendations. For all other stains, the tissue sections were blocked with 1% BSA in Tris-buffered saline for 30 min prior to incubation with the primary antibody. Sections were then incubated with biotin-conjugated anti-rabbit/rat/goat IgG and ABC reagent (Vector Laboratories) for 30 to 45 min at room temperature. DAB was used as a detection system (Vector Laboratories) according to the manufacturer's instructions. The following primary antibodies were used: mouse anti-αSMA (Sigma) 1:200, rabbit anti-FSP1 (a gift from Dr. Eric Nielson, Northwestern University Feinberg School of Medicine) 1:50, biotinylated anti-HABP (Amsbio) 1:200, rabbit anti-CD31 (Abcam) 1:50, and rabbit antivimentin (Cell Signaling) 1:100. For all stainings, DAB positivity was analyzed in five to eight visual fields at an original magnification of 10×, 20×, or 40×. Control and treated mice within an experimental set (at least three mice per group) were analyzed. All stainings were quantified using NIH ImageJ analysis software with the same threshold for each stain; results were expressed as percentage staining per visual field.

Immunofluorescence

Harvested tumors were embedded in O.C.T. medium (TissueTek). Frozen sections 4 to 5 μm thick were fixed in ice-cold acetone for 20 min, blocked

Figure 5. GEM Treatment Does Not Improve Survival of Mice with Myofibroblast-Depleted Tumors

(A) Representative micrographs of H&E stained pancreatic samples (scale bar represents 100 μm) and pathological scores of indicated experimental groups. Control, n = 16; depleted, n = 17; GEM, n = 8; and GEM depleted, n = 8.

(B) Representative micrographs (scale bar represents 200 μm) of the apoptosis marker TUNEL and corresponding quantification (n = 3 in each group).

(C) Representative micrographs (scale bar represents 100 μm) of FSP1 IHC and corresponding quantification (n = 4 in each group).

(D) Representative micrographs (scale bar represents 100 μm) of CD31 IHC and corresponding quantification (n = 3 in each group).

(E) Representative ^{18}F-FDG PET/CT (top, frontal section; bottom, sagittal section) and associated maximum standard update value (SUVmax) (n = 3 in each group).

(F) Hydroxyproline release reflecting collagen content in control and myofibroblast-depleted tumors (n = 4 in each group). Significance was determined using t tests.

(G) Survival analyses of indicated experimental groups.

Data are represented as mean ± SEM. Unless otherwise noted, significance was determined using one-way ANOVA with Tukey post hoc analysis (*$p < 0.05$, **$p < 0.01$). ns, not significant.

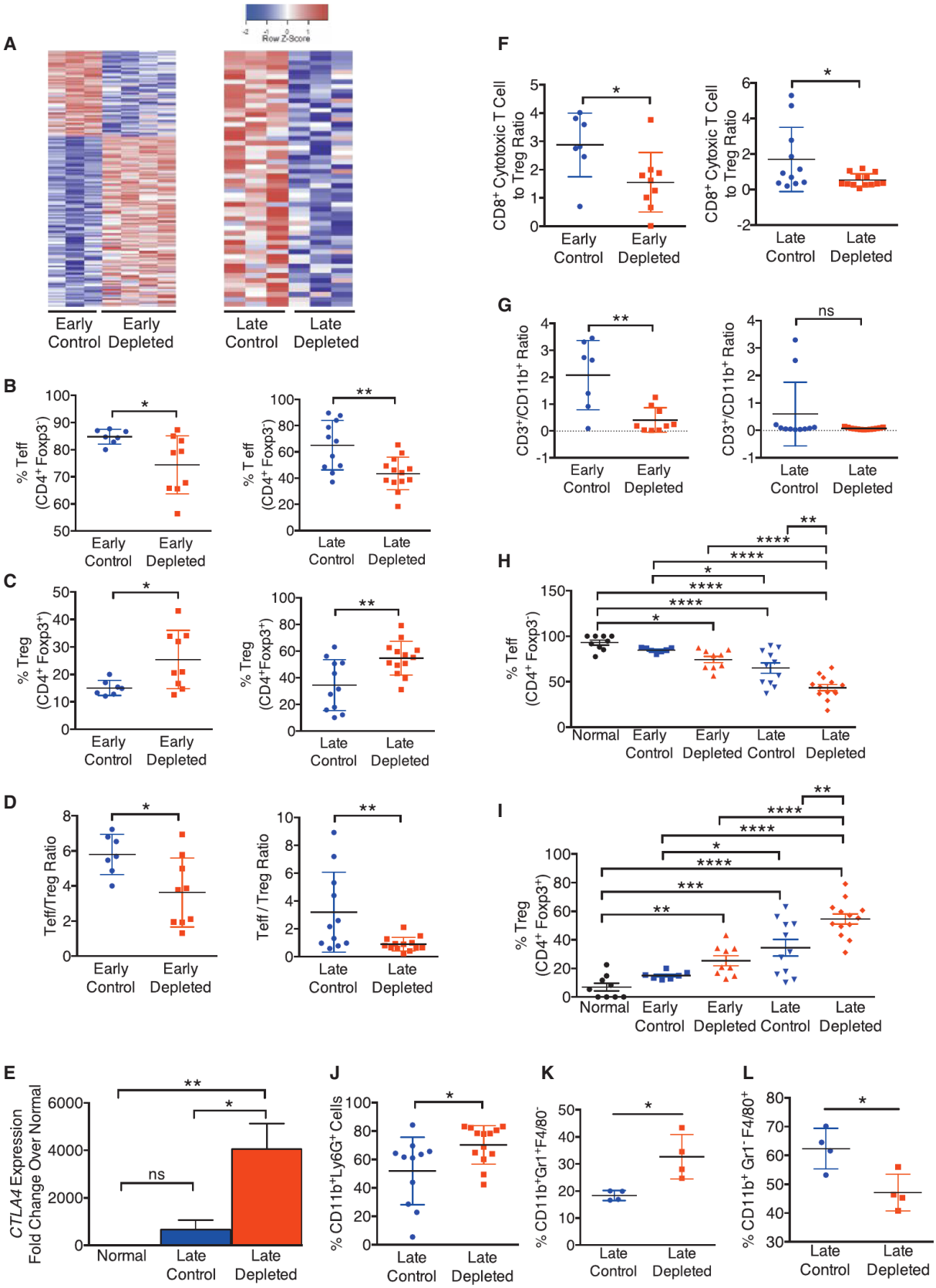

(legend on next page)

with 1% BSA in PBS, and immunostained using standard protocols. Primary antibodies used were goat anti-collagen 1 (Southern Biotech) 1:200, mouse anti-αSMA-FITC/mouse anti-αSMA-Cy3 (Sigma) 1:200, rat antimouse Ki-67 (abcam) 1:200, rabbit anti-FAP (Abcam) 1:200, rat anti-foxp3 (eBioscience) 1:150, rabbit anti-NG2 (Millipore) 1:200, rat anti-CD31 (BD PharMingen) 1:200, mouse 4.3.11.3 (Hypoxyprobe) 1:50, and rabbit anti-LOX (Imgenex) 1:200. Stainings for pimonidazole adduct (Hypoxyprobe) was processed using the M.O.M. Kit according to the manufacturer's recommendations. Apoptosis was assessed using In Situ Cell Death Detection Kit, TMR red (Roche). DAPI was used to stain cell nuclei.

Flow Cytometry

Weighed tumors were minced and allowed to digest in a 2 ml mixture of collagenase (400 U type II collagenase; Worthington) and 0.2 mg/ml DNase I in RPMI media at 37°C for 1 hr. The mixture was gently vortexed every 10 to 20 min. The tissue lysate was filtered through a 40 μm mesh prior to immunostaining. The resulting single-cell suspension was stained with fixable viability dye eFluor 780, anti-CD45.2 Pacific Blue, anti-CD3 PE-Cy7, anti-CD3 Alexa Fluor 700, anti-Foxp3 Alexa Fluor 700, anti-CD11c eFluor 615, and anti-NK1.1 PE (all from eBioscience); anti-Granzyme B APC and anti-CD4 Qdot 605 (Life Technologies); anti-CD8 Brilliant Violet 650, anti-CD11b Brilliant Violet 570, anti-CD19 Brilliant Violet 650, and anti-F4/80 FITC (all from BioLegend); and anti-Ly6C APC, anti-Ly6G PE-Cy7, and anti-Ki-67 PE (BD Biosciences). The percentage positive cells were analyzed by FlowJo and gated on CD45 positivity. To analyze the number of $CD133^+CD44^+$ cells, the single-cell suspension was incubated in the dark, on ice, with Aqua LIVE/DEAD Fixable Dead Cell Stain (Molecular Probes) 1:1,000 for 30 min, followed by staining with anti-CD44 APC 1:400 (eBioscience) and anti-CD133 PE 1:200 (eBioscience). Unstained, LIVE/DEAD only, and single stain served as control. Doublets were gated out using forward-scatter width/height and sideward-scatter width/height event characteristics.

Tumor Spheres and Limiting Dilution Tumor Formation Assay

Tumors were digested as described above, and cell suspension was filtered through a 100 μm mesh. Two million cells were plated in a low-adherence dish with 1% fetal bovine serum, Dulbecco's modified Eagle's medium, and penicillin/streptomycin/amphotericin. Three to 4 weeks later, the formed spheres were counted at 200× magnification. For the limiting dilution assay, flow cytometry purified YFP^+ cancer cells (from PKT mice crossed to R26-stop-EYFP reporter mice) were pelleted and resuspended in PBS prior to subcutaneous injection in nude mice. Six nude mice received injections of YFP^+ cells (100, 1,000 or 10,000 cells) from tumors of PKT mice without myofibroblast depletion (control; two donor mice were used) or with myofibroblast depletion (depleted; two donor mice were used).

Gene Expression Profiling

Total RNA was isolated from tumors of PKT control mice (n = 3 at early stage, n = 3 at late stage) and myofibroblast-depleted mice (n = 4 at early stage, n = 3 at late stage, n = 2 at late stage and treated with anti-CTLA4) using RNeasy Plus Mini Kit (Qiagen) and submitted to the Microarray Core Facility at MD Anderson Cancer Center. Gene expression analysis was performed using Mouse Ref6 Gene Expression BeadChip (Illumina), and the Limma package from R Bioconductor (Carey et al., 2005) was used to analyze differentially expressed genes of myofibroblast-depleted mice versus control mice ($p \leq 0.05$, fold change ≥ 1.5). Gene ontology and pathway analyses of differentially expressed genes are performed using the Web-accessible program Database for Annotation, Visualization and Integrated Discovery (Huang et al., 2009). Pathways that enrich differentially expressed genes are selected ($p < 0.05$). For RNA sequencing analyses, sequencing of the whole transcriptome was performed using the SOLiD system. Lifescope Genomic Analysis Software version 2.5.1 was used to map the raw data to the mouse genome (build mm10) and to quantify the counts per gene. The count data were used to perform differential expression analysis using the R package, DEseq. Quantitative real-time PCR analyses are detailed in Supplemental Experimental Procedures.

Vascular Leakage

Vascular leakage was assayed and quantified as previously described (Cooke et al., 2012). Quantification was performed using a grading system ranging from 0 to 5, representing 0% to 100% extravascular FITC-dextran. Results were plotted as scores.

Clinical Studies

Resected tumors were obtained from 53 patients (Table S1) with invasive pancreatic adenocarcinoma who underwent surgical resection at Johns Hopkins Hospital after approval by the Johns Hopkins Hospital institutional review board (IRB). The cases were obtained under an IRB-exempt protocol. Clinical information was obtained from the electronic medical records. Tissue sections from paraffin-embedded specimens were stained for αSMA (Sigma) as described above, and staining intensity was scored blinded. Each tissue section was surveyed entirely for αSMA stain intensity in interstitial fibroblasts. αSMA^+ vessels of all sizes were easily distinguishable from interstitial fibroblasts. Overall, few αSMA^+ vessels were detected in the tumors, and these were not included in the score. A scale of 0 to 3 was used (0 = no detected staining, 1 = weak staining, 2 = moderate staining, 3 = strong staining). Patients were then divided into two groups: a "low αSMA" group, as defined by scores of 0 and 1, and a "high αSMA" group, as defined by scores of 2 and 3. Kaplan-Meier plots were drawn for each group and statistical differences evaluated using the log rank Mantel-Cox test.

Statistics

Statistical analyses of pathological scores, flow cytometry, and immunohistochemical quantifications were performed by using Student's t test, one-way ANOVA, or Fisher's exact test with GraphPad Prism (GraphPad Software). Limiting dilution assay was evaluated using SPSS (SPSS) with chi-square tests. For survival analyses, Kaplan-Meier plots were drawn and statistical differences evaluated using the log rank Mantel-Cox test. A p value < 0.05 was considered statistically significant.

ACCESSION NUMBERS

The microarray data are deposited at Gene Expression Omnibus under accession numbers GSE52812 (gene expression changes comparing pancreas tumors from PKT mice with pancreas tumors from PKT; αSMA-tk mice) and GSE55871 (gene expression changes comparing myofibroblasts from pancreas tumors of PKT mice with myofibroblasts from pancreas tumors of PKT; αSMA-tk mice).

SUPPLEMENTAL INFORMATION

Supplemental Information includes Supplemental Experimental Procedures, six figures, and three tables and can be found with this article online at http://dx.doi.org/10.1016/j.ccr.2014.04.005.

Figure 6. Myofibroblast Depletion Results in Increased Frequency of $FoxP3^+$ Treg Cells in PDAC

(A) Heatmap of differentially regulated genes pertaining to tumor immunity in early- and late-treated tumors.
(B–D) Percentage Teff (B), percentage Treg (C), and Teff/Treg ratio (D) in early- and late-treated tumors.
(E) Relative *Ctla4* expression in late-treated tumors (n = 6).
(F and G) $CD8^+$ cytotoxic T cell/Treg ratio (F) and CD3/CD11b ratio (G) in early- and late-treated tumors.
(H and I) Percentages Teff (H) and Treg (I) in normal pancreas and in early- and late-treated tumors.
(J–L) Percentages $CD11b^+Ly6G^+$ (J), $CD11b^+Gr1^+F4/80^-$ (K), and $CD11b^+Gr1^-F4/80^+$ (L) cells in late-treated tumors.
Data are represented as mean ± SEM. Significance was determined using t tests, except for multiple-group comparisons, for which significance was determined using one-way ANOVA with Tukey post hoc analysis (*$p < 0.05$, **$p < 0.01$, **$p < 0.001$, ****$p < 0.0001$). ns, not significant. See also Figure S5.

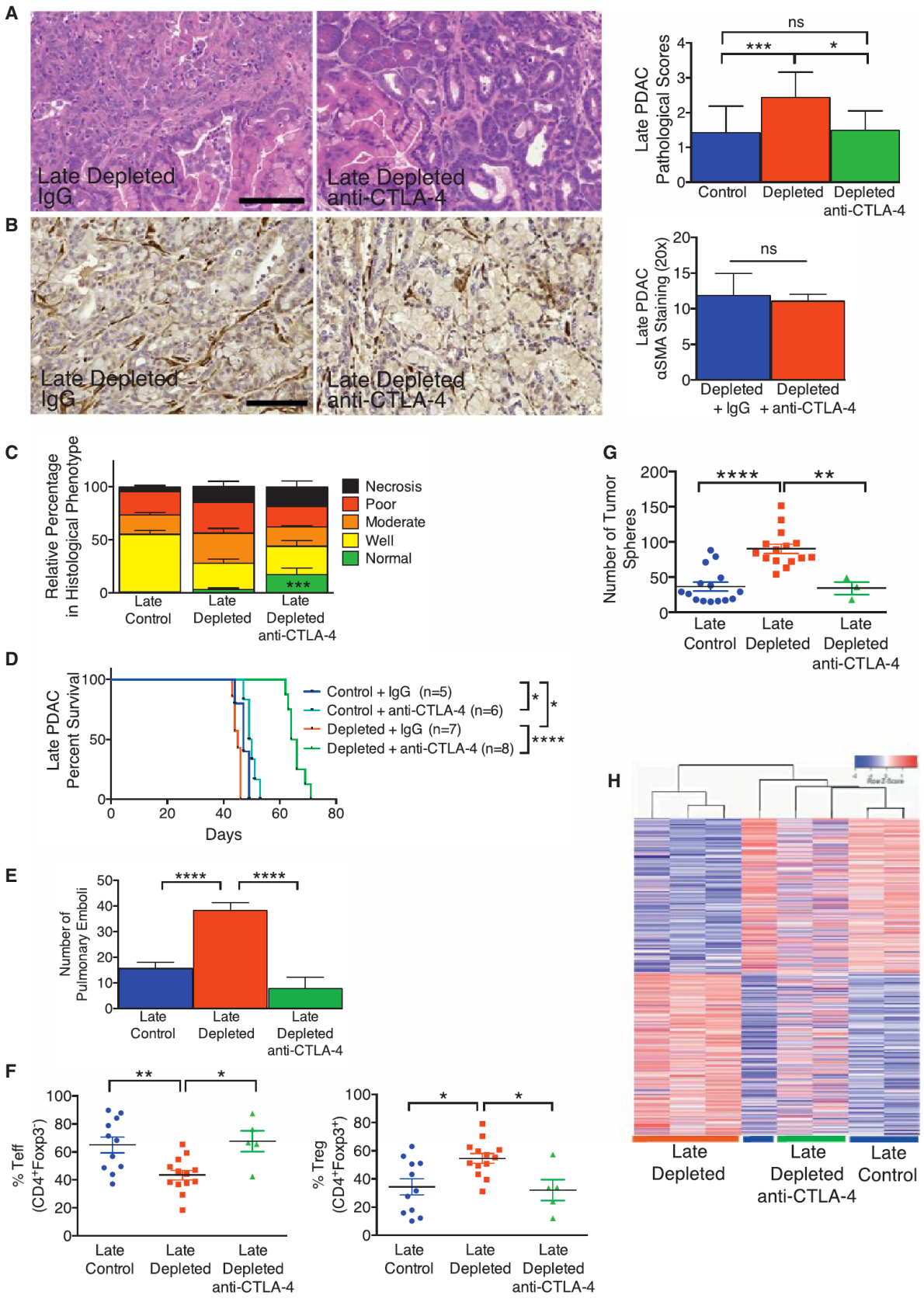

(legend on next page)

ACKNOWLEDGMENTS

We wish to thank Travis Hardcastle, Lauren Bizarro, Judith Kaye, Laura Gibson, and Sara Lovisa for genotyping and animal husbandry support; Donna Reynolds for IHC stainings; and Travis Hardcastle, Dr. Ganiraju C. Manyam, Dr. Jing Wang, and the Bioinformatics and Computational Biology Department at MDACC for bioinformatic support. This study was supported primarily by NIH grant UO1 CA151925. B.C.O. received funding from the OncoSuisse MD/PhD Scholarship (323630-128865/1) and the Swiss National Science Foundation Fellowship (PBBEP3_144809). C.K. is funded by a Research Fellowship of Deutsche Forschungsgemeinschaft. A.M. is supported by NIH grant CA113669. R.K. is supported by the Cancer Prevention and Research Institute of Texas and the Metastasis Research Center at MD Anderson Cancer Center, NIH grants DK55001, DK81976, CA125550, CA155370, and CA163191. J.P.A. is an inventor of intellectual property owned by the University of California, Berkeley, and licensed to Bristol Myers-Squibb.

Received: January 6, 2014
Revised: February 8, 2014
Accepted: April 10, 2014
Published: May 22, 2014

REFERENCES

Aguirre, A.J., Bardeesy, N., Sinha, M., Lopez, L., Tuveson, D.A., Horner, J., Redston, M.S., and DePinho, R.A. (2003). Activated Kras and Ink4a/Arf deficiency cooperate to produce metastatic pancreatic ductal adenocarcinoma. Genes Dev. *17*, 3112–3126.

Amakye, D., Jagani, Z., and Dorsch, M. (2013). Unraveling the therapeutic potential of the Hedgehog pathway in cancer. Nat. Med. *19*, 1410–1422.

Angeli, F., Koumakis, G., Chen, M.C., Kumar, S., and Delinassios, J.G. (2009). Role of stromal fibroblasts in cancer: promoting or impeding? Tumour Biol. *30*, 109–120.

Armstrong, T., Packham, G., Murphy, L.B., Bateman, A.C., Conti, J.A., Fine, D.R., Johnson, C.D., Benyon, R.C., and Iredale, J.P. (2004). Type I collagen promotes the malignant phenotype of pancreatic ductal adenocarcinoma. Clin. Cancer Res. *10*, 7427–7437.

Bardeesy, N., Aguirre, A.J., Chu, G.C., Cheng, K.H., Lopez, L.V., Hezel, A.F., Feng, B., Brennan, C., Weissleder, R., Mahmood, U., et al. (2006a). Both p16(Ink4a) and the p19(Arf)-p53 pathway constrain progression of pancreatic adenocarcinoma in the mouse. Proc. Natl. Acad. Sci. USA *103*, 5947–5952.

Bardeesy, N., Cheng, K.H., Berger, J.H., Chu, G.C., Pahler, J., Olson, P., Hezel, A.F., Horner, J., Lauwers, G.Y., Hanahan, D., and DePinho, R.A. (2006b). Smad4 is dispensable for normal pancreas development yet critical in progression and tumor biology of pancreas cancer. Genes Dev. *20*, 3130–3146.

Bayne, L.J., Beatty, G.L., Jhala, N., Clark, C.E., Rhim, A.D., Stanger, B.Z., and Vonderheide, R.H. (2012). Tumor-derived granulocyte-macrophage colony-stimulating factor regulates myeloid inflammation and T cell immunity in pancreatic cancer. Cancer Cell *21*, 822–835.

Bissell, M.J., and Radisky, D. (2001). Putting tumours in context. Nat. Rev. Cancer *1*, 46–54.

Bissell, M.J., Kenny, P.A., and Radisky, D.C. (2005). Microenvironmental regulators of tissue structure and function also regulate tumor induction and progression: the role of extracellular matrix and its degrading enzymes. Cold Spring Harb. Symp. Quant. Biol. *70*, 343–356.

Carey, V.J., Dudoit, R., Irizarry, R., Huber, W., and Gentleman, R. (2005). Bioinformatics and Computational Biology Solutions Using R and Bioconductor. (Bioconductor), http://www.bioconductor.org/help/publications/books/bioinformatics-and-computational-biology-solutions/

Cheresh, D.A., and Stupack, D.G. (2008). Regulation of angiogenesis: apoptotic cues from the ECM. Oncogene *27*, 6285–6298.

Clark, C.E., Hingorani, S.R., Mick, R., Combs, C., Tuveson, D.A., and Vonderheide, R.H. (2007). Dynamics of the immune reaction to pancreatic cancer from inception to invasion. Cancer Res. *67*, 9518–9527.

Cooke, V.G., LeBleu, V.S., Keskin, D., Khan, Z., O'Connell, J.T., Teng, Y., Duncan, M.B., Xie, L., Maeda, G., Vong, S., et al. (2012). Pericyte depletion results in hypoxia-associated epithelial-to-mesenchymal transition and metastasis mediated by met signaling pathway. Cancer Cell *21*, 66–81.

Coussens, L.M., and Werb, Z. (2002). Inflammation and cancer. Nature *420*, 860–867.

Dvorak, H.F. (1986). Tumors: wounds that do not heal. Similarities between tumor stroma generation and wound healing. N. Engl. J. Med. *315*, 1650–1659.

Erez, N., Truitt, M., Olson, P., Arron, S.T., and Hanahan, D. (2010). Cancer-associated fibroblasts are activated in incipient neoplasia to orchestrate tumor-promoting inflammation in an NF-kappaB-dependent manner. Cancer Cell *17*, 135–147.

Erkan, M., Michalski, C.W., Rieder, S., Reiser-Erkan, C., Abiatari, I., Kolb, A., Giese, N.A., Esposito, I., Friess, H., and Kleeff, J. (2008). The activated stroma index is a novel and independent prognostic marker in pancreatic ductal adenocarcinoma. Clin. Gastroenterol. Hepatol. *6*, 1155–1161.

Feig, C., Gopinathan, A., Neesse, A., Chan, D.S., Cook, N., and Tuveson, D.A. (2012). The pancreas cancer microenvironment. Clin. Cancer Res. *18*, 4266–4276.

Gidekel Friedlander, S.Y., Chu, G.C., Snyder, E.L., Girnius, N., Dibelius, G., Crowley, D., Vasile, E., DePinho, R.A., and Jacks, T. (2009). Context-dependent transformation of adult pancreatic cells by oncogenic K-Ras. Cancer Cell *16*, 379–389.

Grassian, A.R., Coloff, J.L., and Brugge, J.S. (2011). Extracellular matrix regulation of metabolism and implications for tumorigenesis. Cold Spring Harb. Symp. Quant. Biol. *76*, 313–324.

Guerra, C., Collado, M., Navas, C., Schuhmacher, A.J., Hernández-Porras, I., Cañamero, M., Rodriguez-Justo, M., Serrano, M., and Barbacid, M. (2011). Pancreatitis-induced inflammation contributes to pancreatic cancer by inhibiting oncogene-induced senescence. Cancer Cell *19*, 728–739.

Hermann, P.C., Huber, S.L., Herrler, T., Aicher, A., Ellwart, J.W., Guba, M., Bruns, C.J., and Heeschen, C. (2007). Distinct populations of cancer stem cells

Figure 7. Anti-CTLA-4 Attenuates PDAC and Improves Survival in Mice with Myofibroblast-Depleted Tumors

(A) Representative micrographs of H&E stained tumors (scale bar represents 100 μm) and pathological scores of tumors in indicated experimental groups. Control, n = 14; depleted, n = 16; depleted plus anti-CTLA-4, n = 6. Significance was determined using one-way ANOVA with Tukey post hoc analysis.

(B) Representative micrographs of αSMA stained pancreatic samples (scale bar represents 100 μm) and corresponding quantification. Depleted, n = 5; depleted plus anti-CTLA-4, n = 7.

(C) Relative percentage of tissue encompassed by each histology hallmark. Control, n = 15; depleted, n = 16; depleted plus anti-CTLA-4, n = 6. Significance was determined using one-way ANOVA with Tukey post hoc analysis.

(D) Survival analysis of the indicated experimental groups.

(E) Number of pulmonary emboli. Control, n = 14; depleted, n = 28; depleted plus anti-CTLA-4, n = 8.

(F) Percentages Teff (left) and Treg (right) cells in tumors of indicated experimental groups.

(G) Number of spheres formed from tumors of indicated experimental groups.

(H) Heatmap of differentially expressed genes in the indicated groups.

Data are represented as mean ± SEM. Unless otherwise noted, significance was determined using t tests (*$p < 0.05$, **$p < 0.01$, **$p < 0.001$, ****$p < 0.0001$). ns, not significant. See also Figure S6.

determine tumor growth and metastatic activity in human pancreatic cancer. Cell Stem Cell *1*, 313–323.

Hidalgo, M. (2010). Pancreatic cancer. N. Engl. J. Med. *362*, 1605–1617.

Hingorani, S.R., Petricoin, E.F., Maitra, A., Rajapakse, V., King, C., Jacobetz, M.A., Ross, S., Conrads, T.P., Veenstra, T.D., Hitt, B.A., et al. (2003). Preinvasive and invasive ductal pancreatic cancer and its early detection in the mouse. Cancer Cell *4*, 437–450.

Hingorani, S.R., Wang, L., Multani, A.S., Combs, C., Deramaudt, T.B., Hruban, R.H., Rustgi, A.K., Chang, S., and Tuveson, D.A. (2005). Trp53R172H and KrasG12D cooperate to promote chromosomal instability and widely metastatic pancreatic ductal adenocarcinoma in mice. Cancer Cell *7*, 469–483.

Hiraoka, N., Onozato, K., Kosuge, T., and Hirohashi, S. (2006). Prevalence of FOXP3+ regulatory T cells increases during the progression of pancreatic ductal adenocarcinoma and its premalignant lesions. Clin. Cancer Res. *12*, 5423–5434.

Hruban, R.H., Pitman, M.B., and Klimstra, D.S. (2007). Tumors of the Pancreas. (Washington: American Registry of Pathology).

Huang, W., Sherman, B.T., and Lempicki, R.A. (2009). Systematic and integrative analysis of large gene lists using DAVID bioinformatics resources. Nat. Protoc. *4*, 44–57.

Ijichi, H., Chytil, A., Gorska, A.E., Aakre, M.E., Fujitani, Y., Fujitani, S., Wright, C.V., and Moses, H.L. (2006). Aggressive pancreatic ductal adenocarcinoma in mice caused by pancreas-specific blockade of transforming growth factor-beta signaling in cooperation with active Kras expression. Genes Dev. *20*, 3147–3160.

Jacobetz, M.A., Chan, D.S., Neesse, A., Bapiro, T.E., Cook, N., Frese, K.K., Feig, C., Nakagawa, T., Caldwell, M.E., Zecchini, H.I., et al. (2013). Hyaluronan impairs vascular function and drug delivery in a mouse model of pancreatic cancer. Gut *62*, 112–120.

Kalluri, R., and Zeisberg, M. (2006). Fibroblasts in cancer. Nat. Rev. Cancer *6*, 392–401.

Kalluri, R., and Weinberg, R.A. (2009). The basics of epithelial-mesenchymal transition. J. Clin. Invest. *119*, 1420–1428.

Karnoub, A.E., Dash, A.B., Vo, A.P., Sullivan, A., Brooks, M.W., Bell, G.W., Richardson, A.L., Polyak, K., Tubo, R., and Weinberg, R.A. (2007). Mesenchymal stem cells within tumour stroma promote breast cancer metastasis. Nature *449*, 557–563.

Korc, M. (2007). Pancreatic cancer-associated stroma production. Am. J. Surg. *194*, S84–S86.

LeBleu, V.S., Taduri, G., O'Connell, J., Teng, Y., Cooke, V.G., Woda, C., Sugimoto, H., and Kalluri, R. (2013). Origin and function of myofibroblasts in kidney fibrosis. Nat. Med. *19*, 1047–1053.

Lu, P., Weaver, V.M., and Werb, Z. (2012). The extracellular matrix: a dynamic niche in cancer progression. J. Cell Biol. *196*, 395–406.

Mani, S.A., Guo, W., Liao, M.J., Eaton, E.N., Ayyanan, A., Zhou, A.Y., Brooks, M., Reinhard, F., Zhang, C.C., Shipitsin, M., et al. (2008). The epithelial-mesenchymal transition generates cells with properties of stem cells. Cell *133*, 704–715.

Merika, E.E., Syrigos, K.N., and Saif, M.W. (2012). Desmoplasia in pancreatic cancer. Can we fight it? Gastroenterol. Res. Pract. *2012*, 781765.

Olive, K.P., Jacobetz, M.A., Davidson, C.J., Gopinathan, A., McIntyre, D., Honess, D., Madhu, B., Goldgraben, M.A., Caldwell, M.E., Allard, D., et al. (2009). Inhibition of Hedgehog signaling enhances delivery of chemotherapy in a mouse model of pancreatic cancer. Science *324*, 1457–1461.

Omary, M.B., Lugea, A., Lowe, A.W., and Pandol, S.J. (2007). The pancreatic stellate cell: a star on the rise in pancreatic diseases. J. Clin. Invest. *117*, 50–59.

Pàez-Ribes, M., Allen, E., Hudock, J., Takeda, T., Okuyama, H., Viñals, F., Inoue, M., Bergers, G., Hanahan, D., and Casanovas, O. (2009). Antiangiogenic therapy elicits malignant progression of tumors to increased local invasion and distant metastasis. Cancer Cell *15*, 220–231.

Phillips, P. (2012). Pancreatic stellate cells and fibrosis. In Pancreatic Cancer and Tumor Microenvironment, P.J. Grippo and H.G. Munshi, eds. (Trivandrum: Transworld Research Network), chap. 3.

Provenzano, P.P., Cuevas, C., Chang, A.E., Goel, V.K., Von Hoff, D.D., and Hingorani, S.R. (2012). Enzymatic targeting of the stroma ablates physical barriers to treatment of pancreatic ductal adenocarcinoma. Cancer Cell *21*, 418–429.

Rasheed, Z.A., Matsui, W., and Maitra, A. (2012). Pathology of pancreatic stroma in PDAC. In Pancreatic Cancer and Tumor Microenvironment, P.J. Grippo and H.G. Munshi, eds. (Trivandrum: Transworld Research Network), chap. 1.

Robert, C., Thomas, L., Bondarenko, I., O'Day, S., Webster, J.W., Garbe, C., Lebbe, C., Baurain, J.F., Testori, A., Grob, J.J., et al. (2011). Ipilimumab plus dacarbazine for previously untreated metastatic melanoma. N. Engl. J. Med. *364*, 2517–2526.

Roberts, E.W., Deonarine, A., Jones, J.O., Denton, A.E., Feig, C., Lyons, S.K., Espeli, M., Kraman, M., McKenna, B., Wells, R.J., et al. (2013). Depletion of stromal cells expressing fibroblast activation protein-α from skeletal muscle and bone marrow results in cachexia and anemia. J. Exp. Med. *210*, 1137–1151.

Royal, R.E., Levy, C., Turner, K., Mathur, A., Hughes, M., Kammula, U.S., Sherry, R.M., Topalian, S.L., Yang, J.C., Lowy, I., and Rosenberg, S.A. (2010). Phase 2 trial of single agent ipilimumab (anti-CTLA-4) for locally advanced or metastatic pancreatic adenocarcinoma. J. Immunother. *33*, 828–833.

Scarlett, C.J., Colvin, E.K., Pinese, M., Chang, D.K., Morey, A.L., Musgrove, E.A., Pajic, M., Apte, M., Henshall, S.M., Sutherland, R.L., et al. (2011). Recruitment and activation of pancreatic stellate cells from the bone marrow in pancreatic cancer: a model of tumor-host interaction. PLoS ONE *6*, e26088.

Scheel, C., and Weinberg, R.A. (2012). Cancer stem cells and epithelial-mesenchymal transition: concepts and molecular links. Semin. Cancer Biol. *22*, 396–403.

Simeone, D.M. (2008). Pancreatic cancer stem cells: implications for the treatment of pancreatic cancer. Clin. Cancer Rese. *14*, 5646–5648.

Tsai, J.H., Donaher, J.L., Murphy, D.A., Chau, S., and Yang, J. (2012). Spatiotemporal regulation of epithelial-mesenchymal transition is essential for squamous cell carcinoma metastasis. Cancer Cell *22*, 725–736.

Vega, S., Morales, A.V., Ocaña, O.H., Valdés, F., Fabregat, I., and Nieto, M.A. (2004). Snail blocks the cell cycle and confers resistance to cell death. Genes Dev. *18*, 1131–1143.

Vonderheide, R.H., Bajor, D.L., Winograd, R., Evans, R.A., Bayne, L.J., and Beatty, G.L. (2013). CD40 immunotherapy for pancreatic cancer. Cancer Immunol. Immunother. *62*, 949–954.

Vong, S., and Kalluri, R. (2011). The role of stromal myofibroblast and extracellular matrix in tumor angiogenesis. Genes Cancer *2*, 1139–1145.

Wang, W.Q., Liu, L., Xu, H.X., Luo, G.P., Chen, T., Wu, C.T., Xu, Y.F., Xu, J., Liu, C., Zhang, B., et al. (2013). Intratumoral α-SMA enhances the prognostic potency of CD34 associated with maintenance of microvessel integrity in hepatocellular carcinoma and pancreatic cancer. PLoS ONE *8*, e71189.

Whatcott, C.J., Posner, R.G., Von Hoff, D.D., and Han, H. (2012). Desmoplasia and chemoresistance in pancreatic cancer. In Pancreatic Cancer and Tumor Microenvironment, P.J. Grippo and H.G. Munshi, eds. (Trivandrum: Transworld Research Network), chap. 8.

Cancer Cell
Article

Cancer-Secreted miR-105 Destroys Vascular Endothelial Barriers to Promote Metastasis

Weiying Zhou,[1,13] Miranda Y. Fong,[1] Yongfen Min,[16] George Somlo,[2] Liang Liu,[1,14] Melanie R. Palomares,[2,3] Yang Yu,[1,14] Amy Chow,[1] Sean Timothy Francis O'Connor,[1] Andrew R. Chin,[1,12] Yun Yen,[4,9] Yafan Wang,[9] Eric G. Marcusson,[15] Peiguo Chu,[5] Jun Wu,[6] Xiwei Wu,[10] Arthur Xuejun Li,[7] Zhuo Li,[11] Hanlin Gao,[1,10] Xiubao Ren,[14] Mark P. Boldin,[8] Pengnian Charles Lin,[16] and Shizhen Emily Wang[1,*]
[1]Department of Cancer Biology
[2]Department of Medical Oncology
[3]Department of Population Sciences
[4]Department of Molecular Pharmacology
[5]Department of Pathology
[6]Department of Comparative Medicine
[7]Department of Information Science
[8]Department of Molecular and Cellular Biology
[9]Core of Translational Research Laboratory
[10]Core of Integrative Genomics
[11]Core of Electron Microscopy
City of Hope Beckman Research Institute and Medical Center, Duarte, CA 91010, USA
[12]City of Hope Irell & Manella Graduate School of Biological Sciences, Duarte, CA 91010, USA
[13]Department of Pharmacology, College of Pharmacy, The Third Military Medical University, Chongqing, 400038, China
[14]Department of Biotherapy and Key Laboratory of Cancer Immunology, Tianjin Medical University Cancer Institute and Hospital, Tianjin, 300060, China
[15]Oncology and Basic Mechanisms, Regulus Therapeutics, San Diego, CA 92121, USA
[16]Center for Cancer Research, National Cancer Institute, Frederick, MD 21702, USA
*Correspondence: ewang@coh.org
http://dx.doi.org/10.1016/j.ccr.2014.03.007

SUMMARY

Cancer-secreted microRNAs (miRNAs) are emerging mediators of cancer-host crosstalk. Here we show that miR-105, which is characteristically expressed and secreted by metastatic breast cancer cells, is a potent regulator of migration through targeting the tight junction protein ZO-1. In endothelial monolayers, exosome-mediated transfer of cancer-secreted miR-105 efficiently destroys tight junctions and the integrity of these natural barriers against metastasis. Overexpression of miR-105 in nonmetastatic cancer cells induces metastasis and vascular permeability in distant organs, whereas inhibition of miR-105 in highly metastatic tumors alleviates these effects. miR-105 can be detected in the circulation at the premetastatic stage, and its levels in the blood and tumor are associated with ZO-1 expression and metastatic progression in early-stage breast cancer.

INTRODUCTION

Metastasis is the leading cause of mortality in cancer patients. Nearly 50% of breast cancer (BC) patients treated with chemotherapeutic and/or hormonal agents develop distant metastatic disease (Nicolini et al., 2006; Rubens, 2001); these patients face a 5-year survival rate of only ~20% (Yardley, 2010). Therefore, there is a great and urgent need to develop predictive or

Significance

In this study, we set out to identify cancer-secreted miRNAs that participate in cancer metastasis by adapting the niche cells. Our results demonstrate an important role of miR-105 in destroying the vascular endothelial barriers in the host during early premetastatic niche formation by targeting the cellular tight junctions. In breast cancer patients, increased levels of miR-105 in the circulation can be detected at the premetastatic stage and correlate with the occurrence of metastasis. Anti-miR-105 treatment suppresses metastasis and abolishes the systemic effect of tumor-derived miR-105 on niche adaptation. Therefore, these observations strongly suggest clinical applications of miR-105 as a predictive or early diagnostic blood-borne marker as well as a therapeutic target for breast cancer metastasis.

early diagnostic markers for metastasis and to elucidate the molecular mechanisms of metastasis that would allow the development of efficient treatment options. In the ''seed and soil'' hypothesis for metastasis (Paget, 1889), migratory tumor cells leave the primary tumor through intravasation, disseminate throughout the body via the circulation, and eventually engraft in a distant organ that provides an appropriate microenvironment. These consecutive steps require close interplay between cancer cells and their microenvironment. Among the multiple factors underlying metastasis, the adaptation of the primary tumor microenvironment and premetastatic or metastatic niches by cancer to facilitate cancer cell dissemination and distant engraftment plays an important prometastatic role that is starting to be recognized (Chambers et al., 2002; Kaplan et al., 2005; Podsypanina et al., 2008; Psaila and Lyden, 2009; Sethi and Kang, 2011). The recent discovery of microRNAs (miRNAs) and their extracellular presence suggest a potential role of these regulatory molecules in defining the metastatic potential of cancer cells and mediating the cancer-host communication.

miRNAs are small noncoding RNAs that base-pair with the 3′ untranslated regions (UTRs) of protein-encoding mRNAs, resulting in mRNA destabilization and/or translational inhibition. The biogenesis of miRNAs is tightly controlled, and dysregulation of miRNAs is linked to cancer (Calin and Croce, 2006; Iorio et al., 2005). miRNAs are also present extracellularly, either through binding to protein or lipid carriers (Arroyo et al., 2011; Turchinovich et al., 2011; Vickers and Remaley, 2012) or as a major RNA component of exosomes (Redis et al., 2012; Valadi et al., 2007). Exosomes are small (30–100 nm) membrane-encapsulated vesicles that are released into the extracellular environment by many cell types, including cancer cells (Skog et al., 2008; Valadi et al., 2007; Yuan et al., 2009). Exosomal RNAs are heterogeneous in size but enriched in small RNAs, such as miRNAs. Cancer-secreted exosomes and miRNAs can be internalized by other cell types in the primary tumor microenvironment and premetastatic or metastatic niches (Hood et al., 2011; Peinado et al., 2012; Skog et al., 2008; Yuan et al., 2009; Zhang et al., 2010; Zhuang et al., 2012). miRNAs loaded in these exosomes, which to a certain extent reflect the dysregulated miRNA profile in cancer cells, can thus be transferred to recipient niche cells to exert genome-wide regulation of gene expression. In addition, cancer-derived exosomal miRNAs may bind as ligands to Toll-like receptors in surrounding immune cells (Fabbri et al., 2012). Therefore, cancer-secreted miRNAs may play a crucial role in regulating various cellular components of the tumor microenvironment in order to facilitate metastasis.

Cancer-derived miRNAs have been detected in the blood of cancer patients, and their levels distinguish cancer patients from healthy controls (Mitchell et al., 2008; Taylor and Gercel-Taylor, 2008). Previous studies by us and by other groups have identified circulating miRNAs associated with the histopathological features of breast tumors and clinical outcomes in BC patients (Heneghan et al., 2010; Jung et al., 2012; Roth et al., 2010; Wu et al., 2012; Zhu et al., 2009). Some of these miRNAs may play a role in the metastatic process. The goal of this study was to identify cancer-secreted miRNAs that participate in cancer metastasis by adapting the niche cells.

RESULTS

Metastatic BC-Secreted Exosomal RNA Regulates the Migration of Endothelial Cells

We chose the MDA-MB-231 metastatic BC (MBC) line and the MCF-10A noncancerous mammary epithelial line as models for studying cancer-secreted exosomes and miRNAs. Exosomes purified from conditioned media by ultracentrifugation exhibited typical cup-shaped morphology by electron microscopy and a size range of 30 to 100 nm (Figure 1A). We focused on endothelial cells in this study for their critical barrier function during metastasis. When exosomes labeled with the fluorescent dye 1,1′-dioctadecyl-3,3,3′,3′-tetramethylindocarbocyanine perchlorate (DiI) were incubated with primary human microvascular endothelial cells (HMVECs), the recipient cells exhibited high uptake efficiency, as indicated by fluorescence microscopy (Figure 1B) and flow cytometry (Figure 1C), without a significant difference between MCF-10A- and MDA-MB-231-derived exosomes. After a 24 hr incubation with labeled exosomes, >90% of recipient cells were positive for DiI fluorescence (Figure 1C). Among a series of cellular analyses in exosome-treated HMVECs, we found that the transwell migration of endothelial cells was significantly stimulated by MDA-MB-231-secreted, but not MCF-10A-secreted, exosomes (Figure 1D). Transfection of total or small RNA extracted from MDA-MB-231 exosomes, but not that from the MCF-10A exosomes, recapitulated the migration-inducing effect (Figure 1E), thereby indicating that the unique small RNA content of MDA-MB-231 exosomes functions as a migratory regulator in endothelial cells.

miR-105 Is Specifically Expressed and Secreted by MBC Cells and Can Be Transferred to Endothelial Cells via Exosome Secretion

To identify the exosome-associated small RNA(s) that induce migration, we selected and profiled all small RNAs in the exosomes by Solexa (Illumina) deep sequencing. Exosomes from MDA-MB-231 and MCF-10A cells exhibited similar small RNA composition (Figure S1A available online). We focused on miRNAs that are known for their gene-regulatory function, identifying a list of miRNAs differentially secreted between the two lines (Table S1). Among these, some showed the corresponding up- or downregulation in the cells and the exosomes, whereas others exhibited opposite changes between the exosomal and cellular compartments, which may suggest cell-type-specific mechanisms for highly selective enrichment or exclusion of the miRNA in exosome-mediated secretion. We further focused on miR-105 that was predicted by multiple algorithms (TargetScan, miRDB, and PicTar) to target *TJP1* (tight junction [TJ] protein 1; also known as zonula occludens 1 [ZO-1]), a migration-related gene. The secretion of mature miR-105 was highly specific to MDA-MB-231, and its expression was significantly higher in these cells compared with MCF-10A (Figures 2A and 2B; Table S1). Although the primary (pri-) and precursor (pre-) miR-105 also exhibited higher intracellular levels in MDA-MB-231, these forms were not detectable in exosomes (Figures S1B and S1C). Among a panel of BC lines, the expression and secretion of miR-105 were specific to highly metastatic cells originally isolated from pleural effusion (Figures 2A and 2B).

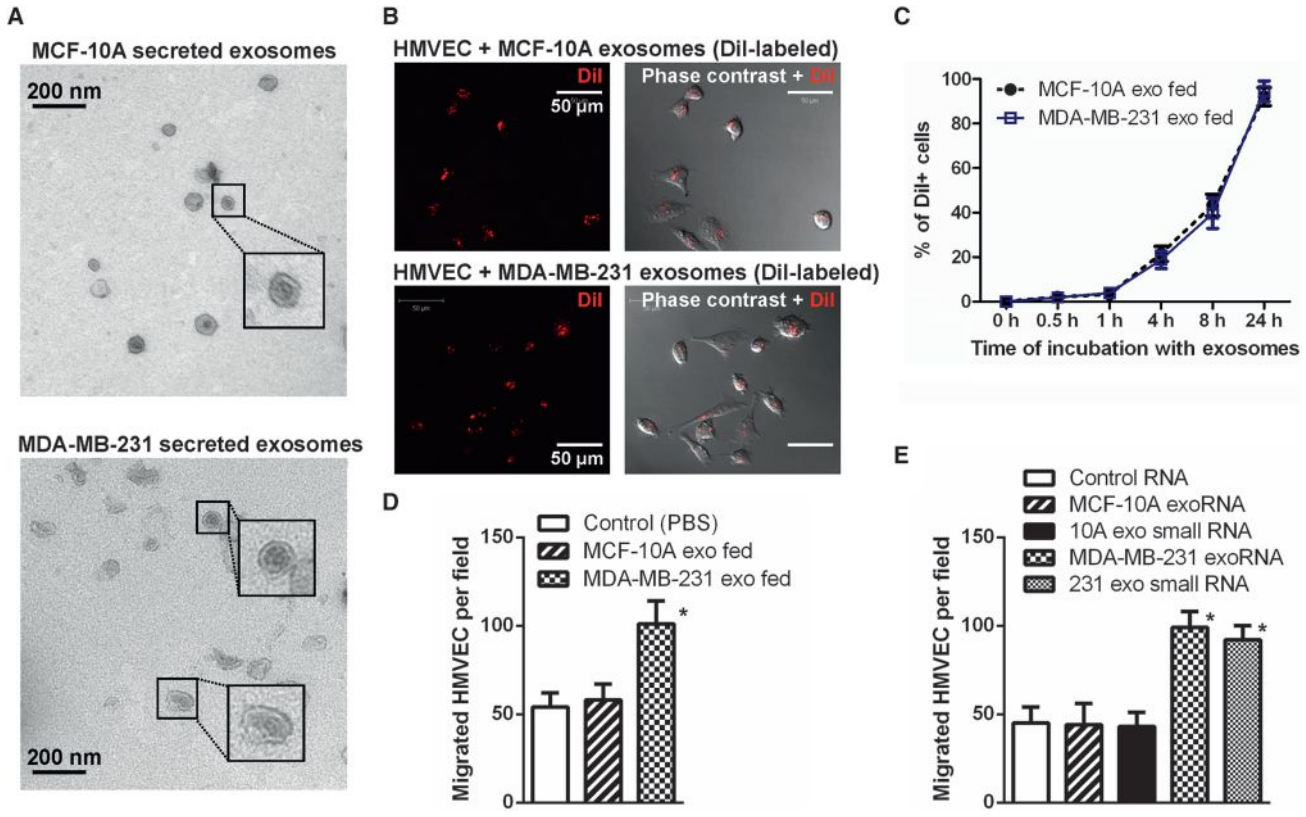

Figure 1. MBC-Secreted Exosomal RNA Regulates Migration of Endothelial Cells

(A) EM images of exosomes secreted by MCF-10A and MDA-MB-231 cells.

(B) Primary HMVECs were incubated with DiI-labeled exosomes (red) for 24 hr before fluorescent and phase contrast images were captured.

(C) HMVECs incubated with DiI-labeled exosomes for indicated time were analyzed by flow cytometry for DiI uptake.

(D) After 48 hr incubation with exosomes or PBS (as control), HMVECs were analyzed for transwell migration, and cells that had migrated within 8 hr were quantified from triplicate wells.

(E) HMVECs transfected with equal amount of total or small (<200 nt) RNA extracted from MCF-10A or MDA-MB-231 (abbreviated as MDA-231 or 231 in figures) secreted exosomes, or control RNA (cel-miR-67), were subjected to transwell migration at 48 hr after transfection.

*$p < 0.005$ compared with control group. Results are presented as mean ± SD.

To confirm that MBC-secreted miR-105 can be transferred to endothelial cells via exosomes, we measured the miR-105 levels in HMVECs treated with exosomes derived from MCF-10A or MDA-MB-231 cells. An increase of the cellular level of mature miR-105, but not pri- or pre-miR-105, was observed in recipient HMVECs following the treatment with MBC-originated exosomes with kinetics starting at 4 hr and peaking at 24 hr (Figures 2C and 2D), similar to that observed for exosome uptake (Figure 1C). We conclude that this increase of miR-105 reflects the exosome-mediated miRNA transfer but not an induction of miR-105's endogenous expression in the recipient cells, as its level in exosome-treated cells was not significantly affected by an RNA polymerase II inhibitor (Figure 2E). When we treated HMVECs with PKH67 (Sigma-Aldrich)-labeled exosomes secreted by MDA-MB-231 cells that were transfected with Cy3-labeled miR-105, the Cy3 fluorescence was observed in >90% of recipient cells, in which it largely colocalized with the PKH67 lipid dye that labeled the exosomal membranes (Figure S1D). In contrast, no internalization of naked Cy3-labeled miR-105 was observed in HMVECs (Figure S1D).

Cancer-Secreted miR-105 Downregulates Tight Junctions and Destroys the Barrier Function of Endothelial Monolayers

We next examined the miR-105 regulation of the putative target ZO-1, a central molecular component of TJs, which comprise a major group of cell-cell adhesion complexes in endothelial and epithelial cells. The four predicted miR-105 binding sites in the 3′UTR of human ZO-1 were cloned into a reporter plasmid and assessed for their responsiveness to miR-105 in HMVECs. Site I and site II, which are conserved among most species, responded to retrovirus-expressed miR-105 by directing a 50% to 65% reduction in reporter gene expression, whereas the other two sites did not. When both sites I and II were present downstream of reporter gene, a greater reduction in gene expression was observed (Figure S2A).

Consistent with the results from the reporter assay, ectopic expression of miR-105, or treatment with exosomes derived from the MDA-MB-231 (high-miR-105) but not the MCF-10A cells (low-miR-105), resulted in a significant decrease of ZO-1 expression at both the mRNA and protein levels in HMVECs (Figures 3A–3C). The effect of MDA-MB-231 exosomes could be abolished

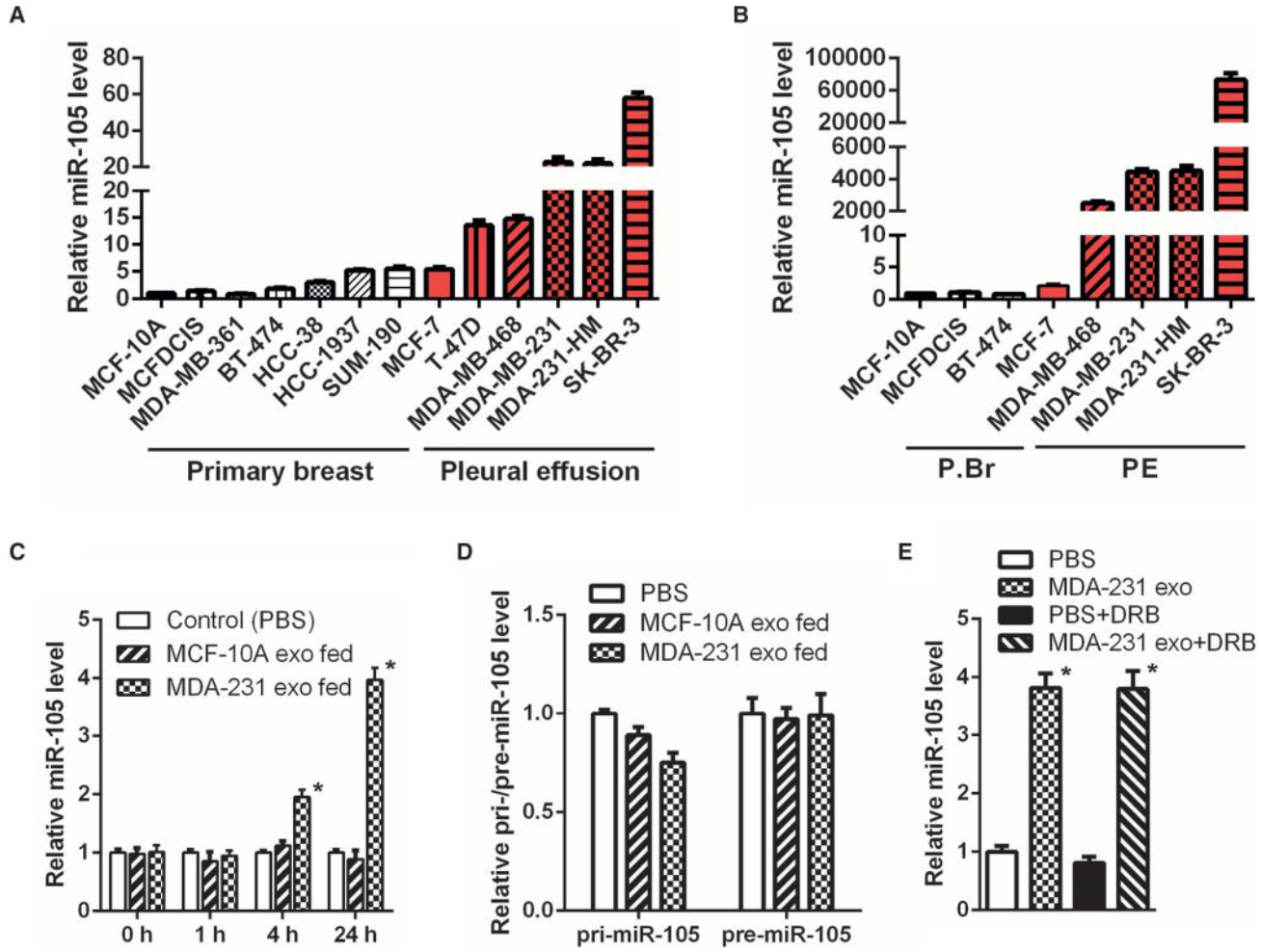

Figure 2. miR-105 Is Specifically Expressed and Secreted by MBC Cells and Can Be Transferred to Endothelial Cells via Exosome Secretion

(A and B) Cellular (A) and exosomal (B) RNA was extracted from various breast cell lines and subjected to miR-105 RT-qPCR. Data were normalized to levels of U6 (cellular; A) or miR-16 (exosomal; B) and compared with the nontumor line MCF-10A. MBC lines originally isolated from pleural effusion (PE) are indicated by red columns.

(C) RNA was extracted from HMVECs incubated with exosomes of different origins for indicated time and analyzed for miR-105 level using U6 as internal control. At each time point, data were compared with PBS-treated cells.

(D) RNA extracted from HMVECs incubated with exosomes of different origins for 24 hr (or PBS as control) was analyzed for the level of pri-miR-105 or pre-miR-105.

(E) MDA-MB-231-secreted exosomes were fed to HMVECs in the presence or absence of 5,6-dichloro-1-β-D-ribofuranosylbenzimidazole (20 μM). After 24 hr, RNA extracted from the recipient cells was analyzed for miR-105 level.

*$p < 0.005$ compared with PBS treatment. Results are presented as mean ± SD (see also Figure S1 and Table S1). P.Br, primary breast.

by transfecting the recipient cells with miR-105 inhibitor (Figures 3B and 3C). It was unlikely to require additional exosomal components that are unique to MDA-MB-231, as exosomes secreted by MCF-10A cells stably overexpressing and secreting miR-105 (Figure S2B) and by other high-miR-105 BC cells but not by low-miR-105 BC cells (Figures 2A and 2B) also downregulated ZO-1 expression in recipient HMVECs (Figure 3C; Figure S2C). When HMVEC monolayers were analyzed by immunofluorescence, those treated with high-miR-105 exosomes (secreted by MCF-10A/miR-105 and MDA-MB-231) exhibited marked reduction of ZO-1 and internalization of another TJ protein occludin from cell junctions, whereas the junctional level of vascular endothelial cadherin (VE-cadherin) was not significantly affected (Figure 3D).

We next performed an in vitro permeability assay by measuring the traversing of rhodamine-labeled dextran (relative molecular mass 70,000) probes through HMVEC monolayers growing on 0.4-μm filters. Similar to the effect induced by vascular endothelial growth factor (VEGF), treatment of the endothelial barrier with MDA-MB-231 exosomes also induced passage of the fluorescent probes from the top to the bottom wells in a manner that was dependent on functional miR-105 and downregulation of ZO-1 (Figure 3E). When the transendothelial electrical resistance was measured in HMVEC monolayers, treatment with MDA-MB-231 exosomes significantly reduced the unit area resistance compared with PBS or MCF-10A exosome treatment. Inhibition of miR-105 and restored

expression of ZO-1 in recipient HMVECs both abolished the effect of MBC-derived exosomes (Figure 3F). The effect of miR-105-containing exosomes on vascular destruction was further tested in a 3D vascular sprouting assay. In this system, endothelial cells formed vascular sprouts after 4 to 5 days in culture. At this time, purified exosomes from MCF-10A/vec (control) or MCF-10A/miR-105 cells were added into the culture media, and the effects on already established vascular structures were analyzed 5 days later. We observed a clear and significant destruction of vascular structures with the treatment of miR-105-containing exosomes (from MCF-10A/miR-105) compared with the control (Figure 3G). Consistent with these results, ectopic expression of miR-105 or treatment with MBC exosomes significantly induced migration in HMVECs through the miR-105/ZO-1-mediated mechanism (Figure 3H). Last, to directly simulate the barrier-traversing step in metastasis, transendothelial invasion of cancer cells was examined using HMVEC monolayers grown on 3-μm filters. The number of GFP-labeled MDA-231-HM cells that had invaded through HMVECs treated with MDA-MB-231 exosomes was significantly greater compared with those that had invaded through untreated or MCF-10A exosome-treated HMVECs, and both miR-105 inhibition and ZO-1 restoration in recipient cells interfered with this effect (Figure 3I).

Cancer-Secreted miR-105 Induces Vascular Permeability and Promotes Metastasis In Vivo

To further demonstrate the in vivo effect of exosomal miR-105 on endothelial barriers, we injected exosomes secreted by MCF-10A/vec (low-miR-105), MCF-10A/miR-105 (high-miR-105), or MDA-MB-231 cells (high-miR-105), or PBS as control, into the tail veins of NOD/SCID/IL2Rγ null (NSG) mice and examined the lung and brain, organs that frequently host BC metastases, after exosome treatment. The results indicated that exosomes with high-miR-105, but not those with low-miR-105, significantly increased miR-105 levels in lung and brain (Figure 4A), accompanied by reduced ZO-1 expression in endothelial cells positive for cluster of differentiation 31 (CD31) (Figure 4B) and enhanced vascular permeability (Figure 4C; Figure S3). In another experiment, mice were pretreated with exosomes secreted by MCF-10A or MDA-MB-231 cells (or PBS as control) before an intracardiac injection of luciferase-labeled MDA-MB-231 cells. Three weeks later, tissues were collected for reverse transcription quantitative PCR (RT-qPCR) of luciferase gene using mouse 18S as internal control to quantify metastases. Consistent with their effect on destroying the endothelial barriers, MDA-MB-231 but not MCF-10A exosomes significantly increased metastases in the lung and brain (Figure 4D).

miR-105 Overexpression in Poorly Metastatic BC Cells Promotes Metastasis In Vivo

To determine if the miR-105 level in primary tumors regulates endothelial barriers and metastasis, we stably overexpressed miR-105 in an MCF-10A-derived tumorigenic line, MCFDCIS, which forms lesions similar to comedo ductal carcinoma in situ that spontaneously progress to invasive tumors (Hu et al., 2008; Miller et al., 2000). Compared with vector-transduced control cells, the miR-105-overexpressing MCFDCIS cells also secreted a higher level of miR-105 (Figure S4A) and showed reduced ZO-1 protein expression and significantly enhanced migration in transwell and wound closure assays (Figures S4B–S4D). Restoration of ZO-1 using an overexpressing plasmid that lacks the 3′UTR abolished the promigratory effect of miR-105. We next established orthotopic xenografts using luciferase-labeled MCFDCIS cells with or without miR-105 overexpression. Although miR-105 did not seem to affect primary tumor growth (Figures S4E and S4F), distant metastases were significantly induced in the lung and brain in mice bearing miR-105-overexpressing tumors at week 6 (Figures 5A and 5B). Histological staining indicated that in contrast to the MCFDCIS/vec tumors, which showed moderate local invasiveness, MCFDCIS/miR-105 tumors displayed no clear margin and extensively infiltrated into the surrounding tissues (Figure 5C). In addition, the in vivo vascular permeability in the lung, liver, and brain of mice bearing miR-105-overexpressing tumors was dramatically increased compared with that in the control group (Figure 5D; Figure S4H), whereas relatively high vascular permeability was observed in the primary tumors of both groups (Figures S4G and S4H). In mice bearing miR-105-overexpressing tumors, miR-105 was detected not only in primary tumors but also in the metastasis-free areas of distant organs (Figure 5E). Reduced level of ZO-1 was observed in the $CD31^+$ vascular endothelial cells in the lung and brain of mice with high-miR-105 xenografts (Figure 5F). These results collectively suggest that tumor cells expressing and consequently secreting higher level of miR-105 acquire greater metastatic potential through the dual advantages of enhanced tumor cell invasion and weakened endothelial barriers in the host.

miR-105 Inhibition Suppresses Metastasis and Restores Vascular Integrity In Vivo

To further explore the potential therapeutic effect of miR-105 intervention, we established xenografts from high-miR-105, high-metastatic MDA-231-HM cells that were generated through explant culture of a spontaneous meningeal metastasis of MDA-MB-231. In vitro treatment of these cells with an anti-miR-105 compound increased ZO-1 expression and suppressed migration (Figures S5A and S5B), consistent with the effect of miR-105 observed in other experiments. In vivo treatment with the anti-miR-105 compound reduced the volume of primary tumors and suppressed distant metastases to the lung and brain compared with the groups receiving PBS or control compound (Figures 6A–6C). Tumors treated with anti-miR-105 had clear margins with significantly reduced tumor cell infiltration into the surrounding tissues (Figure 6D). Although Ki-67 staining did not show a significant difference among the tumor groups, anti-miR-105-treated tumors showed higher levels of ZO-1 and higher percentages of apoptotic cells, as indicated by cleaved caspase-3 (Figure 6E). The in vivo vascular permeability assay indicated a lack of rhodamine-dextran penetration into various tissues in tumor-free mice; conversely, leakage of the dye into these tissues in tumor-bearing animals occurred even at a premetastatic stage (Figure 6F; Figure S5C), which suggests an effect of tumor-secreted factors in destroying the vascular integrity of a distant organ during early premetastatic niche formation. Notably, treatment with anti-miR-105 efficiently blocked this effect, restoring the vascular integrity in tumor-bearing animals (Figure 6F; Figure S5C). Restored ZO-1 expression in $CD31^+$ vascular endothelial cells was observed in the lung and brain

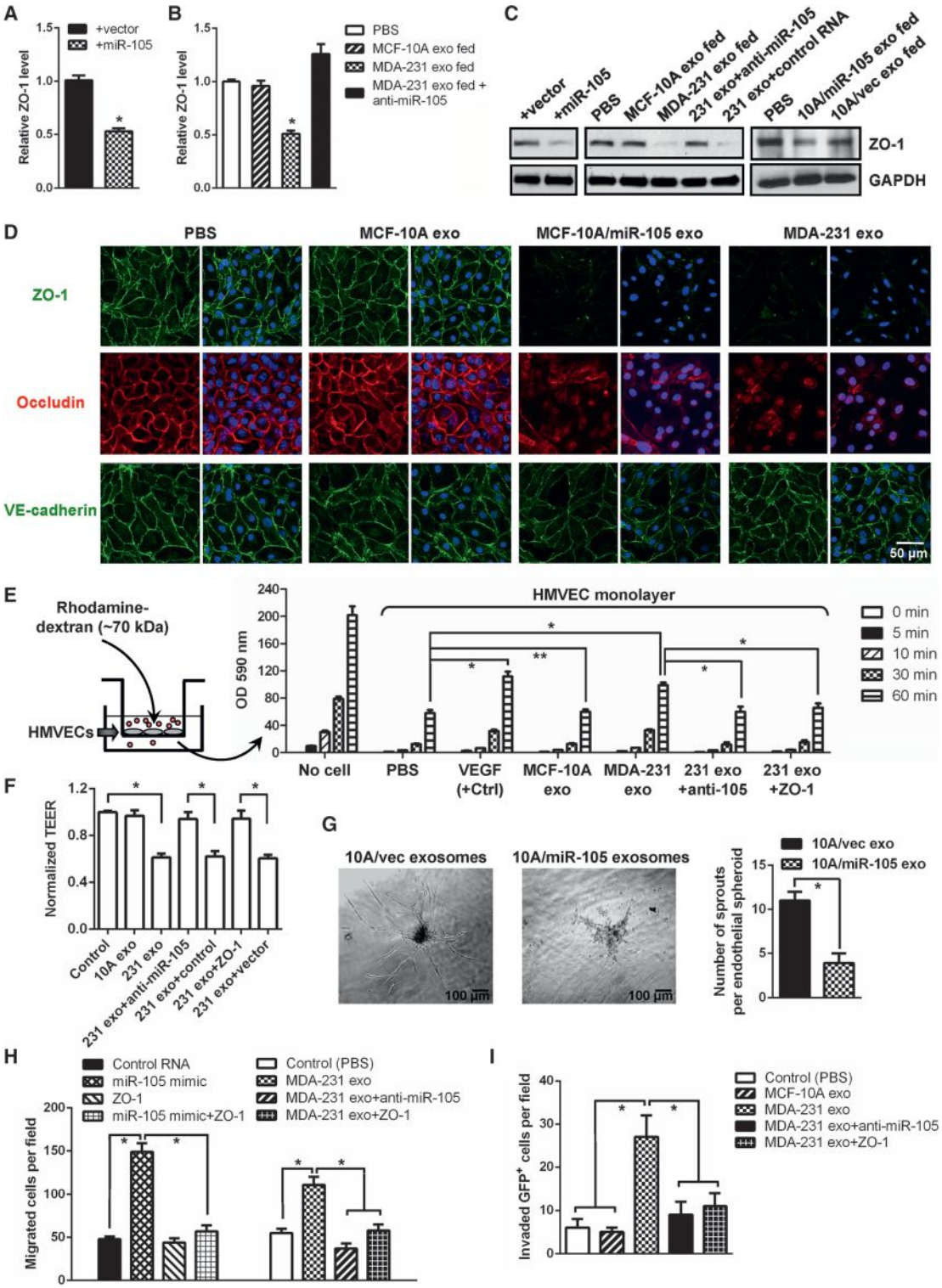

Figure 3. Cancer-Secreted miR-105 Downregulates TJs and Destroys the Barrier Function of Endothelial Monolayer

(A) HMVECs transduced with miR-105 or vector were analyzed for ZO-1 expression by RT-qPCR.

(B) HMVECs treated as indicated were analyzed for the RNA level of ZO-1.

(C) HMVECs treated as indicated were analyzed by Western blot.

(D) HMVEC monolayers were treated as indicated for 48 hr and analyzed by immunofluorescence (IF) for ZO-1 (green), occludin (red), and VE-cadherin (green). DAPI (blue): cell nuclei.

(legend continued on next page)

of tumor-bearing mice treated with anti-miR-105 compound (Figure 6G). Thus, anti-miR-105 treatment suppresses metastasis by reducing tumor invasiveness and restoring the barrier function of endothelial niche cells.

miR-105 Is Associated with ZO-1 Expression and Metastatic Progression in BC

Because miR-105 is uniquely expressed and secreted by MBC cells, it is possible that cancer-secreted miR-105 can be detected in the circulation of BC patients, such that miR-105 may serve as a prognostic marker for metastatic potential. To explore this, we first measured the serum miRNA levels in mice bearing MDA-231-HM xenograft tumors at either the premetastatic (week 3 after cancer cell implantation) or metastatic (week 6 after cancer cell implantation) stage in comparison with tumor-free animals. Circulating miR-105, but not two other miRNAs (miR-155 and miR-375), was significantly elevated in tumor-bearing animals at both premetastatic and metastatic stages (Figure 7A), suggesting that miR-105 derived from primary tumors with high miR-105 levels and high metastatic potential can be detected in the blood at an early stage before the clinical detection of metastasis. We next compared serum miRNA levels among 38 stage II and III BC patients. By comparing miRNA levels in circulating exosomes and the corresponding exosome-depleted serum fraction, we found that circulating miR-105 and miR-181a predominantly existed in exosomes, whereas two other miRNAs (miR-375 and miR-422b) were detected in both exosomes and exosome-depleted fraction at comparable levels (Figure S6). In circulating exosomes purified from sera, levels of miR-105, but not two other miRNAs (miR-181a and miR-375), were significantly higher in patients who later developed distant metastases during the 4.2 years of mean follow-up (n = 16) than those who did not (n = 22) (Figure 7B). To further determine if circulating miR-105 in BC patients is functionally active in regulating endothelial cells, we treated established 3D vascular structures with serum from a healthy donor or a BC patient with a high level of circulating miR-105. The patient serum but not normal serum resulted in a destruction of vascular structures, which was abolished by the anti-miR-105 compound (Figure 7C).

In patients with paired serum and tumor specimens, we further detected a strong positive correlation between circulating (exosomal) and tumor miR-105 levels ($r = 0.85$, $p < 0.01$). In contrast, significant inverse correlations were detected between tumor miR-105 and ZO-1 ($r = -0.48$, $p = 0.03$) and between circulating (exosomal) miR-105 and tumor-adjacent vascular ZO-1 expression ($r = -0.49$, $p = 0.04$) (Figures 7D and 7F). These observations are consistent with the role of miR-105 in downregulating ZO-1. In addition, higher levels of tumor miR-105 and lower levels of tumor and vascular ZO-1 were observed in patients who later developed distant metastases compared with those who did not and compared with normal mammary tissues (Figures 7E and 7F), thus supporting the functional association of these genes with cancer metastasis. In a BC tissue array, significantly higher miR-105 and lower ZO-1 levels were detected in the primary tumors with distant or lymph node metastases (n = 15) compared with those without (n = 60), and the inverse correlation between miR-105 and ZO-1 remained significant among all cases ($r = -0.24$, $p = 0.04$) (Figure 7G). Overall, our clinical data suggest that cancer-derived miR-105 can serve as a blood-based marker for the prediction or early diagnosis of BC metastasis and may play a role in promoting cancer progression by targeting ZO-1.

DISCUSSION

Exchange of cellular materials between cells through various paracrine and endocrine mechanisms is an important means of intercellular communication and can be mediated by exosomes. The tumor-derived adaptation of endothelial cells by miR-105 occurs during early premetastatic niche formation. Enhanced vascular permeability could then enhance cancer cell dissemination and growth at distant sites through multiple means, including (1) plasma protein leakage that results in enhanced entrapment and hence concentration of tumor cells; (2) enhanced dissemination of tumor cells to distant sites, resulting in autocrine signaling that overwhelms any inhibitory signaling at the distant site; and (3) additional exosome cargos and/or plasma proteins that leak into secondary organs and alter cellular physiology toward a prometastatic/tumor-supportive phenotype. In fact, vascular destabilization at the premetastatic lung niche has been previously described and involves a synergistic effect among angiopoietin 2, matrix metalloproteinase (MMP) 3, and MMP10 (Huang et al., 2009). Thus, therapies targeting miR-105 and these protein factors, in combination with existing conventional therapies, may serve as an effective treatment for cancer patients with high risk for metastasis (e.g., indicated by high levels of circulating miR-105). Understanding mechanisms leading to miR-105 overexpression in MBC, which is an ongoing direction in our laboratory, may reveal additional strategies for miR-105 intervention.

(E) The permeability of treated HMVEC monolayers grown on 0.4 μm filters was measured by the appearance of rhodamine-dextran, which was added to the top well at the beginning of the experiment, in the bottom well during a 1 hr time course. The absorbance at 590 nm at each time point was indicated. Treatment of the HMVEC monolayer with VEGF (50 ng/ml) for 8 hr was included as a positive control to show cytokine-induced permeability. The absorbance at the 1 hr time point was compared with the PBS (control) condition. *$p < 0.005$. **$p > 0.05$.

(F) HMVEC monolayers grown on filters and treated as indicated were analyzed for transendothelial electrical resistance. Calculated unit area resistance from triplicate wells was normalized to the control (PBS) treatment.

(G) Treatment with miR-105-containing exosomes resulted in a vascular destruction. Vascular sprouting assay was established for 5 days, at which time 1 μg of purified exosomes from MCF-10A/vec (control) or MCF-10A/miR-105 cells were added into the culture media. Vascular structures were imaged 5 days after the treatment, and representative images are shown (left). Vascular sprouts per spheroid were counted and graphed (right). At least 50 spheroids were counted in each experiment, and the experiment was repeated three times. *$p < 0.05$.

(H) HMVECs treated as indicated were subjected to transwell migration. Cells that had migrated within 8 hr were quantified from triplicate wells. *$p < 0.005$.

(I) HMVEC monolayers grown on 3 μm filters were treated as indicated before GFP-labeled MDA-231-HM cells were seeded in the transwell inserts. After 10 hr, the GFP^+ cells on the bottom side of filters were quantified under a fluorescent microscope. *$p < 0.005$.

Results are presented as mean ± SD (see also Figure S2). GAPDH, glyceraldehyde 3-phosphate dehydrogenase.

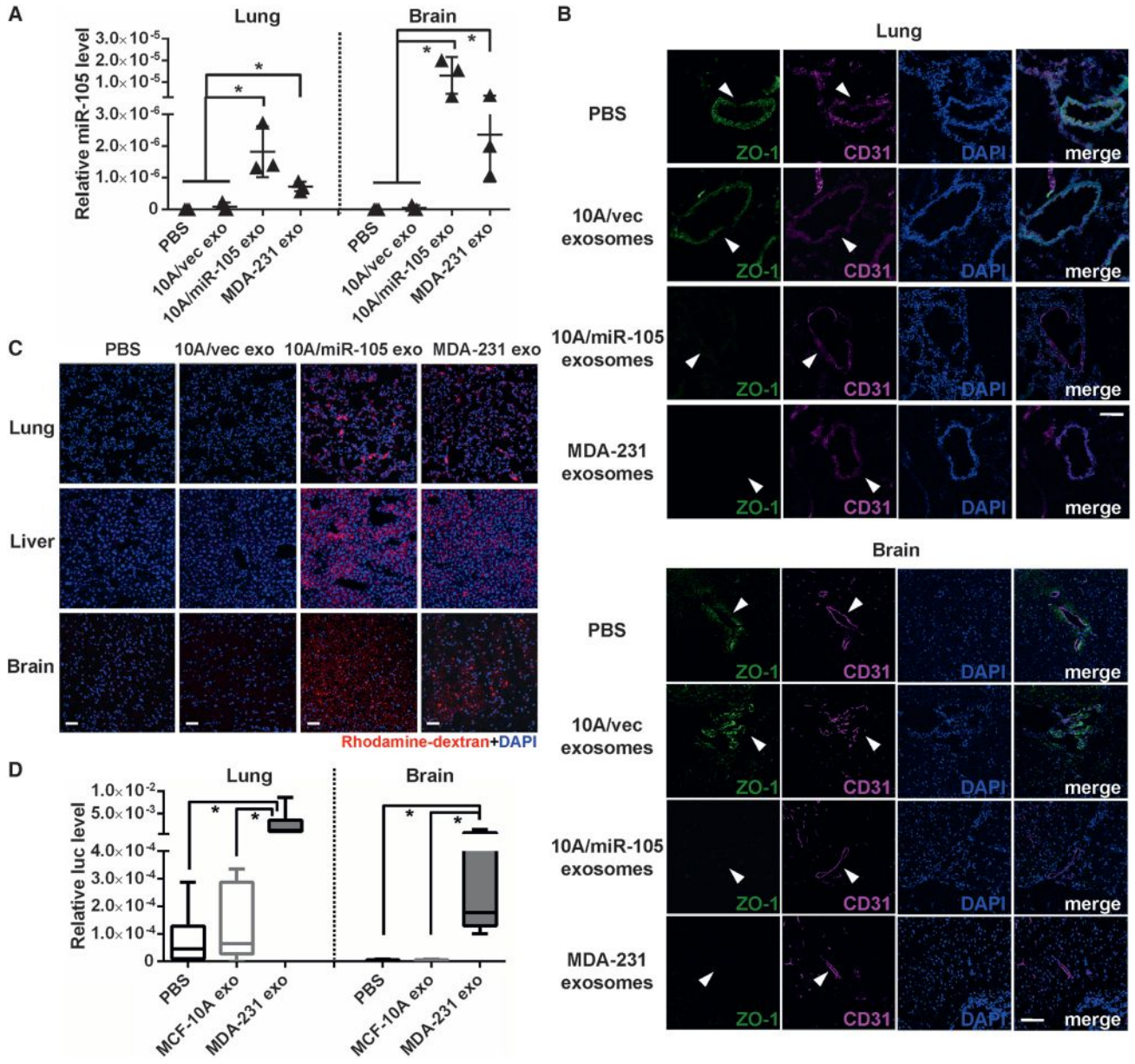

Figure 4. Cancer-Secreted miR-105 Induces Vascular Permeability and Promotes Metastasis In Vivo

(A) Exosomes secreted by MCF-10A/vec, MCF-10A/miR-105, or MDA-MB-231 cells, or PBS (as control), were intravenously injected into the tail veins of NSG mice (n = 3) twice a week. After five injections, tissues were collected for RT-qPCR of miR-105 using U6 as internal control. *$p < 0.05$.

(B) Collected lung and brain tissues were subjected to double-label IF for ZO-1 (green) and CD31 (pink). Structures positive for CD31 are indicated by arrowheads. The scale bar represents 100 μm.

(C) In vivo vascular permeability determined by the appearance of intravenously injected rhodamine-dextran (red) (n = 3). Representative images are shown. DAPI (blue): cell nuclei. The scale bar represents 100 μm.

(D) Exosomes secreted by MCF-10A or MDA-MB-231 cells, or PBS (as control), were intravenously injected into the tail veins of NSG mice (n = 6) twice a week. After five injections, all mice received intracardiac injection of luciferase-labeled MDA-MB-231 cells. Three weeks later, tissues were collected for RT-qPCR of luciferase gene using mouse 18S as internal control to quantify metastases. *$p < 0.05$.

Results are presented as mean ± SD (see also Figure S3).

Downregulation or loss of TJs, frequently as a result of reduced expression of TJ-associated proteins, contributes to cancer progression by altering cell migration, proliferation, polarity, and differentiation (Brennan et al., 2010; Georgiadis et al., 2010; Itoh and Bissell, 2003; Martin and Jiang, 2009). Reduction of TJ-associated ZO-1 in primary breast tumors due to decreased expression or cytoplasmic localization is associated with metastasis in BC patients (Martin et al., 2004; Polette et al., 2005). Our study identifies miR-105 as a key regulator of ZO-1, suggesting one mechanism of TJ disruption associated

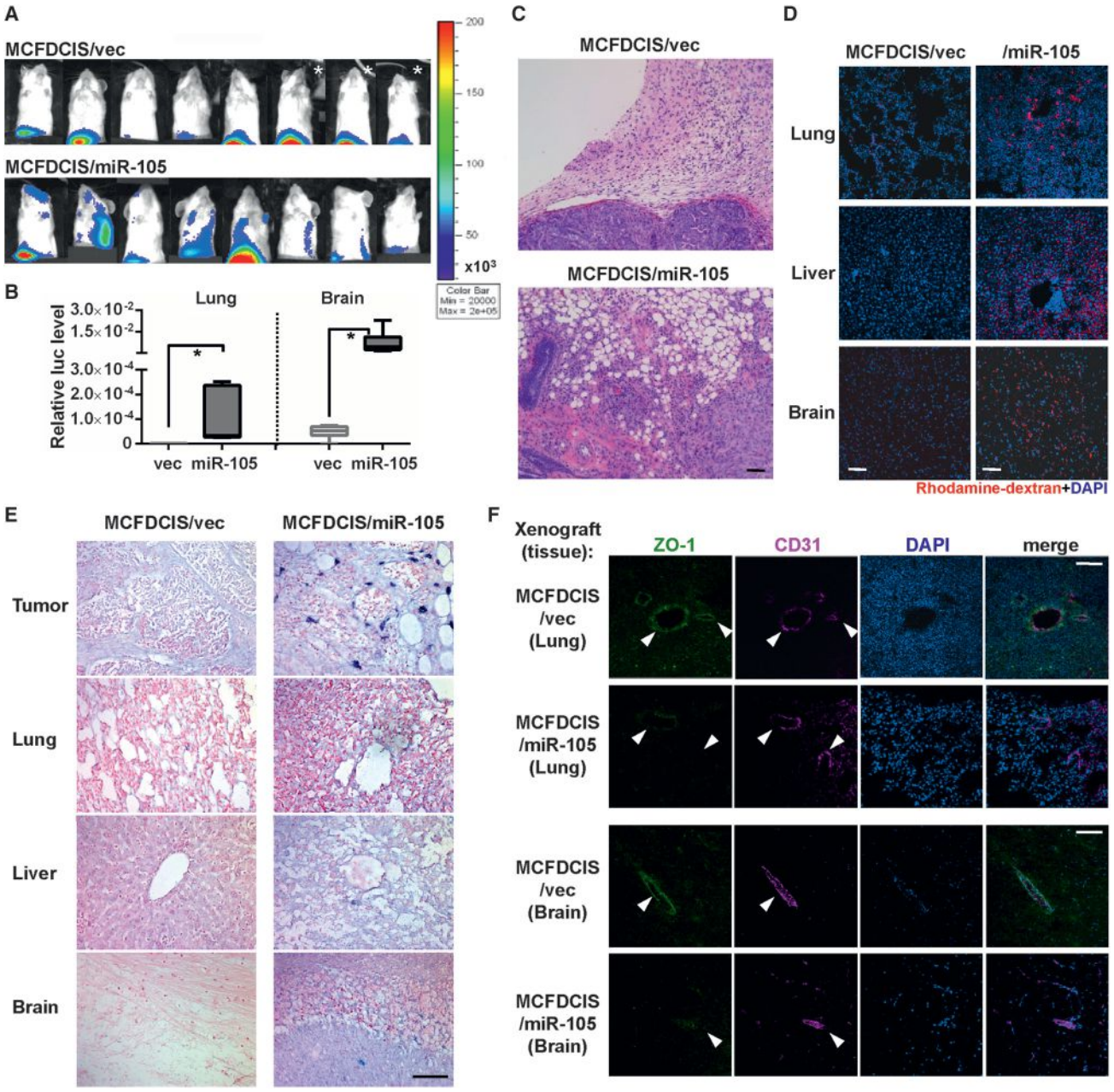

Figure 5. miR-105 Overexpression in Poorly Metastatic BC Cells Promotes Metastasis In Vivo

(A) Luciferase-labeled MCFDCIS/vec or MCFDCIS/miR-105 cells were injected into the number 4 mammary fat pads of NSG mice (n = 8). Bioluminescent imaging (BLI) at week 6 is shown. *Because of the extensive tumor burden, these three mice were sacrificed at week 5.5; their images at week 5 are shown.

(B) Quantification of metastases in the lung and brain. Mice shown in (A) were sacrificed at week 6, and tissues were subjected to RT-qPCR of luciferase gene using mouse 18S as internal control (n = 8). Results are presented as mean ± SD. *$p < 0.05$.

(C) Representative hematoxylin and eosin (H&E) stained images of the tumor edges showing local invasiveness. The scale bar represents 50 μm.

(D) In vivo vascular permeability determined by the appearance of intravenously injected rhodamine-dextran (red) in various organs. Tissues were collected from mice bearing MCFDCIS/vec or MCFDCIS/miR-105 xenografts (n = 3) that were sacrificed at week 6. Representative images are shown. DAPI (blue): cell nuclei. The scale bar represents 100 μm.

(E) Representative images of miR-105 in situ hybridization (ISH) in tissues collected from the two groups. The scale bar represents 50 μm.

(F) Collected tissues were subjected to double-label IF for ZO-1 (green) and CD31 (pink). Structures positive for CD31 are indicated by arrowheads. The scale bar represents 100 μm.

See also Figure S4.

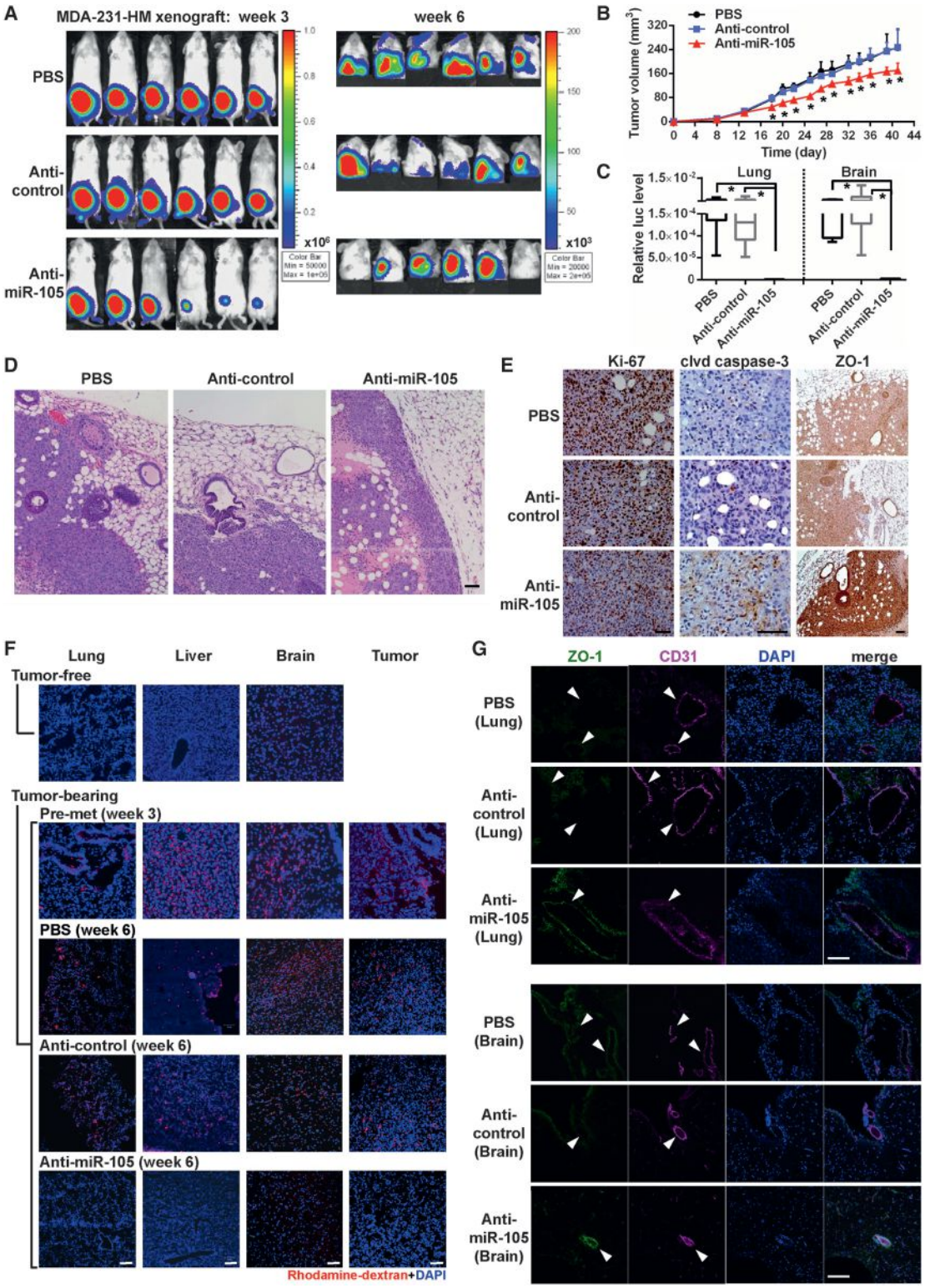

Figure 6. miR-105 Inhibition Suppresses Metastasis and Restores Vascular Integrity In Vivo

(A) Luciferase-labeled MDA-231-HM cells were injected into the number 4 mammary fat pads of NSG mice. Mice were divided into three groups (n = 6) for treatment with PBS, anti-miR-105 compound, or control compound. BLI at week 3 and week 6 is shown.

(B) Tumor volume determined in the three groups. *$p < 0.005$ compared with the other two groups.

(C) Quantification of metastases in the lung and brain. Mice shown in (A) were sacrificed at week 6 and tissues were subjected to RT-qPCR of luciferase gene using mouse 18S as internal control (n = 6). *$p < 0.01$.

(legend continued on next page)

with cancer progression and metastasis. The Rho family of small guanosine triphosphatases (GTPases) has been implicated in the regulation and function of TJs (Connolly et al., 2002; González-Mariscal et al., 2008; Jou et al., 1998; Shen et al., 2006). The Rho-associated protein kinase, a downstream effector of RhoA, regulates actomyosin contractility, TJ assembly, and endothelial capillary formation through phosphorylation of the regulatory myosin light chain (MLC2). Relevant to our study, junctional proteins including ZO-1 have been reported to regulate Rho GTPases through interacting with guanine nucleotide exchange factors and GTPase activating proteins (Citi et al., 2011). In our study, overexpression of miR-105 or treatment with exosomes carrying miR-105 did not alter the activity of RhoA, Rac1/2/3, or Cdc42, or the phosphorylation of MLC2, in recipient HMVECs (data not shown), suggesting that the small GTPases are not downstream effectors of the herein identified miR-105/ZO-1 pathway. In endothelial cells that normally express low miR-105 levels (data not shown), ectopic, cancer-derived miR-105 transferred via exosomes can effectively reduce ZO-1 expression and disrupt the barrier function of these cells both in vitro and in vivo. Although miR-105 secreted by the primary tumor may only affect a fraction of endothelial niche cells, this would be sufficient to open "gates" in these natural monolayer barriers for traversal of cancer cells, thereby facilitating metastasis. In addition, contact-dependent intercellular miRNA transfer between two adjacent cells through the transmembrane channel protein SIDT1 has recently been reported (Elhassan et al., 2012). Through this pathway, cancer-derived miRNAs (e.g., miR-105) that are transferred to a distant organ via circulating exosomes may further extend their regulatory effect to those interconnected niche cells without direct exosome uptake. In patients with familial hypercholesterolemia but not normal subjects, circulating miR-105 can be detected on high-density lipoprotein, which delivers the miRNA to recipient cells as an exosome-independent mechanism (Vickers et al., 2011). It would be interesting to determine the noncancer source of circulating miR-105 and its role in regulating vascular permeability through the herein demonstrated pathway in these patients.

It is likely that additional target genes and pathways regulated by miR-105 also contribute to its prometastatic effect. Although overexpression of miR-105 in MCFDCIS xenografts did not significantly affect primary tumor growth, anti-miR-105 treatment in animals bearing MDA-231-HM xenografts reduced tumor volume and induced apoptosis of tumor cells. This may suggest a cancer- or/and niche-specific effect of miR-105 that facilitates cancer cell survival and, therefore, promotes metastasis. Interestingly, miR-105 has been reported as a tumor suppressor that inhibits proliferation through downregulating cyclin-dependent kinase 6 in prostate cancer cells (Honeywell et al., 2013). This miRNA may also have an anti-inflammatory effect in gingival keratinocytes through targeting Toll-like receptor 2 (Benakanakere et al., 2009). In several cancer cell lines of non-breast origin, mature miR-105 is undetectable, possibly because of the nuclear retention of miR-105 precursors (Lee et al., 2008). These suggest important tissue-specific mechanisms controlling the biogenesis and function of miR-105. Understanding these mechanisms and their relevance to cancer progression and metastasis will provide further rationales for targeting miR-105 as a treatment for MBC.

miRNA transfer between cancer cells and the genetically normal niche cells is apparently bidirectional. In addition to the cancer-derived adaptation of niche cells, normal epithelial cells also secrete and transfer antiproliferative miRNAs (e.g., miR-143) to cancer cells, as a potential strategy to maintain tissue homeostasis at an early stage in cancer formation (Kosaka et al., 2012). In contrast, exosomes secreted by stromal fibroblasts promote BC cell protrusion and motility through Wnt-planar cell polarity signaling (Luga et al., 2012). Because exosomes are secreted by multiple types of normal cells and mediate their natural functions such as antigen presentation (Théry et al., 2002), targeting exosome secretion as a potential means of blocking this mode of cancer-host crosstalk requires the identification of cancer-specific molecules or pathways that control exosome production. The recently reported high expression of Rab27A in cancer and the effect of Rab27A interference by reducing exosome production in multiple melanoma cell lines may provide an approach to specifically inhibit cancer-derived exosomes (Peinado et al., 2012). In addition, as the exosomal secretion of miRNAs exhibits a highly selective pattern that differs between cancer and normal cells (Table S1) (Pigati et al., 2010), understanding the cellular selection mechanism for miRNA secretion, which may involve RNA-binding proteins, recognizing the primary or secondary structures of miRNA and its dysregulation in cancer may reveal unique strategies to block cancer-specific miRNA secretion. Last, characterization of cancer-secreted messengers and effectors, such as miR-105, will enable the selection of patients for the corresponding targeted therapy and eventually combination therapy simultaneously targeting multiple secretory miRNAs and/or proteins. Such patient selection may be achieved by a quantitative blood test for circulating miR-105, which correlates with metastasis in early-stage BC patients. In developing personalized diagnostics and therapeutics, a combination of miR-105 with other miRNA and/or protein markers in the blood that would better specify the disease traits at the individual level will likely enhance our ability to select BC patients with high risk for metastasis for preventive treatment that targets miR-105 and other effectors.

(D) Representative H&E images of the tumor edges showing local invasiveness. The scale bar represents 50 μm.
(E) Immunohistochemistry (IHC) was performed in xenograft tumors using antibodies of Ki-67, cleaved (clvd) caspase-3, and ZO-1. Representative images are shown. The scale bar represents 50 μm.
(F) In vivo vascular permeability indicated by the penetration of rhodamine-dextran (red) into various organs. Tissues were collected from tumor-free NSG mice as well as mice bearing MDA-231-HM tumors that were untreated when sacrificed at week 3 after tumor cell implantation (the premetastatic [pre-met] group) or treated as indicated and sacrificed at week 6 (n = 4). Representative images are shown. DAPI (blue): cell nuclei. The scale bar represents 100 μm.
(G) Tissues were subjected to double-label IF for ZO-1 (green) and CD31 (pink). Structures positive for CD31 are indicated by arrowheads. The scale bar represents 100 μm.
Results are presented as mean ± SD (see also Figure S5).

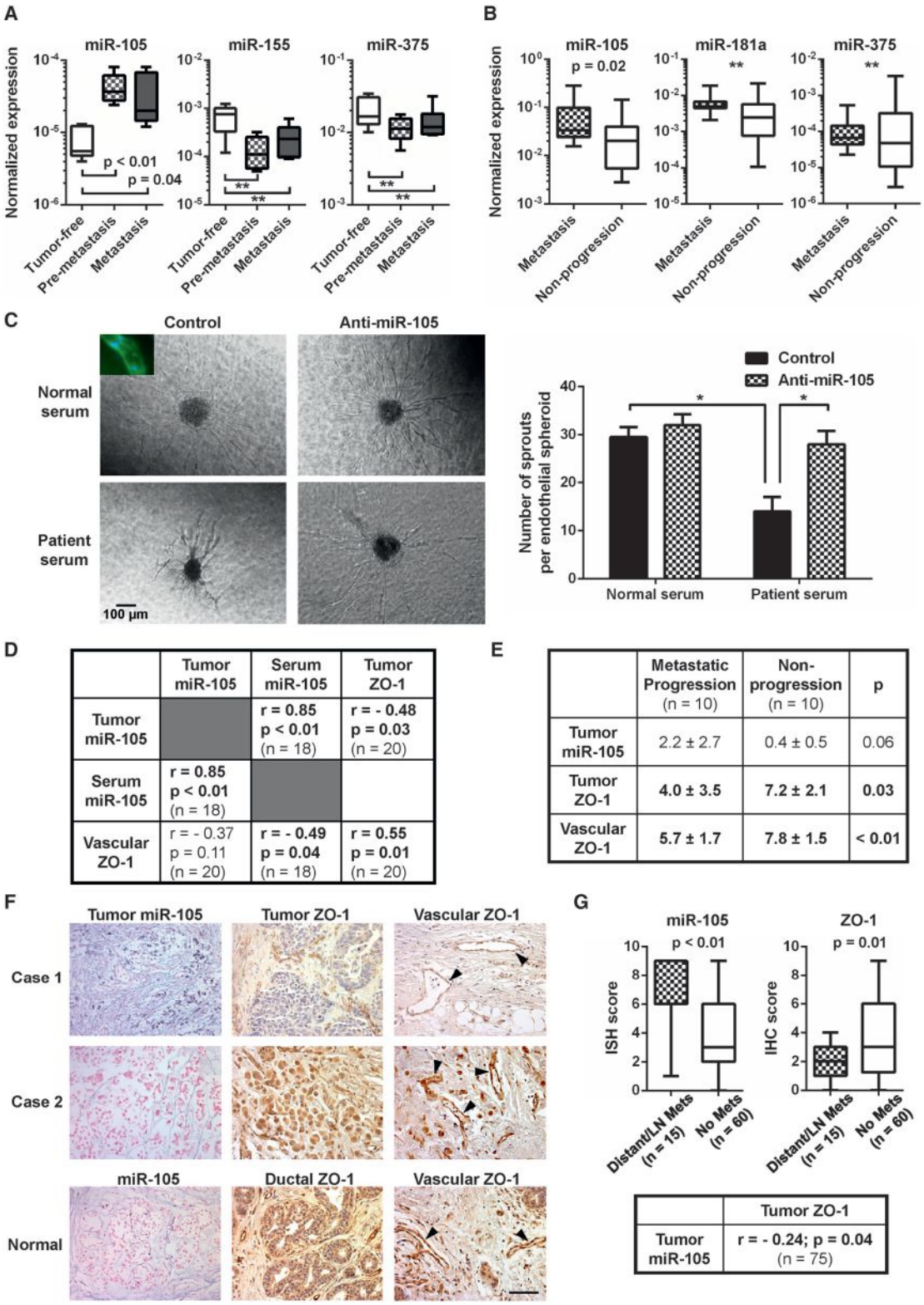

	Tumor miR-105	Serum miR-105	Tumor ZO-1
Tumor miR-105		r = 0.85 p < 0.01 (n = 18)	r = - 0.48 p = 0.03 (n = 20)
Serum miR-105	r = 0.85 p < 0.01 (n = 18)		
Vascular ZO-1	r = - 0.37 p = 0.11 (n = 20)	r = - 0.49 p = 0.04 (n = 18)	r = 0.55 p = 0.01 (n = 20)

	Metastatic Progression (n = 10)	Non-progression (n = 10)	p
Tumor miR-105	2.2 ± 2.7	0.4 ± 0.5	0.06
Tumor ZO-1	4.0 ± 3.5	7.2 ± 2.1	0.03
Vascular ZO-1	5.7 ± 1.7	7.8 ± 1.5	< 0.01

	Tumor ZO-1
Tumor miR-105	r = - 0.24; p = 0.04 (n = 75)

Figure 7. miR-105 Is Associated with ZO-1 Expression and Metastatic Progression in BC

(A) miRNA levels in the sera of tumor-free or MDA-231-HM tumor-bearing mice (premetastasis: serum collected at week 3; metastasis: serum collected at week 6; n = 5 or 6) were measured by RT-qPCR and normalized to miR-16. **p > 0.05.

(B) Circulating exosomes were isolated from serum samples of stage II and III BC patients. miRNAs were measured by RT-qPCR, normalized to miR-16, and compared among patients who developed distant metastases (mets) during follow-up (n = 16) and those who did not (n = 22). **p > 0.05.

(legend continued on next page)

EXPERIMENTAL PROCEDURES

Clinical Specimens

Human specimens were obtained from voluntarily consenting patients at the City of Hope Medical Center (Duarte, CA) under institutional review board-approved protocols. The clinical information is summarized in Tables S2–S5. Details can be found in Supplemental Experimental Procedures.

Cells, Plasmids, and Viruses

Please see Supplemental Experimental Procedures.

Exosome Purification and Electron Microscopy

Detailed protocols for preparing exosomes by ultracentrifugation can be found in Supplemental Experimental Procedures. For electron microscopy (EM), exosomes were fixed with 2% paraformaldehyde, loaded on 200-mesh Formvar-coated grids, and then contrasted and embedded as previously described (Thery et al., 2006). Solexa deep sequencing of exosomal and cellular RNA and genome-wide interrogation were performed as described (Wu et al., 2012); data sets were submitted to Gene Expression Omnibus (GEO) (GSE50429).

RNA Extraction, RT-qPCR, Western Blot Analysis, and Immunofluorescence

These procedures were performed as described previously (Tsuyada et al., 2012; Wang et al., 2011; Yu et al., 2010). See Supplemental Experimental Procedures for details.

Transendothelial Electrical Resistance, Endothelial Permeability, and 3D Vascular Sprouting Assays

Detailed protocols can be found in Supplemental Experimental Procedures. Vascular sprouting assay was performed as described using microcarrier beads coated with endothelial cells and embedded in 3D fibrin gel (Newman et al., 2011).

Wound Closure, Transwell Migration, and Transendothelial Invasion Assays

Wound closure and transwell migration assays were performed as previously described (Wang et al., 2006). Detailed protocols for transendothelial invasion assay can be found in Supplemental Experimental Procedures.

Animals

All animal experiments were approved by the institutional animal care and use committee at City of Hope. Detailed procedures can be found in Supplemental Experimental Procedures. The control and miR-105 targeted compounds used in the miR-105 intervention study had the same chemical modification pattern, chimeric 2′-fluoro and 2′-methoxyethyl modifications on a phosphorothioate backbone (Davis et al., 2006), and were synthesized at Regulus Therapeutics. The same compounds were also used in vitro to transfect MDA-231-HM cells (Figures S5A and S5B).

In Situ Hybridization and Immunohistochemistry

Please see Supplemental Experimental Procedures.

Statistical Analyses

All results were confirmed in at least three independent experiments, and data from one representative experiment were shown. All quantitative data are presented as mean ± SD. The statistical analysis was performed using SAS 9.2 software (SAS Institute). Student's t tests were used for comparisons of means of quantitative data between groups. The correlations between serum and tumor miR-105 and between miR-105 and ZO-1 expression were evaluated using Pearson's correlation coefficient (r). Values of $p < 0.05$ were considered significant.

ACCESSION NUMBERS

The GEO accession number for the exosomal and cellular RNA sequencing data reported in this paper is GSE50429.

SUPPLEMENTAL INFORMATION

Supplemental Information includes Supplemental Experimental Procedures, six figures, and five tables and can be found with this article online at http://dx.doi.org/10.1016/j.ccr.2014.03.007.

ACKNOWLEDGMENTS

This work was supported by the City of Hope Women's Cancer Program, National Institutes of Health (NIH)/National Cancer Institute (NCI) grants R01CA166020 (to S.E.W.) and R01CA163586 (to S.E.W.), California Breast Cancer Research Program grant 17IB-0054 (to S.E.W.), Breast Cancer Research Foundation-American Association for Cancer Research grant 12-60-26-WANG (to S.E.W.), and National Key Basic Research Development Program (973 Program) of China No. 2012CB9333004 (to X.R.). Research reported in this publication included work performed at core facilities supported by the NIH/NCI under grant P30CA33572. We thank the Center for Cancer Research, NCI, for funding support to P.C.L. We acknowledge Dr. Alan Fanning for kindly providing the ZO-1 plasmid. We also thank Drs. John Rossi, Hua Yu, John Shively, Linda Malkas, Andrew Raubitschek, Ren-Jang Lin, Michael Barish, Susan Kane, Shiuan Chen, and Joanne Mortimer for valuable comments as well as the City of Hope Core Facilities for highly professional services. G.S. had grant support from Celgene. E.G.M. was a full-time employee of a company developing miRNA therapeutics, Regulus Therapeutics.

Received: March 7, 2013
Revised: August 23, 2013
Accepted: March 7, 2014
Published: April 14, 2014

REFERENCES

Arroyo, J.D., Chevillet, J.R., Kroh, E.M., Ruf, I.K., Pritchard, C.C., Gibson, D.F., Mitchell, P.S., Bennett, C.F., Pogosova-Agadjanyan, E.L., Stirewalt, D.L., et al. (2011). Argonaute2 complexes carry a population of circulating microRNAs

(C) Circulating miR-105 in patient serum resulted in a vascular destruction. Vascular structures established from HMVECs that were transfected with anti-miR-105 compound or control compound were treated with human serum from a healthy donor or a BC patient with a high level of circulating miR-105. Representative images of the treated vascular structures are shown (left). Inset: Structures were stained with CD31 antibody (green) and DAPI (blue). Vascular sprouts per spheroid were counted and graphed (right). At least 50 spheroids were counted in each experiment, and the experiment was repeated three times. *$p < 0.05$.
(D) Correlation analyses of tumor miR-105, serum (exosomal) miR-105, and ZO-1 levels in BC patients. miR-105 levels in tumor cells and ZO-1 levels in tumor cells (tumor ZO-1) or tumor-adjacent vascular structures (vascular ZO-1) were determined by ISH and IHC, respectively, and scored as described in Experimental Procedures. Serum (exosomal) miR-105 levels were determined by PCR using miR-16 as a normalizer. Correlation analyses were carried out between two sets of quantified data as indicated. Pearson's correlation coefficient (r) and p value are shown.
(E) The scores of tumor miR-105, tumor ZO-1, and vascular ZO-1 staining were compared between stage II and III BC patients who developed distant metastases (n = 10) and those who did not (n = 10). Mean and SD of the staining scores in each group are shown.
(F) Representative images of miR-105 and ZO-1 staining in tumor and normal breast tissue sections. Vascular structures are indicated by arrowheads. The scale bar represents 100 μm.
(G) Levels of tumor miR-105 and ZO-1 determined in a BC tissue array. The ISH or IHC scores were compared between primary tumors with distant or lymph node (LN) metastases (n = 15) and those without (n = 60). The correlation between miR-105 and ZO-1 was analyzed among all cases (n = 75).
Results are presented as mean ± SD (see also Figure S6 and Tables S2–S5).

independent of vesicles in human plasma. Proc. Natl. Acad. Sci. USA *108*, 5003–5008.

Benakanakere, M.R., Li, Q., Eskan, M.A., Singh, A.V., Zhao, J., Galicia, J.C., Stathopoulou, P., Knudsen, T.B., and Kinane, D.F. (2009). Modulation of TLR2 protein expression by miR-105 in human oral keratinocytes. J. Biol. Chem. *284*, 23107–23115.

Brennan, K., Offiah, G., McSherry, E.A., and Hopkins, A.M. (2010). Tight junctions: a barrier to the initiation and progression of breast cancer? J. Biomed. Biotechnol. *2010*, 460607.

Calin, G.A., and Croce, C.M. (2006). MicroRNA signatures in human cancers. Nat. Rev. Cancer *6*, 857–866.

Chambers, A.F., Groom, A.C., and MacDonald, I.C. (2002). Dissemination and growth of cancer cells in metastatic sites. Nat. Rev. Cancer *2*, 563–572.

Citi, S., Spadaro, D., Schneider, Y., Stutz, J., and Pulimeno, P. (2011). Regulation of small GTPases at epithelial cell-cell junctions. Mol. Membr. Biol. *28*, 427–444.

Connolly, J.O., Simpson, N., Hewlett, L., and Hall, A. (2002). Rac regulates endothelial morphogenesis and capillary assembly. Mol. Biol. Cell *13*, 2474–2485.

Davis, S., Lollo, B., Freier, S., and Esau, C. (2006). Improved targeting of miRNA with antisense oligonucleotides. Nucleic Acids Res. *34*, 2294–2304.

Elhassan, M.O., Christie, J., and Duxbury, M.S. (2012). Homo sapiens systemic RNA interference-defective-1 transmembrane family member 1 (SIDT1) protein mediates contact-dependent small RNA transfer and microRNA-21-driven chemoresistance. J. Biol. Chem. *287*, 5267–5277.

Fabbri, M., Paone, A., Calore, F., Galli, R., Gaudio, E., Santhanam, R., Lovat, F., Fadda, P., Mao, C., Nuovo, G.J., et al. (2012). MicroRNAs bind to Toll-like receptors to induce prometastatic inflammatory response. Proc. Natl. Acad. Sci. USA *109*, E2110–E2116.

Georgiadis, A., Tschernutter, M., Bainbridge, J.W., Balaggan, K.S., Mowat, F., West, E.L., Munro, P.M., Thrasher, A.J., Matter, K., Balda, M.S., and Ali, R.R. (2010). The tight junction associated signalling proteins ZO-1 and ZONAB regulate retinal pigment epithelium homeostasis in mice. PLoS ONE *5*, e15730.

González-Mariscal, L., Tapia, R., and Chamorro, D. (2008). Crosstalk of tight junction components with signaling pathways. Biochim. Biophys. Acta *1778*, 729–756.

Heneghan, H.M., Miller, N., Lowery, A.J., Sweeney, K.J., Newell, J., and Kerin, M.J. (2010). Circulating microRNAs as novel minimally invasive biomarkers for breast cancer. Ann. Surg. *251*, 499–505.

Honeywell, D.R., Cabrita, M.A., Zhao, H., Dimitroulakos, J., and Addison, C.L. (2013). miR-105 inhibits prostate tumour growth by suppressing CDK6 levels. PLoS ONE *8*, e70515.

Hood, J.L., San, R.S., and Wickline, S.A. (2011). Exosomes released by melanoma cells prepare sentinel lymph nodes for tumor metastasis. Cancer Res. *71*, 3792–3801.

Hu, M., Yao, J., Carroll, D.K., Weremowicz, S., Chen, H., Carrasco, D., Richardson, A., Violette, S., Nikolskaya, T., Nikolsky, Y., et al. (2008). Regulation of in situ to invasive breast carcinoma transition. Cancer Cell *13*, 394–406.

Huang, Y., Song, N., Ding, Y., Yuan, S., Li, X., Cai, H., Shi, H., and Luo, Y. (2009). Pulmonary vascular destabilization in the premetastatic phase facilitates lung metastasis. Cancer Res. *69*, 7529–7537.

Iorio, M.V., Ferracin, M., Liu, C.G., Veronese, A., Spizzo, R., Sabbioni, S., Magri, E., Pedriali, M., Fabbri, M., Campiglio, M., et al. (2005). MicroRNA gene expression deregulation in human breast cancer. Cancer Res. *65*, 7065–7070.

Itoh, M., and Bissell, M.J. (2003). The organization of tight junctions in epithelia: implications for mammary gland biology and breast tumorigenesis. J. Mammary Gland Biol. Neoplasia *8*, 449–462.

Jou, T.S., Schneeberger, E.E., and Nelson, W.J. (1998). Structural and functional regulation of tight junctions by RhoA and Rac1 small GTPases. J. Cell Biol. *142*, 101–115.

Jung, E.J., Santarpia, L., Kim, J., Esteva, F.J., Moretti, E., Buzdar, A.U., Di Leo, A., Le, X.F., Bast, R.C., Jr., Park, S.T., et al. (2012). Plasma microRNA 210 levels correlate with sensitivity to trastuzumab and tumor presence in breast cancer patients. Cancer *118*, 2603–2614.

Kaplan, R.N., Riba, R.D., Zacharoulis, S., Bramley, A.H., Vincent, L., Costa, C., MacDonald, D.D., Jin, D.K., Shido, K., Kerns, S.A., et al. (2005). VEGFR1-positive haematopoietic bone marrow progenitors initiate the pre-metastatic niche. Nature *438*, 820–827.

Kosaka, N., Iguchi, H., Yoshioka, Y., Hagiwara, K., Takeshita, F., and Ochiya, T. (2012). Competitive interactions of cancer cells and normal cells via secretory microRNAs. J. Biol. Chem. *287*, 1397–1405.

Lee, E.J., Baek, M., Gusev, Y., Brackett, D.J., Nuovo, G.J., and Schmittgen, T.D. (2008). Systematic evaluation of microRNA processing patterns in tissues, cell lines, and tumors. RNA *14*, 35–42.

Luga, V., Zhang, L., Viloria-Petit, A.M., Ogunjimi, A.A., Inanlou, M.R., Chiu, E., Buchanan, M., Hosein, A.N., Basik, M., and Wrana, J.L. (2012). Exosomes mediate stromal mobilization of autocrine Wnt-PCP signaling in breast cancer cell migration. Cell *151*, 1542–1556.

Martin, T.A., and Jiang, W.G. (2009). Loss of tight junction barrier function and its role in cancer metastasis. Biochim. Biophys. Acta *1788*, 872–891.

Martin, T.A., Watkins, G., Mansel, R.E., and Jiang, W.G. (2004). Loss of tight junction plaque molecules in breast cancer tissues is associated with a poor prognosis in patients with breast cancer. Eur. J. Cancer *40*, 2717–2725.

Miller, F.R., Santner, S.J., Tait, L., and Dawson, P.J. (2000). MCF10DCIS.com xenograft model of human comedo ductal carcinoma in situ. J. Natl. Cancer Inst. *92*, 1185–1186.

Mitchell, P.S., Parkin, R.K., Kroh, E.M., Fritz, B.R., Wyman, S.K., Pogosova-Agadjanyan, E.L., Peterson, A., Noteboom, J., O'Briant, K.C., Allen, A., et al. (2008). Circulating microRNAs as stable blood-based markers for cancer detection. Proc. Natl. Acad. Sci. USA *105*, 10513–10518.

Newman, A.C., Nakatsu, M.N., Chou, W., Gershon, P.D., and Hughes, C.C. (2011). The requirement for fibroblasts in angiogenesis: fibroblast-derived matrix proteins are essential for endothelial cell lumen formation. Mol. Biol. Cell *22*, 3791–3800.

Nicolini, A., Giardino, R., Carpi, A., Ferrari, P., Anselmi, L., Colosimo, S., Conte, M., Fini, M., Giavaresi, G., Berti, P., and Miccoli, P. (2006). Metastatic breast cancer: an updating. Biomed. Pharmacother. *60*, 548–556.

Paget, S. (1889). The distribution of secondary growths in cancer of the breast. Lancet *133*, 571–573.

Peinado, H., Alečković, M., Lavotshkin, S., Matei, I., Costa-Silva, B., Moreno-Bueno, G., Hergueta-Redondo, M., Williams, C., García-Santos, G., Ghajar, C., et al. (2012). Melanoma exosomes educate bone marrow progenitor cells toward a pro-metastatic phenotype through MET. Nat. Med. *18*, 883–891.

Pigati, L., Yaddanapudi, S.C., Iyengar, R., Kim, D.J., Hearn, S.A., Danforth, D., Hastings, M.L., and Duelli, D.M. (2010). Selective release of microRNA species from normal and malignant mammary epithelial cells. PLoS ONE *5*, e13515.

Podsypanina, K., Du, Y.C., Jechlinger, M., Beverly, L.J., Hambardzumyan, D., and Varmus, H. (2008). Seeding and propagation of untransformed mouse mammary cells in the lung. Science *321*, 1841–1844.

Polette, M., Gilles, C., Nawrocki-Raby, B., Lohi, J., Hunziker, W., Foidart, J.M., and Birembaut, P. (2005). Membrane-type 1 matrix metalloproteinase expression is regulated by zonula occludens-1 in human breast cancer cells. Cancer Res. *65*, 7691–7698.

Psaila, B., and Lyden, D. (2009). The metastatic niche: adapting the foreign soil. Nat. Rev. Cancer *9*, 285–293.

Redis, R.S., Calin, S., Yang, Y., You, M.J., and Calin, G.A. (2012). Cell-to-cell miRNA transfer: from body homeostasis to therapy. Pharmacol. Ther. *136*, 169–174.

Roth, C., Rack, B., Müller, V., Janni, W., Pantel, K., and Schwarzenbach, H. (2010). Circulating microRNAs as blood-based markers for patients with primary and metastatic breast cancer. Breast Cancer Res. *12*, R90.

Rubens, R.D. (2001). 7. Management of advanced breast cancer. Int. J. Clin. Pract. *55*, 676–679.

Sethi, N., and Kang, Y. (2011). Unravelling the complexity of metastasis - molecular understanding and targeted therapies. Nat. Rev. Cancer *11*, 735–748.

Shen, L., Black, E.D., Witkowski, E.D., Lencer, W.I., Guerriero, V., Schneeberger, E.E., and Turner, J.R. (2006). Myosin light chain phosphorylation regulates barrier function by remodeling tight junction structure. J. Cell Sci. *119*, 2095–2106.

Skog, J., Würdinger, T., van Rijn, S., Meijer, D.H., Gainche, L., Sena-Esteves, M., Curry, W.T., Jr., Carter, B.S., Krichevsky, A.M., and Breakefield, X.O. (2008). Glioblastoma microvesicles transport RNA and proteins that promote tumour growth and provide diagnostic biomarkers. Nat. Cell Biol. *10*, 1470–1476.

Taylor, D.D., and Gercel-Taylor, C. (2008). MicroRNA signatures of tumor-derived exosomes as diagnostic biomarkers of ovarian cancer. Gynecol. Oncol. *110*, 13–21.

Théry, C., Zitvogel, L., and Amigorena, S. (2002). Exosomes: composition, biogenesis and function. Nat. Rev. Immunol. *2*, 569–579.

Thery, C., Amigorena, S., Raposo, G., and Clayton, A. (2006). Isolation and characterization of exosomes from cell culture supernatants and biological fluids. Curr. Protoc. Cell Biol., Chapter 3, Unit 3.22.

Tsuyada, A., Chow, A., Wu, J., Somlo, G., Chu, P., Loera, S., Luu, T., Li, A.X., Wu, X., Ye, W., et al. (2012). CCL2 mediates cross-talk between cancer cells and stromal fibroblasts that regulates breast cancer stem cells. Cancer Res. *72*, 2768–2779.

Turchinovich, A., Weiz, L., Langheinz, A., and Burwinkel, B. (2011). Characterization of extracellular circulating microRNA. Nucleic Acids Res. *39*, 7223–7233.

Valadi, H., Ekström, K., Bossios, A., Sjöstrand, M., Lee, J.J., and Lötvall, J.O. (2007). Exosome-mediated transfer of mRNAs and microRNAs is a novel mechanism of genetic exchange between cells. Nat. Cell Biol. *9*, 654–659.

Vickers, K.C., and Remaley, A.T. (2012). Lipid-based carriers of microRNAs and intercellular communication. Curr. Opin. Lipidol. *23*, 91–97.

Vickers, K.C., Palmisano, B.T., Shoucri, B.M., Shamburek, R.D., and Remaley, A.T. (2011). MicroRNAs are transported in plasma and delivered to recipient cells by high-density lipoproteins. Nat. Cell Biol. *13*, 423–433.

Wang, S.E., Narasanna, A., Perez-Torres, M., Xiang, B., Wu, F.Y., Yang, S., Carpenter, G., Gazdar, A.F., Muthuswamy, S.K., and Arteaga, C.L. (2006). HER2 kinase domain mutation results in constitutive phosphorylation and activation of HER2 and EGFR and resistance to EGFR tyrosine kinase inhibitors. Cancer Cell *10*, 25–38.

Wang, Y., Yu, Y., Tsuyada, A., Ren, X., Wu, X., Stubblefield, K., Rankin-Gee, E.K., and Wang, S.E. (2011). Transforming growth factor-β regulates the sphere-initiating stem cell-like feature in breast cancer through miRNA-181 and ATM. Oncogene *30*, 1470–1480.

Wu, X., Somlo, G., Yu, Y., Palomares, M.R., Li, A.X., Zhou, W., Chow, A., Yen, Y., Rossi, J.J., Gao, H., et al. (2012). De novo sequencing of circulating miRNAs identifies novel markers predicting clinical outcome of locally advanced breast cancer. J. Transl. Med. *10*, 42.

Yardley, D.A. (2010). Visceral disease in patients with metastatic breast cancer: efficacy and safety of treatment with ixabepilone and other chemotherapeutic agents. Clin. Breast Cancer *10*, 64–73.

Yu, Y., Wang, Y., Ren, X., Tsuyada, A., Li, A., Liu, L.J., and Wang, S.E. (2010). Context-dependent bidirectional regulation of the MutS homolog 2 by transforming growth factor β contributes to chemoresistance in breast cancer cells. Mol. Cancer Res. *8*, 1633–1642.

Yuan, A., Farber, E.L., Rapoport, A.L., Tejada, D., Deniskin, R., Akhmedov, N.B., and Farber, D.B. (2009). Transfer of microRNAs by embryonic stem cell microvesicles. PLoS ONE *4*, e4722.

Zhang, Y., Liu, D., Chen, X., Li, J., Li, L., Bian, Z., Sun, F., Lu, J., Yin, Y., Cai, X., et al. (2010). Secreted monocytic miR-150 enhances targeted endothelial cell migration. Mol. Cell *39*, 133–144.

Zhu, W., Qin, W., Atasoy, U., and Sauter, E.R. (2009). Circulating microRNAs in breast cancer and healthy subjects. BMC Res. Notes *2*, 89.

Zhuang, G., Wu, X., Jiang, Z., Kasman, I., Yao, J., Guan, Y., Oeh, J., Modrusan, Z., Bais, C., Sampath, D., and Ferrara, N. (2012). Tumour-secreted miR-9 promotes endothelial cell migration and angiogenesis by activating the JAK-STAT pathway. EMBO J. *31*, 3513–3523.

Cancer Cell
Article

Disrupting the Interaction of BRD4 with Diacetylated Twist Suppresses Tumorigenesis in Basal-like Breast Cancer

Jian Shi,[1,4] Yifan Wang,[1,4,5] Lei Zeng,[6] Yadi Wu,[2,4] Jiong Deng,[7] Qiang Zhang,[6] Yiwei Lin,[1,4] Junlin Li,[1,4] Tiebang Kang,[5] Min Tao,[8] Elena Rusinova,[6] Guangtao Zhang,[6] Chi Wang,[4] Haining Zhu,[1] Jun Yao,[9] Yi-Xin Zeng,[5] B. Mark Evers,[1,3,4] Ming-Ming Zhou,[6,*] and Binhua P. Zhou[1,4,5,*]

[1]Department of Molecular and Cellular Biochemistry, College of Medicine, University of Kentucky, Lexington, KY 40506, USA
[2]Department of Molecular and Biomedical Pharmacology, College of Medicine, University of Kentucky, Lexington, KY 40506, USA
[3]Department of Surgery, College of Medicine, University of Kentucky, Lexington, KY 40506, USA
[4]Markey Cancer Center, College of Medicine, University of Kentucky, Lexington, KY 40506, USA
[5]Sun Yat-sen University Cancer Center, State Key Laboratory of Oncology in South China, and Collaborative Innovation Center of Cancer Medicine, Guangzhou 510060, China
[6]Department of Structural and Chemical Biology, Icahn School of Medicine at Mount Sinai, New York, NY 10029, USA
[7]Department of Pathophysiology, Shanghai Key Laboratory for Tumor Microenvironment and Inflammation, and Translation Medicine Center, Shanghai Chest Hospital, Shanghai Jiao Tong University School of Medicine, Shanghai 200025, China
[8]Department of Oncology, the First Affiliated Hospital of Soochow University, Suzhou 215006, China
[9]Department of Molecular and Cellular Oncology, University of Texas M.D. Anderson Cancer Center, Houston, TX 77030, USA
*Correspondence: ming-ming.zhou@mssm.edu (M.-M.Z.), peter.zhou@uky.edu (B.P.Z.)
http://dx.doi.org/10.1016/j.ccr.2014.01.028

SUMMARY

Twist is a key transcription activator of epithelial-mesenchymal transition (EMT). It remains unclear how Twist induces gene expression. Here we report a mechanism by which Twist recruits BRD4 to direct *WNT5A* expression in basal-like breast cancer (BLBC). Twist contains a "histone H4-mimic" GK-X-GK motif that is diacetylated by Tip60. The diacetylated Twist binds the second bromodomain of BRD4, whose first bromodomain interacts with acetylated H4, thereby constructing an activated Twist/BRD4/P-TEFb/RNA-Pol II complex at the *WNT5A* promoter and enhancer. Pharmacologic inhibition of the Twist-BRD4 association reduced *WNT5A* expression and suppressed invasion, cancer stem cell (CSC)-like properties, and tumorigenicity of BLBC cells. Our study indicates that the interaction with BRD4 is critical for the oncogenic function of Twist in BLBC.

INTRODUCTION

Recruitment and activation of RNA-Pol II at gene promoters are two key steps required for a productive transcription (Zhou et al., 2012). After RNA-Pol II recruitment to a gene promoter, TFIIH phosphorylates serine 5 of the heptapeptide repeats in the C-terminal domain (CTD) of RNA-Pol II, resulting in initial synthesis of short RNA species. However, RNA-Pol II pauses in the proximal promoter and requires a second phosphorylation event on serine 2 of the CTD that is carried out by the pause release factor P-TEFb, a complex composed of CDK9 and cyclin T1/2. Importantly, the recruitment of P-TEFb to RNA-Pol II is mediated, in part, by BRD4 (Jang et al., 2005).

BRD4 is a member of the BET (bromodomain and extra terminal domain) family proteins that are characteristic of two tandem bromodomains (BDs) located in the N terminus. The BDs of BET proteins recognize acetylated-lysine residues in nucleosomal histones (Filippakopoulos et al., 2012), facilitating the

Significance

BLBC is associated with an aggressive clinical history, development of recurrence, distant metastasis, and shorter patient survival. BLBC contains abundant EMT transcription factor Twist and possesses many CSC-like characteristics, suggesting that the Twist-activated EMT program confers growth advantages to BLBC. However, the absence of a clear ligand-binding domain in Twist creates a formidable hurdle toward developing inhibitors that can suppress its function. We found that Twist interacts with and recruits the BRD4/P-TEFb/RNA-Pol II transcription complex to the *WNT5A* superenhancer for gene activation. BET-specific inhibitors disrupted the Twist-BRD4 interaction and resulted in significant Wnt5a reduction, leading to inhibition of invasion and tumorigenicity of BLBC in vitro and in vivo. Our study indicates that targeting the Twist-BRD4 interaction provides an effective approach for treating BLBC.

recruitment of transcriptional proteins to chromatin. Recent studies have shown that pharmacologic inhibition of BRD4 with BET-specific BD inhibitors effectively blocks *MYC* expression in multiple myeloma (Delmore et al., 2011), Burkitt's lymphoma, and acute myeloid leukemia (Dawson et al., 2011; Zuber et al., 2011). However, many mechanistic questions about BRD4 functions as a chromatin regulator in gene transcription are still unanswered, including (1) how BRD4 interacts and works with transcription factors at the target gene promoter and enhancer sites and (2) whether and how the two BDs in BRD4 function differently in gene transcription.

Breast cancer is a heterogeneous disease that can be divided into four major subtypes based on gene expression profiling: luminal A, luminal B, ErbB2, and basal like. Basal-like breast cancer (BLBC) is characterized by the lack of expression of estrogen receptor (ER), progesterone receptor (PR), and epidermal growth factor receptor 2 (HER2) and positive expression of basal markers (Cytokeratin 5/6 [CK5/6] and CK14) (Rakha et al., 2008). The absence of effective targeted therapies and poor response to standard chemotherapy often results in a rapidly fatal clinical outcome for this disease. Notably, BLBC has activated the epithelial-mesenchymal transition (EMT) program, which provides cells with increased plasticity and stem-cell-like properties required during embryonic development, tissue remodeling, wound healing, and metastasis (Thiery et al., 2009).

Twist and Snail are two key members of EMT-activating transcriptional factors. During mesoderm development in *Drosophila*, Snail functions as a transcriptional repressor to prevent expression of genes that belong to ectoderm, whereas Twist serves as a transcriptional activator to induce mesodermal gene expression (Leptin, 1991). A complete loss of all mesodermal characteristics occurs only when both Snail and Twist are absent. These results suggest that Snail and Twist work synergistically, controlling distinct sets of genes, to coordinate EMT induction and mesoderm formation (Zeitlinger et al., 2007). We previously showed that Snail interacts with several transcriptional repressive complexes to suppress gene expression. However, the mechanism underlying gene transcriptional activation by Twist has remained elusive. In this study, we sought to identify Twist-interacting proteins and determine the mechanism by which Twist controls gene transcriptional activation in EMT and BLBC.

RESULTS

BRD4-BD2 Interacts with Lysine-Acetylated Twist

We sought to identify Twist-interacting proteins from a stable HeLa S3 cell line expressing Flag-Twist. Affinity protein purification, followed by SDS-PAGE and analysis by mass spectrometry, revealed the presence of BRD4 and TRRAP/EP400 (data not shown). To validate the interaction between Twist and BRD4, we coexpressed hemagglutinin (HA)-Twist and Flag-BRD4 in HEK293 cells in the presence or absence of the histone deacetylase inhibitor Trichostatin (TSA). After immunoprecipitating Twist, we detected the associated BRD4, and vice versa (Figure 1A and Figure S1A available online). Although similar amounts of Twist were immunoprecipitated from cells with and without TSA treatment, Twist was more acetylated and interacted with more BRD4 in cells treated with TSA. In addition, immunoprecipitation with a pan-acetylated-lysine (pan-AcK) antibody pulled down Twist and BRD4 in cells treated with TSA. Similar observations were made in Twist-expressing HeLa S3 cells (Figures 1B and S1B). We further confirmed the interaction between the endogenous Twist and BRD4 and acetylation of the endogenous Twist in four BLBC cell lines, both of which were substantially enhanced with TSA treatment (Figures 1C and S1C). The Twist-BRD4 interaction is specific because Twist did not associate with other BET members (BRD2, BRD3, and BRDT) or lysine specific demethylase 1 (LSD1), and BRD4 did not associate with TCF4 (Figure S1D). The increased Twist-BRD4 interaction by TSA could not be due to an altered subcellular localization of these two proteins as TSA did not affect their localization (Figure S1E).

We next generated BRD4 deletion constructs and coexpressed them with Twist in HEK293 cells. We found that only N-terminal fragments containing both BDs, but not other regions of BRD4, retained the ability to interact with Twist (Figure 1D). When BD1 or BD2 was coexpressed with Twist in HEK293 cells, only $BD2^{WT}$, but not $BD1^{WT}$, bound to Twist (Figures 1E and S1F). Mutation of the conserved tyrosine and asparagine residues in the acetyllysine binding pocket of BD2 to alanine ($BD2^{YN}$) reduced its binding to Twist. The Twist-BRD4 interaction was readily disrupted when JQ1, a BET-specific BD inhibitor, was added to the immunoprecipitation reaction (Figures 1F, 1G, S1G, and S1H). Similarly, MS417, a BET-specific BD inhibitor with approximately 10-fold higher binding affinity than JQ1 (Zhang et al., 2012), effectively blocked the Twist-BRD4 interaction in four BLBC cell lines (Figures S1I and S1J). These results indicate that the Twist-BRD4 interaction is mediated by the BD2 of BRD4 binding to lysine-acetylated Twist.

Twist Diacetylation at K73 and K76 by Tip60 Is Required for Twist-BRD4 Interaction

The N-terminal half of Twist contains an acidic segment and two lysine/arginine-rich basic motifs that share high sequence similarity to histones H2B and H4, respectively (Figure S2A). We generated Twist deletion constructs DL1 (residues 15–202), DL2 (residues 31–202), and DL3 (residues 47–202) and coexpressed them individually with Flag-BRD4 in HEK293 cells. DL1 retained, whereas DL2 and DL3 lost, interaction with BRD4 (Figures 2A and S2B). Surprisingly, in contrast to DL1, DL2 and DL3 also completely lost acetylation (Figures 2B and S2C). Because the first 30 N-terminal residues in Twist do not contain lysine, the loss of acetylation in DL2 and DL3 suggests that the N-terminal region is critical for Twist acetylation. In our mass spectrometry analysis, the NuA4 histone acetyltransferase complex proteins, including TRRAP and EP400 (Doyon and Côté, 2004), were identified as Twist association partners. We postulated that Tip60, the acetyltransferase of NuA4 complex, was responsible for Twist acetylation. Indeed, when $Twist^{WT}$, DL1, DL2, and DL3 were coexpressed with Tip60 in HEK293 cells, we found that $Twist^{WT}$ and DL1, but not DL2 or DL3, interacted with Tip60 (Figures 2C and S2D). Endogenous Twist-Tip60 interaction was confirmed in three BLBC cell lines, which was markedly enhanced by TSA treatment (Figure S2E). We further observed that ectopic expression of Tip60 in BT549 and SUM1315 cells resulted in enhanced acetylation of Twist and the association of Twist with BRD4 even in the absence of

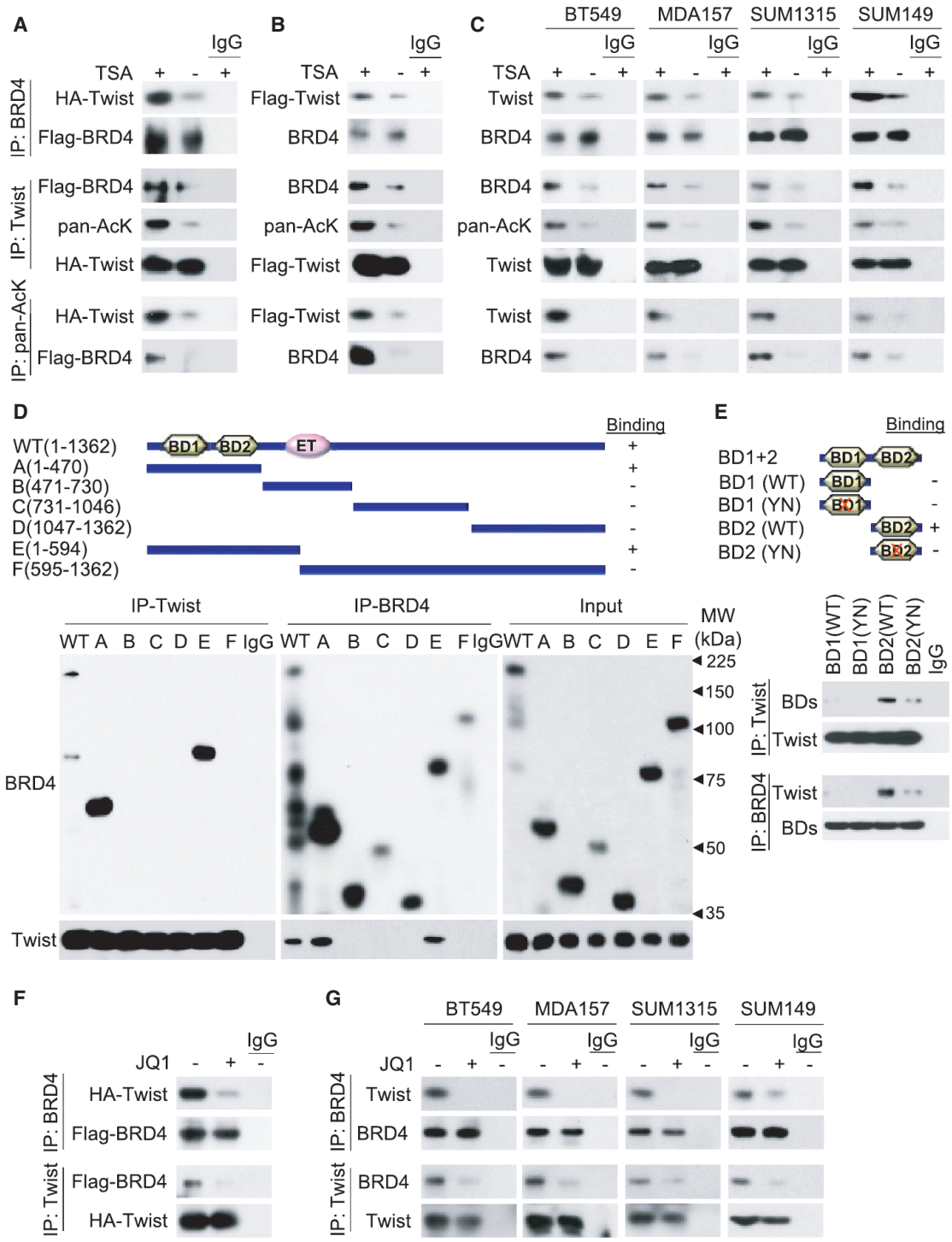

Figure 1. BD2 of BRD4 Is Required for Its Interaction with Acetylated Twist

(A) HA-Twist and Flag-BRD4 were coexpressed in HEK293 cells. After treatment of cells with TSA (2 μM) for 12 hr, Twist, BRD4, and acetylated Twist were immunoprecipitated with HA, Flag, and pan-acetylated-lysine (pan-AcK) antibodies, respectively, and analyzed by western blotting.

(B) HeLa cells stably expressing Flag-Twist were treated with TSA as in (A). Flag-Twist, endogenous BRD4, and acetylated Twist were immunoprecipitated and examined by western blotting.

(C) Cells were treated as described in (A). Endogenous Twist, BRD4, and acetylated Twist were immunoprecipitated and examined by western blotting.

(D) Schematic depiction of the functional domains of BRD4 and deletion constructs used (top). ET, extraterminal domain. Flag-tagged wild-type (WT) or deletion mutants of BRD4 were coexpressed with HA-Twist in HEK293 cells. After being immunoprecipitated with HA or Flag antibody, the bound BRD4 or Twist was examined by western blotting (bottom).

(legend continued on next page)

TSA, whereas knockdown of Tip60 yielded opposite effects even in the presence of TSA (Figures 2D and S2F).

Twist contains five lysine residues (K33, K38, K73, K76, and K77) in its N-terminal region, which are highly conserved among different species (Figure S2A). Point mutation of K33R, K73R, and K76R showed a reduced level of acetylation compared to that of Twist^{WT} (Figures 2E and S2G). Twist^{WT}, K33R, K38R, and K77R showed a similar interaction with BD2, whereas K73R and K76R exhibited clearly weaker binding to BD2 (Figures 2F and S2H). The K73R/K76R double mutant showed an almost complete loss of acetylation and interaction with BD2 (Figures 2G and S2I). We further confirmed the Tip60-mediated Twist acetylation on K73/K76 by mass spectrometry analysis (Figures 2H and S2J). There are 12 nuclear histone acetyltransferases (HATs), divided into three major groups: (1) the GNAT family (e.g., PCAF), (2) the MYST family (e.g., Tip60), and (3) the p300/CBP family (e.g., p300 and CBP) (Rekowski and Giannis, 2010). To examine whether other HATs can also acetylate Twist, we knocked down the expression of p300, CBP, PCAF, or Tip60 individually in BT549 and SUM1315 cells (Figure S2K). We found that knockdown of Tip60, but not p300, CBP, or PCAF, suppressed Twist acetylation at K73/K76. Taken together, these data support our contention that Tip60 is the major HAT responsible for the K73/K76 acetylation on Twist and that diacetylation of Twist is required for its association with BRD4-BD2.

Histone H4 Mimicry in Twist Is Responsible for Its Interaction with BRD4

Diacetylations of the N-terminal tail of H4 at K5 and K8 are often required for the interaction of H4 with BDs of BET family proteins (Filippakopoulos et al., 2012; Morinière et al., 2009). The Twist sequence at K73 and K76 shares high similarity to the N-terminal tail of H4 at K5 and K8 (Figure 3A). To investigate this "histone mimicry" in the interaction between Twist and BRD4, we performed a pull-down study using biotinylated H4 and Twist peptides and lysate of HEK293 cells expressing BRD4-BD2. We observed that biotinylated H4-K5ac/K8ac peptide (residues 1–21) was bound to BD2 and that this interaction was disrupted by nonbiotinylated H4-K5ac/K8ac peptide (Figure 3B, lane 2 versus lane 1). This interaction was also markedly reduced by a Twist-K73ac/K76ac peptide (residues 61–80) but not by the unacetylated corresponding peptide (Figure 3B, lanes 3 and 4 versus lane 1). Similarly, the interaction of a biotinylated Twist-K73ac/K76ac peptide with BD2 was disrupted by a Twist-K73ac/K76ac, but not unacetylated, peptide (Figure 3B, lanes 7 and 8 versus lane 5). Notably, acetylated H4 peptide also disrupted the acetylated Twist and BD2 association (Figure 3B, lane 6 versus lane 5), indicating that diacetylated K5/K8 in H4 and diacetylated K73/K76 in Twist function similarly as a recognition motif for BRD4-BD2.

We then developed a specific antibody against Twist-K73ac/K76ac. Twist recognition by this antibody was disrupted by a Twist-K73ac/K76ac peptide, but not the corresponding nonacetylated peptide (Figures 3C and S3A). This antibody recognized immunoprecipitated Twist^{WT}, but not Twist$^{K73R/K76R}$ that harbored mutated K73 and K76 (Figures 3D and S3B). In line with our contention that Tip60 acetylates Twist at K73/K76, both Twist and H4 acetylated by purified Tip60 in vitro were recognized by this Twist-K73ac/K76ac antibody and a pan-acetylated antibody (Figure 3E). Furthermore, this antibody readily detected endogenous Twist-K73ac/K76ac that was immunoprecipitated from four BLBC cell lines (Figures 3D and S3B). Although immunoprecipitation of the endogenous Twist by this antibody was weak, it was robustly increased by the addition of JQ1 to the binding buffer, indicating that the K73ac/K76ac site is masked by binding to BRD4 in cells (Figure 3F).

We further characterized the functional importance of this diacetylation-dependent Twist-BRD4 interaction in human mammary epithelial (HMLE) cells. Ectopic expression of Twist^{WT} resulted in an induction of EMT, as indicated by the downregulation of E-cadherin and upregulation of vimentin (Figures 3G and S3C). While localized in the nucleus (Figure S3D), Twist$^{K73R/K76R}$ expression failed to induce EMT, indicating that the interaction with BRD4 is critical for the function of Twist.

Molecular Basis of BRD4 Binding to Lysine-Acetylated Twist

To determine the molecular basis of diacetylation-dependent Twist-BRD4 association, we characterized binding of the two BDs of BRD4 to a series of Twist peptides (residues 68–79) bearing no, single-acetylated, or diacetylated lysine at K73 and K76 by nuclear magnetic resonance (NMR) titration. As shown in 2D ^{1}H-^{15}N HSQC spectra (Figure S4A), BRD4-BD2 exhibited substantially more extended chemical shift perturbations upon binding to the single-acetylated, and even more to the diacetylated, Twist peptides than those produced by BRD4-BD1, confirming that BRD4-BD2 is largely responsible for BRD4 association with the diacetylated Twist. The preferred recognition of Twist-K73ac/K76ac by BRD4-BD2 was supported in a fluorescence anisotropy competition binding study using a fluorescein-labeled H4K5ac/K8ac peptide as an assay probe, yielding a K_i of 800 μM and >3,000 μM for BRD4-BD2 and BRD4-BD1, respectively (Figure S4B). Furthermore, BRD4-BD1 and other BDs, including those from CBP and PCAF, showed almost no interaction with the single- or diacetylated Twist peptides (data not shown).

We next solved the 3D structure of BRD4-BD2 bound to Twist-K73ac/K76ac peptide using NMR spectroscopy to determine the molecular basis of this selective interaction (Figures 4A, 4B, and S4C and Table S1). As revealed in the 3D structure, the Twist-K73ac/K76ac peptide is bound in the protein across

(E) Schematic diagram showing the double bromodomain (BD1+BD2) of BRD4 and individual BD constructs used (top). Flag-BD1^{WT}, BD1^{YN}, BD2^{WT}, and BD2^{YN} were coexpressed with HA-Twist in HEK293 cells treated with TSA as in (A). Twist and BDs were immunoprecipitated with HA and Flag antibodies, respectively, and analyzed by western blotting (bottom).
(F) HA-Twist and Flag-BRD4 were coexpressed in HEK293 cells treated with TSA as in (A). Twist and BRD4 were immunoprecipitated with HA and Flag antibodies, respectively, in the presence or absence of JQ1 (1 μM) and analyzed by western blotting.
(G) Cells were treated with TSA as in (A). Endogenous Twist and BRD4 were immunoprecipitated with Twist and BRD4 antibodies, respectively, in the presence or absence of JQ1 (1 μM) and examined by western blotting.
See also Figure S1.

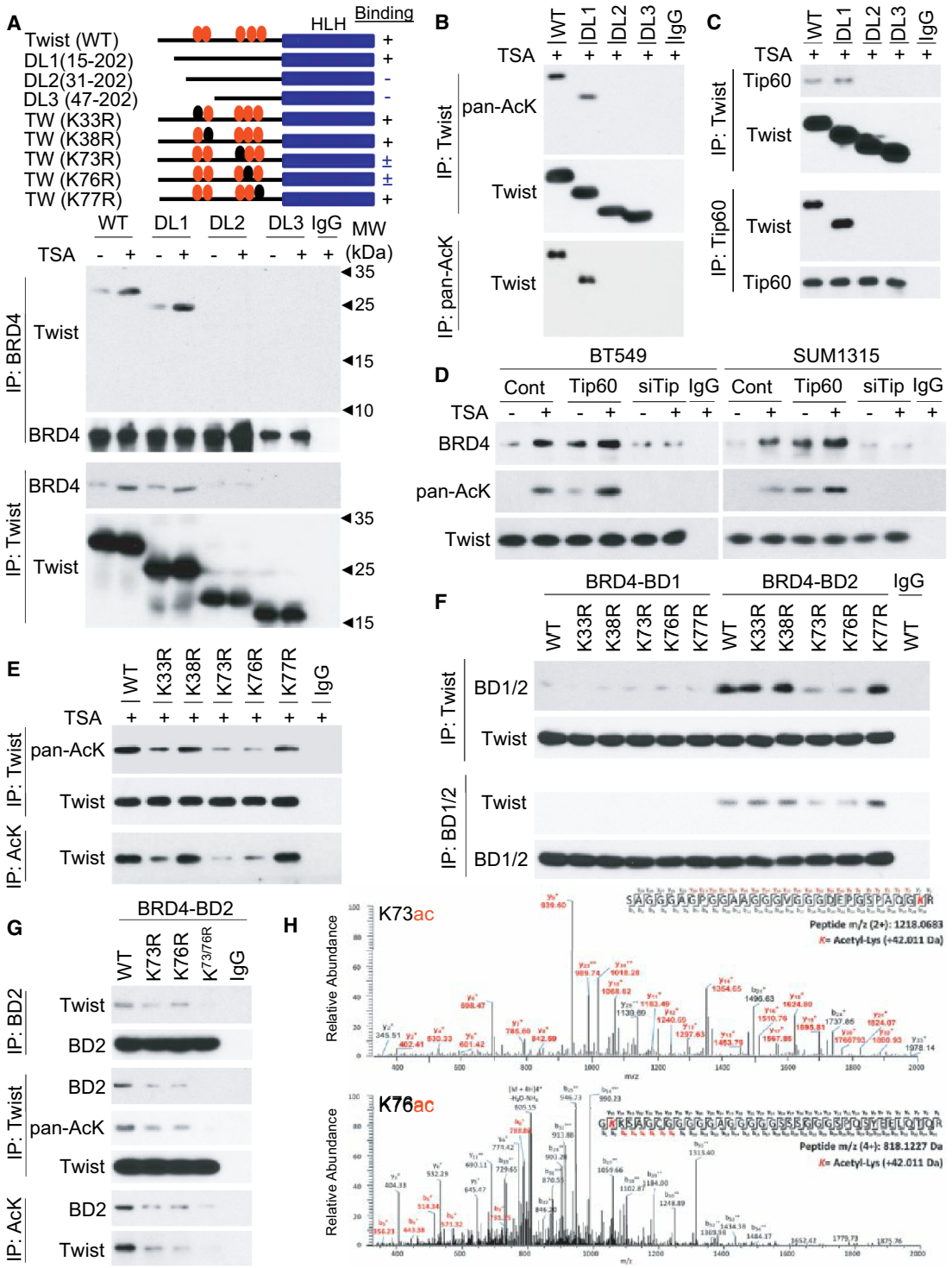

Figure 2. Twist Diacetylation at K73/K76 by Tip60 Is Required for Interaction with BRD4

(A) Schematic diagram showing the domain organization of Twist, with deletion and mutation constructs used (top). HA-tagged WT or deletion mutants of Twist were coexpressed with Flag-BRD4 in HEK293 cells treated with or without TSA. Twist and BRD4 were immunoprecipitated with HA and Flag antibodies, respectively, and analyzed by western blotting (bottom).

(B) HA-tagged WT or deletion mutants of Twist were expressed in HEK293 cells treated with TSA. Twist and acetylated Twist were immunoprecipitated with HA and pan-AcK antibodies, respectively, and analyzed by western blotting.

(C) Flag-tagged WT or deletion mutants of Twist were coexpressed with HA-Tip60 in HEK293 cells treated with TSA. Twist and Tip60 were immunoprecipitated with Flag and HA antibodies, respectively, and analyzed by western blotting.

(legend continued on next page)

an elongated cavity formed between the ZA and BC loops of this left-handed four-helical bundle structure. Specifically, acetylated K73 is bound in the canonical acetyllysine binding site, forming a hydrogen bond between its carbonyl oxygen and the side-chain nitrogen of the conserved Asn433. Acetylated K76 is recognized, next to K73ac, by the BD2 in a small hydrophobic cavity that is lined with Trp374, Val380, Leu385, and Val439. While the overall recognition of the diacetylated K73/K76 in Twist by BD2 is similar to that of the diacetylated K5/K8 in H4 by the BD1 of BRD4, several additional interactions observed in the former complex explain its selectivity. For instance, the imidazole nitrogen atom of His437 of BD2 is within hydrogen bond distance to the backbone carbonyl oxygen of the K73ac (Figures 4A and 4B). Notably, within this highly conserved acetyllysine binding pocket, His437 in BRD4-BD2, which corresponds to Asp144 in BRD4-BD1, is unique. Asp144 was not engaged in any interaction with the H4 peptide as shown in the crystal structure of the BD1/H4-K5ac/K8ac peptide complex (Filippakopoulos et al., 2012), explaining the failed binding of BRD4-BD1 to Twist-K73ac/K76ac. To further examine the role of His437 in BRD4/Twist association, we engineered two point mutants by switching His437 and Asp144 in the two BDs, generating BD2-H437D and BD1-D144H mutants. Remarkably, we found that BD2-H437D almost completely lost its ability to bind to the diacetylated Twist, whereas BD1-D144H gained binding ability for the acetylated Twist (Figure 4C), confirming the important function of His437 in the Twist-K73ac/K76ac recognition.

We observed additional intermolecular interactions in the complex structure that contribute to the selectivity of BRD4-BD2/Twist recognition. For instance, the methyl group of Ala70 of Twist interacts with the aromatic side chain of the conserved Tyr432 in BRD4-BD2, whereas side chains of Ser78 of Twist and Glu438 of the BD2 form electrostatic interactions. Importantly, both Ala70 and Ser78 in Twist are located outside the diacetylation GK-X-GK motif and are not conserved in H4. Ala70 has no corresponding residue in H4, whereas the corresponding residue for Ser78 in H4 is Leu10, which could not form a favorable interaction with Glu438 in BD2, or even Asp145 in BD1. Collectively, our structural insights provide a detailed understanding of the molecular basis for the selective recognition of Twist-K73ac/K76ac by BRD4-BD2.

Histone H4 and Twist Synergistically Interact with BRD4

Because single BD2 of BRD4 can interact with H4 or Twist, we examined their interactions in a cellular context by expressing Twist or Twist$^{K73R/K76R}$ with single or double BDs of BRD4 in HEK293 cells. After immunoprecipitation of Twist, BDs, or H4 individually, the association and acetylation of the other two molecules were analyzed by western blotting (Figures 4D and S4D). First, we immunoprecipitated Twist and examined the presence of other two molecules (Figure 4D, left panel). We found that Twist$^{K73R/K76R}$ did not associate with any of the BDs (Figure 4D, left panel, lanes 7–9), whereas Twist associated with BD2 and BD1+BD2 but not BD1. Notably, the associated BD1+BD2 also contained H4 (Figure 4D, left panel, lanes 4–6). Second, we immunoprecipitated BD1, BD2, or BD1+BD2 and examined the presence and acetylation of Twist and H4 (Figure 4D, middle panel). BD1 associated with H4 but not Twist, whereas BD2 interacted with both Twist and H4, indicating that Twist and H4 can compete for interaction with BD2 (Figure 4D, middle panel, lanes 4–6). BD1+BD2 also associated with Twist and H4. Intriguingly, the amount of H4 associated with single BD (BD1 or BD2) is similar to that with double BDs in BD1+BD2 (Figure 4D, middle panel, lanes 2 and 3 versus lane 1), suggesting that only one BD in BD1+BD2 binds to H4. In the presence of Twist, the binding of BD1+BD2 to H4 did not alter (Figure 4D, middle panel, lane 4 versus lane 1). Because Twist interacts with BD2 but not BD1, H4 likely only interacts with BD1 when BD1+BD2, Twist, and H4 are all present. Consistent with this contention, the amount of Twist associated with BD1+BD2 was more than that with BD2 (Figure 4D, middle panel, lane 4 versus lane 5), where Twist and H4 competed for the binding to the BD2. Lastly, we immunoprecipitated H4 and examined the association of Twist and BDs (Figure 4D, right panel). We found that levels of BD1, BD2, and BD1+BD2 appeared to be equivalent, suggesting that H4 interacted equally with BD1, BD2, and BD1+BD2 and that only one BD interacted with H4 in BD1+BD2. In the presence of Twist, the immunoprecipitated BD2 was reduced (Figure 4D, right panel, lane 5 versus lane 2), suggesting that Twist and H4 compete for the interaction with single BD2. However, when the double BDs (BD1+BD2) were present, only one BD was engaged in interaction with H4, since the intensity of immunoprecipitated BD1+BD2 was about equal to that of Twist (Figure 4D, right panel, lane 1 versus lane 4). Consistent with the results from immunoprecipitated Twist, the immunoprecipitated BD1+BD2 by H4 contained Twist, reaffirming the association of three protein molecules in cells. Taken together, these results indicate that Twist and H4 can simultaneously interact with the double BDs of BRD4, in which BD1 binds to H4, whereas BD2 associates with Twist. This distinct binding selectivity of the two BDs of BRD4 is supported by our structural analysis.

Twist-BRD4 Interaction Is Required for *WNT5A* Expression

To identify the transcriptional target of the Twist-BRD4 complex, we performed cDNA microarray analysis of HMLE and luminal

(D) Ectopic expression of Tip60 or knockdown of endogenous Tip60 was performed in BT549 and SUM1315 cells. After endogenous Twist was immunoprecipitated, acetylation of Twist and the bound BRD4 were examined by western blotting.
(E) HA-tagged WT and mutant Twist were expressed in HEK293 cells, acetylated Twist was immunoprecipitated with HA and pan-AcK antibodies, respectively, and examined by western blotting.
(F) HA-tagged WT or mutant Twist was coexpressed with Flag-tagged BD1 and BD2 in HEK293 cells treated with TSA. Twist and BDs were immunoprecipitated with HA and Flag antibodies, respectively, and examined by western blotting.
(G) HA-tagged WT or mutant Twist was coexpressed with Flag-tagged BD2 in HEK293 cells treated with TSA. Twist, BRD4, and acetylated Twist were immunoprecipitated with HA, Flag, and pan-AcK antibodies, respectively, and analyzed by western blotting.
(H) Determination of Tip60 catalyzed acetylation sites in Twist by mass spectrometry. Peptides contain K73 and K76 acetylations are shown at the top and bottom, respectively.
See also Figure S2.

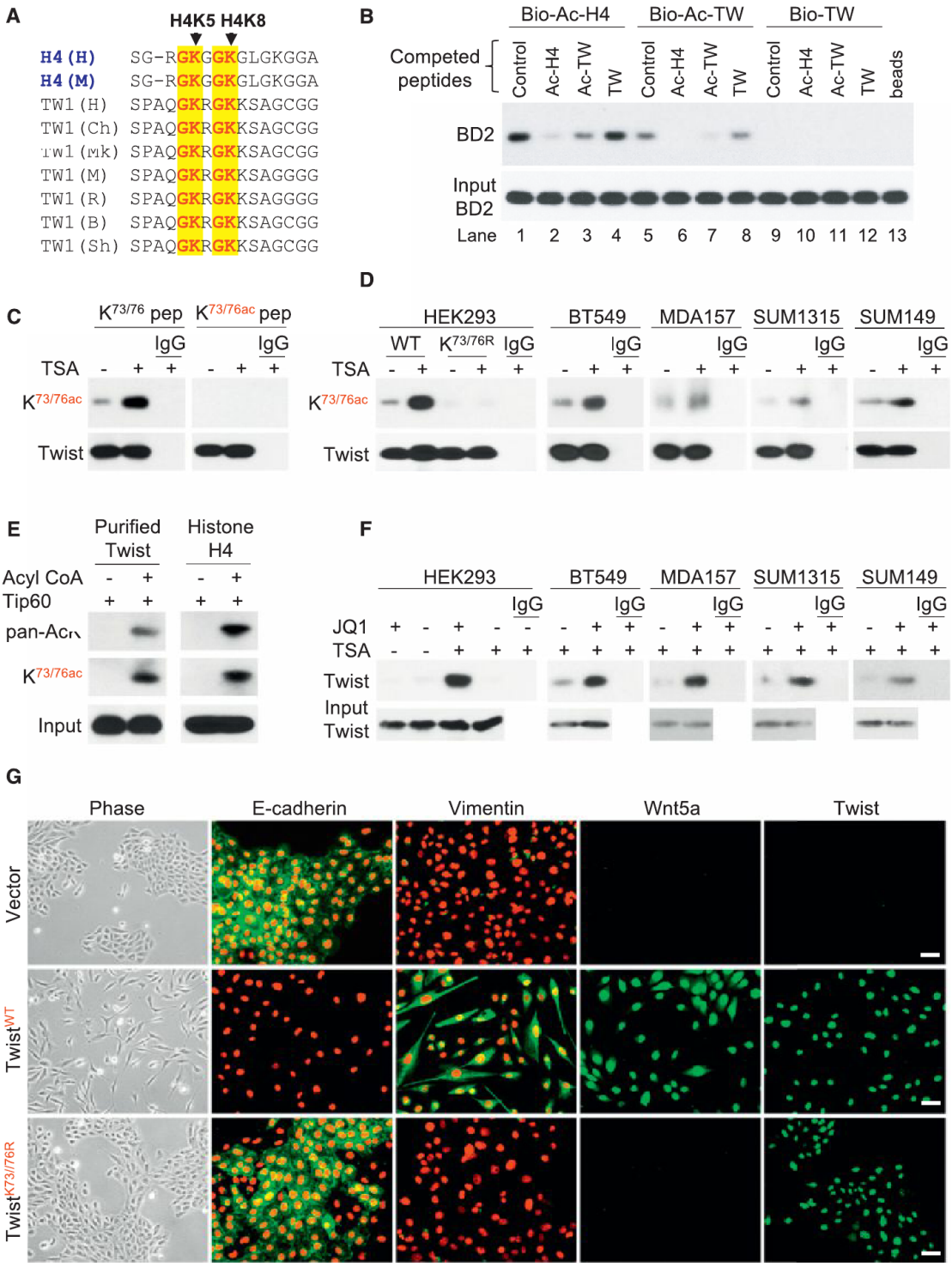

Figure 3. K73ac/K76ac Twist and BRD4 Interaction Is Critical for the Function of Twist

(A) Sequence alignment between K5/8 of histone H4 and K73/76 of Twist. H, human; M, mouse; Ch, chimpanzee; Mk, monkey; R, rat; B, bovine; Sh, sheep.

(B) The indicated biotinylated peptides were mixed with lysates from HEK293 cells expressing BD2 without or with indicated nonbiotinylated competing peptides. The bound BD2 was analyzed by western blotting after pull-down of the biotinylated peptides.

(C) HA-Twist was expressed in HEK293 cells treated with or without TSA. The immunoprecipitated Twist was analyzed on western blots using indicated antibody in the presence of Twist-K73/K76 or Twist-K73ac/K76ac peptides.

(D) HA-tagged or endogenous Twist was immunoprecipitated from cells treated with or without TSA using HA and Twist antibodies, respectively, and analyzed by K73ac/K76ac antibody.

(legend continued on next page)

T47D cells that have undergone Twist-mediated EMT (Figures 3G and S5A). We reasoned that genes that are transcriptionally active in Twist/HMLE and Twist/T47D cells but are downregulated by JQ1 in these cells but not in vector control cells are likely targets of the Twist-BRD4 complex (Figure 5A). Among the 29 overlapping genes, *WNT5A* is noted to encode a critical ligand of both canonical (controlling pluripotency) and noncanonical (regulating motility and planar cell polarity) Wnt pathways. Upregulation of Wnt5a is correlated with an aggressive phenotype in melanoma, as well as breast, lung, and prostate tumors (Witze et al., 2008). We thus selected *WNT5A* as an example to characterize the transcriptional mechanism of Twist. We noticed that $Twist^{WT}$ but not $Twist^{K73R/76R}$ induced Wnt5a expression (Figures 3G and S3C). Similarly, $Twist^{WT}$ induced EMT and Wnt5a expression in T47D cells (Figure S5A). In addition, *TWIST* expression positively correlates with *WNT5A* expression in eight microarray data sets from human breast cancer (Figure S5B). Using Twist and Wnt5a antibodies that detect Twist and Wnt5a, respectively, in xenograft tumors derived from SUM1315 cells, which express high levels of Twist and Wnt5a, but not MCF7 cells, which express low levels of Twist and Wnt5a (Figure S5C), we found that Twist is also positively correlated with Wnt5a expression in breast cancer specimens, with both increased expression found predominantly in estrogen receptor negative (ER^-) breast cancer (Figure S5D). Further, in 14 breast cell lines (Figure 5B), both the mRNA and protein levels of Twist and Wnt5a were found to be largely correlated, with elevated expressions found in BLBC cell lines. BRD4 expression is relatively constant among normal breast, luminal, and BLBC cell lines (Figure 5B). Consistently, no significant difference in BRD4 mRNA was found between ER^+ and ER^- breast cancers from a 477 sample microarray data set (Figure S5E).

We generated a clone of SUM1315 cells with stable knockdown of Twist. Twist knockdown reduced the mesenchymal phenotype as these cells were clustered together; cells also gained expression of epithelial markers and reduced the expression of mesenchymal markers (Figures 5C and S5F). Ectopic expression of $Twist^{WT}$, but not $Twist^{K73R/K76R}$, restored the mesenchymal phenotype in these cells. Twist knockdown also resulted in suppression of Wnt5a expression. Ectopic expression of $Twist^{WT}$, but not $Twist^{K73R/K76R}$, recovered Wnt5a expression (Figure 5C) and restored the invasiveness and mammosphere formation in these cells (Figure S5G). These results are in line with observations in HMLE cells (Figure 3G) and indicate that the Twist-BRD4 interaction is critical in maintaining mesenchymal phenotype/characteristics in BLBC cells. Consistently, JQ1 suppressed Wnt5a expression in both Twist/HMLE and Twist/T47D EMT cells (Figure S5H). In addition, knockdown of Twist or BRD4 in five BLBC cell lines resulted in reduced Wnt5a expression; double knockdown of these two molecules almost completely abolished Wnt5a expression (Figure 5D). The downregulation of Wnt5a by BRD4-knockdown is specific, because knockdown of other BET members did not alter Wnt5a expression (Figure S5I). In addition, knockdown of BRD4 did not change the expression of either epithelial or mesenchymal markers (Figure S5J). The downregulation of Wnt5a correlated with inhibition of invasiveness in BLBC cells; addition of recombinant Wnt5a partially restored invasiveness (Figure S5K). Collectively, these results indicate that the Twist-BRD4 interaction is most likely conserved in HMLE and BLBC cells for EMT and that this interaction is required for the expression of Wnt5a, which may represent as a bona fide target of Twist for promoting tumorigenicity in BLBC.

Twist-BRD4 Interaction Is Required for the Recruitment of BRD4 at the *WNT5A* Superenhancer

To delineate how the Twist-BRD4 complex activates *WNT5A* expression, we constructed a Twist-Gal4 fusion protein by fusing Twist N-terminal residues 1–100 to Gal4 DNA-binding domain (DBD). We also generated several N-terminal deletion mutants of Twist fused with Gal4-DBD, including DL1-Gal4, DL2-Gal4, DL3-Gal4, and KR-Gal4 (Figure S6A). When these Twist-Gal4 constructs were coexpressed with the Gal4-luciferase reporter, Gal4-luciferase activity was moderately increased by about 2-fold compared to the control; coexpression of BRD4 with the Twist-Gal4 fusion constructs that contain the N-terminal region required for Tip60-mediated acetylation (i.e., TW and DL1) greatly enhanced luciferase activity to approximately 8-fold, suggesting that the N-terminal half of Twist contains transactivation activity and its interaction with BRD4 boosts this activity.

The *WNT5A* promoter contains two Twist-responsive E boxes, conserved in human and mouse, and located at −160 bp and −67 bp from transcription start site (TSS) (Figure 6A). We cloned the human *WNT5A* promoter (−2,000 bp upstream of the translation start site) and generated several deletion and E box mutants of the promoter-luciferase constructs, including Luc1 (−2,000 bp), Luc2 (−760) and LucEM (−760, two E box mutations). As expected, Twist alone induced Luc1 and Luc2 promoter luciferase activity; coexpression of BRD4 further enhanced the Twist-induced Luc1 and Luc2 promoter luciferase activities (Figure 6A, left panel). In addition, mutation of each E box (E1M and E2M) in this region reduced, whereas mutation of both E boxes (EM) completely abolished, Twist-BRD4-mediated activation of the *WNT5A* promoter luciferase activity, suggesting that both E boxes are required for Twist-BRD4-induced transcriptional activation. $Twist^{K73R/K76R}$ mutant partially decreased *WNT5A* promoter luciferase activity and was completely insensitive to BRD4-mediated transcriptional activation (Figure 6A, right panel). BRD4-mediated enhancement of Twist transcriptional activity is specific because other BET members did not possess this capability, and treatment with JQ1 or MS417 disrupted this BRD4-mediated enhancement (Figure S6B).

(E) Purified human Twist or histone H4 was incubated with purified Tip60 in the absence or presence of acetyl-CoA. The acetylation of Twist and histone H4 was examined by pan-AcK and anti-K73ac/K76ac antibodies.
(F) K73ac/K76ac Twist was immunoprecipitated with K73ac/K76ac antibody in the presence or absence of JQ1. The bound Twist was examined by western blotting.
(G) HMLE cells expressing the vector or the WT or K73/76R Twist were examined for morphological changes indicative of EMT by phase microscopy and the expression of E-cadherin, vimentin, Wnt5a, and Twist (green) by immunofluorescence staining. Nuclei were stained with DAPI (red). Scale bars, 50 μM.
See also Figure S3.

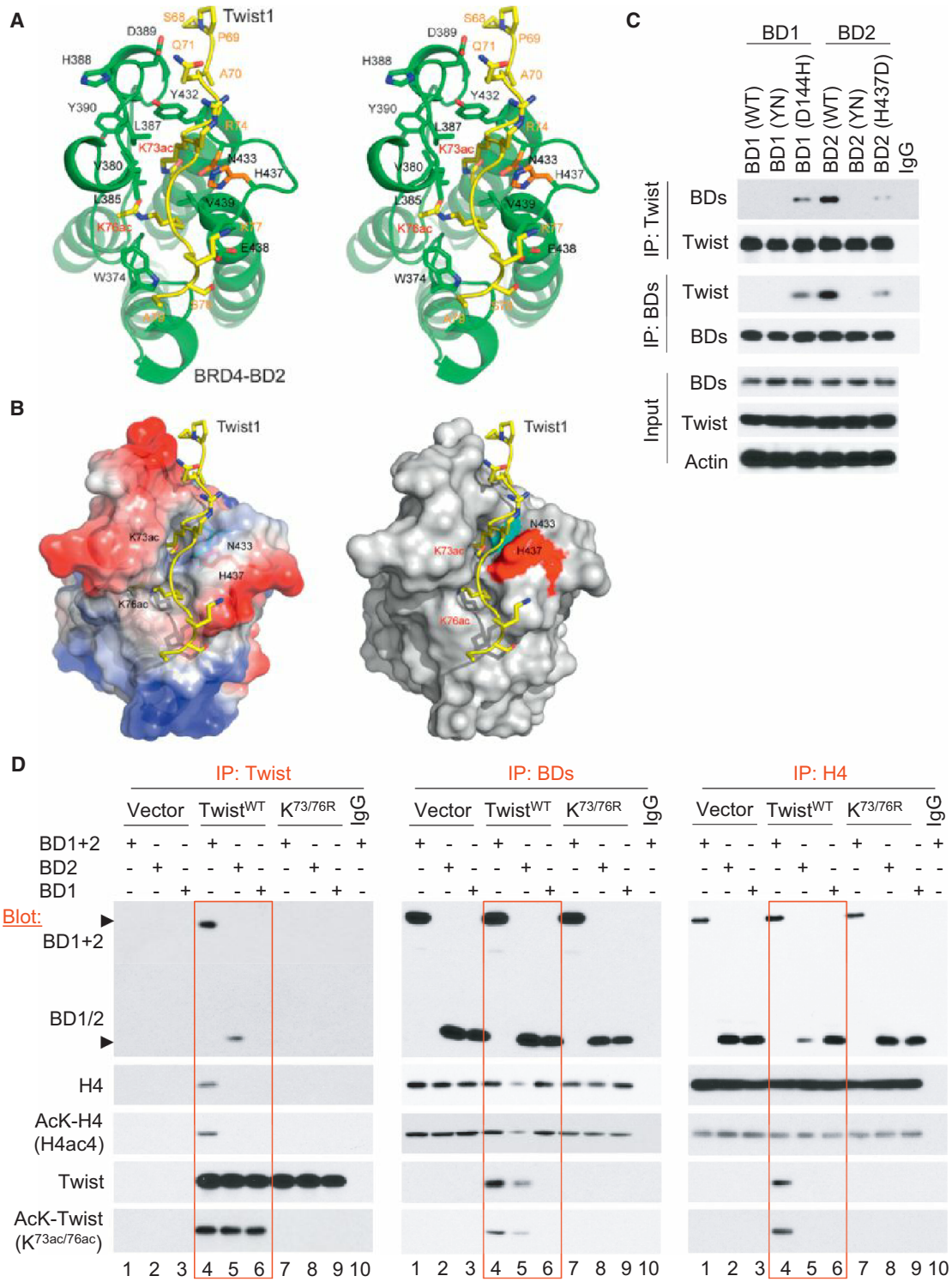

Figure 4. The Structural and Molecular Basis of Twist-K73ac/K76ac Recognition by BRD4

(A) Stereo ribbon diagram of the 3D solution structure of the BRD4-BD2 bound to a diacetylated K73ac/K76ac Twist peptide (yellow). Side chains of key residues engaged at the protein/peptide interactions are depicted and color coded by atom type.

(B) Surface electrostatic potential (left) or space-filled (right) representation of the BRD4-BD2/Twsit-K73ac/K76ac complex structure highlights His437 (red) at the acetyllysine binding site that is responsible for the BRD4-BD2′ specificity of this molecular recognition.

(legend continued on next page)

Chromatin immunoprecipitation (ChIP) analysis revealed that Twist, BRD4, and acetylated H4 associated at the *WNT5A* promoter in BT549 and SUM1315 cells, together with P-TEFb and RNA-Pol II (Figure 6B). A recent study indicated that BRD4 preferentially occupied a small subset of superenhancers in transcriptional active key oncogenes that are critical for proliferation and survival of tumor cells (Lovén et al., 2013). Intriguingly, *WNT5A* is one of these key oncogenes that contain BRD4-associated superenhancer, which covers exon1, promoter, and a region up to 30 kb upstream of the TSS in the *WNT5A* genomic sequence in chromosome 3. To examine whether Twist and BRD4 also bind the *WNT5A* superenhancer in BLBC, we designed two sets of ChIP primers that are 22 and 28 kb upstream of the TSS. ChIP experiments indicated that Twist and BRD4 indeed occupied the *WNT5A* enhancer together with H3K27ac, a mark of active enhancer (Figure 6C). Knockdown of Twist or JQ1 treatment inhibited the association of BRD4 at the *WNT5A* enhancer (data not shown). Knockdown of Twist or JQ1 treatment also reduced the presence of BRD4, P-TEFb, and RNA-Pol II at the *WNT5A* promoter (Figure 6D). However, JQ1 treatment did not affect the association of Twist at the *WNT5A* promoter, suggesting that Twist is required for the recruitment of the BRD4/P-TEFb/RNA-Pol II complex to the *WNT5A* promoter. Consistent with these observations, $Twist^{KR}$, which could not interact with BRD4 and failed to rescue Wnt5a expression (Figure 5C), was unable to recruit the BRD4/P-TEFb/RNA-Pol II complex to the *WNT5A* promoter (data not shown). In addition, ectopic expression of BRD4 increased Twist interaction with P-TEFb and RNA-Pol II, whereas knockdown of BRD4 reduced the association of Twist with P-TEFb and RNA-Pol II (Figure 6E). Our results indicate that Twist recruits BRD4 and acts together with P-TEFb and RNA-Pol II at the *WNT5A* promoter/enhancer to activate transcription.

The direct transcriptional activation of *WNT5A* by the Twist-BRD4 complex prompted us to investigate the stimuli responsible for Twist acetylation and *WNT5A* expression. We found that several stimuli, including TNFα and EGF plus insulin, could induce Twist acetylation at K73/K76 (Figure S6C). TNFα and EGF/insulin treatments greatly enhanced the interaction of Twist with BRD4 and with Tip60, increased K73ac/K76ac of Twist, and promoted Wnt5a expression (Figure 6F, left panel); JQ1 blocked the interaction of Twist with BRD4 and thus suppressed Wnt5a expression (Figure 6F, right panel). Consistent with these findings, TNFα or EGF/insulin treatment greatly enhanced the association of Twist, BRD4, P-TEFb, and RNA-Pol II at the *WNT5A* promoter (Figure S6D). Knockdown of Twist suppressed the association of BRD4 and Twist at the *WNT5A* promoter; however, JQ1 treatment did not inhibit the binding of Twist at the *WNT5A* promoter (Figure S6E). These data suggest that the association of BRD4 at the *WNT5A* promoter is mediated by Twist.

Although JQ1 was reported to reduce c-Myc expression, we noticed that JQ1 (1 μM) caused a decrease of c-Myc expression only in one of five examined BLBC cell lines (Figure 6G). However, JQ1 reduced Wnt5a expression in all cell lines. The low sensitivity to JQ1 in Hs578T cells is likely due to the remarkably high expression levels of Twist and Wnt5a in this particular cell line (Figure 5B). Increased JQ1 concentration resulted in Wnt5a downregulation in a dose-dependent manner in this cell line (Figure S6F). The downregulation of Wnt5a by JQ1 correlated with its inhibition of invasion and tumorsphere formation of these cells; addition of recombinant Wnt5a could partially restore this inhibitory effect (Figures 6H, S6F, and S6G). Together, these data indicate that the Twist-BRD4 interaction, enhanced by extracellular signals, is required for the recruitment of P-TEFb/RNA-Pol II complex to the *WNT5A* superenhancer for transcription of *WNT5A*, which executes, at least in part, the oncogenic function of Twist. JQ1 disrupts this interaction and thereby suppresses *WNT5A* expression in BLBC.

The Twist-BRD4-Wnt5a Axis Is Critical for Tumorigenicity in Breast Cancer

To further examine the oncogenic role of the Twist-BRD4-Wnt5a axis and explore the therapeutic potential of BET-specific inhibitors for targeting this axis in BLBC in vivo, we established two Wnt5a knockdown clones in SUM1315 cells. Knockdown of Wnt5a inhibited the noncanonical Wnt pathway, exemplified by the downregulation of JNK phosphorylation (Figure 7A). Wnt5a knockdown also suppressed the canonical Wnt/β-catenin pathway, indicated by the downregulation of β-catenin and the suppression of Akt/GSK-3β phosphorylation. These effects were further confirmed by β-catenin reporter assay (Figure S7A). Although Wnt5a knockdown did not alter the expression of epithelial or mensenchymal markers, it did reduce the expression of several pluripotent molecules (CD44, Sox2, and Oct4). Consistently, Wnt5a knockdown suppressed invasion and tumorsphere formation in these cells (Figure 7B).

In vivo studies were performed by injection of SUM1315 vector control cells or Wnt5a knockdown clones into the mammary fat pads of NOD-SCID mice. When control tumors were approximately 100 mm^3, mice were divided into three groups to receive daily treatments of JQ1 (50 mg/kg), MS417 (20 mg/kg), or solvent control for 2 weeks. We found that knockdown of Wnt5a completely inhibited tumor growth in SUM1315 cells and that both JQ1 and MS417 treatments significantly inhibited tumor growth (Figure 7C). The growth inhibitory effect of JQ1 and MS417 correlated with suppression of Wnt5a expression and downregulation of proliferative marker Ki67 in these tumors (Figure S7B). These results suggest that Wnt5a is critical for the tumorigenicity of BLBC. BET-specific inhibitors suppress the tumorigenicity of BLBC by inhibiting the Twist-BRD4 interaction and *WNT5A* expression.

DISCUSSION

Our study provides several mechanistic insights into how Twist and BRD4 function cooperatively to activate gene transcription in EMT and BLBC. First, we show that Twist uses a unique

(C) HA-tagged Twist was coexpressed with Flag-tagged WT or mutant BD1 and BD2 in HEK293 cells. Twist and BDs were immunoprecipitated with HA and Flag antibodies, respectively, and the bound BDs and Twist were analyzed by western blotting.
(D) HA-tagged Twist was coexpressed with Flag-tagged BD1, BD2, and BD1+BD2 in HEK293 cells. After immunoprecipitation of Twist, BDs, and H4, the association and acetylation of these molecules were examined by western blotting.
See also Figure S4 and Table S1.

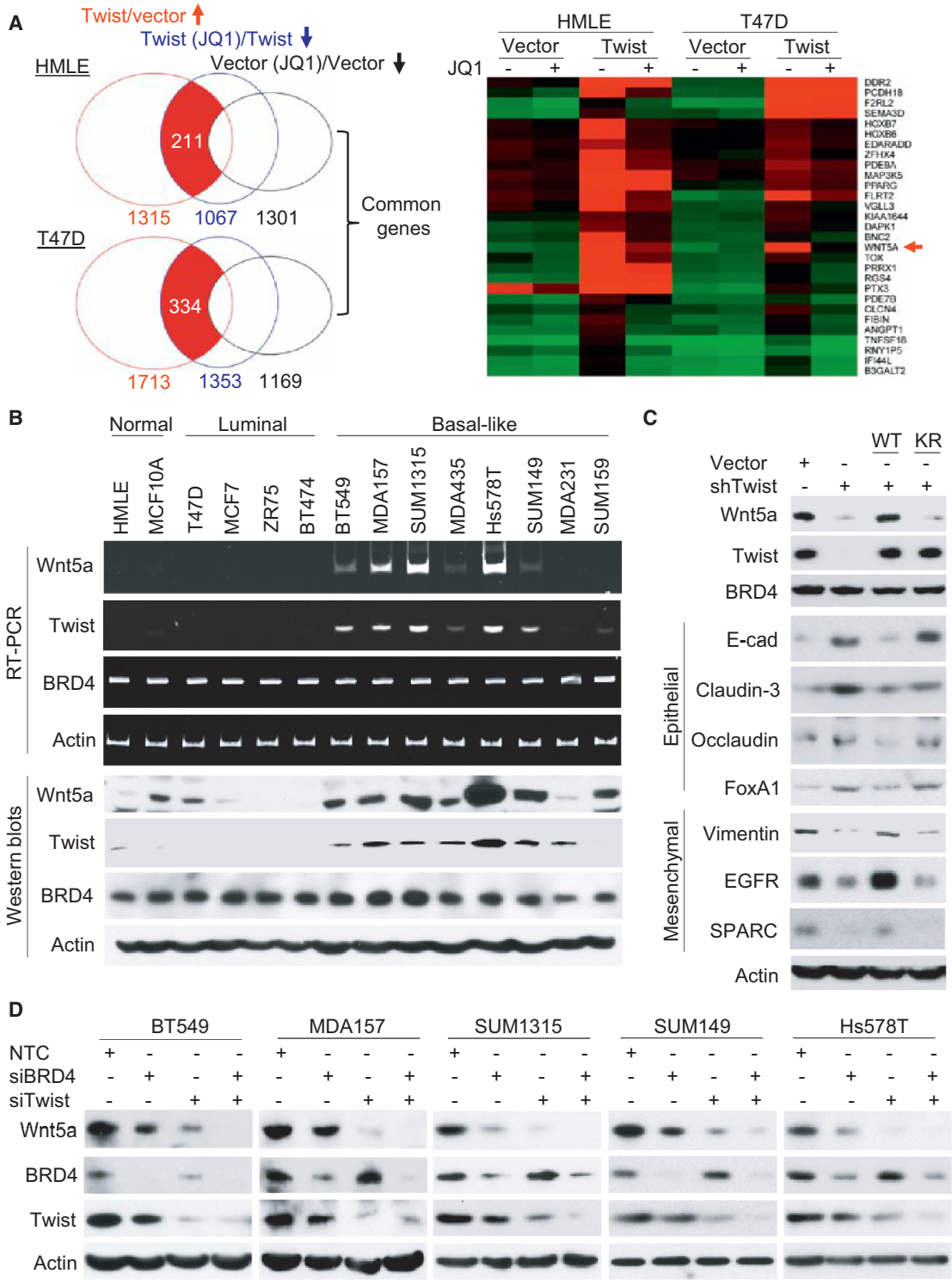

Figure 5. Twist Positively Correlates with Wnt5a Expression in Breast Cancer

(A) Gene expression profiling analysis (left) was used to identify potential Twist target genes. Common Twist target genes between HMLE and T47D cells are shown in the heatmap (right).

(B) The mRNA and protein levels of Twist, Wnt5a, and BRD4 were analyzed by RT-PCR and western blotting.

(C) The effects of stable small hairpin RNA knockdown of endogenous Twist in SUM1315 cells that were transiently transfected with WT or mutant (KR) Twist on the expression of Wnt5a and various molecules was evaluated by western blotting.

(D) Wnt5a expression in five BLBC cell lines with knockdown of Twist and/or BRD4 was analyzed by western blotting. NTC, nontarget control small interfering RNA. See also Figure S5.

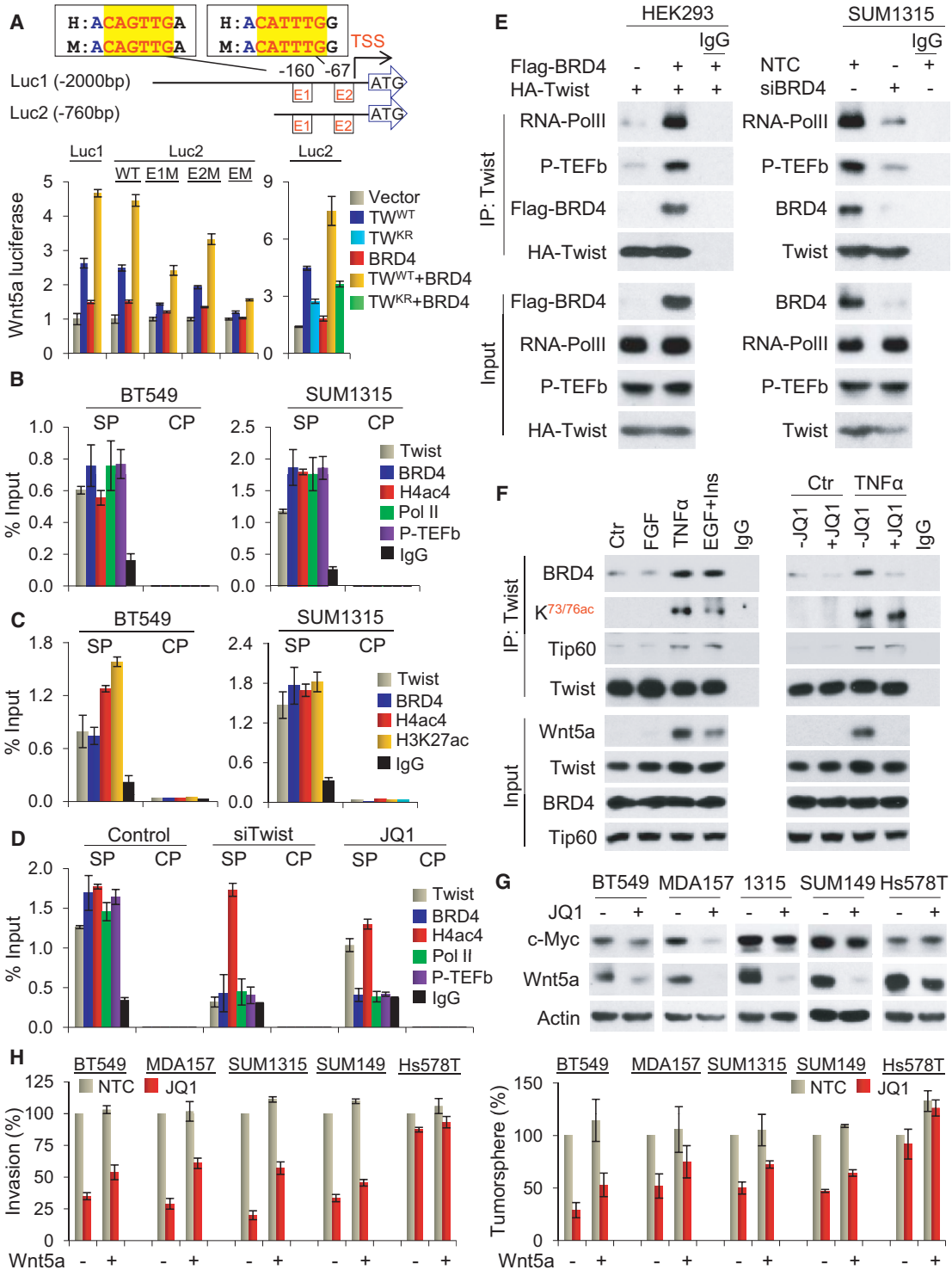

Figure 6. The Twist-BRD4 Complex Directly Activates *WNT5A* Transcription

(A) Schematic depiction of the *WNT5A* promoter and *WNT5A* reporter luciferase constructs used (top). Enhancement of Wnt5a luciferase activity by coexpression of Twist and BRD4 in HEK293 cells is shown (bottom).

(B) Twist, BRD4, H4ac4, RNA-Pol II, and P-TEFb (CDK9) association at the *WNT5A* promoter as assessed by ChIP. SP, specific primer; CP, control primer (5 kb downstream of the 3′ untranslated region).

(C) Twist, BRD4, H4ac, and H3K27ac association at the *WNT5A* enhancer as assessed by ChIP. SP, specific primer (22 kb upstream of the TSS); CP, control primer (5 kb downstream of the 3′ untranslated region).

(legend continued on next page)

mechanism for recruiting BRD4 in gene transcription (Figure 7D). Although BRD4 is the key transcriptional regulator, it lacks specific DNA binding motif. How BRD4 and its associated transcriptional complex are recruited to gene-specific promoters/enhancers remains elusive. We found that Twist contains an "H4-mimic" GK-X-GK motif and becomes diacetylated by Tip60, which also acetylates multiple lysine residues in histone H4 including K5 and K8. By binding to BRD4-BD2 via the K73ac/K76ac motif, Twist recruits BRD4 to target gene promoters/enhancers through the recognition of and interaction with E boxes by its bHLH domain. Once localized in the chromatin, BRD4-BD1 binds with acetylated H4-K5ac/K8ac to facilitate the docking of the BRD4 complex on promoters/enhancers and thereby activates pause release factor P-TEFb to phosphorylate and release RNA-Pol II for *WNT5A* transcription.

Our study demonstrates that the two BDs of BRD4 have distinct functions and binding specificities for acetylated proteins in transcription. Although a single BD1 or BD2 of BRD4 is individually capable of interacting with acetylated H4 in vitro, only BD1 is engaged in the binding with acetylated H4 in the tandem BD1+BD2. This is consistent with the observation that a single BD1 of Brdt binds to acetylated histone H4 nearly as well as Brdt (full length; contains BD1+BD2) (Morinière et al., 2009) and that BRD4-BD1 specifically recognizes acetylation marks on H4, whereas BRD4-BD2 has broad binding specificity for diacetylated substrates (Filippakopoulos et al., 2012). In line with this contention, only BRD4-BD2 interacts with Twist-K73ac/K76ac. We found that charged amino acid residues (D144 in BD1, H437 in BD2) surrounding the acetyllysine-binding pocket of BDs contributed to the binding specificity of BD1 and BD2. Additional residues beyond the diacetylation motif further contribute to Twist's association with BRD4-BD2. Notably, it has recently been reported that BRD4 is phosphorylated by CK2 on several Ser residues in the C-terminal region of BD2 and that these phosphorylations were suggested to affect the interaction of BRD4 with acetylated histones and transcriptional cofactors (Wu et al., 2013). Although a single BD2 of BRD4 can interact with either acetylated H4 or Twist-K73ac/K76ac individually, the tandem BD1+BD2 of BRD4 apparently form a ternary complex with two acetylated proteins in that diacetylated H4 is bound to BD1 and diacetylated Twist is bound to BD2. These results suggest that BRD4 utilizes its tandem BDs as an integration platform to cooperatively interact with H4 and Twist in assembling the integrated transcriptional complex containing P-TEFb and RNA-Pol II at target gene promoters/enhancers. Notably, several transcription-associated proteins that contain tandem binding modules have been shown to engage in combinatorial recognition of different posttranslational modifications (PTMs) in histones for the assembly of transcriptional complexes (Zeng et al., 2010). For example, the tandem PHD-BD module in BPTF specifically recognizes a combination of H3K4me3 and H4K16ac in gene activation (Ruthenburg et al., 2011). Our results not only support this notion, but also extend the functionality of these tandem binding modules in directing gene transcriptional activation as exemplified by the tandem BDs of BRD4 in bridging histone and nonhistone transcription factor.

Notably, these histone-mimic sequences contain lysine/arginine-rich resides, which are often viewed conventionally as a nuclear-localization signal (NLS), as in the case of Twist. However, Twist^{KR} mutant, which cannot be acetylated but still resides in the nucleus, fails to interact with BRD4 and is unable to induce EMT and *WNT5A* expression. Our results suggest that theses lysine/arginine-rich "potential" NLS motifs in transcription factors may have previously unrecognized histone-mimic functions. Consistent with our findings, histone-mimic sequences are deployed by influenza nonstructural protein 1 (NS1) in inhibiting human transcription elongation complex in the antivirus response and by HP1 in forming HP1-chromatin complex (Canzio et al., 2013; Marazzi et al., 2012). We believe that PTMs on histone-mimic sequences present in nonhistone proteins likely play an important role, via conserved molecular mechanisms as seen with those PTMs in histone, in governing the assembly and function of transcriptional complexes in chromatin.

Second, our study demonstrates that Twist is a transcriptional activator responsible for *WNT5A* expression in BLBC. Twist has been shown to bind to the E-cadherin promoter to repress transcription in a way similar to that of Snail. However, this contradicts the role of Twist in development, where it acts as a transcriptional activator to upregulate mesoderm-specific genes in *Drosophila*. When the bHLH domain of Twist was replaced with Gal4-DBD, we found that the Twist-Gal4-DBD fusion was sufficient to activate gene expression, indicating that Twist functions as a transcriptional activator. We further show that Twist recruits BRD4 and the associated P-TEFb and RNA-Pol II to the *WNT5A* promoter/enhancer to directly activate *WNT5A* expression, which is required for invasion and the maintenance of CSC-like properties of BLBC. Notably, Wnt5a is induced in epithelial cells during EMT and required for maintenance of CSC-like properties in the resulting mesenchymal cells (Scheel et al., 2011). In addition, Wnt5a expression is required for the loss of cell-cell contacts, allowing cells to migrate to the edge

(D) Effects of Twist knockdown or JQ1 treatment on the association of Twist, BRD4, RNA-Pol II, and P-TEFb (CDK9) and H4ac4 at the *WNT5A* promoter as assessed by ChIP in SUM1315 cells. SP and CP primers are same as in (B).
(A–D) Statistical analysis (mean ± SD) from three separate experiments in triplicates is shown.
(E) Assessment of the effects of transient expression of HA-Twist and/or Flag-BRD4 on their association with RNA-Pol II and P-TEFb (CDK9) in HEK293 cells (left) and assessment of the effect of endogenous BRD4 knockdown on the association of Twist, BRD4, RNA-Pol II, and P-TEFb (CDK9) in SUM1315 cells (right) are shown.
(F) SUM1315 cells were serum starved for overnight followed by stimulation with FGF, TNFα, or EGF plus insulin for 3 hr in the absence or presence of JQ1 (right). Twist was immunoprecipitated and K73ac/K76ac of Twist and the association of Tip60 and BRD4 were analyzed. Expression of Wnt5a, Twist, BRD4 and Tip60 were also examined by western blotting (left).
(G) BLBC cells were treated with JQ1. Expression of c-Myc and Wnt5a was analyzed by western blotting.
(H) Invasion (left) and tumorsphere formation (right) assays of cells treated as in (G) were examined in the absence or present of recombinant Wnt5a (100 ng/ml). Statistical analysis (mean ± SD) from three independent experiments with duplicates is shown.
See also Figure S6.

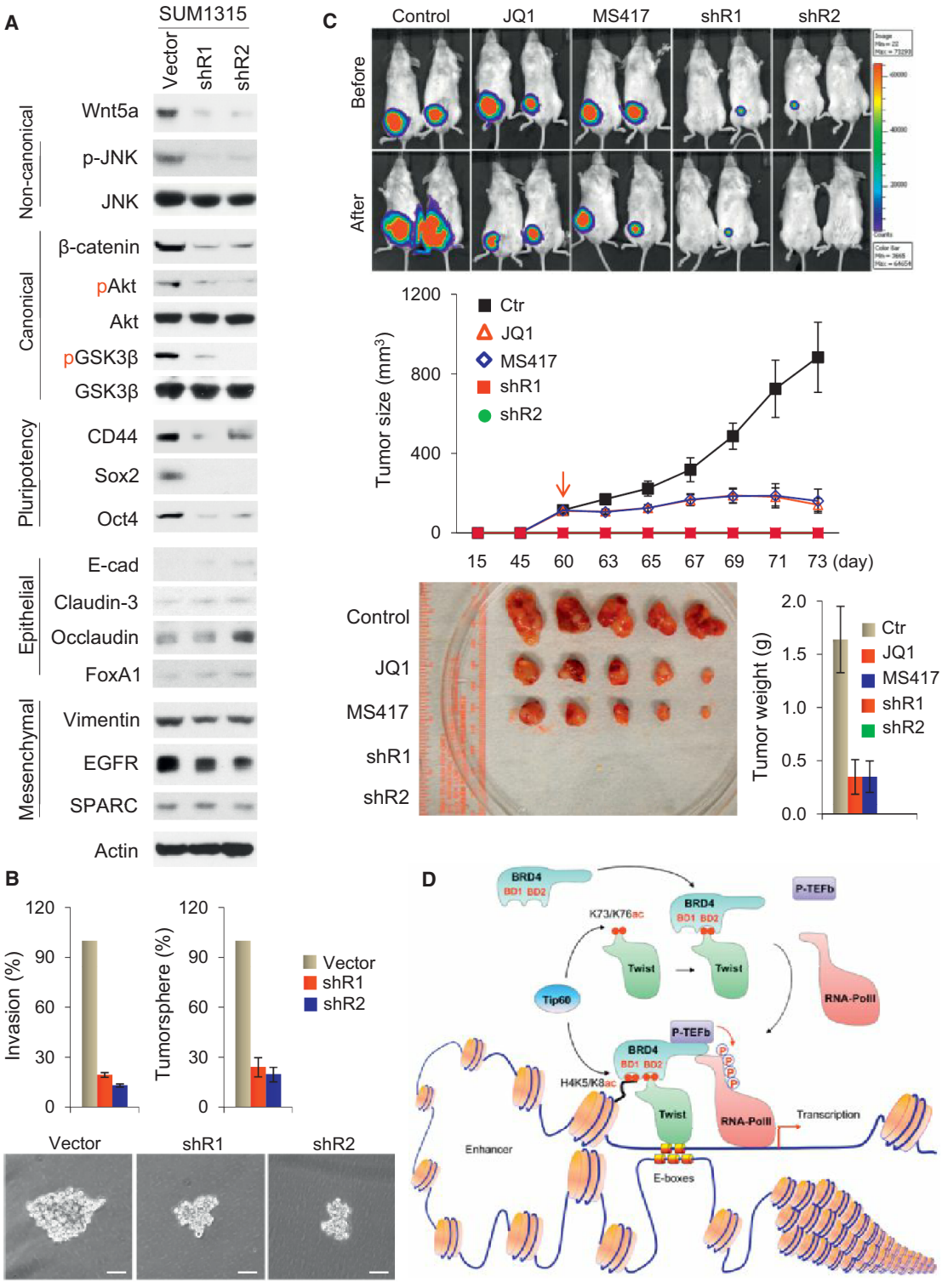

Figure 7. The Twist-BRD4-Wnt5a Axis Is Critical for Tumorigenicity In Vitro and In Vivo

(A) Expression of various molecules in SUM1315 cells with Wnt5a knockdown.

(B) Invasion and tumorsphere formation in SUM1315 cells with Wnt5a knockdown. Data are presented as a percentage of vector control values (mean ± SD in three separate experiments in duplicates). Representative pictures of tumorspheres are shown at the bottom. Scale bar, 100 μM.

(C) Vector control and Wnt5a knockdown SUM1315 cells were injected into the mammary fat pad of NOD-SCID mice. When tumors from mice injected with control cells reached 100 mm^3, mice were divided into three groups and treated with JQ1 (50 mg/Kg), MS417 (20 mg/Kg), or solvent control, respectively. The size

(legend continued on next page)

of wounds, and is also necessary for intestinal epithelial stem cells to regenerate damage tissues during wound healing and tissue repair (Miyoshi et al., 2012). The correlated expression of Twist and Wnt5a in BLBC supports our contention that the Twist-BRD4-Wnt5a signaling axis plays a critical role in the development and progression of BLBC.

Third, our study indicates that the Twist-BRD4 interaction represents a druggable target for treating BLBC. Although Twist is highly expressed in BLBC, the absence of a clear ligand-binding domain in Twist creates a formidable obstacle toward developing small molecules that inhibit its activity as a transcription factor. We found that BET-specific BD inhibitors disrupted the Twist-BRD4 interaction and resulted in significant Wnt5a reduction, leading to inhibition of invasion and tumorigenicity of BLBC cells in vitro and in vivo. Based on our mechanistic understanding of Twist-BRD4 interaction in gene transcription, we predict that selective chemical inhibition of BRD4/H4 interaction would result in a broad inhibition of BRD4 functions as chromatin regulator in gene transcription, whereas selective inhibition of the BRD4/transcription factor association might affect specific transcription factor's ability in their target gene activation. BD inhibitors selectively target BD2 over BD1 of BRD4 are needed to address these questions; they will also further functionally validate the effectiveness and therapeutic benefits of targeting BRD4 for treating BLBC.

EXPERIMENTAL PROCEDURES

Protein Purification and Mass Spectrometry Analysis

We generated a clone of HeLa S3 cells with stable expression of Flag-Twist (Li and Zhou, 2011). After enriching the nuclear extracts from 40 l of suspension culture, we carried out affinity protein purification with Flag affinity columns. The final eluted immunocomplexes were separated on SDS-PAGE, and the bound proteins were excised from the gel and subjected to nano-liquid chromatography-tandem mass spectrometry (nano-LC-MS/MS) analysis (Applied Biomics). For identification of the acetylated lysine residues on Twist, the acetylated Twist was digested with trypsin, and the tryptic peptides were analyzed by LC-MS/MS using an LTQ Velos Orbitrap mass spectrometer (Thermo Fisher Scientific) coupled with a nano-LC Ultra/CHiPLC Nanoflex high-performance liquid chromatography system (Eksigent) through a nanoelectrospray ionization source (Li et al., 2013). MS/MS data were acquired using CID fragmentation of selected peptides during the information-dependent acquisition. The LC-MS/MS results were subjected to protein identification and acetylation sites determination using ProteomeDiscoverer 1.3 software (Thermo Fisher Scientific) and MASCOT server.

Protein Structure Analysis by NMR

The NMR spectral collection, analysis, and structure determination of the BRD4-BD2 with Twist-K73ac/K76ac were performed as previously reported (Zhang et al., 2012). In brief, NMR samples contained a protein/peptide complex of 0.5 mM in a 100 mM sodium phosphate buffer (pH 6.5) that contains 5 mM perdeuterated dithiothreitol and 0.5 mM EDTA in $H_2O/^2H_2O$ (9/1) or ^2H_2O. All NMR spectra were collected at 30°C on NMR spectrometers of 800, 600, or 500 MHz. The ^1H, ^{13}C, and ^{15}N resonances of the protein in the complex were assigned by triple-resonance NMR spectra collected with a $^{13}C/^{15}N$-labeled and 75% deuterated BRD4-BD2 bound to an unlabeled Twist peptide (Clore and Gronenborn, 1994). The distance restraints were obtained from 3D ^{13}C-NOESY or ^{15}N-NOESY spectra. Protein structures were calculated with a distance geometry-simulated annealing protocol using X-PLOR (Brunger, 1993) that was aided with iterative automated NOE assignment by ARIA for refinement (Nilges and O'Donoghue, 1998). Structure quality was assessed by PROCHECK-NMR (Laskowski et al., 1996). The structure of the protein/ligand complex was determined using intermolecular NOE-derived distance restraints that were obtained from ^{13}C-edited (F_1), $^{13}C/^{15}N$-filtered (F_3) 3D NOESY spectra.

Immunoprecipitation, Immunoblotting, Immunofluorescence, Immunohistochemical Staining, RT-PCR, and ChIP

Detailed methods are provided in the Supplemental Experimental Procedures.

Tumorigenesis Assay

All procedures were approved by the Institutional Animal Care and Use Committee at the University of Kentucky College of Medicine and conform to the legal mandates and federal guidelines for the care and maintenance of laboratory animals. Animals were maintained and treated under pathogen-free conditions. Female NOD-SCID mice (6–8 weeks old; Taconic) were injected with breast cancer SUM1315 (2×10^6 cells/mouse) cells via mammary fat pad, and mice had three groups: vector control and two stable clones with Wnt5a-knockdown expression. Tumor growth was monitored with caliper measurements. When tumors were approximately 1.0 cm in size, mice were euthanized and tumors excised. Data were analyzed by Student's t test; $p < 0.05$ was considered significant.

Statistical Analysis

Data are presented as mean ± SD. A Student's t test (two-tailed) was used to compare two groups ($p < 0.05$ was considered significant) unless otherwise indicated.

ACCESSION NUMBERS

Microarray data of Twist expression in HMLE and T47D cells with or without JQ1 treatment were deposited at the Gene Expression Omnibus database with the accession number GSE53222. Structure factors and coordinates for the second bromodomain of BRD4 in complex with K73ac/K76ac diacetylated Twist peptide were deposited at the Protein Data Bank under ID code 2MJV, and the NMR spectral data were deposited at the BioMagResBank (BMRB) under BMRB accession number 19738.

SUPPLEMENTAL INFORMATION

Supplemental Information includes Supplemental Experimental Procedures, seven figures, and one table and can be found with this article online at http://dx.doi.org/10.1016/j.ccr.2014.01.028.

ACKNOWLEDGMENTS

We thank Cathy Anthony for critical reading and editing of this manuscript. We also thank Dr. Jing Chen for technical assistance on mass spectrometry analysis. We are grateful to Dr. James E. Bradner for providing JQ1, Dr. Robert A. Weinberg for HMLE cells, Dr. Michael Rosenblatt for SUM1315 cells, and Dr. Bruno Amati for Tip60 antibodies as valuable reagents for this study. This work was supported in part by grants from the National Institute of Health (CA125454 to B.P.Z., P20CA153043 to B.M.E., and HG004508 and CA87658 to M.-M.Z.), the American Cancer Society (RSG13187 to Y.W.), and the Nature Science Foundation of China (91129303 to J.D.). We acknowledge the University of Kentucky Proteomics Core, which is partially supported

of tumor was recorded by bioluminescence imaging before or after 2 week treatment. Tumor weight was also measured. Data are represented as a mean ± SEM from five mice.

(D) A proposed model illustrating the interaction of Twist and BRD4 at the enhancer/promoter of *WNT5A*, which leads to the transcriptional activation of *WNT5A* expression in EMT and BLBC.

See also Figure S7.

by grants from the National Cancer Institute (P30CA177558) and the National Institute of General Medical Sciences (P20GM103486).

Received: June 9, 2013
Revised: September 23, 2013
Accepted: January 24, 2014
Published: February 10, 2014

REFERENCES

Brunger, A.T. (1993). X-PLOR version 3.1: A system for X-ray Crystallography and NMR (version 3.1 edit.). (New Haven: Yale University Press).

Canzio, D., Liao, M., Naber, N., Pate, E., Larson, A., Wu, S., Marina, D.B., Garcia, J.F., Madhani, H.D., Cooke, R., et al. (2013). A conformational switch in HP1 releases auto-inhibition to drive heterochromatin assembly. Nature *496*, 377–381.

Clore, G.M., and Gronenborn, A.M. (1994). Multidimensional heteronuclear nuclear magnetic resonance of proteins. Methods Enzymol. *239*, 349–363.

Dawson, M.A., Prinjha, R.K., Dittmann, A., Giotopoulos, G., Bantscheff, M., Chan, W.I., Robson, S.C., Chung, C.W., Hopf, C., Savitski, M.M., et al. (2011). Inhibition of BET recruitment to chromatin as an effective treatment for MLL-fusion leukaemia. Nature *478*, 529–533.

Delmore, J.E., Issa, G.C., Lemieux, M.E., Rahl, P.B., Shi, J., Jacobs, H.M., Kastritis, E., Gilpatrick, T., Paranal, R.M., Qi, J., et al. (2011). BET bromodomain inhibition as a therapeutic strategy to target c-Myc. Cell *146*, 904–917.

Doyon, Y., and Côté, J. (2004). The highly conserved and multifunctional NuA4 HAT complex. Curr. Opin. Genet. Dev. *14*, 147–154.

Filippakopoulos, P., Picaud, S., Mangos, M., Keates, T., Lambert, J.P., Barsyte-Lovejoy, D., Felletar, I., Volkmer, R., Müller, S., Pawson, T., et al. (2012). Histone recognition and large-scale structural analysis of the human bromodomain family. Cell *149*, 214–231.

Jang, M.K., Mochizuki, K., Zhou, M., Jeong, H.S., Brady, J.N., and Ozato, K. (2005). The bromodomain protein Brd4 is a positive regulatory component of P-TEFb and stimulates RNA polymerase II-dependent transcription. Mol. Cell *19*, 523–534.

Laskowski, R.A., Rullmannn, J.A., MacArthur, M.W., Kaptein, R., and Thornton, J.M. (1996). AQUA and PROCHECK-NMR: programs for checking the quality of protein structures solved by NMR. J. Biomol. NMR *8*, 477–486.

Leptin, M. (1991). twist and snail as positive and negative regulators during Drosophila mesoderm development. Genes Dev. *5*, 1568–1576.

Li, J., and Zhou, B.P. (2011). Activation of β-catenin and Akt pathways by Twist are critical for the maintenance of EMT associated cancer stem cell-like characters. BMC Cancer *11*, 49.

Li, X., Zhou, Q., Sunkara, M., Kutys, M.L., Wu, Z., Rychahou, P., Morris, A.J., Zhu, H., Evers, B.M., and Huang, C. (2013). Ubiquitylation of phosphatidylinositol 4-phosphate 5-kinase type I γ by HECTD1 regulates focal adhesion dynamics and cell migration. J. Cell Sci. *126*, 2617–2628.

Lovén, J., Hoke, H.A., Lin, C.Y., Lau, A., Orlando, D.A., Vakoc, C.R., Bradner, J.E., Lee, T.I., and Young, R.A. (2013). Selective inhibition of tumor oncogenes by disruption of super-enhancers. Cell *153*, 320–334.

Marazzi, I., Ho, J.S., Kim, J., Manicassamy, B., Dewell, S., Albrecht, R.A., Seibert, C.W., Schaefer, U., Jeffrey, K.L., Prinjha, R.K., et al. (2012). Suppression of the antiviral response by an influenza histone mimic. Nature *483*, 428–433.

Miyoshi, H., Ajima, R., Luo, C.T., Yamaguchi, T.P., and Stappenbeck, T.S. (2012). Wnt5a potentiates TGF-β signaling to promote colonic crypt regeneration after tissue injury. Science *338*, 108–113.

Morinière, J., Rousseaux, S., Steuerwald, U., Soler-López, M., Curtet, S., Vitte, A.L., Govin, J., Gaucher, J., Sadoul, K., Hart, D.J., et al. (2009). Cooperative binding of two acetylation marks on a histone tail by a single bromodomain. Nature *461*, 664–668.

Nilges, M., and O'Donoghue, S. (1998). Ambiguous NOEs and automated NOE assignment. Prog. Nucl. Magn. Reson. Spectrosc. *32*, 107–139.

Rakha, E.A., Reis-Filho, J.S., and Ellis, I.O. (2008). Basal-like breast cancer: a critical review. J. Clin. Oncol. *26*, 2568–2581.

Rekowski, Mv., and Giannis, A. (2010). Histone acetylation modulation by small molecules: a chemical approach. Biochim. Biophys. Acta *1799*, 760–767.

Ruthenburg, A.J., Li, H., Milne, T.A., Dewell, S., McGinty, R.K., Yuen, M., Ueberheide, B., Dou, Y., Muir, T.W., Patel, D.J., and Allis, C.D. (2011). Recognition of a mononucleosomal histone modification pattern by BPTF via multivalent interactions. Cell *145*, 692–706.

Scheel, C., Eaton, E.N., Li, S.H., Chaffer, C.L., Reinhardt, F., Kah, K.J., Bell, G., Guo, W., Rubin, J., Richardson, A.L., and Weinberg, R.A. (2011). Paracrine and autocrine signals induce and maintain mesenchymal and stem cell states in the breast. Cell *145*, 926–940.

Thiery, J.P., Acloque, H., Huang, R.Y., and Nieto, M.A. (2009). Epithelial-mesenchymal transitions in development and disease. Cell *139*, 871–890.

Witze, E.S., Litman, E.S., Argast, G.M., Moon, R.T., and Ahn, N.G. (2008). Wnt5a control of cell polarity and directional movement by polarized redistribution of adhesion receptors. Science *320*, 365–369.

Wu, S.Y., Lee, A.Y., Lai, H.T., Zhang, H., and Chiang, C.M. (2013). Phospho switch triggers Brd4 chromatin binding and activator recruitment for gene-specific targeting. Mol. Cell *49*, 843–857.

Zeitlinger, J., Zinzen, R.P., Stark, A., Kellis, M., Zhang, H., Young, R.A., and Levine, M. (2007). Whole-genome ChIP-chip analysis of Dorsal, Twist, and Snail suggests integration of diverse patterning processes in the Drosophila embryo. Genes Dev. *21*, 385–390.

Zeng, L., Zhang, Q., Li, S., Plotnikov, A.N., Walsh, M.J., and Zhou, M.M. (2010). Mechanism and regulation of acetylated histone binding by the tandem PHD finger of DPF3b. Nature *466*, 258–262.

Zhang, G., Liu, R., Zhong, Y., Plotnikov, A.N., Zhang, W., Zeng, L., Rusinova, E., Gerona-Nevarro, G., Moshkina, N., Joshua, J., et al. (2012). Down-regulation of NF-κB transcriptional activity in HIV-associated kidney disease by BRD4 inhibition. J. Biol. Chem. *287*, 28840–28851.

Zhou, Q., Li, T., and Price, D.H. (2012). RNA polymerase II elongation control. Annu. Rev. Biochem. *81*, 119–143.

Zuber, J., Shi, J., Wang, E., Rappaport, A.R., Herrmann, H., Sison, E.A., Magoon, D., Qi, J., Blatt, K., Wunderlich, M., et al. (2011). RNAi screen identifies Brd4 as a therapeutic target in acute myeloid leukaemia. Nature *478*, 524–528.

Find your way with Cell Press Reviews

Whether you're looking for answers to fundamental questions, brushing up on a new subject or looking for a synthesis on a hot topic, turn to Cell Press Reviews. We publish reviews in a vast array of disciplines spanning the life sciences.

Propel your research forward, faster with Cell Press Reviews. Our insightful, authoritative reviews—published in our primary research and Trends journals—go beyond synthesis and offer a point of view.

www.cell.com/reviews

CellPress
Your work is our life

Cancer Cell
Article

Stromal Elements Act to Restrain, Rather Than Support, Pancreatic Ductal Adenocarcinoma

Andrew D. Rhim,[1,2,8] Paul E. Oberstein,[3,8] Dafydd H. Thomas,[4,5,8] Emily T. Mirek,[2] Carmine F. Palermo,[4,5] Stephen A. Sastra,[4,5] Erin N. Dekleva,[2] Tyler Saunders,[6] Claudia P. Becerra,[5] Ian W. Tattersall,[5] C. Benedikt Westphalen,[4] Jan Kitajewski,[5] Maite G. Fernandez-Barrena,[7] Martin E. Fernandez-Zapico,[7] Christine Iacobuzio-Donahue,[6] Kenneth P. Olive,[4,5,*] and Ben Z. Stanger[2,*]

[1]Division of Gastroenterology, Department of Internal Medicine and Comprehensive Cancer Center, University of Michigan Medical School, Ann Arbor, MI 48109, USA
[2]Gastroenterology Division, Department of Medicine and Abramson Family Cancer Research Institute, Perelman School of Medicine, University of Pennsylvania, Philadelphia, PA 19104, USA
[3]Division of Hematology and Oncology
[4]Division of Digestive and Liver Diseases in the Department of Medicine
[5]Department of Pathology and Cell Biology
Herbert Irving Comprehensive Cancer Center, Columbia University Medical Center, New York, NY 10032, USA
[6]Sol Goldman Pancreatic Cancer Research Center and Department of Pathology, Johns Hopkins University, Baltimore, MD 21287, USA
[7]Schulze Center for Novel Therapeutics, Mayo Clinic, Rochester, MN 55905, USA
[8]Co-first author
*Correspondence: kenolive@columbia.edu (K.P.O.), bstanger@exchange.upenn.edu (B.Z.S.)
http://dx.doi.org/10.1016/j.ccr.2014.04.021

SUMMARY

Sonic hedgehog (Shh), a soluble ligand overexpressed by neoplastic cells in pancreatic ductal adenocarcinoma (PDAC), drives formation of a fibroblast-rich desmoplastic stroma. To better understand its role in malignant progression, we deleted Shh in a well-defined mouse model of PDAC. As predicted, Shh-deficient tumors had reduced stromal content. Surprisingly, such tumors were more aggressive and exhibited undifferentiated histology, increased vascularity, and heightened proliferation—features that were fully recapitulated in control mice treated with a Smoothened inhibitor. Furthermore, administration of VEGFR blocking antibody selectively improved survival of Shh-deficient tumors, indicating that Hedgehog-driven stroma suppresses tumor growth in part by restraining tumor angiogenesis. Together, these data demonstrate that some components of the tumor stroma can act to restrain tumor growth.

INTRODUCTION

Pancreatic ductal adenocarcinoma (PDAC) is notable for its profuse desmoplastic stroma comprised of activated fibroblasts, leukocytes, and extracellular matrix (Olive et al., 2009; Theunissen and de Sauvage, 2009). Studies utilizing in vitro assays and transplantation models have concluded that various stromal elements can enhance cancer cell proliferation and invasion (Hwang et al., 2008; Ikenaga et al., 2010; Lonardo et al., 2012; Vonlaufen et al., 2008; Xu et al., 2010). Various stromal cells can also contribute to immune suppression, further supporting tumor survival and growth. Together, these observations have led to the paradigm that tumor stroma functions to support and promote the growth of cancer (Hanahan and Weinberg, 2011). Based on this paradigm, the concept of "antistromal" therapy has emerged as a

Significance

Numerous therapies are being developed based on the premise that tumor stroma functions to promote cancer growth and invasion while simultaneously limiting the delivery of chemotherapy. Here, we demonstrate that depletion of stromal cells from pancreatic tumors—through genetic or pharmacological targeting of the Hh pathway—results in a poorly differentiated histology, increased vascularity and proliferation, and reduced survival. The study thus provides insight into the failure of Smoothened inhibitors, an antistromal therapy, in pancreatic cancer clinical trials. Moreover, we report that Hh-deficient tumors exhibit an increased sensitivity to VEGFR inhibition. Because poorly differentiated human pancreatic tumors are well-vascularized, in contrast to most pancreatic cancers, our results suggest that this patient subset may be susceptible to angiogenesis inhibitors.

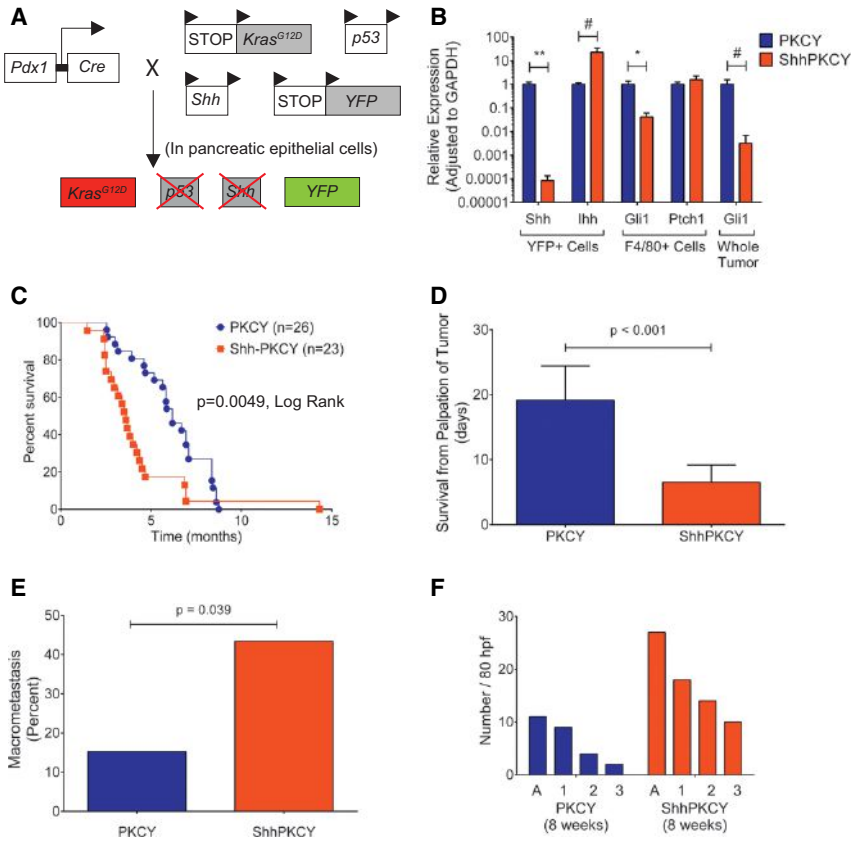

Figure 1. Sonic Hedgehog Behaves as a Tumor Suppressor in a Genetically Engineered Mouse Model of PDAC

(A) Schematic of the ShhPKCY mouse model used in this study, which employs the *Kras*^{G12D} (K), *Pdx1-Cre* (C), *p53* (P), *Rosa*^{YFP} (Y), and *Shh* alleles. Cre-mediated deletion results in simultaneous activation of *Kras*, deletion of one allele of *p53*, and both alleles of *Shh* and recombination of the *YFP* lineage label.

(B) Confirmation of Shh knockdown in ShhPKCY animals. Quantitative PCR analysis of Hedgehog signaling components in YFP$^+$ sorted pancreatic epithelial derived cells and F4/80$^+$ cells from tumors as well as whole tumor derived from PKCY (blue) and ShhPKCY (red) mice (n = 5 for each group; bars represent means ± SD).

(C) Kaplan-Meier survival analysis for PKCY (n = 26) and ShhPKCY mice (n = 23). $p < 0.005$ by Mantel-Cox (log rank) test.

(D) Survival of mice from first clinical palpation of tumor. Presence of tumor was confirmed by ultrasound. Bars represent means ± SD; $p < 0.001$.

(E) Fraction of mice with any macrometastatic lesion by visual inspection at the time of tissue harvest by genotype (n = 26 and 23 for PKCY and ShhPKCY mice, respectively). $p = 0.039$.

(F) Quantitation of acinar to ductal metaplasia (bar A) and PanIN lesions by grade (bars 1–3) in 8-week-old PKCY and ShhPKCY mice. Eighty nonoverlapping high powered fields in which pancreas tissue covered at least 90% of the entire field were analyzed (n = 3 for each group).

Data are presented as the aggregate number of ADMs and PanINs (by grade) for each genotype. #, $p < 0.05$; *, $p < 0.01$; **, $p < 0.001$ by two-tailed Student's t test. See also Figure S1.

promising, albeit unproven, therapeutic approach (Engels et al., 2012).

The Hedgehog (Hh) signaling pathway contributes to stromal desmoplasia in multiple solid tumor systems. Although normally absent in the adult pancreas, this developmental morphogen pathway is reactivated during inflammation and neoplasia. Both sonic hedgehog (Shh) ligand and downstream signaling are induced de novo in preneoplastic lesions and increase significantly during PDAC progression as the stromal compartment enlarges (Thayer et al., 2003). Although ectopic activation of Hh signaling within pancreatic epithelial cells can accelerate tumorigenesis (Mao et al., 2006; Morton et al., 2007; Pasca di Magliano et al., 2006), deletion of the Hh signaling mediator Smoothened (Smo) from the epithelium has no impact on PDAC progression (Nolan-Stevaux et al., 2009). Hence, canonical Hh signaling in PDAC is likely to occur in a paracrine fashion, whereby Shh ligand secreted from epithelial cells activates Smo-dependent downstream signaling in adjacent stromal cells, promoting desmoplasia (Bailey et al., 2008; Tian et al., 2009). The notion that Hh-dependent tumor stroma facilitates tumorigenesis is supported by the finding that inhibiting Hh signaling retards pancreatic tumor growth and metastasis in transplantation models (Bailey et al., 2008; Feldmann et al., 2008a, 2008b) and through our own study of the effects of acute inhibition of Smo in genetically engineered mouse models (Olive et al., 2009). In this study, we sought to interrogate the role of the tumor stroma by using both genetic deletion and long-term pharmacologic inhibition to eliminate stroma-promoting Hh signaling.

RESULTS

Shh Loss Accelerates PDAC Progression

To explore the role of paracrine Hh signaling in an autochthonous mouse model of PDAC, we conditionally deleted *Shh*, the predominant Hh ligand expressed in the diseased pancreas, by breeding Shh^{fl} alleles into the *Pdx1-Cre;Kras*$^{LSL\text{-}G12D/+}$*;p53*$^{fl/+}$*;Rosa26*$^{LSL\text{-}YFP/+}$ (PKCY) model (Rhim et al., 2012). Because *Pdx1-Cre* mediates recombination exclusively in the epithelial cells of the pancreas (Rhim et al., 2012), this combination of alleles results in the simultaneous activation of mutant *Kras* and deletion of *Shh* and *p53* within this tissue compartment (Figure 1A). *Shh* deletion had no effect on pancreatic development (Figure S1A available online), and the resulting *Shh*$^{fl/fl}$*;Pdx1-Cre;Kras*$^{LSL\text{-}G12D/+}$*;p53*$^{fl/+}$*;Rosa26*$^{LSL\text{-}YFP}$ (ShhPKCY) mice were born at expected Mendelian ratios and were phenotypically normal at birth.

To confirm the deletion of *Shh* in the pancreatic epithelial compartment, we performed transcriptional analysis on FACS-sorted yellow fluorescent protein (YFP$^+$) cells from 10- to 16-week-old PKCY and ShhPKCY mice (Rhim et al., 2012). As predicted, Shh transcripts were markedly reduced in YFP$^+$ pancreatic epithelial cells from ShhPKCY mice (Figure 1B).

Interestingly, this decrease in Shh transcription was accompanied by a 10-fold increase in the expression of Indian hedgehog (Ihh), another Hh ligand, although absolute levels of Ihh remained significantly lower than Shh. Desert hedgehog was undetectable under all conditions (data not shown). We then determined the impact of Shh deletion on signaling within the stromal compartment by measuring the expression of the Hh target genes Ptch1 and Gli1 in sorted PDAC-associated F4/80$^+$ monocytes and whole pancreas, as previously described (El-Zaatari et al., 2013). Although Ptch1 expression was similar, transcript levels for Gli1 were significantly decreased in ShhPKCY samples as compared to PKCY samples, indicating that overall Hh signaling was reduced following Shh deletion (Figure 1B).

Given the important role of Shh in promoting the desmoplastic stroma of PDAC, we expected that Shh loss would impair tumorigenesis. Surprisingly, however, pancreatic tumors arose in both PKCY and ShhPKCY mice, demonstrating that Shh is dispensable for tumorigenesis. Remarkably, ShhPKCY mice developed tumors earlier and had a significantly decreased survival compared to PKCY mice ($p < 0.001$ by log rank [Mantel-Cox] test; Figure 1C). Specifically, ShhPKCY mice had a median survival of 3.61 ± 1.97 months as compared to a median survival of 6.17 ± 2.65 months for PKCY mice (Figure S1B). Heterozygous *Shh$^{fl/+}$;Pdx-Cre; Kras$^{LSL\text{-}G12D/+}$;p53$^{fl/+}$;Rosa26$^{LSL\text{-}YFP}$* (*Shh$^{fl/+}$*PKCY) mice that retained one copy of *Shh* also had reduced median survival compared to PKCY mice (4.14 ± 1.57 months, $p = 0.004$; Figure S1B). ShhPKCY tumors were more aggressive than PKCY tumors, because mean survival from first detection of tumor was significantly shorter in ShhPKCY mice (19.2 ± 5.27 versus 6.5 ± 2.7 days, $p < 0.001$; Figure 1D), and the frequency of gross metastasis was higher in ShhPKCY mice than in PKCY mice (43.4 versus 15.3%, $p = 0.039$ by chi-squared test; Figure 1E), although the tissue distribution of macrometastases was similar (Figure S1C). Moreover, histological analysis revealed a higher frequency of acinar-to-ductal metaplasia (ADM) and pancreatic intraepithelial neoplasia (PanIN) of all grades in 8-week-old ShhPKCY compared to PKCY mice (Figure 1F). These data indicate that Shh is not merely dispensable for pancreatic tumorigenesis, but that it somehow restrains tumor progression and aggressiveness.

Shh Loss Is Associated with Changes in Stromal Composition

Next, we compared the histology of ShhPKCY and PKCY tumors. In contrast to the well-differentiated to moderately differentiated histology of most PKCY tumors, ShhPKCY tumors exhibited predominantly undifferentiated and poorly differentiated histology, with few of the ductal elements observed in most PKCY and human pancreatic tumors (Figures 2A and 2B; Figure S2A). ShhPKCY tumors also exhibited a significant increase in Zeb1 and Slug expression, two markers of epithelial-to-mesenchymal transition, consistent with the predominance of poorly differentiated and undifferentiated histology (Singh et al., 2009; Watanabe et al., 2009) (Figure S2B; $p < 0.05$).

Using the YFP lineage label to distinguish epithelial-derived cancer cells from mesenchyme-derived stromal cells, we found that Shh-deficient tumors had significantly reduced stroma, as indicated by decreased numbers of YFP-negative alpha smooth muscle actin (SMA)-positive myofibroblasts (3.7% ± 0.7% versus 16.7% ± 3.2% of all DAPI+ cells within pancreas tumors; $p = 0.016$; Figures 2C and 2D). Despite their increased aggressiveness (but consistent with stromal loss), ShhPKCY tumors exhibited a trend toward decreased weight (Figure S1B). In addition, ShhPKCY tumors had fewer CD45$^+$ myeloid cells (4.9% ± 0.9% versus 36.7% ± 5.2%; $p = 0.0039$; Figures 2E and 2F) and F4/80$^+$ monocytes (2.8% ± 0.5% versus 15.5% ± 2.7%; $p = 0.010$; Figures 2G and 2H). Indeed, the stromal cell composition of ShhPKCY tumors was similar to that of normal pancreas tissue from *Pdx1-Cre;Rosa26$^{LSL\text{-}YFP/+}$* mice (data not shown). These results demonstrate that robust tumor formation can occur in the absence of a fibroblast- and leukocyte-rich desmoplastic stroma.

Because ShhPKCY tumors progressed more rapidly than their PKCY counterparts, we hypothesized that parallel but opposite changes in tumor vasculature might influence tumor growth. Hence, we examined the endothelial compartment in tumors with and without Shh by CD31 staining. Consistent with this hypothesis, ShhPKCY tumors exhibited a substantial increase in the number of blood vessels within the tumor (32.4 ± 7.2 versus 11.2 ± 3.8 CD31$^+$ vessels per high powered field; $p = 0.0004$; Figures 3A and 3B). In addition, the autofluorescent drug doxorubicin was delivered more effectively to ShhPKCY tumors, suggesting that increased vascular density was accompanied by greater perfusion (Figures 3C and 3D). To assess whether this increase in vasculature was associated with changes in autophagy or proliferation, we stained for the autophagosome marker LC3 and the proliferation marker proliferating cell nuclear antigen (PCNA). This analysis revealed a decrease in YFP$^+$LC3$^+$ cells in ShhPKCY tumors (Figures 3E and 3F) and an increase in the frequency of YFP$^+$PCNA$^+$ proliferating tumor cells (Figures 3G and 3H). These data therefore suggest that undifferentiated ShhPKCY tumors are better perfused than PKCY tumors, a change that was associated with enhanced nutrient delivery, decreased autophagy, and increased proliferation.

Chronic Smoothened Inhibition Phenocopies Shh Deletion

We next sought to learn whether the effect of Shh deletion in pancreatic cancer is mediated by canonical Hh signaling. We utilized IPI-926 (Infinity Pharmaceuticals), a targeted inhibitor of Smo, to inhibit canonical Hh signaling in KPC mice (a PDAC model closely related to the PKCY model). We previously performed a preclinical evaluation of IPI-926 in KPC mice harboring large (6–9 mm) pancreatic tumors and found that the combination of IPI-926 and the nucleoside analog gemcitabine (gem) resulted in extension of overall survival (Olive et al., 2009), a finding at odds with the observed effect of genetic Shh deletion. We reasoned that long-term, chronic exposure to Smo inhibition might unveil indirect responses related to the depletion of stroma from tumors rather than the acute response to improved drug delivery. Therefore, we treated KPC mice with IPI-926 alone or vehicle beginning at 8 weeks of age, a time point at which ADM and PanIN lesions are present but at which mice have not yet developed tumors (Figure S3A; see Supplemental Experimental Procedures for additional details).

Strikingly, IPI-926-treated KPC mice exhibited a reduction in overall survival compared to vehicle-treated mice (121 versus 156 days, $p < 0.0001$ by log rank test; Figure 4A). This result

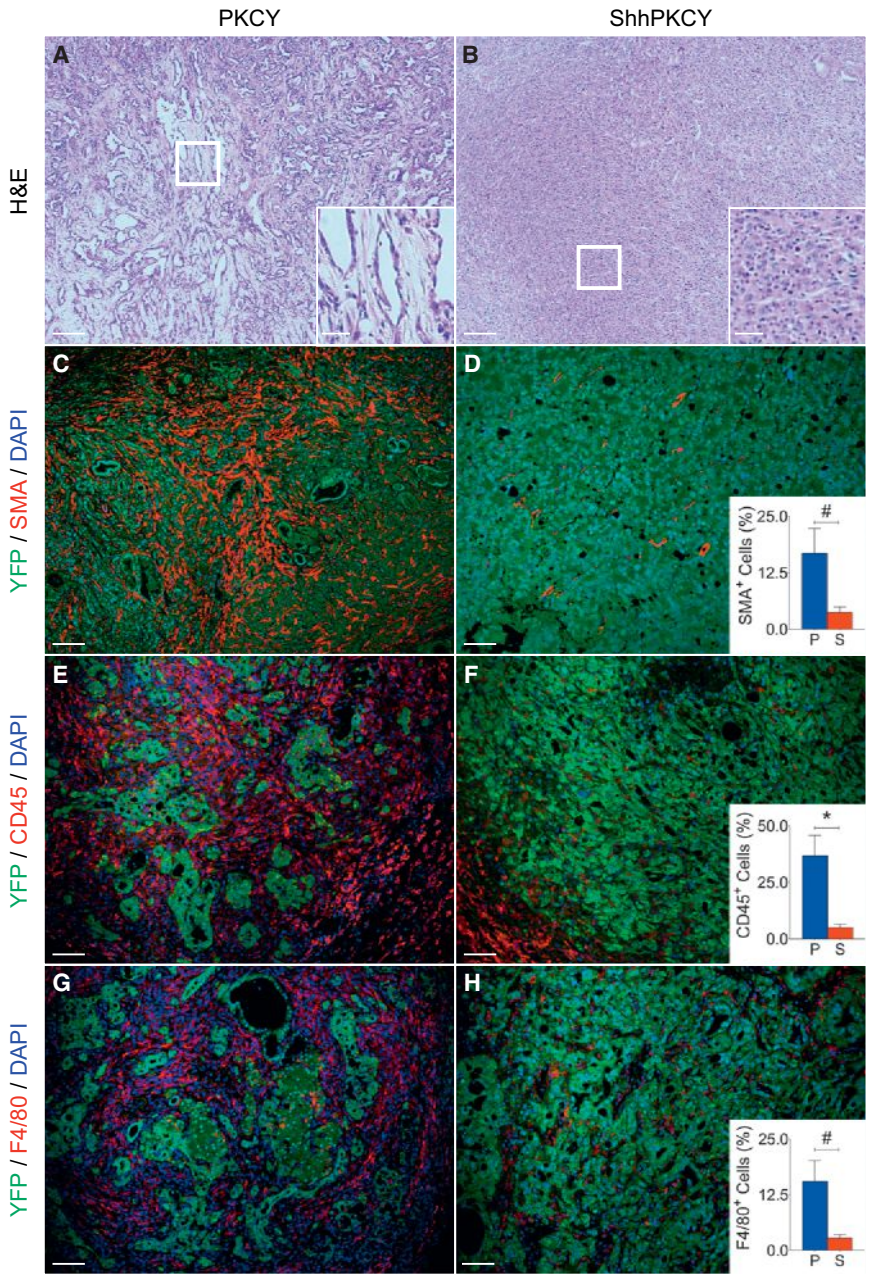

Figure 2. Loss of Shh Leads to a Shift in Pancreatic Tumor Histopathology

(A and B) H&E staining showing representative histology from PKCY (A) and ShhPKCY (B) tumors. Insets show higher magnified view of sections marked by the box.

(C–H) Multicolor immunofluorescence images of PKCY (left column) and ShhPKCY tumors (right column) assessed for myofibroblasts (C and D), total leukocytes (E and F), or macrophages (G and H).

(C and D) Fluorescent images showing staining with the pancreas epithelial lineage label YFP (green) and the myofibroblast marker alpha-SMA (red). Inset, quantitation of SMA+ cells as a percentage of all nucleated (DAPI+) cells within PKCY (blue) and ShhPKCY (red) tumors (n = 3–5; #, p = 0.016; bars represent means ± SD).

(E and F) Fluorescent images showing staining with YFP (green) and the pan-leukocyte marker CD45 (red). Inset, quantitation of $CD45^+$ cells as a percentage of all nucleated ($DAPI^+$) cells (n = 3–5; *, p = 0.0039; bars represent means ± SD).

(G and H) Fluorescent images showing staining with YFP (green) and the macrophage marker F4/80 (red). Inset, quantitation of $F4/80^+$ cells as a percentage of all nucleated (DAPI+) cells (n = 3–5; #, p = 0.010; bars represent means ± SD).

Scale bars, 40 μm for main panels and 20 μm for insets. See also Figure S2.

diverged dramatically from those obtained in our previous intervention study (Olive et al., 2009), despite the fact that the model, drug, dose, route, and schedule were all identical. In an effort to replicate this result and also determine whether coadministration of gemcitabine might change the dynamics of tumor response, we treated a separate cohort of mice with the combination of gemcitabine + IPI-926 or gemcitabine + vehicle. As shown in Figure 4B, the addition of gemcitabine provided a minor extension of survival over IPI-926 monotherapy (p = 0.01, log rank), but the IPI-926-gem combination therapy still resulted in shortened survival compared to vehicle-treated mice from the previous cohort. These results suggest that any benefit afforded by improved drug availability following Smo inhibition is outweighed by other effects on tumor biology in the chronic setting.

Analysis of 3D high resolution ultrasound data (Sastra and Olive, 2013) demonstrated that KPC mice treated with IPI-926 or IPI-926-gemcitabine succumbed more rapidly following initial tumor detection (Figure 4C) and that tumor size was significantly smaller at sacrifice (Figure 4D), similar to the reduced tumor weight observed in ShhPKCY mice (Figure S1B). Indeed, several mice met endpoint criteria before it was possible to detect tumors in their pancreas by ultrasound. However, all but one of these mice was found to have tumors upon careful histopathological analysis. There was no difference in the age at which tumors developed between the two groups, suggesting that IPI-926 treatment accelerates tumor progression after initiation without reducing latency (Figure 4E). Complete tumor volume data for these mice are presented in Figures 4F and 4G.

To better understand why IPI-926-treated mice with very small tumors were dying, we performed detailed necropsies on each mouse and assigned a "proximal cause of death" to each animal. Vehicle- or gem-treated KPC mice typically succumbed to the consequences of locally destructive disease (e.g., local invasion into the gut or abdominal hemorrhage) or high metastatic burden, with only a small subset exhibiting severe weight loss. By contrast, nearly all of the IPI-926-treated mice were euthanized following a period of rapid and severe weight loss

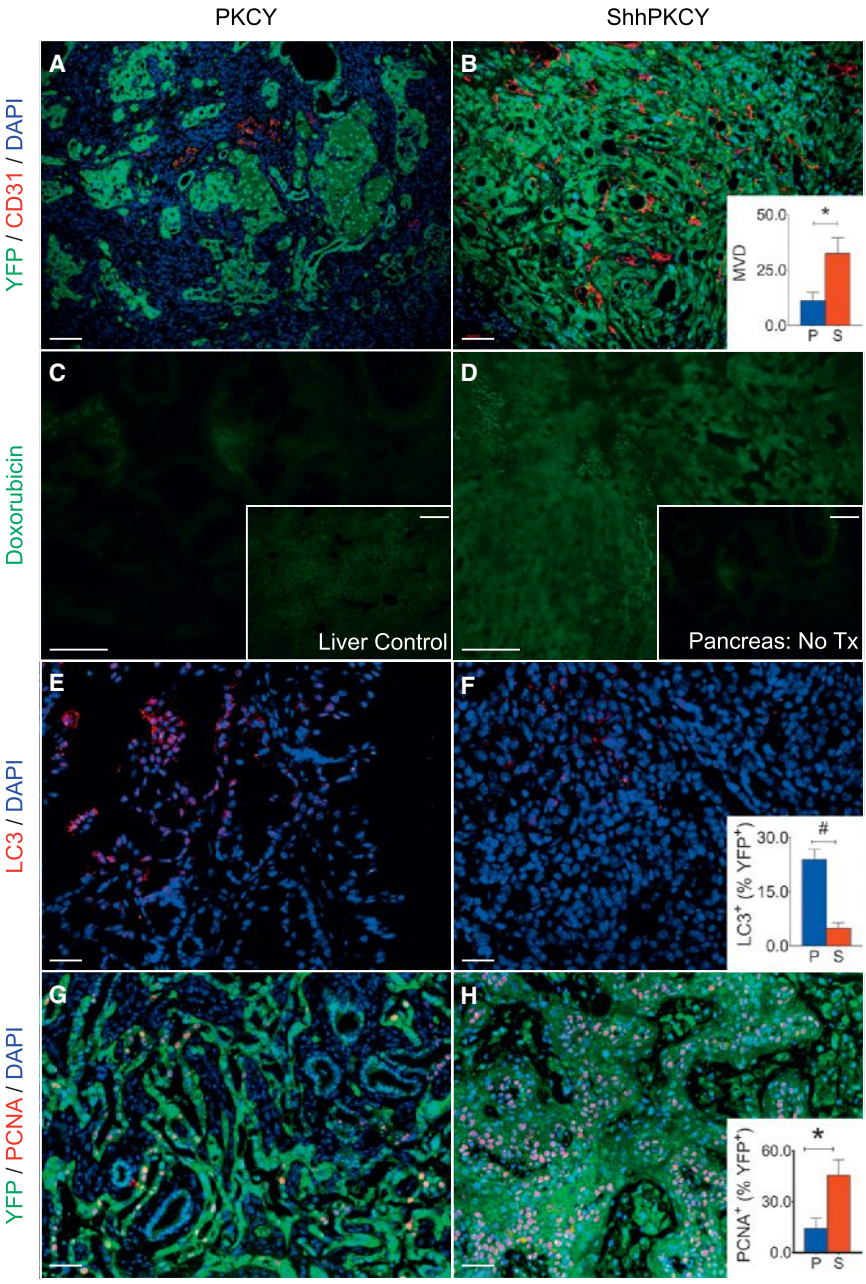

Figure 3. Shh Deletion Results in Greater Vascular Density and Proliferation within Pancreatic Tumors

(A and B) Blood vessel density in PKCY and ShhPKCY tumors was determined by staining for the endothelial marker CD31 (red) and the tumor cell lineage marker YFP (green). Inset, measurement of mean vascular density (MVD) within PKCY (blue) and ShhPKCY (red) tumors (quantified as number of $CD31^+$ vessels per high powered field; n = 3–5; *, p = 0.004; bars represent means ± SD). No Tx, no treatment.

(C and D) Cellular perfusion in PKCY and ShhPKCY tumors was determined by intravascular delivery of the autofluorescent drug doxorubicin. The inset in C shows fluorescence of a liver section from the same PKCY mouse (positive control). The inset in D shows fluorescence of a ShhPKCY tumor injected with PBS (negative control).

(E and F) Autophagy in PKCY and ShhPKCY tumors was determined by staining for the autophagosomal protein LC3 (red). Inset, percentage of $LC3^+$ cells within the YFP^+ tumor cell population in PKCY (blue) and ShhPKCY (red) tumors (n = 3–5; #, p = 0.002; bars represent means ± SD).

(G and H) Proliferation in PKCY and ShhPKCY tumors was determined by staining for the cell cycle marker PCNA (red). Inset, percentage of $PCNA^+$ cells within the YFP^+ tumor cell population in PKCY (blue) and ShhPKCY (red) tumors (n = 3–5; *, p = 0.004; bars represent means ± SD). Scale bars, 40 μm.

(Figures S3B and S3C), a phenomenon also observed in ShhPKCY animals (data not shown).

The tumors arising in IPI-926-treated mice were more poorly differentiated than those arising in controls treated with vehicle or gem alone (Figures 5A–5F), consistent with the observation that ShhPKCY mice developed poorly differentiated tumors. It is worth highlighting a pair of noteworthy exceptions that emphasize the relationship between differentiation state and tumor progression: one IPI-926-treated tumor was extremely well-differentiated and progressed slowly, whereas one vehicle-treated mouse succumbed at an early time point from a small tumor that was 50% poorly differentiated (Figure 4F, highlighted). Examination of pancreatic tissues adjacent to the tumors revealed an exceptionally high content of ADMs and PanINs in IPI-926-treated mice (Figures S4A–S4D). This feature was not shared in IPI-926+gemcitabine-treated mice, possibly because of the impact of genotoxic chemotherapy on the proliferation of preneoplastic lesions. Immunohistochemical analyses revealed that IPI-926-treated tumors were more highly proliferative (Figure 5G; Figures S4E–S4H) and had increased vascular content (Figure 5H; Figures S4I–S4L). Together, these data demonstrate that pharmacologic inhibition of canonical Hedgehog signaling accelerates tumor growth, phenocopying the effect of genetic deletion of Shh in pancreatic tumors.

Hedgehog Signaling Acts in a Paracrine Fashion in PDAC

During embryonic endoderm development, Hedgehog ligand is secreted by gut epithelial cells and acts on adjacent mesenchymal cells to pattern the submucosal layers of the gut (Roberts et al., 1998; Sukegawa et al., 2000). Given strong evidence from previous literature that Hedgehog signaling acts in a paracrine fashion during pancreatic carcinogenesis (Bailey et al., 2008; Tian et al., 2009), we sought to determine whether a similar signaling relay was operating in the autochthonous models. To this end, we introduced a *Gli1*^{GFP} reporter (Brownell et al., 2011) into the KPC background and assessed the distribution

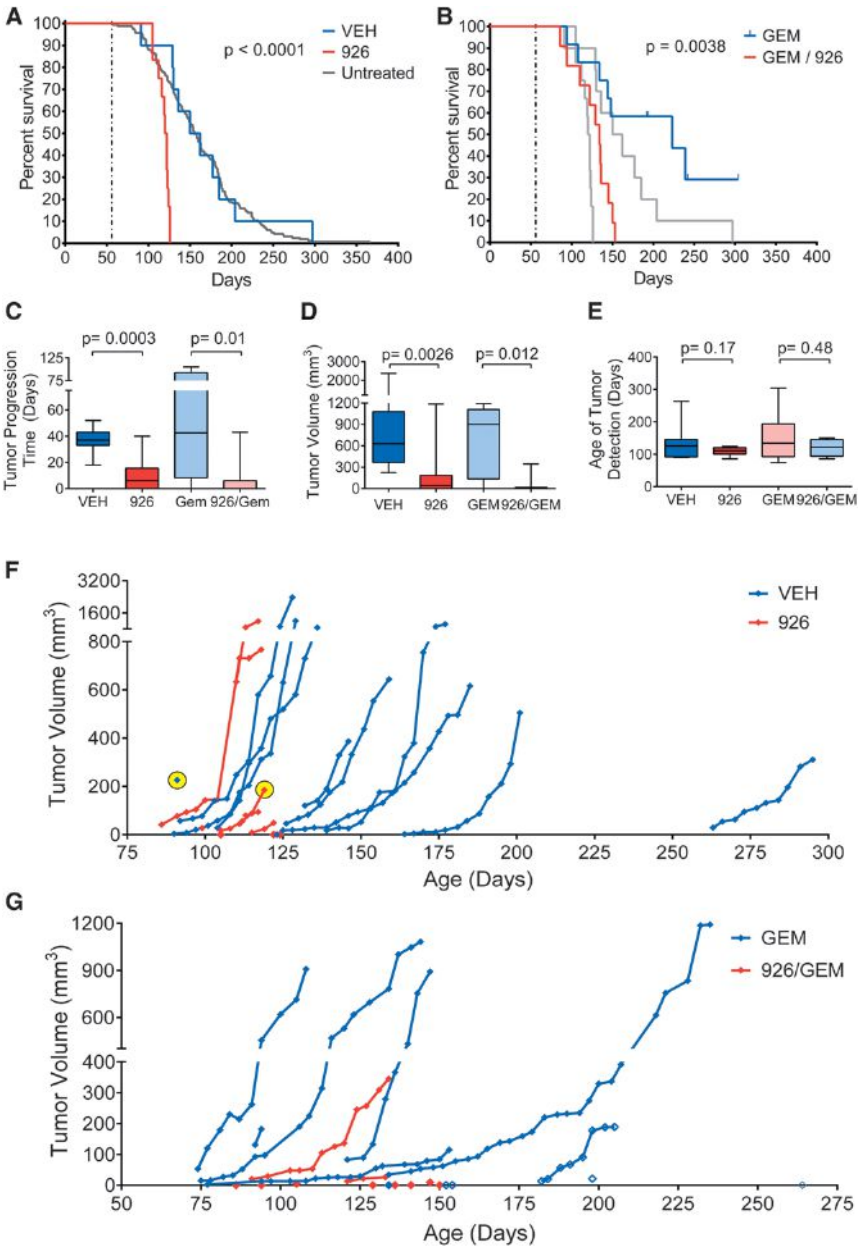

Figure 4. Smoothened Inhibition Accelerates Pancreatic Tumor Development

(A–G) Two separate cohorts of KPC mice were treated with vehicle (VEH) versus IPI-926 (926), or gemcitabine (GEM) versus IPI-926 + gemcitabine (926/GEM), beginning at 8 weeks of age, as described in Supplemental Experimental Procedures. High resolution 3D ultrasound was used to monitor tumor development and to quantify tumor volumes. Treatment continued until mice met endpoint criteria.

(A) Kaplan-Meier curve showing IPI-926 treated KPC mice (red, n = 12), vehicle-treated KPC mice (blue, n = 12) ($p < 0.0001$, log rank test, vehicle versus IPI-926), and an historical collection of untreated KPC mice (gray, n = 165) ($p < 0.0001$, log rank test, historical cohort versus IPI-926).

(B) Kaplan-Meier curve showing IPI-926 + gemcitabine-treated KPC mice (red, n = 11) and vehicle + gemcitabine-treated KPC mice (blue, n = 12) ($p < 0.004$, log rank test, gemcitabine + vehicle versus gemcitabine + IPI-926). The data from panel A are overlaid in gray ($p = 0.01$, log rank test, IPI-926 versus IPI-926 + gemcitabine).

(C) Graph of time from first detection of tumor (by 3D ultrasound) to death in animals among the four treatment groups, comparing animals that received IPI-926 to those that did not ($p = 0.0003$ in monotherapy group, $p = 0.006$ in combination group). Animals with microscopic tumors on necropsy but no measurable tumor on ultrasound were included as 0 days. The data are presented as standard box and whisker plots.

(D) Final tumor volumes (measured by 3D ultrasound) among the four treatment groups, comparing animals that received IPI-926 to those that did not ($p = 0.0026$ in monotherapy group, $p = 0.012$ in the combination group). Several IPI-926-treated mice met endpoint criteria prior to the detection of tumors by ultrasound and are included as 0 mm^3. The data are presented as standard box and whisker plots.

(E) Age of tumor detection (by 3D ultrasound) among the four treatment groups ($p = 0.17$ for monotherapy, $p = 0.48$ for combination). The data are presented as standard box and whisker plots.

(F) Graph showing tumor volumes of mice treated with IPI-926 (red) or vehicle (blue) plotted versus the mouse's age in days. Two exceptional tumors noted in the text are highlighted in yellow.

(G) Graph showing tumor volumes of mice treated with gemcitabine + IPI-926 (red) or gemcitabine + vehicle (blue) are plotted versus the mouse's age in days. Lethal tumors that were undetectable by ultrasound were assigned a volume of 0 on the day of death. Animals still alive at the time of submission are denoted with open diamonds.

See also Figure S3.

of GFP^+ cells in the resulting KPC-$Gli1^{GFP}$ mice by immunofluorescence. GFP staining was readily observed in the E-cadherin-negative (stromal) portions of KPC-$Gli1^{GFP}$ mice but was absent from E-cadherin-positive (epithelial) cells (Figures 6A and 6B). Consistent with this observation, spheroid formation of a KPC pancreatic tumor cell line was unaffected by treatment with recombinant Shh protein or IPI-926 (Figure S5A). In contrast, nearly all alpha-SMA^+ myofibroblasts were found to be $Gli1^{GFP}$ positive, indicating active Hh pathway signaling in this mesenchymally derived cell type (Figures 6A and 6C). This is consistent with previous reports demonstrating a proliferative effect from Hh pathway signaling in fibroblasts (Walter et al., 2010). However, further examination of these tissue sections revealed that many $Gli1^{GFP}$-positive cells (43%) were alpha-SMA negative (Figures 6A and 6C), indicating that multiple stromal cell types can respond to Hh signaling. Importantly, treatment of KPC-$Gli1^{GFP}$ mice with IPI-926 for 10 days completely abrogated GFP staining, indicating that GFP staining was accurately reporting canonical Hedgehog signaling (Figures 6D and 6E). Taken together, these experiments confirm that canonical Hh signaling

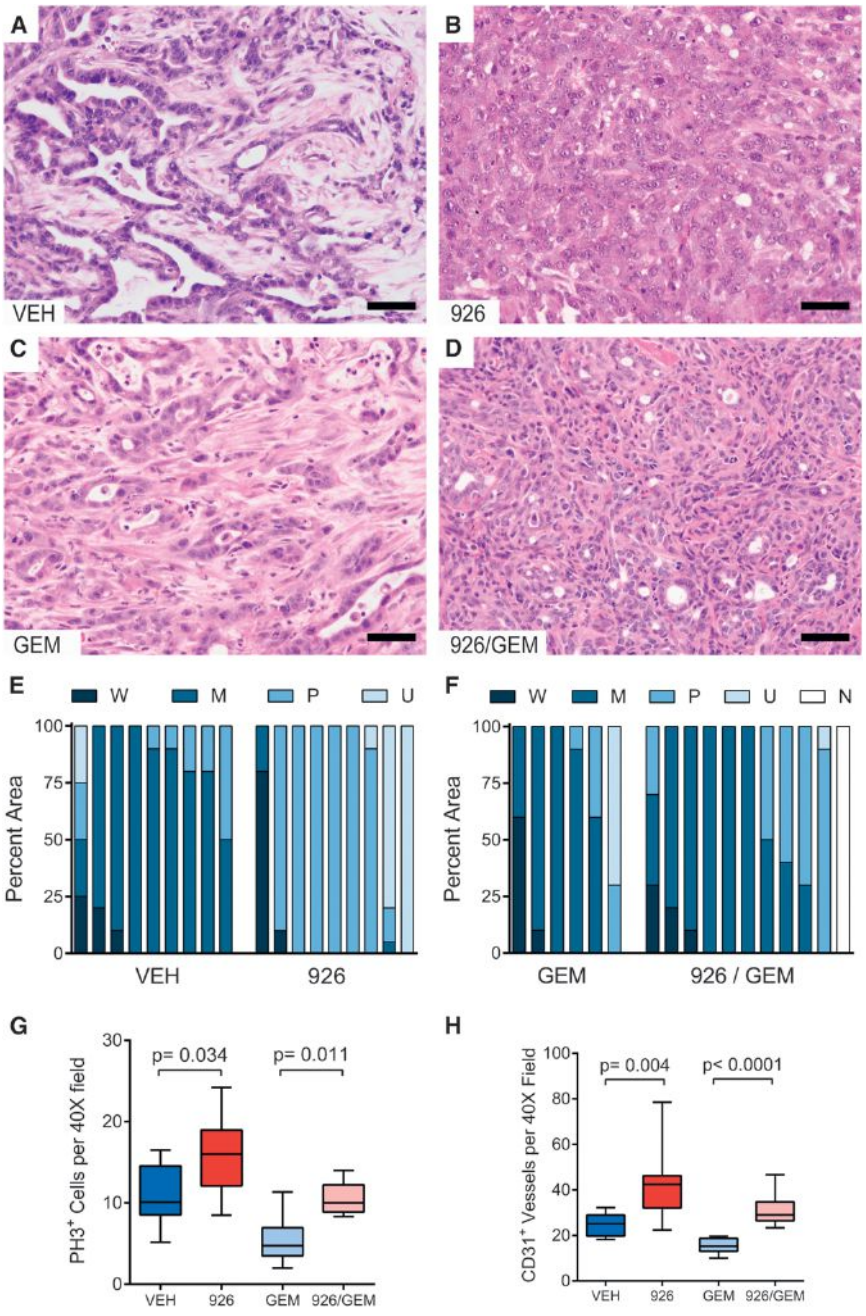

Figure 5. Long-Term Smoothened Inhibition Yields Poorly Differentiated Pancreatic Tumors with Increased Proliferation and Vascularity

(A–D) Representative histology (hematoxylin and eosin stain) of KPC tumors arising after long-term treatment with vehicle (A, VEH), IPI-926 (B), gemcitabine + vehicle (C), or gemcitabine + IPI-926 (D).

(E and F) Quantification of the differentiation state for each cohort. The fraction of each tumor that was observed to be well-differentiated (W), moderately differentiated (M), poorly differentiated (P), or undifferentiated (U) was scored in a blinded manner, and compared between the treatments. No tumor could be located in one IPI-926 + gemcitabine-treated mouse (N).

(G) Quantification of phospho-histone $H3^+$ cells per 40[times] field in each treatment group ($p = 0.034$ for monotherapy, $p = 0.011$ for combination). The data are presented as standard box and whisker plots.

(H) Quantification of $CD31^+$ vessel structures by IHC in each treatment cohort ($p = 0.004$ for monotherapy, $p < 0.0001$ for combination). The data are presented as standard box and whisker plots. Two-tailed Mann-Whitney U tests were used for all unpaired tests. Scale bars, 50 μm. See also Figure S4.

operates in a paracrine fashion in PDAC, as it does during embryonic development.

Shh-Deficient Tumors Are Sensitive to VEGF Inhibition

We next investigated the surprising increase in vasculature in ShhPKCY mice and in IPI-926-treated KPC mice. We first sought to determine whether increased angiogenesis was a direct result of reduced Hh pathway signaling in endothelial cells. We performed coimmunofluorescence on untreated KPC-$Gli1^{GFP}$ mice for GFP and the endothelial marker endomucin but found that Hh pathway signaling is absent in nearly all tumor endothelial cells (Figures 6A and 6F). Consistent with this observation, capillary sprouting of cultured human umbilical venous endothelial cells was unaffected by exposure to recombinant Shh or IPI-926 (Figure S5B). These results suggest that the proangiogenic effect of Hh pathway inhibition is mediated indirectly by signals from mesenchyme-derived stromal cells.

VEGF is a well-known soluble angiogenic factor. As a group, mouse and human PDAC are unaffected by treatment with VEGF receptor inhibitors, consistent with their poor vascularization (Singh et al., 2010). However, undifferentiated tumors comprise approximately 5%–10% of all advanced PDAC (Iacobuzio-Donahue et al., 2009). We hypothesized that the higher vessel density and paucity of stroma of undifferentiated tumors might render them sensitive to angiogenesis inhibitors. To test this hypothesis, we treated tumor-bearing ShhPKCY and control PKCY mice with DC101, a blocking antibody against VEGFR2. Similar to previous studies (Singh et al., 2010), VEGFR inhibition had little effect on tumor size or survival in PKCY mice (Figure 7A; Figure S6A). However, treatment of ShhPKCY mice with DC101 led to significantly improved overall survival compared to treatment with Ig control (median survival 22.4 versus 12.5 days from enrollment; $p = 0.028$; Figure 7B). DC101 treatment was associated with the appearance of large areas of necrosis on hematoxylin and eosin (H&E) (Figures 7C and 7D), and immunofluorescence staining demonstrated a reduced

A

Gli1-GFP$^+$ / E-Cadherin$^+$	11
Total E-Cadherin$^+$ Cells Counted	968
% Double Positive	1.14%

Gli1-GFP$^+$ / Blood Vessel	9
Total Blood Vessels Counted	400
% Double Positive	2.25%

Gli1-GFP/SMA	Total: 496	
Gli1-GFP$^+$ SMA$^+$	Gli1-GFP$^+$ SMA$^-$	Gli1-GFP$^-$ SMA$^+$
276	217	3
55.65%	43.75%	0.60%

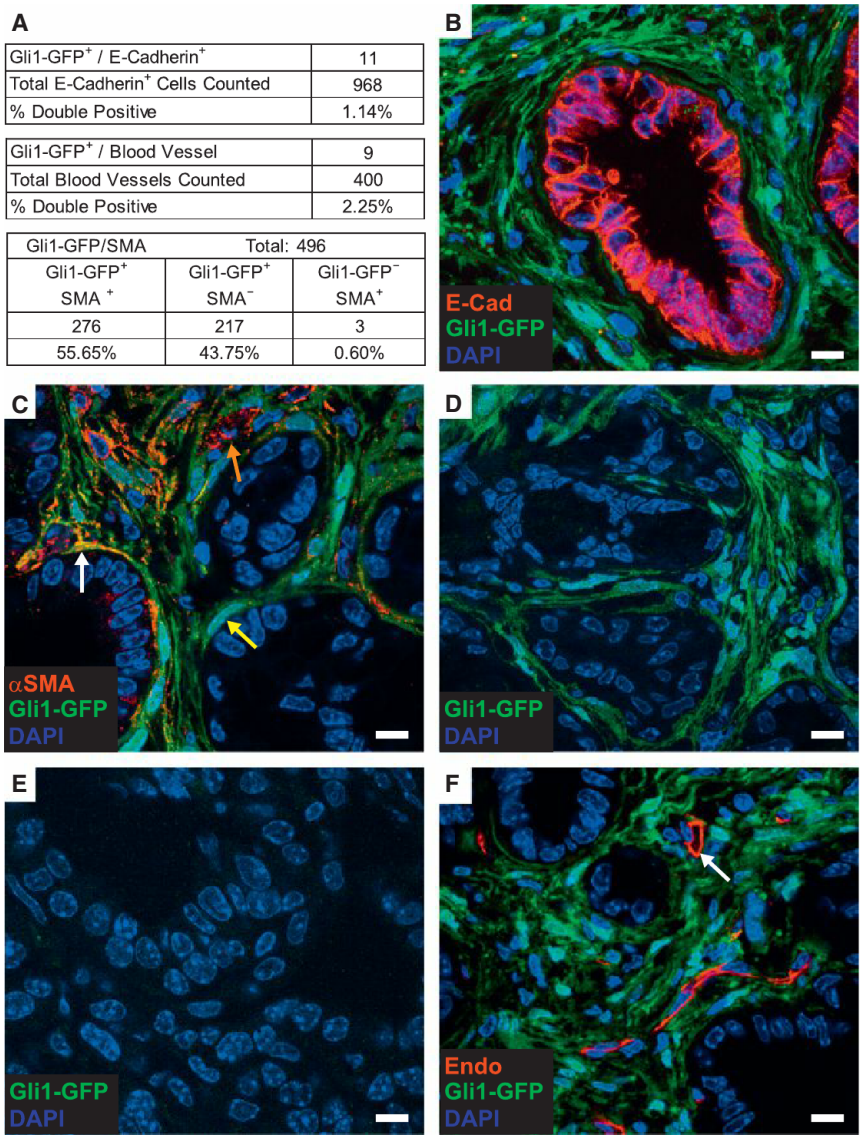

Figure 6. Hh Pathway Activity Is Restricted to Mesenchymally Derived Stromal Cells

(A) Quantification of coimmunofluorescence (Co-IF) for the Gli1^{GFP} Hh reporter and markers of various tumor and stromal populations.

(B) Co-IF for Gli1^{GFP} (green) and E-Cadherin (red, E-Cad) in KPC-Gli1^{GFP} tumors.

(C) Co-IF for Gli1^{GFP} (green) and alpha-SMA (red, αSMA) in in KPC-Gli1^{GFP} tumors. White arrow denotes an alpha-SMA$^+$, Gli1$^+$ cell. Yellow arrow denotes an alpha-SMA$^-$, Gli1$^+$ cell. Orange arrow denotes an aSMA$^+$, Gli1$^-$ cell.

(D and E) Co-IF for Gli1^{GFP} reporter on an untreated KPC-Gli1^{GFP} tumor (D) or after 10 days of IPI-926 treatment (E).

(F) Co-IF for Gli1^{GFP} (green) and the endothelial marker endomucin (red, Endo) in KPC-Gli1^{GFP} tumors. Arrow denotes a Gli1$^-$ endothelial cell.

Scale bars, 10 μm. See also Figure S5.

number of CD31$^+$ blood vessels (Figure 7E; Figures S6B and S6C), an increase in the percentage of tumor cells with LC3$^+$ autophagosomes (Figure 7F; Figures S6D and S6E), and reduced proliferation (Figure 7G; Figures S6F and S6G) in DC101-treated ShhPKCY mice. Interestingly, there was no difference in tumor VEGF expression between ShhPCKY versus PKCY mice or between IPI-926- versus vehicle-treated KPC tumors (data not shown). Thus, the depletion of Hh-dependent stroma from pancreatic tumors leads to a greater utilization and dependence on existing VEGF-mediated angiogenic pathways rather than a de novo induction of VEGF ligand.

Finally, we examined human pancreatic tumors to determine whether similar relationships between histology, Hedgehog signaling, and vascularity were present. In a set of 225 prospectively collected and analyzed human PDAC, undifferentiated tumors had significantly less Gli1 expression compared to all other tumors with well, moderately, and poorly differentiated histology (1.42 versus 2.99; p = 0.0102 by Student's t test, two-tailed; Figure S6H). However, no statistically significant difference was detected in Shh expression. Thus, undifferentiated human PDAC may be associated with attenuated canonical Hedgehog signaling, as predicted by our studies of genetically engineered mice. In a separate, independently collected and analyzed set of human PDAC, we examined 13 total human pancreatic tumors stratified into differentiated (n = 5) and undifferentiated (n = 8) histology to determine whether differentiation status correlated with vessel density in patients. Similar to mice, undifferentiated human pancreatic tumors exhibited significantly greater vascular density and less stroma compared to differentiated tumors, even when both components were present within the same primary carcinoma (Figures 7H–7J). Surprisingly, undifferentiated PDAC had a similar vascular density as normal human pancreas tissue (Figure 7J). These data indicate that like murine ShhPKCY tumors, undifferentiated pancreatic tumors in patients also have a more prominent vasculature.

DISCUSSION

Nearly 50 years have passed since Stoker's pioneering studies of epithelial/stromal interactions in cancer demonstrated that normal fibroblasts restrain the growth of transformed baby hamster kidney cells (Stoker et al., 1966). This "neighbor suppression" effect may be part of an evolved microenvironment surveillance against the development of preneoplasia (Klein, 2014). Nevertheless, in the context of established tumors, the prevailing paradigm of the tumor microenvironment field has been that tumor stroma supports, rather than inhibits, neoplastic growth and progression (Hanahan and Weinberg, 2011). This concept has been bolstered by work on pancreatic

tumors, which are associated with a particularly dense "desmoplastic" stroma. Such studies, which have mostly relied on cell transplantation or in vitro assays, have affirmed that the stroma plays a supportive role in of pancreatic cancer progression (Bailey et al., 2008; Feldmann et al., 2008a, 2008b; Hwang et al., 2008; Ikenaga et al., 2010; Lonardo et al., 2012; Xu et al., 2010). In this study, we have examined the effects of perturbing the tumor microenvironment by genetically deleting sonic hedgehog or pharmacologically inhibiting its essential signaling mediator Smoothened. These interventions greatly reduced stromal desmoplasia, but such tumors unexpectedly exhibited accelerated tumor growth, increased systemic morbidity, and increased metastasis, ultimately leading to earlier mortality. Thus, our findings demonstrate that at least some stromal constituents can act to restrain, rather than promote, tumor progression.

We previously reported that acute administration of IPI-926 to KPC mice bearing large tumors leads to stromal collapse and increased vascularity, consistent with the results shown here (Olive et al., 2009). In that study, treatment with Smo inhibitor alone had minimal effects on tumor size or survival, whereas combined treatment with the Smo inhibitor and gemcitabine led to transient stabilizations and regressions, producing a modest survival benefit (Olive et al., 2009). These results were interpreted as an indication that stromal inhibition could lead to improved drug delivery without a direct effect on tumor growth. However, because most animals in our previous study experienced less than 3 weeks of IPI-926 treatment, there was little opportunity to detect accelerated tumor progression in this acute setting. Indeed, despite the success of IPI-926 in treating basal cell carcinoma (Jimeno et al., 2013), the poor clinical performance of Smo inhibitors in pancreatic cancer trials has led to uncertainty regarding the approach of stromal targeting. Our current data suggest that the short-term, beneficial effects of increased drug delivery are eventually overcome by the negative effects of long-term Smo inhibition.

What is responsible for the increase in tumor cell proliferation and overall mortality in ShhPKCY (and IPI-926-treated) tumors? At present, the precise mechanism for increased tumor cell proliferation remains unknown and is likely to be complex. Nevertheless, the nearly 3-fold increase in blood vessel density in ShhPKCY tumors compared to PKCY tumors—an association that has been previously observed in IPI-926-treated KPC mice (Olive et al., 2009)—is likely to be a major contributor to this effect. This inference is supported by the observation that the more vascular ShhPKCY tumors had a nearly 5-fold decrease in autophagy, a process of cellular autodigestion used by nutrient-deprived cells (Kondo et al., 2005). Moreover, ShhPKCY tumors exhibited a responsiveness to antiangiogenic therapy that was absent in PKCY tumors, suggesting that the more highly vascular Shh-deficient tumors were dependent on this enhanced blood supply. Thus, our study suggests that the interaction between the tumor and its microenvironment is complex, with certain components of the microenvironment (i.e., vasculature) having a tumor-promoting role and other components (i.e., myofibroblasts) having an inert or tumor-suppressive role.

A paradoxical result of our study was the observation that the tumors lacking Hedgehog signaling—following either genetic ablation or treatment with IPI-926—were smaller despite their more aggressive and lethal phenotype, a finding that may reflect the fact that the stroma normally comprises a large percentage of PDAC tumor volume (Chu et al., 2007). Although we do not fully understand the accelerated mortality of Shh-deficient tumors, one possibility is suggested by the finding that tumor-bearing animals treated with IPI-926 exhibited significantly more weight loss and wasting prior to death than vehicle- or gem-treated tumors. It is conceivable that stromal inhibition (and associated changes in tumor metabolism) may lead to increased cachexia, a wasting syndrome common in human PDAC patients. Importantly, we do not believe that IPI-926 contributes to increased mortality or wasting independent of PDAC, because extensive clinical follow-up (Jimeno et al., 2013) and our own observations treating tumor-free animals (data not shown) failed to demonstrate any such toxicity.

There are several models that could account for the finding that ShhPKCY tumors have a reduction in myofibroblasts and leukocytes and an increase in blood vessels. Our data demonstrate that Hh signaling is nearly absent in the endothelial population, arguing against a direct role in angiogenesis. Rather, our findings are consistent with a model in which mesenchymal stromal cells exert an antiangiogenic effect on endothelial cells, possibly acting either directly or indirectly to elevate interstitial fluid pressure, which then represses blood vessel growth (Jacobetz et al., 2013; Provenzano et al., 2012). Importantly, these possibilities are not mutually exclusive, and future studies will be needed to understand the nature of cellular crosstalk between different components of the microenvironment and the role that Shh plays in each.

It is worth noting that global deletion of Gli1, a known mediator of Hedgehog signaling, completely blocks the development of $Kras^{G12D}$-driven pancreatic tumors (Mills et al., 2013). However, because Gli1 can be activated by signals other than Smoothened, it is unclear whether this reported requirement for Gli1 is due to so-called "canonical" (Smo-mediated) Hedgehog signaling or is mediated by other Gli1-dependent signaling pathways. Moreover, because the $Gli1^{GFP}$ reporter showed little if any activity within the tumor epithelium, it is unlikely that the effects we observed are due to a Hh-Smo-Gli1 signaling relay within the tumor cells themselves. Importantly, we employed autochthonous models that harbor mutant *Kras* and *p53*—mutations that are present in 95% and 75%–90% of human PDAC patients, respectively—and it remains to be determined whether the observed effects of Hedgehog deficiency on tumor biology occur only in the context of these genetic lesions or are more generalizable.

It is remarkable that the genetic or pharmacologic manipulation of Hedgehog signaling was associated with a dramatic change in tumor histology, illustrating the high degree of plasticity of differentiation status that exists within tumors in vivo. These data are corroborated by our analysis of human pancreatic tumors. Because poorly differentiated histopathology is strongly associated with poor outcome in PDAC (Han et al., 2006; Yonemasu et al., 2001), this finding has potential clinical implications. Specifically, the observation that inhibition of the Hedgehog pathway leads to the development of less differentiated and more aggressive tumors may explain the lack of benefit observed in clinical trials.

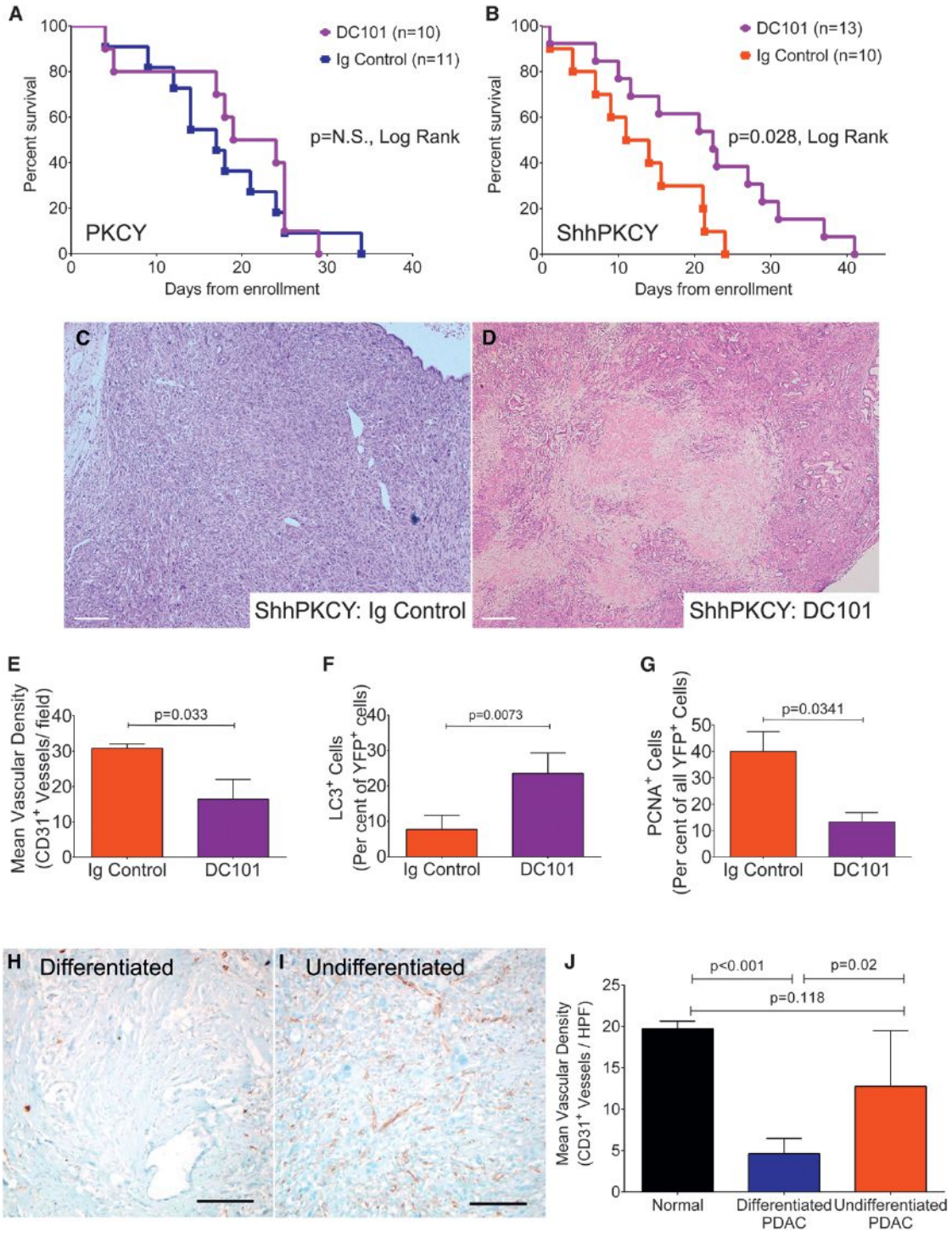

Figure 7. VEGFR2 Antagonism Leads to Selective Inhibition of Tumor Growth in ShhPKCY Mice

(A) Kaplan-Meier survival curve for tumor-bearing PKCY mice treated with bi-weekly DC101 (purple, n = 10) or Ig control (blue, n = 11).

(B) Kaplan-Meier survival curve for tumor-bearing ShhPKCY mice treated with bi-weekly DC101 (purple, n = 13) or Ig control (red, n = 10).

(C and D) H&E analysis of ShhPKCY tumors showing a large area of necrosis upon DC101 treatment (D). Scale bars, 250 μm.

(E) Quantification of $CD31^+$ vessel density in ShhPKCY mice treated with DC101 compared to Ig control, depicted as mean (±SD) number of $CD31^+$ vessels per high powered field (n = 3–5).

(F) Quantification of YFP^+ cells containing $LC3^+$ autophagosomes in ShhPKCY mice treated with DC101 compared to Ig control, depicted as percentage (±SD) of YFP^+ tumor cells exhibiting LC3 staining (n = 3–5).

(legend continued on next page)

Finally, our discovery that undifferentiated tumors were sensitive to VEGFR inhibition points to a possible biomarker of sensitivity to angiogenesis inhibitors in pancreatic cancer. The marked response of ShhPKCY tumors to an antiangiogenesis agent suggests that such undifferentiated tumors are dependent on a plentiful vascular network. Although clinical trials of antiangiogenesis agents failed to show benefit in PDAC, a portion of patients treated with bevacizumab did exhibit a durable response (Kindler et al., 2010). Approximately 5%–10% of advanced human pancreatic tumors exhibit an undifferentiated histology (Iacobuzio-Donahue et al., 2009), and the data we present here suggest that such tumors have a higher blood vessel density. Given our finding that poorly differentiated but well-vascularized pancreatic tumors respond to VEGF receptor blockade, it may be worth reconsidering antiangiogenesis treatment strategies for the subset of patients who harbor predominantly undifferentiated PDAC.

EXPERIMENTAL PROCEDURES

Mouse Models

All studies were conducted in compliance with the institutional guidelines of their respective locations. Two genetically engineered mouse models were used in these studies: $p53^{fl/+}$; $Kras^{LSL\text{-}G12D/+}$;*Pdx1-Cre*;$Rosa26^{YFP}$ (PKCY) (Rhim et al., 2012) and $Kras^{LSL\text{-}G12D/+}$;$p53^{LSL\text{-}R172H}$;*Pdx1-Cre* (KPC) (Hingorani et al., 2005). ShhPKCY and PKCY mice were used to determine the effect of Shh deletion in tumorigenesis and cancer progression. KPC mice were used in a chronic treatment trial of IPI-926. The $Gli1^{eGFP/+}$ allele was crossed into the KPC mouse for immunofluorescence studies (Brownell et al., 2011).

Analysis of Tumor Progression and Survival in PKCY and ShhPKCY Mice

All experiments involving mice were performed in accordance with relevant institutional and national guidelines and were approved by the institutional animal care and use committees at the University of Pennsylvania, Columbia University, and University of Michigan prior to experimentation. Starting at 2 months of age, mice were palpated twice weekly for evidence of tumor. If a potential mass was appreciated, transabdominal ultrasound was performed using a SonoSite M-Turbo ultrasound. If the presence of a tumor was confirmed, mice were examined weekly using ultrasound and general physical exam. If the mouse appeared moribund (decreased spontaneous physical activity, decreased toe pinch reflex, tachycardia, tachypnea, failure to groom, and ruffled coat), indicating low probability of surviving for greater than 24 hr, it was sacrificed for analysis. The tumors were immediately removed and weighed; the dimensions were measured; and the animals were analyzed for evidence of macrometastatic disease.

In Vivo DC101 T1rial

Upon detection of tumor by ultrasound, ShhPKCY and PKCY mice were randomized to two treatment arms: DC101 or IgG1 control (800 μg per mouse; Bio X Cell, West Hanover, NH) administered intraperitoneally every Monday and Thursday. Technicians were blinded to treatment group.

Analysis of Human Pancreatic Tumors

Studies involving all human pancreas tumors were approved by the institutional review boards of Johns Hopkins University and Mayo School of Medicine, and informed consent was obtained from all patients prior to tissue procurement and subsequent analysis. Paraffin-embedded sections (4 μm thickness) of eight human ductal adenocarcinomas with undifferentiated features from the Johns Hopkins Gastrointestinal Rapid Medical Donation Program (Iacobuzio-Donahue et al., 2009) were used and compared to five conventional PDACs and three samples of normal pancreas. Immunolabeling for CD31 was performed using standard histologic methods with prediluted anti-human CD31 monoclonal antibody (Ventana, clone JC70) and detected using the Dako universal liquid DAB+ substrate chromagen system per the manufacturer's instructions (catalog K3468). Slides were counterstained with hematoxylin for 30 s. Microvascular density was calculated as the number of $CD31^+$ vessels per field using a 40[times] objective and a minimum of four fields per sample.

Statistics

All statistics, including Kaplan-Meier statistics (log rank) and results from chi-squared tests, Mann-Whitney U tests, and Student's t tests, were calculated using GraphPad Prism v.5.04 or v.6. The p values from Student's t tests are listed unless otherwise specified. In all graphs, means (bars) and standard deviations (lines) are denoted.

SUPPLEMENTAL INFORMATION

Supplemental Information includes Supplemental Experimental Procedures and six figures and can be found with this article online at http://dx.doi.org/10.1016/j.ccr.2014.04.021.

AUTHOR CONTRIBUTIONS

A.D.R. planned and led all studies using PKCY mice. P.E.O. planned and led the survival study of KPC mice treated with IPI-926. D.H.T. planned and led studies using KPC-Gli1-GFP mice.

ACKNOWLEDGMENTS

We thank E. Collisson, R. Hruban, A. Rustgi, R. Vonderheide, and T. Wang for helpful discussions, as well as B. Orelli, M. Badgley, and J. Eberle for assistance in preparing the manuscript. We also thank Infinity Pharmaceuticals for providing IPI-926 and A. Joyner for providing Gli1-GFP mice. This study was funded by the NIH (DK088945, CA177857, DK034933, and CA046952 [to A.D.R.]; T32CA009503 [to D.H.T.]; CA136526 [to M.E.F.Z.]; CA157980 [to K.P.O.]; and CA169123, DK083355, and DK083111 [to B.Z.S.]) and AGA/FDHN (Fellow to Faculty Transition Award [to A.D.R.] and Bernard L. Schwartz Designated Research Award in Pancreatic Cancer [to K.P.O.]). This work was supported in part by the NIH/NIDDK Center for Molecular Studies in Digestive and Liver Diseases (P30DK050306) and its core facilities (Molecular Pathology and Imaging Core, Molecular Biology/Gene Expression Core, Transgenic and Chimeric Mouse Core, and Cell Culture Core) at the University of Pennsylvania and by the Molecular Pathology Shared Resource, the Confocal and Specialized Imaging Shared Resource, and the Small Animal Imaging Shared Resource within the Columbia University Herbert Irving Comprehensive Cancer Center (P30CA013696). The confocal microscope was purchased with grant S10RR025686.

Received: May 16, 2013
Revised: March 18, 2014
Accepted: April 25, 2014
Published: May 22, 2014

(G) Quantification of YFP^+ cells staining with the proliferation in ShhPKCY mice treated with DC101 compared to Ig control, depicted as percentage (±SD) of YFP+ tumor cells that were PCNA positive (n = 3 YFP 5).
(H and I) IHC for CD31 in differentiated (H) and undifferentiated (I) portions of human pancreas tumor A21. Scale bars, 200 μm.
(J) Mean vascular density of normal pancreas (n = 3), differentiated human PDAC (n = 5), and undifferentiated human PDAC (n = 8). Bars represent p values by two-sided Student's t test.
See also Figure S6.

REFERENCES

Bailey, J.M., Swanson, B.J., Hamada, T., Eggers, J.P., Singh, P.K., Caffery, T., Ouellette, M.M., and Hollingsworth, M.A. (2008). Sonic hedgehog promotes desmoplasia in pancreatic cancer. Clin. Cancer Res. *14*, 5995–6004.

Brownell, I., Guevara, E., Bai, C.B., Loomis, C.A., and Joyner, A.L. (2011). Nerve-derived sonic hedgehog defines a niche for hair follicle stem cells capable of becoming epidermal stem cells. Cell Stem Cell *8*, 552–565.

Chu, G.C., Kimmelman, A.C., Hezel, A.F., and DePinho, R.A. (2007). Stromal biology of pancreatic cancer. J. Cell. Biochem. *101*, 887–907.

El-Zaatari, M., Kao, J.Y., Tessier, A., Bai, L., Hayes, M.M., Fontaine, C., Eaton, K.A., and Merchant, J.L. (2013). Gli1 deletion prevents Helicobacter-induced gastric metaplasia and expansion of myeloid cell subsets. PLoS ONE *8*, e58935.

Engels, B., Rowley, D.A., and Schreiber, H. (2012). Targeting stroma to treat cancers. Semin. Cancer Biol. *22*, 41–49.

Feldmann, G., Fendrich, V., McGovern, K., Bedja, D., Bisht, S., Alvarez, H., Koorstra, J.B., Habbe, N., Karikari, C., Mullendore, M., et al. (2008a). An orally bioavailable small-molecule inhibitor of Hedgehog signaling inhibits tumor initiation and metastasis in pancreatic cancer. Mol. Cancer Ther. *7*, 2725–2735.

Feldmann, G., Habbe, N., Dhara, S., Bisht, S., Alvarez, H., Fendrich, V., Beaty, R., Mullendore, M., Karikari, C., Bardeesy, N., et al. (2008b). Hedgehog inhibition prolongs survival in a genetically engineered mouse model of pancreatic cancer. Gut *57*, 1420–1430.

Han, S.S., Jang, J.Y., Kim, S.W., Kim, W.H., Lee, K.U., and Park, Y.H. (2006). Analysis of long-term survivors after surgical resection for pancreatic cancer. Pancreas *32*, 271–275.

Hanahan, D., and Weinberg, R.A. (2011). Hallmarks of cancer: The next generation. Cell *144*, 646–674.

Hingorani, S.R., Wang, L., Multani, A.S., Combs, C., Deramaudt, T.B., Hruban, R.H., Rustgi, A.K., Chang, S., and Tuveson, D.A. (2005). Trp53R172H and KrasG12D cooperate to promote chromosomal instability and widely metastatic pancreatic ductal adenocarcinoma in mice. Cancer Cell *7*, 469–483.

Hwang, R.F., Moore, T., Arumugam, T., Ramachandran, V., Amos, K.D., Rivera, A., Ji, B., Evans, D.B., and Logsdon, C.D. (2008). Cancer-associated stromal fibroblasts promote pancreatic tumor progression. Cancer Res. *68*, 918–926.

Iacobuzio-Donahue, C.A., Fu, B., Yachida, S., Luo, M., Abe, H., Henderson, C.M., Vilardell, F., Wang, Z., Keller, J.W., Banerjee, P., et al. (2009). DPC4 gene status of the primary carcinoma correlates with patterns of failure in patients with pancreatic cancer. J. Clin. Oncol. *27*, 1806–1813.

Ikenaga, N., Ohuchida, K., Mizumoto, K., Cui, L., Kayashima, T., Morimatsu, K., Moriyama, T., Nakata, K., Fujita, H., and Tanaka, M. (2010). CD10+ pancreatic stellate cells enhance the progression of pancreatic cancer. Gastroenterology *139*, 1041–1051.

Jacobetz, M.A., Chan, D.S., Neesse, A., Bapiro, T.E., Cook, N., Frese, K.K., Feig, C., Nakagawa, T., Caldwell, M.E., Zecchini, H.I., et al. (2013). Hyaluronan impairs vascular function and drug delivery in a mouse model of pancreatic cancer. Gut *62*, 112–120.

Jimeno, A., Weiss, G.J., Miller, W.H., Jr., Gettinger, S., Eigl, B.J., Chang, A.L., Dunbar, J., Devens, S., Faia, K., Skliris, G., et al. (2013). Phase I study of the hedgehog pathway inhibitor IPI-926 in adult patients with solid tumors. Clin. Cancer Res. *19*, 2766–2774.

Kindler, H.L., Niedzwiecki, D., Hollis, D., Sutherland, S., Schrag, D., Hurwitz, H., Innocenti, F., Mulcahy, M.F., O'Reilly, E., Wozniak, T.F., et al. (2010). Gemcitabine plus bevacizumab compared with gemcitabine plus placebo in patients with advanced pancreatic cancer: Phase III trial of the Cancer and Leukemia Group B (CALGB 80303). J. Clin. Oncol. *28*, 3617–3622.

Klein, G. (2014). Evolutionary aspects of cancer resistance. Semin. Cancer Biol. *25C*, 10–14.

Kondo, Y., Kanzawa, T., Sawaya, R., and Kondo, S. (2005). The role of autophagy in cancer development and response to therapy. Nat. Rev. Cancer *5*, 726–734.

Lonardo, E., Frias-Aldeguer, J., Hermann, P.C., and Heeschen, C. (2012). Pancreatic stellate cells form a niche for cancer stem cells and promote their self-renewal and invasiveness. Cell Cycle *11*, 1282–1290.

Mao, J., Ligon, K.L., Rakhlin, E.Y., Thayer, S.P., Bronson, R.T., Rowitch, D., and McMahon, A.P. (2006). A novel somatic mouse model to survey tumorigenic potential applied to the Hedgehog pathway. Cancer Res. *66*, 10171–10178.

Mills, L.D., Zhang, Y., Marler, R.J., Herreros-Villanueva, M., Zhang, L., Almada, L.L., Couch, F., Wetmore, C., Pasca di Magliano, M., and Fernandez-Zapico, M.E. (2013). Loss of the transcription factor GLI1 identifies a signaling network in the tumor microenvironment mediating KRAS oncogene-induced transformation. J. Biol. Chem. *288*, 11786–11794.

Morton, J.P., Mongeau, M.E., Klimstra, D.S., Morris, J.P., Lee, Y.C., Kawaguchi, Y., Wright, C.V., Hebrok, M., and Lewis, B.C. (2007). Sonic hedgehog acts at multiple stages during pancreatic tumorigenesis. Proc. Natl. Acad. Sci. USA *104*, 5103–5108.

Nolan-Stevaux, O., Lau, J., Truitt, M.L., Chu, G.C., Hebrok, M., Fernández-Zapico, M.E., and Hanahan, D. (2009). GLI1 is regulated through Smoothened-independent mechanisms in neoplastic pancreatic ducts and mediates PDAC cell survival and transformation. Genes Dev. *23*, 24–36.

Olive, K.P., Jacobetz, M.A., Davidson, C.J., Gopinathan, A., McIntyre, D., Honess, D., Madhu, B., Goldgraben, M.A., Caldwell, M.E., Allard, D., et al. (2009). Inhibition of Hedgehog signaling enhances delivery of chemotherapy in a mouse model of pancreatic cancer. Science *324*, 1457–1461.

Pasca di Magliano, M., Sekine, S., Ermilov, A., Ferris, J., Dlugosz, A.A., and Hebrok, M. (2006). Hedgehog/Ras interactions regulate early stages of pancreatic cancer. Genes Dev. *20*, 3161–3173.

Provenzano, P.P., Cuevas, C., Chang, A.E., Goel, V.K., Von Hoff, D.D., and Hingorani, S.R. (2012). Enzymatic targeting of the stroma ablates physical barriers to treatment of pancreatic ductal adenocarcinoma. Cancer Cell *21*, 418–429.

Rhim, A.D., Mirek, E.T., Aiello, N.M., Maitra, A., Bailey, J.M., McAllister, F., Reichert, M., Beatty, G.L., Rustgi, A.K., Vonderheide, R.H., et al. (2012). EMT and dissemination precede pancreatic tumor formation. Cell *148*, 349–361.

Roberts, D.J., Smith, D.M., Goff, D.J., and Tabin, C.J. (1998). Epithelial-mesenchymal signaling during the regionalization of the chick gut. Development *125*, 2791–2801.

Sastra, S.A., and Olive, K.P. (2013). Quantification of murine pancreatic tumors by high-resolution ultrasound. Methods Mol. Biol. *980*, 249–266.

Singh, A., Greninger, P., Rhodes, D., Koopman, L., Violette, S., Bardeesy, N., and Settleman, J. (2009). A gene expression signature associated with "K-Ras addiction" reveals regulators of EMT and tumor cell survival. Cancer Cell *15*, 489–500.

Singh, M., Lima, A., Molina, R., Hamilton, P., Clermont, A.C., Devasthali, V., Thompson, J.D., Cheng, J.H., Bou Reslan, H., Ho, C.C., et al. (2010). Assessing therapeutic responses in Kras mutant cancers using genetically engineered mouse models. Nat. Biotechnol. *28*, 585–593.

Stoker, M.G., Shearer, M., and O'Neill, C. (1966). Growth inhibition of polyoma-transformed cells by contact with static normal fibroblasts. J. Cell Sci. *1*, 297–310.

Sukegawa, A., Narita, T., Kameda, T., Saitoh, K., Nohno, T., Iba, H., Yasugi, S., and Fukuda, K. (2000). The concentric structure of the developing gut is regulated by Sonic hedgehog derived from endodermal epithelium. Development *127*, 1971–1980.

Thayer, S.P., di Magliano, M.P., Heiser, P.W., Nielsen, C.M., Roberts, D.J., Lauwers, G.Y., Qi, Y.P., Gysin, S., Fernández-del Castillo, C., Yajnik, V., et al. (2003). Hedgehog is an early and late mediator of pancreatic cancer tumorigenesis. Nature *425*, 851–856.

Theunissen, J.W., and de Sauvage, F.J. (2009). Paracrine Hedgehog signaling in cancer. Cancer Res. *69*, 6007–6010.

Tian, H., Callahan, C.A., DuPree, K.J., Darbonne, W.C., Ahn, C.P., Scales, S.J., and de Sauvage, F.J. (2009). Hedgehog signaling is restricted to the stromal compartment during pancreatic carcinogenesis. Proc. Natl. Acad. Sci. USA *106*, 4254–4259.

Vonlaufen, A., Phillips, P.A., Xu, Z., Goldstein, D., Pirola, R.C., Wilson, J.S., and Apte, M.V. (2008). Pancreatic stellate cells and pancreatic cancer cells: An unholy alliance. Cancer Res. *68*, 7707–7710.

Walter, K., Omura, N., Hong, S.M., Griffith, M., Vincent, A., Borges, M., and Goggins, M. (2010). Overexpression of Smoothened activates the sonic hedgehog signaling pathway in pancreatic cancer-associated fibroblasts. Clin. Cancer Res. *16*, 1781–1789.

Watanabe, S., Ueda, Y., Akaboshi, S., Hino, Y., Sekita, Y., and Nakao, M. (2009). HMGA2 maintains oncogenic RAS-induced epithelial-mesenchymal transition in human pancreatic cancer cells. Am. J. Pathol. *174*, 854–868.

Xu, Z., Vonlaufen, A., Phillips, P.A., Fiala-Beer, E., Zhang, X., Yang, L., Biankin, A.V., Goldstein, D., Pirola, R.C., Wilson, J.S., and Apte, M.V. (2010). Role of pancreatic stellate cells in pancreatic cancer metastasis. Am. J. Pathol. *177*, 2585–2596.

Yonemasu, H., Takashima, M., Nishiyama, K.I., Ueki, T., Yao, T., Tanaka, M., and Tsuneyoshi, M. (2001). Phenotypical characteristics of undifferentiated carcinoma of the pancreas: A comparison with pancreatic ductal adenocarcinoma and relevance of E-cadherin, alpha catenin and beta catenin expression. Oncol. Rep. *8*, 745–752.

CellPress

Cancer Cell
Article

Targeting Tumor-Associated Macrophages with Anti-CSF-1R Antibody Reveals a Strategy for Cancer Therapy

Carola H. Ries,[1,13,*] Michael A. Cannarile,[1,13] Sabine Hoves,[1] Jörg Benz,[2] Katharina Wartha,[1] Valeria Runza,[1] Flora Rey-Giraud,[1] Leon P. Pradel,[1] Friedrich Feuerhake,[3] Irina Klaman,[1] Tobin Jones,[1] Ute Jucknischke,[1] Stefan Scheiblich,[1] Klaus Kaluza,[1] Ingo H. Gorr,[1] Antje Walz,[4] Keelara Abiraj,[4] Philippe A. Cassier,[5] Antonio Sica,[6,7] Carlos Gomez-Roca,[8] Karin E. de Visser,[9] Antoine Italiano,[10] Christophe Le Tourneau,[11] Jean-Pierre Delord,[8] Hyam Levitsky,[12] Jean-Yves Blay,[5] and Dominik Rüttinger[1]

[1]Roche Innovation Center Penzberg, Oncology Division, Roche Pharmaceutical Research and Early Development, 82377 Penzberg, Germany
[2]Roche Innovation Center Basel, Small Molecule Research, Roche Pharmaceutical Research and Early Development, 4070 Basel, Switzerland
[3]Institute for Pathology, Hannover Medical School, 30625 Hannover, Germany
[4]Roche Innovation Center Basel, Pharmaceutical Sciences and Oncology Division, Roche Pharmaceutical Research and Early Development, 4070 Basel, Switzerland
[5]Department of Medicine, Centre Léon Bérard, 69008 Lyon, France
[6]Humanitas Clinical and Research Center, 20089 Milan, Italy
[7]Department of Pharmaceutical Sciences, University of Piemonte, 28100 Novara, Italy
[8]Department of Medicine, Institut Claudius Regaud, 31000 Toulouse, France
[9]Division of Immunology, Netherlands Cancer Institute, 1066 CX Amsterdam, the Netherlands
[10]Department of Medical Oncology, Institut Bergonié, 33076 Bordeaux, France
[11]Department of Medical Oncology, Institut Curie, 75248 Paris, France
[12]Roche Innovation Center Zurich, Oncology Division, Roche Pharmaceutical Research and Early Development, 8952 Zurich, Switzerland
[13]Co-first author
*Correspondence: carola.ries@roche.com
http://dx.doi.org/10.1016/j.ccr.2014.05.016

SUMMARY

Macrophage infiltration has been identified as an independent poor prognostic factor in several cancer types. The major survival factor for these macrophages is macrophage colony-stimulating factor 1 (CSF-1). We generated a monoclonal antibody (RG7155) that inhibits CSF-1 receptor (CSF-1R) activation. In vitro RG7155 treatment results in cell death of CSF-1-differentiated macrophages. In animal models, CSF-1R inhibition strongly reduces F4/80$^+$ tumor-associated macrophages accompanied by an increase of the CD8$^+$/CD4$^+$ T cell ratio. Administration of RG7155 to patients led to striking reductions of CSF-1R$^+$CD163$^+$ macrophages in tumor tissues, which translated into clinical objective responses in diffuse-type giant cell tumor (Dt-GCT) patients.

INTRODUCTION

Colony-stimulating factor 1 (CSF-1) and its receptor, CSF-1R, regulate the migration, differentiation, and survival of macrophages and their precursors (Hume and MacDonald 2012; Chitu and Stanley 2006). CSF-1R is a member of the receptor protein tyrosine kinase (rPTK) family of growth factor receptors, which includes several known proto-oncogenes. The molecular pathology of the diffuse-type giant cell tumor (Dt-GCT; formerly known as pigmented villonodular synovitis [PVNS or Dt-PVNS]), a rare proliferative disease affecting large joints, vividly demonstrates the effects of deregulated CSF-1 production. In the majority of

Significance

Preclinical data indicate that tumor-associated macrophages (TAMs) represent an attractive therapeutic target as they represent key orchestrators of various tumor-promoting processes, such as escape of immune surveillance. Here, we report that treatment with an anti-CSF-1R antibody (RG7155) depletes TAMs from the tumor tissue of cancer patients across various tumor types. Moreover, in Dt-GCT patients, a neoplastic disorder characterized by CSF-1 overexpression, RG7155-induced reduction of CSF-1R$^+$ mononuclear cells provided significant clinical benefits and offers a therapeutic option other than surgery, which is associated with a high likelihood of relapse. Furthermore, our work forms the basis for exploring combination therapies especially in those tumor entities in which TAMs contribute to tumor pathogenesis.

Dt-GCT patients, chromosomal translocations involving the gene encoding CSF-1 result in overexpression of this cytokine by cells within the synovial lining (West et al., 2006). This leads to massive recruitment of CSF-1R-expressing cells, mainly nonmalignant mononuclear and multinucleated cells that form the bulk tumorous mass (Cupp et al., 2007; West et al., 2006). Marginal excision or complete synovectomy remain the treatments of choice (Ravi et al., 2011) for Dt-GCT, but the disorder sometimes necessitates mutilating surgery due to locally destructive and recurring tumor growth. Another investigational approach for treating Dt-GCT patients exploits the CSF-1R-targeting component of the tyrosine kinase inhibitor imatinib mesylate (Gleevec), thus suggesting that this receptor represents an attractive target for development of cancer therapies (Cassier et al., 2012; Blay et al., 2008).

In solid tumors, such as those in breast and pancreatic cancer, infiltrating $CD68^+$ or $CD163^+$ tumor-associated macrophages (TAMs) correlate with poor outcome (DeNardo et al., 2011; Kurahara et al., 2011; Shabo et al., 2008). The tumor-promoting function of TAMs is based on their capacity to secrete proangiogenic and growth factors, as well as to potently suppress T cell effector function by releasing immunosuppressive cytokines and affecting their metabolism (Wynn et al., 2013; Biswas and Mantovani 2010; Gordon and Martinez 2010; Hoves et al., 2006). Macrophages exerting these protumorigenic functions are also termed M2-type macrophages, in contrast to the antitumorigenic M1 subtype (Mantovani et al., 2002).

Here, we investigate the effect of blocking CSF-1R signaling by a humanized anti-CSF-1R antibody (RG7155) and the resulting effect on TAMs in vitro, in in vivo animal models, and in RG7155-treated Dt-GCT patients and patients with various other malignancies.

RESULTS

Antibody RG7155 Blocks CSF-1R Dimerization

We generated and characterized RG7155, a humanized anti-human CSF-1R immunoglobulin G1 (IgG1) monoclonal antibody that binds to human and cynomolgus CSF-1R with high affinity (K_D = 0.2 nM, as determined by surface plasmon resonance [SPR]; Figure 1A). The binding epitope and the mode of action of RG7155 was characterized using the crystal structure of the full-length CSF-1R extracellular domain (ECD) bound to the RG7155 Fab fragment in a 1:1 ratio (Figure 1B and Table S1). In the structure, the ligand binding domains D1–D3 of CSF-1R (Ma et al., 2012) are assembled into a helical-like arrangement, in contrast to the planar surface of the receptor dimerization interface formed by domains D4 and D5. RG7155 blocks the receptor dimerization interface with its epitope being located within D4 and D5 (Figures 1C and 1D). Previously, it has been shown for the homologous type III receptor tyrosine kinase (RTK) c-Kit that homotypic D4-D4 contacts between a strictly conserved Arg-Glu residue pair are essential for formation of the receptor dimer interface (Yuzawa et al., 2007). In our structure, the corresponding residues ^{D4}Arg370 and ^{D4}Glu375 form salt bridge contacts with Asp98 and Arg100 of the heavy chain CDR3 of RG7155, thereby preventing lateral receptor contacts (Figure 1C). Mutation analysis of the CSF-1R ECD confirmed that binding of RG7155 was abolished in constructs lacking D4 or D5 as determined by SPR (Figure 1E).

High-affinity binding of dimeric CSF-1 to CSF-1R requires receptor dimerization (Verstraete and Savvides 2012; Elegheert et al., 2011). This cooperative formation of the ligand receptor complex is inhibited by RG7155's blocking the receptor dimerization interface. As a consequence, the antibody inhibits binding of both CSF-1 and the other ligand, interleukin-34 (IL-34), to CSF-1R in a competitive manner (Figure 1F). Additionally, RG7155 blocks the transforming activity of a ligand-independent CSF-1R mutant, resulting in significantly reduced cell viability of NIH 3T3-CSF-1R L301S Y969F recombinant cells (Roussel et al., 1990) (Figure S1A) and OCI-AML-5 (wild-type [WT] CSF-1R; Figure S1B). Other human type III RTKs such as c-Kit and platelet-derived growth factor, or mouse CSF-1R, are not targeted by RG7155 (data not shown), thus confirming the selectivity of this antibody. Taking these data together, we conclude that RG7155 is a selective CSF-1R receptor dimerization inhibitor that blocks ligand-dependent and ligand-independent receptor activation.

RG7155 Depletes $CSF\text{-}1R^+CD163^+$ Macrophages In Vitro and In Vivo

Human macrophages were differentiated from monocytes in vitro in the presence of either CSF-1 or granulocyte macrophage (GM)-CSF. CSF-1-differentiated macrophages were characterized by the expression of CSF-1R and CD163, whereas differentiation with GM-CSF resulted in $CD80^+MHC\text{-}II^{high}$-expressing macrophages with undetectable CD163 and CSF-1R (Figure 2A). This profile indicates an M2-like polarization of macrophages in the presence of CSF-1 (Geissmann et al., 2010; Martinez et al., 2008). RG7155 potently inhibited the viability of CSF-1-differentiated macrophages with an IC_{50} of 0.3 nM by inducing cell death (Figures 2B and S1C). Moreover, cross-titration of GM-CSF and CSF-1 revealed that addition of small amounts of GM-CSF can protect macrophages from RG7155-induced apoptosis (Figure 2B).

To mimic the physiologic concentrations of these two cytokines in the tumor context, we investigated the effect of RG7155 on macrophages (TC-Macs) differentiated with tumor-conditioned media (TCM). Differentiation of TC-Macs susceptible to RG7155 was enabled by TCM with high CSF-1 and low GM-CSF levels, in contrast to tumor cells secreting high concentrations of GM-CSF (Figure 2C). Furthermore, these TC-Macs differentiated with high CSF-1 TCM displayed an M2-like phenotype characterized by a principal component analysis (PCA) using the first, second, and third PC, based on 23 selected receptors, cytokines, chemokines, and growth factors (Figure S2). TC-Macs differentiated with TCM containing high GM-CSF showed a mixed M1/M2 phenotype. (Figure S2). Blockade of both GM-CSF and CSF-1 signaling pathways resulted in cell death of GM-CSF/CSF-1 polarized TC-Macs, while blockade of each single cytokine did not (Figure 2D), confirming again the dominating influence of GM-CSF on TC-Mac survival in the presence of RG7155.

M2 macrophages are also characterized by their ability to suppress T cell activation, which was confirmed for macrophages susceptible to RG7155 in coculture assays with autologous T cells: CSF-1-differentiated macrophages potently suppressed

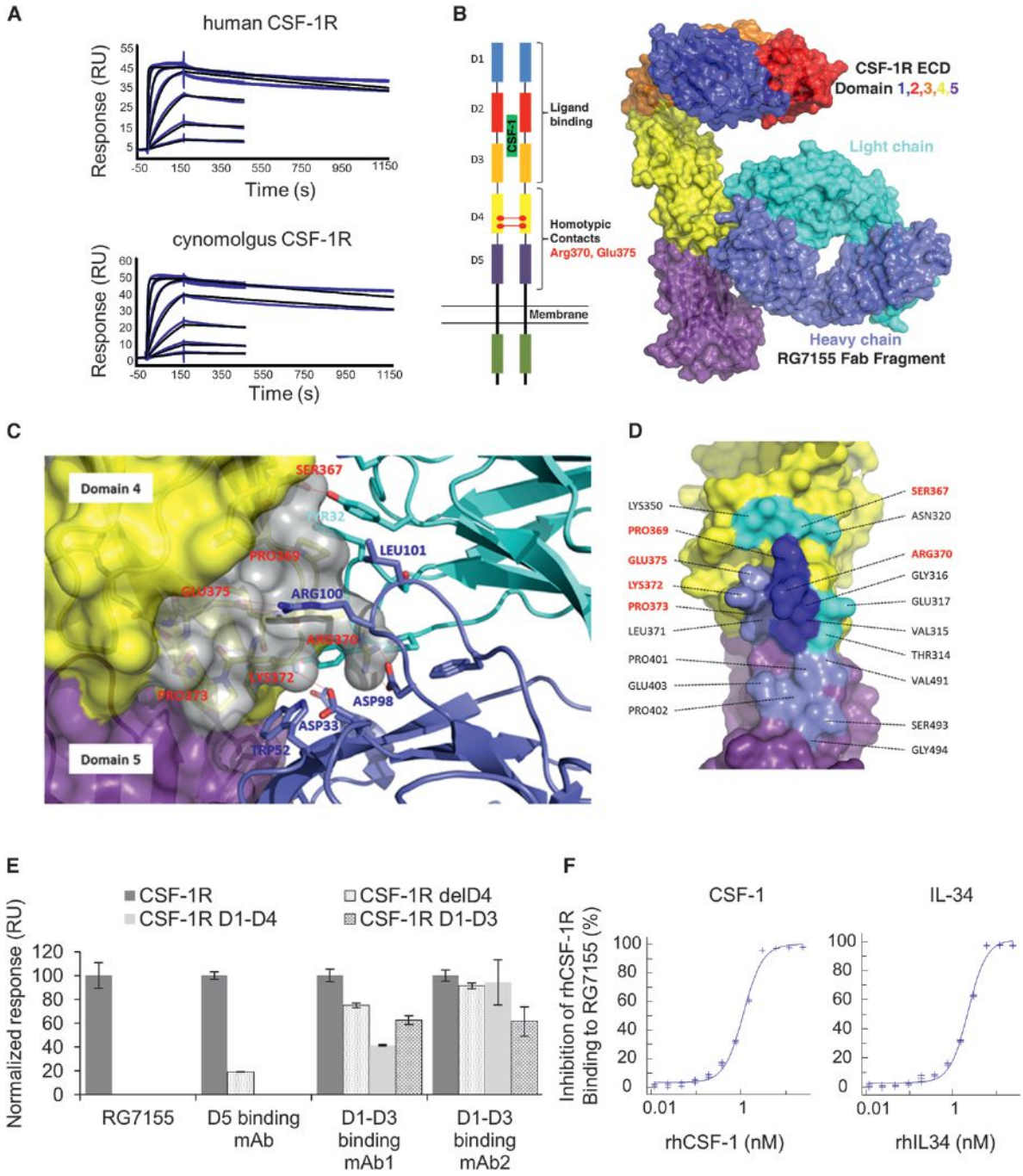

Figure 1. RG7155 Binds to the Human CSF-1R Dimerization Interface

(A) SPR sensorgrams showing binding of a series of concentrations of human and cynomolgus CSF-1R ECD to RG7155 captured onto a Biacore sensor chip.

(B) Schematic representation (left) of the CSF-1R ECD dimer. Key residues Arg370 and Glu375 most likely involved in dimerization in domain 4 are highlighted. The overall structure of the CSF-1R ECD monomer complex with Fab fragment of RG7155 is shown in surface representation (right).

(C) Close-up view of the Fab fragment binding site. Important Fab fragment residues for interaction with domains 4 and 5 of the receptor are shown as sticks. The surface patch in light gray resembles the receptor dimerization interface (based on an overlay with the c-KIT structure; Protein Data Bank [PDB] entry 2E9W) in domains 4 and 5 of the CSF-1R ECD, which is blocked by RG7155.

(D) Mapping of the Fab (RG7155) epitope on the CSF-1R ECD domain 4 (surface in yellow) and domain 5 (surface in purple). Residues interacting with the Fab (RG7155) HC (light blue), LC (cyan), or both HC and LC (dark blue) are labeled. Labels of residues involved in dimerization are shown in red.

(E) RG7155 requires both the D4 and D5 domains for binding. Full-length ECD/Fc (CSF-1R), dimeric CSF-1R delD4, D1-D4/Fc, and D1-D3/Fc were amine coupled onto a Biacore sensor chip, and binding of RG7155 and comparator monoclonal antibodies recognizing the ligand binding domain (Amgen and Imclone) or domain D5 (Sherr et al., 1989) was determined at 5 nM. Signals were corrected for the level of immobilization and are reported for each monoclonal antibody normalized to its binding of the full-length receptor = 100%.

(legend continued on next page)

CD4 and CD8 T cell proliferation induced by CD3/CD28 antibodies (Figure 2E). In contrast, macrophages polarized toward a M1 phenotype by the TCM from MDA-MB231 are least susceptible to RG7155 mediated killing (Figure 2C). Indeed, these TC-Macs were able to stimulate T cell proliferation (Figure 2F), indicating that RG7155 efficiently eliminates immunosuppressive M2-like macrophages.

The activity profile of RG7155 was tested in vivo using the cross-reactive nonhuman primate *Macaca fascicularis* (Figure 1A). The pharmacokinetic (PK) and pharmacodynamic (PD) profiles of RG7155 were assessed for various dose levels in a single-dose and repeat-dose study. Two doses of 30 and 100 mg/kg were administered weekly for analysis of tissue-resident macrophages. The PK profile was nonlinear, suggesting a target-mediated elimination pathway, pronounced at very low doses and saturated at higher doses (Figure 3A). Plasma CSF-1 concentrations increased at all tested doses immediately after RG7155 infusion and returned to baseline with declining drug levels (Figure 3B). RG7155 mediated rapid elimination of nonclassical $CD14^+CD16^+$, but not of classical $CD14^+CD16^-$, monocytes in peripheral blood of cynomolgus monkeys. With increasing doses, more durable reduction of nonclassical monocytes was observed. Of note, a strong rebound effect on these monocytes occurred with decay of RG7155 levels, most likely due to a stimulatory feedback mechanism mediated by increased CSF-1 levels. The extent and duration of the rebound phase of $CD14^+CD16^+$ monocytes was dose dependent and transient (Figure 3C). RG7155 efficiently reduced $CSF\text{-}1R^+$ and $CD68^+163^+$ macrophages in the liver (Kupffer cells) and colon of cynomologus monkeys. However, reduction of alveolar macrophages in the lung was rather minor (Figure 3D).

Mouse CSF-1R Inhibition Results in Depletion of TAMs and a Shift toward Higher CD8/CD4 T Cell Ratio

Since RG7155 does not cross-react with mouse CSF-1R (data not shown), we generated a chimeric mouse IgG1 antagonistic antibody (2G2) that binds to mouse CSF-1R with high affinity (K_D = 0.2 nM; Figure S3A). This antibody enables specific and long-term CSF-1R inhibition in immune-competent mice. Antibody 2G2 reduces survival of CSF-1-dependent murine M-NFS-60 cells (Nakoinz et al., 1990), confirming its bioactivity (Figure S3B). Both MC38 colorectal adenocarcinoma and MCA1 fibrosarcoma represent tumor models that are dominated by TAMs (Figures 4A and S3D). Flow-cytometric analysis of MC38 tumor-associated immune cells revealed significant reduction in TAMs (Figures 4A and S3F), accompanied by a relative increase of other types of immune cells including $Ly6G^{high}$ neutrophils, natural killer (NK) cells, and both $CD4^+$ and $CD8^+$ T cells (Figures 4A, 4B, S3F, and S3G). Importantly, tumors recovered from 2G2 antibody-treated mice showed a pronounced increase of $CD8^+$ compared with $CD4^+$ T cells, resulting in a positive shift of the CD8 to CD4 ratio toward cytotoxic effector T cells (Figure 4B). This changed ratio was associated with a decrease in $FoxP3^+$ T regulatory cells, which represent the tumor-promoting subset of the CD4 T cell population (Figure 4C). These findings suggest that aside from the strong reduction of TAMs in the tumor infiltrate, other immune effector cells are indirectly influenced by CSF-1R blockade.

The direct functional relationship between TAMs isolated from MC38 tumors and T cells was investigated in coculture experiments. TAMs markedly suppressed the in vitro expansion of CD3/CD28-activated $CD8^+$ T cells in a dose-dependent fashion (Figure 4D). Hence, TAMs not only affect the frequency of T cells, but also their functional activity. In both MC38 and MCA1 tumor models, we observed that in vivo administration of 2G2 antibody caused a delay in tumor growth (Figures 4E and S3C) associated to a dramatic reduction of TAMs that contribute to the tumorous mass (Figures 4A and S3D). Furthermore, 2G2 therapy reduced the number of spontaneously developed metastases in the MCA1 model (Figure S3E).

RG7155 Treatment Results in Marked Clinical Benefit for Patients with Diffuse-Type Giant Cell Tumors

A phase 1 clinical trial was initiated with RG7155 that included patients suffering from Dt-GCT. Eligible patients were treated every 2 weeks by intravenous infusion and monitored by (18F)-fluorodeoxy-glucose-positron emission tomography (FDG-PET) and tumor biopsies at baseline and on treatment after two administrations of RG7155 (at 4 weeks of treatment). Concurrently, whole blood was taken to investigate RG7155 infusion-related PK and PD effects (Figure 5A). Clinical activity was demonstrated by high metabolic response rate based on FDG-PET and objective clinical responses according to RECIST 1.1 accompanied by significant symptomatic improvement in all Dt-GCT patients as early as 4 weeks after treatment initiation. All seven evaluable patients showed partial metabolic response in FDG-PET imaging (according to the European Organization for Research and Treatment of Cancer, EORTC; Young et al., 1999), with two patients approaching a complete metabolic response. Five of the seven patients went on to achieve partial responses (RECIST) at the first assessment (Figure 5B).

The FDG-PET and magnetic resonance imaging (MRI) images of a 19-year-old female patient with recurring, nonresectable Dt-GCT of the right ankle clearly confirmed the disaggregation of the tumorous mass by RG7155 treatment (Figure 5C). Clinical activity correlated with a significant reduction of $CD68^+/CD163^+$ macrophages and of $CSF\text{-}1R^+$ cells in matching tumor biopsies (Figure 5D). The analysis of monocytes in the peripheral blood of this patient revealed rapid and sustained elimination of nonclassical $CD14^+CD16^+$ monocytes between 5 and 96 hr after RG7155 infusion. Classical $CD14^+CD16^-$ monocytes did not show a sustained alteration (Figure 5E). Accordingly, CSF-1R expression was significantly increased on nonclassical monocytes compared to classical activated and intermediate monocytes analyzed from healthy donors (Figure 5F).

(F) Binding of RG7155 to CSF-1R is competitive with ligand binding. Binding of CSF-1R/Fc (4 nM) to sensor-chip-captured RG7155 was determined in the presence of increasing concentrations of CSF-1 or IL-34. The amount of free receptor bound was calculated using a calibration curve and depicted as the percent inhibition of the maximal signal.

See also Figure S1 and Table S1.

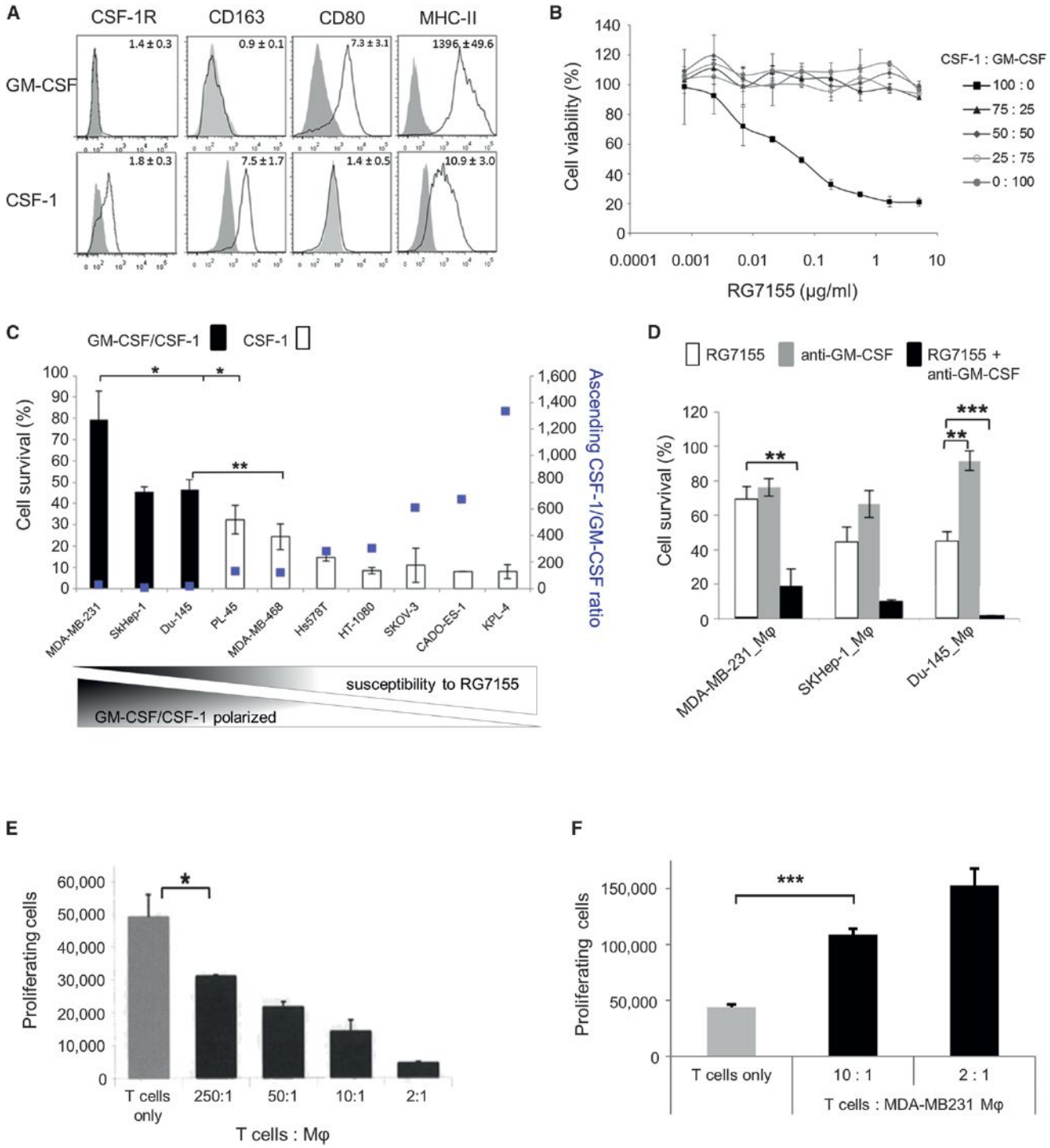

Figure 2. RG7155 Induces Cell Death of In Vitro-Differentiated Human M2-like, but Not M1-like, Macrophages

(A) Surface marker profile of GM-CSF (M1)- or CSF-1 (M2)-differentiated macrophages was assessed by flow cytometry. The given numbers indicate the mean ratio fluorescence intensity (MRFI ± SD; $n \geq 5$) calculated from the antigen's MFI (empty profiles) relative to the matching isotype (filled profiles).

(B) Macrophages were differentiated using different ratios of CSF-1 and/or GM-CSF in presence of RG7155. Cell viability was determined at day 7 using CellTiter-Glo. Data are pooled from four independent experiments and are shown as means ± SD (each sample run in triplicate; pairwise comparisons by Tukey-Kramer test; $p < 0.0001$).

(C) RG7155 inhibits monocyte survival during differentiation by TCM. Monocytes were cultured for 6 days in TCM with 30 μg/ml RG7155 or huIgG, and survival was analyzed by DAPI staining. Columns depicted were normalized to viable cells in the corresponding huIgG control (at least three donors; mean ± SEM; pairwise t test; *$p < 0.05$, **$p < 0.01$). The corresponding M-CSF/GM-CSF ratio of TCM is indicated on the secondary scale (blue squares). TC-Macs were classified as GM-CSF/CSF-1 polarized and are depicted by black bars at a CSF-1/GM-CSF ratio <50.

(legend continued on next page)

RG7155 Decreases CSF-1R$^+$CD163$^+$ TAMs in Patients with Various Types of Solid Malignancies and Alters T Cell Tumor Microenvironment Composition

Macrophage reduction by RG7155 in Dt-GCT patients was further confirmed and extended in patients with various advanced solid tumors, using doses every 2 weeks from 200 mg up to 3000 mg RG7155 in monotherapy and in combination with paclitaxel. Again, RG7155 treatment induced significant reduction of CSF-1R$^+$ cells and CD68$^+$CD163$^+$ macrophages in on-treatment biopsies from tumor lesions compared to matched biopsies taken from the same lesion prior to treatment in all patients analyzed after 4 weeks of therapy (Figures 6A and 6B). The results from the phase 1 dose escalation trial demonstrate that anti-CSF-1R treatment induces macrophage depletion in tumors and indicate proof of mechanism in patients with various types of malignant neoplasms. In patients who received doses of 600 mg or higher (to ensure saturation of the target based on PK and PD assessments), we additionally analyzed the respective T cell infiltrate. The baseline T cell infiltrate was dominated by CD4$^+$ T cells and switched to a predominantly CD8$^+$ lymphocyte infiltrate upon therapy. This is reflected in the increased CD8/CD4 ratio in five out of seven patients treated with RG7155 (Figure 6C), thus mirroring observations in mouse models. Baseline infiltrate in these patients of either CSF-1R$^+$ cells or CD68$^+$CD163$^+$ TAMs varied from 10% to 60%. However, the dramatic TAM reduction was independent of the degree of basal macrophage infiltrate (Figures 6B and 6C).

DISCUSSION

Here we describe a specific and potent CSF-1R targeting antibody, RG7155, that shows significant clinical activity in Dt-GCT patients and reduces TAMs in tumors of patients suffering from various cancers. In contrast to RG7155's blocking both ligand-dependent and -independent receptor activation, all other blocking CSF-1R antibodies currently known to be in phase 1 clinical development for advanced solid tumors (antibody AMG820, identifier NCT01444404; antibody IMC-CS4, identifier NCT01346358) target the ligand binding domains (Amgen, human *C-FMS* antigen binding proteins US2008/073611, 2009; Imclone, antibodies against CSF-1R, US2011/030148, 2011). Further clinical evaluation is needed to explore whether targeting of different CSF-1R epitopes will impact efficacy and safety as shown for other therapeutic antibodies targeting an RTK (King and Wong 2012) and the impact of direct versus indirect competition in settings in which the ligand concentration increases as much as 1,000-fold after receptor blockade. Additional toxicities triggered by less-specific CSF-1R small-molecule tyrosine kinase inhibitors have been discussed as another limiting factor of CSF-1R blockade in tumor tissue (El-Gamal et al., 2013), such as imatinib, which is a weak CSF-1R inhibitor compared with its primary targets, ABL and c-KIT (Taylor et al., 2006; Dewar et al., 2005). Imatinib mesylate and its more potent and better-tolerated successor, nilotinib, have been tested in small series of Dt-GCT patients with only limited clinical activity (Gelderblom et al., 2013; Cassier et al., 2012) compared to the objective clinical responses in 74% of Dt-GCT patients treated with RG7155 as described here. The overall safety profile for RG7155 was acceptable, with the most frequent adverse event being periorbital edema, which mirrored the findings from the monkey study. Thus far, none of these patients was reported to have progressive disease, with the longest follow-up being 12 months.

The molecular pathology of Dt-GCT represents a model disease for CSF-1R targeting agents, with a few aberrant cells producing CSF-1, resulting in massive recruitment of CSF-1R positive macrophages. Additionally, in solid malignancies such as sarcoma or breast cancer CSF-1, overexpression by tumor cells and an extensive CD68$^+$ or CSF-1R$^+$ macrophage infiltrate are associated with poor prognosis (Espinosa et al., 2009; Kluger et al., 2004). In solid malignancies, additional chemokines such as MCP-1 or SDF-1 might support recruitment of monocytes (Pollard, 2009; Murdoch et al., 2008). However, GM-CSF or CSF-1 control TCM macrophage survival, as shown in our in vitro studies. Since CSF-1 (unlike GM-CSF) is systemically available (Hamilton and Achuthan 2013), we postulate that TAMs are amenable to anti-CSF-1R therapy independently of their recruitment mechanism. Hence, patients enrolled in the phase 1 trial with RG7155 were not preselected for CSF-1 levels in tumor, serum, or TAM infiltrate. Yet, in all paired tumor biopsies, a significant reduction of CSF-1R$^+$ TAMs upon RG7155 therapy was detectable. Analysis into whether patients with a stronger macrophage infiltrate benefit more from RG7155 therapy is ongoing, a question that will require treatment of a larger patient cohort to answer. As our in vitro data show that the presence of GM-CSF during macrophage differentiation inhibits RG7155 induced cell death, which has been demonstrated previously also for a small-molecule CSF-1R inhibitor (Pyonteck et al., 2013), it will be important to address in future clinical studies the role of tumor-derived GM-CSF on the efficacy of RG7155-mediated TAM depletion. In particular, pancreatic cancer has been described to express GM-CSF, and the role of this growth factor in inducing immunosuppressive myeloid-derived suppressor cells in mouse models has been reported (Bayne et al., 2012; Dolcetti et al., 2010; Bronte et al., 2000). Even if TAM depletion is diminished in GM-CSF-expressing tumors, inhibition of CSF-1R signaling can alter the polarization of macrophages and hence be therapeutically beneficial (Pyonteck et al., 2013). However, tumor types to be treated with RG7155 will have to be selected carefully, taking into account that TAMs have been also attributed good prognostic relevance, e.g., in colorectal cancer (Zhang et al., 2012).

(D) Macrophages were differentiated for 6 days followed by incubation with 30 μg/ml RG7155 and/or 10 μg/ml GM-CSF-neutralizing antibody for 6 days. Survival was determined by DAPI staining, and data were normalized to live cells observed in huIgG control (mean ± SEM of at least four donors; $^{**}p < 0.01$, $^{***}p < 0.001$).
(E) Constant numbers of autologous T cells were cocultured with the indicated amounts of CSF-1-differentiated macrophages and activated by anti-CD3/CD28 beads. Proliferation was determined by CFSE dilution. Data are representative of five different donors and are given as means + SD of triplicates ($^{*}p < 0.05$).
(F) MDA-MB231 conditioned-media-differentiated macrophages were cocultured with T cells and activated as described above. Data are representative of two donors and are given as means + SD of triplicates ($^{*}p < 0.05$).
See also Figure S2.

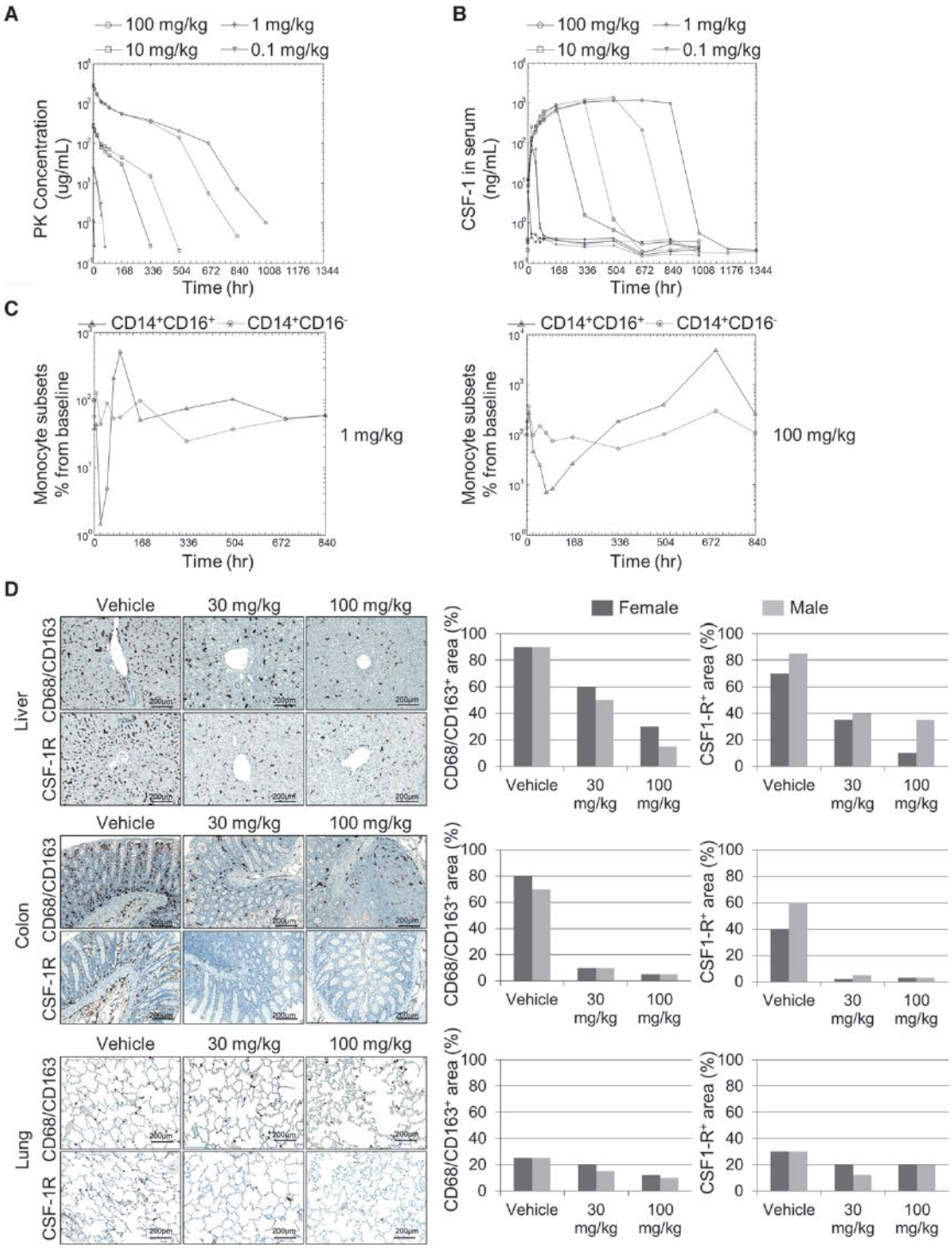

Figure 3. PK/PD Effects in RG7155-Treated Nonhuman Primates' Peripheral Blood and Tissue

(A) RG7155 serum concentration-time profiles at different doses shown for the two individual animals treated per dose cohort.

(B) Increase of CSF-1 concentration in serum at the same time points as for PK analytics.

(C) Nonclassical $CD14^+CD16^+$ and classical $CD14^+CD16^-$ monocytes determined by flow cytometry at baseline and after single RG7155 doses. One representative individual dosed at 1 mg/kg (left) and 100 mg/kg (right) as the percent change from the baseline is depicted.

(D) Representative immunohistochemistry (IHC) images from one cynomolgus male animal is shown for each liver, colon, and lung from the vehicle-, 30 mg/kg RG7155-, and 100 mg/kg RG7155-treated groups (left). Each group is represented by one male and one female treated once weekly for 2 weeks. Individual scores for the percent area coverage of the different cell types are shown for both animals per vehicle and dosing groups tested (right).

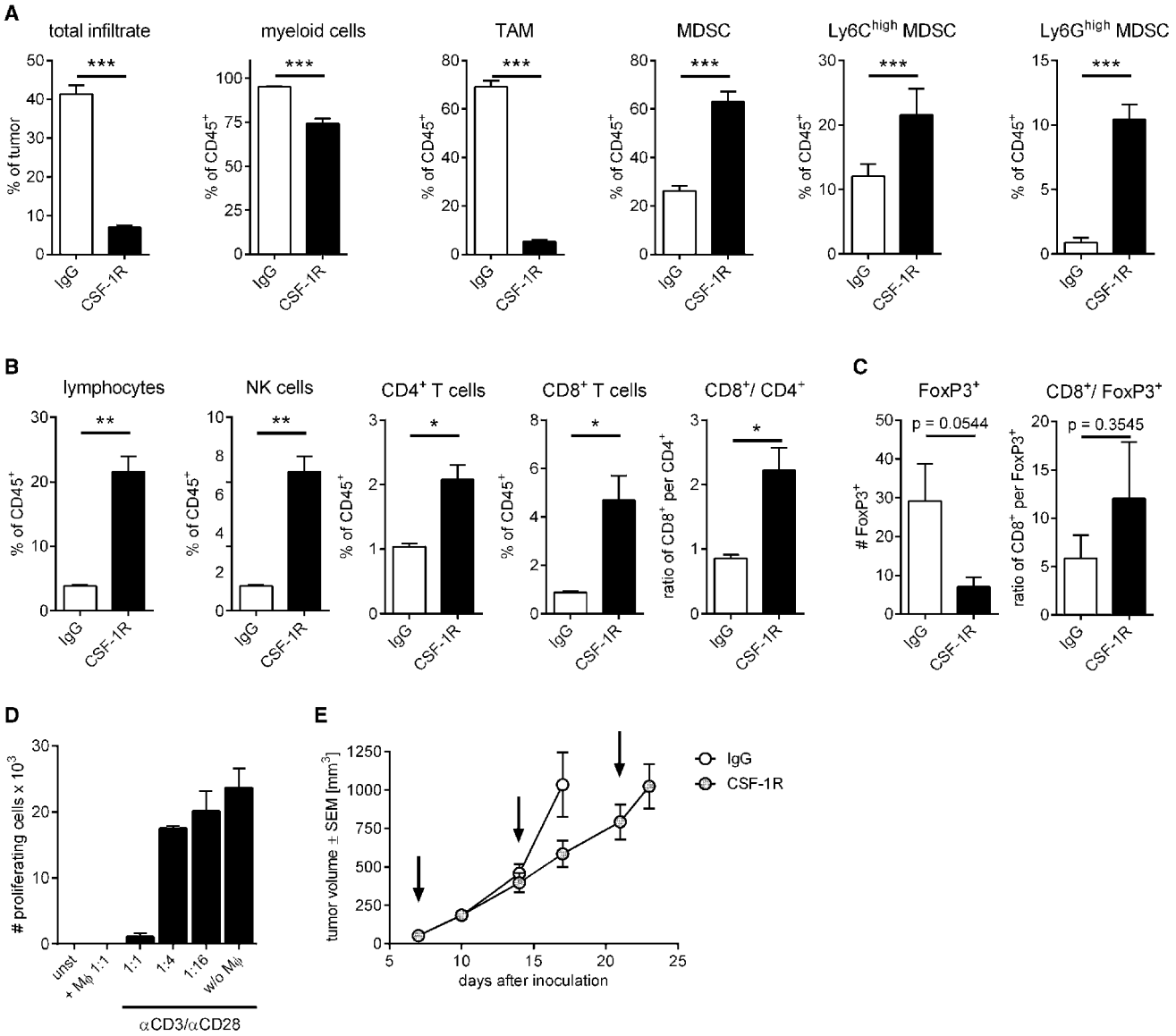

Figure 4. CSF-1R Inhibition Depletes TAMs and Increases Lymphocyte Infiltration into MC38 Colon Carcinomas

(A–C) Female C57BL/6N mice were inoculated subcutaneously with 10^6 MC38 tumor cells and treated with 30 mg/kg of either murine IgG1 control (clone MOPC-21) or anti-CSF-1R (clone 2G2) when tumor size reached 50 mm^3 (day 7). Mice were treated twice (days 7 and 14 after tumor inoculation), and tumor infiltrate was analyzed on day 16 by flow cytometry (A and B) or immunohistochemistry (C). Total tumor leukocyte and myeloid cell infiltrate were analyzed from n = 6 animals per group (A), and lymphocyte infiltrate was analyzed from n ≥ 3 per group (B). The graphs depict data pooled from two independent experiments for subpopulations relative to total infiltrate ($CD45^+$). $FoxP3^+$ regulatory T cell and CTL infiltrate were analyzed from n = 5 per group by IHC; total cell counts were summarized from five high power fields (HPF) each (C). The graphs in (A)–(C) show means ± SEM and were analyzed using an unpaired t test plus Bonferroni post test (*p < 0.05, **p < 0.01, ***p < 0.001; n.s., not significant).

(D and E) TAM were isolated from MC38 tumors and cocultured at the ratios indicated with CFSE-labeled $CD8^+$ T cells in the presence of CD3/CD28 stimulation (D). T cell proliferation was analyzed in triplicates after 3 days using bead quantification of $CFSE^{low}$ dividing cells (shown as means + SEM). MC38 tumors were treated continuously in weekly intervals (indicated by black arrows), and tumor growth was monitored every 3 to 4 days for n = 10 mice per group (E). In (D) and (E), one representative experiment is depicted as means ± SEM.

See also Figure S3.

Furthermore, the Langerhans cell infiltrate in skin biopsies from RG7155-treated patients will be analyzed since keratinocyte derived IL-34 was identified as their survival factor (Greter et al., 2012). Microglia, the other macrophage population regulated by neural progenitor and glial cell-derived IL-34, was not affected in the RG7155-treated monkey brain tissue (data not shown). Currently, it is unclear whether, in the context of glioblastoma accompanied with an impaired blood-brain barrier, a sufficient amount of antibody would reach the tumor. Proneural glioblastoma (GBM) might be a promising avenue for further development of RG7155 since this resembles a tumor type in which inhibition of CSF-1R resulted in TAM re-education instead

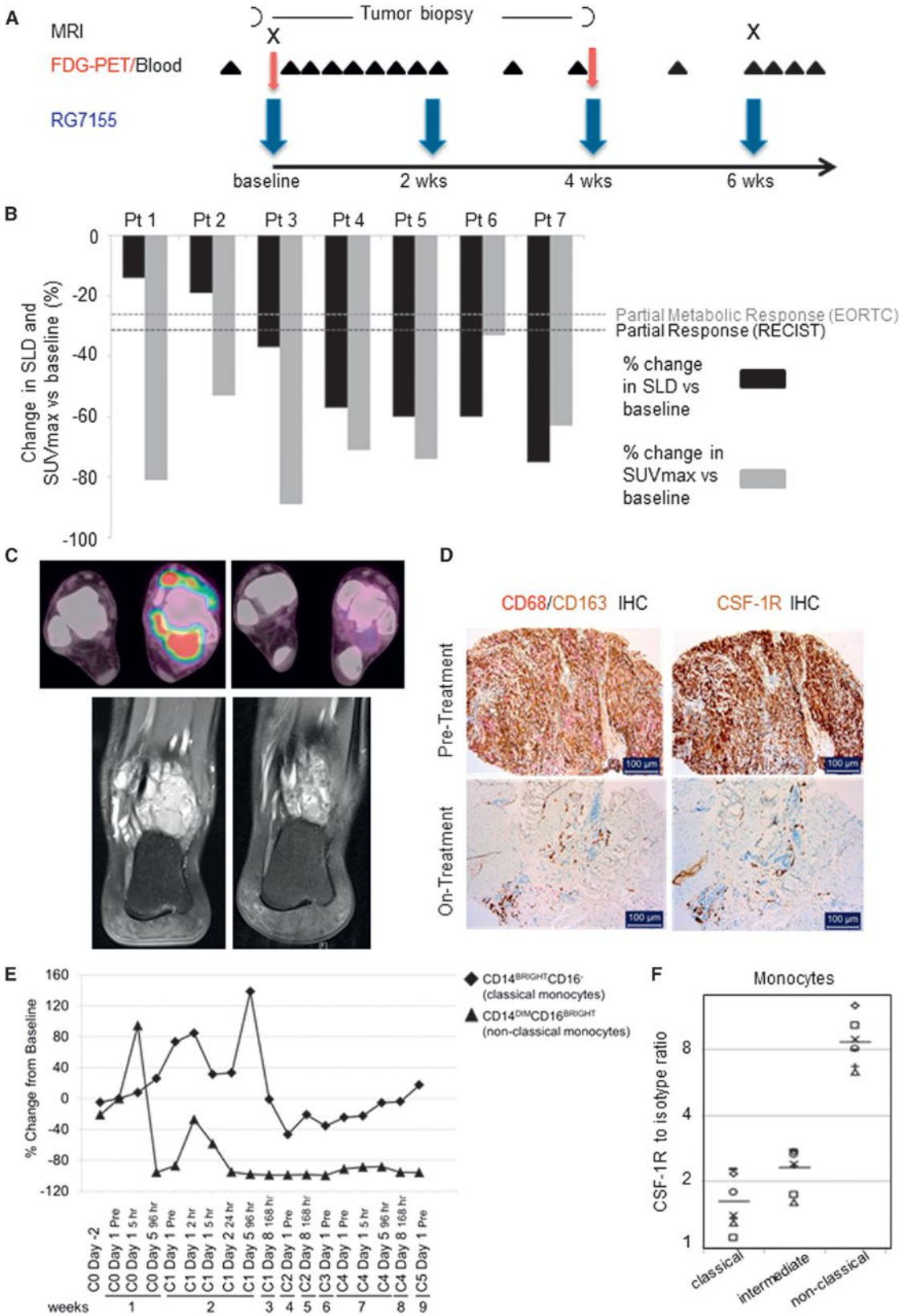

(legend on next page)

of depletion (Pyonteck et al., 2013). Furthermore, the presence of IL-34 has been shown to inhibit GBM cell line proliferation via its second receptor protein-tyrosine phosphatase (Nandi et al., 2013), which we expect to be similarly elevated upon RG7155 administration as CSF-1. Hence, the use of a CSF-1R inhibitor in GBM might not only indirectly effect tumor growth by reducing TAM suppressive function and re-educating their antitumoral state, but also directly target GBM tumor cells via IL-34.

Targeting of macrophages is a promising therapeutic approach, considering their role in mediating resistance to cancer therapies. TAMs have been shown to blunt chemotherapy-induced antitumor responses by secreting chemoprotective factors such as MMP-9 and cathepsins (De Palma and Lewis 2013; Shree et al., 2011). A previous report of small-molecule CSF-1R inhibitors used for macrophage depletion in PyMT mice (DeNardo et al., 2011) described increased $CD8^+$ T cell levels, but only when administered in combination with chemotherapy. In contrast, our 2G2 antibody mediated macrophage depletion and relatively increased $CD8^+$ T cells and NK cells in tumors when delivered in monotherapy. These differences might be attributed to the dominating role of macrophages in the MC38 and MCA1 models employed for our studies or to differences in the CSF-1R inhibitors used. The latter is more likely since an increase of $CD8^+$ T cells has been observed in PyMT using another CSF-1R small-molecule inhibitor, BLZ945 (Strachan et al., 2013). The immunosuppressive function of TAMs is well documented (Cavnar et al., 2013) and was also confirmed here for the CSF-1-dependent human in vitro-differentiated and ex vivo-isolated murine TAMs. Most strikingly, we report that targeting of CSF-1R results in a higher CD8/CD4 T cell ratio in tumor lesions in the majority of the cancer patients analyzed. However, we were unable to identify a correlation between the grade of macrophage depletion or the severity of basal macrophage infiltrate and the changes in the T cell composition, due to the low number of patients analyzed. Of note, patients with a tumor type in which macrophages have been associated with its etiopathology, such as mesothelioma (Yang et al., 2008), were among those patients that showed the most pronounced changes in lymphocyte infiltrate. Taken together, these observations provide rationale for future testing of combinations of RG7155 with currently available immunostimulatory therapies, such as sipuleucel-T and anti-CTLA-4 (Chen and Mellman 2013). Accordingly, an obstacle limiting the efficacy of such immune-activating therapies may well be the presence of an immunosuppressive myeloid infiltrate, which now can be targeted by RG7155. While some studies have suggested an antitumorigenic activity of TAM subpopulations (Weiskopf et al., 2013; Beatty et al., 2011), targeting of the strong immunosuppressive function of TAMs at the cost of their potential tumoricidal activity is expected to be therapeutically beneficial, given that T cells are considered to be the more powerful effector cells, due to their capability to expand by proliferation.

In summary, we report the characterization of a specific CSF-1R inhibitor, RG7155, that offers Dt-GCT patients a highly active therapeutic agent. In contrast to surgical resection as the current mainstay of treatment and investigational approaches such as imatinib and nilotinib therapy and radiation therapy, RG7155 shows promising activity in Dt-GCT patients. In addition, we speculate that patients with some types of solid tumors may also benefit from the TAM-depleting effects of RG7155, especially when combined with "standard of care" treatments such as chemotherapeutic drugs or immunotherapies. In this regard, the effects of RG7155 are not limited only to reducing TAMs, but also are likely to be manifested by increases within tumors of other immune effector cells, as reflected by the increased CD8/CD4 T cell ratio that we observed clinically in a broad range of cancers.

EXPERIMENTAL PROCEDURES

X-Ray Crystallography

Prior to crystallization experiments, the Fab-ectodomain complex was deglycosylated with peptide-N-glycosidase. Crystallization screening was performed at a concentration of 20 mg/ml in sitting-drop plates at 21°C. The largest crystals were obtained from 0.2 M lithium sulfate, 25% PEG 3350, and 0.1 M HEPES (pH 7.5). Diffraction data were collected at a wavelength of 1.0000 Å using a PILATUS 6M detector at the beamline X10SA of the Swiss Light Source.

Data were processed with XDS (Kabsch 2010) and scaled with SADABS (BRUKER). The structure was determined at a resolution of 2.55 Å by molecular replacement with PHASER (McCoy et al., 2007) using the coordinates of an in-house Fab fragment and of PDB entries 3EJJ and 2EC8 for Ig domains 1–4 of the receptor. Domain 5 was directly traced into difference electron density. Coordinates were refined by rigid-body and positional refinement using the CCP4 suite (Collaborative Computational Project, Number 4, 1994) and BUSTER (Bricogne et al., 2011). Difference electron density was used to change amino acids according to sequence differences by real-space refinement. Manual rebuilding of the protein was performed using COOT (Emsley et al., 2010). The final structure includes residues 21 to 500 of the receptor ectodomain.

Construction of Antibodies

RG7155 was generated by immunization of nuclear MRI mice with an expression vector pDisplay (Invitrogen) encoding the ECD of huCSF-1R by

Figure 5. RG7155 Treatment Reduces Tumor Burden in Patients with Diffuse-type Giant Cell Tumors

(A) RG7155 treatment and biomarker assessment schedule. Patients were intravenously infused biweekly and underwent tumor biopsy sampling, FDG-PET, and MRI assessment at baseline prior to the first RG7155 dose and on treatment at 4 weeks (FDG-PET and biopsy) and 6 weeks (MRI), i.e., after two or three RG7155 infusions. Additionally, blood sampling was performed as indicated (solid triangle) for assessment of PK/PD markers.

(B) Changes in standard uptake value maximum (SUVmax) by FDG-PET and the sum of the largest diameter (SLD) assessed by MRI in Dt-GCT patients compared with the baseline. Partial metabolic response in FDG-PET imaging (EORTC criteria) was observed in seven out of seven patients, two of whom had near-complete metabolic response. Partial response (RECIST 1.1.) was seen in five out of seven patients at first assessment.

(C) Top: FDG-PET of the left ankle of a 19-year-old Dt-GCT patient (left, pretreatment; right, on treatment). Bottom: MRI assessment of the same patient at 6 weeks revealing significant disaggregation of the tumor.

(D) Corresponding immunohistochemistry of $CD68^+CD163^+$ TAM and $CSF\text{-}1R^+$ cells in pretreatment and on-treatment tumor biopsy from the same patient (n = 2). RG7155 treatment reduced $CD68^+CD163^+$ macrophages by 88% and $CSF\text{-}1R^+$ cells by 91%.

(E) Whole-blood samples from Dt-GCT patients were analyzed for monocyte subpopulations pretreatment and on treatment by flow cytometry. $CD14^+CD16^-$ and $CD14^-CD16^+$ cells are shown as relative change from the baseline.

(F) Analysis of CSF-1R expression on monocyte subsets from healthy volunteers given as ratio of CSF-1R relative to the matching isotype.

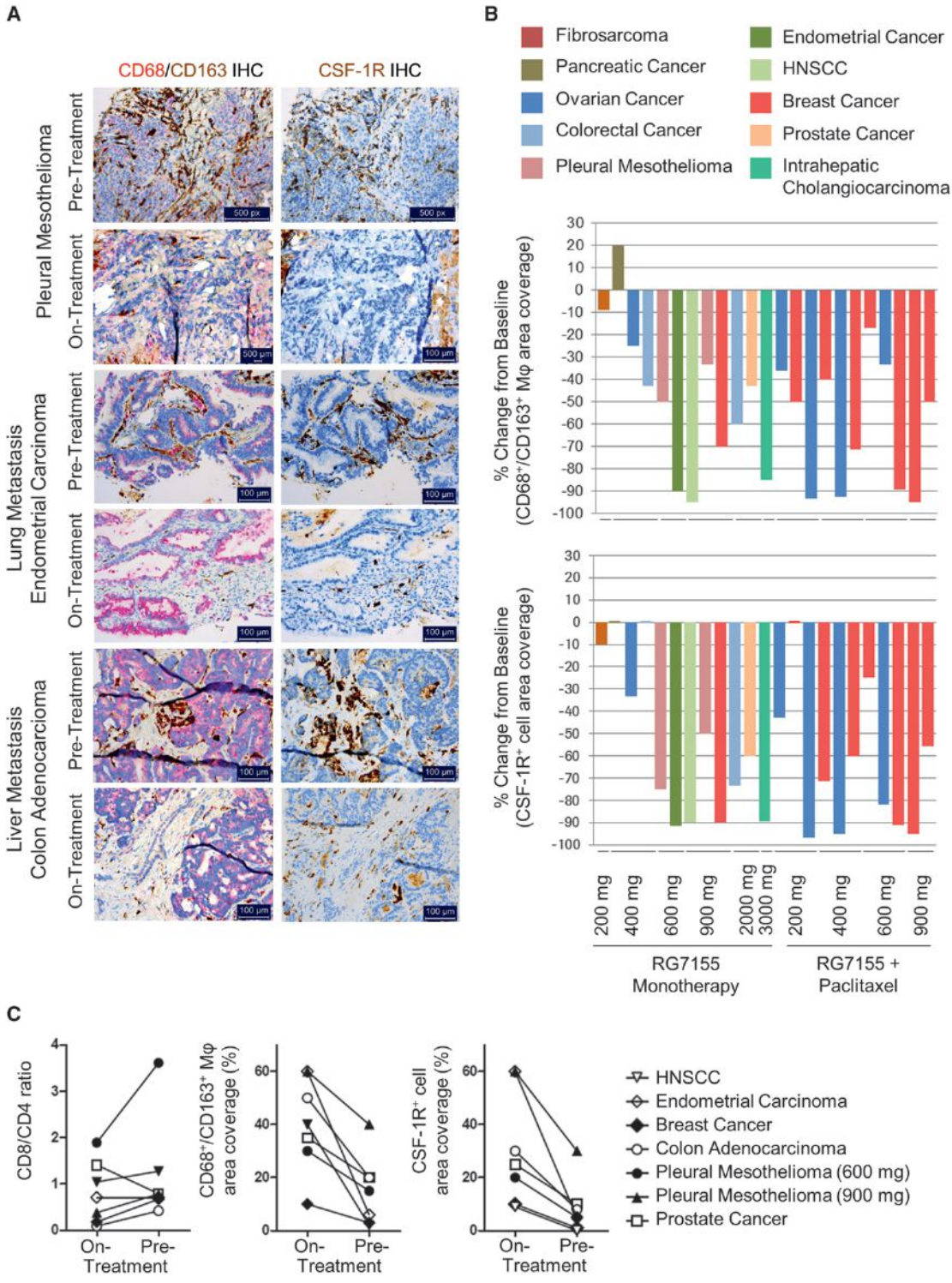

Figure 6. RG7155 Decreases CSF-1R$^+$CD163$^+$ TAM in Patients with Various Types of Solid Tumors and Alters Intratumoral T Cell Composition

(A) Detection of CD68$^+$CD163$^+$ TAM or CSF-1R$^+$ cells in representative pretreatment and on-treatment tumor biopsies from patients with metastatic primary pleural mesothelioma, endometrial carcinoma, and colorectal cancer treated with 600 and 2,000 mg (colorectal cancer) RG7155 as assessed by IHC (20× magnification).

(B) The relative decrease of area coverage of CD68$^+$CD163$^+$ macrophages and CSF-1R$^+$ cells is depicted as the change from the baseline, which is derived from the pretreatment biopsy of patients treated in RG7155 monotherapy and in combination with weekly paclitaxel.

(C) Absolute numbers of CD8$^+$ and CD4$^+$ lymphocyte infiltrates were analyzed by IHC from the indicated patients treated with RG7155 at doses of 600 mg and higher and are depicted as CD8/CD4 ratios of pretreatment and on-treatment biopsies with a different symbol for each individual patient. In addition, the corresponding CD68$^+$CD163$^+$ TAM and CSF-1R$^+$ cells in pretreatment and on-treatment biopsies are shown.

electroporation. Splenocyte-derived hybridomas were subcloned and screened for inhibition of receptor-ligand interaction by ELISA and inhibition of phosphorylation in human WT CSF-1R overexpressing NIH 3T3 cells. RG7155 was selected as the lead candidate after extensive screening of subcloned hybridomas in additional cell-based assays (Figures 2B, S1A, and S1B).

2G2 was generated by immunizing hamster with mouse CSF-1R ECD protein (Wang et al., 1993). Subcloned hybridomas were screened for inhibition of M-NFS-60 cell viability. The parental hamster antibody was chimerized to mouse IgG1.

Monocyte-Derived Macrophages

The study was approved by the local ethics committee (Bayerische Landesärztekammer). Monocytes were enriched from whole blood by negative selection using the Rosette Sep (STEMCELL Technologies) according to the manufacturer's instructions. Monocytes were differentiated into macrophages for 6 days in RPMI plus 10% fetal bovine serum (FBS), 4 mM L-glutamine with recombinant human (rhu)-CSF-1, or rhuGM-CSF for M2 or M1 macrophages, respectively. Monocytes were also treated with different ratio of rhu-CSF-1/rhu-GM-CSF (total 100 ng/ml) for 6 days in the absence or presence of RG7155 or human IgG as a control (data not shown).

Tumor-derived macrophages were generated by culturing freshly isolated monocytes in TCM for 6 days. These media were prepared by culturing of tumor cell lines overnight in media containing 10% FBS followed by 3 days in 1% FBS.

Animal Studies

Monkey

A 90-day pharmacokinetic study was conducted in male cynomolgus monkeys (*Maccaca fascicularis* of Mauritius origin) to assess monocyte subsets in blood, in order to determine the CSF-1 concentration-time profiles in plasma and serum concentration-time profiles of RG7155 after single intravenous (i.v.) administration of 0.1, 1, 10, 30, and 100 mg/kg (n = 2 per dose group). Details of quantification of RG7155 in monkey serum can be found in the Supplemental Experimental Procedures. A 2-week toxicity study was conducted, and IHC tissue analysis of lung, liver, and colon tissue was performed after repeated i.v. doses of 0, 30, and 100 mg/kg given once weekly for 2 weeks to male and female cynomolgus (n = 1 per dose group and per sex). The in vivo studies are in compliance with the Animal Welfare Act, the Guide for the Care and Use of Laboratory Animals, and the Office of Animal Welfare. The study design was based on the principles of the Food and Drug Administration Center for Drug Evaluation and Research (CDER)/International Conference on Harmonisation (ICH) Harmonised Tripartite Guidelines ICH-M3 and Nonclinical Safety Studies for the Conduct of Human Clinical Trials for Pharmaceuticals (CDER, January 2010) and was approved by the Institutional Animal Care and Use Committee (IACUC) at our Association for Assessment and Accreditation of Laboratory Animal Care International (AAALAC)-accredited facility.

Mouse

Female C57BL/6N mice (Charles River) were inoculated subcutaneously with 10^6 MC38 or injected intramuscularly with 10^4 MN/MCA1 tumor cells in the left hind leg. Treatment of ten mice per group with control antibody (MOPC-21; Bio X Cell) and anti-CSF-1R antibody 2G2 at a weekly intraperitoneal dose of 30 mg/kg was initiated when a tumor volume of 50 mm^3 was established (for MC38) or 1 week after injection (for MN/MCA1). Tumor growth was monitored by measurement of tumor size bycaliper two to three times a week. For MN/MCA1, lung metastases were estimated 4 weeks after tumor cell injection, as previously described (Bottazzi et al., 1986). All procedures were performed in accordance with the National Institutes of Health Guidelines for the Care and Use of Laboratory Animals and European Union directives and guidelines and were approved by the local ethics committees (for studies conducted at Roche: Regierung von Oberbayern, Munich, Germany; for studies conducted at the Humanitas Clinical and Research Center: Scientific Board of Humanitas Clinical and Research Center, Milan, Italy).

Clinical Phase 1 Trial

Data are taken from an ongoing multicenter, open-label study at five study sites in France (clinicaltrials.gov identifier NCT01494688). The study is being conducted in accordance with the Declaration of Helsinki, current International Conference on Harmonisation of Technical Requirements for Registration of Pharmaceuticals for Human Use (ICH) guidelines, and all applicable regulatory and ethical requirements. All subjects provided written informed consent before study-related procedures were performed. Patients with relapsed and histologically confirmed diffuse-type giant cell tumors (formerly known as pigmented villonodular synovitis) were enrolled, as well as patients with solid malignancies who were not amenable to standard treatment. In the dose escalation, RG7155 was administered every 2 weeks as an intravenous infusion as monotherapy and in combination with a fixed weekly dose of paclitaxel. The study protocol was approved by the local ethics committee (Comité de la Protection des Personnes of Sud-Est IV) on Octover 26, 2011, and by the French Health Products Safety Agency (ANSM) on November 10, 2011.

Metabolic-Response Assessment by FDG-PET

PET acquisition procedures were standardized across the sites, and images were analyzed centrally. The metabolic response (MR) was assessed using the modified guidelines of the EORTC. MR was classified in relation to the percentage change from the baseline in the sum of the SUVmax for up to five lesion values for each individual patient. Complete MR was defined as the complete resolution of FDG uptake in all lesions, which becomes indistinguishable from surrounding normal tissue. Partial MR (PMR) was defined as a reduction of 25% or more in the sum of the SUVmax after two i.v. administrations of RG7155, with no new lesions detected and no progression of those lesions not selected for SUVmax measurement.

Flow-Cytometric Analysis

Six-week-old female C57BL/6 mice were inoculated with 10^6 MC38 tumor cells and treated with either murine IgG1 or 2G2 twice (days 7 and 14 after tumor inoculation). Leukocyte infiltrate was analyzed 2 days after the second 2G2 administration. Tumors were excised, mechanically and enzymatically processed, and analyzed on a BD FACS Canto II (BD Biosciences). The following antibodies (clones) were used to analyzed leukocyte infiltrate: CD45 (30-F11), CD11b (M1/70), F4/80 (BM8), Ly6G (1A8), Ly6C (AL-21), NK1.1 (PK136), CD4 (RM4-5), CD8 (53-6.7), and the matching isotype controls (all from BioLegend). Viability was determined with either DAPI or Zombie Aqua (BioLegend) dyes.

TAM Suppression Assay

TAMs were enriched from single-cell suspensions of MC38 tumors after enzymatic digest using a two-step protocol. Single cells were stained with CD11b-FITC (clone M1/70) and positively enriched over MACS columns by anti-FITC beads (Miltenyi). Upon removal from the column, anti-FITC beads were detached using release buffer protocol as provided by the manufacturer. Finally, TAMs were isolated by addition of anti-Ly6G and anti-Ly6C positive selection beads in order to remove granulocytic and monocytic cells from TAM preparations. Final cell purity was analyzed and was usually >90%. Subsequently, TAMs were titrated in the indicated ratios to total $CD3^+$ T cells labeled with CFSE in U-bottom plates coated with anti-CD3, and soluble anti-CD28 was added. Cell proliferation was determined from $CFSE^{low}$ cells using blank Sphero beads as previously described after 3 days of incubation (Hoves et al., 2006, 2011).

Statistical Analyses

Results are shown as means ±SEM or ±SD as indicated. Dose-response fits and the calculation of the area under the curve (AUC) were performed using the Excel plug-in XLfit. Statistical analyses were performed using GraphPad Prism and SAS-JMP. For pairwise comparisons, the Tukey-Kramer method was used for multiple testing correction. Individual t tests were performed for significance assessment of the differences between treatments at different cell states.

Further or detailed experimental procedures can be found in the Supplemental Experimental Procedures.

ACCESSION NUMBERS

Coordinates and structure factors have been deposited in the PDB database under accession number 4LIQ.

SUPPLEMENTAL INFORMATION

Supplemental Information includes Supplemental Experimental Procedures, three figures, and one table and can be found with this article online at http://dx.doi.org/10.1016/j.ccr.2014.05.016.

AUTHOR CONTRIBUTIONS

C.H.R., M.A.C. and D.R., with support from J.Y.B., designed and conceptualized the overall research. C.H.R., M.A.C., D.R., and S.H. analyzed data and wrote the manuscript.

ACKNOWLEDGMENTS

We thank Hubert Hertenberger for his support of crystallization efforts, Claudia Kirstenpfad for her work on macrophages, Alexander Fidler and Gudrun Geiselmann for performing hybridoma screening, Maria Grazia Totaro and Theresia Manger-Harasim for their work on the mouse models, Barbara Threm for flow cytometry analyses, Tisee Hau for IHC analysis, Sandra Bunte for T cell isolation, Dominqiue Burger for protein analytics, Expose and the team at the beam line X10SA of the Swiss Light Source in Villigen, Dr. Stefan Ries for valuable strategic advice and review, Dr. Ann-Marie Broeske for scientific support, the Study Management team for managing the phase 1 clinical trial, Dr. Mike Burgess for supporting the clinical development of RG7155, Dr. Sascha Dimitrijevic for helpful discussions, and Dr. John C. Reed for critical review. We thank Dr. Pin Lu (Rx Communications, Mold, UK), who provided support in formatting the manuscript funded by Roche. C.H.R., M.A.C., S.H., J.B., K.W., V.R., F.R.-G., L.P.P., F.F., I.K., T.J., U.J., S.S., K.K., I.H.G., A.W., K.A., H.L., and D.R. are or have been employees of Roche. The clinical trial was funded by F. Hoffmann-La Roche AG. A.S., K.E.d.V., and J.Y.B. received research support from Roche.

Received: October 31, 2013
Revised: February 5, 2014
Accepted: May 21, 2014
Published: June 1, 2014

REFERENCES

Bayne, L.J., Beatty, G.L., Jhala, N., Clark, C.E., Rhim, A.D., Stanger, B.Z., and Vonderheide, R.H. (2012). Tumor-derived granulocyte-macrophage colony-stimulating factor regulates myeloid inflammation and T cell immunity in pancreatic cancer. Cancer Cell *21*, 822–835.

Beatty, G.L., Chiorean, E.G., Fishman, M.P., Saboury, B., Teitelbaum, U.R., Sun, W., Huhn, R.D., Song, W., Li, D., Sharp, L.L., et al. (2011). CD40 agonists alter tumor stroma and show efficacy against pancreatic carcinoma in mice and humans. Science *331*, 1612–1616.

Biswas, S.K., and Mantovani, A. (2010). Macrophage plasticity and interaction with lymphocyte subsets: cancer as a paradigm. Nat. Immunol. *11*, 889–896.

Blay, J.Y., El Sayadi, H., Thiesse, P., Garret, J., and Ray-Coquard, I. (2008). Complete response to imatinib in relapsing pigmented villonodular synovitis/tenosynovial giant cell tumor (PVNS/TGCT). Ann. Oncol. *19*, 821–822.

Bottazzi, B., Mantovani, A., Taraboletti, G., and Giavazzi, R. (1986). Characterization of spontaneous metastases from autochthonous 3-methylcholanthrene-induced tumors. Invasion Metastasis *6*, 44–57.

Bricogne, G., Blanc, E., Brandl, M., Flensburg, C., Keller, P., Paciorek, W., Roversi, P., Sharff, A., Smart, O.S., Vonrhein, C., et al. (2011). BUSTER version X.Y.Z.. (Cambridge: Global Phasing).

Bronte, V., Apolloni, E., Cabrelle, A., Ronca, R., Serafini, P., Zamboni, P., Restifo, N.P., and Zanovello, P. (2000). Identification of a CD11b(+)/Gr-1(+)/CD31(+) myeloid progenitor capable of activating or suppressing CD8(+) T cells. Blood *96*, 3838–3846.

Cassier, P.A., Gelderblom, H., Stacchiotti, S., Thomas, D., Maki, R.G., Kroep, J.R., van der Graaf, W.T., Italiano, A., Seddon, B., Dômont, J., et al. (2012). Efficacy of imatinib mesylate for the treatment of locally advanced and/or metastatic tenosynovial giant cell tumor/pigmented villonodular synovitis. Cancer *118*, 1649–1655.

Cavnar, M.J., Zeng, S., Kim, T.S., Sorenson, E.C., Ocuin, L.M., Balachandran, V.P., Seifert, A.M., Greer, J.B., Popow, R., Crawley, M.H., et al. (2013). KIT oncogene inhibition drives intratumoral macrophage M2 polarization. J. Exp. Med. *210*, 2873–2886.

Chen, D.S., and Mellman, I. (2013). Oncology meets immunology: the cancer-immunity cycle. Immunity *39*, 1–10.

Chitu, V., and Stanley, E.R. (2006). Colony-stimulating factor-1 in immunity and inflammation. Curr. Opin. Immunol. *18*, 39–48.

Collaborative Computational Project, Number 4 (1994). The CCP4 suite: programs for protein crystallography. Acta Crystallogr. D Biol. Crystallogr. *50*, 760–763.

Cupp, J.S., Miller, M.A., Montgomery, K.D., Nielsen, T.O., O'Connell, J.X., Huntsman, D., van de Rijn, M., Gilks, C.B., and West, R.B. (2007). Translocation and expression of CSF1 in pigmented villonodular synovitis, tenosynovial giant cell tumor, rheumatoid arthritis and other reactive synovitides. Am. J. Surg. Pathol. *31*, 970–976.

De Palma, M., and Lewis, C.E. (2013). Macrophage regulation of tumor responses to anticancer therapies. Cancer Cell *23*, 277–286.

DeNardo, D.G., Brennan, D.J., Rexhepaj, E., Ruffell, B., Shiao, S.L., Madden, S.F., Gallagher, W.M., Wadhwani, N., Keil, S.D., Junaid, S.A., et al. (2011). Leukocyte complexity predicts breast cancer survival and functionally regulates response to chemotherapy. Cancer Discov. *1*, 54–67.

Dewar, A.L., Cambareri, A.C., Zannettino, A.C., Miller, B.L., Doherty, K.V., Hughes, T.P., and Lyons, A.B. (2005). Macrophage colony-stimulating factor receptor c-fms is a novel target of imatinib. Blood *105*, 3127–3132.

Dolcetti, L., Peranzoni, E., Ugel, S., Marigo, I., Fernandez Gomez, A., Mesa, C., Geilich, M., Winkels, G., Traggiai, E., Casati, A., et al. (2010). Hierarchy of immunosuppressive strength among myeloid-derived suppressor cell subsets is determined by GM-CSF. Eur. J. Immunol. *40*, 22–35.

El-Gamal, M.I., Anbar, H.S., Yoo, K.H., and Oh, C.H. (2013). FMS kinase inhibitors: current status and future prospects. Med. Res. Rev. *33*, 599–636.

Elegheert, J., Desfosses, A., Shkumatov, A.V., Wu, X., Bracke, N., Verstraete, K., Van Craenenbroeck, K., Brooks, B.R., Svergun, D.I., Vergauwen, B., et al. (2011). Extracellular complexes of the hematopoietic human and mouse CSF-1 receptor are driven by common assembly principles. Structure *19*, 1762–1772.

Emsley, P., Lohkamp, B., Scott, W.G., and Cowtan, K. (2010). Features and development of Coot. Acta Crystallogr. D Biol. Crystallogr. *66*, 486–501.

Espinosa, I., Beck, A.H., Lee, C.H., Zhu, S., Montgomery, K.D., Marinelli, R.J., Ganjoo, K.N., Nielsen, T.O., Gilks, C.B., West, R.B., and van de Rijn, M. (2009). Coordinate expression of colony-stimulating factor-1 and colony-stimulating factor-1-related proteins is associated with poor prognosis in gynecological and nongynecological leiomyosarcoma. Am. J. Pathol. *174*, 2347–2356.

Geissmann, F., Manz, M.G., Jung, S., Sieweke, M.H., Merad, M., and Ley, K. (2010). Development of monocytes, macrophages, and dendritic cells. Science *327*, 656–661.

Gelderblom, H., Pérol, D., Chevreau, C., Tattersall, M.H.N., Stacchiotti, S., Casali, P.G., Cropet, C., Piperno-Neumann, S., Le Cesne, A., Italiano, A., et al. (2013). An open-label international multicentric phase II study of nilotinib in progressive pigmented villo-nodular synovitis (PVNS) not amenable to a conservative surgical treatment. 2013 ASCO Annual Meeting Proceedings. J. Clin. Oncol. *31*, (suppl.; abstr. 10516).

Gordon, S., and Martinez, F.O. (2010). Alternative activation of macrophages: mechanism and functions. Immunity *32*, 593–604.

Greter, M., Lelios, I., Pelczar, P., Hoeffel, G., Price, J., Leboeuf, M., Kündig, T.M., Frei, K., Ginhoux, F., Merad, M., and Becher, B. (2012). Stroma-derived interleukin-34 controls the development and maintenance of langerhans cells and the maintenance of microglia. Immunity *37*, 1050–1060.

Hamilton, J.A., and Achuthan, A. (2013). Colony stimulating factors and myeloid cell biology in health and disease. Trends Immunol. *34*, 81–89.

Hoves, S., Krause, S.W., Schütz, C., Halbritter, D., Schölmerich, J., Herfarth, H., and Fleck, M. (2006). Monocyte-derived human macrophages mediate

anergy in allogeneic T cells and induce regulatory T cells. J. Immunol. *177*, 2691–2698.

Hoves, S., Sutton, V.R., Haynes, N.M., Hawkins, E.D., Fernández Ruiz, D., Baschuk, N., Sedelies, K.A., Schnurr, M., Stagg, J., Andrews, D.M., et al. (2011). A critical role for granzymes in antigen cross-presentation through regulating phagocytosis of killed tumor cells. J. Immunol. *187*, 1166–1175.

Hume, D.A., and MacDonald, K.P. (2012). Therapeutic applications of macrophage colony-stimulating factor-1 (CSF-1) and antagonists of CSF-1 receptor (CSF-1R) signaling. Blood *119*, 1810–1820.

Kabsch, W.X.D.S. (2010). Integration, scaling, space-group assignment and post-refinement. Acta Crystallogr. D Biol. Crystallogr. *66*, 133–144.

King, E.R., and Wong, K.K. (2012). Insulin-like growth factor: current concepts and new developments in cancer therapy. Recent Patents Anticancer. Drug Discov. *7*, 14–30.

Kluger, H.M., Dolled-Filhart, M., Rodov, S., Kacinski, B.M., Camp, R.L., and Rimm, D.L. (2004). Macrophage colony-stimulating factor-1 receptor expression is associated with poor outcome in breast cancer by large cohort tissue microarray analysis. Clin. Cancer Res. *10*, 173–177.

Kurahara, H., Shinchi, H., Mataki, Y., Maemura, K., Noma, H., Kubo, F., Sakoda, M., Ueno, S., Natsugoe, S., and Takao, S. (2011). Significance of M2-polarized tumor-associated macrophage in pancreatic cancer. J. Surg. Res. *167*, e211–e219.

Ma, X., Lin, W.Y., Chen, Y., Stawicki, S., Mukhyala, K., Wu, Y., Martin, F., Bazan, J.F., and Starovasnik, M.A. (2012). Structural basis for the dual recognition of helical cytokines IL-34 and CSF-1 by CSF-1R. Structure *20*, 676–687.

Mantovani, A., Sozzani, S., Locati, M., Allavena, P., and Sica, A. (2002). Macrophage polarization: tumor-associated macrophages as a paradigm for polarized M2 mononuclear phagocytes. Trends Immunol. *23*, 549–555.

Martinez, F.O., Sica, A., Mantovani, A., and Locati, M. (2008). Macrophage activation and polarization. Front. Biosci. *13*, 453–461.

McCoy, A.J., Grosse-Kunstleve, R.W., Adams, P.D., Winn, M.D., Storoni, L.C., and Read, R.J. (2007). Phaser crystallographic software. J. Appl. Cryst. *40*, 658–674.

Murdoch, C., Muthana, M., Coffelt, S.B., and Lewis, C.E. (2008). The role of myeloid cells in the promotion of tumour angiogenesis. Nat. Rev. Cancer *8*, 618–631.

Nakoinz, I., Lee, M.T., Weaver, J.F., and Ralph, P. (1990). Differentiation of the IL-3-dependent NFS-60 cell line and adaption to growth in macrophage colony-stimulating factor. J. Immunol. *145*, 860–864.

Nandi, S., Cioce, M., Yeung, Y.G., Nieves, E., Tesfa, L., Lin, H., Hsu, A.W., Halenbeck, R., Cheng, H.Y., Gokhan, S., et al. (2013). Receptor-type protein-tyrosine phosphatase ξ is a functional receptor for interleukin-34. J. Biol. Chem. *288*, 21972–21986.

Pollard, J.W. (2009). Trophic macrophages in development and disease. Nat. Rev. Immunol. *9*, 259–270.

Pyonteck, S.M., Akkari, L., Schuhmacher, A.J., Bowman, R.L., Sevenich, L., Quail, D.F., Olson, O.C., Quick, M.L., Huse, J.T., Teijeiro, V., et al. (2013). CSF-1R inhibition alters macrophage polarization and blocks glioma progression. Nat. Med. *19*, 1264–1272.

Ravi, V., Wang, W.L., and Lewis, V.O. (2011). Treatment of tenosynovial giant cell tumor and pigmented villonodular synovitis. Curr. Opin. Oncol. *23*, 361–366.

Roussel, M.F., Downing, J.R., and Sherr, C.J. (1990). Transforming activities of human CSF-1 receptors with different point mutations at codon 301 in their extracellular domains. Oncogene *5*, 25–30.

Shabo, I., Stål, O., Olsson, H., Doré, S., and Svanvik, J. (2008). Breast cancer expression of CD163, a macrophage scavenger receptor, is related to early distant recurrence and reduced patient survival. Int. J. Cancer *123*, 780–786.

Sherr, C.J., Ashmun, R.A., Downing, J.R., Ohtsuka, M., Quan, S.G., Golde, D.W., and Roussel, M.F. (1989). Inhibition of colony-stimulating factor-1 activity by monoclonal antibodies to the human CSF-1 receptor. Blood *73*, 1786–1793.

Shree, T., Olson, O.C., Elie, B.T., Kester, J.C., Garfall, A.L., Simpson, K., Bell-McGuinn, K.M., Zabor, E.C., Brogi, E., and Joyce, J.A. (2011). Macrophages and cathepsin proteases blunt chemotherapeutic response in breast cancer. Genes Dev. *25*, 2465–2479.

Strachan, D.C., Ruffell, B., Oei, Y., Bissell, M.J., Coussens, L.M., Pryer, N., and Daniel, D. (2013). CSF1R inhibition delays cervical and mammary tumor growth in murine models by attenuating the turnover of tumor-associated macrophages and enhancing infiltration by CD8(+) T cells. OncoImmunology *2*, e26968.

Taylor, J.R., Brownlow, N., Domin, J., and Dibb, N.J. (2006). FMS receptor for M-CSF (CSF-1) is sensitive to the kinase inhibitor imatinib and mutation of Asp-802 to Val confers resistance. Oncogene *25*, 147–151.

Verstraete, K., and Savvides, S.N. (2012). Extracellular assembly and activation principles of oncogenic class III receptor tyrosine kinases. Nat. Rev. Cancer *12*, 753–766.

Wang, Z.E., Myles, G.M., Brandt, C.S., Lioubin, M.N., and Rohrschneider, L. (1993). Identification of the ligand-binding regions in the macrophage colony-stimulating factor receptor extracellular domain. Mol. Cell. Biol. *13*, 5348–5359.

Weiskopf, K., Ring, A.M., Ho, C.C., Volkmer, J.P., Levin, A.M., Volkmer, A.K., Ozkan, E., Fernhoff, N.B., van de Rijn, M., Weissman, I.L., and Garcia, K.C. (2013). Engineered SIRPα variants as immunotherapeutic adjuvants to anticancer antibodies. Science *341*, 88–91.

West, R.B., Rubin, B.P., Miller, M.A., Subramanian, S., Kaygusuz, G., Montgomery, K., Zhu, S., Marinelli, R.J., De Luca, A., Downs-Kelly, E., et al. (2006). A landscape effect in tenosynovial giant-cell tumor from activation of CSF1 expression by a translocation in a minority of tumor cells. Proc. Natl. Acad. Sci. USA *103*, 690–695.

Wynn, T.A., Chawla, A., and Pollard, J.W. (2013). Macrophage biology in development, homeostasis and disease. Nature *496*, 445–455.

Yang, H., Testa, J.R., and Carbone, M. (2008). Mesothelioma epidemiology, carcinogenesis, and pathogenesis. Curr. Treat. Options Oncol. *9*, 147–157.

Young, H., Baum, R., Cremerius, U., Herholz, K., Hoekstra, O., Lammertsma, A.A., Pruim, J., and Price, P.; European Organization for Research and Treatment of Cancer (EORTC) PET Study Group (1999). Measurement of clinical and subclinical tumour response using [18F]-fluorodeoxyglucose and positron emission tomography: review and 1999 EORTC recommendations. Eur. J. Cancer *35*, 1773–1782.

Yuzawa, S., Opatowsky, Y., Zhang, Z., Mandiyan, V., Lax, I., and Schlessinger, J. (2007). Structural basis for activation of the receptor tyrosine kinase KIT by stem cell factor. Cell *130*, 323–334.

Zhang, Q.W., Liu, L., Gong, C.Y., Shi, H.S., Zeng, Y.H., Wang, X.Z., Zhao, Y.W., and Wei, Y.Q. (2012). Prognostic significance of tumor-associated macrophages in solid tumor: a meta-analysis of the literature. PLoS ONE *7*, e50946.

Cancer Cell
Article

Identification of Distinct Basal and Luminal Subtypes of Muscle-Invasive Bladder Cancer with Different Sensitivities to Frontline Chemotherapy

Woonyoung Choi,[1] Sima Porten,[1] Seungchan Kim,[6] Daniel Willis,[1] Elizabeth R. Plimack,[7] Jean Hoffman-Censits,[8] Beat Roth,[1] Tiewei Cheng,[1,5] Mai Tran,[1,5] I-Ling Lee,[1] Jonathan Melquist,[1] Jolanta Bondaruk,[3] Tadeusz Majewski,[3] Shizhen Zhang,[3] Shanna Pretzsch,[1] Keith Baggerly,[4] Arlene Siefker-Radtke,[2] Bogdan Czerniak,[3] Colin P.N. Dinney,[1] and David J. McConkey[1,5,*]

[1]Department of Urology, University of Texas MD Anderson Cancer Center, Houston, TX 77030, USA
[2]Department of Genitourinary Medical Oncology, University of Texas MD Anderson Cancer Center, Houston, TX 77030, USA
[3]Department of Pathology, University of Texas MD Anderson Cancer Center, Houston, TX 77030, USA
[4]Department of Bioinformatics, University of Texas MD Anderson Cancer Center, Houston, TX 77030, USA
[5]The University of Texas-Graduate School of Biomedical Sciences (GSBS) at Houston, Houston, TX 77030, USA
[6]Computational Biology Division, Translational Genomics Research Institute, 445N, Fifth Street, Phoenix, AZ 85004, USA
[7]Department of Medical Oncology, Fox Chase Cancer Center, 333 Cottman Avenue, Philadelphia, PA 19111-2497, USA
[8]Department of Medical Oncology, Thomas Jefferson University Hospital, 1025 Walnut Street, Suite 700, Philadelphia, PA 19107, USA
*Correspondence: dmcconke@mdanderson.org
http://dx.doi.org/10.1016/j.ccr.2014.01.009

SUMMARY

Muscle-invasive bladder cancers (MIBCs) are biologically heterogeneous and have widely variable clinical outcomes and responses to conventional chemotherapy. We discovered three molecular subtypes of MIBC that resembled established molecular subtypes of breast cancer. Basal MIBCs shared biomarkers with basal breast cancers and were characterized by p63 activation, squamous differentiation, and more aggressive disease at presentation. Luminal MIBCs contained features of active PPARγ and estrogen receptor transcription and were enriched with activating *FGFR3* mutations and potential FGFR inhibitor sensitivity. p53-like MIBCs were consistently resistant to neoadjuvant methotrexate, vinblastine, doxorubicin and cisplatin chemotherapy, and all chemoresistant tumors adopted a p53-like phenotype after therapy. Our observations have important implications for prognostication, the future clinical development of targeted agents, and disease management with conventional chemotherapy.

INTRODUCTION

Bladder cancer progresses along two distinct pathways that pose distinct challenges for clinical management (Dinney et al., 2004). Low-grade non-muscle invasive ("superficial") cancers, which account for 70% of tumor incidence, are not immediately life-threatening, but they have a propensity for recurrence that necessitates costly lifelong surveillance (Botteman et al., 2003). In contrast, high-grade muscle-invasive bladder cancers (MIBCs) progress rapidly to become metastatic and generate the bulk of patient mortality (Shah et al., 2011). Radical cystectomy with perioperative cisplatin-based combination chemotherapy is the current standard of care for high-risk MIBC. Treatment selection depends heavily on clinico-pathologic features, but current staging systems are woefully inaccurate and result in an unacceptably high rate of clinical understaging and consequently inadequate treatment (Svatek et al., 2011). Furthermore, cisplatin-based chemotherapy is only effective in 30%–40% of cases, and it is not yet possible to prospectively identify the patients who are likely to obtain benefit (Shah

Significance

Using whole genome mRNA expression profiling, we identified three molecular subtypes of muscle-invasive bladder cancer (MIBC) that shared molecular features with basal and luminal breast cancers. Tumors in one of them expressed an active p53 gene signature, and these "p53-like" MIBCs were consistently resistant to frontline neoadjuvant cisplatin-based combination chemotherapy. Furthermore, comparison of matched gene expression profiles before and after chemotherapy revealed that all resistant tumors expressed wild-type p53 gene expression signatures. Together, the data indicate that "p53-ness" plays a central role in chemoresistance in bladder cancer and suggest that it should be possible to prospectively identify the patients who most likely will not benefit from neoadjuvant chemotherapy.

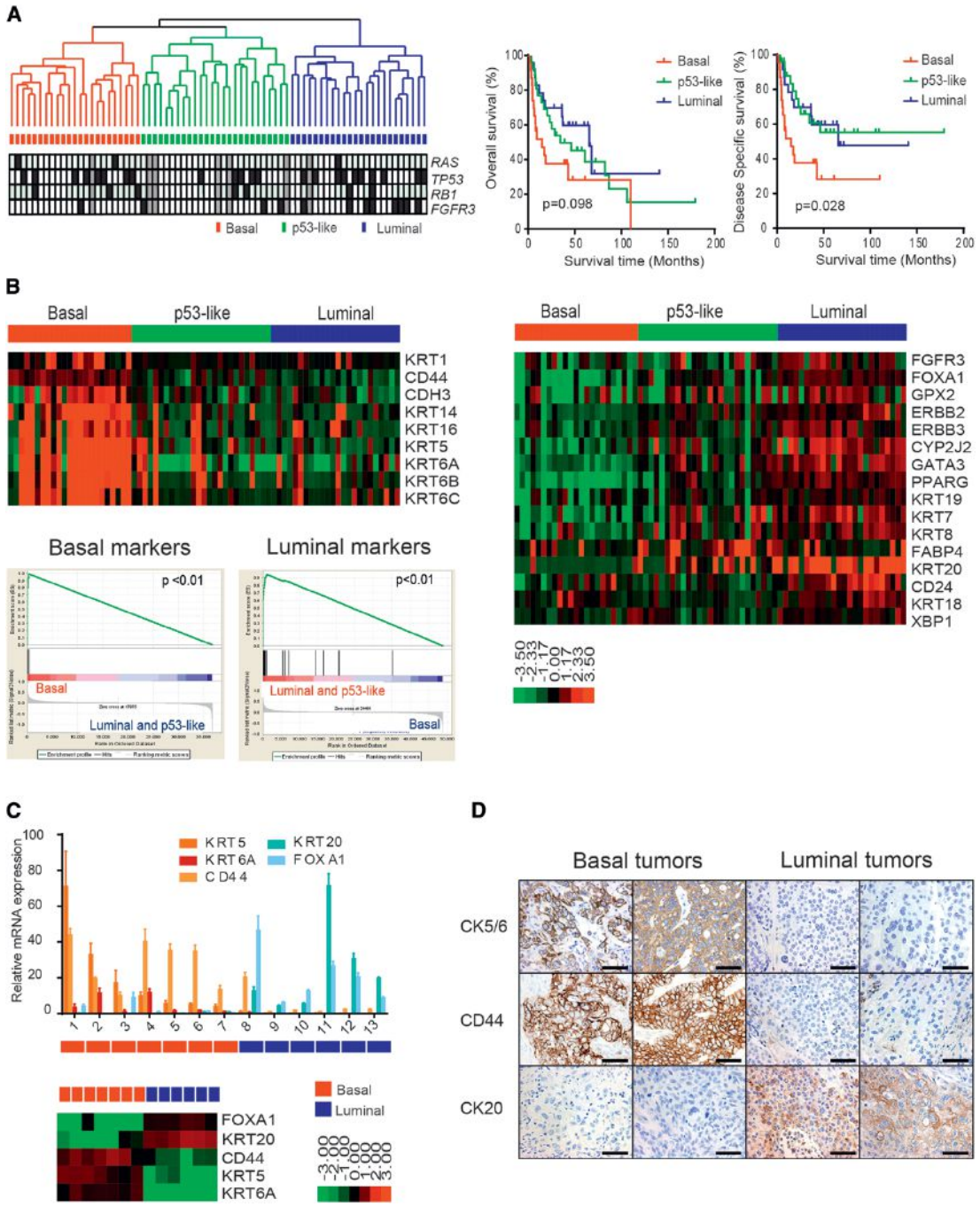

Figure 1. Basal and Luminal Subtypes of Bladder Cancer

(A) Left: whole genome mRNA expression profiling and hierarchical cluster analysis of a cohort of 73 MIBCs. RNA from fresh frozen tumors was analyzed using Illumina arrays. *RAS*, *TP53*, *RB1*, and *FGFR3* mutations were detected by sequencing and are indicated in the color bars below the dendrogram. Black, mutation; white, wild-type; gray, mutation data were unavailable. Right: Kaplan-Meier plots of overall survival ($p = 0.098$) and disease-specific survival ($p = 0.028$) in the three tumor subtypes.

(B) Expression of basal and luminal markers in the three subtypes. The heat maps depict relative expression of basal (left) and luminal (right) biomarkers. GSEA analyses (below, left) were used to determine whether basal and luminal markers were enriched in the subtypes.

(C) Quantitative RT-PCR was used to evaluate the accuracy of the gene expression profiling results. Relative levels of the indicated basal (red shades) and luminal (blue shades) biomarkers measured by RT-PCR were compared to the levels of the same markers measured by gene expression profiling on RNA isolated from macrodissected FFPE sections of the same tumors. Results are presented as relative quantitation (RQ) and the error bars indicate the range of RQ values as defined by 95% confidence level. RT-PCR results are shown on top, DASL gene expression profiling results are shown below.

(D) Analysis of basal and luminal marker expression by immunohistochemistry. Results from two representative basal (left) and luminal (right) tumors as defined by gene expression profiling are displayed. The scale bars correspond to 100 μm.

See also Figure S1.

Table 1. Clinicopathologic Characteristics of the MDACC Discovery Cohort

Characteristic	Total	Basal	p53-like	Luminal	p Value
Cohort size	73	23 (32%)	26 (36%)	24 (33%)	
Mean age (years) ± SD	68.8 ± 10.2	70.1 ± 9.4	69.8 ± 8.9	66.4 ± 12.1	0.371
Gender					
Female	19 (26%)	10 (44%)	6 (23%)	3 (13%)	0.133
Male	54 (74%)	13 (57%)	20 (77%)	21 (88%)	
Race					
Caucasian	54 (74%)	14 (61%)	21 (81%)	19 (79%)	0.352
African American	12 (16%)	6 (26%)	2 (7%)	4 (17%)	
Hispanic	7 (10%)	3 (13%)	3 (12%)	1 (4%)	
Clinical stage at TUR (N0,M0)					
≤cT1	0 (0%)	0 (0%)	0 (0%)	0 (0%)	0.990
cT2	37 (51%)	9 (39%)	16 (62%)	12 (50%)	
cT3	16 (22%)	4 (17%)	7 (27%)	5 (21%)	
cT4	6 (8%)	2 (9%)	2 (8%)	2 (8%)	
Positive clinical lymph nodes, cN+	11 (15%)	5 (22%)	1 (4%)	5 (21%)	0.137
Positive clinical metastasis, cM+	7 (10%)	5 (22%)	0 (0%)	2 (8%)	0.035
Primary treatment					
Cystectomy	57 (78%)	15 (65%)	25 (96%)	17 (71%)	0.019
Other[a]	16 (22%)	8 (35%)	1 (4%)	7 (29%)	
Neoadjuvant Chemotherapy, NAC	18 (25%)	5 (22%)	7 (27%)	6 (25%)	0.910
Response to NAC[b]					
Yes	6 (33%)	2 (40%)	0 (0%)	4 (67%)	0.018
No	12 (67%)	3 (60%)	7 (100%)	2 (33%)	
Pathologic T stage (n = 57)					
pT0	4 (7%)	2 (13%)	0 (0%)	2 (12%)	0.001
pTa, pT1, pTis	6 (11%)	2 (13%)	1 (4%)	3 (18%)	
pT2	10 (18%)	1 (7%)	4 (16%)	5 (29%)	
pT3	25 (44%)	4 (27%)	18 (72%)	3 (18%)	
pT4	12 (21%)	6 (40%)	2 (8%)	4 (22%)	
Positive pathologic lymph nodes	23 (40%)	3 (13%)	14 (54%)	6 (25%)	0.010
Variant histology in specimen					
Squamous differentiation	18 (32%)	13 (57%)	4 (15%)	1 (4%)	<0.001
Sarcomatoid differentiation	3 (5%)	3 (13%)	0 (0%)	0 (0%)	
Other (micropapillary, glandular, adenocarcinoma)	3 (5%)	0 (0%)	3 (12%)	0 (0%)	
Median overall survival (months)	37.2	14.9	34.6	65.6	0.098
Median disease-specific survival (months)	46.3	14.9	not reached	65.6	0.028

The Kruskal-Wallis test was used to compare differences in mean age between groups. Log-rank test was used to compare differences in survival (overall and disease-specific) between groups. For the remainder of categorical variables, Fisher's exact test was used to determine differences between subtypes. p values < 0.05 were considered significant.

[a]Chemotherapy was recommended for all 16 patients, based on available medical records; nine patients had documentation of completion.

[b]Decrease in stage to pT0 or pT1 (for patients with high-risk features at TUR: lymphovascular invasion, variant histology, hydronephrosis, or abnormal exam under anesthesia) at cystectomy.

et al., 2011). To add to the quandary, no effective alternative to cisplatin-based chemotherapy has been identified for resistant tumors. Therefore, there is an urgent need to develop a more precise, biology-based approach to the classification of bladder cancer to inform clinical management.

Gene expression profiling has been used to identify molecular heterogeneity in other human cancers. For example, Perou and coworkers (Perou et al., 2000) used gene expression profiling to identify molecular subtypes of breast cancer (basal/triple negative, HER2$^+$, luminal A, and luminal B) that behave clinically as though they are distinct disease entities—luminal breast cancers respond to estrogen receptor (ER)-targeted therapy, HER2$^+$ tumors to Herceptin and other ErbB2-blocking agents, and basal tumors to chemotherapy only (Rouzier et al., 2005). Previous studies in bladder cancer identified signatures associated with stage and outcomes (Blaveri et al., 2005; Dyrskjøt et al., 2003; Sanchez-Carbayo et al., 2006; Sjodahl et al., 2012) and progression (Kim et al., 2010; Lee et al., 2010), but the biological and

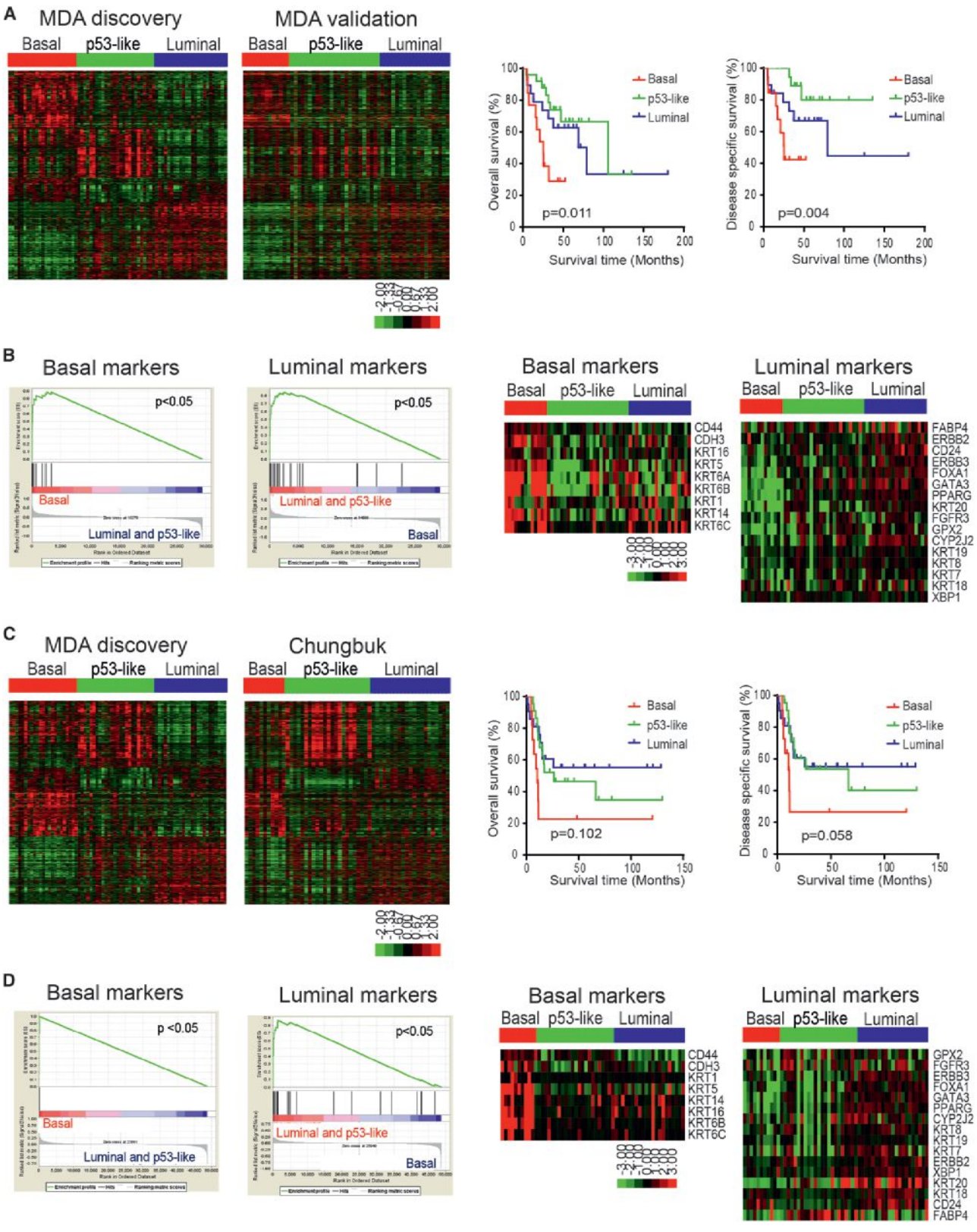

(legend on next page)

clinical significance of these signatures remain unclear. Here we also used gene expression profiling and unsupervised analyses to identify molecular subtypes of MIBC with the goal of defining the biological basis for the molecular heterogeneity that is observed in them.

RESULTS

Muscle-Invasive Bladder Cancers Can Be Grouped into Basal and Luminal Subtypes

We performed whole genome mRNA expression profiling and unsupervised hierarchical cluster analyses on a cohort of 73 primary fresh-frozen MIBCs obtained by transurethral resection at our institution. We identified three distinct molecular subtypes (Figure 1A; Table 1). The upregulated genes (fold changes) that determined subtype assignments contained signature biomarkers for basal (CD44, KRT5, KRT6, KRT14, and CDH3) and luminal (CD24, FOXA1, GATA3, ERBB2, ERBB3, XBP1, and KRT20) breast cancers, respectively (Figure 1B, heat maps; Figure S1A available online; Perou et al., 2000), and formal gene set enrichment analyses (GSEA) confirmed that the subtypes were enriched with basal and luminal markers (Figure 1B, below). In control experiments, we confirmed that the array-based measurements of basal and luminal marker expression correlated well with the results obtained with quantitative RT-PCR (Figure 1C) or immunohistochemistry (Figure 1D) in some of the same tumors. We therefore propose the names "basal" and "luminal" for two of the MIBC subtypes. Although the tumors in the third subtype also expressed luminal biomarkers (Figure 1B; Figure S1A), we have termed this MIBC subtype "p53-like" because its distinguishing feature was an activated wild-type p53 gene expression signature that we will discuss further below.

Table 1 depicts the clinical and pathologic characteristics of the discovery cohort by molecular subtype. Basal tumors were enriched with sarcomatoid features and metastatic disease at presentation (Table 1) and were associated with shorter overall survival (14.9 months, p = 0.098), and disease-specific survival (median 14.9 months, p = 0.028; Figure 1A, right). Although they expressed epithelial cytokeratins, basal tumors also contained "mesenchymal" biomarkers (i.e., TWIST1/2, SNAI2, ZEB2, and VIM; McConkey et al., 2010; Peinado et al., 2007; Figure S1B), as do basal breast cancers (Chaffer et al., 2013). In addition, basal tumors expressed high levels of the epidermal growth factor receptor (EGFR) and several of its ligands (Figure S1B), similar to basal breast and head and neck squamous cell carcinomas (Perou et al., 2000; Romano et al., 2009; Sørlie et al., 2001). On the other hand, luminal tumors were enriched with "epithelial" biomarkers (E-cadherin/CDH1 and members of the miR-200 family; Gregory et al., 2008; Figure S1B), high levels of fibroblast growth factor receptor-3 (FGFR3), and activating *FGFR3* mutations (Figures 1A and 1B; Figure S1C). *TP53* mutation frequencies were similar in all of the subtypes (Figure S1C). To examine cluster stability, we calculated silhouette scores for each subtype. All of the basal and luminal tumors were stable, whereas 9/26 of the p53-like tumors were not (Figure S1D); five of these unstable tumors were most similar to the luminal subtype (data not shown).

We developed a classifier using the differentially expressed genes associated with subtype membership in the discovery cohort and applied it to whole genome mRNA expression data from an independent cohort of formalin-fixed paraffin-embedded MIBCs (n = 57, MD Anderson validation cohort; Figure 2A; Table S1). Like the discovery cohort, basal tumors in the validation cohort were associated with shorter overall survival (median 25.0 months, p = 0.011) and disease-specific survival (median 25.3 months, p = 0.004; Figure 2A, right side) and were enriched with basal biomarkers compared to tumors in the other subtypes (Figure 2B). We then used the classifier to make additional predictions in the MIBCs (n = 55) from a third, publicly available gene expression profiling data set ("Chungbuk cohort"; Kim et al., 2010; Figure 2C; Table S2). The Chungbuk basal tumors were also associated with shorter median disease-specific survival (11.2 months, p = 0.102) and overall survival (10.4 months, p = 0.058; Figure 2C, right side) and were enriched with basal biomarkers (Figure 2D). In addition, GSEA confirmed that luminal biomarkers were enriched in luminal subtypes in both of the validation cohorts (Figures 2B and 2D).

Basal Tumors Are Characterized by Squamous Differentiation

Bladder cancers with squamous histological features are generally considered distinct from conventional urothelial cancers. However, the basal MIBCs in the discovery and validation cohorts were significantly enriched with squamous features (Figure 3A; Table 1; Table S1), and the basal tumors with squamous features also expressed higher basal biomarker mRNA levels than did basal tumors without squamous features (data not shown). The high molecular weight keratins (KRT5, KRT6, and KRT14) that characterized basal MIBCs were also enriched in a lethal "squamous cell carcinoma" MIBC subtype that was

Figure 2. Characterization of Basal and Luminal Subtypes in other MIBC Cohorts

(A) Subtype classification of the MD Anderson validation cohort (n = 57). RNA was isolated from macrodissected FFPE tumor sections and whole genome mRNA expression was measured using Illumina's DASL platform. Kaplan-Meier plots of overall survival (p = 0.011) and disease-specific survival (p = 0.004) associated with the three subtypes are presented on the right.

(B) Expression of basal and luminal markers in the molecular subtypes in the MD Anderson validation cohort. The results of GSEA of basal and luminal marker expression in the subtypes are displayed on the left, and heat maps depicting relative basal and luminal marker levels in the subtypes are displayed on the right.

(C) Subtype classification of the Chungbuk cohort (n = 55). Whole genome mRNA expression profiling (Illumina platform) and clinical data were downloaded from GEO (GSE13507), and the oneNN classifier was used to assign tumors to subtypes. Tumors were assigned to subtypes using the oneNN prediction model (left). Kaplan-Meier plots of overall survival (p = 0.102) and disease-specific survival (p = 0.058) as a function of tumor subtype (right).

(D) Expression of basal and luminal markers in the molecular subtypes in the Chungbuk cohort. The results of GSEA of basal and luminal marker expression in the subtypes are displayed on the left, and heat maps depicting basal and luminal marker expression are displayed on the right.

See also Tables S1 and S2.

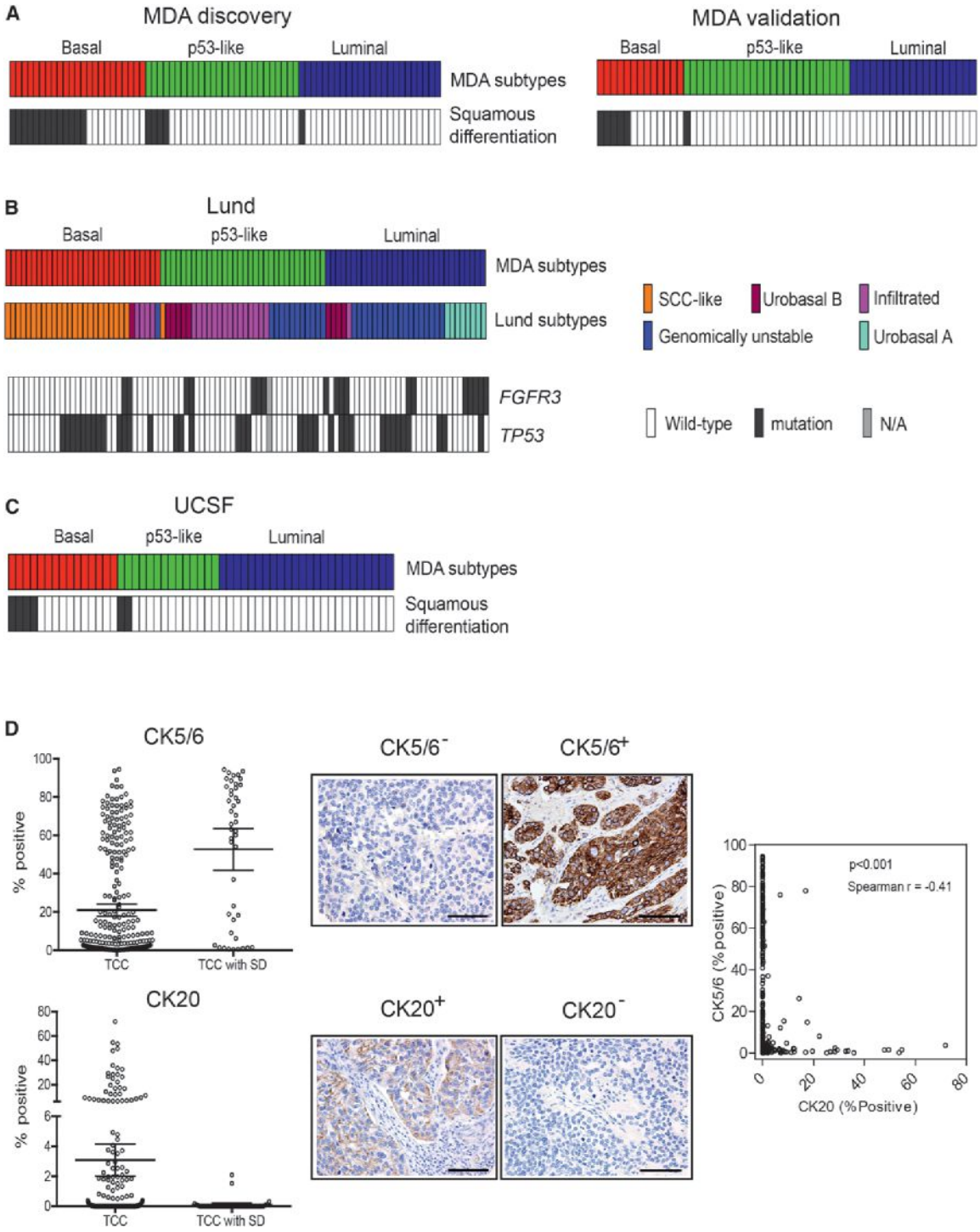

Figure 3. Presence of Squamous Features in the Subtypes

(A) Tumor squamous feature content in the MD Anderson discovery and validation cohorts. Subtype designations are indicated by the top color bars, and the presence of squamous features (in black) is indicated in the color bars below.

(B) Relationship between the MD Anderson subtypes and the molecular taxonomy developed by Sjodahl and colleagues (Sjodahl et al., 2012). Whole genome mRNA expression (Illumina platform) and clinical data were downloaded from GEO (GSE32894), and the oneNN classifier was used to assign the Lund tumors to subtypes. Subtype membership is indicated by the top color bars, and *FGFR3* and *TP53* mutations in the Lund tumors are indicated in color bars below. Black, mutant; white, wild-type; gray (N/A), mutation data were not available.

(C) Presence of squamous features in the UCSF data set. Gene expression profiling (in-house platform) and clinical data were downloaded from GEO (GSE1827), and the oneNN classifier was used to assign the UCSF tumors to the subtypes. Subtype memberships for each tumor are indicated in the top color bars, and the presence of squamous features (in black) is indicated in the color bar below.

(legend continued on next page)

identified recently by another group (Sjodahl et al., 2012). We applied our subtype classifier to the other group's data set ("Lund cohort"; Sjodahl et al., 2012) and confirmed that the Lund squamous cell carcinoma subtype (Sjodahl et al., 2012) corresponded to the basal subtype identified here ("Lund" tumors, Figure 3B; Table S3). Furthermore, like the MD Anderson discovery and validation cohorts, the Lund basal/SCC-like tumors were enriched with squamous differentiation (Sjodahl et al., 2012). Other Lund features also correlated with the subtypes described here—the MD Anderson p53-like subtype and the Lund "infiltrated" (MS2b.1) tumors were enriched with extracellular matrix biomarkers (Figure 3B; also see Figure S2; Sjodahl et al., 2012), and all of the Lund "urobasal A" tumors were confined to the MD Anderson luminal subtype (Figure 3B). In addition, as was the case in the MD Anderson discovery cohort, the Lund luminal tumors were enriched with activating *FGFR3* mutations ($p < 0.05$; Figure 3B; Figure S1C). High molecular weight keratins (KRT5 and KRT14) also characterized a bladder cancer "squamous cluster" (cluster D) identified by a group at the University of California-San Francisco ("UCSF cohort"; Blaveri et al., 2005). We applied our classifier to the UCSF data set and confirmed that the UCSF basal tumors were also enriched with squamous features (Figure 3C; "UCSF," Table S4). Finally, we stained a tissue microarray containing 332 pT3 MIBCs (Table S5) with clinical-grade antibodies specific for basal (CK5/6) or luminal (CK20) cytokeratins, quantified antigen expression across the tissue microarray by image analysis, and correlated cytokeratin levels with the presence of squamous features (Figure 3D). Mean CK5/6 levels were significantly higher in tumors with squamous differentiation, whereas CK20 was expressed at higher levels in conventional MIBCs, and expression of CK5/6 correlated inversely with CK20 across the cohort (Figure 3D). Expression of CK5/6 did not correlate with adverse outcomes (data not shown) because careful stage matching had been performed in the tumor cohort. Together, the results demonstrate that squamous differentiation is a common feature of basal MIBCs and that the subtypes described here are similar to those identified independently by other groups.

p63 and PPARγ Control Basal and Luminal Biomarker Expression

To more clearly define the transcription factors that controlled basal and luminal gene expression, we used the "upstream regulators" function in Ingenuity Pathway Analysis (IPA, Ingenuity Systems; http://www.ingenuity.com) and the gene expression profiling data from the MD Anderson discovery cohort to identify the transcription factors that were responsible for the gene expression signatures observed in the MIBC subtypes (Figure 4; Table S6). Because the silhouette analyses revealed that nine of the p53-like tumors were unstable, we compared the IPA results obtained with (n = 73) and without (n = 64) the unstable tumors (Table S7). Transcription factors that have been implicated in the biology of the basal/stem cell compartment of the normal urothelium (Stat-3, NFκB, Hif-1, and p63; Ho et al., 2012) were predicted to be significantly "activated" in basal MIBCs (Figure 4; Table S6; Figure S3A). TP63 has been identified as a biomarker for lethal MIBCs (Choi et al., 2012; Karni-Schmidt et al., 2011), and we used quantitative RT-PCR to confirm that TP63 levels were elevated in the basal MIBCs in the MD Anderson discovery cohort (Figure S3B). Six of the top ten upregulated basal MIBC biomarkers (KRT5, KRT6A, KRT6C, PI3, KRT14, and S100A7) based on fold changes are known direct ΔNp63α transcriptional targets in other tissues (Boldrup et al., 2007; Celis et al., 1996; Romano et al., 2009; Figure 4, also Figure 1B). Basal tumors were also enriched for MYC expression, which is controlled by p63 in human bladder cancer cells (Marquis et al., 2012).

Luminal MIBCs exhibited strong peroxisome proliferator activator receptor (PPAR) pathway activation as well as high-level expression of PPARG and its direct transcriptional target and coactivator, FABP4 (Figures 1B and 4; Table S6; Ayers et al., 2007). In addition, the estrogen receptor (ER) and its coactivator Trim-24 (Hatakeyama, 2011; Tsai et al., 2010) were among the top "activated" upstream regulators in the luminal MIBCs, whereas the basal Stat-3 and NFκB transcriptional networks were downregulated in them (Table S6; Figures S3C and S3D). Conversely, breast luminal transcriptional pathways (ER, Gata-3, and Trim-24) were all downregulated in the basal MIBCs (Table S6). The p53-like luminal MIBCs could be distinguished from the luminal tumors by their expression of an active p53-associated gene expression signature that was not associated with the presence of wild-type *TP53* (Figure 4; also Figures 1 and 3B; Tables S6 and S7). The p53-like tumors also contained an active p16 (CDKN2A) gene signature (Figure S3E).

To more directly define p63's role in controlling basal gene expression, we stably transduced human UM-UC14 bladder cancer cells with nontargeting or TP63-specific shRNAs and used whole genome mRNA expression profiling to create a bladder cancer p63 pathway gene expression signature. IPA analyses indicated that TP63 knockdown decreased basal (p63 and Myc) pathway gene expression, and interestingly, it also increased PPAR pathway gene expression (Figure 5A; Figure S4A). GSEA analyses in the discovery cohort confirmed that the p63 gene signature was significantly enriched in primary basal MIBCs (Figure 5B).

To determine PPARγ's role in controlling luminal gene expression, we generated PPARγ gene expression signatures using whole genome mRNA expression profiling data collected from two human bladder cancer cell lines (UM-UC7 and UM-UC9) that had been exposed to the PPARγ-selective agonist rosiglitazone. IPA analyses confirmed that rosiglitazone activated PPAR

(D) Tissue microarray analysis of CK5/6 (basal) and CK20 (luminal) cytokeratin expression. Cytokeratin protein expression was measured by immunohistochemistry and optical image analysis in the MD Anderson Pathology Core on a tissue microarray containing 332 high-grade pT3 tumors. The percentages of positive tumor cells as determined by image analysis are shown. Left panels: mean levels of CK5/6 (top) and CK20 (bottom) in tumors without (TCC) or with (TCC with SD) squamous features. Bars indicate mean values with 95% confidence intervals. Middle panels: representative images of stained cores from tumors that expressed high or low levels of CK5/6 or CK20. The scale bars correspond to 100 μm. Right panel: relationship between CK5/6 and CK20 expression across the cohort.
See also Tables S3–S5 and Figure S2.

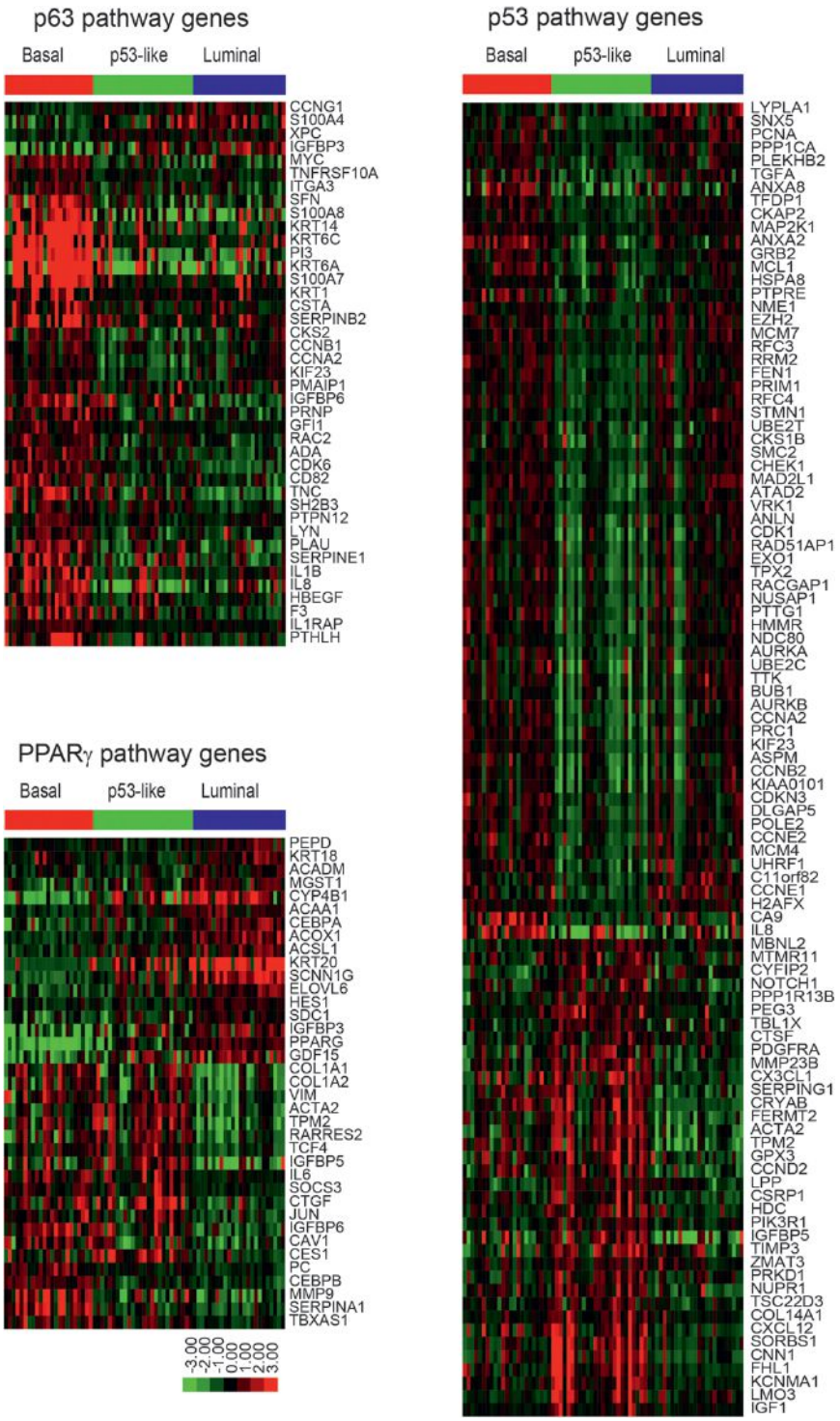

Figure 4. Subtype-Associated Gene Expression Signatures

Signatures were identified using the whole genome mRNA expression profiling data from the MD Anderson discovery cohort and the upstream regulators tool in Ingenuity Pathway Analysis (IPA, Ingenuity Systems; http://www.ingenuity.com). Each heat map displays the expression of the corresponding IPA gene signature as a function of tumor subtype membership; note that genes can be either up- or downregulated by an active transcription factor. Top left: p63-associated gene expression. Bottom left: PPARγ-associated gene expression. Right: p53-associated gene expression.

See also Tables S6 and S7 and Figure S3.

and other luminal transcriptional pathways in both cell lines (Figure 5A; Figures S4B and S4C). GSEA revealed that the UM-UC7 and UM-UC9 PPARγ gene signatures were significantly enriched in primary luminal MIBCs in the discovery cohort (Figure 5B). Interestingly, rosiglitazone also decreased basal transcription factor activation (Figure 5A; Figure S4C). Therefore, PPARγ activation plays an important role in regulating the luminal MIBC gene expression signature, and p63 and PPARγ antagonize each other.

p53-like MIBCs Are Resistant to Neoadjuvant Chemotherapy

Presurgical (neoadjuvant) cisplatin-based chemotherapy (NAC) is the current standard-of-care for high-risk MIBC (Shah et al., 2011), and pathological response to NAC (downstaging to ≤pT1 at cystectomy) is a strong predictor of disease-specific survival (Grossman et al., 2003), as it is in breast cancer (Esserman et al., 2012b). We noticed that all of the p53-like MIBCs from patients treated with NAC in the discovery cohort (n = 7) were resistant to chemotherapy (Table 1). To examine this relationship further, we explored the chemoresistance of p53-like MIBCs in an expanded NAC cohort (n = 34) and in an additional cohort of 23 archival tumors treated uniformly with methotrexate, vinblastine, doxorubicin and cisplatin (MVAC) within the context of a Phase III clinical trial (Millikan et al., 2001). The p53-like MIBCs in both cohorts were resistant to NAC (Figure 6A; Tables S8 and S9). We applied the primary tumor p53 signature to a panel of human bladder cancer cell lines and identified a subset of them that expressed the signature, not all of which retained wild-type *TP53* (Figure 6B). The p53-like cell lines were also resistant to cisplatin-induced apoptosis in vitro (Figure 6C). In addition, four of five of the *TP53* wild-type cell lines that did not contain the "p53-like" signature at baseline were cisplatin-resistant (Figures 6B and 6C).

To further examine whether chemoresistance was a consistent feature of the p53-like subtype, we used gene expression profiling and our classifier to perform molecular subtype

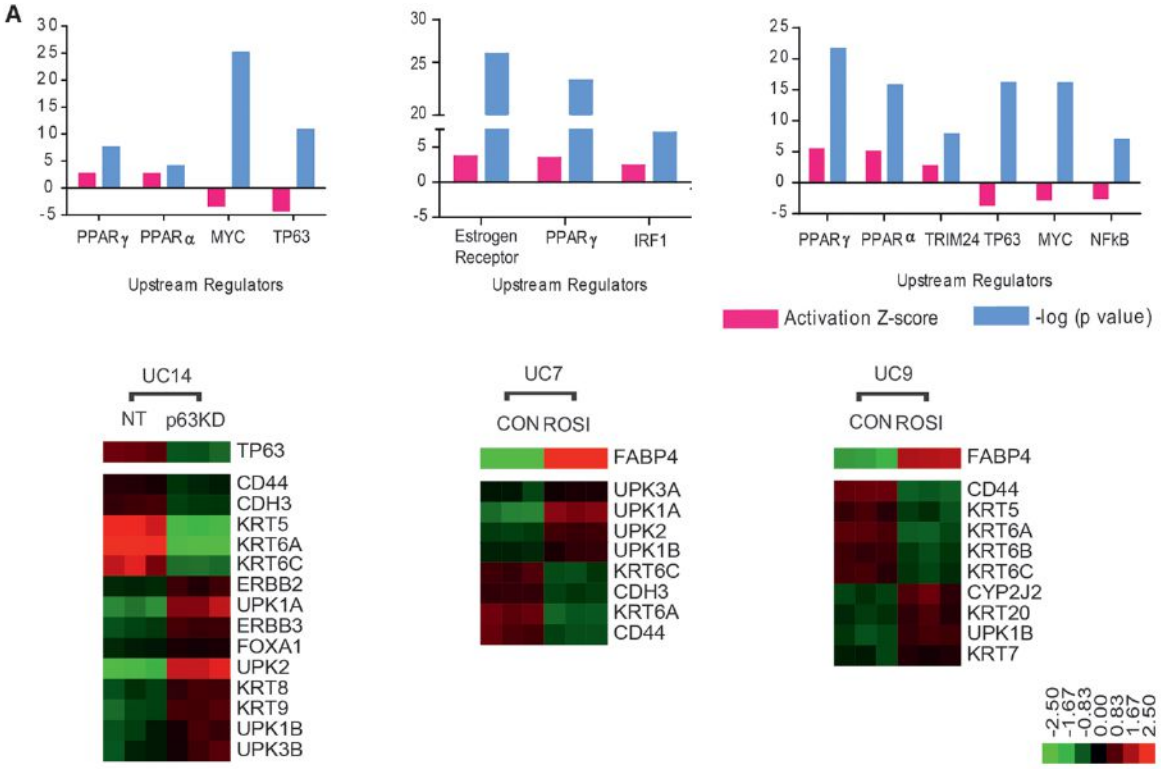

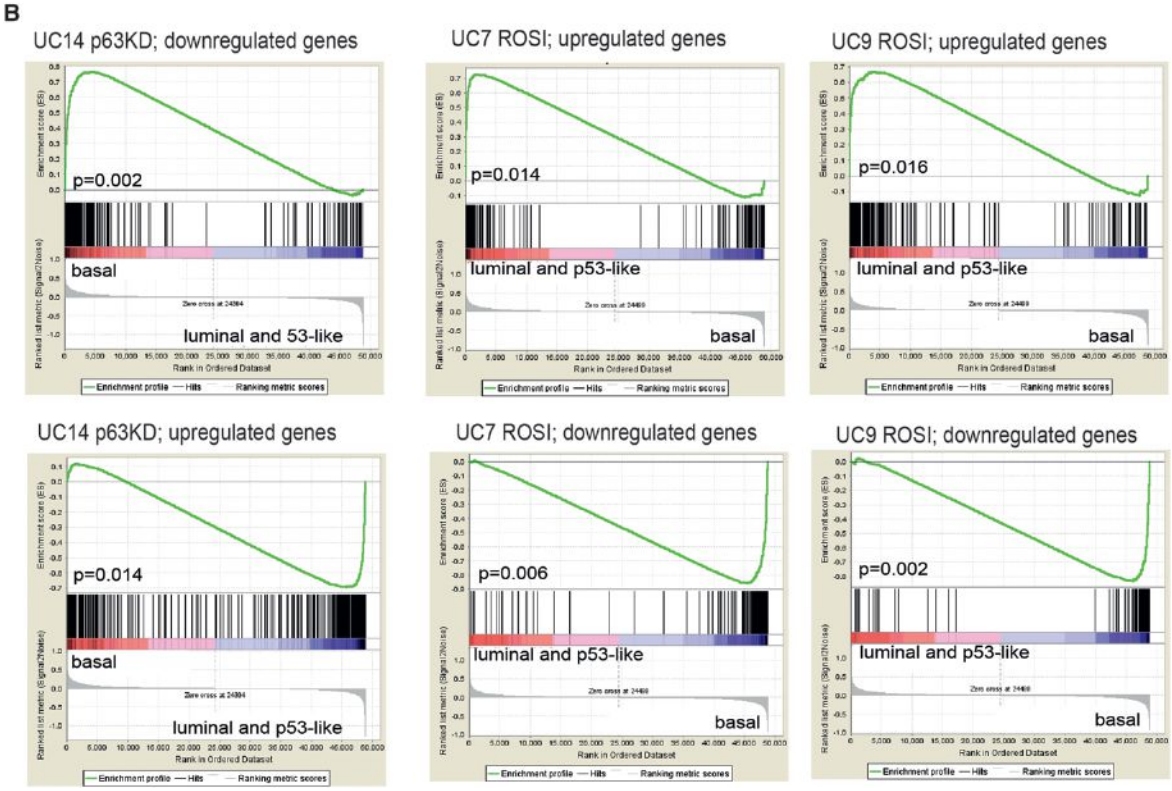

(legend on next page)

assignments on matched pre- and post-treatment MIBCs collected within the context of a prospective Phase II clinical trial of neoadjuvant dose-dense MVAC (DDMVAC), conducted at Fox Chase Cancer Center and Thomas Jefferson University Hospital (Table S10). All of the pretreatment tumors with squamous features in this ''Philadelphia'' cohort were confined to the basal cluster (Table S10; $p = 0.012$). In addition, and consistent with what we had observed in the MD Anderson cohorts, many of the Philadelphia basal (7/14) and luminal (12/20) tumors responded to NAC, whereas the response rate in the p53-like tumors was significantly lower at 11% (1/9; Figure 7A). Furthermore, chemoresistant tumors were enriched with the p53-like subtype after NAC (Figure 7B).

To further characterize the molecular mechanisms underlying chemoresistance, we compared the matched pre- and post-treatment gene expression profiles of the chemoresistant Philadelphia tumors using the ''upstream regulators'' function of IPA (data not shown). The results indicated that chemotherapy caused all of the tumors to express an active p53 pathway gene signature after NAC (Figure 7C; Table S11). Importantly, this chemotherapy-induced p53 signature was not very similar to the one that dictated tumor membership within the p53-like subtype (13 overlapping probes, Table S11).

Finally, we searched for pretreatment gene signatures within the Philadelphia basal and luminal MIBC subtypes that might predict chemosensitivity. We were unable to detect such a signature in the luminal tumors (data not shown), but the chemosensitive Philadelphia basal tumors were enriched for biomarkers reflective of immune infiltration (Figure 7D). Similarly, all of the chemosensitive basal tumors from the MD Anderson MVAC cohort were also enriched with these immune biomarkers (Figure S5).

DISCUSSION

We conclude that MIBCs can be grouped into basal and luminal subtypes reminiscent of those observed in human breast cancers (Perou et al., 2000). Basal MIBCs were associated with shorter disease-specific and overall survival, presumably because patients with these cancers tended to have more invasive and metastatic disease at presentation. The invasive/metastatic phenotype was associated with expression of ''mesenchymal'' and bladder cancer stem cell (Chan et al., 2009) biomarkers, and the tumors were enriched with sarcomatoid and squamous features (Blaveri et al., 2005; Sjodahl et al., 2012). The link between squamous features and aggressive behavior is consistent with other recent observations (Kim et al., 2012; Mitra et al., 2013), and the presence of EMT and bladder cancer stem cell biomarkers in basal tumors provides a biological explanation for their aggressive behaviors. Transcription factor p63 plays a central role in controlling the basal gene signature, and our preliminary data suggest that the EGFR, Stat-3, NFκB, and Hif-1α are also involved. Importantly, immune-infiltrated basal MIBCs responded to NAC, as do some basal breast cancers (Esserman et al., 2012a, 2012b). Because NAC pathological complete response is associated with excellent long-term survival (Grossman et al., 2003), aggressive early management of basal MIBCs with NAC offers the best chance for improved survival for patients with this potentially deadly form of this disease. It also seems likely that T cell modulators (i.e., anti-CTLA4) and EGFR-, NFκB, Hif-1α/VEGF, and/or Stat-3-targeted agents will also be active within this subtype.

Like luminal breast cancers (Perou et al., 2000; Sørlie et al., 2001), luminal MIBCs displayed active ER/TRIM24 pathway gene expression and were enriched with FOXA1, GATA3, ERBB2, and ERBB3. Agents that target the ER (George et al., 2013; Hoffman et al., 2013; Shen et al., 2006) and/or ErbB2 and -3 may therefore be clinically active in luminal MIBCs. In addition, luminal MIBCs contained active PPAR gene expression and activating *FGFR3* mutations, so PPARγ- and FGFR-3-targeted agents may be active in this subtype. Because many luminal MIBCs responded to NAC, targeted therapies should probably be combined with conventional chemotherapy for maximum efficacy.

The idea that wild-type p53 is required for DNA damage-induced apoptosis is a central tenet in cancer biology (Lowe et al., 1993, 1994). Therefore, it was surprising to us that de novo and induced chemoresistance in MIBCs was associated with wild-type p53 gene expression signatures. Nevertheless, this link between ''p53-ness'' and chemoresistance is another shared property of MIBCs and luminal breast cancers. The recently completed I-SPY 1 TRIAL (''Investigation of Serial Studies to Predict Your Therapeutic Response With Imaging and Molecular Analysis,'' CALGB150007/150012) examined the correlation between pathological complete response (pCR) rates and recurrence-free and overall survival in women treated with NAC. One of its main conclusions was that pCR rates varied markedly within the different breast cancer subtypes such that tumors with luminal A and/or wild-type p53-like gene expression signatures responded very poorly to NAC (Esserman et al., 2012a, 2012b). Wild-type p53-induced reversible senescence has also recently been implicated in chemoresistance in a mouse model of breast cancer (Jackson et al., 2012), and more generally, quiescence is considered an important mechanism of chemoresistance. Importantly, *TP53* mutation frequencies

Figure 5. Transcriptional Control of the Basal and Luminal Gene Expression

Whole genome mRNA expression profiling was used to analyze the effects of stable p63 knockdown or rosiglitazone-induced PPARγ activation in human bladder cancer cell lines, and the data were used to generate gene expression signatures characteristic of p63 and PPARγ activation. GSEA was then used to determine whether these signatures were present in the MD Anderson discovery cohort tumor subtypes.

(A) Effects of p63 or PPARγ modulation on basal and luminal transcriptional signatures. Top panels: significantly activated/inhibited transcriptional pathways after p63 knockdown in UM-UC14 cells (top left), PPARγ activation in UM-UC7 (top middle), or PPARγ activation in UM-UC9 (top right) based on IPA analyses. The heat maps below each graph indicate significant changes in basal and luminal marker expression.

(B) p63 and PPARγ gene expression signatures in the subtypes of primary MIBCs. Separate results and p values are shown for the signatures derived from the up- and downregulated genes in each condition. ROSI, rosiglitazone.

See also Figure S4.

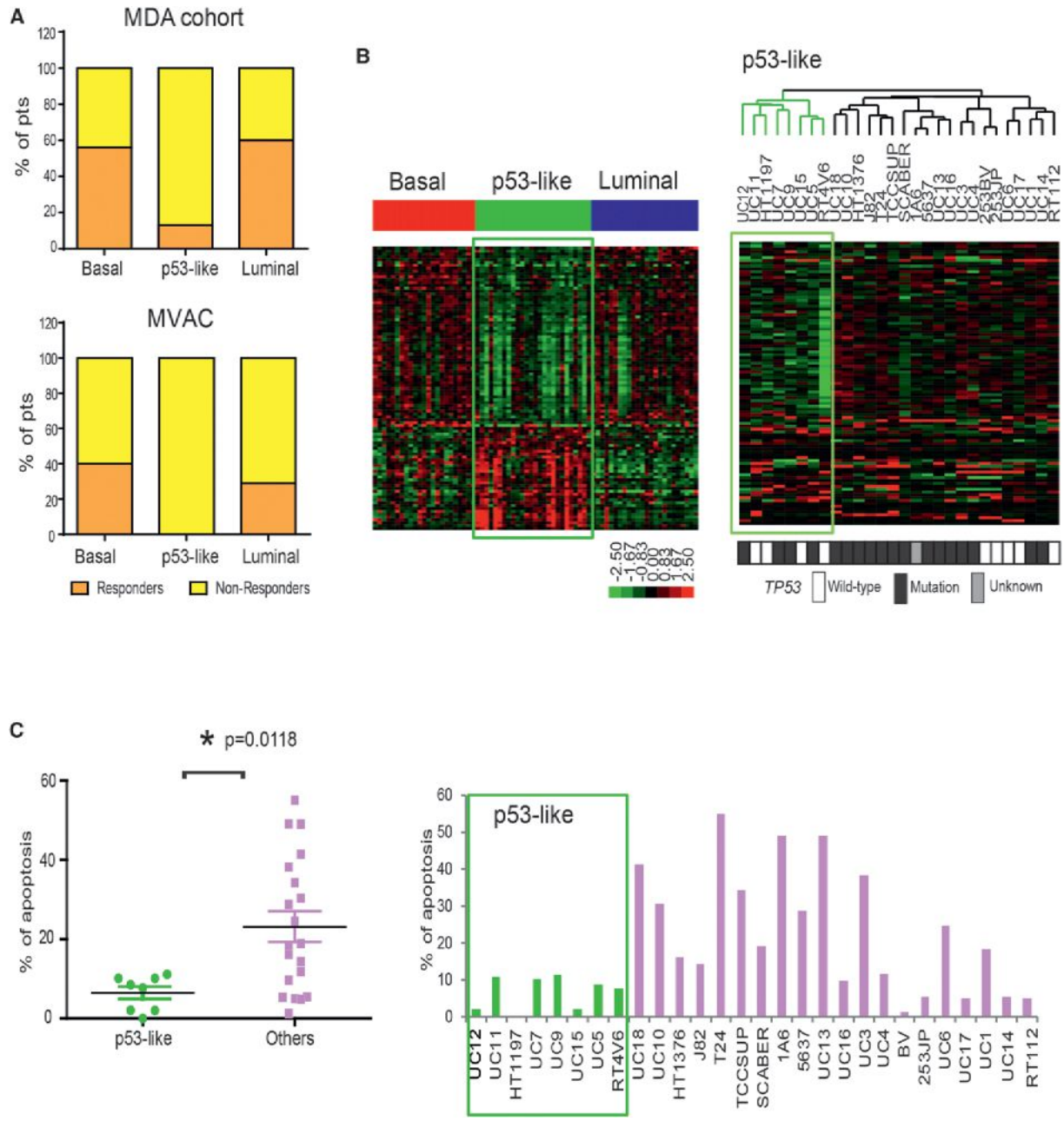

Figure 6. Relationship between Subtype Membership and Chemotherapy Sensitivity

(A) Responses to neoadjuvant chemotherapy in the MD Anderson NAC (n = 34) and MVAC (n = 23) cohorts. Subtype membership was determined using whole genome mRNA expression profiling data obtained from untreated (TURBT) tumors and the oneNN classifier. Pathological response was defined as downstaging to ≤pT1.

(B) The IPA-defined p53 gene expression signature from the p53-like primary MIBCs was used to perform unsupervised hierarchical cluster analysis on whole genome expression data from a panel of human bladder cancer cell lines (n = 28). The green boxes on the heat maps indicate expression of the signature in the MD Anderson discovery cohort (left) or the cell lines (right). *TP53* mutational status was determined by sequencing and is indicated by the color bar below the heat map (black, mutant; white, wild-type; gray, data were not available).

(C) Cells were incubated with or without 10 μM cisplatin for 48 hr and apoptosis-associated DNA fragmentation was quantified by propidium iodide staining and FACS analysis in three independent experiments. The left panel displays a scatter gram comparing the levels within the two subsets of cell lines (mean ± SEM). The right panel displays the mean value of induced apoptosis in each cell line across the entire cohort.

See also Tables S8 and S9.

were similar in all three MIBC subtypes, indicating that wild-type p53 was not responsible for the baseline and chemotherapy-induced p53-like gene expression signatures reported here. We therefore propose that "p53-ness" as measured by mRNA expression would be a more accurate predictor of de novo and induced MIBC chemoresistance than would analyses of *TP53*

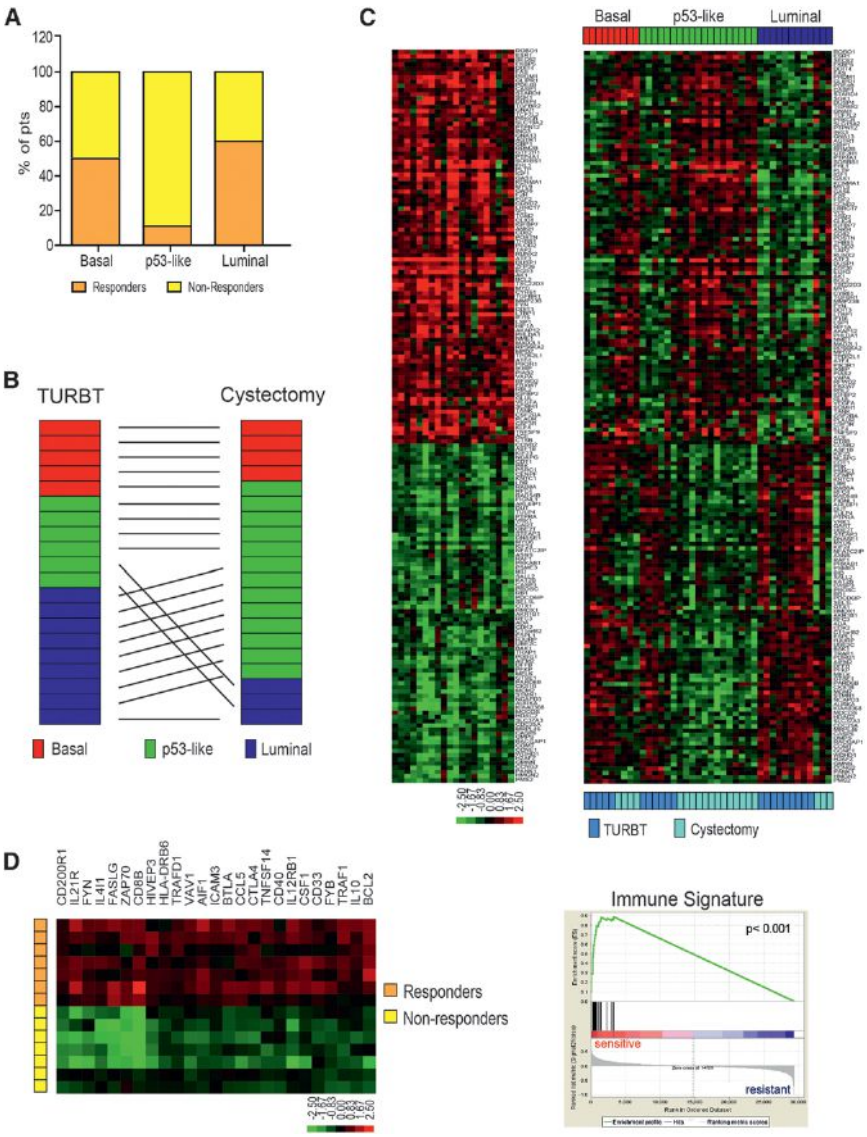

Figure 7. Wild-Type p53 Gene Signatures in Tumors before and after Treatment with NAC

(A) Relationship between subtype membership and response to NAC in the Philadelphia DDMVAC cohort. Subtype membership was determined using pretreatment (TURBT) specimens. Pathological response was defined as downstaging to $\leq$ pT1.

(B) Comparison of subtype membership in the chemoresistant Philadelphia tumors before and after NAC. Whole genome mRNA expression profiling was performed on matched tumors before and after NAC, and the oneNN classifier was used to assign tumors to subtypes. "TURBT" refers to the pretreatment tumors and "cystectomy" to the post-treatment tumors.

(C) Expression of a wild-type p53 gene signature in matched pre- and post-treatment tumors. Left: heat map displaying expression of an active p53 gene signature after NAC (log ratio cystectomy/TURBT of matched tumors). Right: relative expression of the p53 signature in matched pre- and post-treatment tumors arranged according to subtype membership.

(D) Analysis of an immune infiltration signature in basal tumors. A supervised analysis was performed to compare the differences in gene expression between basal tumors that were either sensitive or resistant to neoadjuvant DDMVAC in the Philadelphia cohort. Left: heat map depicting the relative expression of immune signature genes in basal responders and non-responders. Right: GSEA analyses of immune biomarkers in the basal tumors.

See also Tables S10 and S11 and Figure S5.

mutational status. It will be important to determine the molecular basis of these p53-like signatures in future studies so that therapeutic approaches can be developed to overcome de novo and/or prevent acquired chemoresistance. We also plan to prospectively test the relationship between the p53-like phenotype and chemoresistance within the context of a SWOG-sponsored multicenter clinical trial (S1314) that is very similar to I-SPY and was designed to prospectively evaluate another gene expression profiling-based algorithm ("CoXEN"; Lee et al., 2007).

EXPERIMENTAL PROCEDURES

Technical details are provided in the Supplemental Experimental Procedures.

Human Specimens

Clinical data were obtained from the MD Anderson Genitourinary Cancers Research Database, from the Gene Expression Omnibus (GEO), or from patient charts (MVAC and Philadelphia cohorts). All MD Anderson patients signed a "front door" informed consent allowing collection of their tissue and of their clinical data that was approved by the MD Anderson Institutional Review Board (IRB). An additional MD Anderson IRB-approved protocol was obtained specifically for genomics analyses. The Philadelphia tissues were collected and analyzed as part of a Phase II clinical trial that was IRB-approved at the Fox-Chase Cancer Center and Thomas Jefferson University. Unstained tissue sections (10 micron, five slides/tumor) and matched hematoxylin and eosin stained sections from the DDMVAC clinical trial were transferred to MD Anderson under an executed materials transfer agreement between MD Anderson and Fox-Chase. A genitourinary pathologist (Bogdan Czerniak) reviewed all of the tissue samples.

Tumor Cohorts

The Chungbuk (n = 55) (Kim et al., 2010), Lund (n = 93) (Sjodahl et al., 2012), and UCSF (n = 53)(Blaveri et al., 2005) cohort data were downloaded from the GEO (GSE13507, GSE32894, and GSE1827, respectively). The discovery cohort consisted of 73 tumors from transurethral resections (TURs) that had been snap-frozen in liquid nitrogen within 5 min of isolation and transferred to the MD Anderson Bladder SPORE Tissue Core. The MD Anderson validation cohort consisted of 57 randomly selected, formalin-fixed, paraffin-embedded (FFPE) tumors that were obtained from the main MD Anderson Cancer Center CCSG-supported Pathology Tissue Bank. The MD Anderson NAC cohort (n = 34) contained a mixture of 18 tumors from the discovery cohort plus 16 additional FFPE tumors from patients treated with neoadjuvant chemotherapy on- and off-protocol. The MD Anderson MVAC cohort (n = 23) consisted of all available FFPE pretreatment tumors (TURs) from a previously reported Phase

III clinical trial (Millikan et al., 2001). The Philadelphia NAC cohort (n = 43 TURs and 20 cystectomies) consisted of all available pre- and post-treatment FFPE tumors from patients enrolled in a Phase II clinical trial of neodjuvant dose-dense MVAC (DDMVAC) that was conducted at Fox-Chase Cancer Center and The Thomas Jefferson University and will be reported elsewhere. NAC response in all of the cohorts was defined as downstaging to no muscle-invasive disease at cystectomy ($\leq$pT1; Millikan et al., 2001).

Gene Expression Profiling Platforms

The MD Anderson discovery cohort and human bladder cancer cell lines were analyzed by direct hybridization on Illumina HT12v3 and HT12v4 chips, respectively (Illumina). Data from all of the FFPE cohorts were generated using Illumina's DASL platform (WG-DASL HT12v4 chips).

Tumor Cluster Assignments

MIBC clusters (subtypes) were determined in the discovery cohort using unsupervised hierarchical cluster analysis (Eisen et al., 1998). The gene signatures associated with each cluster were then used to generate a one nearest neighbor (oneNN; Dudoit et al., 2002) prediction model that was used in all subsequent analyses to assign tumors to specific subtypes.

Micro RNA Expression

Levels of miR-200b and miR-200c were measured in the discovery cohort by quantitative RT-PCR as described in the Supplemental Experimental Procedures.

Analysis of Cytokeratin Protein Expression

Basal (CK5/6) and luminal (CK20) cytokeratin protein expression was analyzed on a tissue microarray (TMA) consisting of stage-matched (pT3, n = 332) MIBCs collected within the context of the International Bladder Cancer Network's Bladder Cancer Bank initiative (Goebell et al., 2005). Immunohistochemical staining was performed using clinical-grade (CLIA) antibodies and protocols in the MD Anderson Pathology Core, and staining intensities were quantified by image analysis.

Generation of p63 and PPARγ Gene Signatures

UM-UC14 human MIBC cells were stably transduced with TP63-specific or nontargeting lentiviral shRNA constructs in the MD Anderson Vector Core. UM-UC7 and UM-UC9 cells were incubated with or without 1 μM rosiglitazone for 48 hr. Triplicate RNA isolates were prepared on different days for each condition, and global changes in gene expression were determined by whole genome expression profiling. The statistically significant changes in gene expression were used to create signatures that were subsequently used in the IPA and GSEA analyses presented in Figure 5.

Statistical Analyses

Clinicodemographic characteristics were compared using Fisher's exact tests and Kruskal-Wallis tests to assess differences between groups in categorical and continuous variables, respectively. Kaplan-Meier analysis with log-rank statistics was used to characterize survival distributions and associations between subtypes and survival outcomes. Statistical analysis was performed using SPSS (version 19) and a p value less than 0.05 was considered significant.

ACCESSION NUMBERS

The GEO accession numbers for the gene expression profiling data presented in this study are GSE48277 and GSE47993.

SUPPLEMENTAL INFORMATION

Supplemental Information includes Supplemental Experimental Procedures, five figures, and eleven tables and can be found with this article online at http://dx.doi.org/10.1016/j.ccr.2014.01.009.

ACKNOWLEDGMENTS

The authors would like to acknowledge Lyndsay Harris (Southwest Oncology Group, Breast Committee, Case Cancer Center) for her help with the DASL assay and Neema Navai and Matthew Wszolek for sharing their miR-200b and miR-200c PCR data. This work was supported by a grant from the Baker Foundation, the MD Anderson Bladder SPORE (P50 CA91846), grant R01 CA151489 (to B.C.), and the MD Anderson CCSG (P30 016672). E.R.P. is supported by grant no. IRG-92-027-17 from the American Cancer Society. This paper is dedicated to the memory of Dexter Baker. The authors wish to disclose that the MD Anderson Cancer Center has submitted a patent that covers some of the findings reported in this manuscript.

Received: December 19, 2012
Revised: October 17, 2013
Accepted: January 13, 2014
Published: February 10, 2014

REFERENCES

Ayers, S.D., Nedrow, K.L., Gillilan, R.E., and Noy, N. (2007). Continuous nucleocytoplasmic shuttling underlies transcriptional activation of PPARgamma by FABP4. Biochemistry *46*, 6744–6752.

Blaveri, E., Simko, J.P., Korkola, J.E., Brewer, J.L., Baehner, F., Mehta, K., Devries, S., Koppie, T., Pejavar, S., Carroll, P., and Waldman, F.M. (2005). Bladder cancer outcome and subtype classification by gene expression. Clin. Cancer Res. *11*, 4044–4055.

Boldrup, L., Coates, P.J., Gu, X., and Nylander, K. (2007). DeltaNp63 isoforms regulate CD44 and keratins 4, 6, 14 and 19 in squamous cell carcinoma of head and neck. J. Pathol. *213*, 384–391.

Botteman, M.F., Pashos, C.L., Redaelli, A., Laskin, B., and Hauser, R. (2003). The health economics of bladder cancer: a comprehensive review of the published literature. Pharmacoeconomics *21*, 1315–1330.

Celis, J.E., Rasmussen, H.H., Vorum, H., Madsen, P., Honoré, B., Wolf, H., and Orntoft, T.F. (1996). Bladder squamous cell carcinomas express psoriasin and externalize it to the urine. J. Urol. *155*, 2105–2112.

Chaffer, C.L., Marjanovic, N.D., Lee, T., Bell, G., Kleer, C.G., Reinhardt, F., D'Alessio, A.C., Young, R.A., and Weinberg, R.A. (2013). Poised chromatin at the ZEB1 promoter enables breast cancer cell plasticity and enhances tumorigenicity. Cell *154*, 61–74.

Chan, K.S., Espinosa, I., Chao, M., Wong, D., Ailles, L., Diehn, M., Gill, H., Presti, J., Jr., Chang, H.Y., van de Rijn, M., et al. (2009). Identification, molecular characterization, clinical prognosis, and therapeutic targeting of human bladder tumor-initiating cells. Proc. Natl. Acad. Sci. USA *106*, 14016–14021.

Choi, W., Shah, J.B., Tran, M., Svatek, R., Marquis, L., Lee, I.L., Yu, D., Adam, L., Wen, S., Shen, Y., et al. (2012). p63 expression defines a lethal subset of muscle-invasive bladder cancers. PLoS ONE *7*, e30206.

Dinney, C.P., McConkey, D.J., Millikan, R.E., Wu, X., Bar-Eli, M., Adam, L., Kamat, A.M., Siefker-Radtke, A.O., Tuziak, T., Sabichi, A.L., et al. (2004). Focus on bladder cancer. Cancer Cell *6*, 111–116.

Dudoit, S., Fridlyand, J., and Speed, T.P. (2002). Comparison of discrimination methods for classification of tumors using DNA microarrays. J. Am. Stat. Assoc. *97*, 77–87.

Dyrskjøt, L., Thykjaer, T., Kruhøffer, M., Jensen, J.L., Marcussen, N., Hamilton-Dutoit, S., Wolf, H., and Orntoft, T.F. (2003). Identifying distinct classes of bladder carcinoma using microarrays. Nat. Genet. *33*, 90–96.

Eisen, M.B., Spellman, P.T., Brown, P.O., and Botstein, D. (1998). Cluster analysis and display of genome-wide expression patterns. Proc. Natl. Acad. Sci. USA *95*, 14863–14868.

Esserman, L.J., Berry, D.A., Cheang, M.C., Yau, C., Perou, C.M., Carey, L., DeMichele, A., Gray, J.W., Conway-Dorsey, K., Lenburg, M.E., et al.; I-SPY 1 TRIAL Investigators (2012a). Chemotherapy response and recurrence-free survival in neoadjuvant breast cancer depends on biomarker profiles: results from the I-SPY 1 TRIAL (CALGB 150007/150012; ACRIN 6657). Breast Cancer Res. Treat. *132*, 1049–1062.

Esserman, L.J., Berry, D.A., DeMichele, A., Carey, L., Davis, S.E., Buxton, M., Hudis, C., Gray, J.W., Perou, C., Yau, C., et al. (2012b). Pathologic complete response predicts recurrence-free survival more effectively by cancer subset: results from the I-SPY 1 TRIAL–CALGB 150007/150012, ACRIN 6657. J. Clin. Oncol. *30*, 3242–3249.

George, S.K., Tovar-Sepulveda, V., Shen, S.S., Jian, W., Zhang, Y., Hilsenbeck, S.G., Lerner, S.P., and Smith, C.L. (2013). Chemoprevention of BBN-Induced Bladder Carcinogenesis by the Selective Estrogen Receptor Modulator Tamoxifen. Translational oncology *6*, 244–255.

Goebell, P.J., Groshen, S., Schmitz-Drager, B.J., Sylvester, R., Kogevinas, M., Malats, N., Sauter, G., Grossman, H.B., Dinney, C.P., Waldman, F., and Cote, R.J. (2005). Concepts for banking tissue in urologic oncology–the International Bladder Cancer Bank. Clinical cancer research: an official journal of the American Association for Cancer Research *11*, 413–415.

Gregory, P.A., Bert, A.G., Paterson, E.L., Barry, S.C., Tsykin, A., Farshid, G., Vadas, M.A., Khew-Goodall, Y., and Goodall, G.J. (2008). The miR-200 family and miR-205 regulate epithelial to mesenchymal transition by targeting ZEB1 and SIP1. Nat. Cell Biol. *10*, 593–601.

Grossman, H.B., Natale, R.B., Tangen, C.M., Speights, V.O., Vogelzang, N.J., Trump, D.L., deVere White, R.W., Sarosdy, M.F., Wood, D.P., Jr., Raghavan, D., and Crawford, E.D. (2003). Neoadjuvant chemotherapy plus cystectomy compared with cystectomy alone for locally advanced bladder cancer. N. Engl. J. Med. *349*, 859–866.

Hatakeyama, S. (2011). TRIM proteins and cancer. Nat. Rev. Cancer *11*, 792–804.

Ho, P.L., Kurtova, A., and Chan, K.S. (2012). Normal and neoplastic urothelial stem cells: getting to the root of the problem. Nat Rev Urol *9*, 583–594.

Hoffman, K.L., Lerner, S.P., and Smith, C.L. (2013). Raloxifene inhibits growth of RT4 urothelial carcinoma cells via estrogen receptor-dependent induction of apoptosis and inhibition of proliferation. Hormones & cancer *4*, 24–35.

Jackson, J.G., Pant, V., Li, Q., Chang, L.L., Quintás-Cardama, A., Garza, D., Tavana, O., Yang, P., Manshouri, T., Li, Y., et al. (2012). p53-mediated senescence impairs the apoptotic response to chemotherapy and clinical outcome in breast cancer. Cancer Cell *21*, 793–806.

Karni-Schmidt, O., Castillo-Martin, M., Shen, T.H., Gladoun, N., Domingo-Domenech, J., Sanchez-Carbayo, M., Li, Y., Lowe, S., Prives, C., and Cordon-Cardo, C. (2011). Distinct expression profiles of p63 variants during urothelial development and bladder cancer progression. Am. J. Pathol. *178*, 1350–1360.

Kim, W.J., Kim, E.J., Kim, S.K., Kim, Y.J., Ha, Y.S., Jeong, P., Kim, M.J., Yun, S.J., Lee, K.M., Moon, S.K., et al. (2010). Predictive value of progression-related gene classifier in primary non-muscle invasive bladder cancer. Mol. Cancer *9*, 3.

Kim, S.P., Frank, I., Cheville, J.C., Thompson, R.H., Weight, C.J., Thapa, P., and Boorjian, S.A. (2012). The impact of squamous and glandular differentiation on survival after radical cystectomy for urothelial carcinoma. J. Urol. *188*, 405–409.

Lee, J.K., Havaleshko, D.M., Cho, H., Weinstein, J.N., Kaldjian, E.P., Karpovich, J., Grimshaw, A., and Theodorescu, D. (2007). A strategy for predicting the chemosensitivity of human cancers and its application to drug discovery. Proc. Natl. Acad. Sci. USA *104*, 13086–13091.

Lee, J.S., Leem, S.H., Lee, S.Y., Kim, S.C., Park, E.S., Kim, S.B., Kim, S.K., Kim, Y.J., Kim, W.J., and Chu, I.S. (2010). Expression signature of E2F1 and its associated genes predict superficial to invasive progression of bladder tumors. Journal of clinical oncology: official journal of the American Society of Clinical Oncology *28*, 2660–2667.

Lowe, S.W., Ruley, H.E., Jacks, T., and Housman, D.E. (1993). p53-dependent apoptosis modulates the cytotoxicity of anticancer agents. Cell *74*, 957–967.

Lowe, S.W., Bodis, S., McClatchey, A., Remington, L., Ruley, H.E., Fisher, D.E., Housman, D.E., and Jacks, T. (1994). p53 status and the efficacy of cancer therapy in vivo. Science *266*, 807–810.

Marquis, L., Tran, M., Choi, W., Lee, I.L., Huszar, D., Siefker-Radtke, A., Dinney, C., and McConkey, D.J. (2012). p63 expression correlates with sensitivity to the Eg5 inhibitor ZD4877 in bladder cancer cells. Cancer Biol. Ther. *13*, 477–486.

McConkey, D.J., Lee, S., Choi, W., Tran, M., Majewski, T., Lee, S., Siefker-Radtke, A., Dinney, C., and Czerniak, B. (2010). Molecular genetics of bladder cancer: Emerging mechanisms of tumor initiation and progression. Urol. Oncol. *28*, 429–440.

Millikan, R., Dinney, C., Swanson, D., Sweeney, P., Ro, J.Y., Smith, T.L., Williams, D., and Logothetis, C. (2001). Integrated therapy for locally advanced bladder cancer: final report of a randomized trial of cystectomy plus adjuvant M-VAC versus cystectomy with both preoperative and postoperative M-VAC. Journal of clinical oncology: official journal of the American Society of Clinical Oncology *19*, 4005–4013.

Mitra, A.P., Bartsch, C.C., Bartsch, G., Jr., Miranda, G., Skinner, E.C., and Daneshmand, S. (2013). Does presence of squamous and glandular differentiation in urothelial carcinoma of the bladder at cystectomy portend poor prognosis? An intensive case-control analysis. Urol. Oncol. *12*, S1078–S1439.

Peinado, H., Olmeda, D., and Cano, A. (2007). Snail, Zeb and bHLH factors in tumour progression: an alliance against the epithelial phenotype? Nat. Rev. Cancer *7*, 415–428.

Perou, C.M., Sørlie, T., Eisen, M.B., van de Rijn, M., Jeffrey, S.S., Rees, C.A., Pollack, J.R., Ross, D.T., Johnsen, H., Akslen, L.A., et al. (2000). Molecular portraits of human breast tumours. Nature *406*, 747–752.

Romano, R.A., Ortt, K., Birkaya, B., Smalley, K., and Sinha, S. (2009). An active role of the DeltaN isoform of p63 in regulating basal keratin genes K5 and K14 and directing epidermal cell fate. PLoS ONE *4*, e5623.

Rouzier, R., Perou, C.M., Symmans, W.F., Ibrahim, N., Cristofanilli, M., Anderson, K., Hess, K.R., Stec, J., Ayers, M., Wagner, P., et al. (2005). Breast cancer molecular subtypes respond differently to preoperative chemotherapy. Clinical cancer research: an official journal of the American Association for Cancer Research *11*, 5678–5685.

Sanchez-Carbayo, M., Socci, N.D., Lozano, J., Saint, F., and Cordon-Cardo, C. (2006). Defining molecular profiles of poor outcome in patients with invasive bladder cancer using oligonucleotide microarrays. Journal of clinical oncology: official journal of the American Society of Clinical Oncology *24*, 778–789.

Shah, J.B., McConkey, D.J., and Dinney, C.P. (2011). New strategies in muscle-invasive bladder cancer: on the road to personalized medicine. Clinical cancer research: an official journal of the American Association for Cancer Research *17*, 2608–2612.

Shen, S.S., Smith, C.L., Hsieh, J.T., Yu, J., Kim, I.Y., Jian, W., Sonpavde, G., Ayala, G.E., Younes, M., and Lerner, S.P. (2006). Expression of estrogen receptors-alpha and -beta in bladder cancer cell lines and human bladder tumor tissue. Cancer *106*, 2610–2616.

Sjodahl, G., Lauss, M., Lovgren, K., Chebil, G., Gudjonsson, S., Veerla, S., Patschan, O., Aine, M., Ferno, M., Ringner, M., et al. (2012). A molecular taxonomy for urothelial carcinoma. Clinical cancer research: an official journal of the American Association for Cancer Research *18*, 3377–3386.

Sørlie, T., Perou, C.M., Tibshirani, R., Aas, T., Geisler, S., Johnsen, H., Hastie, T., Eisen, M.B., van de Rijn, M., Jeffrey, S.S., et al. (2001). Gene expression patterns of breast carcinomas distinguish tumor subclasses with clinical implications. Proc. Natl. Acad. Sci. USA *98*, 10869–10874.

Svatek, R.S., Shariat, S.F., Novara, G., Skinner, E.C., Fradet, Y., Bastian, P.J., Kamat, A.M., Kassouf, W., Karakiewicz, P.I., Fritsche, H.M., et al. (2011). Discrepancy between clinical and pathological stage: external validation of the impact on prognosis in an international radical cystectomy cohort. BJU Int. *107*, 898–904.

Tsai, W.W., Wang, Z., Yiu, T.T., Akdemir, K.C., Xia, W., Winter, S., Tsai, C.Y., Shi, X., Schwarzer, D., Plunkett, W., et al. (2010). TRIM24 links a non-canonical histone signature to breast cancer. Nature *468*, 927–932.

Make your point
with Cell Reports

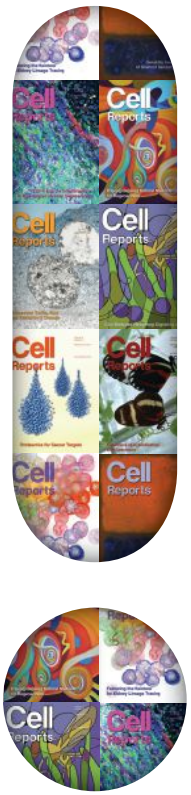

Share your discoveries as you find them. Every breakthrough should get the attention it deserves. *Cell Reports* puts a spotlight on groundbreaking research with shorter, single-point stories.

Cell Reports is an open access journal that offers the quality, rigor, and visibility you've come to expect from Cell Press.

Do you have a new biological insight? Submit your paper to *Cell Reports*.

For more information www.cell.com/cell-reports

An open access journal with impact.
From Cell Press.

Cell Reports

Cancer Cell
Article

CellPress

Metabolic Reprogramming of Stromal Fibroblasts through p62-mTORC1 Signaling Promotes Inflammation and Tumorigenesis

Tania Valencia,[1] Ji Young Kim,[1] Shadi Abu-Baker,[2] Jorge Moscat-Pardos,[1] Christopher S. Ahn,[3] Miguel Reina-Campos,[1] Angeles Duran,[1] Elias A. Castilla,[2] Christian M. Metallo,[3,4] Maria T. Diaz-Meco,[1,5,*] and Jorge Moscat[1,5,*]
[1]Sanford-Burnham Medical Research Institute, 10901 N. Torrey Pines Road, La Jolla, CA 92037, USA
[2]University of Cincinnati Medical College, Cincinnati, OH 45267, USA
[3]Department of Bioengineering, University of California, San Diego, 9500 Gilman Drive, La Jolla, CA 92093, USA
[4]Moores Cancer Center, University of California, San Diego, 9500 Gilman, Drive, La Jolla, CA 92093
[5]Co-senior author
*Correspondence: mdmeco@sanfordburnham.org (M.T.D.-M.), jmoscat@sanfordburnham.org (J.M.)
http://dx.doi.org/10.1016/j.ccr.2014.05.004

SUMMARY

The tumor microenvironment plays a critical role in cancer progression, but the precise mechanisms by which stromal cells influence the epithelium are poorly understood. Here we show that p62 levels were reduced in the stroma of several tumors and that its loss in the tumor microenvironment or stromal fibroblasts resulted in increased tumorigenesis of epithelial prostate cancer cells. The mechanism involves the regulation of cellular redox through an mTORC1/c-Myc pathway of stromal glucose and amino acid metabolism, resulting in increased stromal IL-6 production, which is required for tumor promotion in the epithelial compartment. Thus, p62 is an anti-inflammatory tumor suppressor that acts through the modulation of metabolism in the tumor stroma.

INTRODUCTION

Primary tumors are initiated as a result of the stepwise acquisition of genetic alterations within the epithelial compartment (Shen and Abate-Shen, 2010). However, increasing evidence supports the notion that the tumor microenvironment also plays a critical role in cancer progression in many types of neoplasias, including prostate cancer (PCa), although relatively little is known about the signaling pathways that mediate communication between the stromal and epithelial compartments (Ammirante et al., 2010; Erez et al., 2010; Santos et al., 2009; Trimboli et al., 2009). Inflammation and metabolism are two critical factors contributing to the protumorigenic properties of the stroma (DeBerardinis and Thompson, 2012; Grivennikov et al., 2010; Hanahan and Coussens, 2012; Metallo and Vander Heiden, 2013; Vander Heiden, 2013). Although not totally understood, some evidence suggests that the metabolic state of the tumor stroma can decisively influence the tumorigenic potential of the tumor epithelial compartment (Lisanti et al., 2013). Here we have addressed this fundamental biological question in the context of p62 deficiency in the nonepithelial tumor compartment. Our laboratory initially identified p62, also known as sequestosome-1, as a scaffold protein for the atypical protein kinase C isozymes and later implicated p62 in other cell stress responses (Diaz-Meco and Moscat, 2012; Moscat and Diaz-Meco, 2012; Moscat et al., 2007; Sanchez et al., 1998). p62 binds Raptor, a key component of the mTOR-orchestrated nutrient-sensing complex and an important activator of anabolic pathways that are instrumental in metabolic reprogramming during cell transformation (Duran et al., 2011; Moscat and Diaz-Meco, 2011). Nonetheless, nothing is known about the signaling cascades that p62 regulates in stromal cells or to

Significance

Inappropriate activation of the stroma as a consequence of the tumorigenic process can potentiate the growth and transformation of epithelial tumor cells, thus facilitating the progression of cancers toward more malignant stages. Using prostate cancer as a model system, we show that the loss of the signaling adaptor p62 in stromal cells triggers an inflammatory response that leads to activation of cancer-associated fibroblasts that enhances tumorigenesis in vitro and in vivo. Deficiency in p62 results in reduced mTORC1 activity and deregulation of metabolic pathways controlling inflammation. Because the stroma is increasingly recognized as a potential source of therapeutic targets, this study suggests that targeting stromal metabolic reprogramming can decisively influence the tumorigenic potential of the tumor epithelial compartment.

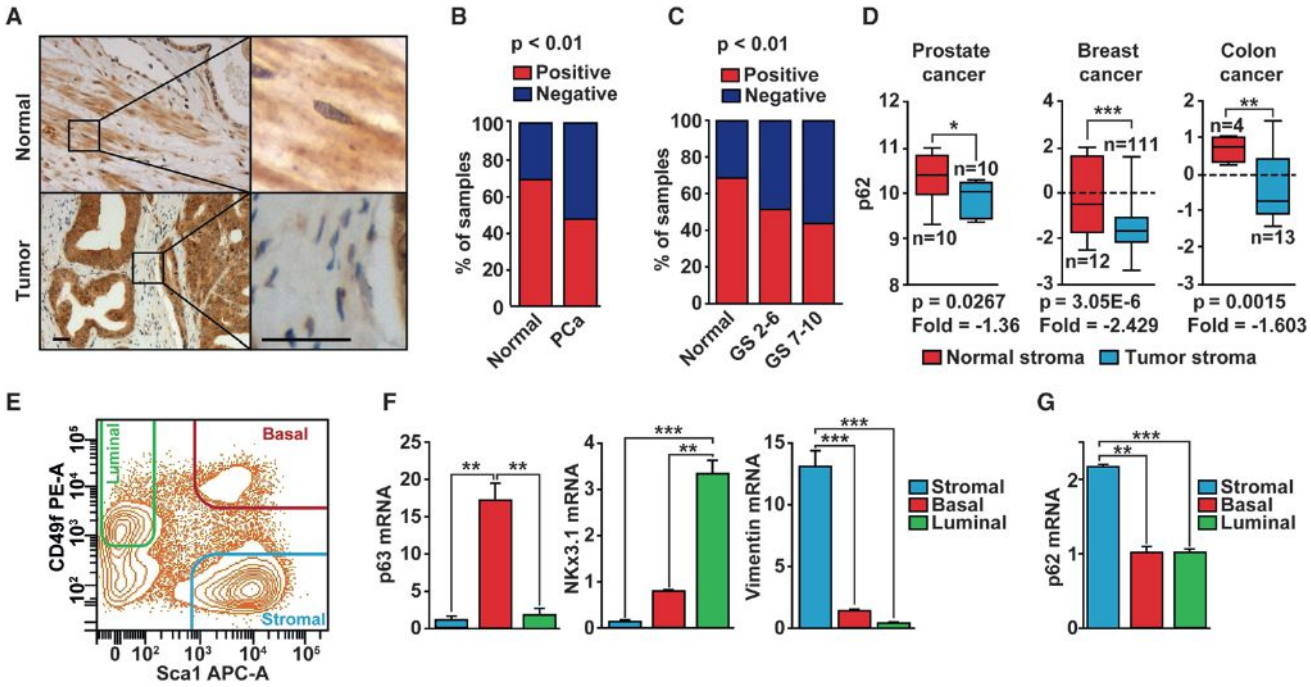

Figure 1. p62 Levels Are Reduced in the Stroma of Human Prostate Tumors

(A) Representative examples of p62 staining of normal and primary prostate cancer (tumor) samples. The scale bars represent 25 μm.

(B) Quantification of p62 staining in the stroma of primary PCa tumors compared with normal; n = 22 (normal), n = 202 (PCa). Fisher's exact test, $p < 0.01$.

(C) p62 levels are reduced upon PCa progression; n = 22 (normal), n = 70 (GS 2–6), n = 132 (GS 7–10). Chi-square test, $p < 0.01$.

(D) p62 mRNA levels in stroma of human cancer samples. Data were collected from public data sets of gene expression in the tumor stroma of several human cancers: GSE34312 (prostate cancer), GSE9014 (breast cancer), and GSE35602 (colon cancer).

(E) FACS-sorted adult murine prostate cell lineages. Prostate basal, luminal, and stromal cells are $Lin^{-}Sca\text{-}1^{+}CD49f^{Hi}$, $Lin^{-}Sca\text{-}1^{-}CD49f^{Low}$, and $Lin^{-}Sca\text{-}1^{+}CD49f^{-}$, respectively.

(F) RT-PCR of specific markers for each prostate cell population (n = 3): p63 (basal), Nkx3.1 (luminal), and vimentin (stromal).

(G) RT-PCR for p62 in prostate cell populations (n = 3).

*$p < 0.05$, **$p < 0.01$, ***$p < 0.001$. Results are presented as mean ± SEM. See also Figure S1.

what extent these pathways influence the epithelial-stromal interaction in the tumor microenvironment. Cancer-associated fibroblasts (CAFs) have been proposed to be key mediators of the crosstalk between malignant tumor cells and their microenvironment (Barron and Rowley, 2012; Franco and Hayward, 2012). CAFs and the complex set of signaling molecules they secrete generate an environment conducive to inflammation, and this in turn maintains the protumorigenic status of the stromal cells. Among these proteins, interleukin-1β (IL-1β), interleukin-8, and interleukin-6 (IL-6) have been implicated as part of the proinflammatory signature of the PCa stroma (Erez et al., 2010; Franco and Hayward, 2012; Schauer et al., 2008). Furthermore, IL-6 has received increasing attention as a key proinflammatory and protumorigenic molecule in many types of cancer, including PCa (Azevedo et al., 2011; De Marzo et al., 2007; Guo et al., 2012; Schafer and Brugge, 2007). Here we address the role of p62 in the stroma in the control of the inflammatory environment in PCa.

RESULTS

p62 Expression Levels in the Tumor Microenvironment

The initial evidence suggesting that p62 plays a role in the regulation of the tumor microenvironment in PCa came from the histological analysis of a tissue panel comprising 202 primary human PCa tumors, 8 metastases, and 22 adjacent normal prostate tissue samples. This study revealed that p62 was expressed in the prostate epithelium and also in the stroma (Figure 1A). p62 protein levels were downregulated in the stroma of human primary PCa tumors compared with the stroma of normal samples (Figures 1A and 1B). Furthermore, when the tumor samples were grouped on the basis of low Gleason score (GS) (2–6) or high GS (7–10), p62 levels in the stroma were significantly reduced upon progression to the most aggressive stage (Figure 1C). p62 was also overexpressed in the epithelial compartment of the PCa human samples (Figure 1A; Figures S1A and S1B available online). This is consistent with previous observations suggesting that p62 is upregulated in many cancers, including lung cancer (Duran et al., 2008; Inoue et al., 2012), liver cancer (Inami et al., 2011), glioblastoma (Galavotti et al., 2013), breast cancer (Rolland et al., 2007; Thompson et al., 2003), and kidney cancer (Li et al., 2013). However, because those studies did not report on expression in the stromal component, it is not clear whether p62 was downregulated in the stroma in those samples, as we have shown in the samples analyzed here. Moreover, bioinformatics analysis of public data sets of stromal gene expression also demonstrated that p62 was significantly downregulated in the tumor stroma, compared

with normal stroma, in several types of cancers, including prostate, breast, and colon cancers (Figure 1D). In addition, fluorescence-activated cell sorting (FACS) analysis of adult mouse prostates showed that p62 is more highly expressed in cells of the stroma than in those of basal or luminal lineages (Figures 1E–1G). Quantitative RT-PCR analyses of the sorted prostate cell populations showed that transcripts for the basal marker p63, the luminal cell marker Nkx3.1, and the stroma marker vimentin were enriched in their corresponding cell populations, demonstrating successful cell fractionation (Figures 1E and 1F). Of note, p62 expression was highly enriched in the stromal compartment compared with the other two cell populations (Figure 1G). These results suggest that p62 could exert its effect as a tumor suppressor in the tumor microenvironment, likely in the stroma.

p62 Is a Suppressor of Inflammation and the CAF Phenotype in the Tumor Microenvironment

To test whether p62 deficiency in the tumor microenvironment is relevant to the transforming properties of epithelial cells, we performed orthotopic injections of syngeneic murine PCa cells (TRAMP-C2Re3) (Olson et al., 2006) into the prostates of wild-type (WT) and p62 knockout (KO) mice and then assessed tumor growth. The resulting tumors were bigger in the prostates of p62 KO mice than in those of WT mice (Figures 2A–2C), supporting the notion that a loss of p62 in the tumor microenvironment promotes PCa growth. We next carried out transcriptomic profiling of the orthotopic tumors in the WT and p62 KO mice. NextBio analysis revealed important correlations between genes upregulated in the p62 KO orthotopic tumors with a gene signature in the category of "response to wounding" (Figure S2A). In addition, gene set enrichment analysis (GSEA) also identified "response to wounding" as significantly enriched of the gene ontology (GO) biological-process categories (Figure 2D; Figures S2B and S2C) and "stromal stimulation" in the C2 curated gene set library (Figures S2D and S2E). Because CAFs acquire an "activated phenotype" during tumor progression that resembles that of fibroblasts during the wound-healing repair process, these results suggested that the p62 KO stroma is likewise activated (Barron and Rowley, 2012; Bissell and Radisky, 2001; Franco and Hayward, 2012; Schäfer and Werner, 2008) and has a more CAF-like phenotype than the WT stroma. In support of this notion, we observed an increase in the expression of α smooth muscle actin (α-SMA) in sections from orthotopic tumors in p62 KO mice compared to WT controls (Figure 2E), as well as an increase in transforming growth factor β (TGF-β) transcripts as determined by RT-PCR in the same samples (Figure 2F). TGF-β and α-SMA are two bona fide markers of the CAF phenotype (Barron and Rowley, 2012; Franco and Hayward, 2012). Consistent with this, Ingenuity Pathway Analysis identified TGF-β1 as a predicted upstream regulator in the p62 KO orthotopic tumors ($p = 1.47 \times 10^{-7}$, activation Z score = 3.890). To determine the potential cell-autonomous effect of p62 in this important function, we used FACS to isolate prostate stromal cells from mice of both genotypes, as described in Figures 1E and 1F. Interestingly, we found that p62-deficient stromal cells also showed characteristics of CAFs, as determined by increased expression levels of α-SMA, TGF-β, and vimentin (Figure 2G). To facilitate subsequent studies, we generated prostate fibroblasts from WT and p62 KO mice and determined their "CAF activation" state. In these cells, the loss of p62 resulted in increased CAF transcript markers (Figure 2H), as well as in the secretion of TGF-β, as determined by ELISA (Figure 2I). This is important because TGF-β is essential for the acquisition and maintenance of the CAF/myofibroblast phenotype (Kojima et al., 2010; Ostman and Augsten, 2009). Therefore, p62 loss modifies the stroma by inducing a CAF phenotype, which in turn drives tumor progression.

Further bioinformatics GSEA revealed a hyperinflammatory phenotype in the p62 KO orthotopic tumors. That is, we found "humoral immune response" and "inflammatory response" as second GO categories enriched in the p62 KO transcriptome profile (Figure 2J; Figures S2F and S2G). RT-PCR analysis of the tumors from p62 KO mice showed increases in the transcripts of inflammatory cytokines such as IL-6, IL-1β, and keratinocyte chemoattractant (Figure 2K), as well as in the secretion of IL-6 as determined by ELISA (Figure 2L). We hypothesized that IL-6 could be an important mediator of the stromal p62-dependent signals that influence PCa progression in the epithelium. To test this possibility, we carried out an orthotopic injection experiment using p62/IL-6 double-KO (DKO) mice as hosts. Notably, the increased tumor growth observed in p62 KO mice was completely reversed in the DKO mice (Figures 2M and 2N), demonstrating that p62 plays a tumor-suppressive role in the tumor microenvironment during PCa progression by inhibiting CAF activation and blocking inflammation.

p62 in Stromal Fibroblasts Regulates an IL-6/TGF-β Cascade Essential for Tumor Invasion

We next set up a 3D organotypic culture model that recapitulates, in a genetically accessible system, the tumor microenvironment and its interactions with the tumor epithelial cell, closely mimicking the physiological situation and the cellular architecture (Gaggioli et al., 2007; Kim et al., 2013; Nyström et al., 2005; Ridky et al., 2010). Because our genome-wide transcriptomic analysis suggested that the loss of p62 in the tumor microenvironment is associated with a CAF-like signature, and because fibroblasts are a critical component of the stroma, we next tested whether p62 KO prostate fibroblasts were able to recapitulate the in vivo phenotype in 3D organotypic cultures. To do this, we cocultured in this organotypic system prostate fibroblasts from p62 KO and WT mice with TRAMP-C2Re3 PCa cells (Figure 3A). Importantly, p62 KO prostate fibroblasts (versus WT counterparts) enhanced the invasiveness and proliferation index of PCa epithelial tumor cells (Figures 3B–3D). Similar results were obtained with other PCa cell lines, such as mouse Myc-CaP (Figure S3A), or human PC3 cells (Figure S3B). Mouse fibroblasts from p62 KO mice also enhanced the invasiveness and proliferation index of human normal prostate epithelial cells compared with similar organotypic cultures with WT fibroblasts (Figure S3C). Altogether, this indicates that p62 deficiency in the stromal fibroblasts has a pivotal role in mediating cancer cell proliferation and invasion.

To follow up on our findings that IL-6 levels were increased in orthotopically injected tissues and that increased IL-6 expression was associated with enhanced tumorigenicity in vivo (Figures 2K–2N), we further investigated the role of this cytokine in the protumorigenic microenvironment created by p62 deficiency

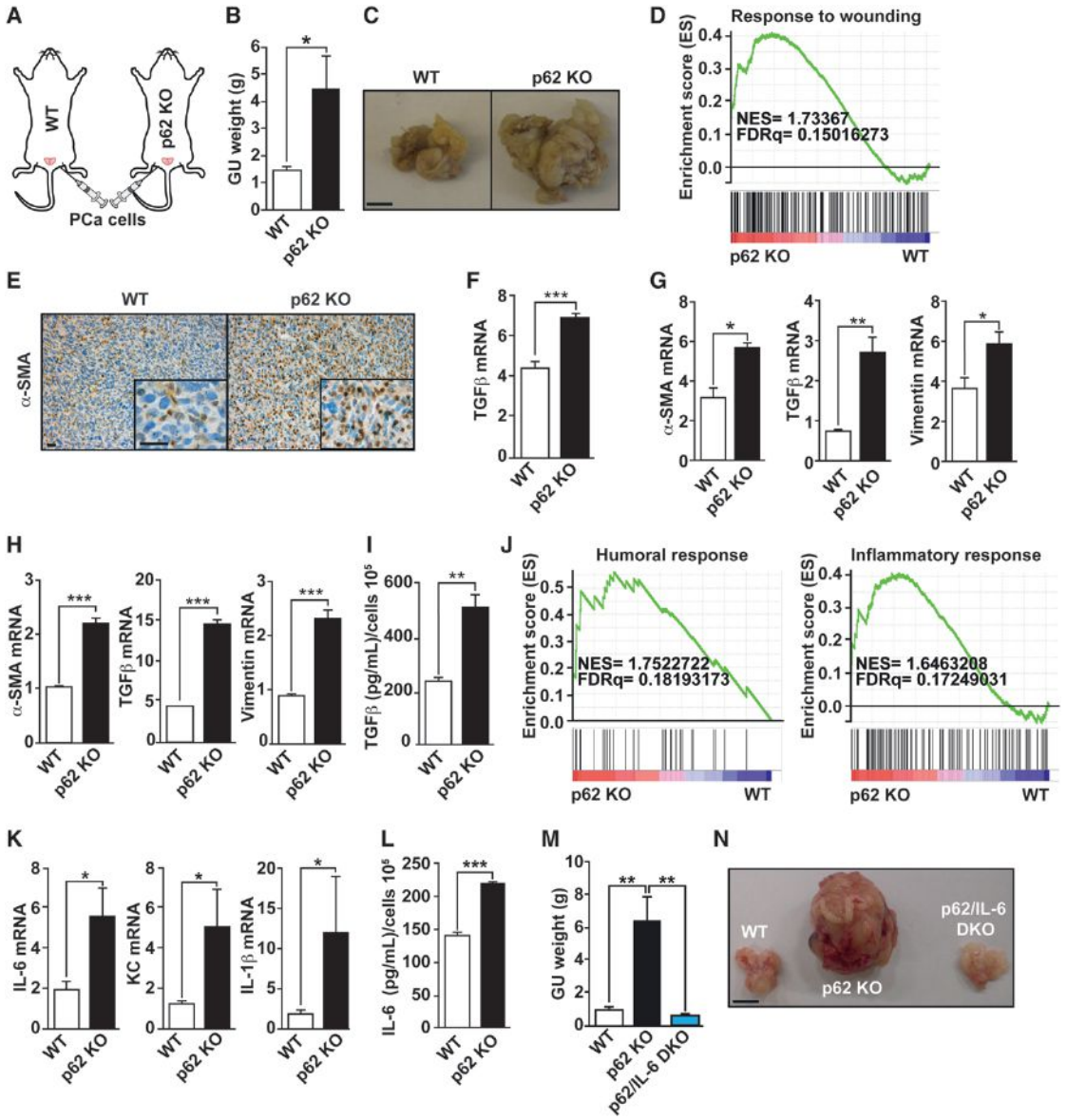

Figure 2. IL-6 Is Required for p62's Role in the Tumor Microenvironment

(A) Orthotopic injection of TRAMP-C2Re3 cells into the prostates of syngeneic WT and p62 KO mice. Orthotopic tumors were allowed to grow for two months.

(B and C) GU tract weight (B) and pictures (C) from (A); n = 5 or 6 mice per genotype. The scale bar represents 1 cm.

(D) "Response to wounding" GSEA plot of enrichment of gene expression in p62 KO orthotopic tumors.

(E) α-SMA staining of orthotopic tumors from WT and p62 KO mice. The scale bars represent 25 μm.

(F) RT-PCR of TGF-β in orthotopic tumors from WT and p62 KO mice (n = 3).

(G and H) RT-PCR of CAF markers (α-SMA, TGF-β, and vimentin) in FACS-sorted prostate stromal fraction from WT and p62 KO mice (G) and in WT and p62 KO prostate fibroblasts (H); n = 3.

(I) TGF-β production in prostate fibroblasts was determined by ELISA.

(J) GSEA plots of enrichment of gene expression in p62 KO orthotopic tumors.

(K) RT-PCR of inflammatory cytokines in orthotopic tumors of WT and p62 KO mice; n = 5 or 6 animals per group versus WT.

(L) IL-6 ELISA in fibroblasts.

(M and N) Orthotopic injection of TRAMP-C2Re3 cells into the prostates of mice of different genotypes (n = 5 or 6 mice). GU weights (M) and pictures (N). The scale bar represents 1 cm.

*$p < 0.05$, **$p < 0.01$, ***$p < 0.001$. Results are presented as mean ± SEM. See also Figure S2.

in the stroma. The two major sources of IL-6 in the tumor microenvironment are macrophages and stromal fibroblasts (Hanahan and Coussens, 2012). Notably, 3D organotypic culture experiments established that fibroblasts (Figures 3B and 3C), but not macrophages (Figure S3D), from p62 KO mice recapitulated the p62 KO phenotype in the orthotopic tissue grafting

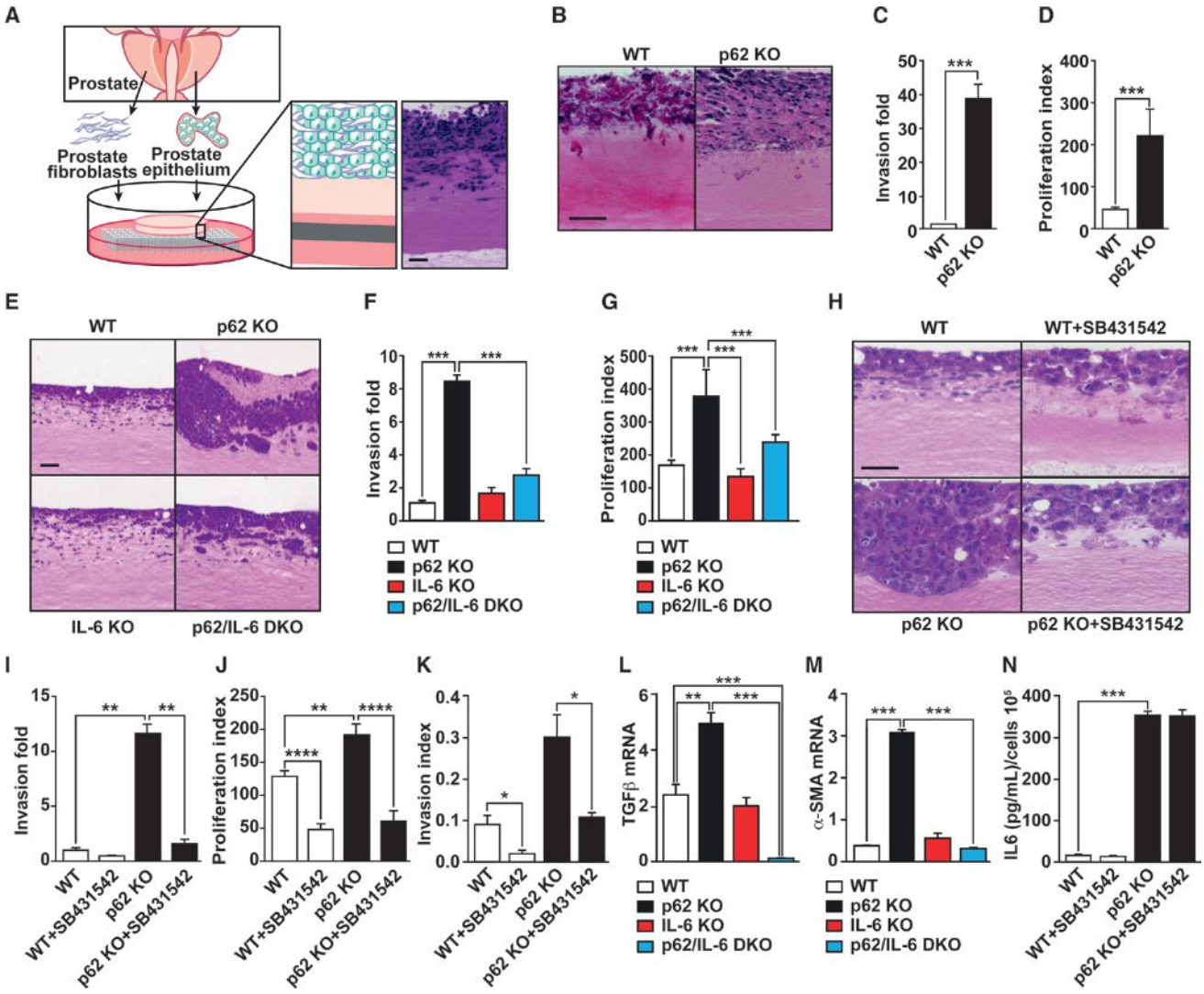

Figure 3. p62-Deficient Stroma-Mediated Invasion Is IL-6 and TGF-β Dependent

(A) Schematic representation of 3D organotypic cultures.

(B) H&E-stained sections of TRAMP-C2Re3 cells cultured in an organotypic system in the presence of primary prostate fibroblasts from WT and p62 KO mice.

(C and D) Quantification of PCa cell invasion (C) and proliferation index (D) of experiment shown in (B); n = 4.

(E) H&E staining of organotypic gels combining Myc-CaP cells with prostate fibroblasts from mice of different genotypes (n = 4).

(F and G) Quantification of PCa cell invasion (F) and proliferation index (G) of experiment shown in (E); n = 4.

(H) H&E staining of organotypic gels combining Myc-CaP cells with prostate fibroblasts from mice WT and p62 KO mice in the presence or absence of the TGF-β inhibitor SB431542 (10 μM).

(I and J) PCa cell invasion quantification (I) and proliferation index (J) of (H); n = 4.

(K) Invasion index determined by modified Boyden chamber assay with conditioned media from WT and p62 KO fibroblasts in the presence or absence of SB431542 (10 μM); n = 3.

(L and M) RT-PCR of TGF-β (L) and α-SMA (M) mRNA levels in fibroblasts of mice of different genotypes (n = 4).

(N) IL-6 production by WT and p62 KO fibroblasts in the presence or absence of the TGF-β inhibitor SB431542 (n = 4).

*p < 0.05, **p < 0.01, ***p < 0.001, ****p < 0.0001. Results are presented as mean ± SEM. The scale bars represent 100 μm. See also Figure S3.

experiment, and this effect was abolished when p62/IL-6 DKO fibroblasts were used in the 3D system (Figures 3E–3G). Furthermore, when TGF-β signaling was inhibited by incubating the organotypic cultures with the TGF-β inhibitor SB431542 (Inman et al., 2002), the protumorigenic phenotype of p62-deficient fibroblasts was reverted, consistent with the notion that TGF-β is important for the CAF phenotype and PCa proliferation (Figures 3H–3J). Likewise, the TGF-β inhibitor reverted the increased invasion index of PCa cells incubated with p62-deficient fibroblast conditioned medium in a Boyden chamber invasion assay (Figure 3K). Results shown in Figure S3E demonstrate the effectiveness of this inhibitor to block the TGF-β pathway. Moreover, the enhanced TGF-β production observed in the p62 KO fibroblasts, as well as that of α-SMA, was completely abrogated in

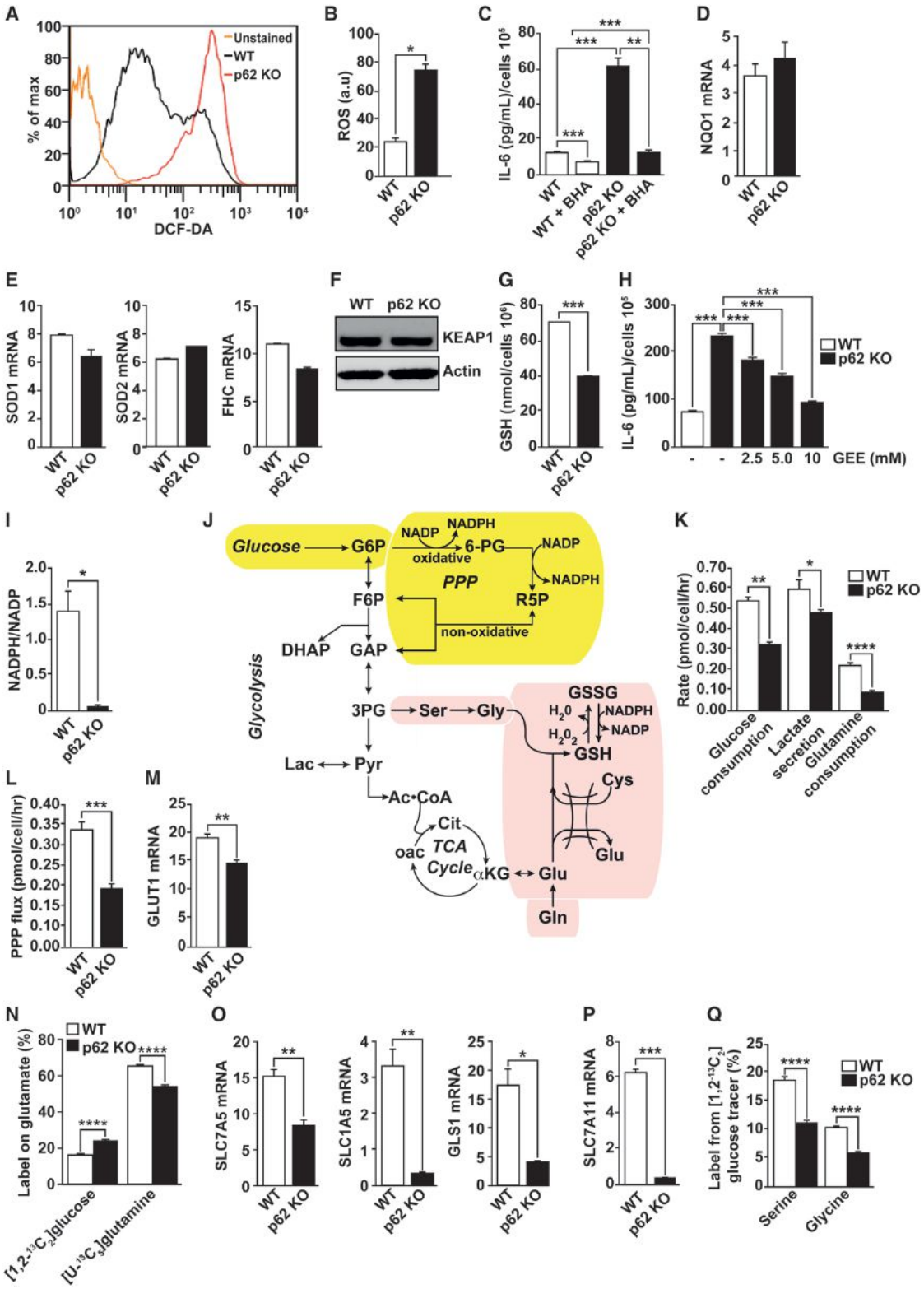

Figure 4. Metabolic Reprogramming in p62-Deficient Stroma

(A and B) Total intracellular levels of ROS in WT and p62 KO fibroblasts (A) and quantification (B); n = 4.

(C) IL-6 ELISA of WT and p62 KO fibroblasts treated with vehicle or the ROS scavenger BHA (100 μM) for 12 hr (n = 4).

(D and E) RT-PCR of NQO1 (D) and SOD1, SOD2, and FHC (E) mRNA levels in fibroblasts (n = 4).

(legend continued on next page)

the DKO fibroblasts (Figures 3L and 3M). Consistently, the knockdown of IL-6 in p62 KO fibroblasts impaired IL-6 secretion and, more important, also reverted TGF-β production and PCa invasion (Figures S3F–S3H). Furthermore, incubation of p62/IL-6 DKO fibroblasts with exogenously added IL-6 restored TGF-β levels to those of p62 KO cells as well as PCa invasion (Figure S3I and S3J). All this is consistent with a cell-autonomous role of the p62-IL-6 axis in the control of the CAF phenotype. However, incubation of p62 KO fibroblasts with the TGF-β signaling inhibitor SB431542 did not affect the overproduction of IL-6 in p62 KO fibroblasts (Figure 3N). These are important observations that establish a sequential p62/IL-6/TGF-β axis in the tumor fibroblastic compartment contributing to the control of epithelial tumorigenesis during PCa progression.

p62 Controls IL-6 Levels by Repressing Reactive Oxygen Species Production through Metabolic Reprogramming

We next sought to determine how p62 controls IL-6 production in fibroblastic stromal cells and whether the mechanisms mediating IL-6 production are relevant to stroma-driven tumorigenesis. It should be noted that p62 KO fibroblasts have increased levels of reactive oxygen species (ROS) (Figures 4A and 4B) and that the inhibition of ROS production (by the ROS scavenger butylated hydroxyanisole [BHA]) completely reverts the IL-6 hyperproduction phenotype (Figure 4C). This indicates that the mechanism whereby p62 represses IL-6 production in fibroblasts involves the control of ROS levels. It has previously been reported that p62 can activate NF-κB and NRF2 (Duran et al., 2008; Komatsu et al., 2010; Moscat and Diaz-Meco, 2009), which suggests that these molecules could play a role in the ability of p62 to repress ROS production and the subsequent activation of IL-6. The expression of critical detoxifying NF-κB- or NRF2-dependent genes (Figures 4D and 4E), as well as the levels of the NRF2 inhibitor Keap1 (Figure 4F), was not affected by the loss of p62 in fibroblasts. However, we found that p62 KO fibroblasts displayed lower levels of reduced glutathione (GSH) than the WT controls (Figure 4G). These are important observations because GSH is central to the control of ROS levels. In fact, treatment of p62 KO fibroblasts with the GSH analog GSH-reduced ethyl ester (GEE) reduced IL-6 to levels comparable with those of WT fibroblasts (Figure 4H). These results demonstrate that the loss of p62 results in lower GSH levels, thus promoting ROS accumulation, which is required for IL-6 overproduction in p62-deficient fibroblasts.

We observed a striking decrease in the reduced nicotinamide adenine dinucleotide phosphate (NADPH)/nicotinamide adenine dinucleotide phosphate (NADP) ratio in p62-deficient fibroblasts (Figure 4I). This ratio provides additional information on the cellular redox status, as the relative concentration of GSH versus oxidized GSH depends on the cellular content of NADPH. Glycolytic metabolism plays a critical role in maintaining NADPH production through the oxidative pentose phosphate pathway (PPP) (Figure 4J, yellow shading). Indeed, p62 KO cells exhibited decreased glucose uptake and lactate secretion (Figure 4K). This reduction in glycolytic rate resulted in decreased flux through the oxidative PPP, as determined by stable isotope tracing with [1,2-$^{13}C_2$]glucose (Figure 4L). These metabolic changes correlated with a reduction in GLUT1 levels in p62-deficient fibroblasts (Figure 4M), providing evidence that transcriptional changes associated with p62 loss influence metabolic flux.

Amino acids are critical for the production of GSH, a peptide composed of glutamate, cysteine, and glycine (Figure 4J, pink shading). Glutamine serves as an important precursor for glutamate, and loss of p62 in fibroblasts leads to lower glutamine consumption compared with WT cells (Figure 4K). We also observed a decrease in the direct conversion of [U-$^{13}C_5$] glutamine to glutamate in p62 KO fibroblasts, with a relative increase in the fraction of glutamate derived from [1,2-$^{13}C_2$]glucose (Figure 4N). In good agreement with these changes in glutamine metabolism, we observed reduced levels of the glutamine transporters SLC7A5 and SLC1A5, as well as glutaminase-1 (GLS1) (Figure 4O), a critical enzyme in the pathway that catalyzes the conversion of glutamine into glutamate (Figure 4J). Consistent with reduced levels of GSH, p62 KO fibroblasts also exhibit a dramatic reduction in the levels of SLC7A11, the xCT cystine/glutamate antiporter, which is the major driver of cystine uptake, a critical and rate-limiting step in the synthesis of GSH in several cell types, including fibroblasts (Figure 4P) (Bannai and Tateishi, 1986; Gout et al., 1997). Finally, we observed significant decreases in labeling of both serine and glycine from [1,2-$^{13}C_2$] glucose (Figure 4Q). Serine serves as a precursor to glycine and cysteine (when synthesized from methionine), so this decrease in label transfer provides evidence that there is less demand for GSH synthesis in p62-deficient cells. These results collectively demonstrate that loss of p62 in fibroblasts influences metabolic pathways controlling cellular redox, including NADPH production in the PPP and GSH synthesis.

p62 Is a Critical Regulator of c-Myc Levels

Previous data from other laboratories have established the critical role of c-Myc in the regulation of glutamine and glucose metabolism (Dang, 2012). We found significantly reduced levels of c-Myc in p62 KO fibroblasts as well as in WT fibroblasts in which p62 has been knocked down by small hairpin RNA (shRNA)

(F) Immunoblot analysis of KEAP1 in cell lysates from WT and p62 KO fibroblasts. Results are representative of three experiments.
(G) Cellular GSH levels in WT and p62 KO fibroblasts (n = 4).
(H) IL-6 ELISA of fibroblasts treated with increasing concentrations of the GSH analog GEE (n = 4).
(I) Cellular NADPH/NADP levels in WT and p62 KO fibroblasts (n = 4).
(J) Metabolic scheme depicting biosynthetic routes to NAPDH (yellow shading) and GSH (pink shading) from glucose and glutamine.
(K) Glucose consumption, lactate secretion, and glutamine consumption rates determined by spent medium analysis from WT and p62 KO fibroblasts (n = 3).
(L) PPP flux estimates from metabolic flux analysis in WT and p62 KO fibroblast cultures labeled with [1,2-$^{13}C_2$]glucose (n = 3).
(M) RT-PCR of GLUT1 mRNA (n = 4).
(N) Glutamate labeling in WT and p62 KO fibroblasts grown in either [1,2-$^{13}C_2$]glucose and unlabeled glutamine or [U-$^{13}C_5$]glutamine and unlabeled glucose (n = 3).
(O and P) RT-PCR of SLC7A5, SLC1A5, and GLS1 (O) and SLC7A11 (P) mRNA levels in WT and p62 KO fibroblasts (n = 3).
(Q) Labeling of serine and glycine from [1,2$^{13}C_2$]glucose (n = 3).
*p < 0.05, **p < 0.01, ***p < 0.001, ****p < 0.0001. Results are presented as mean ± SEM.

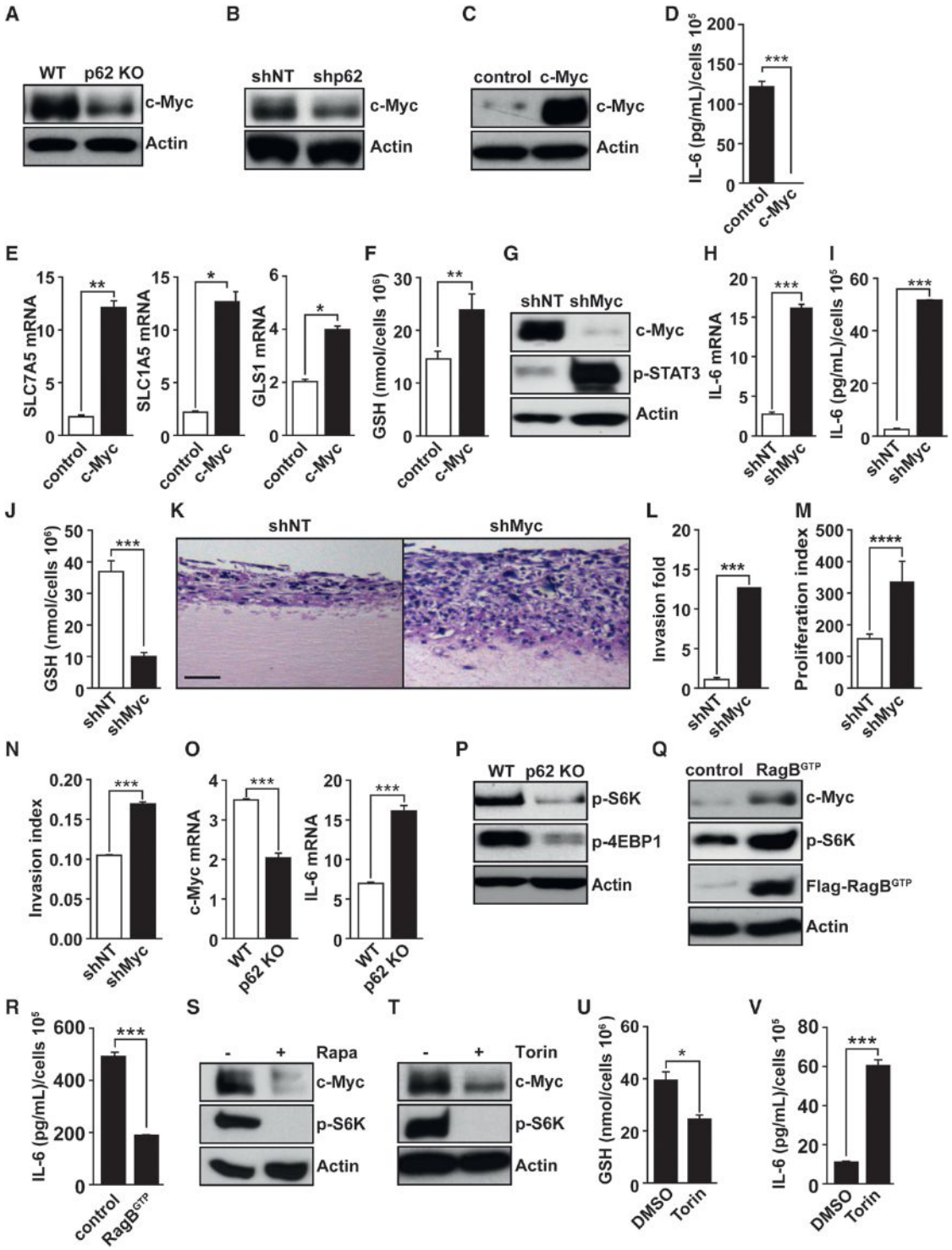

Figure 5. c-Myc-Mediated Metabolism in p62-Deficient Stroma

(A–C) Immunoblot analysis of c-Myc levels in WT and p62 KO fibroblasts (A), in WT fibroblasts lentivirally infected with shRNA nontargeted control (shNT) or shRNA specific for p62 (shp62) (B), and in p62 KO fibroblasts retrovirally infected with control vector (control) or with c-Myc expression vector (c-Myc) (C). Results are representative of three experiments.

(D) IL-6 ELISA in control and c-Myc cells (n = 4) as in (C).

(E) RT-PCR of SLC7A5, SLC1A5, and GLS1 mRNA in control and c-Myc cells (n = 3).

(F) Intracellular GSH levels in control and c-Myc cells (n = 3).

(G) Immunoblot analysis of c-Myc and p-STAT3 in WT fibroblasts infected with shNT or shRNA for c-Myc (shMyc).

(legend continued on next page)

(Figures 5A and 5B) and reductions in the levels of the key glutamine transporters SLC7A5 and SLC1A5, and GLS1 (Figure 4O), which are targets of c-Myc (Dang, 2012). Interestingly, ectopic expression of c-Myc in p62 KO fibroblasts (Figure 5C) reverted the p62-deficient phenotype in terms of IL-6 production (Figure 5D) and the levels of glutamine transporters and GLS1 (Figure 5E) and GSH (Figure 5F). On the contrary, c-Myc knockdown in WT fibroblasts (Figure 5G) resulted in increased IL-6 production at the mRNA and protein levels (Figures 5H and 5I). c-Myc knockdown in fibroblasts led to decreased levels of GSH (Figure 5J), as well as enhanced PCa cell invasion and proliferation in organotypic cell cultures (Figures 5K–5M). Also, the knockdown of c-Myc in fibroblasts resulted in increased PCa cell invasion index in a Boyden chamber assay (Figure 5N). Of note, this cause-and-effect correlation between p62 deficiency, c-Myc expression, and IL-6 production was also found in FACS-isolated prostate stromal cells from WT and p62 KO mice (Figure 5O). Collectively these results demonstrate that p62 repression of c-Myc expression in the stroma fibroblasts accounts for its tumor suppressive role in PCa.

IL-6 Is Regulated by a p62/mTORC1/c-Myc Cascade

Consistent with previously published observation (Duran et al., 2011), we found that p62 KO cells displayed reduced mTORC1 activity (Figure 5P). We hypothesized that the reduction in c-Myc levels found in p62 KO fibroblasts could be the consequence of mTORC1 inhibition. Importantly, we rescued c-Myc inhibition in p62 KO fibroblasts by expressing a permanently active mutant of the small-guanosine triphosphatase RagB, which is a critical activator of mTORC1 (Figure 5Q). IL-6 levels were likewise reduced under these conditions (Figure 5R). These results demonstrate that reduced mTORC1 activity in p62 KO fibroblasts accounts for the low levels of c-Myc and the subsequent increase in IL-6 production in these mutant cells. Treatment of WT fibroblasts with rapamycin or Torin, two different inhibitors of mTORC1, effectively reduced c-Myc levels (Figures 5S and 5T), promoting a significant reduction in GSH levels (Figure 5U) and a concomitant increase in IL-6 production (Figure 5V). Therefore, p62's ability to regulate mTORC1 in the stroma is essential for its control of the c-Myc/GSH/IL-6 axis.

p62 KO Mice Develop Prostate Hyperplasia and Prostatic Intraepithelial Neoplasia upon Aging

On the basis of these results, we hypothesized that the loss of p62 at an organismal level, which would include both the prostate stroma and epithelium, might be sufficient to drive prostate epithelium toward neoplasia. We characterized the prostates of p62 KO mice by histological analysis, which revealed no abnormalities in development or morphology at early stages. However, at 9 months of age, prostates from p62 KO mice developed hyperplasia, with a concomitant increase in Ki67 staining (Figures 6A and 6B). These lesions progressed to prostatic intraepithelial neoplasia (PIN) at 1 year of age (Figure 6C). This indicated that, whereas in xenograft experiments PCa epithelial cells with reduced p62 displayed inhibited tumorigenesis (Duran et al., 2011), the total loss of p62 in vivo promoted prostate epithelial cell growth. These observations are in good agreement with our model whereby p62 in the stromal fibroblasts normally acts as a tumor suppressor, and the total KO of p62 results in p62-deficient stromal fibroblasts that drive the prostate epithelium to a malignancy-prone state. To further test this hypothesis, we crossed total p62 KO mice with two well-established mouse models of PCa ($PTEN^{+/-}$ and $TRAMP^{+}$) (Di Cristofano et al., 1998; Greenberg et al., 1995) and asked whether total ablation of p62 inhibited or promoted prostate tumor development. Figures 6D and 6E show hematoxylin and eosin (H&E) analyses of $PTEN^{+/-}$/p62 KO prostrates demonstrating an increase in the percentage of glands with high-grade PIN at the age of 6 months. Furthermore, $TRAMP^{+}$/p62 KO mice had reduced survival (Figure 6F), increased percentages of poorly differentiated adenocarcinoma (Figure 6G) and neuroendocrine tumors (Figure 6H), as well as a larger number of metastases (Figure 6I), of which a higher percentage were in the liver (Figure 6J). Consistent with our model, prostate fibroblasts from $PTEN^{+/-}$/p62 KO mice showed increased IL-6 and reduced c-Myc expression compared with those from p62-proficent $PTEN^{+/-}$ mice (Figures S4A–S4C). Interestingly, immunohistochemical analysis of prostates from $PTEN^{+/-}$ mice confirmed reduced expression of p62 in the stromal compartment compared with those from WT mice (Figure S4D). To further support the role of p62 deficiency in the stroma in driving tumorigenesis in vivo, we coinjected syngeneic PCa cells (TRAMP-C2Re3) with WT or p62 KO fibroblasts and assessed the effect that fibroblasts exert on tumor growth. Tumors coinjected with p62 KO fibroblasts grew significantly faster and were larger than tumors in mice injected with WT fibroblasts, consistent with the cell-autonomous tumor-promoting activity of p62-deficient fibroblasts on epithelial PCa cells (Figures 6K and 6L). In agreement with this, bromodeoxyuridine (BrdU) incorporation was increased in the p62 KO fibroblast-driven tumors (Figures 6M and 6N).

(H and I) RT-PCR of IL-6 mRNA (H) and IL-6 ELISA (I) in the same cells (n = 3) as in (G).
(J) Quantification of intracellular GSH levels in WT shNT and shMyc cells (n = 3).
(K) H&E-stained organotypic gels of TRAMP-C2Re3 cells with shNT or shMyc fibroblasts. The scale bar represents 100 μm.
(L and M) Quantification of PCa cell invasion (L) and proliferation index (M) of experiment shown in (K).
(N) Invasion index determined by modified Boyden chamber assay of Myc-CaP cells cocultured with shNT and shMyc fibroblasts.
(O) RT-PCR of c-Myc and IL-6 mRNA levels in FACS-isolated prostate stromal cells from WT and p62 KO mice (n = 3).
(P) Immunoblot analysis with the indicated antibodies of cell lysates of WT and p62 KO fibroblasts.
(Q) Immunoblot analysis for the specified proteins of cell lysates from p62 KO fibroblasts retrovirally infected with control vector (control) or FLAG-$RagB^{GTP}$ expression vector ($RagB^{GTP}$). Results are representative of three experiments.
(R) IL-6 ELISA (n = 3) in cells shown in (Q).
(S and T) Immunoblot analysis of c-Myc and p-S6K in fibroblasts treated with rapamycin (S) or Torin1 (T) for 12 hr.
(U) Intracellular GSH levels in fibroblasts treated with Torin1.
(V) IL-6 ELISA in fibroblasts treated with Torin1 (n = 3).
*p < 0.05, **p < 0.01, ***p < 0.001, ****p < 0.0001. Results are presented as mean ± SEM.

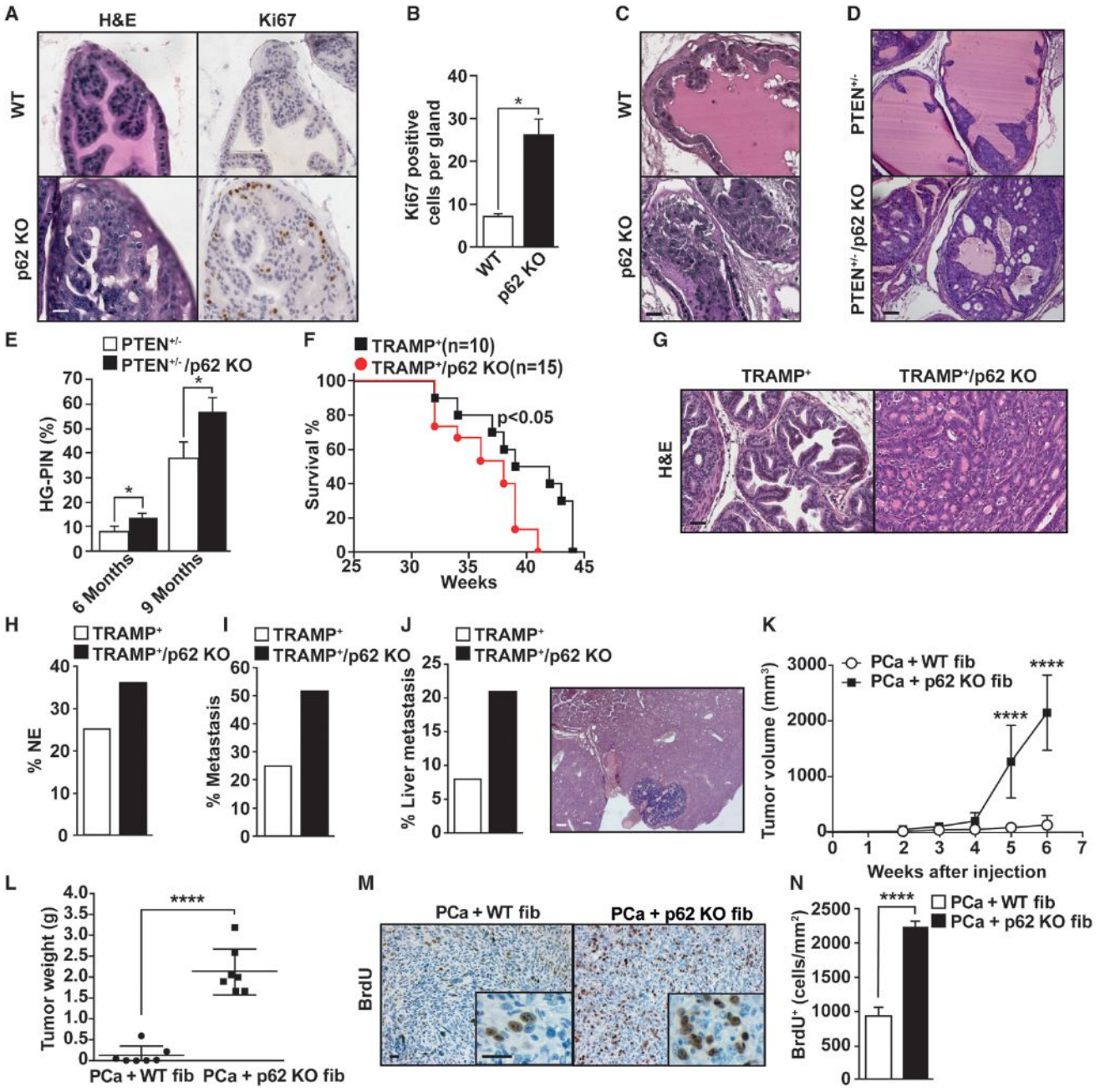

Figure 6. p62 Deficiency Accelerates Prostate Tumor Progression in Different Mouse Models of Prostate Cancer

(A) Hyperplasia in the prostatic anterior lobe of p62 KO mice. H&E and Ki67 staining of prostates from 9-month-old WT and p62 KO mice (n = 5).

(B) Quantification of Ki67-positive cells in the prostate sections shown in (A). Results are the means ± SD of counts from 10 different fields per mouse (n = 5).

(C) PIN in the dorsolateral lobes of prostates from 12-month-old p62 KO mice.

(D) Representative examples of H&E staining of dorsolateral lobes of prostates from $PTEN^{+/-}$ and $PTEN^{+/-}$/p62 KO mice at 6 months of age (n = 5).

(E) Percentage of glands with HG-PIN (n = 5 mice).

(F) Kaplan-Meier survival curve of $TRAMP^{+}$ mice (n = 10), compared with $TRAMP^{+}$/p62 KO mice (n = 15).

(G) Representative H&E staining of mouse prostate sections from $TRAMP^{+}$ and $TRAMP^{+}$/p62 KO mice (n = 10).

(H) Incidence of neuroendocrine tumors in $TRAMP^{+}$ (n = 12) and $TRAMP^{+}$/p62 KO mice (n = 19).

(I and J) Incidence of metastasis (I) and liver metastasis (J) in $TRAMP^{+}$ compared with $TRAMP^{+}$/p62 KO mice.

(K–M) Coinjection of syngeneic TRAMPC2-Re3 PCa cells with either WT or p62 KO fibroblasts in C57BL/6 mice. (K) Tumor volume assessed at different time points after injection (n = 7 mice). (L) Tumor weight at 6 weeks after injection (n = 7 mice). (M) BrdU staining in tumor sections.

(N) Quantification of BrdU positive cells of (M).

Results are presented as mean ± SEM (n = 10). *p < 0.05, ****p < 0.001. The scale bars represent 25 μm. See also Figure S4.

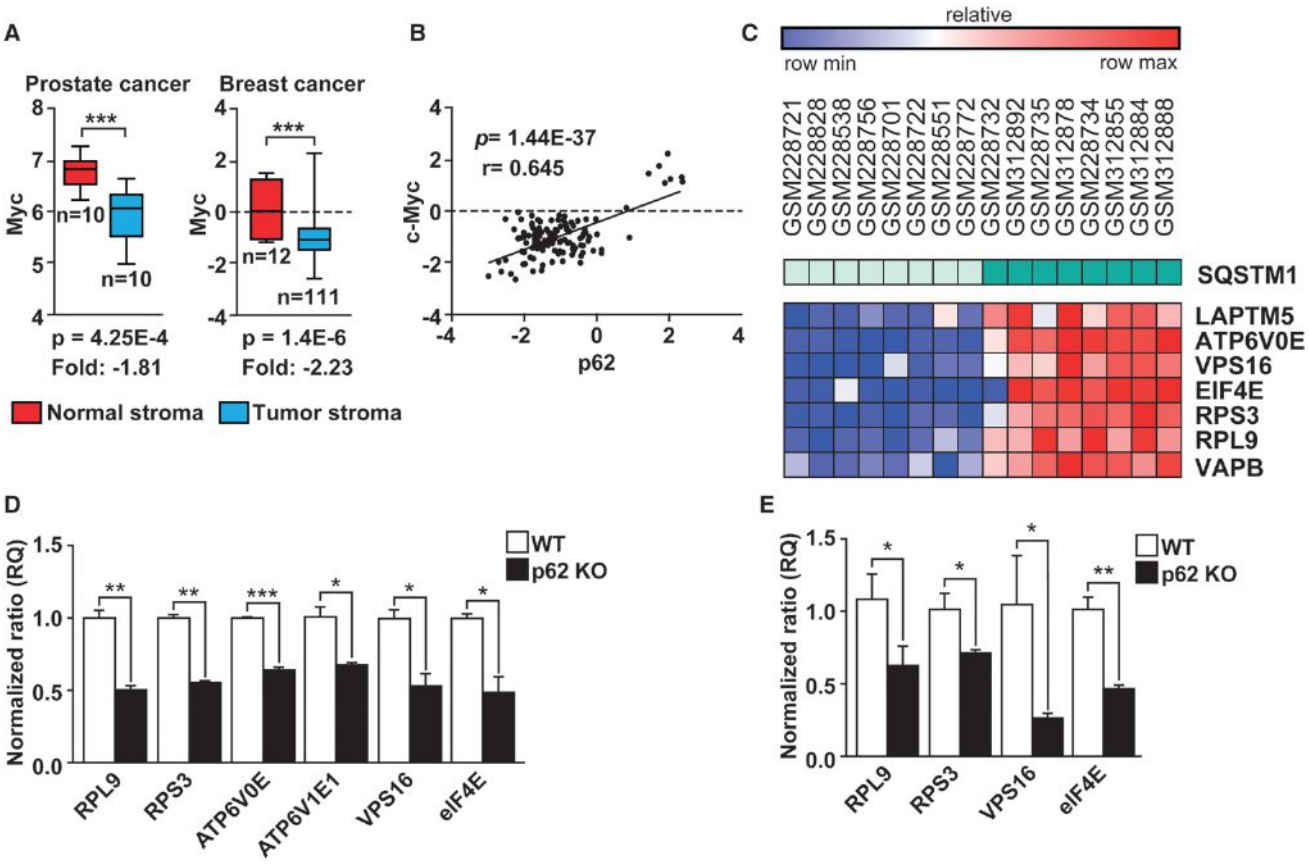

Figure 7. The p62-Myc-mTORC1 Cassette Is Downregulated in Prostate Tumor-Associated Stroma in Human Samples

(A) Myc levels are downregulated in the tumor stroma of human tissue samples. Data were collated from public data sets of gene expression in tumor stroma in several human cancers: GSE34312 (prostate cancer) and GSE9014 (breast cancer). The p value, fold change of expression, and size of the sample (n) for each study are indicated in the corresponding panels.

(B) Positive correlation between p62 and Myc levels in the stroma.

(C) Heatmap of mTORC1 signature selected from p62 neighboring genes in human stroma. p62 levels are indicated as SQSTM1.

(D and E) RT-PCR analysis of mTORC1 genes in WT and p62 KO fibroblasts (D) and in FACS sorted mouse prostate stromal fraction (E).

*p < 0.05, **p < 0.01, ***p < 0.001. Results are presented as mean ± SEM (n = 3). See also Figure S5.

p62/mTORC1/c-Myc Connection in Human Cancer Stroma

To determine whether the identified link between p62 and c-Myc through mTORC1 has relevance to the role of the stroma in human cancer, we used bioinformatics to analyze c-Myc transcript levels in two sets of human gene-expression arrays from prostate and breast cancer stroma. Stroma of human tumors displayed reduced levels of c-Myc (Figure 7A), and there was a statistically significant correlation between c-Myc and p62 expression in tumor stroma (Figure 7B), emphasizing the clinical relevance of the p62-Myc connection in the stroma. To further explore the link between p62 and mTORC1 in the tumor stroma of human cancers, we identified expression neighbors of p62. We developed this gene signature by using the human cancer stroma data set shown in Figure 7A, in which we classified tumors on the basis of p62 expression levels and selected for analysis only those samples in the top and bottom 25%. Interestingly, this analysis revealed a statistically significant correlation between p62 expression and that of genes previously reported to be controlled by mTORC1 activity (Figure 7C; Figure S5) (Peña-Llopis et al., 2011). We determined the expression levels of a selection of these genes by RT-PCR and found that their expression was reduced in p62 KO fibroblasts compared with WT (Figure 7D). The same results were obtained when these were analyzed in prostate stromal cell preparations from p62 KO and WT mice (Figure 7E). Furthermore, we found a clear statistically significant correlation between p62 expression and that of these genes in human cancer stroma (Figures S5B–S5H). Altogether, these results demonstrate that the p62/mTORC1/c-Myc connection is not only relevant in the mouse prostate stroma but it is also important in human cancer stroma.

DISCUSSION

Tumorigenesis is a slow process that is initiated by the successive accumulation of genetic and epigenetic changes that result in the activation of cell growth and survival genes and the inactivation of tumor suppressors (Hanahan and Weinberg, 2011). However, for tumor development to take place, initiation is not sufficient. Other signals are required to drive tumor promotion

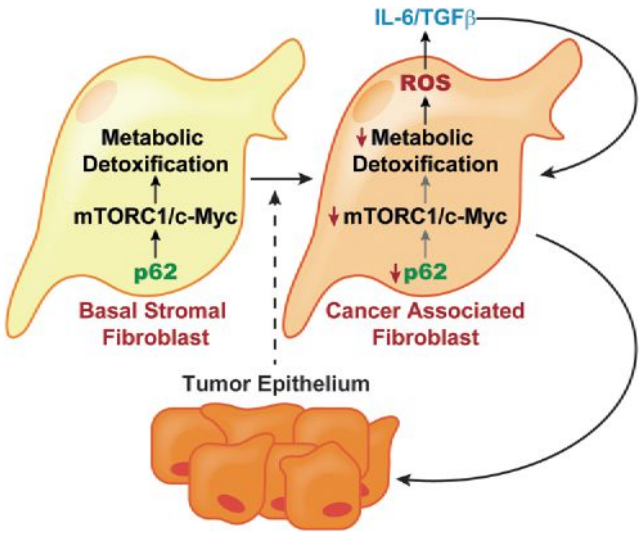

Figure 8. Stromal Activation by p62 Deficiency in Cancer
Tumor epithelium promotes the downregulation of p62 in stromal fibroblasts, leading to reduced mTORC1 activity and c-Myc expression, which results in impaired metabolic detoxification and the subsequent release of ROS and IL-6. An autocrine pathway promotes TGF-β and the induction of CAF phenotype, which further increases epithelial invasion and tumorigenesis.

and progression and the development of the fully malignant stage. The progression phase is most likely orchestrated via the tumor microenvironment by nonepithelial cells in which metabolic stress and inflammation create an environment in which epithelial tumor-derived cells propagate and acquire more aggressive phenotypes (Hanahan and Coussens, 2012; Hanahan and Weinberg, 2011). Immune cells, such as tumor-associated macrophages, are among the cell types in the tumor microenvironment that contribute to inflammation (Coussens and Werb, 2002; Johansson et al., 2008). On the other hand, a crosstalk between metabolic pathways in the stromal and epithelial compartments of the tumor may drive the survival and growth of epithelial cancer cells (Lisanti et al., 2013). However, it has not been thoroughly investigated whether metabolic reprogramming in the stromal cells of the tumor microenvironment exerts any control over inflammation and the malignant characteristics of the transformed epithelium.

Here we demonstrate that the inactivation of mTORC1 in p62-deficient stromal fibroblasts results in metabolic reprogramming through c-Myc inactivation (Figure 8). This reprogramming leads to increased levels of IL-6, which promotes epithelial cell invasion and proliferation. Therefore, because of its regulation of mTORC1, p62 emerges as a tumor suppressor that acts by regulating c-Myc and thus inducing an inflammatory response. These results are in marked contrast to the role played by p62 and mTORC1 in epithelial cancer cells. That is, we have recently demonstrated that p62 inactivation in PCa and lung adenocarcinoma epithelial cells inhibits the proliferation and tumorigenic properties of these cells and correlates with decreased mTORC1 activation. Moreover, the increased IL-6 phenotype can be reverted by expression of a permanently active mutant of the mTORC1 activator RagB. This has important implications from a therapeutic point of view because inhibition of p62 and/or mTORC1 may result in opposite effects in the stroma and the epithelium of the tumor, thus reducing the efficacy of broadly applied mTORC1-based chemotherapeutic approaches. In this regard, these results are reminiscent of the dual role that mTORC1 might play as a regulator of autophagy, which can have a tumor-suppressing or a tumor-promoting effect, depending of the stage of the tumor (Guo et al., 2013; Levine and Kroemer, 2008), and also on whether the manipulation takes place in the epithelium or in the stroma (Lisanti et al., 2013). Our data using KO mice clearly reveal that p62 deficiency creates a protumorigenic environment for p62-proficient PCa cells in orthotopic experiments and also show that, even under normal conditions, it drives PIN formation in the endogenous epithelium in the absence of any other induced mutations. Furthermore, in two PCa models, the lack of p62 at an organismal level results in increased tumorigenesis, despite the fact that p62 is absent not only in the stroma but also in the transformed epithelium. These results are very important because they demonstrate that even though p62 is required for epithelial cancer cells to proliferate in vitro and in xenografts (Duran et al., 2011), the p62-deficient tumor microenvironment overrides the requirement for p62 in the epithelium. Our in vitro and in vivo findings establish that increased IL-6 levels generated by stromal fibroblasts are a critical event in that process. Therefore, it can be predicted that total ablation of p62 at an organismal level, either genetically or pharmacologically, may increase tumorigenesis, rather than inhibiting it, depending on the contribution of the stroma and the ability of p62 deficiency to reprogram stromal metabolism to generate ROS and inflammation. Our data shown here demonstrate that this is the case in prostate tumorigenesis and suggest that it could be a relevant mechanism in other tumor types as well. The proinflammatory microenvironment in the p62-deficient stroma results in a CAF-activated phenotype that is maintained by stromal TGF-β production. This is consistent with previous results in colon cancer demonstrating that a TGF-β-activated tumor microenvironment is critical for fully aggressive cancer cells to metastasize (Calon et al., 2012).

Metabolic reprogramming in cancer is emerging as a central process in tumor cell survival and growth (DeBerardinis and Thompson, 2012; Metallo and Vander Heiden, 2013; Vander Heiden, 2013). The so-called Warburg effect supports the importance of an atypical glucose metabolism tailored to the cancer cell's need for efficient anabolic utilization of nutrients (Vander Heiden et al., 2009). More recently, different types of reprogramming events have been unveiled that constitute specific responses of the tumor cell to a nutrient-deficient environment. These include the metabolism of serine or the utilization of the PPP to alleviate oxidative stress conditions during tumorigenesis (Locasale, 2013; Ma et al., 2013; Possemato et al., 2011; Vander Heiden et al., 2010). In the current study, we show that metabolic reprogramming triggered by p62 deficiency in the tumor stroma is critical for the creation of a protumorigenic inflammatory environment driven by IL-6. Moreover, we have shown that this involves an mTORC1/c-Myc/ROS cascade that is controlled by p62. In this regard, previous results from our and other laboratories have shown that p62 represses ROS by inducing the activation of NF-κB- or NRF2-dependent detoxifying molecules (Duran et al., 2008; Komatsu et al., 2010; Ling et al., 2012). Surprisingly, neither of these two transcription factors nor Keap1

levels were affected in p62-deficient stromal fibroblasts, indicating that p62 may use diverse cascades in different cellular compartments of the tumor. Interestingly, our previous data demonstrate that under conditions of Ras-induced transformation, p62 deficiency leads to increased cell death and reduced tumorigenesis due to enhanced ROS production (Duran et al., 2008). In contrast, we show here that the enhanced ROS observed in the untransformed stromal fibroblasts does not result in increased cell death but rather in the creation of a proinflammatory phenotype. The main conclusion of these results is that increased ROS production induced by p62 deficiency has different outcomes depending on the cell type and the mechanisms whereby ROS is produced. The outcome also depends on whether or not the levels of ROS are high enough to engage a c-Jun N-terminal kinase-driven cell-death pathway, as found in the Ras-tumor cell, as opposed to increased IL-6 production and a protumorigenic effect on epithelial cells, as we demonstrated in the stromal nontransformed fibroblasts.

Importantly, we were able to show that the implication of the p62/mTORC1/c-Myc cascade is relevant not only in mouse model systems but also in human samples, in which this pathway is inactivated in the tumor stroma. Therefore, our findings support a more comprehensive approach when devising therapeutic strategies in cancer, which should take into account not only the altered pathways in the transformed epithelial compartment but also how the inhibition of these cascades might affect the surrounding stroma. Our observations suggest that pharmacological inhibition of IL-6 and/or TGF-β to target stromal activation could be beneficial in combination with epithelial-targeted therapies.

EXPERIMENTAL PROCEDURES

Mice

WT, p62 KO, PTEN$^{+/-}$, and TRAMP^{+} mice were previously described (Durán et al., 2004; Di Cristofano et al., 1998; Greenberg et al., 1995). All mouse strains were generated in a C57BL/6 background. All mice were born and maintained under pathogen-free conditions. All genotyping was done by PCR. Mice were sacrificed and genitourinary (GU) sections were dissected. Mice were injected with 5-bromo-2′-deoxyuridine intraperitoneally and sacrificed 2 hr after injection. Animal handling and experimental procedures conformed to institutional guidelines (Sanford-Burnham Medical Research Institute Institutional Animal Care and Use Committee).

Cell Lysis and Western Immunoblotting

Cells were rinsed once with ice-cold PBS and lysed in radioimmunoprecipitation assay buffer (1 × PBS, 1% Nonidet P-40, 0.5% sodium deoxycholate, 0.1% SDS, 1 mM phenyl methyl sulfonyl fluoride, and protease inhibitors). Cell extracts were denatured, subjected to 8% to 14% SDS-PAGE, transferred to nitrocellulose-enhanced chemiluminescence membranes (GE Healthcare), and immunoblotted with the specific antibodies. Chemiluminescence was used to detect the proteins (Thermo Scientific).

Statistical Analysis

Significant differences between groups were determined using Student's t test. Scoring of immunostaining of human prostate tissue microarrays was analyzed using Fisher's exact test. The significance level for statistical testing was set at $p < 0.05$.

ACCESSION NUMBERS

The Gene Expression Omnibus accession number for the microarray data reported in this paper is GSE55587.

SUPPLEMENTAL INFORMATION

Supplemental Information includes Supplemental Experimental Procedures and five figures and can be found with this article online at http://dx.doi.org/10.1016/j.ccr.2014.05.004.

AUTHOR CONTRIBUTIONS

T.V., J.Y.K., S.A.-B. and A.D. performed experiments. J.M.-P. and M.R.-C. performed bioinformatics analysis. E.A.C. provided pathologist expertise for histological analysis. C.S.A. and T.V. performed the metabolic experiments. C.M.M., M.D.M., and J.M. designed and analyzed metabolic data. M.D.M. and J.M conceived and supervised the project with equal contribution. M.D.M. and J.M. wrote the manuscript with assistance from all the authors.

ACKNOWLEDGMENTS

This work was funded by grants R01CA132847 (J.M.), R01CA172025 (J.M.), R01CA134530 (M.T.D.-M.), and 5P30CA030199 (M.T.D-M. and J.M.) from the NIH. Additional support was provided by grants W81XWH-13-1-0353 (M.T.D-M.), W81XWH-13-1-0354 (J.M.), and W81XWH-13-1-0105 (C.M.M.) from the U.S. Department of Defense. We thank Maryellen Daston for editing this manuscript; Diantha LaVine for the artwork; and Tomoko Yajima, Tom Hudson, Jessica Leung, and the personnel of the Cancer Metabolism, Flow Cytometry, Cell Imaging, Animal Facility, Histology, Functional Genomics and Viral Vectors Shared Resources at the Sanford-Burnham Medical Research Institute for technical assistance. We thank Neil Bhowmick for assistance in the preparation of prostate fibroblasts.

Received: December 24, 2013
Revised: March 17, 2014
Accepted: May 7, 2014
Published: July 3, 2014

REFERENCES

Ammirante, M., Luo, J.L., Grivennikov, S., Nedospasov, S., and Karin, M. (2010). B-cell-derived lymphotoxin promotes castration-resistant prostate cancer. Nature *464*, 302–305.

Azevedo, A., Cunha, V., Teixeira, A.L., and Medeiros, R. (2011). IL-6/IL-6R as a potential key signaling pathway in prostate cancer development. World J. Clin. Oncol. *2*, 384–396.

Bannai, S., and Tateishi, N. (1986). Role of membrane transport in metabolism and function of glutathione in mammals. J. Membr. Biol. *89*, 1–8.

Barron, D.A., and Rowley, D.R. (2012). The reactive stroma microenvironment and prostate cancer progression. Endocr. Relat. Cancer *19*, R187–R204.

Bissell, M.J., and Radisky, D. (2001). Putting tumours in context. Nat. Rev. Cancer *1*, 46–54.

Calon, A., Espinet, E., Palomo-Ponce, S., Tauriello, D.V., Iglesias, M., Céspedes, M.V., Sevillano, M., Nadal, C., Jung, P., Zhang, X.H., et al. (2012). Dependency of colorectal cancer on a TGF-β-driven program in stromal cells for metastasis initiation. Cancer Cell *22*, 571–584.

Coussens, L.M., and Werb, Z. (2002). Inflammation and cancer. Nature *420*, 860–867.

Dang, C.V. (2012). MYC on the path to cancer. Cell *149*, 22–35.

De Marzo, A.M., Platz, E.A., Sutcliffe, S., Xu, J., Grönberg, H., Drake, C.G., Nakai, Y., Isaacs, W.B., and Nelson, W.G. (2007). Inflammation in prostate carcinogenesis. Nat. Rev. Cancer *7*, 256–269.

DeBerardinis, R.J., and Thompson, C.B. (2012). Cellular metabolism and disease: what do metabolic outliers teach us? Cell *148*, 1132–1144.

Di Cristofano, A., Pesce, B., Cordon-Cardo, C., and Pandolfi, P.P. (1998). Pten is essential for embryonic development and tumour suppression. Nat. Genet. *19*, 348–355.

Diaz-Meco, M.T., and Moscat, J. (2012). The atypical PKCs in inflammation: NF-κB and beyond. Immunol. Rev. *246*, 154–167.

Durán, A., Serrano, M., Leitges, M., Flores, J.M., Picard, S., Brown, J.P., Moscat, J., and Diaz-Meco, M.T. (2004). The atypical PKC-interacting protein p62 is an important mediator of RANK-activated osteoclastogenesis. Dev. Cell *6*, 303–309.

Duran, A., Linares, J.F., Galvez, A.S., Wikenheiser, K., Flores, J.M., Diaz-Meco, M.T., and Moscat, J. (2008). The signaling adaptor p62 is an important NF-kappaB mediator in tumorigenesis. Cancer Cell *13*, 343–354.

Duran, A., Amanchy, R., Linares, J.F., Joshi, J., Abu-Baker, S., Porollo, A., Hansen, M., Moscat, J., and Diaz-Meco, M.T. (2011). p62 is a key regulator of nutrient sensing in the mTORC1 pathway. Mol. Cell *44*, 134–146.

Erez, N., Truitt, M., Olson, P., Arron, S.T., and Hanahan, D. (2010). Cancer-associated fibroblasts are activated in incipient neoplasia to orchestrate tumor-promoting inflammation in an NF-kappaB-dependent manner. Cancer Cell *17*, 135–147.

Franco, O.E., and Hayward, S.W. (2012). Targeting the tumor stroma as a novel therapeutic approach for prostate cancer. Adv. Pharmacol. *65*, 267–313.

Gaggioli, C., Hooper, S., Hidalgo-Carcedo, C., Grosse, R., Marshall, J.F., Harrington, K., and Sahai, E. (2007). Fibroblast-led collective invasion of carcinoma cells with differing roles for RhoGTPases in leading and following cells. Nat. Cell Biol. *9*, 1392–1400.

Galavotti, S., Bartesaghi, S., Faccenda, D., Shaked-Rabi, M., Sanzone, S., McEvoy, A., Dinsdale, D., Condorelli, F., Brandner, S., Campanella, M., et al. (2013). The autophagy-associated factors DRAM1 and p62 regulate cell migration and invasion in glioblastoma stem cells. Oncogene *32*, 699–712.

Gout, P.W., Kang, Y.J., Buckley, D.J., Bruchovsky, N., and Buckley, A.R. (1997). Increased cystine uptake capability associated with malignant progression of Nb2 lymphoma cells. Leukemia *11*, 1329–1337.

Greenberg, N.M., DeMayo, F., Finegold, M.J., Medina, D., Tilley, W.D., Aspinall, J.O., Cunha, G.R., Donjacour, A.A., Matusik, R.J., and Rosen, J.M. (1995). Prostate cancer in a transgenic mouse. Proc. Natl. Acad. Sci. USA *92*, 3439–3443.

Grivennikov, S.I., Greten, F.R., and Karin, M. (2010). Immunity, inflammation, and cancer. Cell *140*, 883–899.

Guo, Y., Xu, F., Lu, T., Duan, Z., and Zhang, Z. (2012). Interleukin-6 signaling pathway in targeted therapy for cancer. Cancer Treat. Rev. *38*, 904–910.

Guo, J.Y., Xia, B., and White, E. (2013). Autophagy-mediated tumor promotion. Cell *155*, 1216–1219.

Hanahan, D., and Weinberg, R.A. (2011). Hallmarks of cancer: the next generation. Cell *144*, 646–674.

Hanahan, D., and Coussens, L.M. (2012). Accessories to the crime: functions of cells recruited to the tumor microenvironment. Cancer Cell *21*, 309–322.

Inami, Y., Waguri, S., Sakamoto, A., Kouno, T., Nakada, K., Hino, O., Watanabe, S., Ando, J., Iwadate, M., Yamamoto, M., et al. (2011). Persistent activation of Nrf2 through p62 in hepatocellular carcinoma cells. J. Cell Biol. *193*, 275–284.

Inman, G.J., Nicolás, F.J., Callahan, J.F., Harling, J.D., Gaster, L.M., Reith, A.D., Laping, N.J., and Hill, C.S. (2002). SB-431542 is a potent and specific inhibitor of transforming growth factor-beta superfamily type I activin receptor-like kinase (ALK) receptors ALK4, ALK5, and ALK7. Mol. Pharmacol. *62*, 65–74.

Inoue, D., Suzuki, T., Mitsuishi, Y., Miki, Y., Suzuki, S., Sugawara, S., Watanabe, M., Sakurada, A., Endo, C., Uruno, A., et al. (2012). Accumulation of p62/SQSTM1 is associated with poor prognosis in patients with lung adenocarcinoma. Cancer Sci. *103*, 760–766.

Johansson, M., Denardo, D.G., and Coussens, L.M. (2008). Polarized immune responses differentially regulate cancer development. Immunol. Rev. *222*, 145–154.

Kim, J.Y., Valencia, T., Abu-Baker, S., Linares, J., Lee, S.J., Yajima, T., Chen, J., Eroshkin, A., Castilla, E.A., Brill, L.M., et al. (2013). c-Myc phosphorylation by PKCζ represses prostate tumorigenesis. Proc. Natl. Acad. Sci. U S A *110*, 6418–6423.

Kojima, Y., Acar, A., Eaton, E.N., Mellody, K.T., Scheel, C., Ben-Porath, I., Onder, T.T., Wang, Z.C., Richardson, A.L., Weinberg, R.A., and Orimo, A. (2010). Autocrine TGF-beta and stromal cell-derived factor-1 (SDF-1) signaling drives the evolution of tumor-promoting mammary stromal myofibroblasts. Proc. Natl. Acad. Sci. U S A *107*, 20009–20014.

Komatsu, M., Kurokawa, H., Waguri, S., Taguchi, K., Kobayashi, A., Ichimura, Y., Sou, Y.S., Ueno, I., Sakamoto, A., Tong, K.I., et al. (2010). The selective autophagy substrate p62 activates the stress responsive transcription factor Nrf2 through inactivation of Keap1. Nat. Cell Biol. *12*, 213–223.

Levine, B., and Kroemer, G. (2008). Autophagy in the pathogenesis of disease. Cell *132*, 27–42.

Li, L., Shen, C., Nakamura, E., Ando, K., Signoretti, S., Beroukhim, R., Cowley, G.S., Lizotte, P., Liberzon, E., Bair, S., et al. (2013). SQSTM1 is a pathogenic target of 5q copy number gains in kidney cancer. Cancer Cell *24*, 738–750.

Ling, J., Kang, Y., Zhao, R., Xia, Q., Lee, D.F., Chang, Z., Li, J., Peng, B., Fleming, J.B., Wang, H., et al. (2012). KrasG12D-induced IKK2/β/NF-κB activation by IL-1α and p62 feedforward loops is required for development of pancreatic ductal adenocarcinoma. Cancer Cell *21*, 105–120.

Lisanti, M.P., Martinez-Outschoorn, U.E., and Sotgia, F. (2013). Oncogenes induce the cancer-associated fibroblast phenotype: metabolic symbiosis and "fibroblast addiction" are new therapeutic targets for drug discovery. Cell Cycle *12*, 2723–2732.

Locasale, J.W. (2013). Serine, glycine and one-carbon units: cancer metabolism in full circle. Nat. Rev. Cancer *13*, 572–583.

Ma, L., Tao, Y., Duran, A., Llado, V., Galvez, A., Barger, J.F., Castilla, E.A., Chen, J., Yajima, T., Porollo, A., et al. (2013). Control of nutrient stress-induced metabolic reprogramming by PKCζ in tumorigenesis. Cell *152*, 599–611.

Metallo, C.M., and Vander Heiden, M.G. (2013). Understanding metabolic regulation and its influence on cell physiology. Mol. Cell *49*, 388–398.

Moscat, J., and Diaz-Meco, M.T. (2009). p62 at the crossroads of autophagy, apoptosis, and cancer. Cell *137*, 1001–1004.

Moscat, J., and Diaz-Meco, M.T. (2011). Feedback on fat: p62-mTORC1-autophagy connections. Cell *147*, 724–727.

Moscat, J., and Diaz-Meco, M.T. (2012). p62: a versatile multitasker takes on cancer. Trends Biochem. Sci. *37*, 230–236.

Moscat, J., Diaz-Meco, M.T., and Wooten, M.W. (2007). Signal integration and diversification through the p62 scaffold protein. Trends Biochem. Sci. *32*, 95–100.

Nyström, M.L., Thomas, G.J., Stone, M., Mackenzie, I.C., Hart, I.R., and Marshall, J.F. (2005). Development of a quantitative method to analyse tumour cell invasion in organotypic culture. J. Pathol. *205*, 468–475.

Olson, M.V., Lee, J., Zhang, F., Wang, A., and Dong, Z. (2006). Inducible nitric oxide synthase activity is essential for inhibition of prostatic tumor growth by interferon-beta gene therapy. Cancer Gene Ther. *13*, 676–685.

Ostman, A., and Augsten, M. (2009). Cancer-associated fibroblasts and tumor growth—bystanders turning into key players. Curr. Opin. Genet. Dev. *19*, 67–73.

Peña-Llopis, S., Vega-Rubin-de-Celis, S., Schwartz, J.C., Wolff, N.C., Tran, T.A., Zou, L., Xie, X.J., Corey, D.R., and Brugarolas, J. (2011). Regulation of TFEB and V-ATPases by mTORC1. EMBO J. *30*, 3242–3258.

Possemato, R., Marks, K.M., Shaul, Y.D., Pacold, M.E., Kim, D., Birsoy, K., Sethumadhavan, S., Woo, H.K., Jang, H.G., Jha, A.K., et al. (2011). Functional genomics reveal that the serine synthesis pathway is essential in breast cancer. Nature *476*, 346–350.

Ridky, T.W., Chow, J.M., Wong, D.J., and Khavari, P.A. (2010). Invasive three-dimensional organotypic neoplasia from multiple normal human epithelia. Nat. Med. *16*, 1450–1455.

Rolland, P., Madjd, Z., Durrant, L., Ellis, I.O., Layfield, R., and Spendlove, I. (2007). The ubiquitin-binding protein p62 is expressed in breast cancers showing features of aggressive disease. Endocr. Relat. Cancer *14*, 73–80.

Sanchez, P., De Carcer, G., Sandoval, I.V., Moscat, J., and Diaz-Meco, M.T. (1998). Localization of atypical protein kinase C isoforms into lysosome-targeted endosomes through interaction with p62. Mol. Cell. Biol. *18*, 3069–3080.

Santos, A.M., Jung, J., Aziz, N., Kissil, J.L., and Puré, E. (2009). Targeting fibroblast activation protein inhibits tumor stromagenesis and growth in mice. J. Clin. Invest. *119*, 3613–3625.

Schafer, Z.T., and Brugge, J.S. (2007). IL-6 involvement in epithelial cancers. J. Clin. Invest. *117*, 3660–3663.

Schäfer, M., and Werner, S. (2008). Cancer as an overhealing wound: an old hypothesis revisited. Nat. Rev. Mol. Cell Biol. *9*, 628–638.

Schauer, I.G., Ressler, S.J., Tuxhorn, J.A., Dang, T.D., and Rowley, D.R. (2008). Elevated epithelial expression of interleukin-8 correlates with myofibroblast reactive stroma in benign prostatic hyperplasia. Urology *72*, 205–213.

Shen, M.M., and Abate-Shen, C. (2010). Molecular genetics of prostate cancer: new prospects for old challenges. Genes Dev. *24*, 1967–2000.

Thompson, H.G., Harris, J.W., Wold, B.J., Lin, F., and Brody, J.P. (2003). p62 overexpression in breast tumors and regulation by prostate-derived Ets factor in breast cancer cells. Oncogene *22*, 2322–2333.

Trimboli, A.J., Cantemir-Stone, C.Z., Li, F., Wallace, J.A., Merchant, A., Creasap, N., Thompson, J.C., Caserta, E., Wang, H., Chong, J.L., et al. (2009). Pten in stromal fibroblasts suppresses mammary epithelial tumours. Nature *461*, 1084–1091.

Vander Heiden, M.G. (2013). Exploiting tumor metabolism: challenges for clinical translation. J. Clin. Invest. *123*, 3648–3651.

Vander Heiden, M.G., Cantley, L.C., and Thompson, C.B. (2009). Understanding the Warburg effect: the metabolic requirements of cell proliferation. Science *324*, 1029–1033.

Vander Heiden, M.G., Locasale, J.W., Swanson, K.D., Sharfi, H., Heffron, G.J., Amador-Noguez, D., Christofk, H.R., Wagner, G., Rabinowitz, J.D., Asara, J.M., and Cantley, L.C. (2010). Evidence for an alternative glycolytic pathway in rapidly proliferating cells. Science *329*, 1492–1499.

Cell Systems

A new journal from Cell Press launching July 2015 offering breadth and visibility for quantitative integrative research.

Launching July 2015, Cell Systems is the home for outstanding research toward systems-level understanding and applications in the life sciences and related areas, offering a venue to reach colleagues across science, engineering, and biomedical disciplines.

- High-quality, cutting-edge basic and applied research
- Broad scope
- Peer review and publication tailored to multidisciplinary data-intensive research
- Flexible open access options

Learn more at www.cell.com/cell-systems

CellPress
Your work is our life

ASHG2015

ASHG 2015 is the largest human genetics meeting in the world, making it the destination for cutting-edge science in all genetics disciplines.

Features:

- **Invited Sessions and Interactive Workshops**
- **Thousands of Poster Presentations**
- **Exhibit Hall and Technology Sessions by Exhibitors**
- **Plenary Sessions organized by ASHG's Program Committee Chair and President**
- **Trainee-Focused Events and Career Resources**
- **Networking and Collaboration Opportunities**

2015 Program Chair:
Chris Gunter, PhD, Marcus Autism Center and Emory University School of Medicine

2015 President:
Neil Risch, PhD, University of California San Francisco

Earn CMEs & CEUs

Reserve Hotel Rooms Now

Where **Science** Meets the **City**

October 6-10 • Baltimore, MD

ashg.org/2015meeting

Abstract Submission Deadline: June 11, 2015

The American Society of Human Genetics
1.866.HUMGENE | General: ashgmeetings@ashg.org | Exhibits: exhibits@ashg.org

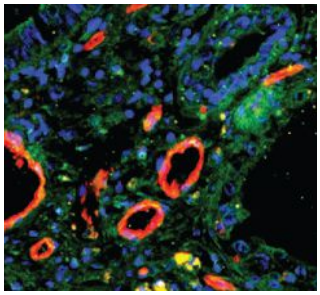

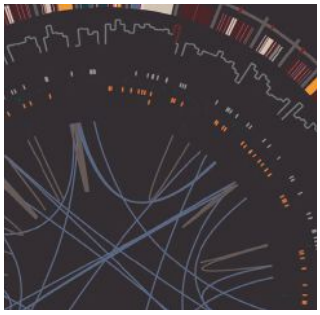

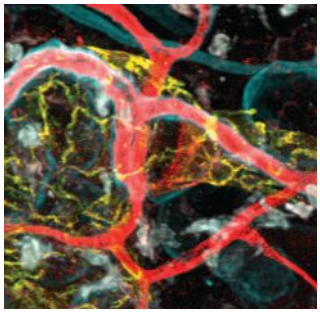

2015-2016 SCIENTIFIC CONFERENCES

Presenting the most significant research on cancer etiology, prevention, diagnosis, and treatment

Metabolism and Cancer
Co-Chairpersons: Ralph J. DeBerardinis, David M. Sabatini, and Almut Schulze
June 7-10, 2015 • Bellevue, WA

AACR Precision Medicine Series: Integrating Clinical Genomics and Cancer Therapy
Co-Chairpersons: Charles L. Sawyers, Elaine R. Mardis, and Arul M. Chinnaiyan
June 13-16, 2015 • Salt Lake City, UT

EACR-AACR-SIC Special Conference on Anticancer Drug Action and Drug Resistance: From Cancer Biology to the Clinic
Co-Chairpersons: Richard M. Marais, Pasi Jänne, and Riccardo Dolcetti
June 20-23, 2015 • Florence, Italy

Chromatin and Epigenetics in Cancer
Co-Chairpersons: Peter A. Jones, Sharon Y. R. Dent, and Charles W. M. Roberts
September 24-27, 2015 • Atlanta, GA

CRI-CIMT-EATI-AACR The Inaugural International Cancer Immunotherapy Conference: Translating Science into Survival
September 27-30, 2015 • New York, NY

Advances in Breast Cancer Research
Co-Chairpersons: Matthew J. Ellis, Charles M. Perou, and Jane E. Visvader
October 17-20, 2015 • Bellevue, WA

Advances in Ovarian Cancer: Exploiting Vulnerabilities
Co-Chairpersons: Kathleen R. Cho, Douglas A. Levine, and Benjamin G. Neel
October 17-20, 2015 • Orlando, FL

Fourth AACR International Conference on Frontiers in Basic Cancer Research
Chairperson: M. Celeste Simon;
Co-Chairpersons: James P. Allison, John E. Dick, Nathanael S. Gray, and Victor E. Velculescu
October 23-26, 2015 • Philadelphia, PA

Basic Science of Sarcomas
Co-Chairpersons: Robert G. Maki, Angelo Paolo Dei Tos, Jonathan A. Fletcher, Lee J. Helman, and Brian Van Tine
November 3-4, 2015 • Salt Lake City, UT

AACR-NCI-EORTC International Conference on Molecular Targets and Cancer Therapeutics
Scientific Committee Co-Chairpersons: Levi A. Garraway, Lee J. Helman, and Jean-Charles Soria
November 5-9, 2015 • Boston, MA

Pediatric Oncology
Co-Chairpersons: Scott Armstrong, Charles G. Mullighan, Kevin M. Shannon, and Kimberly Stegmaier
November 9-12, 2015 • Fort Lauderdale, FL

New Horizons in Cancer Research
Co-Chairpersons: Lewis C. Cantley and Carlos L. Arteaga
November 12-15, 2015 • Shanghai, China

Eighth AACR Conference on the Science of Cancer Health Disparities in Racial/Ethnic Minorities and the Medically Underserved
Co-Chairpersons: John M. Carethers, Marcia R. Cruz-Correa, Mary Jackson Scroggins, Edith A. Perez, Beti Thompson, and Cheryl L. Willman
November 13 - 16, 2015 Atlanta, GA

Developmental Biology and Cancer
Co-Chairpersons: Hans Clevers, Stuart Orkin, and Suzanne Baker
November 30-December 3, 2015 • Boston, MA

Tumor Metastasis
Co-Chairpersons: Bruce R. Zetter, Melody A. Swartz, and Jeffrey W. Pollard
November 30-December 3, 2015 • Austin, TX

Noncoding RNAs and Cancer
Co-Chairpersons: Howard Y. Chang, Jeannie T. Lee, and Joshua Mendell
December 4-7, 2015 • Boston, MA

San Antonio Breast Cancer Symposium
Co-Directors: Carlos L. Arteaga, Virginia Kaklamani, and C. Kent Osborne
December 8-12, 2015 • San Antonio, TX

Tenth AACR-JCA Joint Conference
Conference Co-Chairpersons: Frank McCormick and Tetsuo Noda
February 16-20, 2016 • Maui, Hawaii

AACR Annual Meeting 2016
Program Committee Chairperson: Scott Armstrong
April 16-20, 2016 • New Orleans, LA

www.AACR.org/Calendar

AACR American Association for Cancer Research

FINDING CURES TOGETHER℠

200

BIO-RAD'S DROPLET DIGITAL™ PCR SYSTEMS

Over 200 Peer-Reviewed Droplet Digital PCR (ddPCR™) Publications*

From detection of rare mutations and cancer biomarkers to quantification of gene expression and miniscule viral loads, the QX100™ and QX200™ Droplet Digital PCR Systems have been used to redefine the limits of absolute nucleic acid quantification. With over 200 peer-reviewed publications, ddPCR platforms have outperformed other digital PCR systems by several orders of magnitude. The third-generation QX200™ AutoDG™ System now brings automation and scalability to digital PCR.

Visit **bio-rad.com/info/cancercell200** for the publication list and to learn more.

BIO-RAD

* Based on PubMed data, February 2015.

nanoString TECHNOLOGIES®

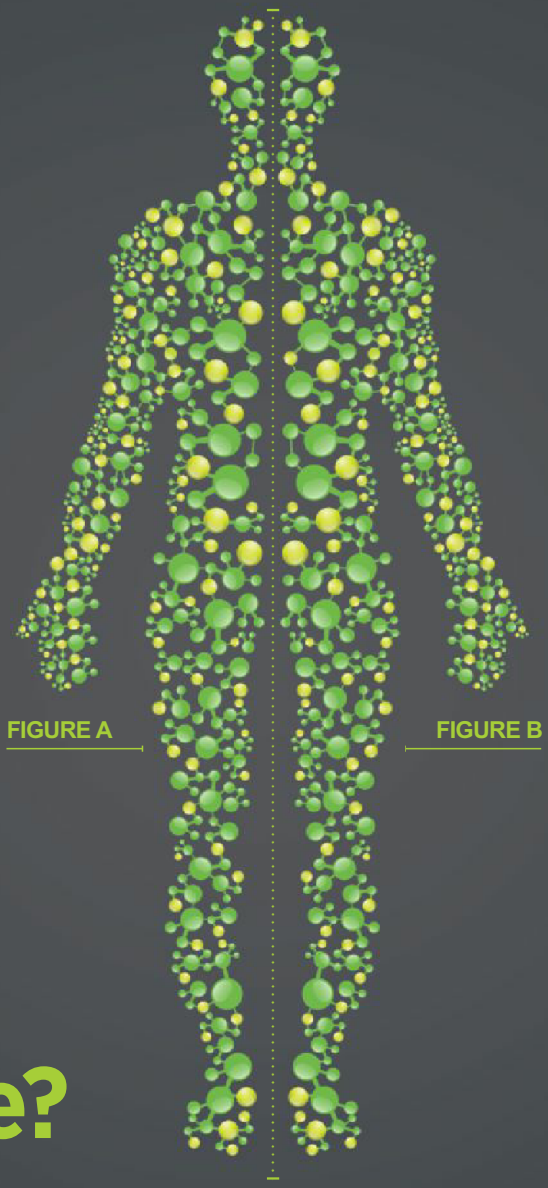

See the difference?

IN TRANSLATIONAL RESEARCH, EVERY DIFFERENCE COUNTS. NO MATTER HOW COMPLEX YOUR SAMPLES OR HOW CHALLENGING YOUR QUESTIONS, WITH nCOUNTER, YOU'LL FIND THE REAL DIFFERENCE—EVERY RUN, EVERY TIME.

With NanoString's nCounter® Analysis System, you can believe the differences you see. nCounter offers streamlined, enzyme-free* technology that eliminates both cDNA synthesis and PCR amplification, so you won't waste your time with artifacts or variable results. You get clinic-ready data that can be validated and trusted today.

www.nanostring.com/see-the-difference

*Single Cell assay requires amplification prior to analysis on the nCounter Analysis System.